

Final Report

August 2022

Development of GFRP Reinforced Single Slope Bridge Rail

Principal investigator:

Gary R. Consolazio, Ph.D.

Co-Principal investigator:

H.R. Trey Hamilton, Ph.D., P.E.

Research assistants:

Uni Y. Chen

Satyajeet R. Patil, Ph.D.

Department of Civil and Coastal Engineering
University of Florida
P.O. Box 116580
Gainesville, Florida 32611

Sponsor:

Florida Department of Transportation (FDOT)
Christina Freeman, P.E. – Project manager

Contract:

UF Project No. P0119525-P0119526
FDOT Contract No. BDV31-977-110

DISCLAIMER

The opinions, findings, and conclusions expressed in this publication are those of the authors and not necessarily those of the State of Florida Department of Transportation.

SI (MODERN METRIC) CONVERSION FACTORS
APPROXIMATE CONVERSIONS TO SI UNITS

SYMBOL	WHEN YOU KNOW	MULTIPLY BY	TO FIND	SYMBOL
LENGTH				
in	inches	25.4	millimeters	mm
ft	feet	0.305	meters	m
yd	yards	0.914	meters	m
mi	miles	1.61	kilometers	km
AREA				
in²	square inches	645.2	square millimeters	mm ²
ft²	square feet	0.093	square meters	m ²
yd²	square yard	0.836	square meters	m ²
ac	acres	0.405	hectares	ha
mi²	square miles	2.59	square kilometers	km ²
VOLUME				
fl oz	fluid ounces	29.57	milliliters	mL
gal	gallons	3.785	liters	L
ft³	cubic feet	0.028	cubic meters	m ³
yd³	cubic yards	0.765	cubic meters	m ³
NOTE: volumes greater than 1000 L shall be shown in m ³				
MASS				
oz	ounces	28.35	grams	g
lb	pounds	0.454	kilograms	kg
T	short tons (2,000 lb)	0.907	Megagrams	Mg (or "t")
TEMPERATURE (exact degrees)				
°F	Fahrenheit	5(F-32)/9 or (F-32)/1.8	Celsius	°C
FORCE and PRESSURE or STRESS				
kip	1,000 pound force	4.45	kilonewtons	kN
lbf	pound force	4.45	newtons	N
lbf/in²	pound force per square inch	6.89	kilopascals	kPa
ksi	kips force per square inch	6.89	Megapascals	MPa

TECHNICAL REPORT DOCUMENTATION PAGE

1. Report No.	2. Government Accession No.	3. Recipient's Catalog No.	
4. Title and Subtitle <p style="text-align: center;">Development of GFRP Reinforced Single Slope Bridge Rail</p>		5. Report Date <p style="text-align: center;">August 2022</p>	
		6. Performing Organization Code	
		8. Performing Organization Report No.	
7. Author(s) <p style="text-align: center;">Gary Consolazio, H.R. Hamilton, Uni Chen, Satyajeet Patil</p>		2022/119525-119526	
9. Performing Organization Name and Address <p style="text-align: center;">University of Florida Department of Civil and Coastal Engineering 365 Weil Hall, P.O. Box 116580 Gainesville, FL 32611-6580</p>		10. Work Unit No. (TRAIS)	
		11. Contract or Grant No. <p style="text-align: center;">BDV31-977-110</p>	
		13. Type of Report and Period Covered <p style="text-align: center;">Final Report</p>	
12. Sponsoring Agency Name and Address <p style="text-align: center;">Florida Department of Transportation Research Management Center 605 Suwannee Street, MS 30 Tallahassee, FL 32399-0450</p>		14. Sponsoring Agency Code	
		15. Supplementary Notes	
16. Abstract <p>In the design of highway bridges in Florida, glass fiber reinforced polymer (GFRP) materials are starting to replace mild carbon steel as the basis for reinforcing structural concrete components. Whereas traditional steel rebar is susceptible to corrosion, GFRP rebar is not, and therefore the use of GFRP has the potential to reduce maintenance costs and mitigate the need for corrosion-related structural rehabilitation. Moreover, GFRP rebar is lightweight in comparison to steel rebar, and consequently its use can simplify construction processes and reduce construction costs. However, GFRP does not possess the ductility that is associated with yielding of mild steel rebar. Instead GFRP is linearly elastic until failure. Additionally, the elastic modulus of GFRP is approximately one-quarter that of steel, resulting in reduced system stiffness. Designing GFRP reinforced concrete elements must therefore include consideration of how these material differences may alter structural performance and failure modes.</p> <p>The Florida Department of Transportation (FDOT) has, to date, implemented the use GFRP-reinforced concrete (GFRP-R/C) for use in the construction of a variety of different bridge structural components (piles, pile caps, decks, etc.). In the present study, a GFRP-reinforced concrete FDOT 36" single slope traffic rail (SSTR) was developed and tested. To minimize potential changes in bridge rail construction processes, the GFRP-reinforced rail was designed using a steel-to-GFRP, bar-for-bar replacement approach wherever possible. However, some modifications in rebar configuration were necessitated by the non-ductile nature of GFRP rebar.</p> <p>Geometrically, the shape of the impact face of a R/C bridge rail that had previously passed full-scale truck crash testing was preserved, without modification, in the GFRP bridge rail. In lieu of full-scale crash testing, dynamic pendulum impact tests were used in this study to evaluate whether the performance of the GFRP reinforced bridge rail. Pendulum testing utilized an impactor that reproduced the transverse impact energy and transverse peak impact force from a MASH test level 4 (TL-4) impact of a 10000S single unit truck (SUT). Tests were performed on steel-reinforced concrete R/C (control) rails and GFRP reinforced concrete rails in structural configurations that represented impacts at both central- and end-locations located longitudinally along rails.</p> <p>Results from pendulum impact testing indicated that the GFRP rail exhibited impact performance characteristics that were compatible with the requirements of bridge rails. For interior (centrally located) impact locations, representing the most common practical design scenarios, a density of GFRP bar equivalent to that of mild steel rebar was determined to be adequate. Under the most severe (end-of-rail) impact conditions tested, however, a greater density of GFRP reinforcement was required, in comparison to mild steel rebar. By introducing additional GFRP bars within a limited end-region zone, deflections for GFRP rails were acceptably small, and observed cracking was manageable (i.e., cracks could, if necessary, be repaired/injected).</p>			
17. Key Words <p>Bridge traffic railing, glass fiber reinforced polymer (GFRP) concrete, vehicle impact load, pendulum impact testing</p>		18. Distribution Statement <p style="text-align: center;">No restrictions.</p>	
19. Security Classif. (of this report) <p style="text-align: center;">Unclassified</p>	20. Security Classif. (of this page) <p style="text-align: center;">Unclassified</p>	21. No. of Pages <p style="text-align: center;">338</p>	22. Price

Form DOT F 1700.7 (8-72). Reproduction of completed page authorized

ACKNOWLEDGEMENTS

The authors thank the Florida Department of Transportation (FDOT) for providing the funding that made this research possible. Additionally, the authors acknowledge contributions made by FDOT Structures Research Center personnel who contributed significantly to this project by providing technical insights, suggestions, and assistance with fabrication and pendulum impact testing. Special thanks to Christina Freeman, William Potter, Stephen Eudy, Justin Robertson, Paul Tighe, Michael Waters, Miguel Ramirez, Ben Allen, and Sam Adeniji.

The authors thank Owens Corning Infrastructure Solutions for technical suggestions, donated materials, and material test data. Special thanks to Douglas Gremel, Jonathan Fischer, Mikhail Vorobiev, Casey Mattson, Shelby Ewart, and Dave Hartman.

EXECUTIVE SUMMARY

In this study, a glass fiber reinforced polymer (GFRP) reinforced concrete FDOT 36” single slope traffic rail (SSTR) was developed and tested as an alternative to the conventional mild steel reinforced concrete (R/C) bridge rail. To minimize potential changes in bridge rail construction processes, the GFRP-reinforced rail was designed using a steel-to-GFRP, bar-for-bar replacement approach wherever possible. However, some modifications in rebar configuration were necessitated by the non-ductile (‘linear elastic to rupture’) nature of GFRP rebar.

To facilitate direct comparisons between the GFRP-reinforced concrete traffic rail and the conventional R/C rail, test specimens of each configuration were pendulum impact tested. Pendulum impact test protocols used during the physical testing phase of this project delivered impact force and impact energy that corresponded to the transverse (perpendicular to rail) components of a test level 4 (TL-4) vehicle impact, as described by AASHTO MASH. Specifically, the pendulum impactor used during testing imparted the transverse components of force and energy from a 10000S single unit truck (SUT) impact under TL-4 conditions.

Steel-reinforced (conventional) and GFRP-reinforced (alternative) concrete bridge rails were tested in two configurations: center-of-rail (COR), and end-of-rail (EOR). Center-of-rail tests were intended to represent vehicle impacts at central (interior) locations along a bridge rail. At such locations, significant length of rail extends in both directions away from the impact zone and serves to partially support the impacted region against transverse deflection. In contrast, end-of-rail impacts were intended to represent conditions at locations where the rail would be discontinuous (e.g., at a rail transition point or at a construction joint). At these locations, only rail length extending in one direction away from the impact zone is available to contribute to resisting transverse load. Consequently, transverse deflections and damage indicators (e.g., crack widths) are expected to be larger for the more severe end-of-rail test conditions.

Pendulum impact testing of the R/C COR specimen produced a maximum deflection of approximately 0.07 in., and no discernible cracking. Corresponding testing of a GFRP COR specimen produced a maximum deflection of approximately 0.09 in., and a single crack with a width of less than 0.004 in. For central (interior) impact locations, performance of the GFRP system was thus comparable to that of the traditional R/C system.

For the more structurally demanding end-of-rail condition, pendulum impact testing of the R/C EOR specimen produced a maximum deflection of 0.42 in. and a maximum crack width of 0.016 in. Pendulum impact testing of a GFRP EOR specimen (design iteration 2) produced a maximum deflection of 0.67 in., residual deflection of 0.25 in., and a maximum crack width of 0.035 in. Deflections and crack widths for the GFRP rail were larger than for the R/C rail, however, the observed levels were considered acceptable given that GFRP rebar is not susceptible to corrosion.

For the center-of-rail test (COR) specimens, the traditional steel rebar layout and the GFRP rebar layout were very similar in terms of bar sizes, bar lengths, and bar spacings. However, for the end-of-rail (EOR) specimens, additional transverse bars were necessary to avoid a failure mode involving progressive rupturing of multiple GFRP bars.

Based on pendulum impact test results, the center and end GFRP rail specimens performed in manner comparable to conventional R/C rails. Deflections for GFRP rails were acceptably small, and observed cracking was manageable (i.e., cracks could, if necessary, be injected and repaired).

TABLE OF CONTENTS

DISCLAIMER	ii
SI (MODERN METRIC) CONVERSION FACTORS	iii
TECHNICAL REPORT DOCUMENTATION PAGE	iv
ACKNOWLEDGEMENTS	v
EXECUTIVE SUMMARY	vi
LIST OF FIGURES	x
CHAPTER 1 INTRODUCTION	1
1.1 Background.....	1
1.1.1 Related FDOT research	2
1.2 Objectives	2
1.3 Scope of work	3
1.4 Overall approach.....	3
CHAPTER 2 LITERATURE REVIEW	4
2.1 Introduction.....	4
2.2 Design specifications: GFRP-reinforced concrete.....	4
2.2.1 Environmental reduction factors	4
2.2.2 Yield line analysis of concrete barrier	4
2.2.3 Resistance factor.....	6
2.3 Material specifications: GFRP rebar	6
2.4 Impact test guidelines: bridge rail vehicular crash test.....	7
2.5 Prior research: GFRP-reinforced concrete under impact load.....	7
2.5.1 Pendulum impact test on TL-4 GFRP reinforced rails.....	7
2.5.2 Vehicle crash test on TL-5 GFRP reinforced barriers.....	10
2.5.3 FRP reinforced beam testing	11
CHAPTER 3 SURROGATE VEHICLE PENDULUM IMPACT TESTING AND SIMULATION	13
3.1 Introduction.....	13
3.2 Full scale impact test	13
3.3 Development of Single-Unit Truck (SUT) 10000S impactor.....	14
3.3.1 Impact energy	14
3.3.2 Impact force.....	15
3.3.3 Single-Unit Truck (SUT) 10000S impactor	18
3.4 Pendulum impact test facility	20
3.5 Finite element modeling and swing simulation.....	21

3.5.1 Impactor model.....	22
3.5.2 Pendulum impact simulation	22
CHAPTER 4 DEVELOPMENT OF RAIL REBAR CONFIGURATION	24
4.1 Introduction.....	24
4.2 Rail impact locations	24
4.3 Reference configuration: steel rebar	24
4.4 Replacement configuration: GFRP rebar.....	26
4.4.1 Material properties.....	26
4.4.2 Center-of-rail (COR) rebar	27
4.4.3 End-of-rail (EOR) rebar	28
CHAPTER 5 FINITE ELEMENT MODELING OF RAIL COMPONENTS	30
5.1 Introduction.....	30
5.2 Concrete modeling.....	30
5.3 Rebar modeling.....	31
5.4 Bond modeling.....	32
CHAPTER 6 DEVELOPMENT OF RAIL TEST SPECIMEN CONFIGURATION	33
6.1 Introduction.....	33
6.2 Simulated impact performance for COR specimen: Steel vs. GFRP	36
6.3 Simulated impact performance for EOR specimen: Steel vs. GFRP.....	39
CHAPTER 7 FULL-SCALE RAIL PENDULUM IMPACT TEST PROGRAM	43
7.1 Overview.....	43
7.2 Construction of test specimens	43
7.3 Installation of test specimen	46
7.4 Instrumentation plan	52
7.4.1 Contact tape switches	53
7.4.2 Optical break beams	54
7.4.3 Accelerometers	55
7.4.4 High speed cameras.....	57
7.4.5 Laser displacement sensors	58
7.4.6 Concrete strain gages.....	59
7.4.7 Rebar strain gages.....	60
7.5 Impact test procedure.....	61
CHAPTER 8 FULL-SCALE CENTER OF RAIL (COR) IMPACT TEST RESULTS	63
8.1 Introduction.....	63
8.2 Standard (R/C) rail.....	63
8.2.1 Impact testing of R/C COR specimen 1	63
8.2.2 Impact testing of R/C COR specimen 2	77
8.3 GFRP reinforced rail.....	89

8.3.1 Impact testing of GFRP reinforced COR specimen 1	89
8.4 Comparison of GFRP and R/C COR test specimen results	102
8.4.1 Comparison of COR acceleration data and pendulum impact forces.....	102
8.4.2 Comparison of COR laser displacement data.....	102
8.4.3 Comparison of COR external concrete strain gage data	103
8.4.4 Comparison of COR internal steel rebar strain gage data	105
CHAPTER 9 FULL-SCALE END OF RAIL (EOR) IMPACT TEST RESULTS	107
9.1 Introduction.....	107
9.2 Standard (R/C) rail.....	109
9.2.1 Impact testing of R/C EOR specimen 1 (R/C test specimen 3).....	109
9.3 GFRP rail	122
9.3.1 Impact testing of GFRP EOR specimen 1 (GFRP test specimen 2).....	122
9.3.2 Impact testing of GFRP EOR specimen 2 (GFRP test specimen 3).....	137
9.4 Comparison of GFRP and R/C EOR test specimen results	150
9.4.1 Overview	150
9.4.2 Comparison of EOR acceleration data and pendulum impact forces.....	150
9.4.3 Comparison of EOR laser displacement data	151
9.4.4 Comparison of EOR external concrete strain gage data and cracking patterns ...	151
9.4.5 Comparison of EOR internal steel rebar strain gage data	154
CHAPTER 10 SUMMARY AND CONCLUSIONS	155
REFERENCES	157
APPENDIX A: CALCULATION OF IMPACT TEST DESIGN	159
APPENDIX B: MATERIAL KEYWORDS FOR FINITE ELEMENT MODELING	184
APPENDIX C: CALCULATION OF 36” SINGLE SLOPE BRIDGE RAIL	186
APPENDIX D: STRUCTURAL DRAWINGS FOR GFRP-REINFORCED TEST SPECIMEN.....	206
APPENDIX E: STRUCTURAL DRAWINGS FOR STEEL-REINFORCED TEST SPECIMEN.....	231
APPENDIX F: CONCRETE MIXTURE DESIGNS AND DELIVERED MIXTURES.....	253
APPENDIX G: ANCHORAGE SEQUENCE.....	276
APPENDIX H: INSTRUMENTATION PLAN	294
APPENDIX I: HARDENED MECHANICAL PROPERTIES OF RAIL CONCRETE MIXTURES	316

LIST OF FIGURES

<u>Figure</u>	<u>Page</u>
Figure 1-1. Corrosion on bridge rail	1
Figure 1-2. Typical FDOT 36” SSTR a) Installed on a typical bridge; b) Cross section	2
Figure 2-1. Yield line analysis of concrete bridge rail (AASHTO LRFD 2017)	5
Figure 2-2. Simplified rail behavior under transverse impact load: a) Top of rail behavior; b) Base of rail behavior (sectional view); c) Isometric view of rail.....	6
Figure 2-3. Pendulum impact test set-up (El-Salakawy et al. 2001): a) Schematic diagram for the test set-up; b) PL-2 barrier field test set up; c) Steel plate and tire arrangement for load distribution; d) Impact test with steel wrecking ball.....	8
Figure 2-4. PL-2 barrier reinforcement layout (El-Salakawy et al. 2001).....	9
Figure 2-5. Cross section of crash-tested barrier (Sennah et al. 2018): a) Tested barrier with 180° hooked end bars; b) Established Canadian Highway Bridge Design Code (CHBDC) barrier with GFRP bars	10
Figure 2-6. GFRP RC beams under impact loading (Goldston et al. 2016): a) Failure of over-reinforced beam; b) Failure of beam with balanced reinforcement ratio	12
Figure 3-1. TL-4 crash test on TxDOT 36-in. SSTR (Sheikh et al. 2011)	14
Figure 3-2. TxDOT 36-in. SSTR after MASH test 4-12 (Sheikh et al. 2011).....	14
Figure 3-3. FE model of the SUT impacting a rigid SSTR under MASH TL-4 impact conditions (Sheikh et al. 2011)	15
Figure 3-4. FEA impact force-time curve for 36-in. single-slope traffic rails (SSTR) (after Sheikh et al. 2011)	16
Figure 3-5. Pendulum impactor design overview (Consolazio et al., 2021).....	16
Figure 3-6. Aluminum honeycomb cartridge and impactor front nose (Consolazio et al., 2021)	17
Figure 3-7. Simplified TTI FEA force-time curve compared to the design crushable nose (see Appendix A for additional details) (Consolazio et al., 2021).....	18
Figure 3-8. Design of the FDOT SUT 10000S impactor (Consolazio et al., 2021)	19

Figure 3-9. FDOT SUT 10000S impactor (without aluminum honeycomb cartridges installed).....	19
Figure 3-10. FDOT SUT 10000S impactor prior of TL-4 pendulum impact test.....	20
Figure 3-11. FDOT pendulum impact facility at M. H. Ansley Structures Research Center (Tallahassee, FL).....	21
Figure 3-12. Pendulum impactor in pulled-back configuration (Note: towers supporting the impactor not shown for clarity).....	21
Figure 3-13. Pendulum impactor finite element model (Note: rigid links connecting hanger frame to back block not shown).....	22
Figure 3-14. Finite element pendulum impact simulation with impactor at: a) Drop height; b) Incipient contact; c) End of impact (Consolazio et al., 2021)	23
Figure 3-15. Finite element pendulum impactor simulation: a) Side elevation view at end of impact; b) Force-time results from simulation (Consolazio et al., 2021)	23
Figure 4-1. Rail impact locations: a) Center-of-rail (COR); b) End-of-rail (EOR).....	24
Figure 4-2. Steel reinforced typical section through traffic rail.....	25
Figure 4-3. Steel bars for steel-reinforced bridge rail: a) bar 4P; b) bar 4V	25
Figure 4-4. Steel and GFRP material properties	26
Figure 4-5. GFRP reinforced typical section through traffic rail (COR).....	27
Figure 4-6. Stirrups of GFRP-reinforced bridge rail: a) bar G401; b) bar G402	28
Figure 4-7. Rail rebar configurations and spacing at center of rail (COR) and end of rail (EOR): a) Steel rebar spacing overview; b) Steel rebar details; c) GFRP rebar spacing overview; d) GFRP COR rebar details; e) GFRP EOR rebar details	29
Figure 5-1. Stress-strain model for concrete (tension and compression) and damage index as reported by the MAT_CSCM material model (adapted from Murray, 2007)	31
Figure 5-2. Stress-strain models for steel rebar and GFRP rebar	32
Figure 6-1. Traffic rail on a typical bridge	33
Figure 6-2. Test specimen deck overhang and thickened edge: a) Cross-sectional view; b) Back view (COR shown, EOR similar)	33
Figure 6-3. Test specimen anchorages on thickened deck.....	34

Figure 6-4. 36-in. SSTR test specimen overview: a) COR; b) EOR	35
Figure 6-5. COR test specimen FEA model: a) Concrete components overview; b) Steel reinforcement; c) GFRP reinforcement	37
Figure 6-6. Rebar models for COR test specimens: a) Steel transverse bars; b) GFRP transverse bars	38
Figure 6-7. Reinforced test specimen rail cross section: a) Steel-reinforced test specimen; b) GFRP reinforced test specimen	38
Figure 6-8. COR rail test specimen FEA swing model maximum concrete damage: a) Steel-reinforced rail (front isometric view); b) Steel-reinforced rail (back isometric view); c) GFRP-reinforced rail (front isometric view); d) GFRP-reinforced rail (back isometric view).....	39
Figure 6-9. EOR test specimen FEA model: a) Concrete components overview; b) Steel reinforcement; c) GFRP reinforcement	40
Figure 6-10. EOR GFRP rail transverse rebar models	41
Figure 6-11. EOR test specimen rail FEA swing model maximum concrete damage: a) Steel-reinforced rail (front isometric view); b) Steel-reinforced rail (back isometric view); c) GFRP-reinforced rail (front isometric view); d) GFRP-reinforced rail (back isometric view).....	42
Figure 7-1 Reinforcing bars positioned inside deck formwork for steel reinforced specimens	43
Figure 7-2 Deck-to-rail connection bars and end-support buttress reinforcement positioned inside deck formwork for steel reinforced specimens	44
Figure 7-3 GFRP bars positioned inside deck formwork for GFRP bar reinforced specimen	44
Figure 7-4 Deck concrete placement	45
Figure 7-5 Construction of rail portion of R/C test specimen 1: (a) Rail reinforcement positioned inside rail formwork; (b) Rail concrete placed and formed	45
Figure 7-6 Formed R/C test specimen 1	46
Figure 7-7 Test specimen lifted out of the formwork by crane	46
Figure 7-8 Test specimen being moved into position on the pendulum foundation.....	47
Figure 7-9 Impact test specimen in position on pendulum foundation.....	47
Figure 7-10 Backside of impact specimen after being positioned onto the pendulum foundation (with temporary HSS lifting element still connected).....	48

Figure 7-11 Diagram of impact test specimen with additional anchoring elements placed: (a) Front isometric view; (b) Back isometric view	49
Figure 7-12 Post-tensioning fourth (front right) threaded bar for anchoring test specimen to pendulum foundation with the FDOT loading assembly	50
Figure 7-13 Anchored test specimen	50
Figure 7-14 Placing grout between test specimen and reaction element (steel slide stopper) as a secondary reaction system to prevent specimen from sliding during impact testing.....	51
Figure 7-15 Aluminum loading wedge adhered to front face of rail	51
Figure 7-16 Pendulum impactor and impact test specimen prepared and ready for testing	52
Figure 7-17 Instrumentation plan used in pendulum impact testing.....	52
Figure 7-18 External instrumentation: (a) Front concrete strain gage and tape switch sensor locations; (b) Back concrete strain gage and laser displacement sensor locations	53
Figure 7-19 Tape switches adhered to the impact face of the aluminum loading wedge	54
Figure 7-20 Optical break beam sensors: (a) Close up of an individual sensor; (b) Break beam sensors positioned for testing	55
Figure 7-21 Accelerometers installed on pendulum impactor (top view)	56
Figure 7-22 Accelerometers installed on the pendulum impactor: (a) AC-1 mounted to the top of the concrete back block; (b) AC-2 mounted to the bottom of the concrete back block; (c) AC-3 mounted to the left mounting plate on the aluminum front nose; (d) AC-4 mounted to the right mounting plate on the aluminum front nose.....	57
Figure 7-23 High-speed digital video camera.....	58
Figure 7-24 Laser displacement sensor mounted behind a test specimen	59
Figure 7-25 Concrete strain gages (3 and 4) adhered to concrete rail surface.....	60
Figure 7-26 Strain gages attached to reinforcing bars and protected with waterproof tape: (a) Attached to steel rebar; (b) Attached to GFRP rebar	61
Figure 7-27. Pendulum impact test on rail test specimen	62
Figure 8-1 Impactor pulled back to 15-ft drop height (prior to release).....	64
Figure 8-2 High-speed video frames from HSC-1 (R/C COR test 1) showing crush deformation of aluminum honeycomb: (a) At initial impact; (b) – (c) Intermediate frames; (f) At peak impact force; (g) – (h) Sliding and separation of loading wedge	65

Figure 8-3 High-speed video frames from HSC-2 (R/C COR test 1): (a) At start of impact; (b) –; (c) Intermediate frames; (d) At peak impact force	66
Figure 8-4 R/C COR 1 test specimen after completion of impact test	66
Figure 8-5 Break beam data for R/C COR test 1	67
Figure 8-6 Tape switch data for R/C COR test 1	68
Figure 8-7 Raw concrete back block acceleration data (AC-1 & AC-2) for R/C COR test 1 (in the impact direction, local Y direction of accelerometer)	69
Figure 8-8 Raw front nose acceleration data (AC-3 & AC-4) for R/C COR test 1 (in the impact direction, local Y direction of accelerometer)	69
Figure 8-9 Computed impact forces from back block for R/C COR test 1	70
Figure 8-10 Computed impact forces from front nose for R/C COR test 1	70
Figure 8-11 Raw and filtered total computed impact force for R/C COR test 1	71
Figure 8-12 Filtered total experimental impact force for R/C COR test 1 compared to FEA prediction	71
Figure 8-13 Laser displacement sensor data for R/C COR test 1	72
Figure 8-14 External concrete strain gage data for locations on the top front face of the rail during R/C COR test 1	73
Figure 8-15 External concrete strain gage data for locations on the lower front face of the rail during R/C COR test 1	73
Figure 8-16 External concrete strain gage data for locations at the toe of the rail and deck during R/C COR test 1	74
Figure 8-17 External concrete strain gage data for locations on the back face of the rail during R/C COR test 1	75
Figure 8-18 Internal rebar strain gage data during R/C COR test 1: (a) Deck rebar; (b) Rail rebar	76
Figure 8-19 High-speed video frames from HSC-1 (R/C COR test 2) showing crush deformation of aluminum honeycomb: (a) At initial impact; (b) – (c) Intermediate frames; (f) At peak impact force	78
Figure 8-20 High-speed video frames from HSC-2 (R/C COR test 2): (a) At start of impact; (b) – (c) Intermediate frames; (d) At peak impact force	79
Figure 8-21 R/C COR test 2 specimen after completion of impact test	79

Figure 8-22 Break beam data for R/C COR test 2	80
Figure 8-23 Tape switch data for R/C COR test 2.....	80
Figure 8-24 Raw concrete back block acceleration data (AC-1 & AC-2) for R/C COR test 2 (in the impact direction, local Y direction of accelerometer)	81
Figure 8-25 Raw front nose acceleration data (AC-3 & AC-4) for R/C COR test 2 (in the impact direction, local Y direction of accelerometer)	81
Figure 8-26 Computed impact forces from back block for R/C COR test 2	82
Figure 8-27 Computed impact forces from front nose for R/C COR test 2.....	82
Figure 8-28 Raw and filtered total computed impact force for R/C COR test 2	83
Figure 8-29 Filtered total experimental impact force for R/C COR test 2 compared to FEA prediction	83
Figure 8-30 Laser displacement sensor data from R/C COR test 2.....	84
Figure 8-31 External concrete strain gage data for locations on the top front face of the rail during R/C COR test 2.....	85
Figure 8-32 External concrete strain gage data for locations on the lower front face of the rail during R/C COR test 2.....	85
Figure 8-33 External concrete strain gage data for locations at the toe of the rail and deck during R/C COR test 2.....	86
Figure 8-34 External concrete strain gage data for locations on the back face of the rail during R/C COR test 2.....	87
Figure 8-35 Internal rebar strain gage data during R/C COR test 2: (a) Deck rebar; (b) Rail rebar	88
Figure 8-36 High-speed video frames from HSC-1 (GFRP COR test 1) showing crush deformation of aluminum honeycomb: (a) At initial impact; (b) – (c) Intermediate frames; (f) At peak impact force.....	90
Figure 8-37 High-speed video frames from HSC-2 (GFRP COR test 1): (a) At start of impact; (b) – (c) Intermediate frames; (d) At peak impact force.....	91
Figure 8-38 GFRP COR test 1 specimen after completion of impact test: (a) front view; (b) back view	92
Figure 8-39 Break beam data for GFRP COR test 1	93
Figure 8-40 Tape switch data for GFRP COR test 1	93

Figure 8-41 Raw concrete back block acceleration data (AC-1 & AC-2) for GFRP COR test 1 (in the impact direction, local Y direction of accelerometer)	94
Figure 8-42 Raw front nose acceleration data (AC-3) for GFRP COR test 1 (in the impact direction, local Y direction of accelerometer)	95
Figure 8-43 Computed impact forces from back block for GFRP COR test 1	95
Figure 8-44 Computed impact forces from front nose for GFRP COR test 1	96
Figure 8-45 Raw and filtered total computed impact force for GFRP COR test 1	96
Figure 8-46 Filtered total experimental impact force for GFRP COR test 1 compared to FEA prediction	97
Figure 8-47 Laser displacement sensor data for GFRP COR test 1	98
Figure 8-48 External concrete strain gage data for locations on the top front face of the rail during GFRP COR test 1	99
Figure 8-49 External concrete strain gage data for locations on the lower front face of the rail during GFRP COR test 1	99
Figure 8-50 External concrete strain gage data for locations at the toe of the rail and deck during GFRP COR test 1	100
Figure 8-51 External concrete strain gage data for locations on the back face of the rail during GFRP COR test 1	100
Figure 8-52 Internal rebar strain gage data during GFRP COR test 1: (a) Deck rebar; (b) Rail rebar	101
Figure 8-53 Total impact force for each traffic rail impact test	102
Figure 8-54 Comparison of captured displacements	103
Figure 8-55 Comparison of external concrete strain gages on the deck near the rail toe (on the front side of the impact specimen)	104
Figure 8-56 Comparison of external concrete strain gages located at the center of the specimen (on back side of the impact specimen)	105
Figure 8-57 Comparison of internal strain gages located on the top deck rebar	106
Figure 9-1 Main components of EOR specimen	107
Figure 9-2 External EOR instrumentation: (a) Front concrete strain gage and tape switch sensor locations; (b) Back concrete strain gage and laser displacement sensor locations	108

Figure 9-3 Poor concrete consolidation of R/C EOR specimen 1 prior to testing: (a) Front face of rail; (b) Bottom of the (cross-sectional) rail face at free end.....	110
Figure 9-4 High-speed video frames from HSC-1 (R/C EOR test 1) showing crush deformation of aluminum honeycomb: (a) At initial impact; (b) – (c) Intermediate frames; (f) At peak impact force.....	111
Figure 9-5 High-speed video frames from HSC-2 (R/C EOR test 1): (a) At start of impact; (b) – (c) Intermediate frames; (d) At peak impact force.....	112
Figure 9-6 R/C EOR test 1 specimen after completion of impact test.....	112
Figure 9-7 Cracking found on R/C EOR test 1 specimen: (a) On front rail face; (b) On back rail face.....	113
Figure 9-8 Break beam data for R/C EOR test 1	114
Figure 9-9 Tape switch data for R/C EOR test 1	114
Figure 9-10 Raw concrete back block acceleration data (AC-1 & AC-2) for R/C EOR test 1 (in the impact direction, local Y direction of accelerometer).....	115
Figure 9-11 Raw front nose acceleration data (AC-3 & AC-4) for R/C COR test 1 (in the impact direction, local Y direction of accelerometer)	115
Figure 9-12 Computed impact forces from back block for R/C EOR test 1.....	116
Figure 9-13 Computed impact forces from front nose for R/C EOR test 1	116
Figure 9-14 Raw and filtered total computed impact force for R/C EOR test 1	117
Figure 9-15 Filtered total experimental impact force for R/C EOR test 1 compared to FEA prediction	117
Figure 9-16 Laser displacement sensor data from R/C EOR test 1	118
Figure 9-17 Concrete strain gage data for locations with out-of-range readings on the front face of the rail (due to cracking) for R/C EOR test 1	119
Figure 9-18 Concrete strain gage data for locations with in-range readings on the front face of the rail for R/C EOR test 1	119
Figure 9-19 External concrete strain gage data for locations on the back face of the rail during R/C EOR test 1	120
Figure 9-20 Internal rebar strain gage data during R/C EOR test 1: (a) Deck rebar; (b) Rail rebar	121

Figure 9-21 GFRP EOR specimen prepared and ready for pendulum impact testing (with instrumentation in place).....	122
Figure 9-22 High-speed video frames from HSC-1 (GFRP EOR test 1) showing crush deformation of aluminum honeycomb: (a) At initial impact; (b) – (c) Intermediate frames; (f) At peak impact force	123
Figure 9-23 High-speed video frames from HSC-2 (GFRP EOR test 1): (a) At start of impact; (b) – (c) Intermediate frames; (d) At peak impact force	124
Figure 9-24 Cracking found on GFRP EOR-1 test specimen after impact: (a) On front rail face; (b) On back rail face.....	125
Figure 9-25 Crack on the back face of GFRP EOR-1 specimen with width wider than 0.10 in.	126
Figure 9-26 Crack in deck with no rail on top (looking towards the back face)	126
Figure 9-27 Break beam data for GFRP EOR test 1	127
Figure 9-28 Tape switch data for GFRP EOR test 1	127
Figure 9-29 Raw concrete back block acceleration data (AC-1 & AC-2) for GFRP EOR test 1 (in the impact direction, local Y direction of accelerometer)	128
Figure 9-30 Raw front nose acceleration data (AC-3 & AC-4) for GFRP EOR test 1 (in the impact direction, local Y direction of accelerometer)	129
Figure 9-31 Computed impact forces from back block for GFRP EOR test 1	129
Figure 9-32 Computed impact forces from front nose for GFRP EOR test 1	130
Figure 9-33 Raw and filtered total computed impact force for GFRP EOR test 1	130
Figure 9-34 Filtered total experimental impact force for GFRP EOR test 1 compared to FEA prediction.....	131
Figure 9-35 Laser displacement sensor data from GFRP EOR test 1.....	132
Figure 9-36 Concrete strain gage data for locations with out-of-range readings (due to cracking) for GFRP EOR test 1	133
Figure 9-37 Concrete strain gage data for locations with in-range readings for GFRP EOR test 1	133
Figure 9-38 Concrete strain gage data for locations on the back (non-impact) face of the rail during GFRP EOR test 1.....	134

Figure 9-39 Internal rebar strain gage data during GFRP EOR test 1: (a) Deck rebar; (b) Rail rebar.....	135
Figure 9-40 Approximate locations at which GFRP bars were dissected from GFRP EOR rail specimen 1	136
Figure 9-41 Dissected top layer GFRP rebars and surrounding concrete: (a) Location near end of rail (EOR); (b) Location distant from EOR.....	136
Figure 9-42 GFRP EOR test 2 specimen prepared and ready for pendulum impact testing (with instrumentation in place).....	137
Figure 9-43 Additional rebar in GFRP EOR test 2 specimen (plan view of deck and rail reinforcement shown)	138
Figure 9-44 Cracks on GFRP EOR test 2 test specimen after impact: (a) On front rail face; (b) On back rail face	139
Figure 9-45 Crack in deck with no rail on top (looking towards the back face)	140
Figure 9-46 Break beam data for GFRP EOR test 2.....	140
Figure 9-47 Tape switch data for GFRP EOR test 2	141
Figure 9-48 Raw concrete back block acceleration data (AC-1 & AC-2) for GFRP EOR test 2 (in the impact direction, local Y direction of accelerometer)	142
Figure 9-49 Raw front nose acceleration data (AC-3 & AC-4) for GFRP EOR test 2 (in the impact direction, local Y direction of accelerometer)	142
Figure 9-50 Computed impact forces from back block for GFRP EOR test 2.....	143
Figure 9-51 Computed impact forces from front nose for GFRP EOR test 2	143
Figure 9-52 Raw and filtered total computed impact force for GFRP EOR test 2.....	144
Figure 9-53 Filtered total experimental impact force for GFRP EOR test 2 compared to FEA prediction.....	144
Figure 9-54 Laser displacement sensor data from GFRP EOR test 2.....	145
Figure 9-55 Concrete strain gage data for locations with out-of-range readings (due to cracking) for GFRP EOR test 2	146
Figure 9-56 Concrete strain gage data for locations with in-range readings for GFRP EOR test 2.....	147
Figure 9-57 Concrete strain gage data for locations on the back (non-impact) face of the rail during GFRP EOR test 2.....	148

Figure 9-58 Internal rebar strain gage data during GFRP EOR test 2: (a) Deck rebar; (b) Rail rebar.....	149
Figure 9-59 Total impact force for each traffic rail impact test.....	150
Figure 9-60 Comparison of displacements	151
Figure 9-61 Comparison of crack pattern on the front (impact) face of EOR rail specimens: (a) GFRP EOR specimen 1; (b) GFRP EOR specimen 2; (c) R/C EOR specimen	152
Figure 9-62 Comparison of crack pattern on the back (non-impact) face of EOR rail specimens: (a) GFRP EOR specimen 1; (b) GFRP EOR specimen 2; (c) R/C EOR specimen	153

LIST OF TABLES

<u>Table</u>	<u>Page</u>
Table 3-1 Comparison between MASH TL-4 impact and designed pendulum impact test	15
Table 3-2 Aluminum honeycomb cartridges: design dimensions and crush forces (Consolazio et al., 2021)	18
Table 4-1 Owens Corning GFRP material properties (without application of C_E)	26
Table 5-1 GFRP material properties (with $C_E=0.7$).....	32
Table 7-1 GFRP material properties for bars used in specimens (with $C_E=0.7$)	44
Table 7-2 Specifications for pressure sensitive tape switches	54
Table 7-3 Specifications for optical break beams.....	55
Table 7-4 Specifications for accelerometers.....	57
Table 7-5 Specifications for high-speed cameras	58
Table 7-6 Specifications for laser displacement sensors	59
Table 7-7 Specifications for concrete strain gages	60
Table 7-8 Specifications for rebar strain gages.....	61
Table 8-1 Full-scale COR impact test summary.....	63
Table 9-1 Full-scale EOR impact test summary	109
Table I-1 Average compressive strength of concrete deck samples at 28 days.....	316
Table I-2 Average compressive strength of concrete deck samples near day of impact testing .	316
Table I-3 Average compressive strength of concrete rail samples at 28 days	316
Table I-4 Average compressive strength of concrete rail samples near day of testing.....	317

CHAPTER 1 INTRODUCTION

1.1 Background

Corrosion related damage to steel reinforced concrete bridge elements exposed to marine (salt water) environments is widely acknowledged. Such corrosion can cause damage not only to bridge pier components, but also to bridge rails (Figure 1-1). As steel corrodes, volumetric expansion induces tensile concrete stresses, cracking, and spalling. Such forms of damage further accelerate deterioration, reduce structural capacity, and ultimately decrease the service life of the structure. The resulting maintenance and repair of steel reinforced concrete can be costly and can disrupt traffic. To mitigate corrosion-related problems, corrosion-resistant composite materials are increasingly being used in bridge construction. Glass fiber reinforced polymer (GFRP) is one such composite material. Rebar manufactured using GFRP offers a corrosion-resistant alternative to steel rebar and is particularly advantageous in extremely aggressive (corrosive) environments.



Figure 1-1. Corrosion on bridge rail

GFRP rebar is manufactured by merging glass fibers, resin, various natural minerals (e.g., silica sand), and other additives. In addition to being non-corrosive, other advantages of GFRP include: high tensile strength and low weight-to-strength ratio. Due to the lightweight nature of GFRP rebar, on-site handling and installation processes are simplified, and potential savings in construction costs may be realized. However, GFRP does not possess the ductility that is associated with yielding of mild steel rebar. Additionally, the elastic modulus of GFRP is approximately one-quarter that of steel, resulting in reduced structural stiffness. Designing GFRP reinforced concrete elements must therefore include consideration of how these material differences may alter structural performance and failure modes.

The Florida Department of Transportation (FDOT) has implemented GFRP-reinforced concrete for use in the construction of a variety of different bridge structural components (piles, pile caps, decks, etc.). To complete a non-corrosive, steel-free bridge plan, in this study, a GFRP reinforced FDOT 36" single-slope traffic rail was designed and impact tested along with a corresponding standard steel-reinforced rail (Figure 1-2). As rebar inside a rail typically overlaps

with rebar extending out of the deck slab, it was necessary to develop a design that made use of GFRP reinforcement both for the rail and the deck. Due to the non-ductile characteristics of GFRP rebar, yield line analysis was not directly applicable; therefore, simplified analytical approaches and advanced nonlinear finite element analyses were used to design the GFRP reinforced rail. Follow-up experimental impact testing focused on evaluating the structural equivalency of GFRP rail strength in comparison to the standard FDOT steel R/C rail under the effects of AASHTO (2016) MASH test level 4 (TL-4) transverse truck impact load.

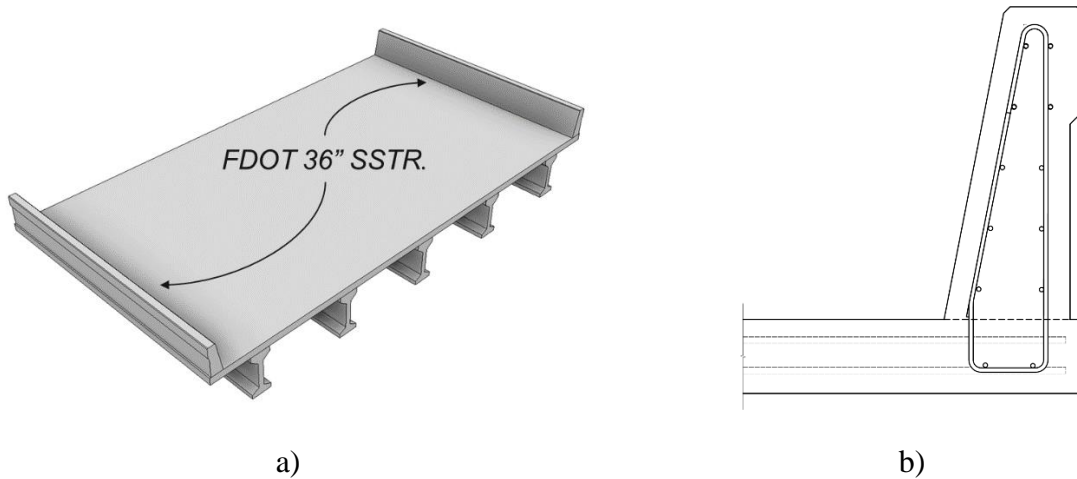


Figure 1-2. Typical FDOT 36” SSTR
a) Installed on a typical bridge; b) Cross section

1.1.1 Related FDOT research

In a related study sponsored by the FDOT (BDV31-977-72), a bridge rail was designed and constructed using steel fiber reinforced concrete (FRC), and subjected to pendulum impact testing (Consolazio et al., 2021). In that study, standardized test specimens suitable for pendulum impact testing were developed for purposes of evaluating the impact performance of FDOT 36” single slope bridge rails (FRC, and conventional R/C). Each test specimen consisted of an appropriate length of rail, bridge deck, and associated support elements. Pendulum impact testing of the rail specimens utilized a newly developed impactor which reproduced the transverse impact energy and transverse peak impact force from a MASH test level 4 (TL-4) impact of a 10000S single unit truck (SUT). In the present GFRP rail study, the standardized test specimen and pendulum impactor developed in the FRC rail study were adapted for use in testing GFRP reinforced rails.

1.2 Objectives

The primary objectives of this study were to design and evaluate the impact performance of a GFRP reinforced rail using pendulum impact testing. Pendulum impact tests, conducted at the FDOT Structures Research Center, were used to evaluate structural equivalency of the GFRP rail to the traditional FDOT R/C rail.

1.3 Scope of work

The scope of work included in this study was organized into the following key phases:

- Adaptation of previously developed pendulum impact test protocols: The pendulum impactor developed in BDV31-977-72 was adapted for use in testing and evaluating the impact performance of a GFRP reinforced concrete TL-4 bridge rail.
- Establishment of a design basis for GFRP-reinforced rail: The design of the GFRP-reinforced rail was based primarily on the existing steel-reinforced rail scheme. However, due to the ‘linear-elastic to rupture’ nature of GFRP material behavior, yield line analysis, as recommended in AASHTO LRFD (2017), was not applicable. Alternative methods were therefore used to evaluate GFRP system capacity. In particular, advanced finite element impact simulation techniques were used to estimate expected system performance under pendulum impact loading conditions.
- Design and test steel- and GFRP-reinforced rail test specimens: Adapting the test specimen and test protocols developed in BDV31-977-72, integrated rail-and-deck GFRP-reinforced test specimens were developed for pendulum impact testing in the present study. Thickened deck edges were incorporated into the specimen to facilitate anchorage to the test foundation and to simulate a bridge deck ‘overhang’ condition by vertically offsetting the deck from the test foundation. Concrete end buttresses with separation plates were added to the test specimen – which were relatively short-span – to approximate the support conditions that would normally be provided by adjacent continuous rail. Specimens were impact tested using a TL-4 pendulum impactor and results were processed to evaluate GFRP bridge rail performance, and to develop design recommendations.

1.4 Overall approach

The overall approach used to design and test the GFRP-reinforced rail combined the following processes:

- Use of applicable design standards: Standard structural design documents such as AASHTO LRFD (2017) and AASHTO GFRP (2018) were used to design the GFRP-reinforced concrete rail. AASHTO MASH was used to develop the pendulum impactor and test protocols. AISC steel design specifications (2017) were used to design and size various components for impactor and to facilitate test specimen fabrication and transport.
- Finite element modeling and simulations: Finite element modeling and dynamic impact simulations were used to design the test specimens and assess anticipated structural responses under impact loading.
- Pendulum impact testing: Pendulum impact tests of the steel- and GFRP-reinforced rail systems were conducted at the FDOT Structures Research Center to experimentally evaluate the structural equivalency of GFRP rail in comparison to the steel R/C rail.

CHAPTER 2 LITERATURE REVIEW

2.1 Introduction

In this chapter, a review is provided of code provisions, design specifications, and prior research studies that pertain to the development and testing of GFRP reinforced concrete bridge elements.

2.2 Design specifications: GFRP-reinforced concrete

As the advantages of GFRP have become more widely recognized in the bridge design and construction industry, organizations have dedicated greater focus to developing standards that can be used for GFRP reinforced concrete design. Specifications for GFRP design first emerged in the Euro-code and Canadian Highway Bridge Design Code (CSA 2014), but are now also widely available in the United States. The AASHTO LRFD Bridge Design Specifications (AASHTO LRFD) (2017) and AASHTO LRFD Bridge Design Guide Specifications for GFRP-Reinforced Concrete (AASHTO GFRP) (2018) were reviewed in detail for this study. Also, ACI 440.0 2R-15 “Guide for the Design and Construction of Structural Concrete Reinforced with Fiber-Reinforced Polymer (FRP) Bars” (ACI 440) (2015) was reviewed and compared to AASHTO GFRP (2018).

2.2.1 Environmental reduction factors

When exposed to a harsh environment over long periods of time, GFRP bars may deteriorate due to a series of physical and chemical changes. In a recent study, the tensile strengths of 127 GFRP bars exposed to various types of environments (D’Antino et al. 2018) were analyzed. Long term exposure to alkaline solution was reported to degrade GFRP bars and reduce the bar tensile strength. In the case of GFRP reinforced concrete, when stress induces cracks in the GFRP rebar composite matrix, alkaline moisture from the concrete can seep into the rebar and deteriorate the glass fibers. Vinyl ester resins are better at resisting moisture seepage in comparison to other resins such as polyester and epoxy. Vinyl ester resin is also the only approved resin system that can be used for FDOT road and bridge construction (FDOT 2020b). To conservatively account for the effects of long-term environmental exposure, as specified in AASHTO GFRP (2018) Section 2.4.2.1, based on the exposure condition, an environmental reduction factor (C_E) must be applied to the ultimate tensile strength and strain reported by manufacturers. When GFRP reinforced concrete is not exposed to earth or weather, C_E shall be 0.80; when such material is exposed to earth or weather, C_E shall be 0.70. The GFRP reinforced bridge rail evaluated in this study is assumed to be subjected to exterior exposure under the service environment. Therefore, the design tensile strength and strain used in this study were determined with C_E specified as 0.7.

2.2.2 Yield line analysis of concrete barrier

For a traditional steel-reinforced concrete bridge rail, the transverse load carrying capacity (i.e. the resistance to impact load) can be computed using the AASHTO yield line calculation procedure documented in AASHTO LRFD (2017) Section 13, and then compared to the design impact load to assess structural adequacy. Yield line analysis assumes that, after yielding, reinforcement elements behave essentially plastically (i.e., rebar stresses remain at an approximately constant level as strain accumulates). As the reinforcement plastically deforms, a

yield line pattern of system damage emerges (Figure 2-1). Under the effect of transverse impact loading, the damage/failure pattern in a bridge is assumed to occur within a distance referred to as the critical length, L_c . In contrast to mild steel bars, GFRP bars do not exhibit yielding; instead, they behave in a linear elastic manner up to the point of abrupt tensile failure. Consequently, the traditional yield line analysis procedure cannot be directly applied to the calculation of GFRP-reinforced rail capacity.

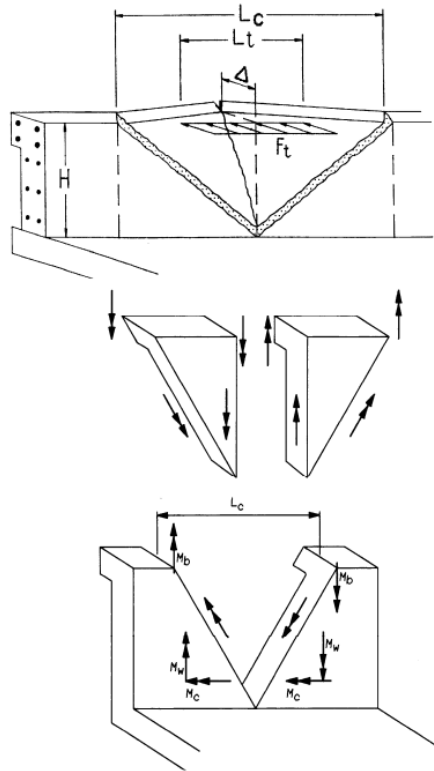


Figure 2-1. Yield line analysis of concrete bridge rail (AASHTO LRFD 2017)

While yield line analysis is not directly applicable to a GFRP reinforced rail, certain overall responses of such a rail are expected to be similar to R/C rails. For example, as indicated in Figure 2-2, the top portion of a GFRP reinforced rail is expected to undergo a deformation condition similar to a simply supported beam, and the bottom portion of the rail is expected to undergo a deformation condition similar to a cantilever wall. These general behaviors formed the basis of simplified structural capacity checks that were performed in this study. Advanced nonlinear finite element analyses were also (subsequently) performed so that no dependency on the assumptions of yielding analysis or simplified behaviors were necessary in order to assess anticipated rail responses under impact loading.

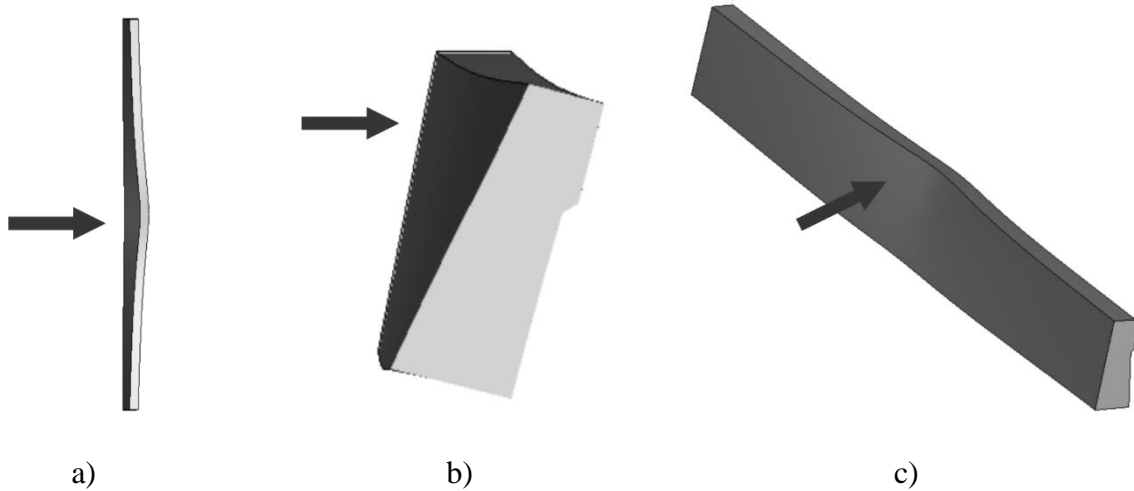


Figure 2-2. Simplified rail behavior under transverse impact load: a) Top of rail behavior; b) Base of rail behavior (sectional view); c) Isometric view of rail

2.2.3 Resistance factor

When assessing the flexural moment capacities for both steel-reinforced and GFRP-reinforced bridge rails, under extreme event (vehicle impact) loading, the resistance (or strength reduction) factor, ϕ , is set equal to 1.0. In general, the resistance factor is determined based on the statistical reliability and variability of the reinforced concrete. Typically, for a GFRP-reinforced flexural beam under sustained loading, due to the lack of ductility, the ϕ factor is lower than it would be for a steel-reinforced counterpart. The use of a reduced ϕ for GFRP reinforced results in a more significant strength penalty in design calculations. As there is limited research regarding appropriate ϕ factors for GFRP reinforced concrete resisting impact loading, it is noted in AASHTO GFRP (2018) Section 2.5.6 that a ϕ factor similar to AASHTO LRFD (2017) Table 3.4.1-1 ($\phi = 1.0$) may be used. The commentary from AASHTO GFRP (2018) Section 2.5.6 notes that the low ductility and limited moment redistribution ability of GFRP RC should be carefully examined. Both effects were carefully evaluated in this study through the use of finite element simulations. Particularly, simulation results for end-of-rail impact conditions indicated progressive failure of certain GFRP rebar elements, as a result of lack of ductility. This issue was addressed by modifying the GFRP rebar configuration to prevent such progressive failure.

2.3 Material specifications: GFRP rebar

Requirements for GFRP bar materials are specified in the FDOT Standard Specifications for Road and Bridge Construction (2020) Section 932-3. Other specifications and standards that were reviewed included ASTM D7205: Standard Test Method for Tensile Properties of Fiber Reinforced Polymer Matrix Composite Bars, and ASTM D7957 Standard Specifications for Solid Round Glass Fiber Reinforced Polymer Bars for Concrete Reinforcement. The design tensile strength of GFRP bars is typically obtained from GFRP bar manufacturers since the process of experimentally quantifying such strength parameters is challenging and sensitive to variations in the experimental setup. For the GFRP materials utilized in this study, test certification for each lot

of materials were obtained from the manufacturer. These certifications included parameters such as tensile strength, tensile strain at rupture, and elastic modulus.

2.4 Impact test guidelines: bridge rail vehicular crash test

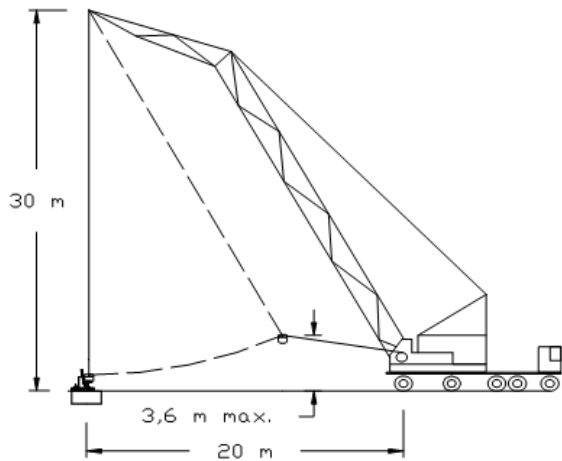
When designing a new bridge rail, a vehicular crash test is usually performed based on the AASHTO Manual for Assessing Safety Hardware (MASH) (2016). AASHTO MASH provides testing guidelines and evaluation criteria for various highway safety features such as bridge rails, barriers, and roadside sign structures. There are six test levels for bridge rails, where Test Level 4 (TL-4) was used for the rail evaluated in this study. Impact conditions and the type of test vehicle are defined for each test level. Test Level 4 considers three test vehicle designations: passenger car, pickup truck, and single-unit truck. The most severe TL-4 impact condition, a '10000S' (10,000 kg) single-unit truck (SUT) impacting at 56 mph and at an angle of 15-deg., was used to design the pendulum-equivalent transverse impact test protocols.

2.5 Prior research: GFRP-reinforced concrete under impact load

In recent years, GFRP reinforced concrete has been studied by researchers and tested in both laboratory settings and in the field to evaluate the structural performance relative to traditional R/C structures. The results and recommendations from these studies provided valuable insight into the design of the FDOT TL-4 GFRP reinforced bridge rail.

2.5.1 Pendulum impact test on TL-4 GFRP reinforced rails

Static tests and dynamic impact tests have been conducted on GFRP reinforced concrete rails to qualify GFRP reinforced rails as adequate alternatives to steel reinforced rails. In 2001, laboratory static tests and pendulum impact tests were conducted on a GFRP reinforced concrete bridge rail segment by the Ministry of Transportation of Quebec (MTQ) and the University of Sherbrooke (El-Salakawy et al. 2001). In 2010, two additional types of bridge rails were tested using a similar test setup and methodology (Ahmed et al. 2013). The pendulum impact tests were conducted on both GFRP-reinforced rails and steel-reinforced counterparts (Figure 2-3). The approach used to design the GFRP-reinforced rail was to maintain the same amount of reinforcement as was present in the previously established steel-reinforced rail.



a)



b)



c)



d)

Figure 2-3. Pendulum impact test set-up (El-Salakawy et al. 2001):

- a) Schematic diagram for the test set-up; b) PL-2 barrier field test set up; c) Steel plate and tire arrangement for load distribution; d) Impact test with steel wrecking ball

Test results indicated that the GFRP-reinforced rails behaved similarly to a traditional R/C rail when subjected to a TL-4 impact load (El-Salakawy et al. 2001, Ahmed et al. 2013). The crack pattern was similar for both steel- and GFRP-reinforced barriers (El-Salakawy et al. 2001, Ahmed et al. 2013). The extent of the cracked section was measured and agreed closely with the critical length defined by AASHTO, predicted using yield line analysis (El-Salakawy et al. 2001). The number of cracks and the crack widths of the GFRP-reinforced rails were both larger but with a smaller spacing as compared to steel-reinforced rails (El-Salakawy et al. 2001).

Due to differences in material characteristics, GFRP and steel bars (Figure 2-4) were found to redistribute impact load differently. In the studies noted above, the strain in the horizontal steel bars was considerably smaller than that in the GFRP bars; for vertical reinforcement, the strain was higher in steel bars as compared to GFRP bars. These observations can be explained by the

relative stiffnesses of the materials, where steel is stiffer (i.e., has a larger elastic modulus) than GFRP. Because vertical bars are closer to the impact face and steel is stiffer than GFRP, the vertical steel reinforcing bars directly carry more load before redistributing to the horizontal bars. Since GFRP is less stiff than steel, the vertical GFRP bars do not carry as much load before redistributing to the horizontal bars. As a result, in a GFRP system, the horizontal bars may carry more impact load than the vertical bars (El-Salakawy et al. 2001).

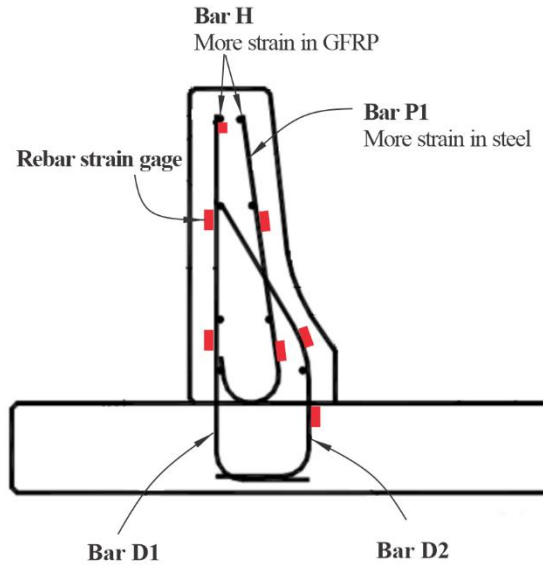


Figure 2-4. PL-2 barrier reinforcement layout (El-Salakawy et al. 2001)

In the current project, a similar type of testing (i.e., pendulum impact testing instead of vehicle crash testing) was conducted to evaluate the performance of a TL-4 GFRP reinforced rail. The transverse kinetic energy of a TL-4 impact was estimated to determine the weight and height of the pendulum impactor. However, the tests conducted in the present study differed from the tests conducted by El-Salakawy et al. (2001) and Ahmed et al. (2013) in several ways. The rail type (FDOT 36" SSTR) tested in the current project was an FDOT single slope rail, while the research mentioned above focused on MTQ F-shape rails. Pendulum impact test protocols used in the present study were significantly improved relative to past projects. Tests performed by MTQ were carried out by swinging a wrecking ball using a mobile crane, where only the peak force and duration of impact load were measured. The impactor designed for the current project produced a realistic truck transverse impact force-time history curve by using carefully sized crushable aluminum honeycomb cartridges. Test specimen scales were also different. While the rails tested by MTQ and the University of Sherbrooke were approximately 36-ft long, to accommodate the FDOT Structures Research Center laboratory and pendulum impact test conditions, the test specimen designed for the current project was 13-ft long. Tests from MTQ and the University of Sherbrooke indicated the feasibility of using GFRP bars as steel alternatives in traffic rails, whereas the current study provides a more detailed assessment of the behavior of a single-sloped traffic rail under a more realistic truck impact loading condition.

2.5.2 Vehicle crash test on TL-5 GFRP reinforced barriers

Sennah et al. (2018) performed a vehicle crash test on a TL-5 GFRP reinforced barrier. A 131-ft long barrier reinforced with GFRP bars was built and tested based on updated AASHTO MASH (2016) crash-test procedures and performance evaluation. A main purpose of this test was to evaluate the effect of GFRP bar configuration on structural performance. Fiber bending and stress concentration in a bend region can reduce the tensile strength compared to a straight bar. Considering the strength reduction that is associated with bent bars, researchers seek alternatives. Sennah et al. replaced bent bars with straight bars that had 180° hooks (Figure 2-5) at the ends. Crash testing of the barrier demonstrated that this alternative configuration of GFRP rebar resulted in a system that was able to sustain the impact load. Cosmetic damage from the tire and minor cracks were observed, but there was no catastrophic failure. The barrier satisfied structural adequacy requirements, met occupant risk criteria, and successfully redirected the test vehicle (Sennah et al. 2018).

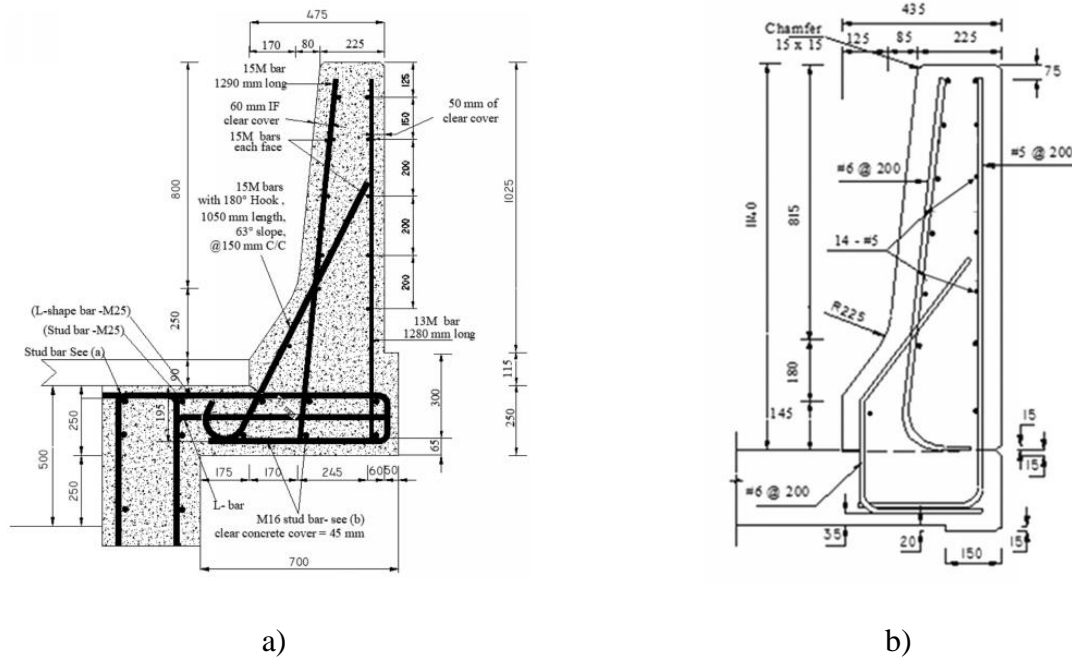


Figure 2-5. Cross section of crash-tested barrier (Sennah et al. 2018):

- a) Tested barrier with 180° hooked end bars; b) Established Canadian Highway Bridge Design Code (CHBDC) barrier with GFRP bars

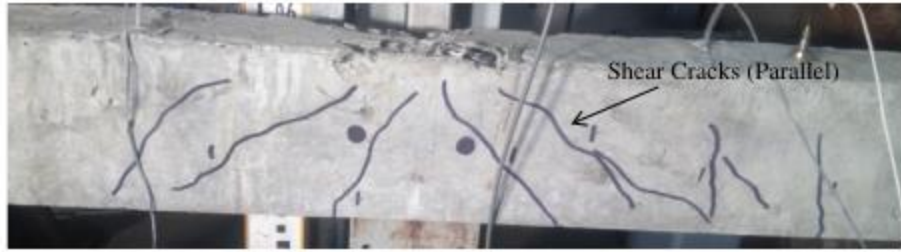
Although the vehicle impact testing performed by Sennah et al. successfully demonstrated that a GFRP-reinforced rail can be designed to adequately resist truck impact loading conditions, the present study differed from this previous work in several ways. Most importantly, the GFRP rail designed by Sennah et al. was a 44-in. tall F-shaped rail with a distinct rebar configuration (size, spacing, and bend). In contrast, the rail evaluated in the current project was a FDOT 36-in. single-sloped rail with similar rebar spacing and configuration to those of the standard steel-reinforced FDOT 36-in. SSTR. Differences between the geometry and reinforcing configuration used by Sennah, and those used in the FDOT SSTR, necessitated separate FDOT-specific analysis

and impact testing. The cross-sectional shape and impact face of the FDOT GFRP rail remained the same as those of the steel-reinforced FDOT 36-in. SSTR. Full-scale vehicle crash testing, as used by Sennah et al., was therefore not necessary in the current study since vehicle redirection and occupant risk measures for the SSTR rail geometry were already known to be satisfactory per MASH. Thus, in the present study, vehicle crash testing (as used by Sennah et al.) was replaced with pendulum impact testing. Additional differences include the fact that steel reinforcement was used in the deck slab by Sennah et al., while GFRP reinforcement was used in the FDOT GFRP reinforced deck. Finally, the TL-5 test condition (Van-Type Tractor-Trailer) investigated by Sennah et al. differs from the TL-4 (Single-Unit Van Truck) test condition that was the focus of the current study.

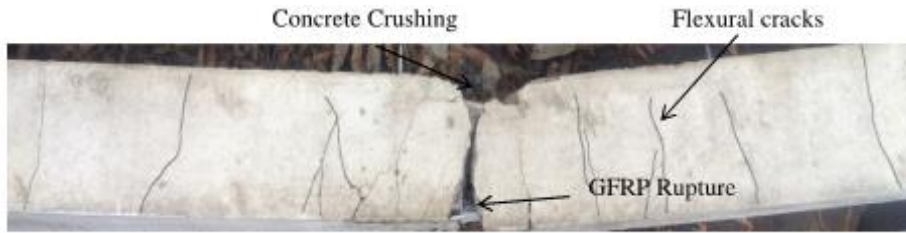
2.5.3 FRP reinforced beam testing

To develop a more general understanding of GFRP reinforced concrete structural behavior, studies have been conducted on GFRP RC beams. Goldston et al. (2016) focused on the strength of GFRP RC beams under static and impact load and the corresponding load-deflection relationship, crack pattern, energy absorption capacity, and failure mode. Beams were cast with variable reinforcement ratios for both static and dynamic tests. For sustained static loads, it is generally considered desirable to design GFRP reinforced beams to be over-reinforced. This stems from the fact that the failure mode of GFRP rebar is sudden tensile rupture (Goldston et al. 2016) rather than yielding, as is the case for mild steel rebar. To provide a level of warning of structural distress in GFRP beams that must carry sustained static loads—and thus facilitate possible evacuation, shoring, or repair—the failure mode of concrete crushing is preferred over the more abrupt rupture mode of GFRP bars in tension.

Under static loading, the GFRP beams tested by Goldston et al. (2016) showed high bending stiffness until cracking, after which the stiffness was significantly reduced. GFRP reinforced beams with a balanced reinforcement ratio failed abruptly and without warning. Over-reinforced beams developed vertical cracks from the tension zone to the compression zone. Under impact loading, a “shear plug” type of failure was observed for over-reinforced beam. Shear cracks were parallel on each side of the impact zone and were oriented at an approximate angle of 45°. Vertical flexural cracks were observed for beams with a balanced reinforcement ratio (Figure 2-6) (Goldston et al. 2016). Tests were also carried out with different concrete strengths; however, results indicated that increasing the concrete strength from normal to high strength had minimal effect on moment capacity.



a)



b)

Figure 2-6. GFRP RC beams under impact loading (Goldston et al. 2016):
a) Failure of over-reinforced beam; b) Failure of beam with balanced reinforcement ratio

CHAPTER 3

SURROGATE VEHICLE PENDULUM IMPACT TESTING AND SIMULATION

3.1 Introduction

Since the rail under investigation was specified by FDOT (2019) as needing to satisfy TL-4 requirements, vehicle impact test conditions prescribed in AASHTO MASH (2016) were used to develop pendulum impact test protocols. Specifically, the most severe TL-4 vehicle impact test was selected: a 56-mph, ‘10000S’ (10,000 kg [22,046 lbm]) single-unit truck (SUT) impact at a 15-deg. impact angle. The geometric configuration of the Florida SSTR bridge rail was previously subjected to vehicular crash testing and passed all criteria for a TL-4 rail. Thus, for the present study, instead of conducting a fully instrumented MASH compliant vehicular crash test, pendulum impact testing was adopted as means of assessing barrier performance under transverse impact loading. Specifically, a gravity pendulum combined with a surrogate impact ‘vehicle’ was used to evaluate impact performance of the R/C and GFRP R/C rails. For a pendulum impact test to be an acceptable alternative to a vehicular test, it must yield similar impact characteristics (e.g., impact energy, force vs. time response).

In the case of the AASHTO MASH 56-mph SUT impact, the impact is oblique (i.e., the vehicle strikes the rail at 15-deg. and is then redirected). Since the longitudinal component of the impact force is considered to have a negligible influence on the transverse capacity of a rail, only the transverse (i.e., perpendicular) component of the impact was considered in this project. Additionally, conducting an oblique impact with the pendulum impactor would not be feasible because such an impact would produce uncontrollable twisting of the impactor—a situation that is considered dangerous with regard to the integrity of the hanger cables and the safety of testing personnel. Therefore, pendulum impact testing was conducted in a direct (i.e., ‘head on’, non-oblique) manner.

Key aspects of the development of the surrogate vehicle (‘impactor’) and high energy pendulum impact test are summarized in this chapter. However, the TL-4 pendulum impact test system was primarily designed in BDV31-977-72 (Consolazio et al., 2021), thus the reader is referred to that report for more detailed information.

3.2 Full scale impact test

In 2011, Texas Transportation Institute (TTI) performed a full-scale TL-4 vehicular impact test (Figure 3-1, MASH test 4-12) on a standard TxDOT 36-in. SSTR (Sheikh et al. 2011)—the same shape that the FDOT adopted for the 36-in. SSTR. The test vehicle and impact conditions complied with MASH test 4-12 requirements, with a 22,150-lbm single-unit box-van truck traveling at an impact speed of 57.2-mph and an impact angle of 16.1-deg. Results demonstrated that the tested rail passed all criteria for a TL-4 rail. The test vehicle was safely contained and redirected with acceptable occupant risk. The rail exhibited only cosmetic damage (e.g., tire marks), and no new cracks were formed, nor was repair needed (Figure 3-2).



a) Overhead view



b) Frontal view

Figure 3-1. TL-4 crash test on TxDOT 36-in. SSTR (Sheikh et al. 2011)



Figure 3-2. TxDOT 36-in. SSTR after MASH test 4-12 (Sheikh et al. 2011)

3.3 Development of Single-Unit Truck (SUT) 10000S impactor

The FDOT pendulum impactor surrogate vehicle was developed in BDV31-977-72 (2021) and was adopted in the present project to produce impact behaviors – in the direction transverse to the rail – comparable to a TL-4 impact test. The pendulum impactor was designed with two main goals: (1) to produce impact energy matching that of the vehicular impact test, and (2) to produce a realistic force-time history response.

3.3.1 Impact energy

A pendulum impact test converts potential energy into kinetic energy by raising an impactor to a specified height, releasing it, and allowing it to swing downward toward a test

specimen. The pendulum impactor mass and drop height, which were carefully chosen to be within the capacity of the FDOT pendulum impact test facility, were designed to produce the same impact energy as the transverse (perpendicular to rail) component of AASHTO MASH TL-4 SUT impact. Based on the condition of an AASHTO MASH TL-4 SUT impact test (a 56-mph SUT impact at 15-deg.), a transverse impact (kinetic) energy of 155 kip-ft was calculated. A 10,000-lbm impactor was then designed in BDV31-977-72 to utilize a drop height of 15 ft in order to convert potential energy into equivalent kinetic impact energy. A comparison of MASH TL-4 vehicle impact test conditions and pendulum impact test conditions is provided in Table 3-1.

Table 3-1 Comparison between MASH TL-4 impact and designed pendulum impact test

	MASH TL-4 SUT impact	Pendulum impact
Transverse kinetic impact energy (kip-ft)	155	155
Impact mass (lbm)	22,046	10,333
Transverse impact velocity (mph)	14.5	21.2
Drop height (ft)	N/A	15

3.3.2 Impact force

In addition to conducting the TxDOT 36-in. SSTR vehicular test, Sheikh et al. (2011) performed finite element impact simulations using LS-DYNA (LSTC 2019), a validated vehicle model of the 10000S (SUT) truck, and a rigid numerical representation of the 36-in. SSTR geometry (Figure 3-3). Based on the simulation results, the researchers quantified the transverse impact force on the rail and produced impact force versus time curves (an example is shown in Figure 3-4). The impactor for the FDOT pendulum was designed to produce a force vs. time curve that had similar characteristics to the TTI data reported by Sheikh et al. (i.e., the FDOT impactor force would ‘ramp up’ to the maximum level at a similar rate).

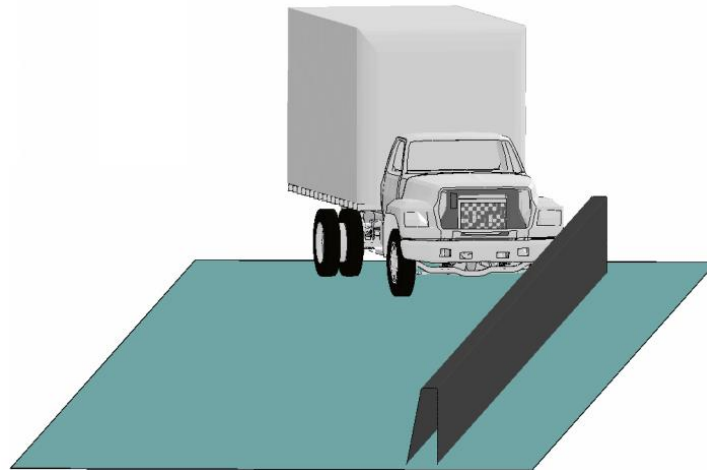


Figure 3-3. FE model of the SUT impacting a rigid SSTR under MASH TL-4 impact conditions (Sheikh et al. 2011)

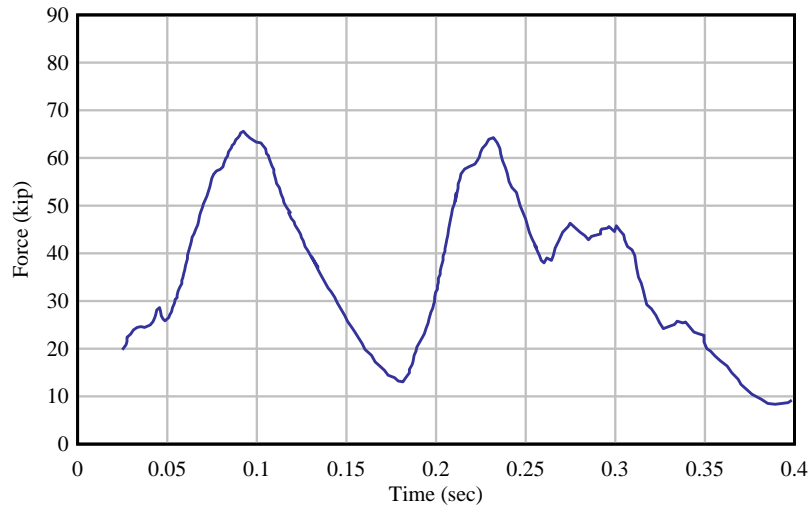


Figure 3-4. FEA impact force-time curve for 36-in. single-slope traffic rails (SSTR) (after Sheikh et al. 2011)

In order to reproduce a force-time curve that was similar to that documented by Sheikh et al. (2011), a crushable nose impactor was developed using aluminum honeycomb cartridges (additional details are available in the report for BDV31-977-72). A series of aluminum honeycomb cartridges of stepwise increasing sizes (Figure 3-5, Figure 3-6) generated increasing impact force as the nose crushed and the kinetic energy of the back block was delivered to the rail specimen being tested.

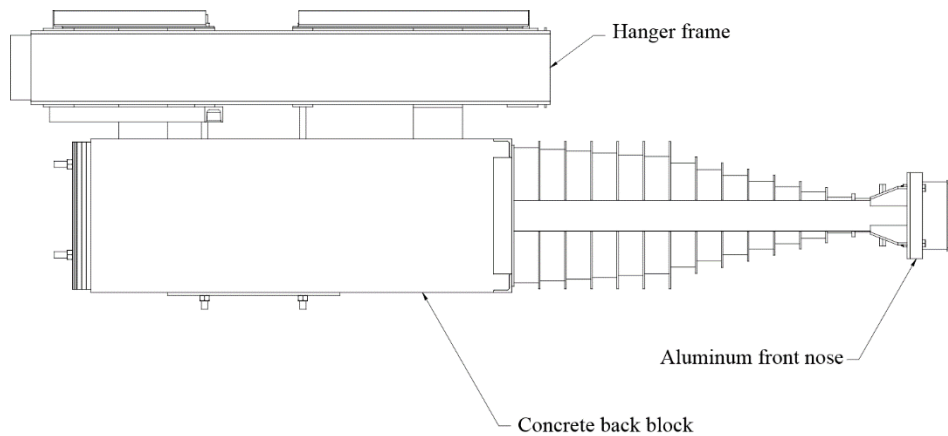


Figure 3-5. Pendulum impactor design overview (Consolazio et al., 2021)

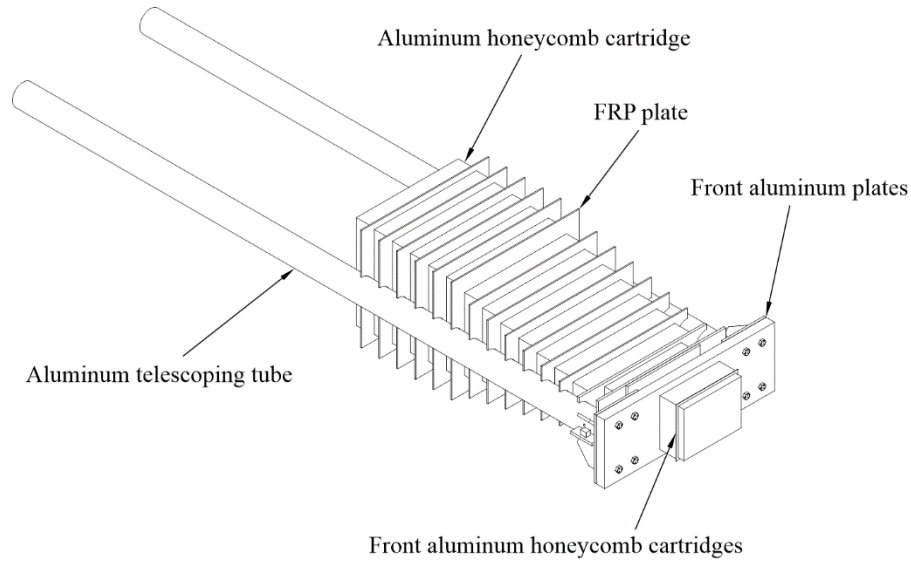


Figure 3-6. Aluminum honeycomb cartridge and impactor front nose (Consolazio et al., 2021)

Based on a pendulum impact velocity of 21.5-mph, a front cartridge (with 6-in. equivalent thickness) and 15 additional 4-in. thick aluminum honeycomb cartridges, with a design compressive strength of 130 psi (Table 3-2), were designed (Appendix A) to deliver the kinetic energy (155 kip-ft) of the pendulum impactor to the test specimen (bridge rail). Of the total of 16 cartridges, the first 12 were required to produce the initial peak of the force-time curve—i.e., from zero until reaching the first 65-kip peak of the force-time curve from Sheikh et al. 2011. The design of the remaining four cartridges produced a force-time curve that conservatively enveloped the TTI curve (recall Figure 3-4). A force-time curve that more ‘realistically’ follows the curves in Figure 3-4—where force increases to 65-kips, subsequently decreases, and then increases again due to vehicle redirection and ‘backslap’ of the rear SUT tandem—was impossible to safely reproduce with the FDOT impact pendulum. Instead, a conservative impact condition was designed in which, once the peak 65-kip force was reached, a nearly constant 65-kip force was maintained until all remaining kinetic energy was consumed (Figure 3-7).

Table 3-2 Aluminum honeycomb cartridges: design dimensions and crush forces
(Consolazio et al., 2021)

Cartridge #	Compressive strength (psi)	Vertical height (in.)	Transverse width (in.)	Thickness (in.)*	Design force (kip)
1A	130	10.5	13.5	2	18.4
1B	130	11	14	4	20
2	130	5	12	4	7.7
3	130	5.5	18	4	12.9
4	130	5.83	24	4	18.2
5	130	7.53	24	4	23.5
6	130	9.26	24	4	28.9
7	130	11.06	24	4	34.5
8	130	12.92	24	4	40.3
9	130	14.87	24	4	46.4
10	130	16.92	24	4	52.8
11	130	19.13	24	4	59.7
12	130	19.66	24	4	61.4
13	130	20.26	24	4	63.2
14	130	20.85	24	4	65.1
15	130	21.44	24	4	66.9
16	130	22.04	24	4	68.8

* Thickness after cartridge pre-crushing

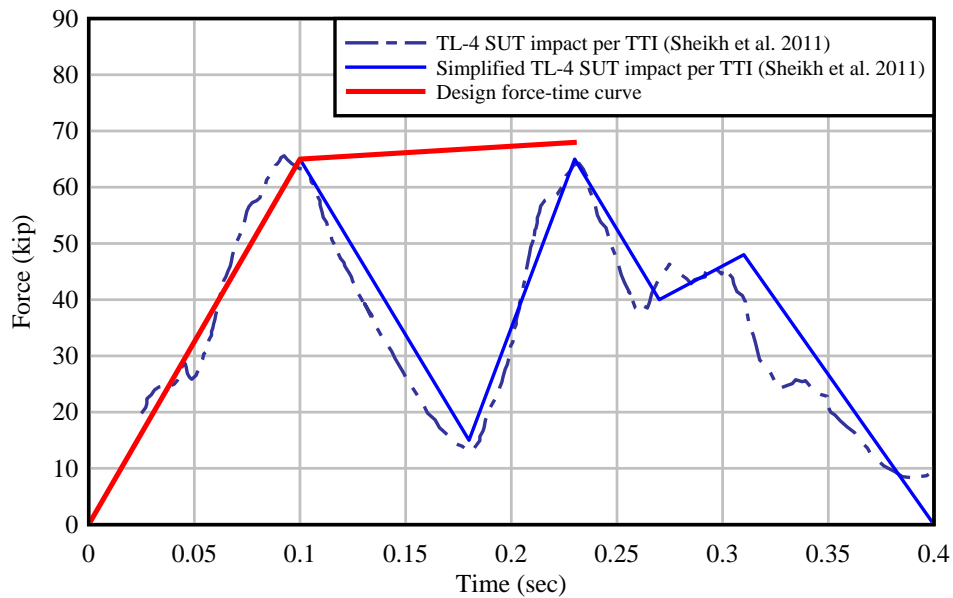


Figure 3-7. Simplified TTI FEA force-time curve compared to the design crushable nose
(see Appendix A for additional details) (Consolazio et al., 2021)

3.3.3 Single-Unit Truck (SUT) 10000S impactor

The complete design of the FDOT pendulum impactor consisted of three main components: (1) the steel hanger frame; (2) the concrete back block; and (3) the aluminum telescoping front nose. The steel hanger frame was used to attach the body of the impactor to the pendulum support towers via cables. The concrete back block was heavily reinforced and accounted for most of the

mass of the impactor. The aluminum telescoping front nose was used to control sequential crushing of the aluminum honeycomb cartridges and thus generated the intended force-time history.

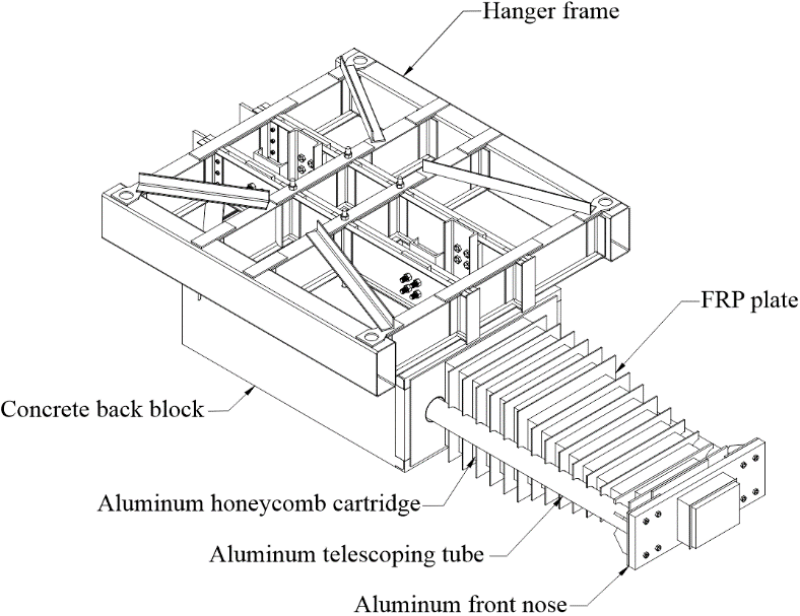


Figure 3-8. Design of the FDOT SUT 10000S impactor (Consolazio et al., 2021)



Figure 3-9. FDOT SUT 10000S impactor (without aluminum honeycomb cartridges installed)



Figure 3-10. FDOT SUT 10000S impactor prior of TL-4 pendulum impact test

3.4 Pendulum impact test facility

The FDOT pendulum impact test facility (Figure 3-11) located at the M.H. Ansley FDOT Structures Research Center in Tallahassee, Florida was used to conduct the impact test experiments. The pendulum consists of three 50-ft-tall towers positioned in a tripod arrangement. The impactor was suspended by cables from two of the towers near the universal foundation on which the impact specimen was securely anchored and pulled back to the desired height by a lifting cable that extended from the third tower. Impact was initiated by releasing the pull-back cable. The impactor would swing freely and produce the maximum kinetic energy at the lowest height of the swing.



Figure 3-11. FDOT pendulum impact facility at M. H. Ansley Structures Research Center (Tallahassee, FL)

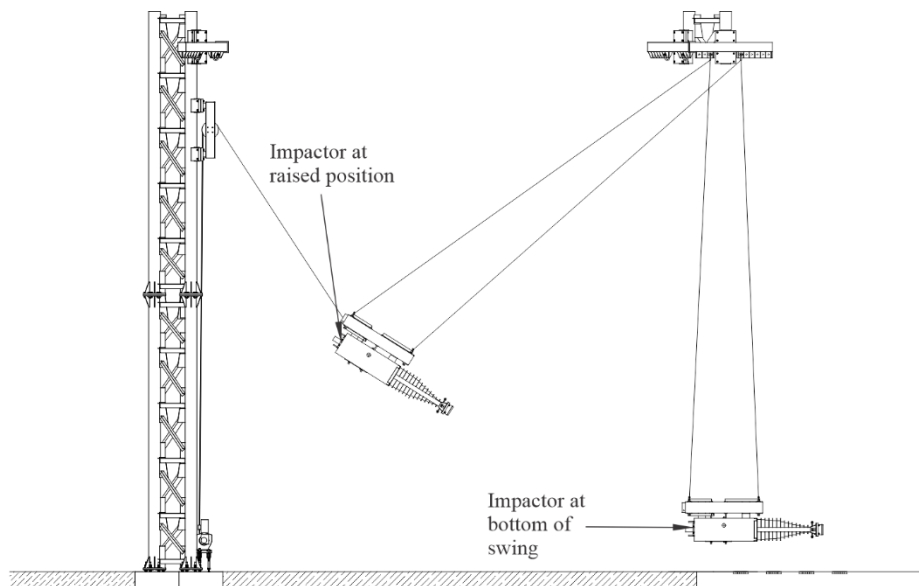


Figure 3-12. Pendulum impactor in pulled-back configuration
(Note: towers supporting the impactor not shown for clarity)

3.5 Finite element modeling and swing simulation

A finite element representation of the FDOT pendulum and impactor was developed in BDV31-977-72 (Consolazio et al., 2021) for analysis using the LS-DYNA finite element code. To evaluate the anticipated impact force-time curve, nonlinear dynamic impact swing simulations were conducted using a detailed model of the FDOT SUT 10000S impactor and a simplified rigid model of the FDOT SSTR. Simulation results were used to iteratively improve the design of the pendulum impactor to achieve the desired force vs. time curve.

3.5.1 Impactor model

The impactor model (Figure 3-13) consisted of a steel hanger frame (supported by cables), a concrete back block, and an aluminum telescoping front nose consisting of structural guide tubes, aluminum honeycomb cartridges, and FRP spacer plates. While the detailed modeling techniques are documented in BDV31-977-72, some notable aspects of the impactor model are:

- Aluminum cartridges: modeled with nonlinear discrete beam elements and material properties of crushable aluminum honeycomb
- Aluminum telescoping tubes: modeled with fully integrated solid elements with aluminum material properties, where material yielding or failure could be observed
- Concrete back block: modeled with fully integrated solid elements with an elastic concrete material model

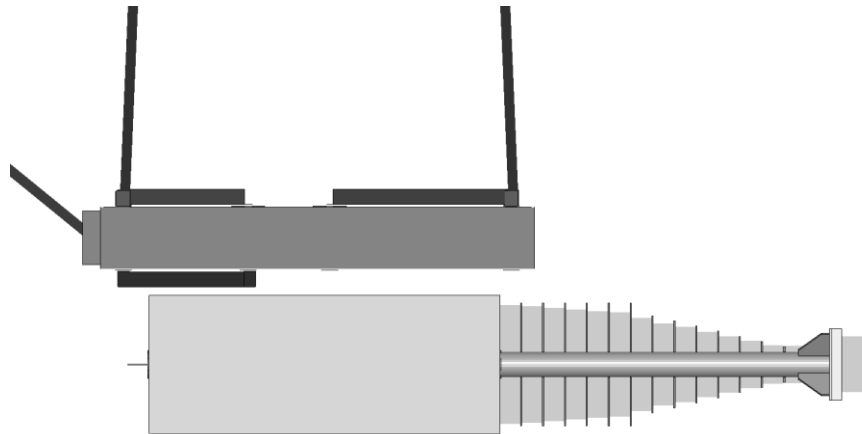


Figure 3-13. Pendulum impactor finite element model
(Note: rigid links connecting hanger frame to back block not shown)

3.5.2 Pendulum impact simulation

Each pendulum impact simulation included three key phases: pull back phase, free-swing phase, and impact phase. During the pull-back phase, the impactor was pulled back (by a cable attached to the hanger frame) to the designed pull-back location and drop height. The impactor was then held at this position until it stabilized (Figure 3-14a). Then, at the beginning of the free-swing phase, the cable (beam) element representing the pull-back cable was deleted (released), and the impactor swung downward freely (Figure 3-14b) until impact occurred. When the front nose came into contact with the concrete bridge rail model, impact was initiated. Aluminum honeycomb beams then started to crush (Figure 3-14c) from the front of the nose (weakest cartridge) to the back (strongest cartridge).

Using multiple cycles of pull-back, swing, and impact simulations, the finite element impactor model was iteratively refined and improved until the motion of the impactor after release was smooth (i.e., impactor oscillations were acceptably small); and differences between the impactor generated force vs. time curve and the target (design) curve were acceptably small (Figure 3-15).

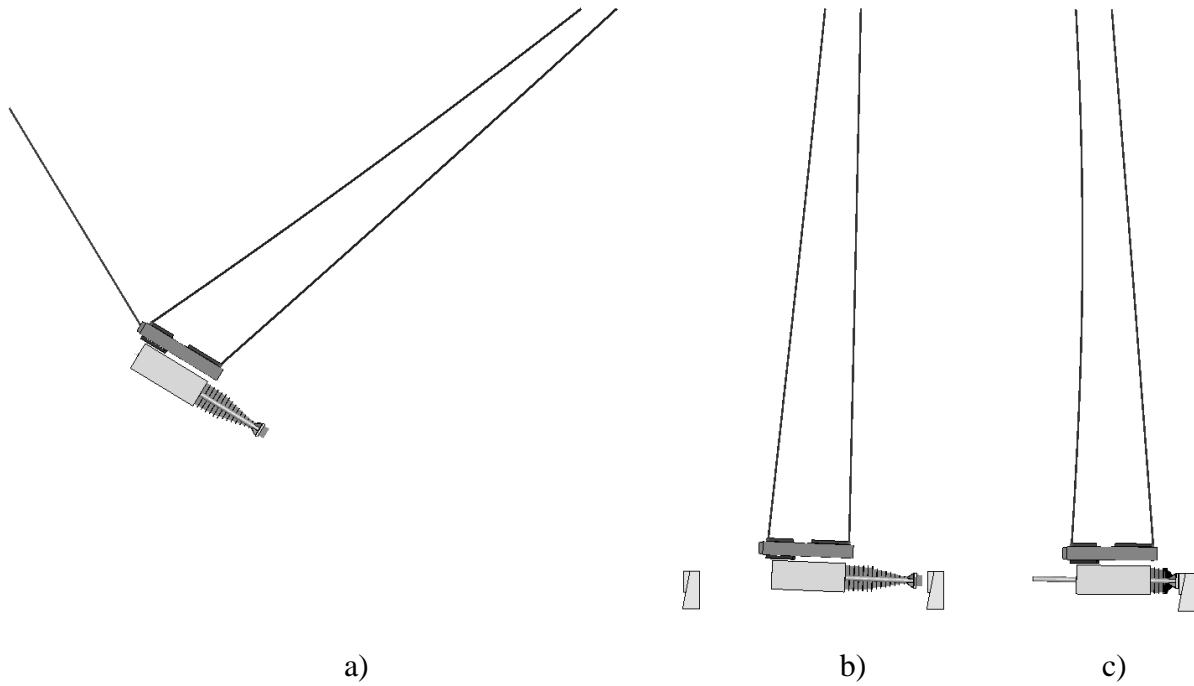


Figure 3-14. Finite element pendulum impact simulation with impactor at:
a) Drop height; b) Incipient contact; c) End of impact (Consolazio et al., 2021)

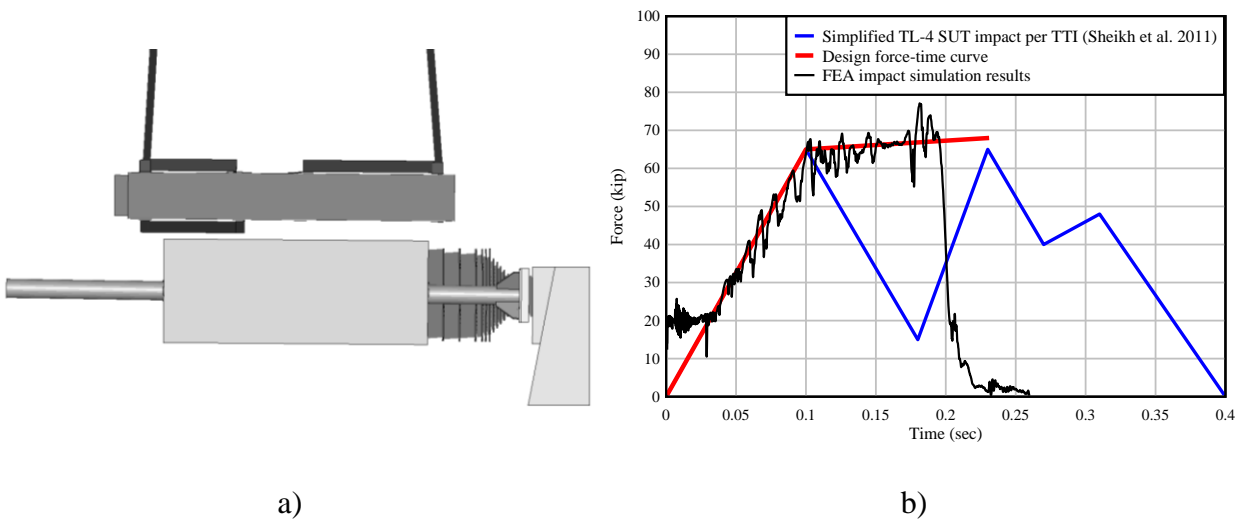


Figure 3-15. Finite element pendulum impactor simulation:
a) Side elevation view at end of impact; b) Force-time results from simulation
(Consolazio et al., 2021)

CHAPTER 4 DEVELOPMENT OF RAIL REBAR CONFIGURATION

4.1 Introduction

As an alternative to the existing steel-reinforced FDOT 36-in. SSTR, a GFRP bridge rail was developed primarily based on a bar-for-bar, GFRP-for-steel replacement approach. The GFRP rebar was selected with the same size and spacing wherever plausible. Due to distinct material properties of GFRP rebar (e.g., low ductility; cannot be bent on-site), GFRP bar bend configurations were adjusted to accommodate current manufacturing capabilities. Finite element models were developed and analyzed to evaluate rail behavior under impact load, identify potential failure modes, and iteratively improve the reinforcement design. Development of the GFRP reinforcement configuration is documented in this chapter.

4.2 Rail impact locations

Considering different rail responses, when impact locations vary from mid span of the rail to a discontinuous section (i.e., rail end, rail transition, bridge joint), two critical locations were evaluated in this project – center of rail and the end of rail (Figure 4-1). For the center-of-rail (COR) impact condition, the collision occurs away from any rail discontinuity and the impact energy can be distributed to both sides from the impact location, allowing an uninterrupted formation of damage pattern. For an end-of-rail (EOR) impact, the collision occurs near a discontinuous rail section and the impact energy is distributed to one side from the impact location.

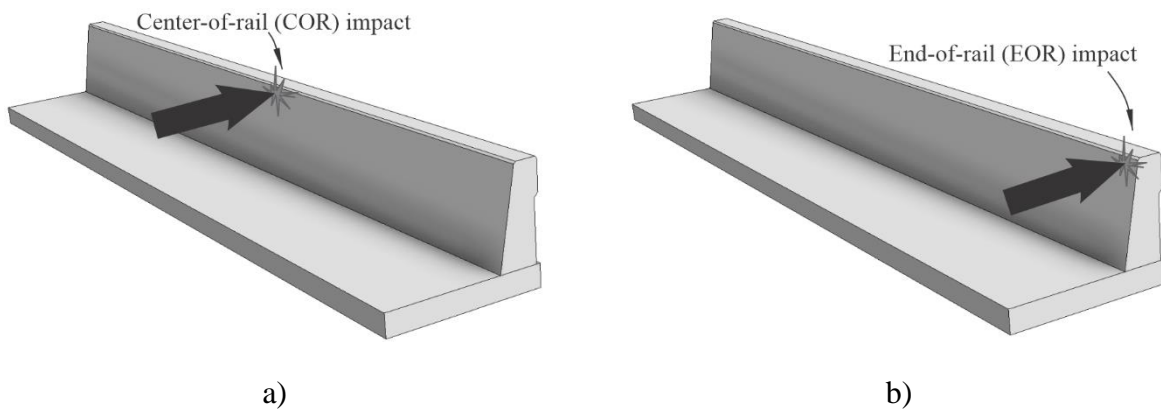


Figure 4-1. Rail impact locations:
a) Center-of-rail (COR); b) End-of-rail (EOR)

4.3 Reference configuration: steel rebar

The standard FDOT 36" SSTR structural plan [Index 521-427, FDOT (2019)] was used as the standard steel reinforced rail in this project. The bridge rail was 36-in. tall and 16-in. wide (Figure 4-2), reinforced with #4 mild steel rebars. A typical section of rail is reinforced with a set of overlapping vertical bars – 4P and 4V (Figure 4-3) and longitudinal (i.e., parallel to traffic) bars 4S. The minimum bar bend diameter for the 4P and 4V bars was 2-in. These bars were overlapped at the front and back rail faces and placed at 6-in. spacing longitudinally along the rail. At least 6-in. of bar 4V length was embedded in the bridge deck. Longitudinal bars (4S) were positioned

adjacent to the vertical bars (4P and 4V) at 7-in. increments of elevation. The typical bridge deck reinforcement was designed based on FDOT Standard Design Guidelines (FDOT 2020a). Both the top and bottom mats of the deck reinforcement consisted of #5 longitudinal bars at 9-in. spacing, and #6 transverse bars at 6-in. spacing. Per SDG 1.4.1, ASTM A615 Grade 60 deformed carbon-steel was used as bridge rail reinforcement and deck reinforcement.

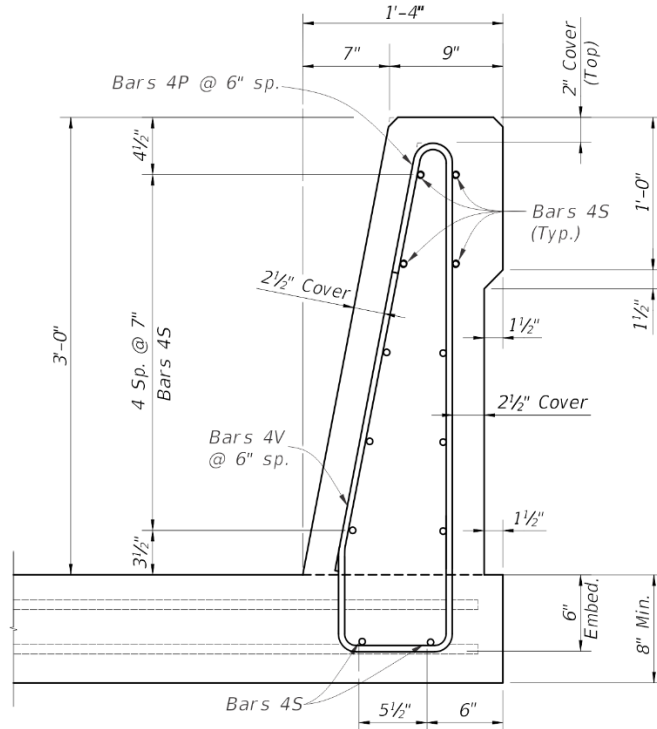


Figure 4-2. Steel reinforced typical section through traffic rail

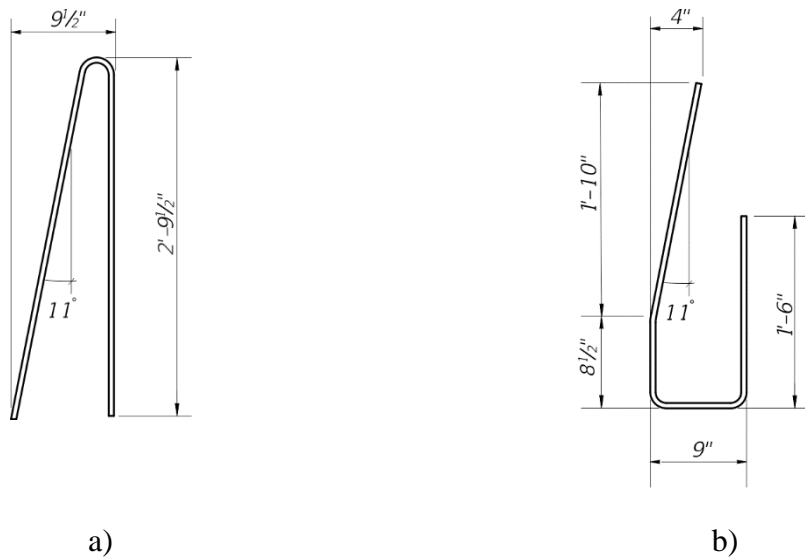


Figure 4-3. Steel bars for steel-reinforced bridge rail: a) bar 4P; b) bar 4V

4.4 Replacement configuration: GFRP rebar

The GFRP bridge rail tested in this study was based on the existing steel-reinforced rail system. A GFRP-for-steel, bar-for-bar replacement option was prioritized, while GFRP bar shapes were adjusted per manufacturer recommendations and availability. The design was also iteratively evaluated and enhanced using finite element simulations.

4.4.1 Material properties

While the modulus of elasticity of GFRP bars is constant across different sizes of bars, the ultimate tensile strengths vary. GFRP rebar exhibits a linear elastic behavior up to the failure strain, then fails abruptly. No plastic deformation of any significance occurs. To model GFRP rebar using finite element analysis, an elastic modulus, ultimate stress, and failure strain were specified, as shown in Table 4-1. These values were obtained from product datasheets provided by the material producer used in this project (Owens Corning). Stress-strain curves for the steel and GFRP rebar elements are presented graphically in Figure 4-4. It is also noted that the GFRP tensile strengths used in this study (i.e., FEA simulations and hand calculations) have been reduced with the consideration of long-term exposure to the environment, as noted in Section 2.2.1. The environmental reduction factor ($C_E = 0.7$) recommended by AASHTO GFRP (2018) was applied to the initial manufacturer GFRP tensile strengths and strains.

Table 4-1 Owens Corning GFRP material properties (without application of C_E)

GFRP Bar Type	Nominal Area (in ²)	Ultimate Tensile Load (kips)	Guaranteed Tensile Strength (ksi)	Ultimate Strain (in./in.)	Modulus of Elasticity (ksi)
#4	0.196	21.56	110	0.0164	6700
#5	0.307	32.24	105	0.0157	6700
#6	0.442	44.20	100	0.0149	6700

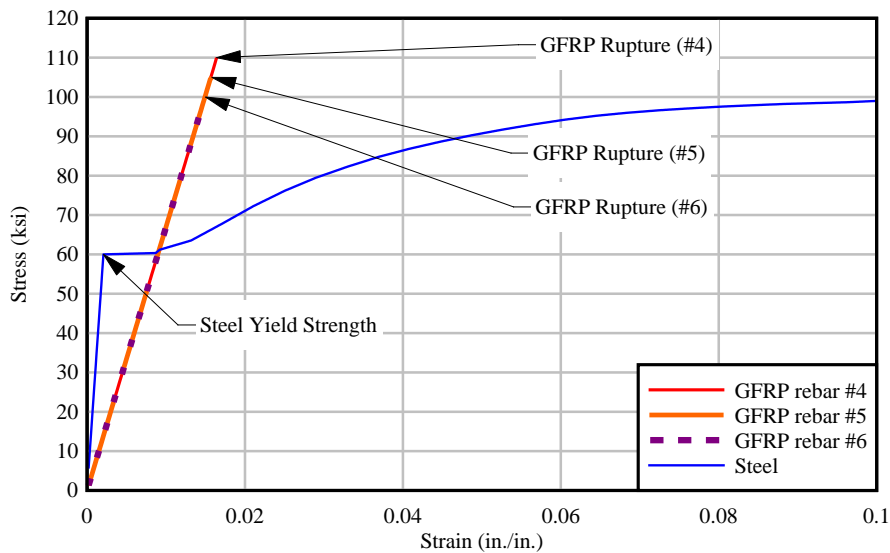


Figure 4-4. Steel and GFRP material properties

4.4.2 Center-of-rail (COR) rebar

GFRP rebar differs from steel bars in several ways, and one of the most significant differences in characteristics is the non-ductile behavior of GFRP. Bends in GFRP bars must be carefully designed to be consistent with manufacturing processes, as all bent bars must be formed in the manufacturer factory (versus in the field). Once resin in a GFRP bar has cured, generally the bar cannot be bent again. The bend radius is predetermined by manufacturers depending on the size of the bars and the bar type. Typically, the design of bent GFRP bars requires communication with the manufacturer to ensure that bars can be produced efficiently and economically.

In this study, Owens Corning was selected to be the producer of all GFRP bars. After discussions with company engineers, an alternative GFRP bar configuration was developed that was as similar as possible to the original steel bars (Figure 4-5, Figure 4-6). The GFRP design utilizes the steel-equivalent bar size (#4), spacing (6-in.), clearance, and embedment depth (6-in. min.). However, rather than using a single, continuous bar bent at the top and bottom of the rail, the GFRP reinforcement utilizes two individual vertical bars. These bars are bent and overlapped at the top and bottom of the rail. The predetermined bar bend radius for a #4 GFRP bar is 2.125 in. (Figure 4-6).

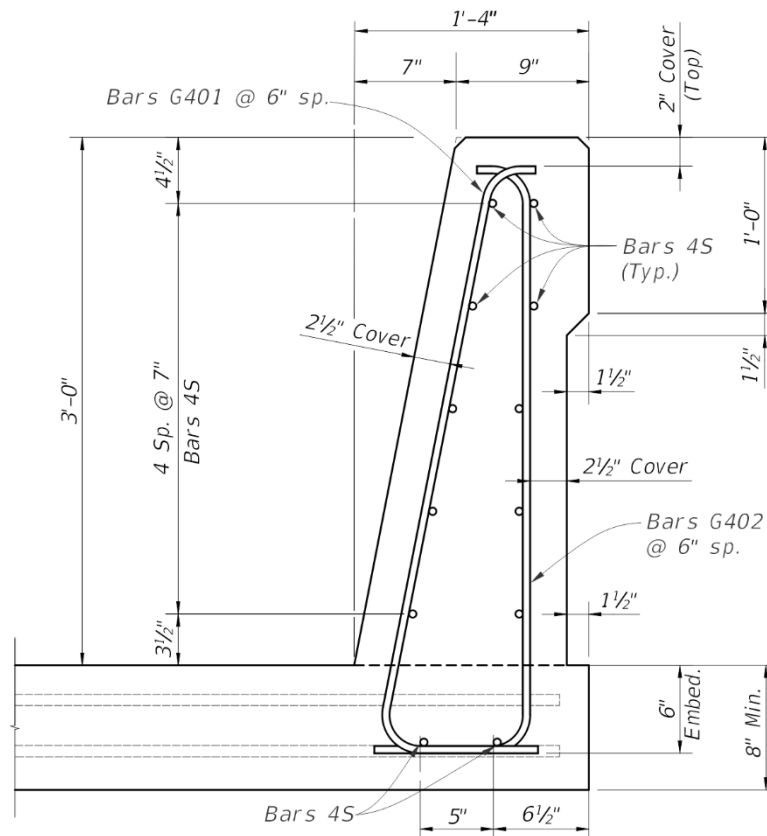


Figure 4-5. GFRP reinforced typical section through traffic rail (COR)

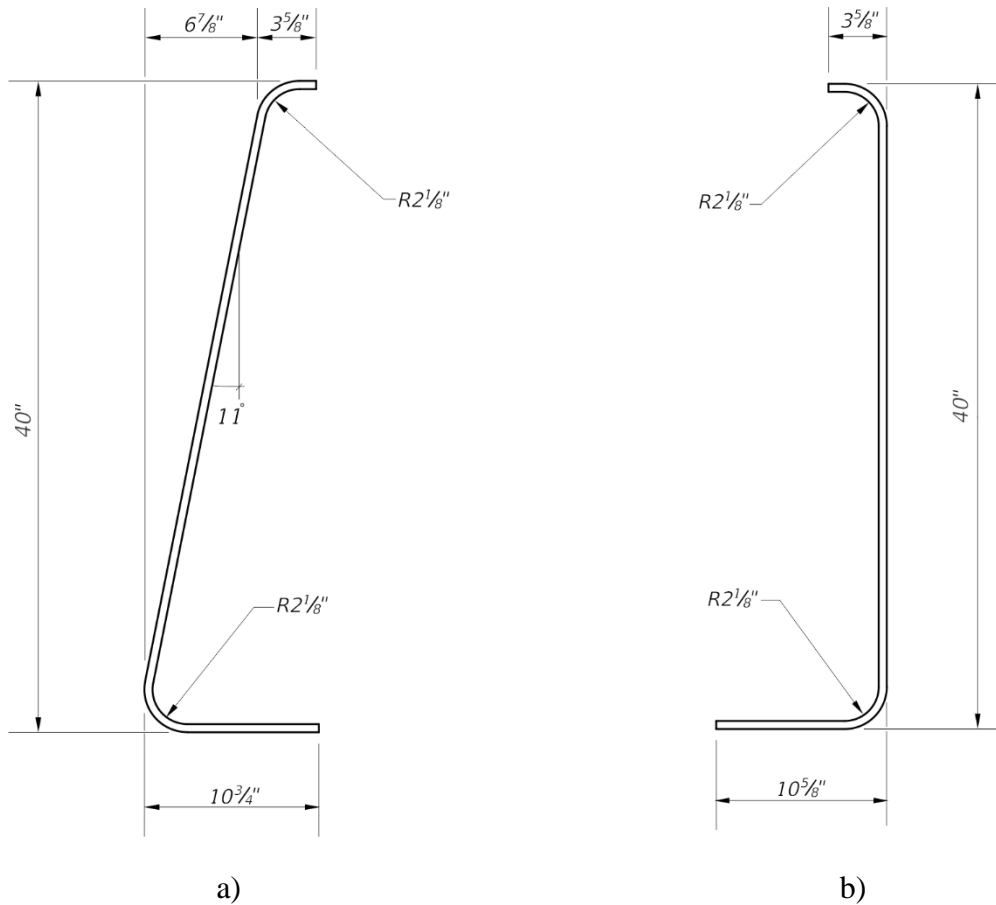


Figure 4-6. Stirrups of GFRP-reinforced bridge rail:
a) bar G401; b) bar G402

4.4.3 End-of-rail (EOR) rebar

Due to the lack of ductility of GFRP rebar, special attention was given to the situation where impact occurs near the end of a rail segment (i.e., bridge joint, rail end). Finite element impact simulations indicated that when an end portion of rail was subjected to the design impact force, progressive rupture of rebar elements occurred, leading to member-level structural failure. This finding necessitated the iterative development of improved end-of-rail (EOR) reinforcement configurations. After using FEA to evaluate various reinforcement options, a configuration of EOR GFRP rebar proposed for testing was established (Figure 4-7).

To minimize reinforcement layout changes during construction, the GFRP bent bar shapes were not altered. Instead, the spacing of bars in the EOR region was reduced from 6 in. to 3 in., over a span of 3 ft. Also, since GFRP rebar has significantly less stiffness than steel rebar, maintaining rail stiffness in the end section required that GFRP bars be bundled to increase the gross cross-sectional area. Specifically, for each EOR bar set, an extra bar G401 was added to the typical COR vertical rebar set.

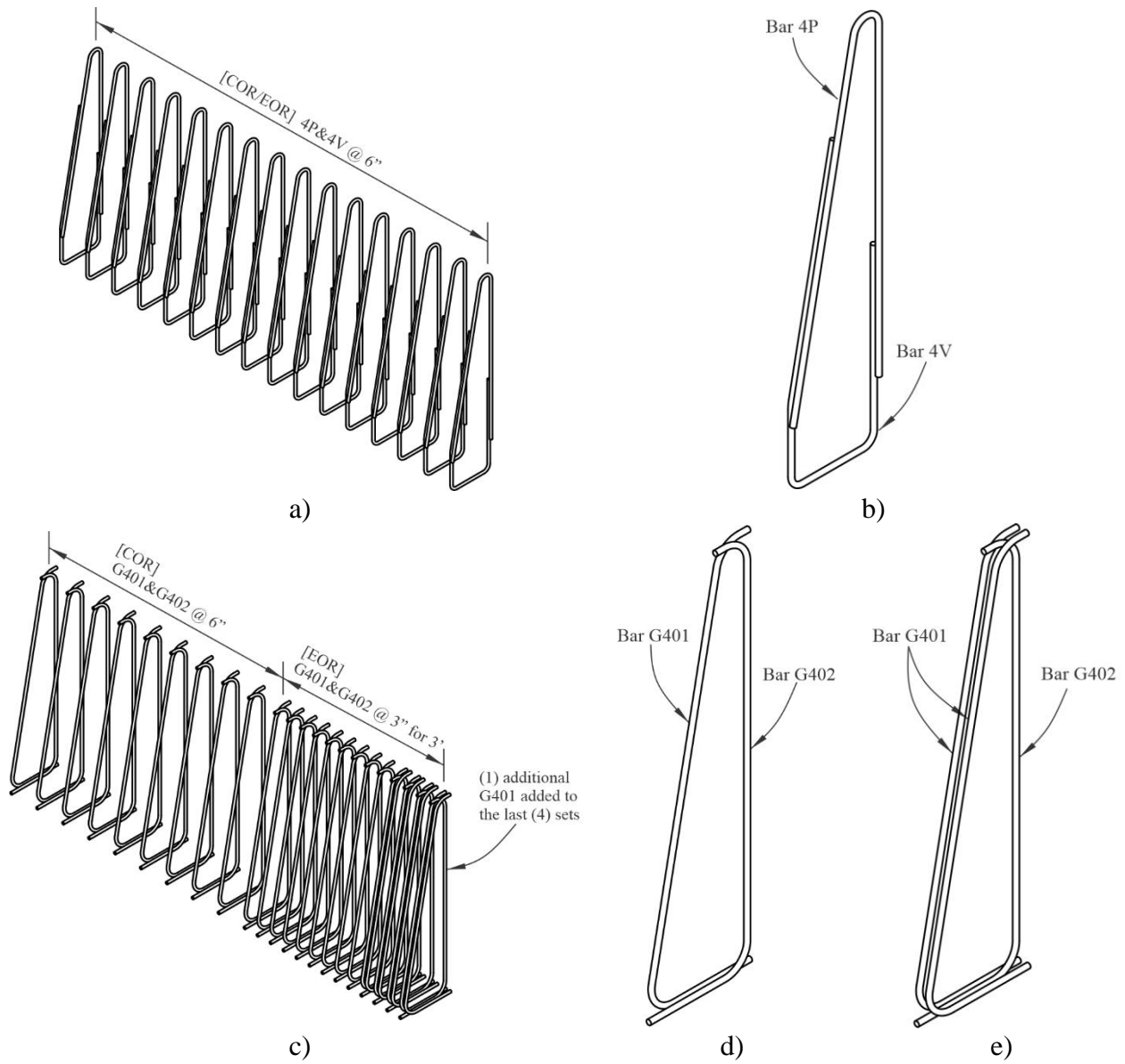


Figure 4-7. Rail rebar configurations and spacing at center of rail (COR) and end of rail (EOR):
 a) Steel rebar spacing overview; b) Steel rebar details; c) GFRP rebar spacing overview; d)
 GFRP COR rebar details; e) GFRP EOR rebar details

CHAPTER 5 FINITE ELEMENT MODELING OF RAIL COMPONENTS

5.1 Introduction

Finite element analyses were used to simulate impacts of the surrogate vehicle (pendulum impactor) against GFRP-reinforced and steel-reinforced rail test specimens (discussed in detail in the following chapter) under MASH test level 4 (TL-4) impact conditions. Modeling techniques (e.g., material models, element types), used to represent each component of the rail test specimens, are documented in this chapter. Detailed LS-DYNA keywords cards for the material models are provided in Appendix B.

5.2 Concrete modeling

Concrete components (e.g., rail and deck) were modeled using 8-node, hexahedral fully integrated solid elements (LS-DYNA solid element formulation `ELFORM=2`). Volumetrically, the rail and deck were meshed with elements that had dimensions of approximately 2"x2"x2", on average. Constitutive (stress-strain) properties of concrete were modeled using the continuous surface cap model (LS-DYNA material model `MAT_CSCM`) which is widely used for simulating concrete subjected to either static or dynamic (impact) loads. The `CSCM` concrete material model incorporates numerical representations of tensile and compressive damage states (Figure 5-1), as well as material failure. Of particular relevance to this study is the fact that this material model has undergone extensive testing and validation for applications relating to vehicle impact loading of roadside safety hardware [e.g., Murray (2007), Murray et al. (2007)]. In accordance with FDOT design standards, compressive strengths specified for the concrete rail and deck portions of the model were 3400 psi and 4500 psi, respectively.

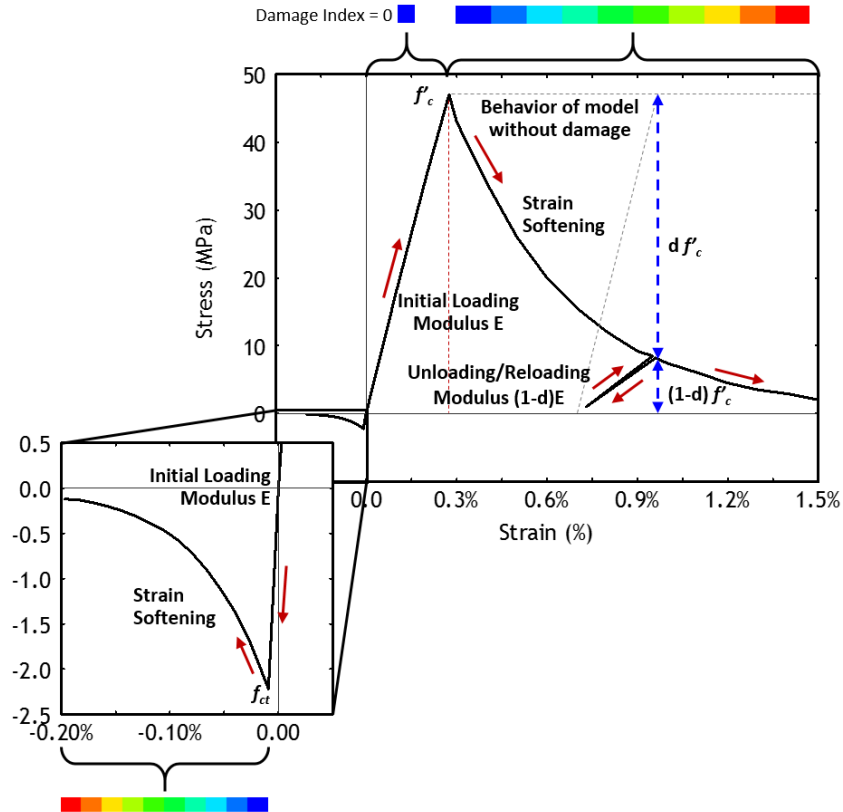


Figure 5-1. Stress-strain model for concrete (tension and compression) and damage index as reported by the MAT_CSCM material model (adapted from Murray, 2007)

5.3 Rebar modeling

Rebar was modeled using LS-DYNA beam elements based on the cross-section integrated Hughes-Liu formulation (ELFORM=1) with a circular cross-sectional shape (CST=1), and a 2x2 pattern of integration points at mid-length of each element. Beam cross-section diameters were defined appropriately for each bar size (#4, #5, and #6), and beam element lengths were approximately 2 in. for bent bars and 4 in. for straight bars. The rebar material models used to represent steel and GFRP were:

- **Steel rebar:** MAT_PIECEWISE_LINEAR_PLASTICITY, an elastic-plastic material model for which stress and strain curves can be defined in a piecewise-linear manner. To model steel rebar linear elastic behavior, plastic yielding, and material hardening, the stress-strain curve for Grade 60 steel rebar developed in the FDOT research project BDV31 977-93 (Consolazio et al. 2022) was used (Figure 5-2).
- **GFRP rebar:** MAT_PLASTIC_KINEMATIC, a nonlinear elastic-plastic material model capable of representing linear elastic behavior, plastic yielding (if appropriate), and material failure. Although GFRP rebar is idealized as exhibiting ‘linear to failure’ structural behavior, MAT_PLASTIC_KINEMATIC was used due to the material ‘failure’ feature of this model. To model GFRP, the ‘yield’ and failure strains were specified as being nearly equal to within a very small numerical tolerance. As such, the material exhibited linear elastic behavior up

to the failure strain, then failed abruptly. No plastic deformation of any significance occurred. For the GFRP rebar material model, the elastic modulus, yield stress, and failure strain were specified as listed in Table 5-1. These values were determined from the producer datasheet obtained from Owens Corning with an environmental reduction value of $C_E=0.7$ applied. Stress-strain curves for the steel and GFRP rebar elements are presented graphically in Figure 5-2.

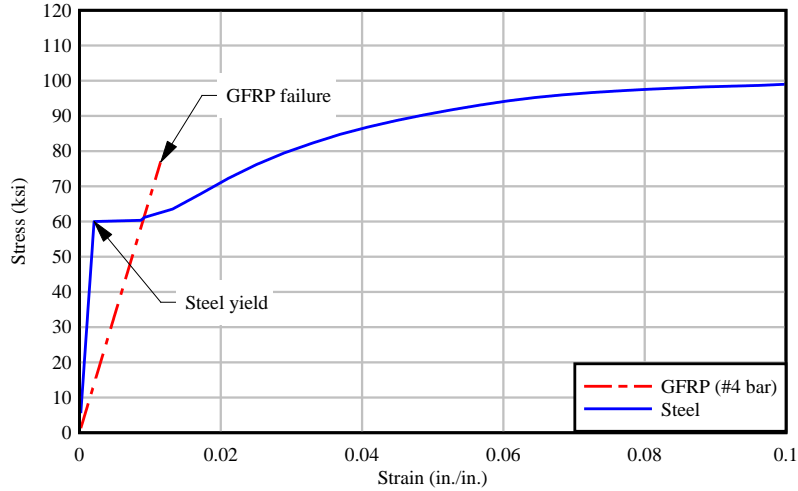


Figure 5-2. Stress-strain models for steel rebar and GFRP rebar

Table 5-1 GFRP material properties (with $C_E=0.7$)

GFRP Bar Type	Tensile Strength (ksi)	Ultimate Strain (in./in.)	Modulus of Elasticity (ksi)
#4	77.0	0.0115	6700
#5	73.5	0.0110	6700
#6	70.0	0.0104	6700

5.4 Bond modeling

To model bond between rebar (beam elements) and concrete (solid elements), the LS-DYNA `CONSTRAINED_BEAM_IN_SOLID` feature was used. This feature automatically generates constraint-based coupling links between the beams (beams) and surrounding solids (concrete). Coupling constraints were generated at all beam end-nodes as well as at two additionally generated coupling points ($NCOUP=2$) interior to each beam element.

CHAPTER 6 DEVELOPMENT OF RAIL TEST SPECIMEN CONFIGURATION

6.1 Introduction

To numerically compare the designed GFRP bridge rail to the standard steel R/C bridge rail, center-of-rail (COR) and end-of-rail (EOR) test specimens of both types (standard steel R/C and GFRP) were designed to emulate the behavior of such rails when installed on a highway bridge. When a rail is installed on a bridge, it is typically cast on the bridge deck overhang (Figure 6-1). Per FDOT SDG 4.2.5, the maximum deck overhang measured from beam/girder centerline is 6 ft for a 36-in. tall rail. To emulate the impact-induced deformation of the deck edge and rail, the 8.5-in. thick deck designed for the test specimen consisted of a 4-ft overhang, raised 8.5 in. above the ground plane by 17-in. deep thickened edges (Figure 6-2). The thickened edges, located at the front (rail impact face) and two sides of the test specimen, were also used during lifting during transportation (Figure 6-3), and to embed anchorages to secure the test specimen onto the laboratory universal foundation.

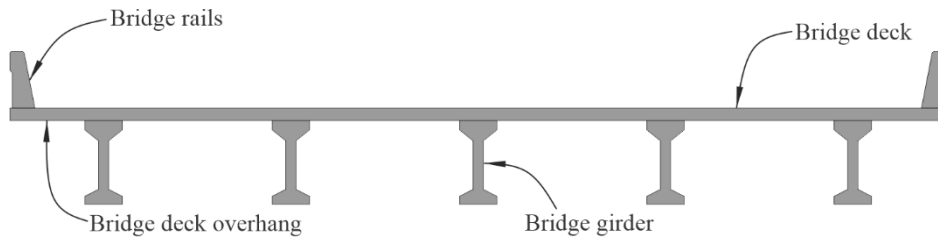


Figure 6-1. Traffic rail on a typical bridge

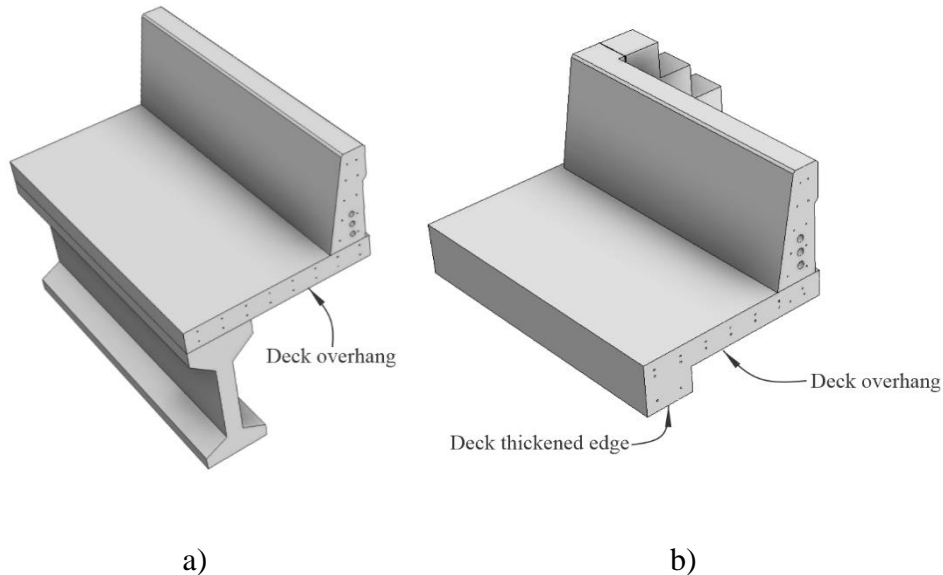


Figure 6-2. Test specimen deck overhang and thickened edge:
a) Cross-sectional view; b) Back view (COR shown, EOR similar)

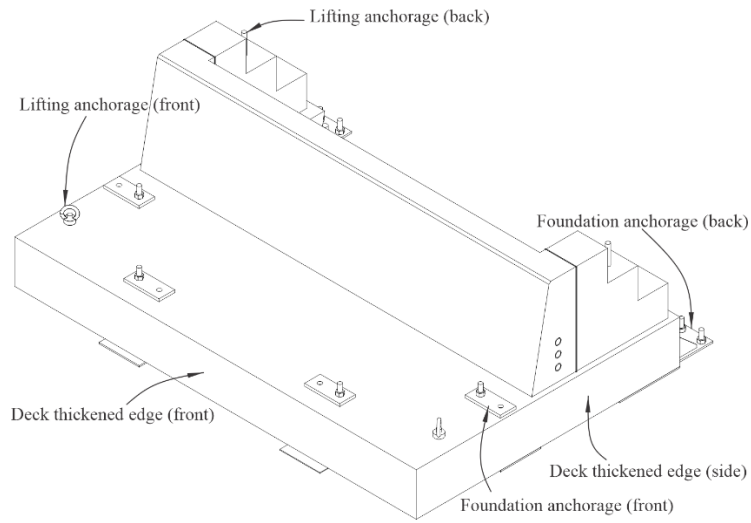
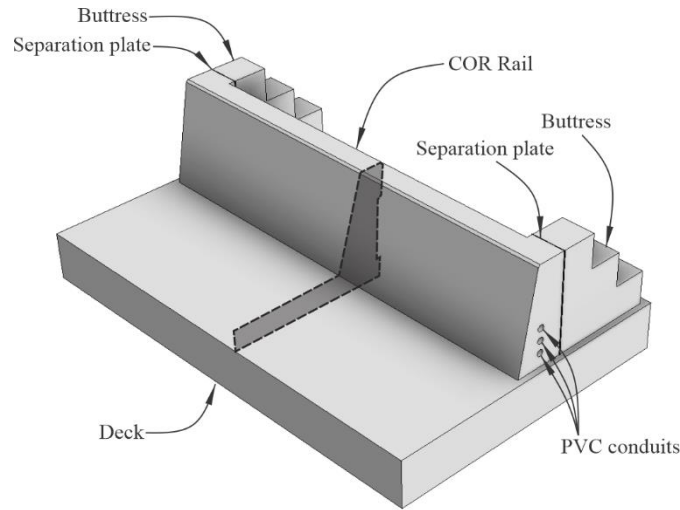
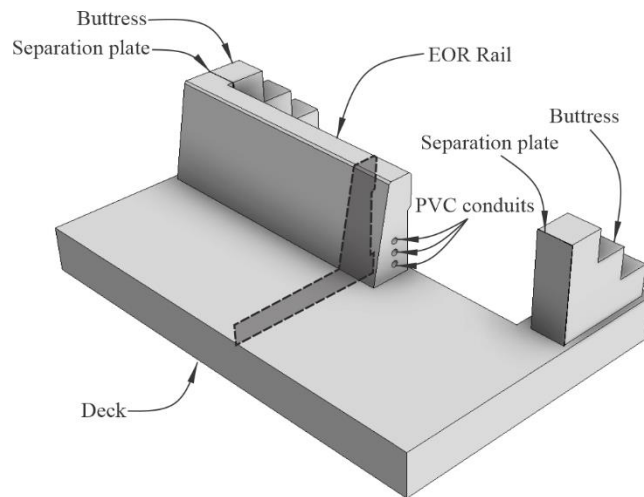


Figure 6-3. Test specimen anchorages on thickened deck

Each test specimen included: COR or EOR reinforced rail, deck, buttresses, separation plates, and PVC conduits (Figure 6-4).



a)



b)

Figure 6-4. 36-in. SSTR test specimen overview: a) COR; b) EOR

Typically, concrete bridge rails are installed over relatively long bridge span lengths. In order to evaluate the vehicle redirection and stability, the crash-test that TTI performed on the TxDOT 36-in. SSTR utilized a rail length of 150-ft (Sheikh et al. 2011). In contrast, the universal foundation of the FDOT pendulum impact test facility could not accommodate such rail length, nor was such a significant length required to evaluate lateral load behavior (as opposed to vehicular motion). To determine a rail test specimen length for pendulum impact testing, both theoretical estimation and FEA simulation were employed. In AASHTO LRFD (2017), critical rail length, L_c , was determined from the length of the yield line failure pattern along the rail. For a TL-4 36-in. SSTR, the critical rail length was found to be 10 ft (Appendix C). Therefore, a COR test specimen rail length of 13 ft, with an 11-ft clear span between end supports, was selected. Furthermore, FEA simulations of the test specimen configuration (13 ft), and a longer rail length (40 ft), indicated

similar deflection and damage patterns. In the EOR test specimen configuration, a portion of the COR rail was removed, and an 8-ft long EOR rail was designed.

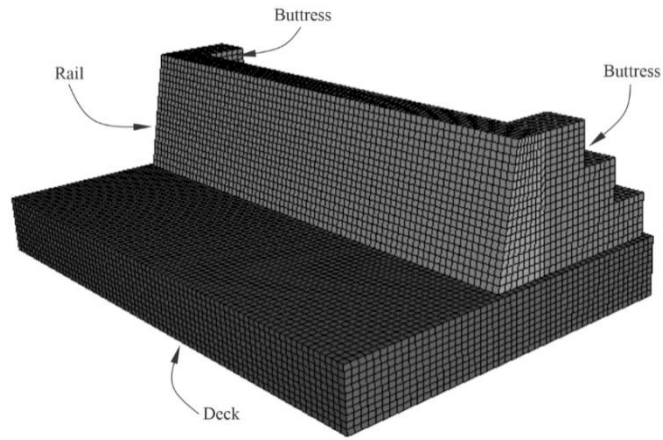
As the rail length was of limited length in the test specimens, end buttresses were incorporated to provide support conditions that otherwise would have been provided by adjacent continuous (upstream and downstream) bridge rail. Initial finite element simulations of a rail segment with integral end buttresses indicated that the buttresses would rotationally over stiffen the rail ends and adversely affect the intended rail damage pattern. To resolve this issue, a steel separation plates were introduced between each buttress and the rail. The discontinuities introduced by these plates allowed the rail ends to rotate independently of the buttresses and thus avoid the rotational constraint that was observed in simulations involving integral buttresses.

To ensure that impact load was applied in the lateral direction, an aluminum loading wedge was attached to the impact face of each rail test specimen. The impact (traffic side) of the rail is oriented at an 11-deg. angle from vertical. Therefore, the aluminum loading wedge had a vertical impact face but an 11-deg. back slope which was adhered to the rail during impact.

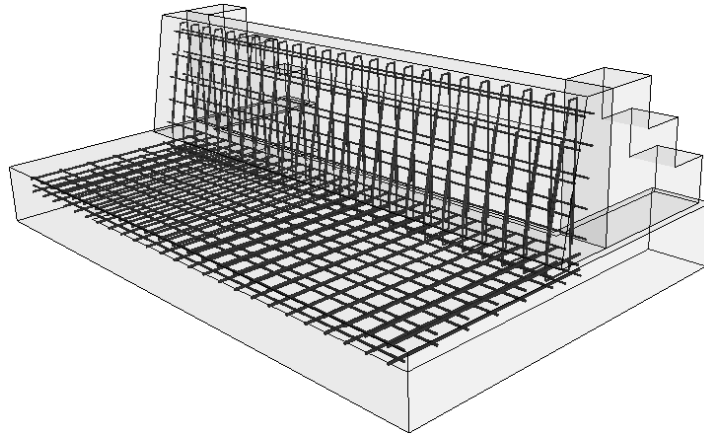
Finite element simulations were carried out to investigate and iterate each rail configuration (R/C, GFRP reinforced, COR, and EOR) so that during subsequent pendulum impact testing the rail specimens would perform as intended. For example, it was through this iterative process that the need for separation plates between the rail and buttresses was determined. Results from the FEA simulations are summarized in the following sections.

6.2 Simulated impact performance for COR specimen: Steel vs. GFRP

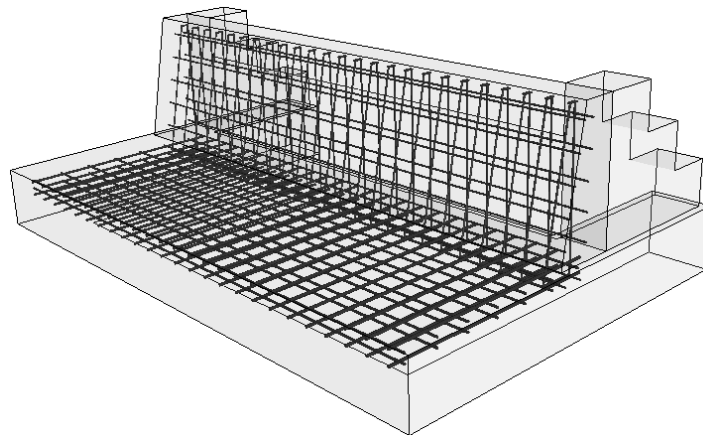
The FEA model of the COR test specimen included a 13-ft long reinforced rail, deck with thickened edges, and buttresses (Figure 6-5). The test specimen model was reinforced with four types of rebar: transverse (impact direction) rail bars, longitudinal rail bars, transverse deck bars, and longitudinal deck bars. The rail was reinforced with transverse bent bars and straight longitudinal bars. The configuration of the steel and GFRP rail reinforcement (rail transverse bars and rail longitudinal bars) was previously summarized in Chapter 4. The steel reinforced COR model consisted of top bar (4P) beams and bottom bar (4V) beams at an offset of 0.5-in. (rebar diameter) (Figure 6-6a). The GFRP reinforced model consisted of front bar (G401) beam elements and back bar (G402) beam elements at an offset of 0.5-in. (rebar diameter) as well (Figure 6-6b). The straight bars (4V) were spaced at 7-in. vertically against the transverse bars with an offset of 0.5-in. The deck was reinforced with two layers of #6 transverse straight bars at 6-in. spacing and #5 longitudinal straight bars at 12-in. spacing. Concrete components (rail, deck and buttresses) were modeled using high-resolution meshes (~2-in. cubes) of 8-node fully integrated solid elements. A contact surface between the loading wedge and concrete rail was defined so that impact force could be calculated for each simulation. Nodes at the interface between the buttresses and the rail were not nodally merged together. Instead, contact detection surfaces were defined at each of these locations to represent the structural effect of introducing steel separation plates.



a)



b)



c)

Figure 6-5. COR test specimen FEA model:
a) Concrete components overview; b) Steel reinforcement; c) GFRP reinforcement



Figure 6-6. Rebar models for COR test specimens:
 a) Steel transverse bars; b) GFRP transverse bars

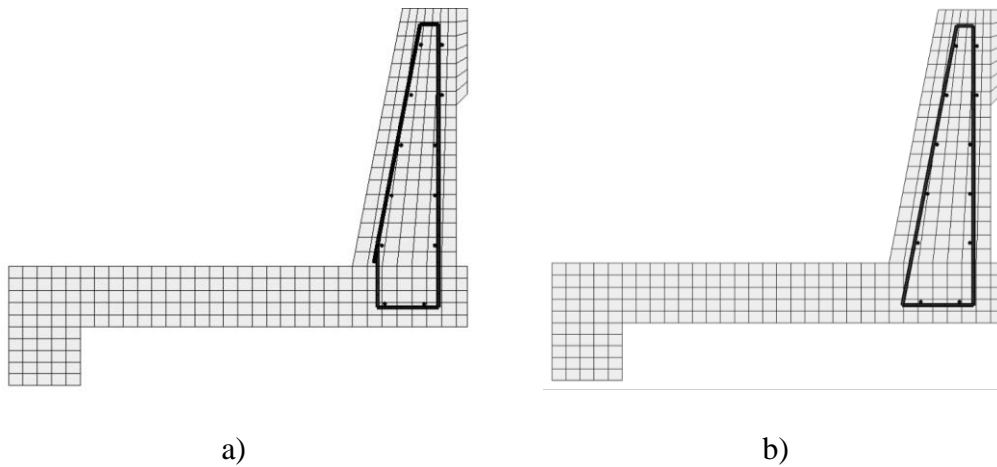


Figure 6-7. Reinforced test specimen rail cross section:
 a) Steel-reinforced test specimen; b) GFRP reinforced test specimen

While both steel and GFRP COR models exhibited the expected “V” shaped damage pattern, the GFRP COR model exhibited considerably more damage and deformation in comparison to the steel counterpart (Figure 6-8). This result was anticipated. As the modulus of GFRP rebar was about a quarter that of steel rebar, the direct bar-for-bar replacement method resulted in a less stiff section and more extensive rail deformation. However, despite the more extensive damage observed in the GFRP rail model, no GFRP rebar rupture or structural failure occurred.

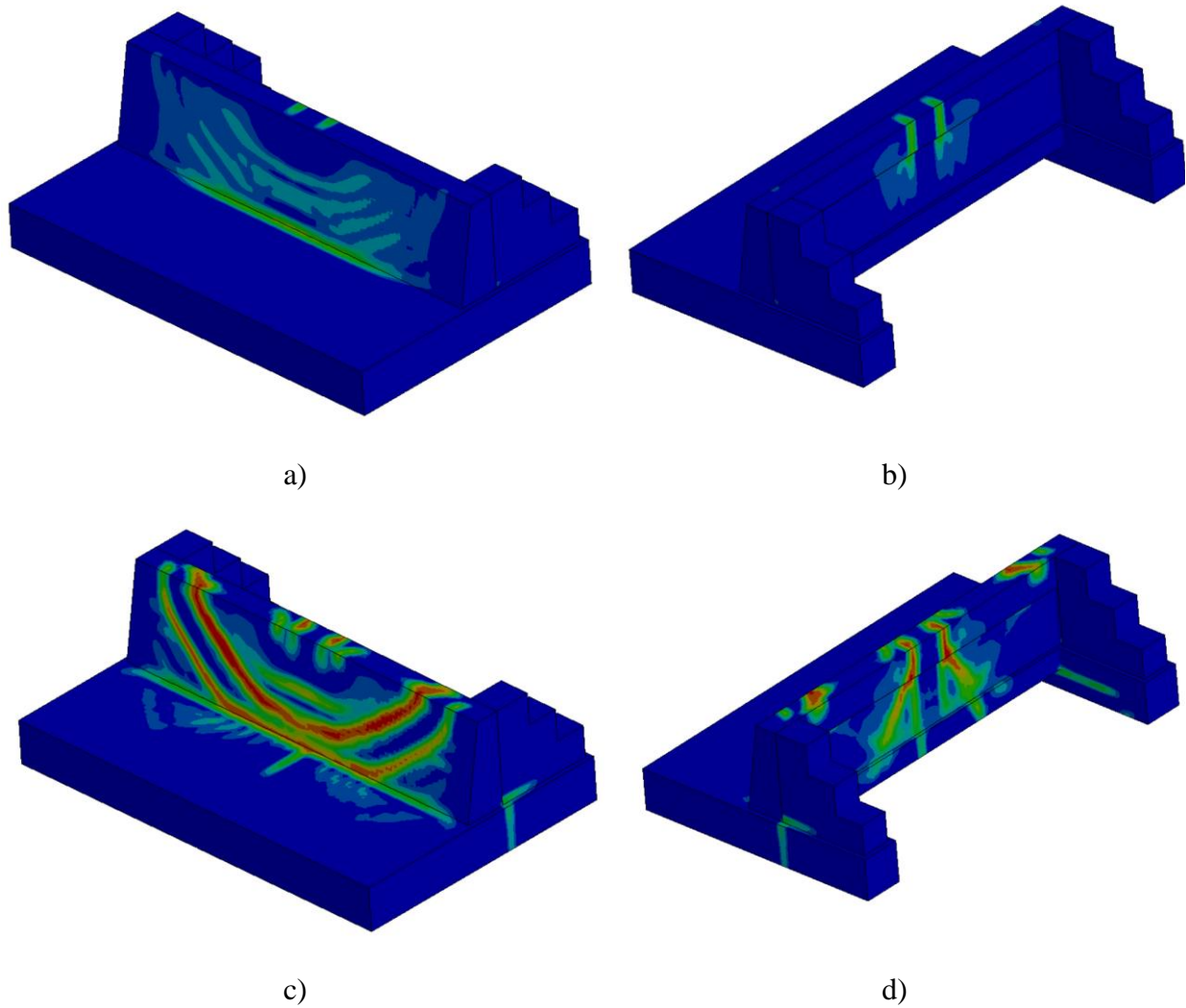
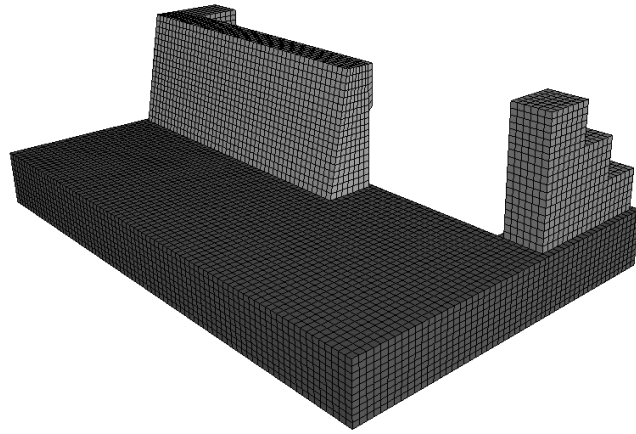


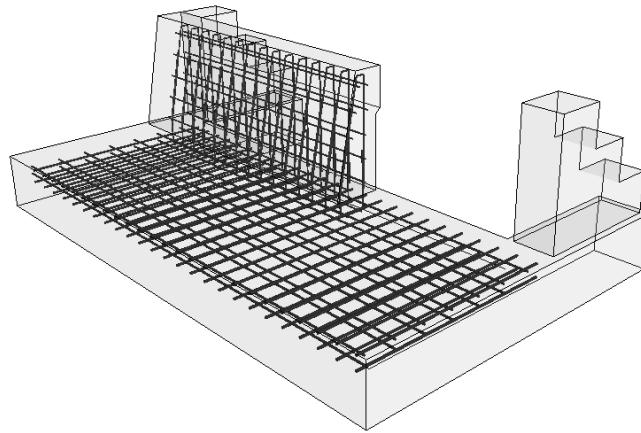
Figure 6-8. COR rail test specimen FEA swing model maximum concrete damage: a) Steel-reinforced rail (front isometric view); b) Steel-reinforced rail (back isometric view); c) GFRP-reinforced rail (front isometric view); d) GFRP-reinforced rail (back isometric view)

6.3 Simulated impact performance for EOR specimen: Steel vs. GFRP

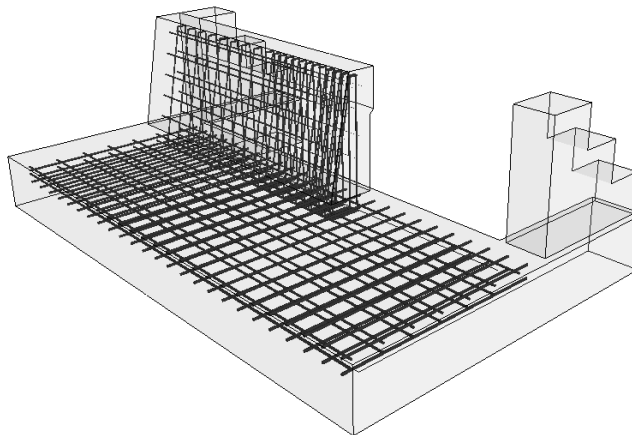
Steel and GFRP EOR test specimen models consisted of an 8-ft long reinforced rail (instead of 13-ft), deck with thickened edges, and buttresses (Figure 6-9). As there was no specific rail end reinforcement adjustment required for the FDOT 36-in. R/C SSTR, the reinforcement layout was unchanged (i.e., 4P and 4V bars at 6-in. spacing). However, to represent the GFRP EOR transverse rebar configuration documented in Chapter 4 (i.e., G401 and G402 at 6-in. spacing throughout the rail), four bundles of end bars were added, and rebar spacing was reduced to 3-in. near the end (Figure 6-10).



a)



b)



c)

Figure 6-9. EOR test specimen FEA model:
a) Concrete components overview; b) Steel reinforcement; c) GFRP reinforcement

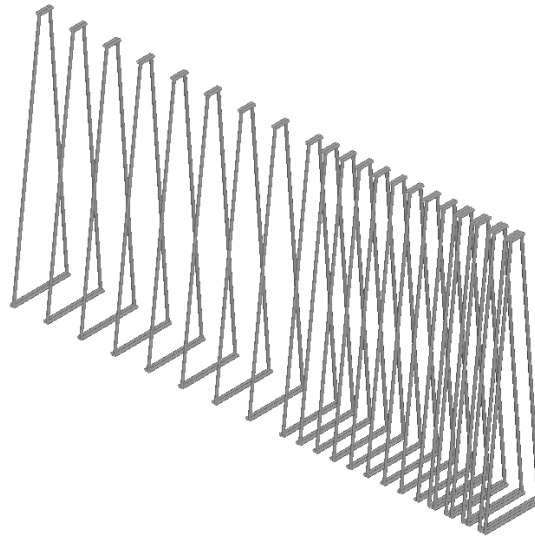


Figure 6-10. EOR GFRP rail transverse rebar models

Whereas the COR specimen consisted of continuous rail extending from both sides of the impact location (to carry load to the buttressed), the EOR specimen did not. As such, the concrete damage (Figure 6-11) in both the steel reinforced and GFRP reinforced EOR models was more significant as compared to the COR models. In both steel reinforced and GFRP reinforced models, noticeable concrete damage was observed in the form of diagonal damage lines at the front face, as well as at the connection between the rail and deck. While more extensive concrete damage was observed in the GFRP EOR test specimen model (as compared to the GFRP COR model), no GFRP rebar rupture occurred and the rail remained structurally intact.

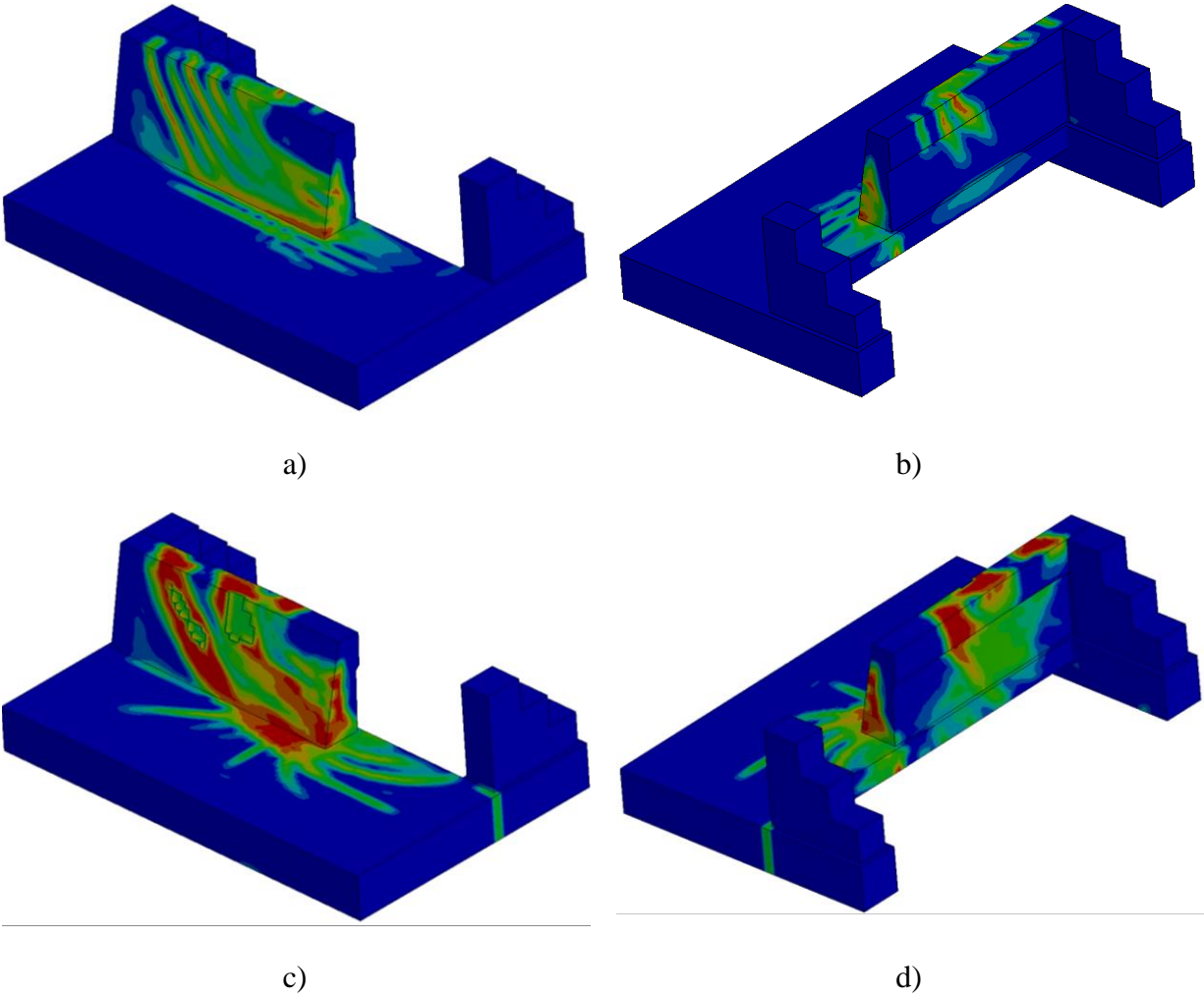


Figure 6-11. EOR test specimen rail FEA swing model maximum concrete damage:
a) Steel-reinforced rail (front isometric view); b) Steel-reinforced rail (back isometric view); c)
GFRP-reinforced rail (front isometric view); d) GFRP-reinforced rail (back isometric view)

CHAPTER 7 FULL-SCALE RAIL PENDULUM IMPACT TEST PROGRAM

7.1 Overview

Full-scale pendulum impact tests were conducted to investigate the structural adequacy of the designed GFRP reinforced bridge rail at both center-of-rail (COR) location and end-of-rail (EOR) location. Four types of test specimens were impact tested: steel reinforced COR (quantity=2), GFRP reinforced COR (quantity=1), steel reinforced EOR (quantity=1), and GFRP reinforced EOR (quantity=2). Note that although all the above mentioned test specimens are documented and discussed in this chapter, the steel reinforced COR test specimens were fabricated and impact tested under the project BDV31-977-72 (Consolazio et al., 2021).

The test specimens were impact tested using the impact pendulum at FDOT Structures Research Center. Impact test components included: crushable-nose pendulum impactor supported by cables and pendulum towers, and rail test specimens installed on the universal foundation. The impactor was designed and fabricated in project BDV31-977-72 (Consolazio et al., 2021) and utilized consumable aluminum honeycomb cartridges. Bridge rail test specimens were fabricated inside the FDOT Structures Research Center, then relocated to the pendulum using a crane, and installed on the universal foundation. Detailed test specimen drawings are provided in Appendix D and Appendix E.

7.2 Construction of test specimens

To begin the construction process for each test specimen, the reinforcing bars (steel or GFRP) for the deck portion of the test specimens were tied together and placed into deck formwork (shown in Appendices D and E). In the case of steel reinforced specimens, connection bars between the deck and rail (i.e., 4V bars), and end-support buttress bars were also installed within the deck formwork (Figure 7-1 and Figure 7-2). In the case of GFRP reinforced specimens, the rail reinforcement (i.e., G401 and G402 bars) and end-support buttress bars were installed within the deck formwork (Figure 7-3). Table 7-1 shows material properties of GFRP bars delivered and used in the test specimens.



Figure 7-1 Reinforcing bars positioned inside deck formwork for steel reinforced specimens



Figure 7-2 Deck-to-rail connection bars and end-support buttress reinforcement positioned inside deck formwork for steel reinforced specimens



Figure 7-3 GFRP bars positioned inside deck formwork for GFRP bar reinforced specimen

Table 7-1 GFRP material properties for bars used in specimens (with $C_E=0.7$)

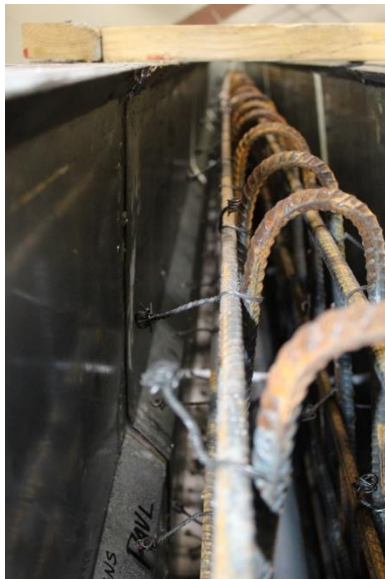
GFRP Bar Type	Tensile Strength (ksi)	Ultimate Strain (in./in.)	Modulus of Elasticity (ksi)
#4 Bent Bar	122.9	0.0151	8152
#4 Straight Bar	110.8	0.0127	8732
#5 Straight Bar	112.4	0.0131	8588
#6 Straight Bar	110.3	0.0123	8935

With bars for the deck portion in place, an FDOT approved Class II deck concrete (a conventional 4500-psi strength concrete that met FDOT mixture design requirements for concrete bridge decks) was placed (Figure 7-4) and adequately vibrated to form the deck portion of each test specimen. Mixture design details and the specific concrete mixture quantities used in the delivered deck concrete are provided in Appendix F. After placement and hardening of the deck concrete, formwork for the rail portion of the test specimen was attached above the deck.



Figure 7-4 Deck concrete placement

To construct each rail, reinforcing bars (steel or GFRP) were installed, and rail formwork was positioned (Figure 7-5a). Then an FDOT approved Class II non-bridge deck conventional 3400-psi strength concrete that meets FDOT mixture design requirements for the 36-in. SSTR was placed and adequately vibrated to form both the rail and buttress regions of the test specimens (Figure 7-5b). Mixture design details and the specific concrete mixture quantities used in the delivered rail concrete are provided in Appendix F. After adequate time for curing – approximately 3 days – had passed, components of the deck and rail formwork were removed and the construction phase was complete (Figure 7-6).



(a)



(b)

Figure 7-5 Construction of rail portion of R/C test specimen 1: (a) Rail reinforcement positioned inside rail formwork; (b) Rail concrete placed and formed



Figure 7-6 Formed R/C test specimen 1

7.3 Installation of test specimen

After providing adequate time for curing – approximately 7 days after placing the rail concrete – the test specimens were lifted by crane out of the formwork (Figure 7-7), moved across the FDOT structures laboratory and placed onto a truck bed. The truck was driven outside to the pendulum, where an additional crane was used to lift the specimen off the truck bed and into position on the pendulum foundation (Figures 7-8 – 7-10). The total weight of each test specimen was approximately 20 kip and no noticeable cracking occurred during the lifting/transportation process.



Figure 7-7 Test specimen lifted out of the formwork by crane



Figure 7-8 Test specimen being moved into position on the pendulum foundation



Figure 7-9 Impact test specimen in position on pendulum foundation



Figure 7-10 Backside of impact specimen after being positioned onto the pendulum foundation (with temporary HSS lifting element still connected)

Once correctly positioned, the test specimen was anchored to the pendulum foundation—using the anchoring process that is presented in Appendix G. As depicted in Figure 7-11, a number of structural steel components were used to anchor each test specimen to the pendulum foundation thus preventing the test specimen from transverse movement or sliding as a rigid body, and only allowing the rail portion of the test specimen to deflect under impact loading.

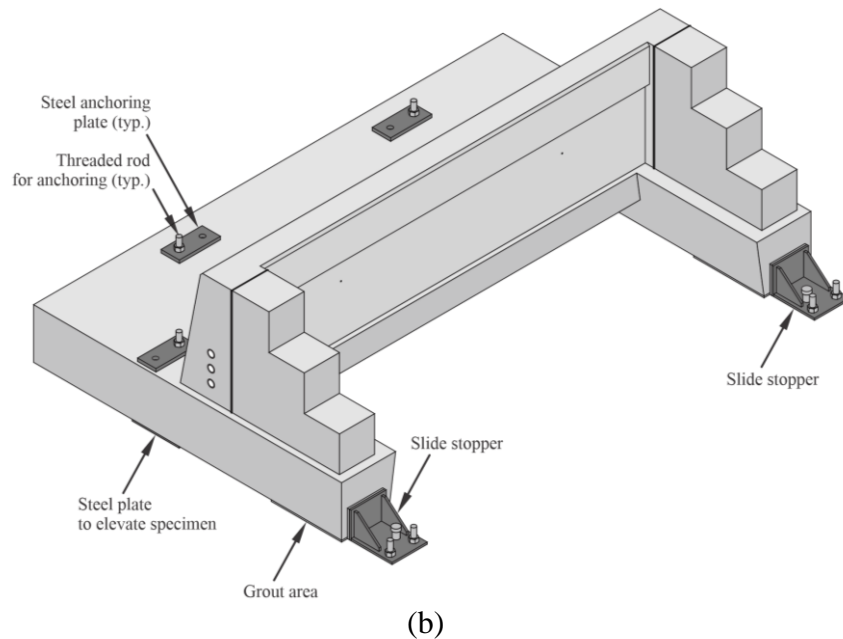
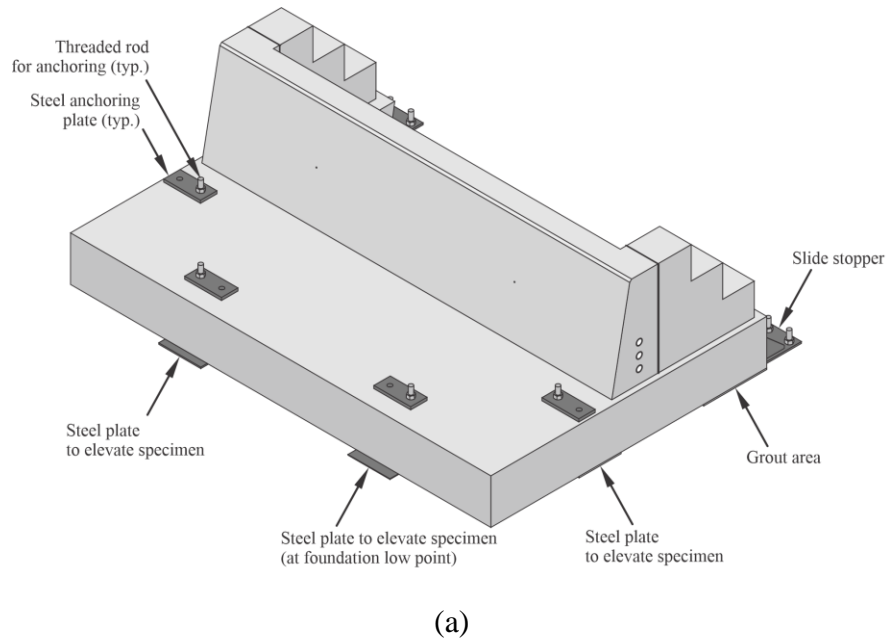


Figure 7-11 Diagram of impact test specimen with additional anchoring elements placed:
 (a) Front isometric view; (b) Back isometric view

During forming of the deck portion of each test specimen, PVC pipes were cast within the deck concrete to create 8 openings, which passed vertically through the deck. Each of these eight openings was positioned within the deck to coincide with an ‘anchor point’—a fixture location—on the pendulum foundation. Anchoring was completed by first passing four threaded rods, which were fastened to the foundation, through the deck at four of the eight openings. Although eight openings were included in the design of the test specimen, it was later determined that only four of the eight were necessary for adequate anchoring. Steel anchoring plates (Figure 7-11), with holes for threaded rods to pass through) were placed on top of the deck with a leveled grout surface

and fastened with a threaded nut. Each of the four threaded rods were then post-tensioned, using a loading assembly provided by FDOT (Figure 7-12), to a 35-kip force. The 35-kip post-tension force (per threaded rod) was selected such that post-tensioning would produce a total 140-kip normal force (acting on the test specimen). Assuming a static coefficient of friction of 0.5, a 70-kip frictional force would then be relied upon to resist—as the primary method for preventing transverse rigid body movement—the impact force applied to the specimen. Photographs taken during the post-tensioning process for one of the threaded rods are shown in Figures 7-12 – 7-13.



Figure 7-12 Post-tensioning fourth (front right) threaded bar for anchoring test specimen to pendulum foundation with the FDOT loading assembly



Figure 7-13 Anchored test specimen

In the unlikely event that post-tensioning would not produce adequate friction to resist transverse (rigid body) sliding of the test specimen, an additional (secondary) mechanism was used with the anchoring/installation process. As depicted in Figure 7-11b, behind each end-support buttress at the foundation/deck level, a steel ‘slide stopper’ was installed. Each slide stopper was designed to transfer up to a 35-kip transverse force from the deck to the foundation and prevent sliding of the test specimen. As part of the developed anchoring plan, and to accommodate possible construction tolerances of the test specimen, a small gap (about 0.5-in.) between each steel slide

stopper and test specimen was included. After the test specimen was post-tensioned, and with the slide stoppers installed on the foundation, grout was used to fill the gap between the slide stopper and test specimen (Figure 7-14), completing the anchoring sequence. With the test specimen anchoring sequence complete, an aluminum loading wedge was adhered to the rail (Figure 7-15), and aluminum honeycomb cartridges were installed in the impactor nose (Figure 7-16), completing the test specimen installation stage.



Figure 7-14 Placing grout between test specimen and reaction element (steel slide stopper) as a secondary reaction system to prevent specimen from sliding during impact testing



Figure 7-15 Aluminum loading wedge adhered to front face of rail



Figure 7-16 Pendulum impactor and impact test specimen prepared and ready for testing

7.4 Instrumentation plan

For each pendulum impact test, a collection of high-speed data acquisition systems was used to record data. Specifically, the following instrumentation components/sensors were used:

- Contact tape switches
- Optical break beams
- Accelerometers
- High-speed cameras
- Laser displacement sensors
- Concrete strain gages
- Rebar strain gages

The overall instrumentation plan for each test specimen (either R/C or GFRP configuration) is depicted in Figure 7-17 and is further detailed in Appendix H. The data acquisition rates were 2000 frames/sec for each high-speed camera and 10 kHz per channel for all other sensors. Sensors positioned on (i.e., attached to) the exterior faces of each test specimen are depicted in Figure 7-18.

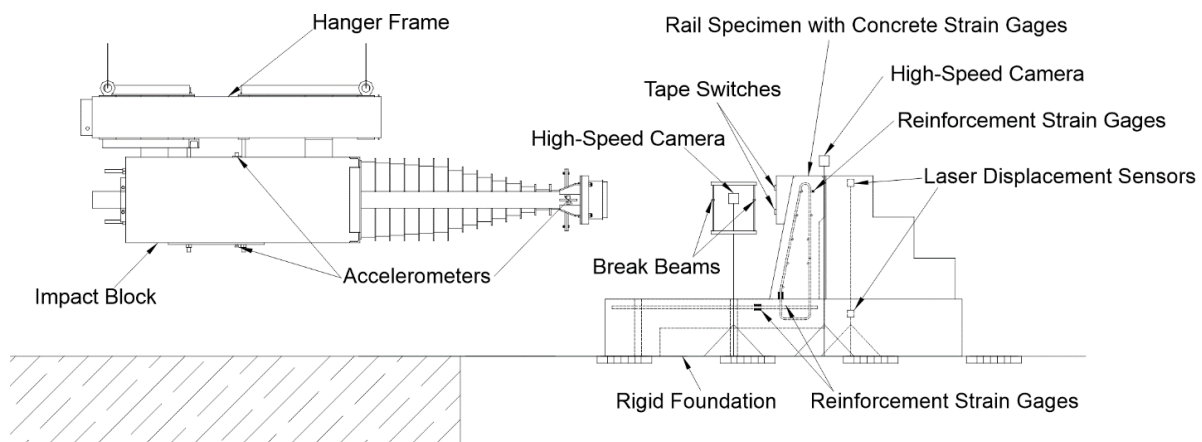
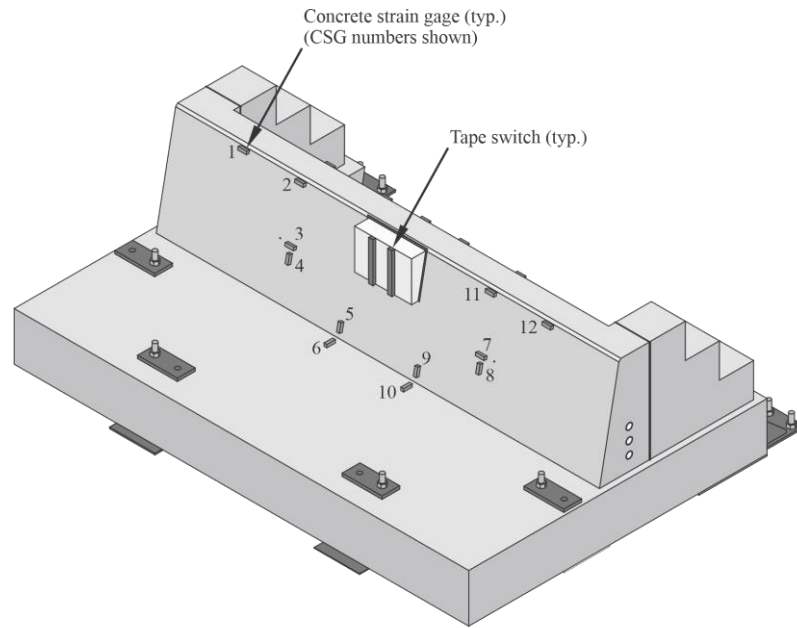
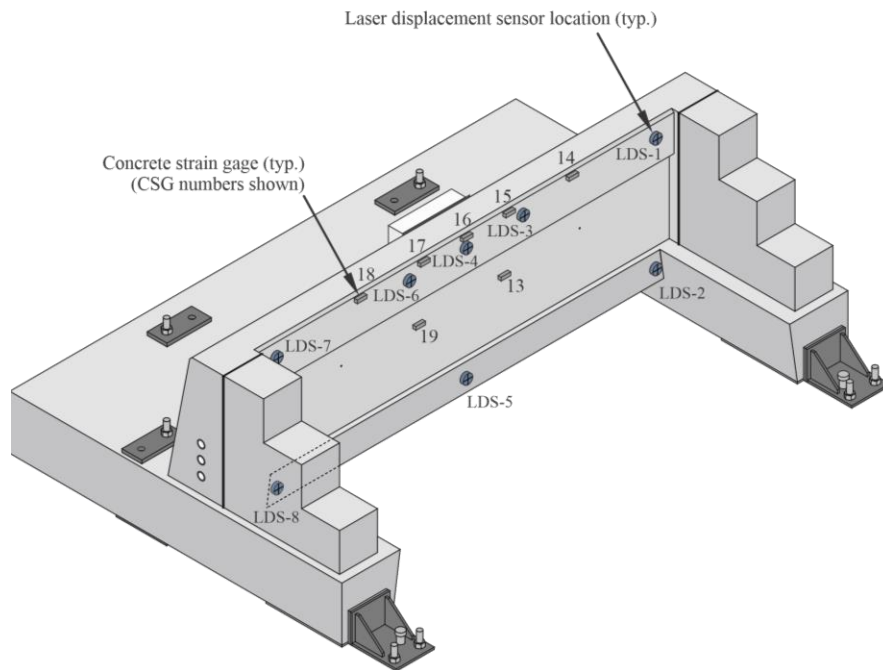


Figure 7-17 Instrumentation plan used in pendulum impact testing



(a)



(b)

Figure 7-18 External instrumentation: (a) Front concrete strain gage and tape switch sensor locations; (b) Back concrete strain gage and laser displacement sensor locations

7.4.1 Contact tape switches

Pressure sensitive contact tape switches were installed on each test specimen to detect the initial time of impact. Specifically, two tape switches were placed on the impact face of the

aluminum loading wedge (Figure 7-19). Tape switches are used to detect a directly applied contact pressure and are activated when the pendulum impactor comes into contact with the loading wedge (i.e., when depressed, the gage produces a change in voltage reading, signaling the starting time of impact). Although each tape switch activates independently, two tape switches were used in each impact test to redundantly ensure that the data acquisition system properly triggered. Specifications of the 18-in. long disposable tape switches are provided in Table 7-2.

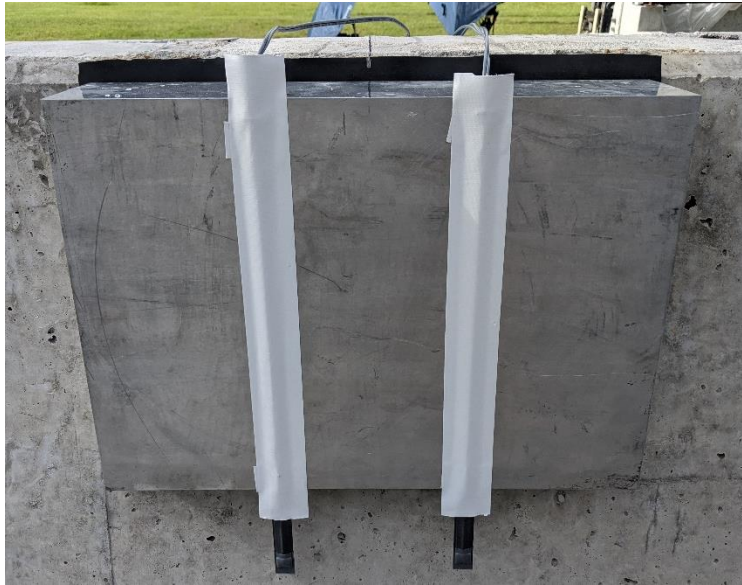


Figure 7-19 Tape switches adhered to the impact face of the aluminum loading wedge

Table 7-2 Specifications for pressure sensitive tape switches

Manufacturer	Tapeswitch Corporation
Ribbon switch type	131-A
Actuation force	60 oz.
Switch lengths used	18 in.
Dimensions	$\frac{3}{4}$ " in. wide, $\frac{3}{16}$ in. thick
Minimum bend radius	1 in.

7.4.2 Optical break beams

Infrared optical break beam sensors were used to quantify the impact velocity of each test. An individual break beam sensor set consists of one transmitter and one receiver. As shown in the instrumentation plan (Appendix H), two sets of break beams were positioned in front of the test specimen at a 12-in. spacing and were mounted on a stand to elevate the sensors to the designated impact height (Figure 7-20). For each break beam set, the transmitter emits an infrared beam and is received by the other receiving end. If the infrared beam is blocked (in this case, when the impactor swings and crosses the path of the beam), an increase in recorded voltage data will be produced. By separating break beam set 1 from break beam set 2 by a distance of 1 ft, and by knowing the duration of time over which the impactor traversed the 1 ft distance, the velocity could

be quantified just prior to impact (and compared to the target/design impact velocity). Break beam specifications are provided in Table 7-3.

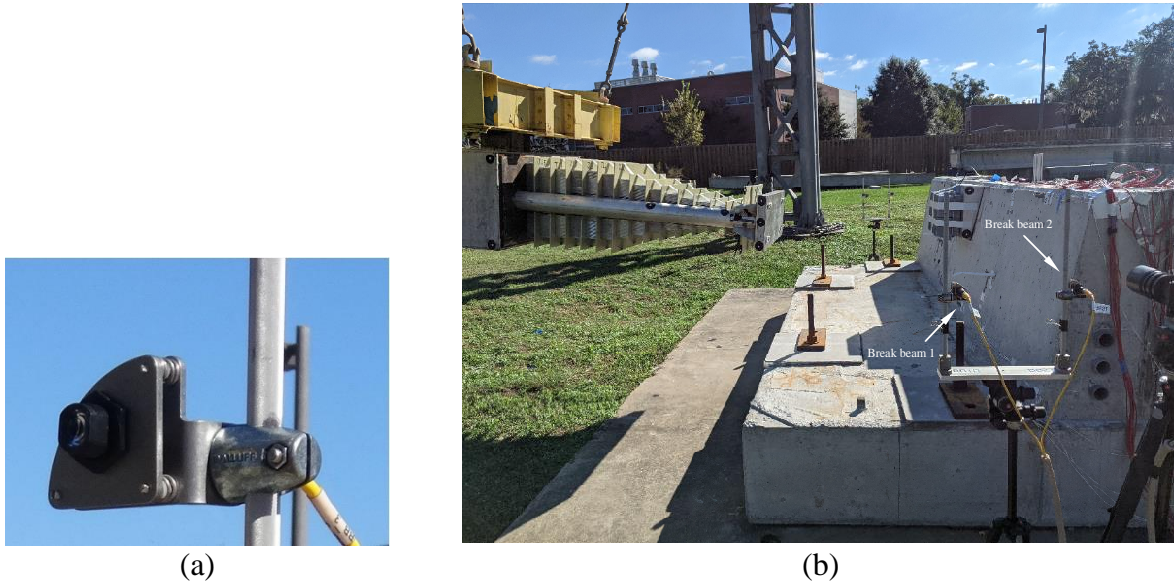


Figure 7-20 Optical break beam sensors: (a) Close up of an individual sensor; (b) Break beam sensors positioned for testing

Table 7-3 Specifications for optical break beams

Manufacturer	Balluff
Receiver model	BLS 18KF-NA-1PP-S4-C
Transmitter model	BLS 18KF-XX-1P-S4-L
Range	65 ft

7.4.3 Accelerometers

Accelerometers were used to measure accelerations on the impactor. Such acceleration data were then multiplied by the impactor mass to indirectly quantify the time-varying impact force that was applied to the test specimen. To measure accelerations at various locations on the impactor, four triaxial accelerometers were utilized with each test:

- One 25g accelerometer on the top of the impactor block
- One 25g accelerometer on the bottom of the impactor block
- One 400g accelerometer on the front left side of the impactor nose
- One 400g accelerometer on the front right side of the impactor nose

Accelerometer locations are depicted as shown in Figure 7-21 and Figure 7-22. For each accelerometer, a calibration datasheet provided by the manufacturer was used to convert voltage readings into acceleration data sets. A summary of accelerometer specifications is provided in Table 7-4.

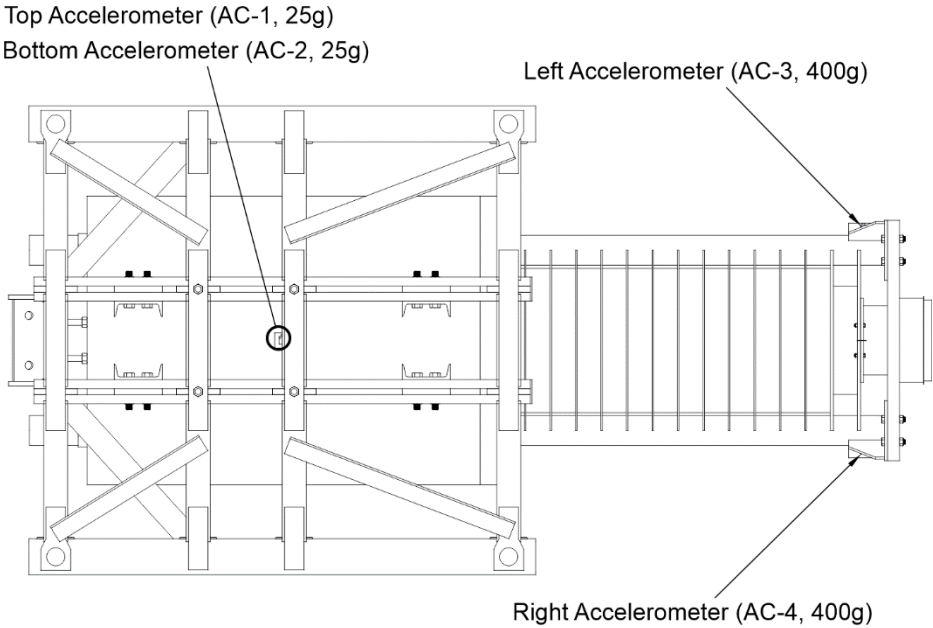


Figure 7-21 Accelerometers installed on pendulum impactor (top view)



(a)



(b)



(c)



(d)

Figure 7-22 Accelerometers installed on the pendulum impactor: (a) AC-1 mounted to the top of the concrete back block; (b) AC-2 mounted to the bottom of the concrete back block; (c) AC-3 mounted to the left mounting plate on the aluminum front nose; (d) AC-4 mounted to the right mounting plate on the aluminum front nose

Table 7-4 Specifications for accelerometers

Manufacturer	Model number	Serial number	Label	Range (g)	Bandwidth (Hz)
Dytran Instruments, Inc	7503D4	11355	AC-1	25	10,000
Dytran Instruments, Inc	7503D4	11356	AC-2	25	10,000
Dytran Instruments, Inc	7503D8	11367	AC-3	400	10,000
Dytran Instruments, Inc	7503D8	11368	AC-4	400	10,000

7.4.4 High speed cameras

High-speed video cameras (Figure 7-23) were used to visually record the impact test at a rate of 2000 frames/sec (Table 7-5). During each impact test, two high-speed cameras were utilized with: (1) one focused on the front impact region of the test (from the side view perspective), and (2) the other focused above the height of the rail (from the side view perspective, looking down

the longitudinal direction of the rail), capturing any transverse rail movement. Both cameras were positioned on the same side of the rail.



Figure 7-23 High-speed digital video camera

Table 7-5 Specifications for high-speed cameras

Manufacturer	Integrated Design Tools (IDT)
Distributor	Dynamic Imaging, LLC
Camera model	MotionXtra N-3
Image resolution	1280 x 1024
Frame rate	1000 fps (frames/sec)
Frame rate (plus mode)	2000 fps (frames/sec)
Memory	1.25GB
Maximum recording time	0.76 sec.

7.4.5 Laser displacement sensors

Laser displacement sensors positioned behind the test specimen (Figure 7-24) were used to capture transverse displacements, and potentially rigid motion of the specimen, at various locations on the specimen, such as on the rail and deck elevations. Specifications of the laser displacement sensors are provided in Table 7-6.



Figure 7-24 Laser displacement sensor mounted behind a test specimen

Table 7-6 Specifications for laser displacement sensors

Manufacturer	MTI Instruments
Model	LTS-300-200
Measurement range	7.8 in.
Accuracy	0.03%

7.4.6 Concrete strain gages

Bonded electrical resistance concrete strain gages (Figure 7-25) were used to measure concrete strain levels at select locations on the rail and deck surfaces of each test specimen. Specifications for concrete strain gages are detailed in Table 7-7.

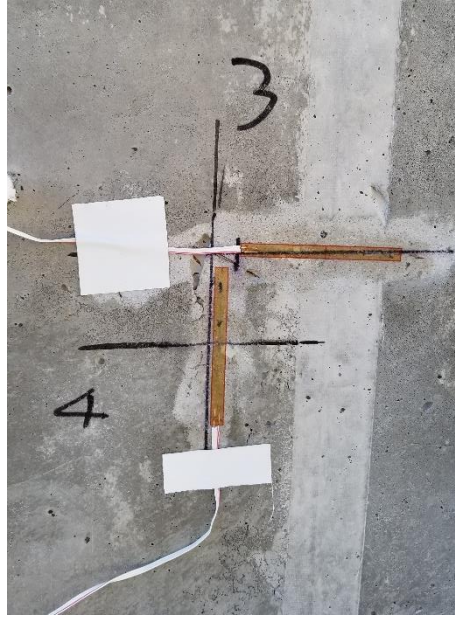


Figure 7-25 Concrete strain gages (3 and 4) adhered to concrete rail surface

Table 7-7 Specifications for concrete strain gages

Manufacturer	Kyowa Electronic Instruments
Model	KC-80-120-A1-11L3M3R
Gage length	80 mm
Gage width	0.6 mm
Strain limit	1.8%

7.4.7 Rebar strain gages

Before the deck or rail portions of the test specimen were cast (i.e., prior to concrete placement), bonded electrical resistance strain gages were attached to select reinforcing bars (see typical example shown in Figure 7-26). Rebar strain gages were used to measure rebar strain and infer rebar stress levels. Specifications for rebar strain gages are detailed in Table 7-8.



(a)



(b)

Figure 7-26 Strain gages attached to reinforcing bars and protected with waterproof tape:
 (a) Attached to steel rebar; (b) Attached to GFRP rebar

Table 7-8 Specifications for rebar strain gages

Manufacturer	Kyowa Electronic Instruments
Model	KFGS-5-120-C1-11L3M3R
Gage length	5 mm
Gage width	1.4 mm
Strain limit	5.0%

7.5 Impact test procedure

Once each test specimen was anchored to the universal foundation, aluminum honeycomb cartridges were installed in the impactor nose, and various instrumentation components (e.g., high-speed cameras, laser displacement sensors) were positioned. The impactor was raised by the pull-back cable to achieve a 15-ft drop height. After being positioned at the designed elevation, the pull-back cable was released, and the impactor was dropped to convert the 155 k-ft of potential energy into kinetic energy at the bottom of the swing. Initial impact against the test rail occurred at an approximate impact speed of 31.1 ft/sec (or 21.5mph). As the impact continued, the aluminum honeycomb cartridges crushed progressively from the front nose towards the back block. After the impactor came to a complete stop, the pendulum impact test was completed.

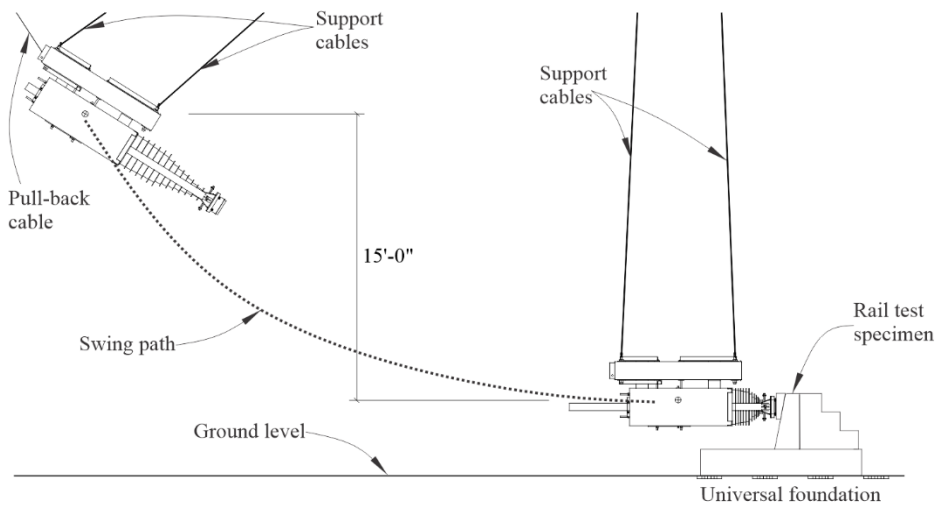


Figure 7-27. Pendulum impact test on rail test specimen

CHAPTER 8 FULL-SCALE CENTER OF RAIL (COR) IMPACT TEST RESULTS

8.1 Introduction

A key objective of this study was to experimentally investigate the structural behavior of the proposed GFRP traffic rail. To achieve this objective, a series of pendulum impact tests were conducted on six rail test specimens following the procedures discussed in Chapter 7. In this chapter, results from three full-scale rail impact tests are discussed. These three specimens are referred to as ‘center of rail’ (COR) test specimens, of which one was reinforced with GFRP bars and two with steel rebars. Note that GFRP reinforced specimens are referred to as GFRP specimens and steel reinforced specimens are referred to as R/C specimens in this report. The test specimens were 13-ft long, were supported at each end (using end-support buttresses), and the impact occurred at the centerline of the specimens in the impact direction (i.e., 6.5 ft from either end).

Results for the COR impact tests are organized by the two rail types (i.e., R/C and GFRP) and are followed by a comparison of the COR test results. A summary of the overall COR test program is provided in Table 8-1. Hardened mechanical properties for the concrete material used to cast and form each pendulum impact test specimen (such as concrete compressive strength) are provided in Appendix I.

Table 8-1 Full-scale COR impact test summary

Impact test specimen	Test date	Drop height (ft)	Impact speed (mph) [ft/sec]	Impact energy (kip-ft)
R/C COR 1	10/30/2020	15	21.2 [31.1]	155.3
R/C COR 2	12/09/2020	15	20.5 [30.0]	144.5
GFRP COR 1	6/4/2021	15	21.2 [31.1]	155.3

8.2 Standard (R/C) rail

8.2.1 Impact testing of R/C COR specimen 1

On October 30, 2020, full-scale pendulum impact testing for R/C COR test specimen 1 was conducted. The pendulum impactor was dropped from the required 15-ft drop height (Figure 8-1). Instrumentation components included in the R/C COR test specimen were accelerometers, break beams, high-speed cameras, tape switches, laser displacement sensors, internal reinforcement strain gages, and external concrete strain gages. Additional details of the instrumentation plan used during impact testing are provided in Appendix H.



Figure 8-1 Impactor pulled back to 15-ft drop height (prior to release)

Sequential images taken from high-speed camera 1 (HSC-1) over the impact duration are provided in Figure 8-2, starting with the first instant of impact and including the point in time when maximum crush depth of the crushable front nose (i.e., maximum impact force) was reached. As shown in Figure 8-2e – 8-2h, about halfway through the impact, the adhesive used to hold the aluminum loading wedge in place on the face of the rail failed. As a result, the latter half of the impact occurred without the adhesive holding the wedge in position, allowing the wedge to slide up the surface of the rail as the impact continued. Once the total kinetic energy of the impactor was delivered to the test specimen, the remaining upward momentum of the loading wedge caused it to continue to slide up the face of the rail, eventually losing contact with the impactor and rail. Although the sliding of the wedge was not preferable and was not anticipated, the maximum design impact force—based on acceleration data (discussed later)—was still achieved, indicating that the test was a success.

Additional images from high-speed camera 2 (HSC-2) are provided in Figure 8-3, where an insignificant horizontal displacement was observed. This was confirmed with laser displacement data, which is discussed later. A photograph of the test specimen after completion of the impact test is shown in Figure 8-4. After completion of the impact test, no damage or cracking was found in the rail or deck concrete.

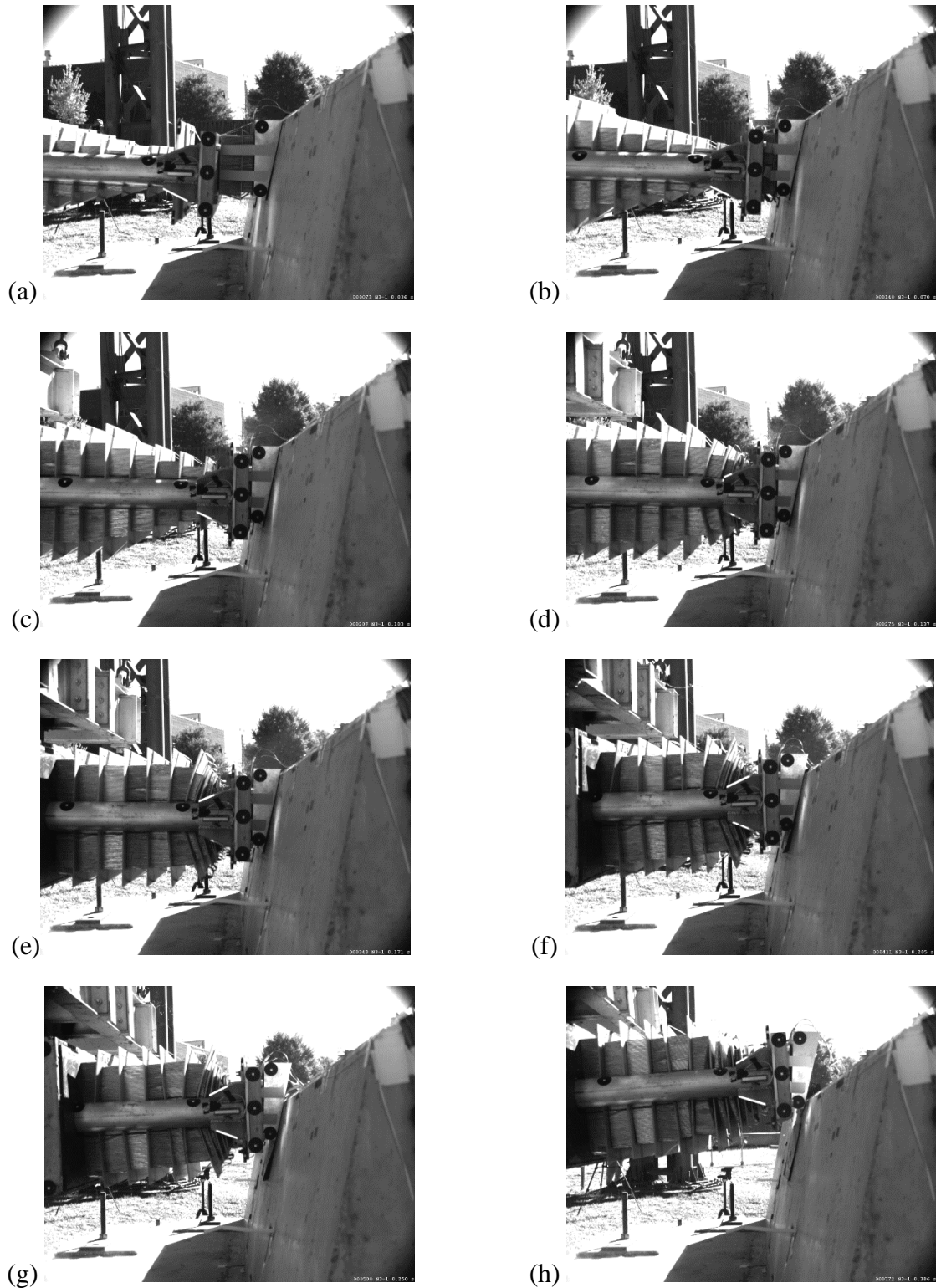


Figure 8-2 High-speed video frames from HSC-1 (R/C COR test 1) showing crush deformation of aluminum honeycomb: (a) At initial impact; (b) – (c) Intermediate frames; (f) At peak impact force; (g) – (h) Sliding and separation of loading wedge

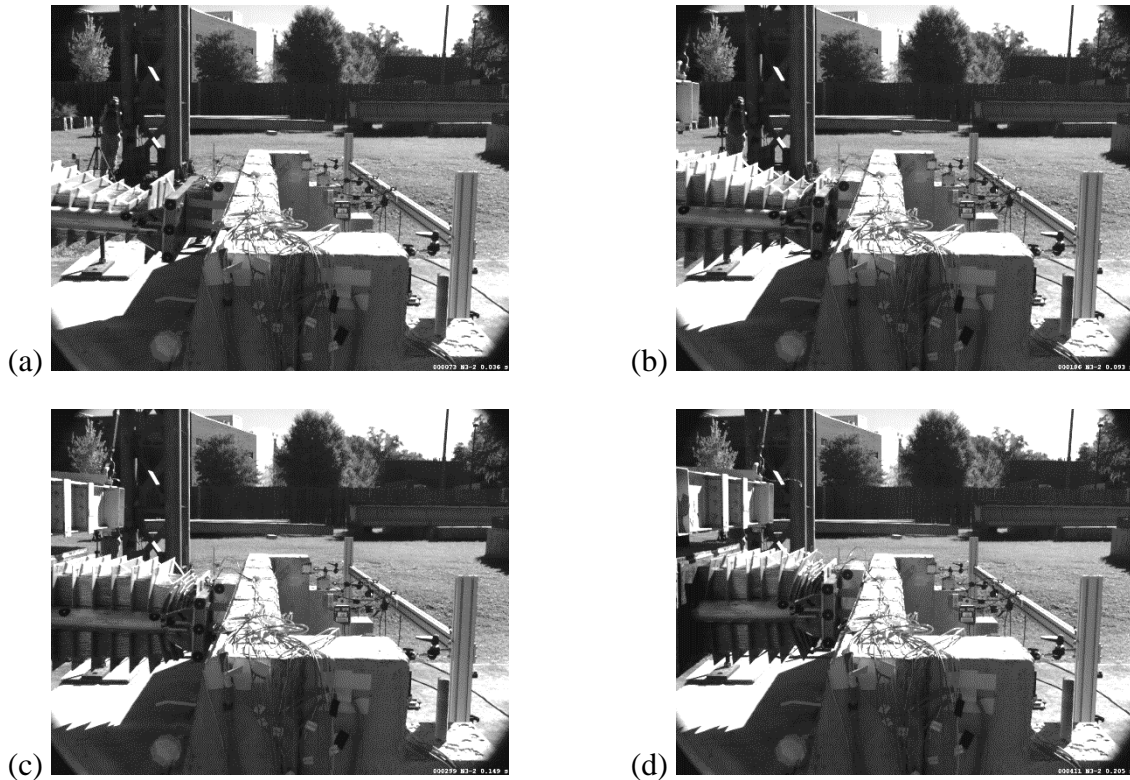


Figure 8-3 High-speed video frames from HSC-2 (R/C COR test 1): (a) At start of impact; (b) –; (c) Intermediate frames; (d) At peak impact force



Figure 8-4 R/C COR 1 test specimen after completion of impact test

Break beam voltage data from R/C impact test 1 are provided in Figure 8-5, and were used to quantify the impact velocity. As shown in the instrumentation plan (Appendix H), two sets of break beams were placed in front of the impact test specimen at a 1-ft spacing. For each break

beam, after the impactor was released and when the impactor crossed the path of the sensor, a change in voltage was observed. The duration of time over which the impactor moved the 1-ft distance from break beam 1 to break beam 2 was used to quantify velocity just prior to impact. For R/C test 1, the impact velocity was determined to be 31.3 ft/sec—compared to the design impact velocity of 31.1 ft/sec (a 0.6% difference). Tape switch data were used to determine the time at which the impact began and are shown in Figure 8-6. Note that all impact test data have been shifted such that the initiation of impact begins at 0.1 s (using the spike in tape switch voltage).

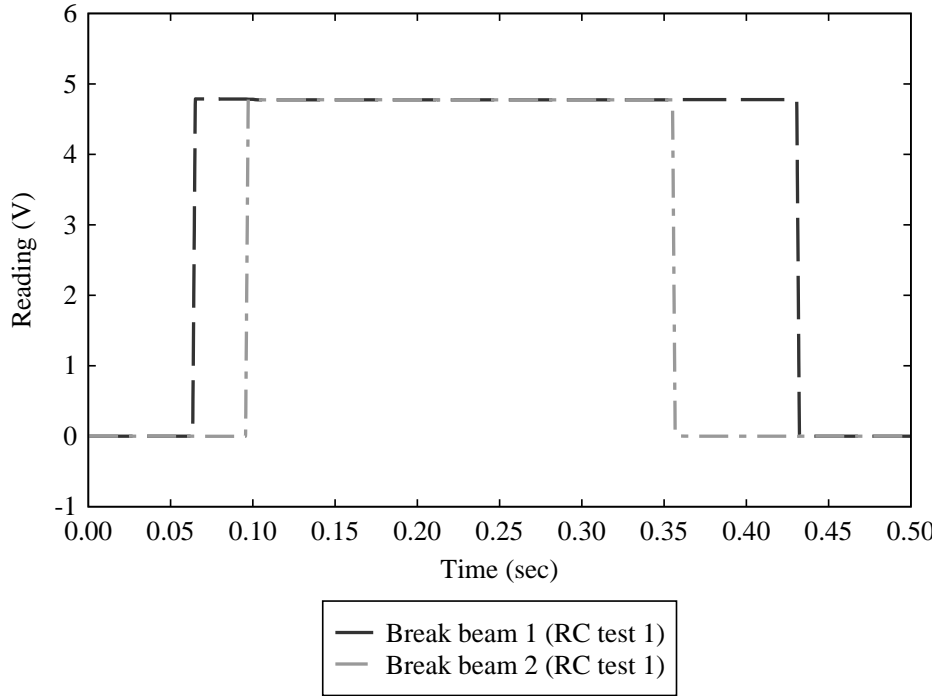


Figure 8-5 Break beam data for R/C COR test 1

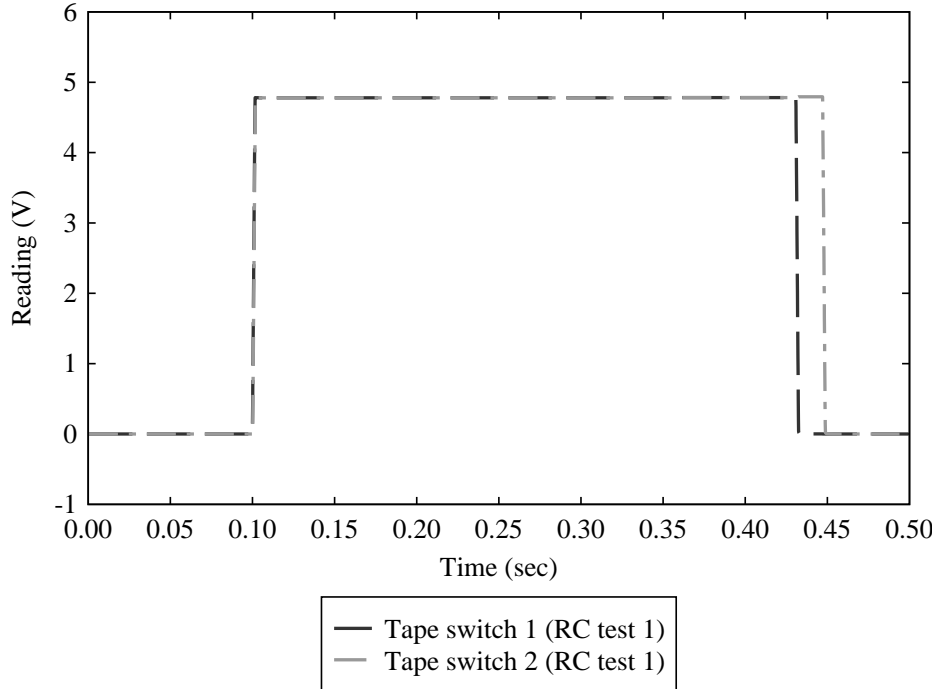


Figure 8-6 Tape switch data for R/C COR test 1

As shown in the instrumentation plan (Appendix H), four triaxial accelerometers—two mounted on the impactor concrete back block and two mounted on the aluminum front nose—were used to measure impactor accelerations during the pendulum impact test. Measured accelerations from the two accelerometers on the concrete back block (AC-1 & AC-2) in the impact direction (i.e., local Y direction of the accelerometer) are shown in Figure 8-7. Correspondingly, measured accelerations from the two accelerometers on the aluminum front nose (AC-3 & AC-4) in the impact direction (local Y direction) are shown in Figure 8-8. As expected, acceleration values are negative, indicating impactor deceleration during impact. Furthermore, a more gradual deceleration of the back block is clearly shown in the AC-1 and AC-2 data when compared with the more instantaneous deceleration that occurred with the front nose (as expected), producing more fluctuations in AC-3 and AC-4 data.

Accelerations were then multiplied by mass to quantify the impact forces that were applied to the standard R/C rail. Specifically, back block accelerations (AC-1 & AC-2) were multiplied by the 9850-lb back block mass (composed of the steel hanger frame and concrete block), while the front nose accelerations (AC-3 & AC-4) were multiplied by the 350-lb front nose mass (composed of the aluminum front nose components). The two back block forces (from AC-1 & AC-2) were then averaged and are shown in Figure 8-9, while the two front nose forces (from AC-3 & AC-4) were averaged and are shown in Figure 8-10.

The total applied impact force was then computed by combining the two averages from the back block and front nose, as shown in Figure 8-11. In comparison to the designed/predicted maximum impact forces (shown in Figure 8-12, which provides the predicted impact force over time from previous FEA impact simulations), the maximum observed impact force from R/C test 1 was found to be 71.5 kip (3.9% greater than the originally designed 68.8-kip peak impact force).

As shown in Figure 8-7, acceleration measurements from AC-2—the accelerometer beneath the concrete back block—were noticeably influenced by the undesired and unexpected

sliding of the aluminum loading wedge. Specifically, the designed gradual increase in acceleration magnitude and peak impact force were not entirely captured with AC-2. However, after averaging and combining data from all four accelerometers, with the total peak impact force and overall duration of impact similar to the designed force-time curve, these results indicate that the wedge sliding only had minimal influence on the impact test.

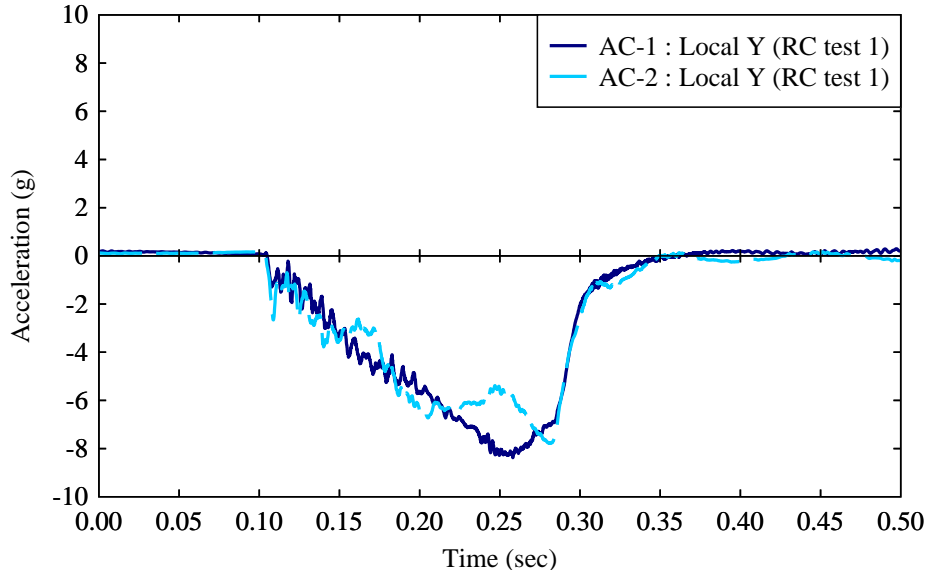


Figure 8-7 Raw concrete back block acceleration data (AC-1 & AC-2) for R/C COR test 1 (in the impact direction, local Y direction of accelerometer)

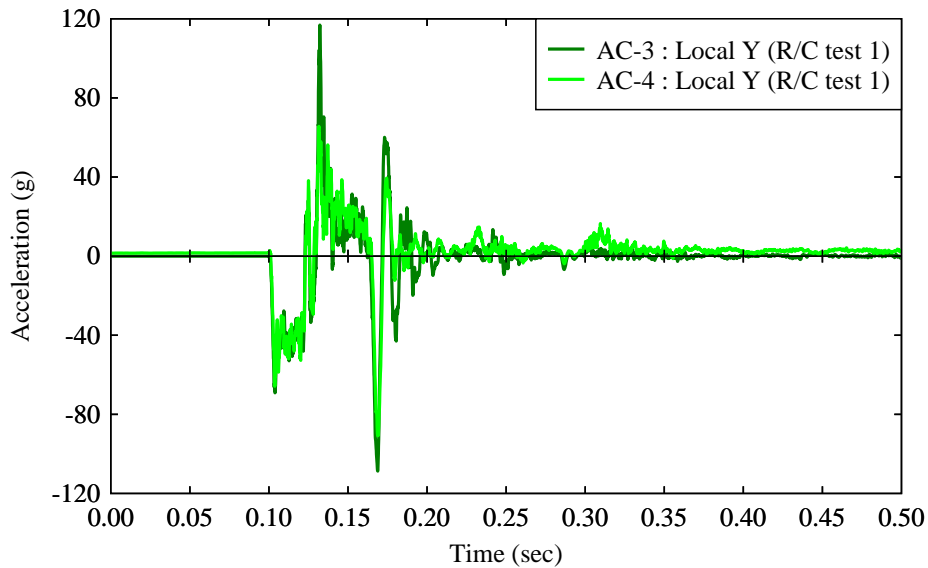


Figure 8-8 Raw front nose acceleration data (AC-3 & AC-4) for R/C COR test 1 (in the impact direction, local Y direction of accelerometer)

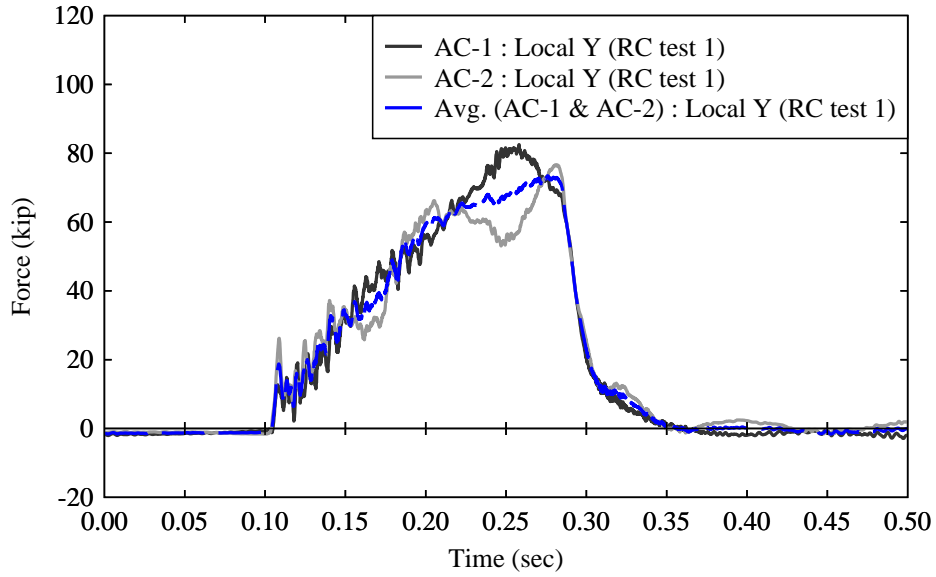


Figure 8-9 Computed impact forces from back block for R/C COR test 1

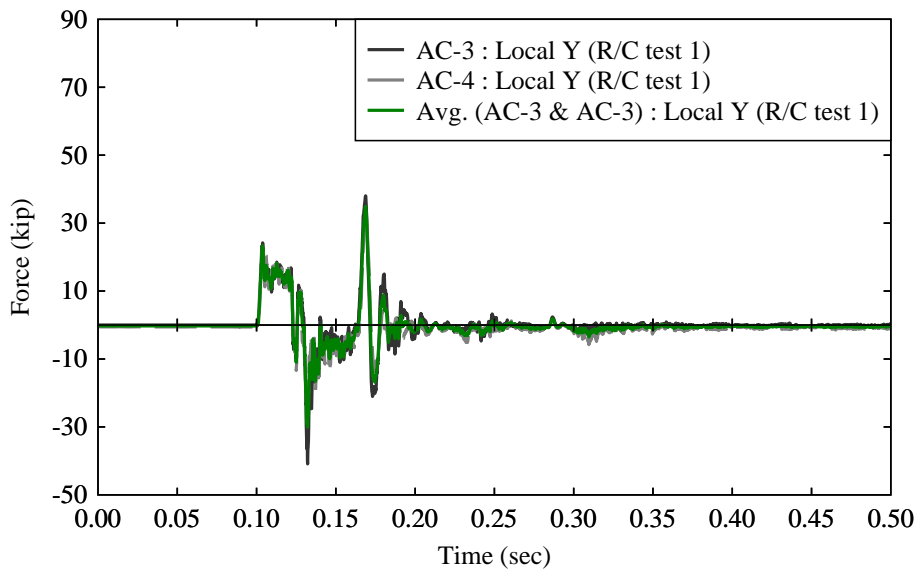


Figure 8-10 Computed impact forces from front nose for R/C COR test 1

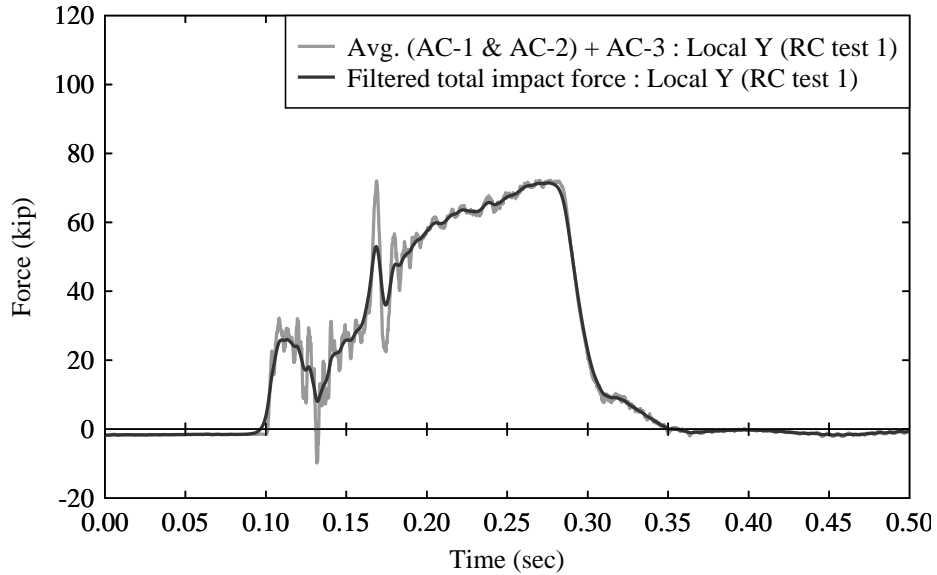


Figure 8-11 Raw and filtered total computed impact force for R/C COR test 1

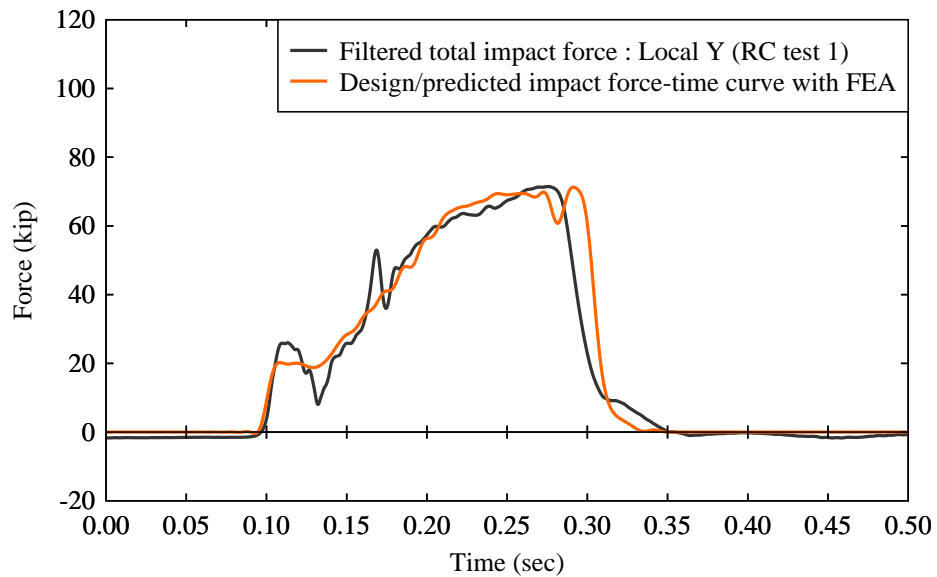


Figure 8-12 Filtered total experimental impact force for R/C COR test 1 compared to FEA prediction

During the impact test, transverse deflections of the rail were measured with laser displacement sensors positioned behind the specimen. Further, external concrete strain measurements on the rail and deck were taken at locations along the front and back faces of the specimen. Specific locations of the laser displacement sensors (LDS) and external concrete strain gages (CSG) are depicted in Figure 7-18 (and further detailed in Appendix H).

Laser displacement data captured during R/C test 1 are provided in Figure 8-13, where it is shown that the maximum displacement occurred at the center of the rail (LDS-4) with a magnitude of 0.067 in., when the peak impact force was applied. After completion of the impact, the measured displacements at the deck elevation did not return to zero, indicating that some

(minimal) horizontal sliding occurred. Had only the rail deflected, and no rigid sliding of the specimen occurred, displacement data at the deck level (LDS-2, LDS-5, LDS-8) would have been zero. Note that data from LDS-1 and LDS-5 are not included, because data from those sensors were inaccurate and no useful information could be discerned.

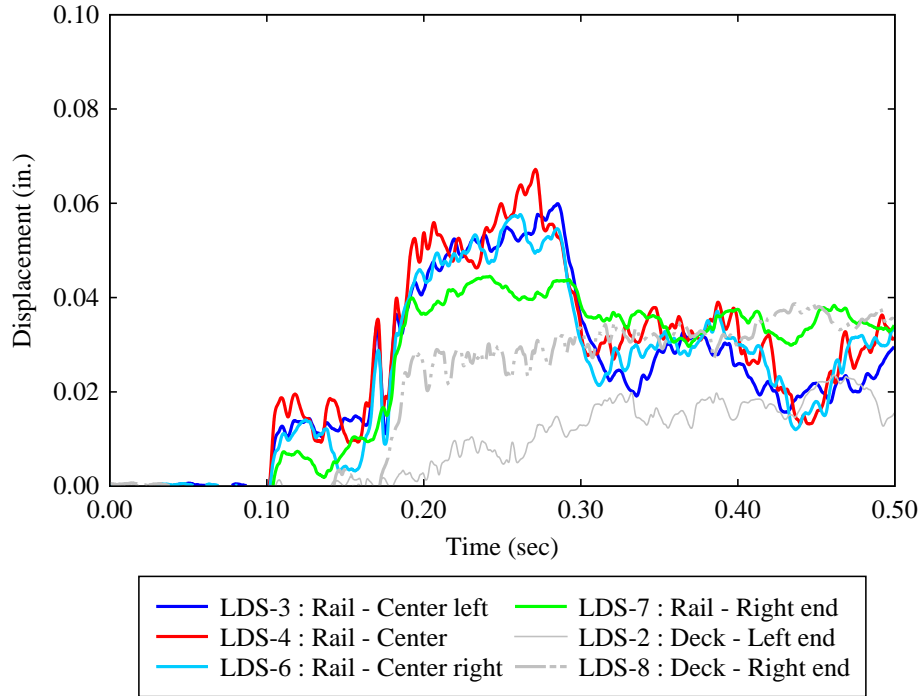


Figure 8-13 Laser displacement sensor data for R/C COR test 1

Readings from external concrete strain gages are provided in Figures 8-14 through 8-17. External gage readings for the top front face of the rail are provided in Figure 8-14. Strain readings for the bottom (i.e., lower half and toe) of the rail front face are provided in Figure 8-15 and Figure 8-16, and readings for the back face of the rail are provided in Figure 8-17. Although some strain levels reached the approximate tensile rupture strain for 3400-psi strength concrete, no discernible cracking was found in the rail or deck after visual inspection.

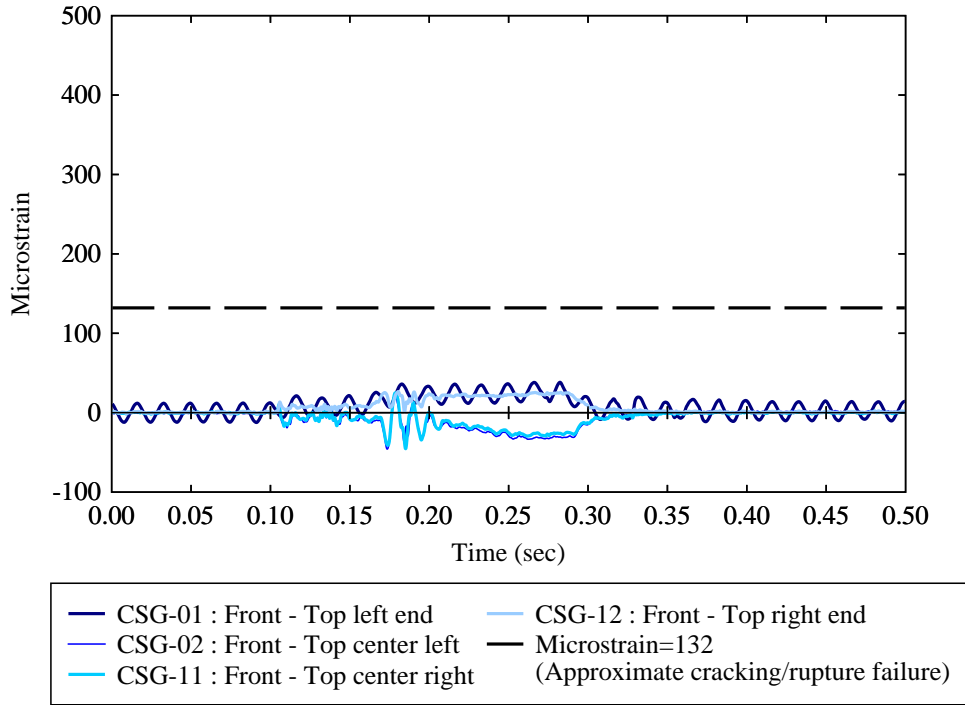


Figure 8-14 External concrete strain gage data for locations on the top front face of the rail during R/C COR test 1

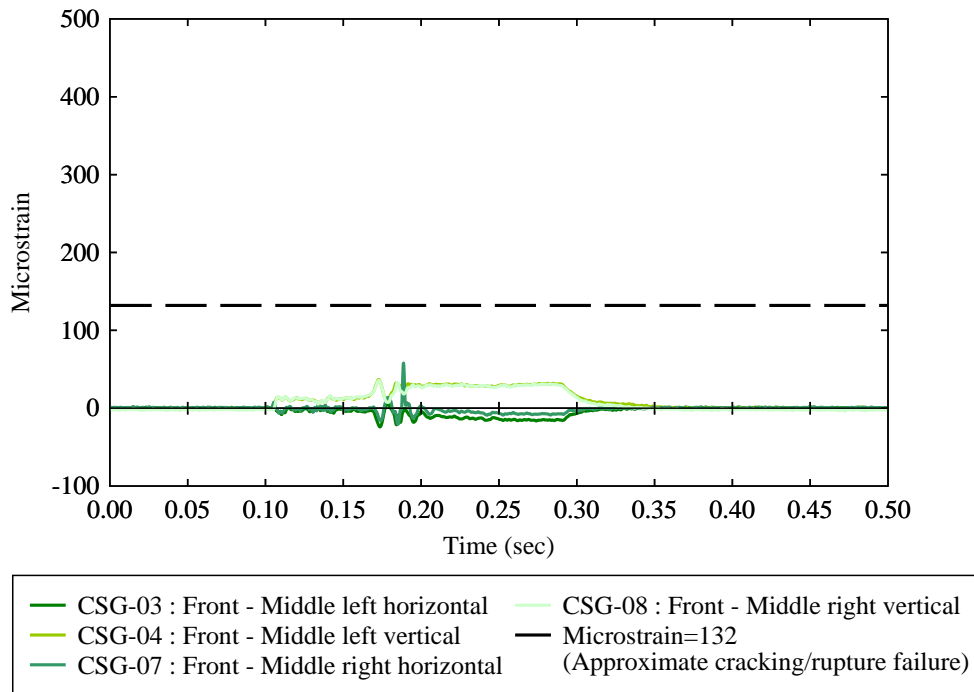


Figure 8-15 External concrete strain gage data for locations on the lower front face of the rail during R/C COR test 1

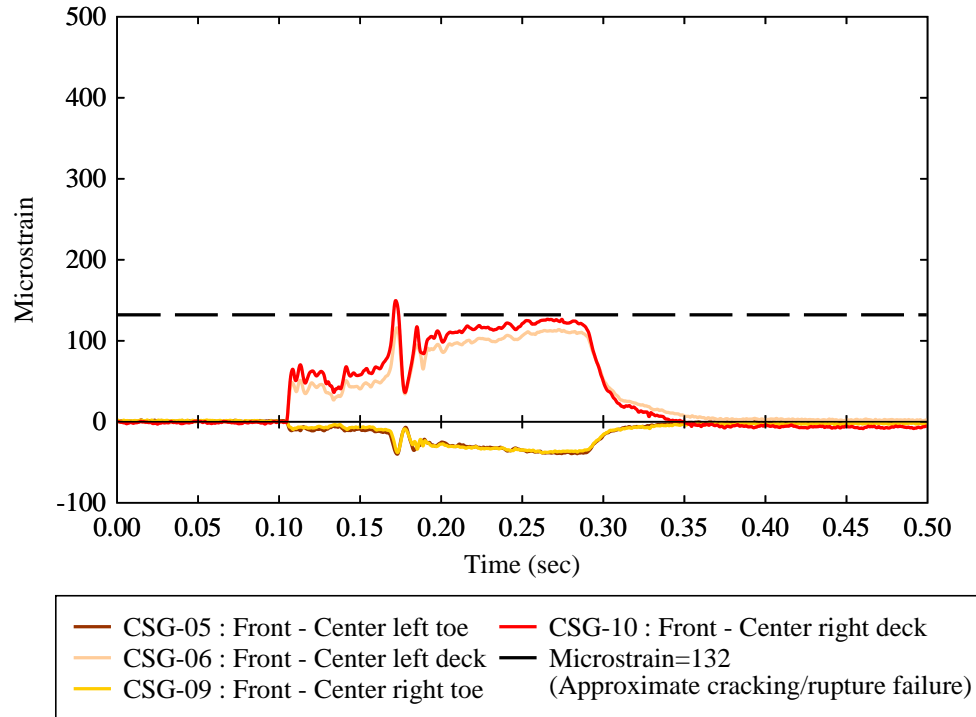


Figure 8-16 External concrete strain gage data for locations at the toe of the rail and deck during R/C COR test 1

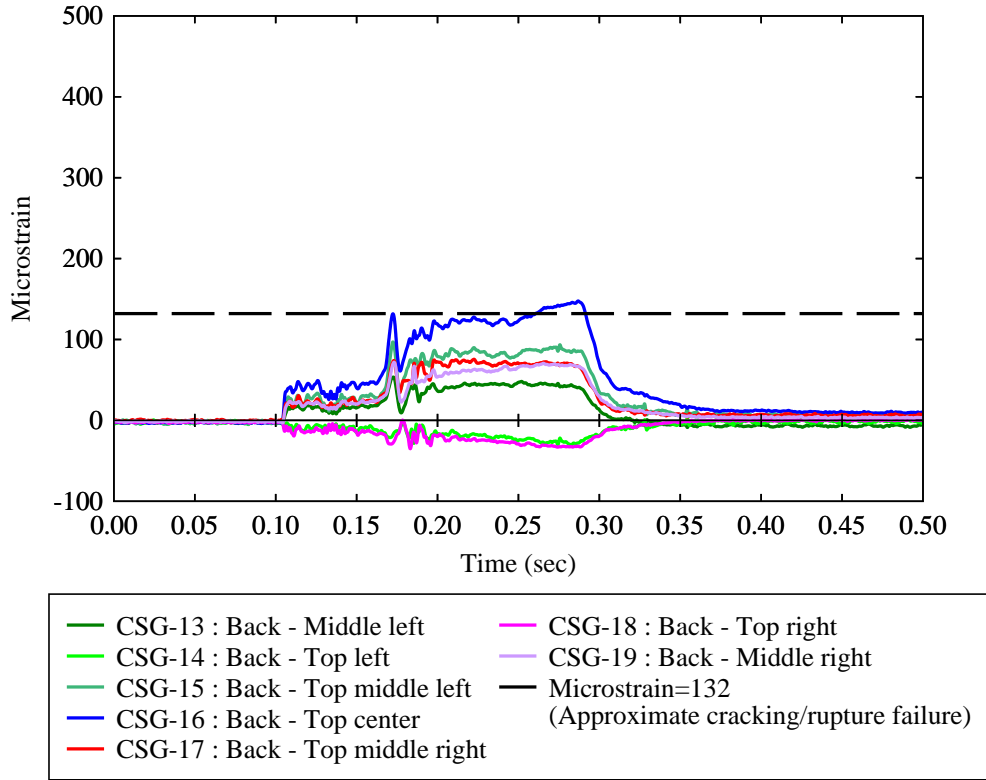
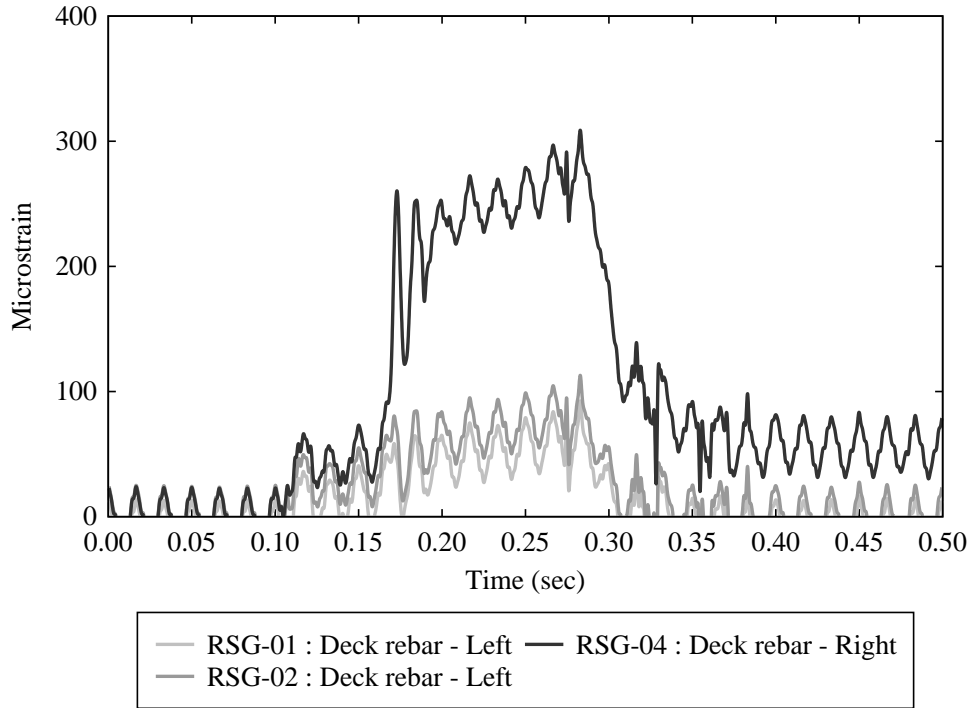
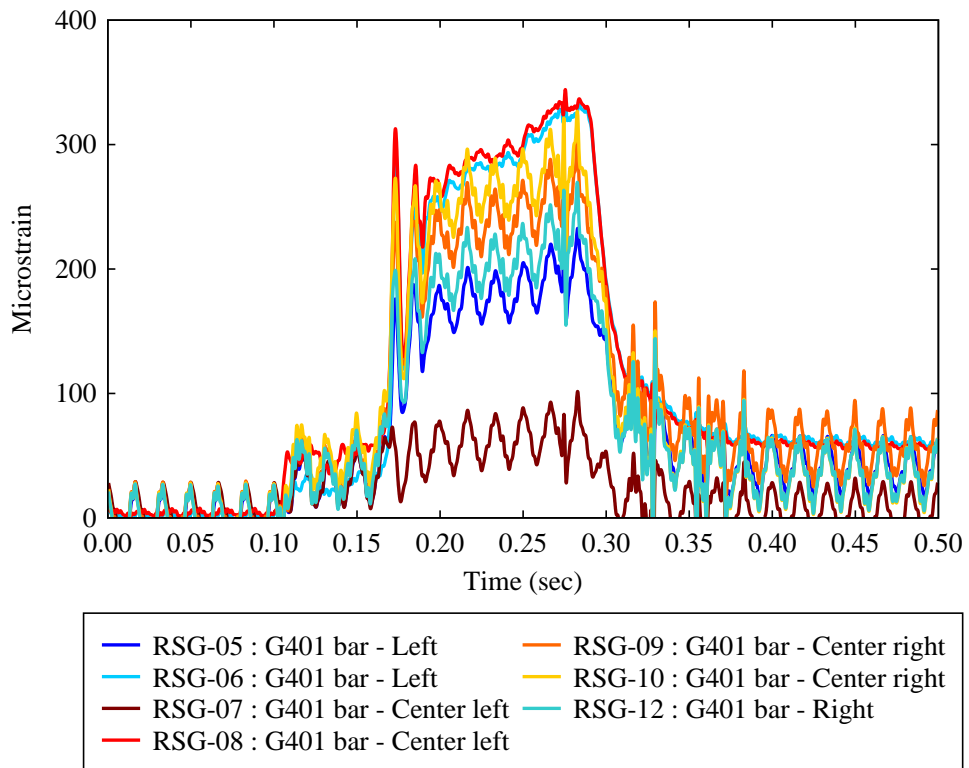


Figure 8-17 External concrete strain gage data for locations on the back face of the rail during R/C COR test 1

Readings from internal rebar strain gages are provided in Figure 8-18. Specific locations of the deck and connection (4V) rebar gages are provided in Appendix H. Maximum strain levels in the deck and rail steel reinforcement are well below yielding strain (2000 microstrain) indicating that the test specimen successfully resisted the pendulum impact with minimal damage. Note that some rebar strain gage readings are not included because the gages were damaged during the casting process and did not provide any data during testing (e.g., RSG-03, RSG-11, RSG-13, RSG-14, RSG-15 had zero readings during the test).



(a)



(b)

Figure 8-18 Internal rebar strain gage data during R/C COR test 1:
(a) Deck rebar; (b) Rail rebar

8.2.2 Impact testing of R/C COR specimen 2

On December 9, 2020, full-scale pendulum impact testing for R/C COR test specimen 2 was conducted—where the pendulum impactor was dropped from 15 ft. Instrumentation included with R/C test specimen 2 was the same as described for R/C test 1. Sequential images taken from high-speed camera 1 (HSC-1) over the impact duration are provided in Figure 8-19, starting with the first instant of impact and including the point in time when the maximum crush depth on the crushable front nose (i.e., maximum impact force) was reached. Unlike R/C COR test 1, for R/C COR test 2, the adhesive used to hold the aluminum loading wedge did not fail. Additional images from high-speed camera 2 (HSC-2) are provided in Figure 8-20, where no sliding was observed neither between the aluminum loading wedge and test specimen, nor between the test specimen and the foundation. A photograph of the test specimen after completion of the impact test is shown in Figure 8-21. After completion of the impact test, no discernible damage or cracking was found in the rail or deck concrete.



Figure 8-19 High-speed video frames from HSC-1 (R/C COR test 2) showing crush deformation of aluminum honeycomb: (a) At initial impact; (b) – (e) Intermediate frames; (f) At peak impact force

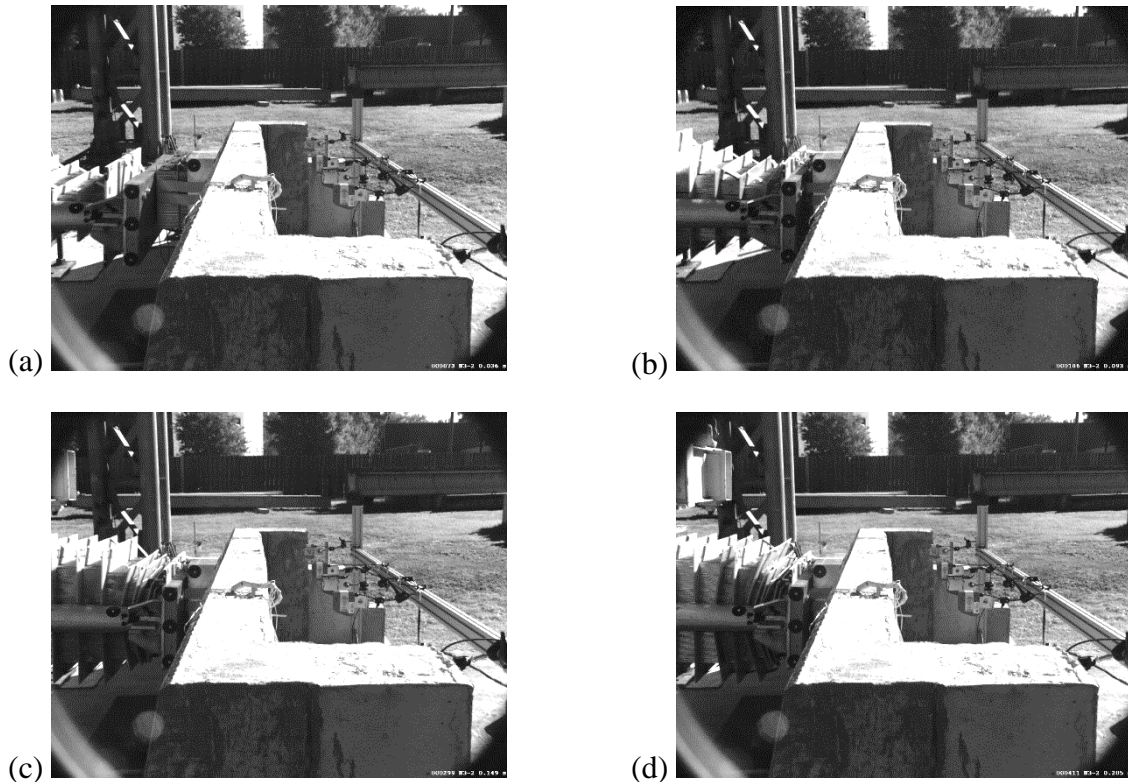


Figure 8-20 High-speed video frames from HSC-2 (R/C COR test 2): (a) At start of impact; (b) – (c) Intermediate frames; (d) At peak impact force



Figure 8-21 R/C COR test 2 specimen after completion of impact test

Break beam voltage data from R/C impact test 2 are provided in Figure 8-22, and were used to quantify the impact velocity. For R/C test 2, the impact velocity was determined to be 30.0 ft/sec—compared to the design impact velocity of 31.1 ft/sec (a 3.5% difference). Tape switch data are shown in Figure 8-23. Note that all impact test data has been shifted such that the initiation of impact begins at 0.1 s, using the spike in tape switch voltage.

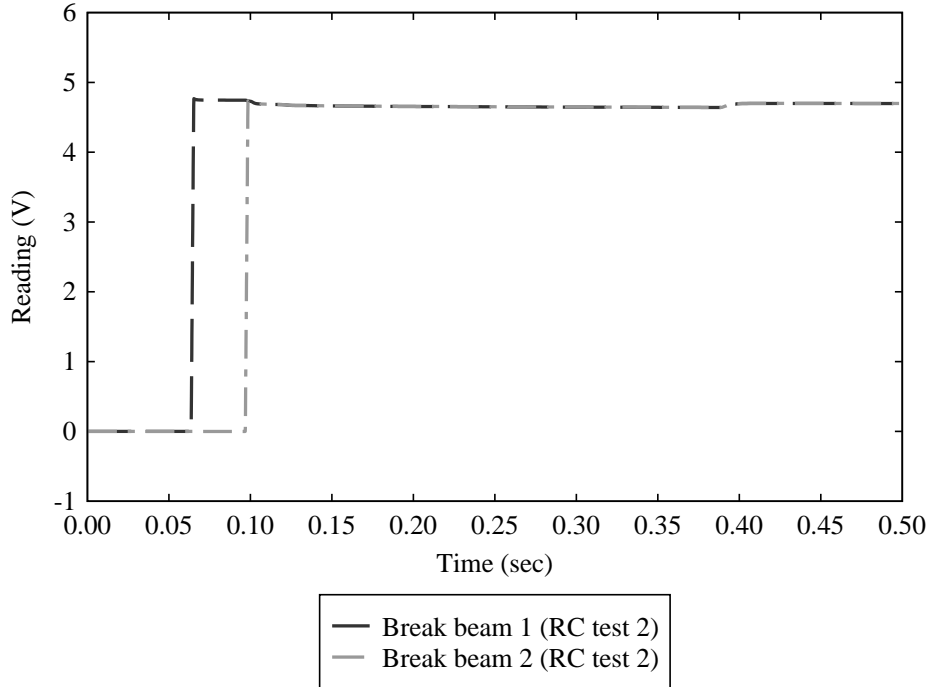


Figure 8-22 Break beam data for R/C COR test 2

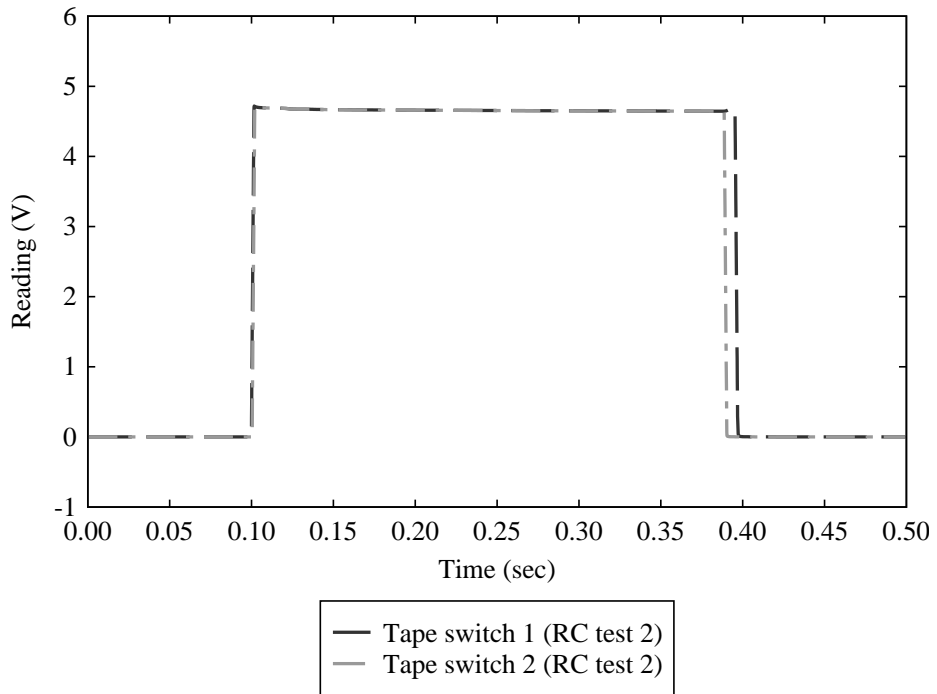


Figure 8-23 Tape switch data for R/C COR test 2

Measured accelerations from the two accelerometers on the concrete back block (AC-1 & AC-2) in the impact direction (i.e., local Y direction of the accelerometer) are shown in Figure 8-24. Correspondingly, measured accelerations from the two accelerometers on the

aluminum front nose (AC-3 & AC-4) in the impact direction (local Y direction) are shown in Figure 8-25. Computed and averaged back block impact forces (from AC-1 & AC-2) are shown in Figure 8-26, while the computed and averaged front nose impact forces (from AC-3 & AC-4) are shown in Figure 8-27.

The total applied impact force – computed by combining the averages of the back block and front nose – is shown in Figure 8-28. In Figure 8-29, the designed/predicted impact force vs. time from previous FEA impact simulations is compared to the experimental results. The maximum observed experimental impact force from R/C test 2 was found to be 74.3 kip (7.9% greater than the originally designed 68.8-kip peak impact force).

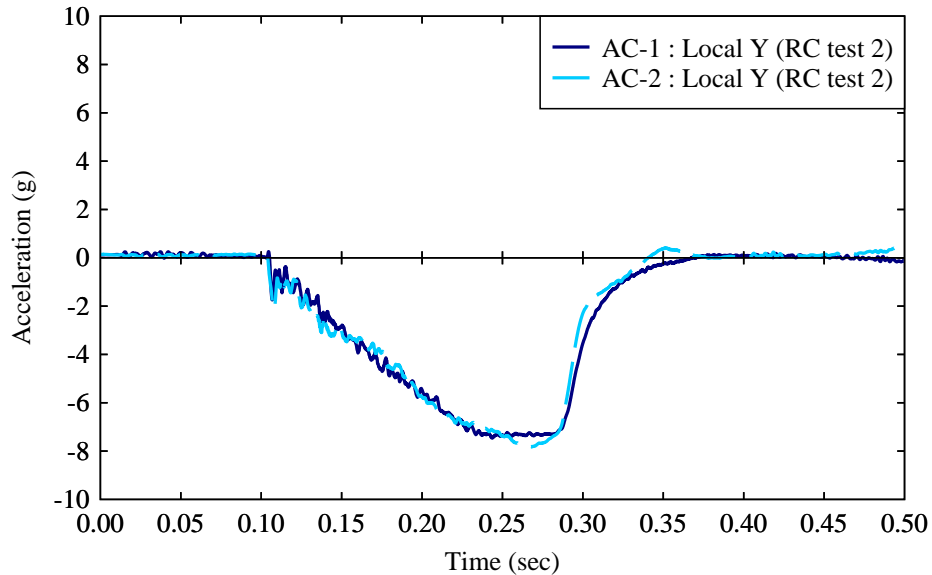


Figure 8-24 Raw concrete back block acceleration data (AC-1 & AC-2) for R/C COR test 2 (in the impact direction, local Y direction of accelerometer)

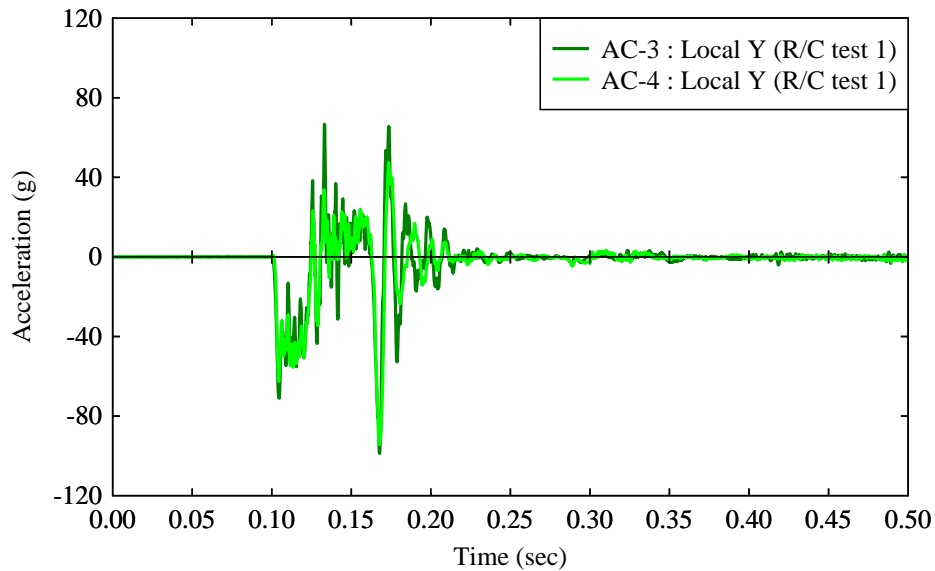


Figure 8-25 Raw front nose acceleration data (AC-3 & AC-4) for R/C COR test 2 (in the impact direction, local Y direction of accelerometer)

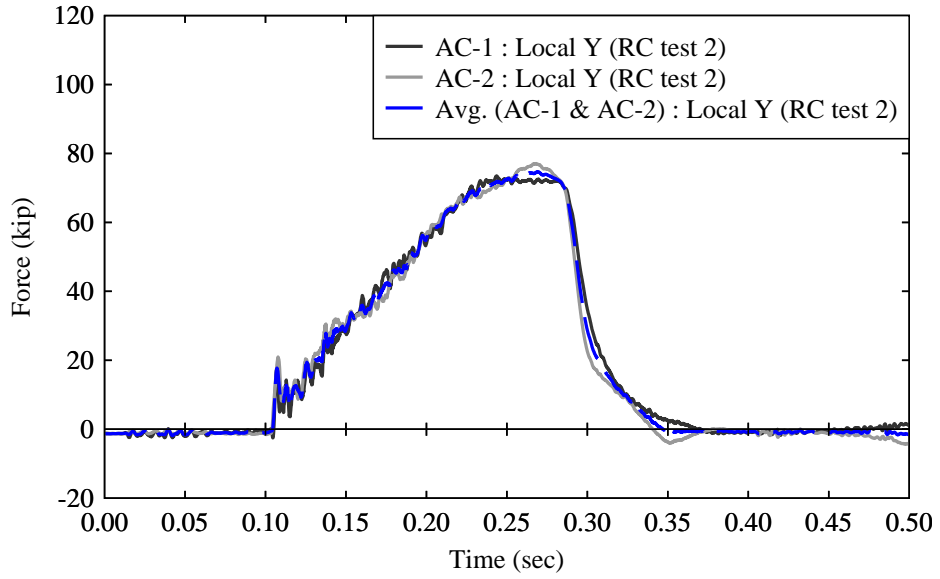


Figure 8-26 Computed impact forces from back block for R/C COR test 2

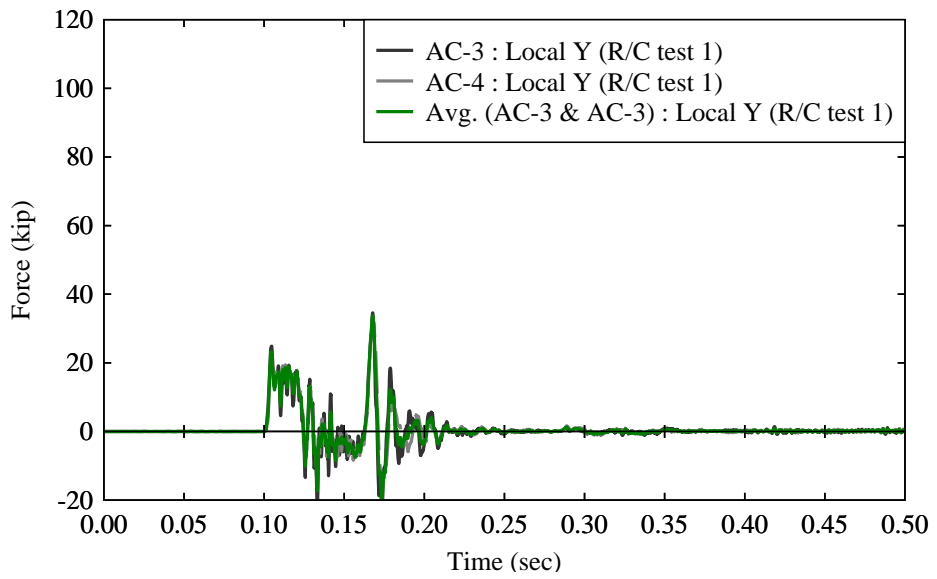


Figure 8-27 Computed impact forces from front nose for R/C COR test 2

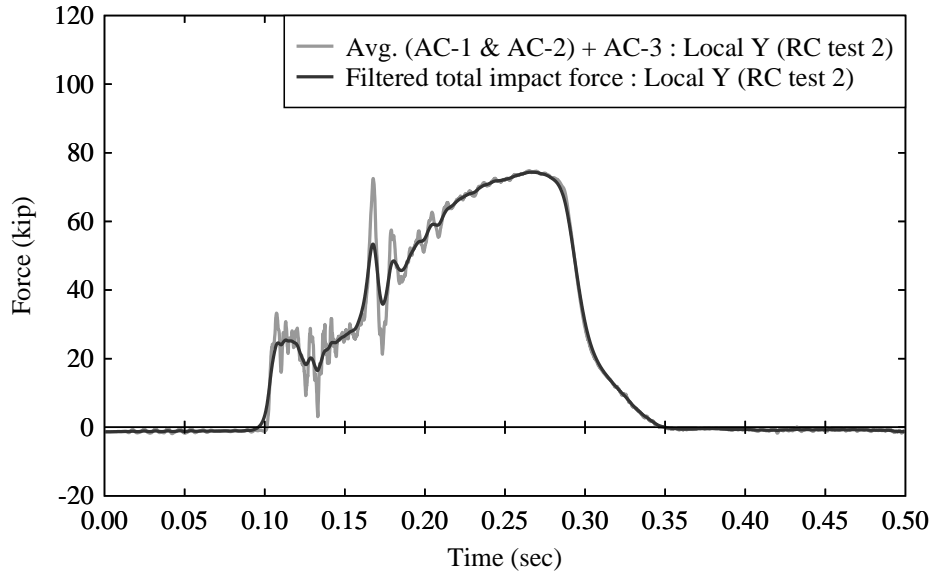


Figure 8-28 Raw and filtered total computed impact force for R/C COR test 2

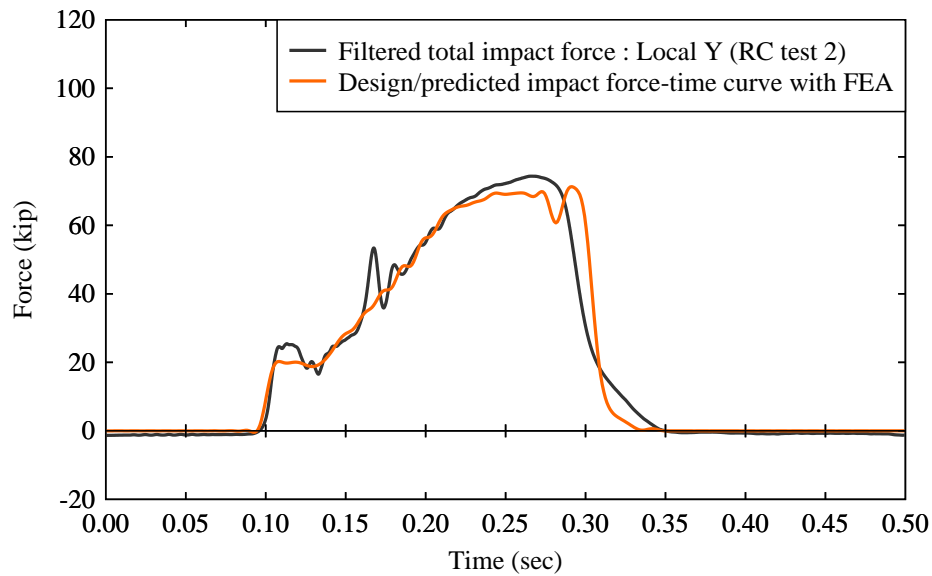


Figure 8-29 Filtered total experimental impact force for R/C COR test 2 compared to FEA prediction

Laser displacement data captured during R/C COR test 2 are provided in Figure 8-30. Based on the unusual and sporadic behavior displayed in the displacement data, it was determined that the laser data from R/C test 2 were not useful and did not provide any discernable trends. The sporadic nature of the data was attributed to undesirable movement (e.g., vibration) of the frame/stand that was used to hold the laser gages in position. Modifications made to the sensor mounting frame, based on this impact test, prevented similar issues from arising in subsequent tests.

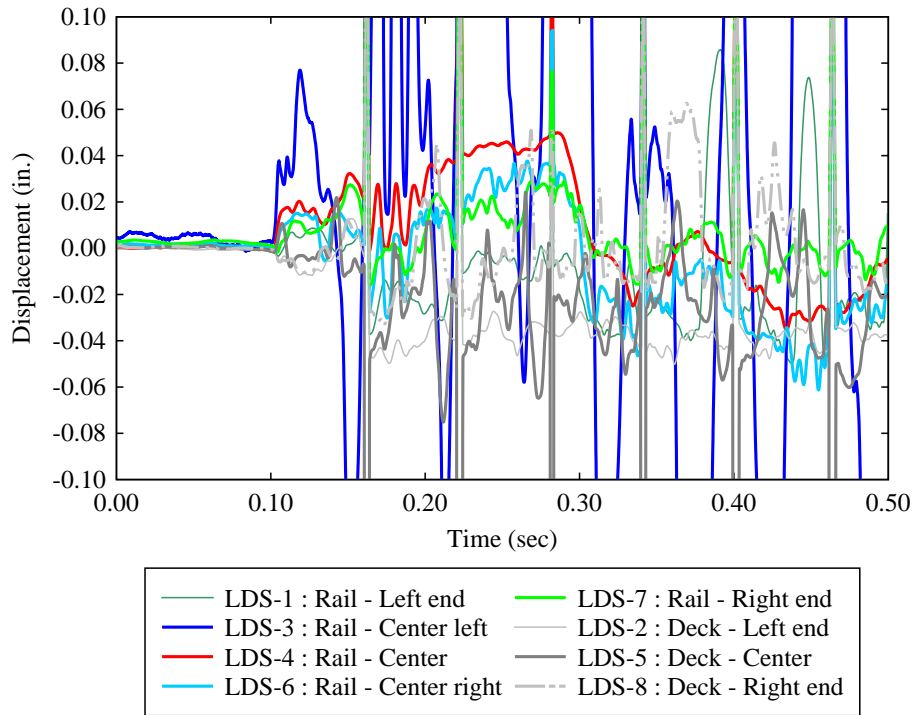


Figure 8-30 Laser displacement sensor data from R/C COR test 2

Concrete strain gage readings for the top front face of the rail are provided in Figure 8-31. Strain readings for the bottom (i.e., lower half and toe) of the rail front face are provided in Figure 8-32 and Figure 8-33, and readings for the back face of the rail are provided in Figure 8-34. Although some strain levels exceeded the approximate rupture strain for 3400-psi strength concrete, no visible cracks were found in the rail or deck during visual inspection.

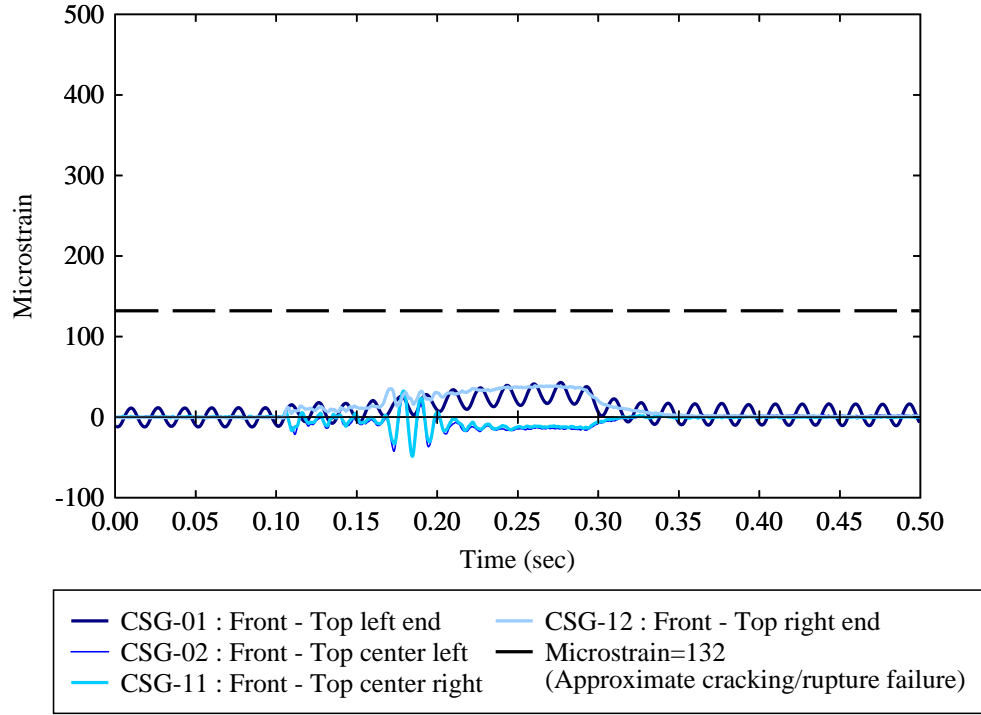


Figure 8-31 External concrete strain gage data for locations on the top front face of the rail during R/C COR test 2

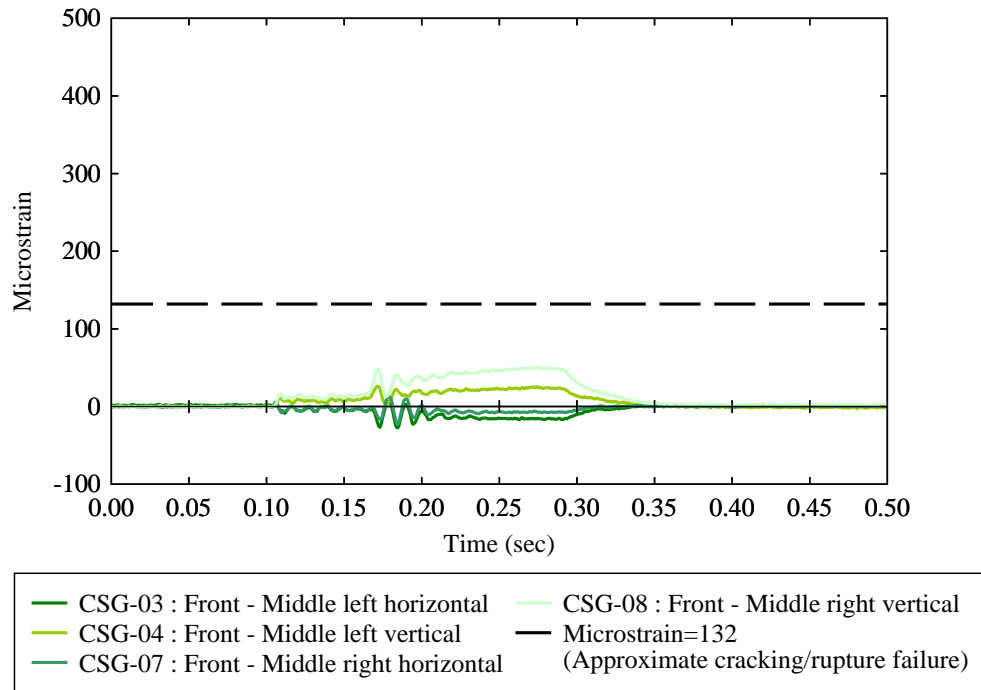


Figure 8-32 External concrete strain gage data for locations on the lower front face of the rail during R/C COR test 2

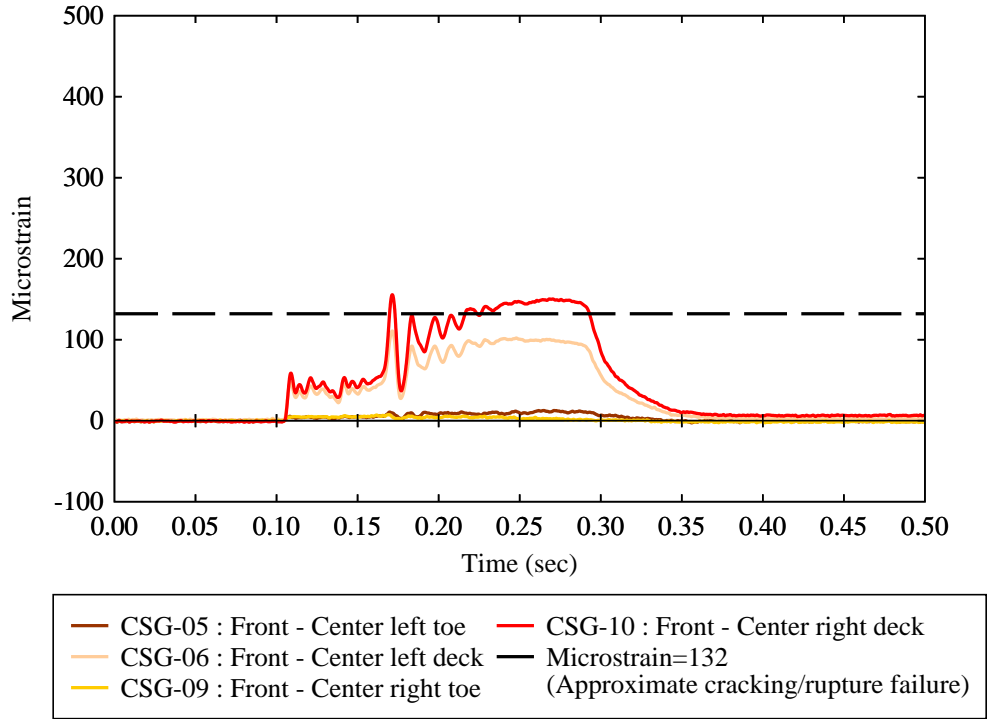


Figure 8-33 External concrete strain gage data for locations at the toe of the rail and deck during R/C COR test 2

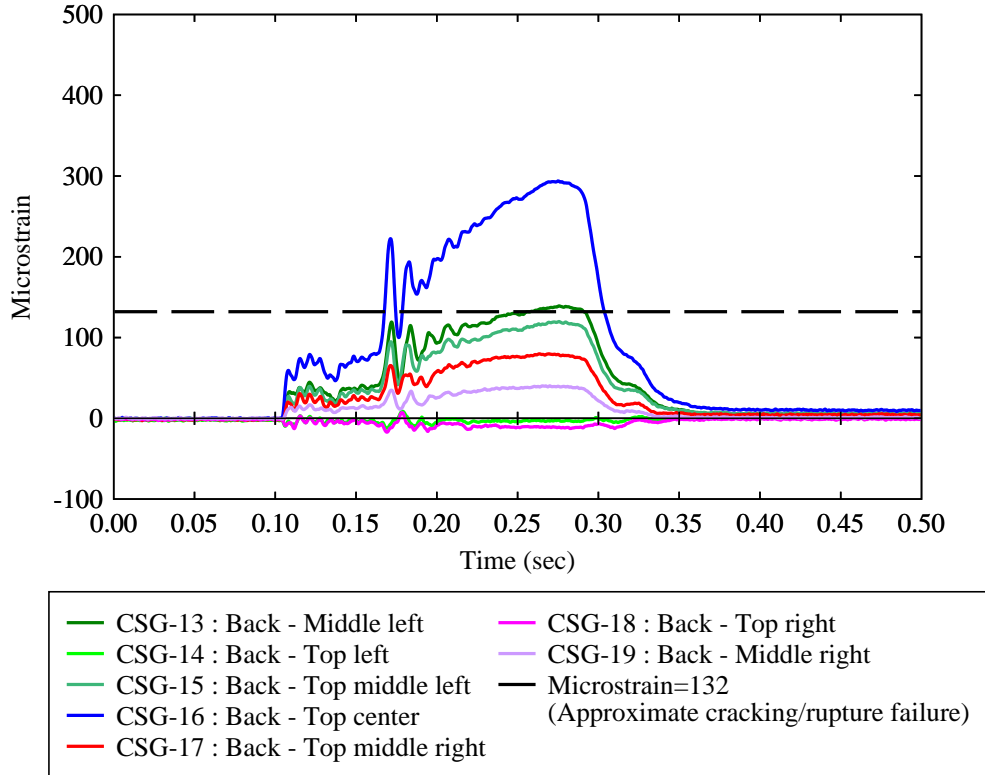
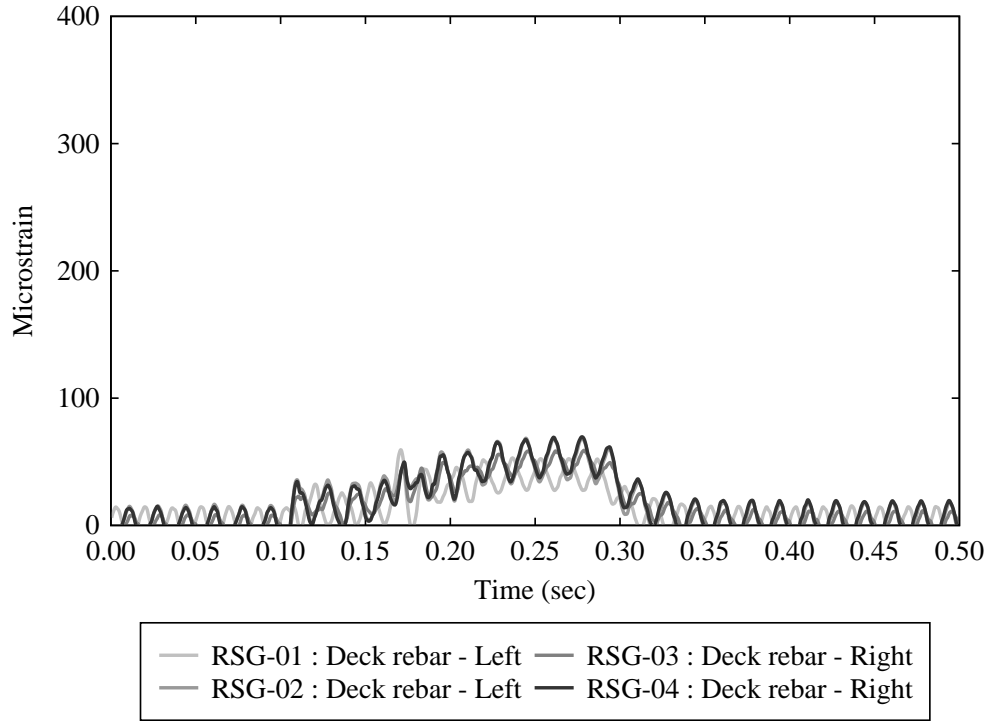
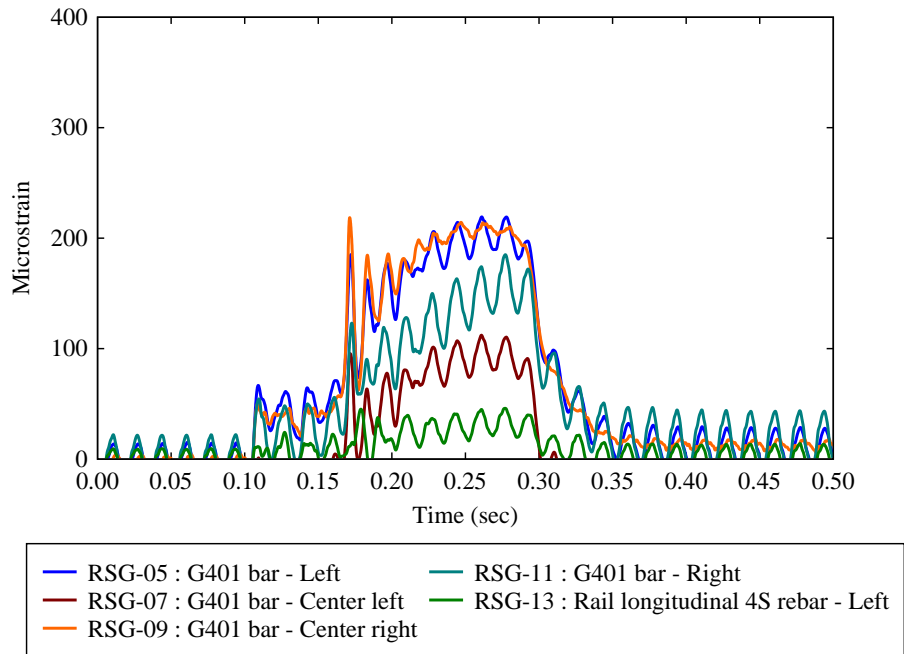


Figure 8-34 External concrete strain gage data for locations on the back face of the rail during R/C COR test 2

Readings from internal rebar strain gages are provided in Figure 8-35. Specific locations of the deck and connection (4V) rebar gages are provided in Appendix H. Maximum strain levels in the deck and rail steel reinforcement are well below yielding strain (2000 microstrain) indicating that the test specimen successfully resisted the pendulum impact. Note that a significant number of rebar strain gage readings are not included because the gages were damaged during the casting process and did not provide data during testing (e.g., RSG-6, RSG-8, RSG-10, RSG-12, RSG-14, RSG-15 are zero).



(a)



(b)

Figure 8-35 Internal rebar strain gage data during R/C COR test 2:
(a) Deck rebar; (b) Rail rebar

8.3 GFRP reinforced rail

8.3.1 Impact testing of GFRP reinforced COR specimen 1

On June 4, 2021, full-scale pendulum impact testing for GFRP COR test specimen 1 was conducted. The pendulum impactor was dropped from the required 15-ft drop height. Instrumentation components included with the first GFRP COR test specimen were accelerometers, break beams, high-speed cameras, tape switches, laser displacement sensors, internal reinforcement strain gages, and external concrete strain gages. Additional details of the instrumentation plan used during impact testing are provided in Appendix H.

Sequential images taken from high-speed camera 1 (HSC-1) over the impact duration are provided in Figure 8-36, starting with the first instant of impact and including the point in time when the maximum crush depth on the crushable front nose (i.e., maximum impact force) was reached. The adhesive used to hold the aluminum loading wedge did not fail during the impact. Additional images from high-speed camera 2 (HSC-2) are provided in Figure 8-37, where no sliding of the test specimen was observed. Photographs of the test specimen after completion of the impact test are shown in Figure 8-38. After completion of the impact test, one crack (of less than 0.004-in. width) was found vertically along the center line in the back face of the rail (Figure 8-38b).

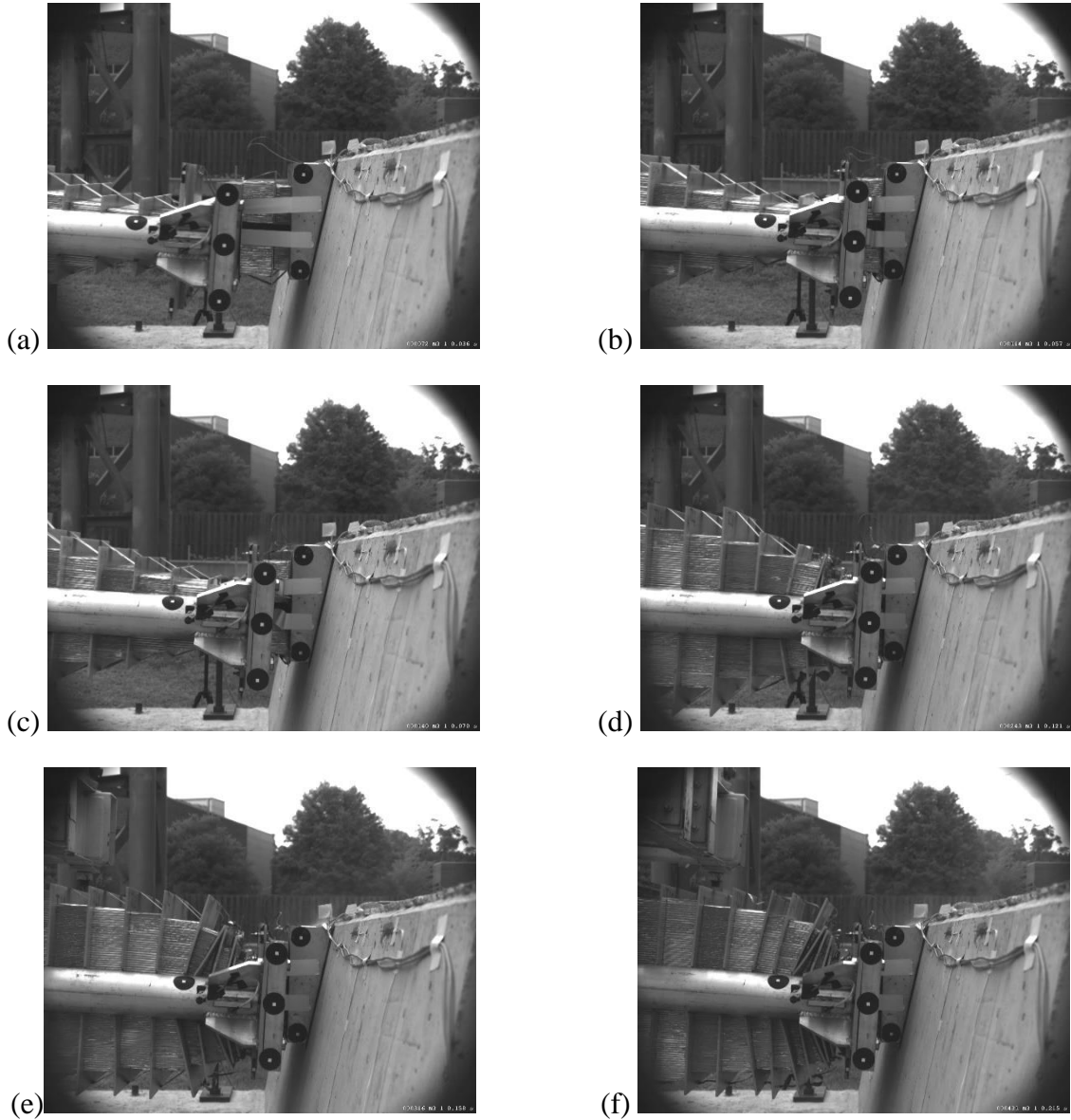


Figure 8-36 High-speed video frames from HSC-1 (GFRP COR test 1) showing crush deformation of aluminum honeycomb: (a) At initial impact; (b) – (c) Intermediate frames; (f) At peak impact force

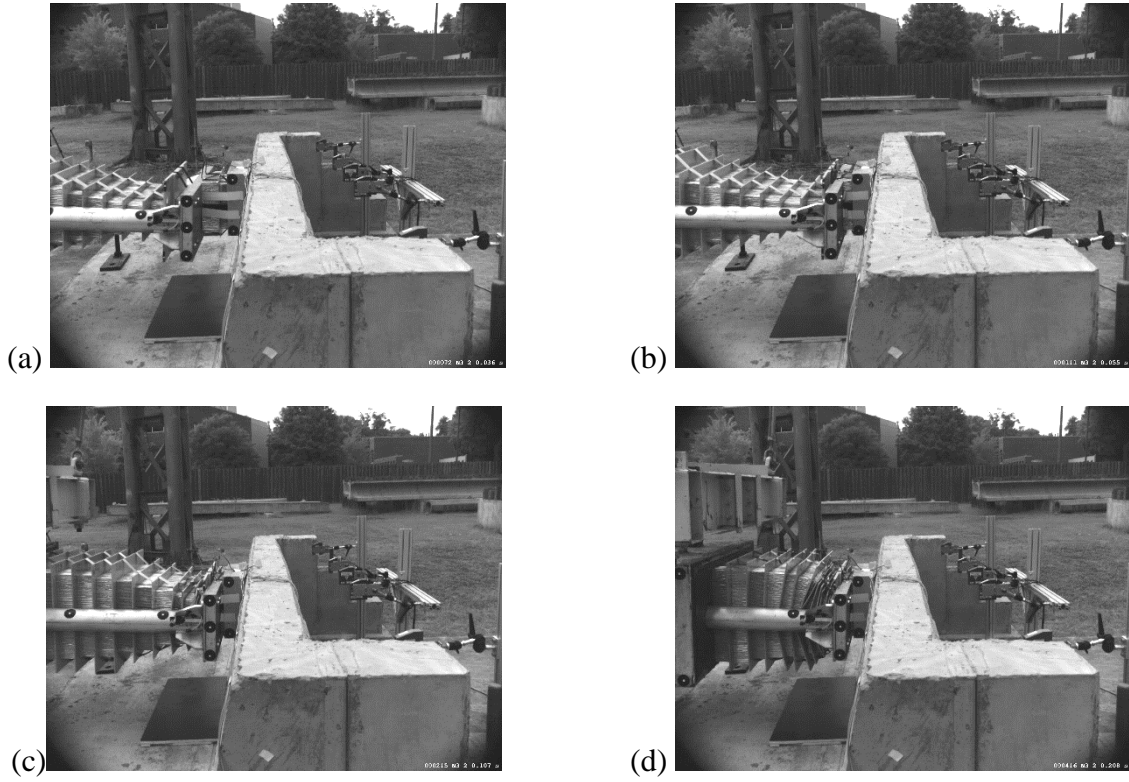


Figure 8-37 High-speed video frames from HSC-2 (GFRP COR test 1): (a) At start of impact; (b) – (c) Intermediate frames; (d) At peak impact force



(a)



(b)

Figure 8-38 GFRP COR test 1 specimen after completion of impact test: (a) front view; (b) back view

Break beam voltage data from GFRP impact test 1 are provided in Figure 8-39, and were used to quantify the impact velocity. For GFRP test 1, the impact velocity was determined to be 31.1 ft/sec—compared to the design impact velocity of 31.1 ft/sec (a 0% difference). Tape switch data are shown in Figure 8-40. Note that all impact test data has been shifted such that the initiation of impact begins at 0.1 s, using the spike in tape switch voltage.

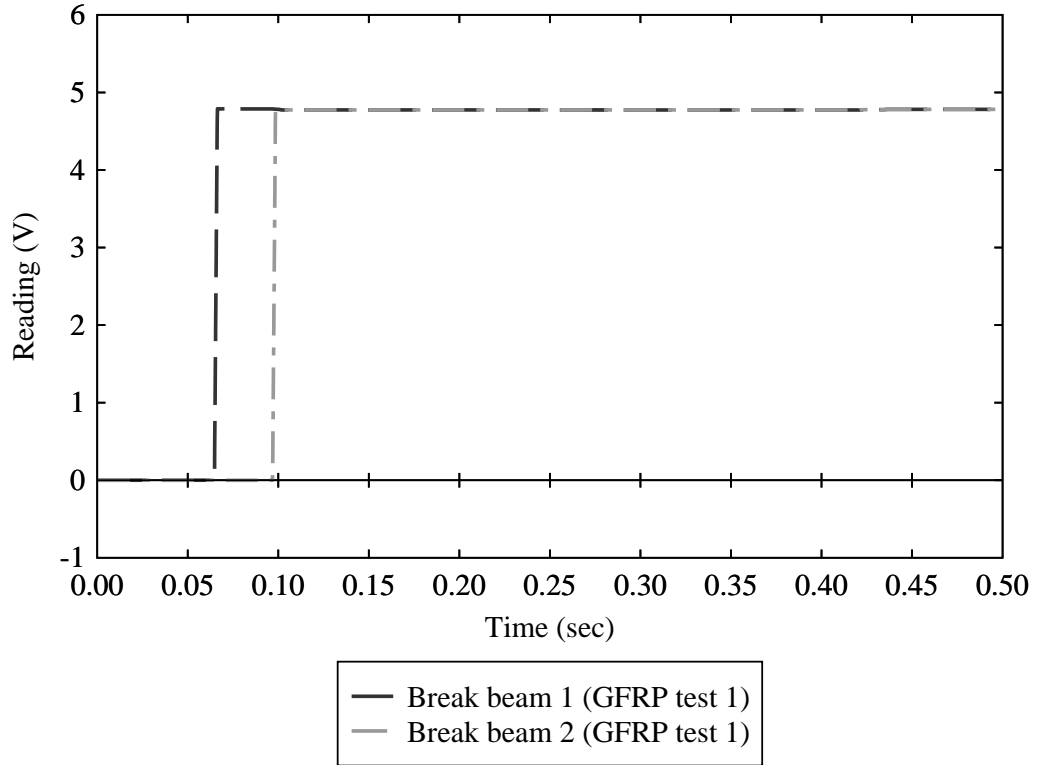


Figure 8-39 Break beam data for GFRP COR test 1

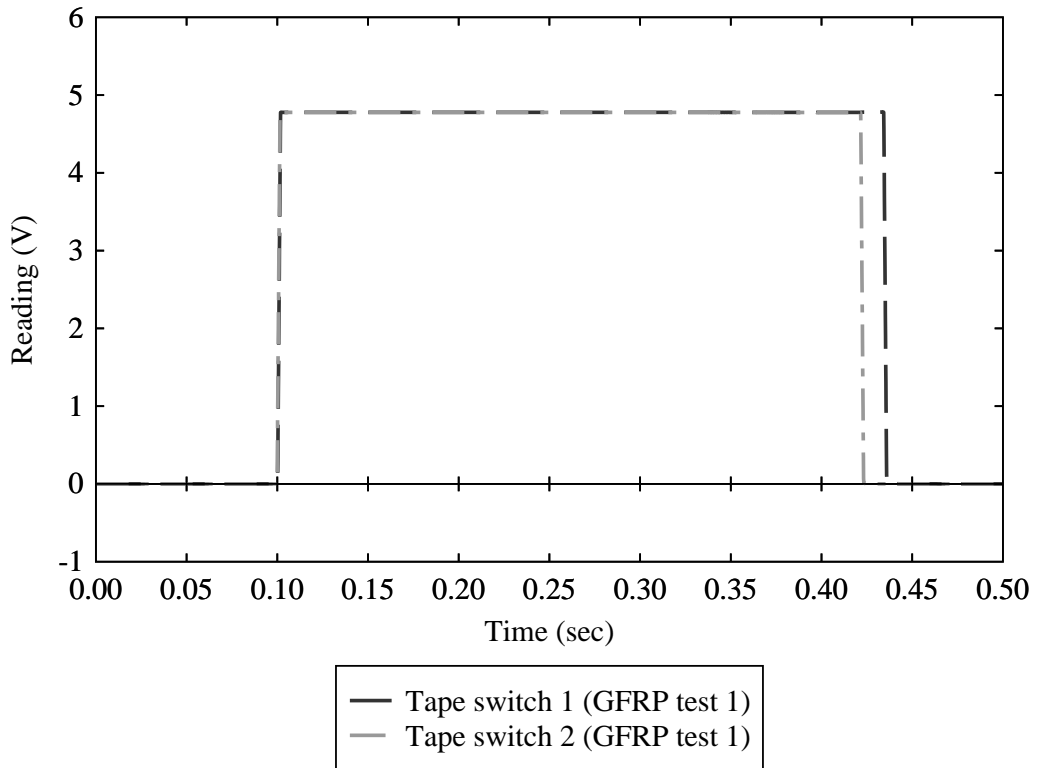


Figure 8-40 Tape switch data for GFRP COR test 1

Measured accelerations from the two accelerometers on the concrete back block (AC-1 & AC-2) in the impact direction (i.e., local Y direction of the accelerometer) are shown in Figure 8-41. Similar to the concrete back block, two accelerometers, AC-3 and AC-4 were mounted on the aluminum front nose to measure acceleration and impact force. However, during testing, the cable connected to AC-4 was damaged immediately after release of the impactor, and no data were recorded for AC-4. The measured accelerations from one accelerometer on the aluminum front nose (AC-3) in the impact direction (local Y direction) are shown in Figure 8-42. Computed and averaged back block impact forces (from AC-1 & AC-2) are shown in Figure 8-43, while the computed front nose impact forces (from AC-3) are shown in Figure 8-44.

The total applied impact force – computed by combining the average of the back block and the front nose – is shown in Figure 8-45. In comparison with the designed/predicted maximum impact forces (shown in Figure 8-46, which provides the predicted impact force over time from previous FEA impact simulations), the maximum observed impact force from GFRP COR test 1 was found to be 76 kip (10% greater than the originally designed 68.8-kip peak impact force).

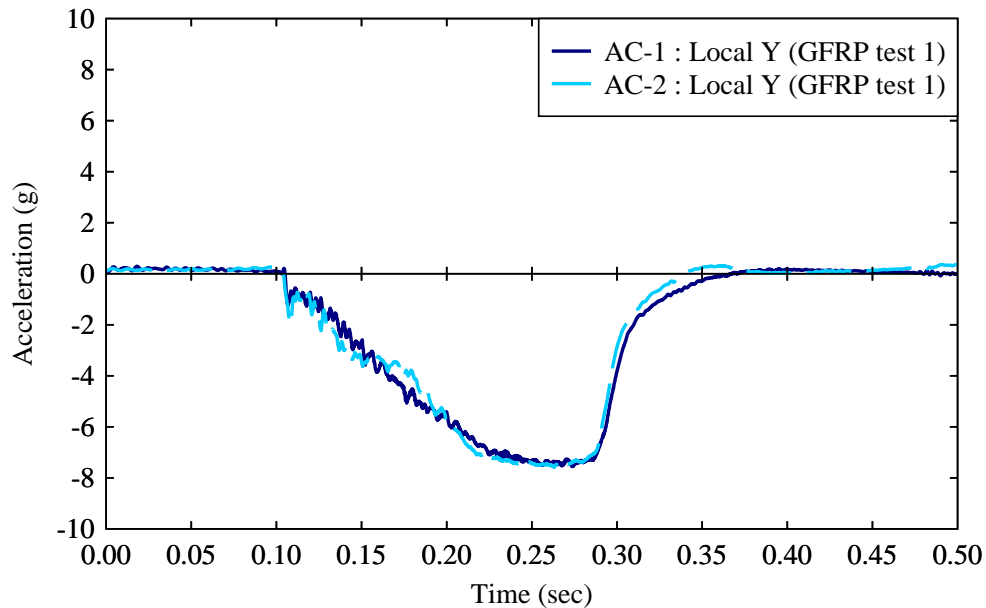


Figure 8-41 Raw concrete back block acceleration data (AC-1 & AC-2) for GFRP COR test 1 (in the impact direction, local Y direction of accelerometer)

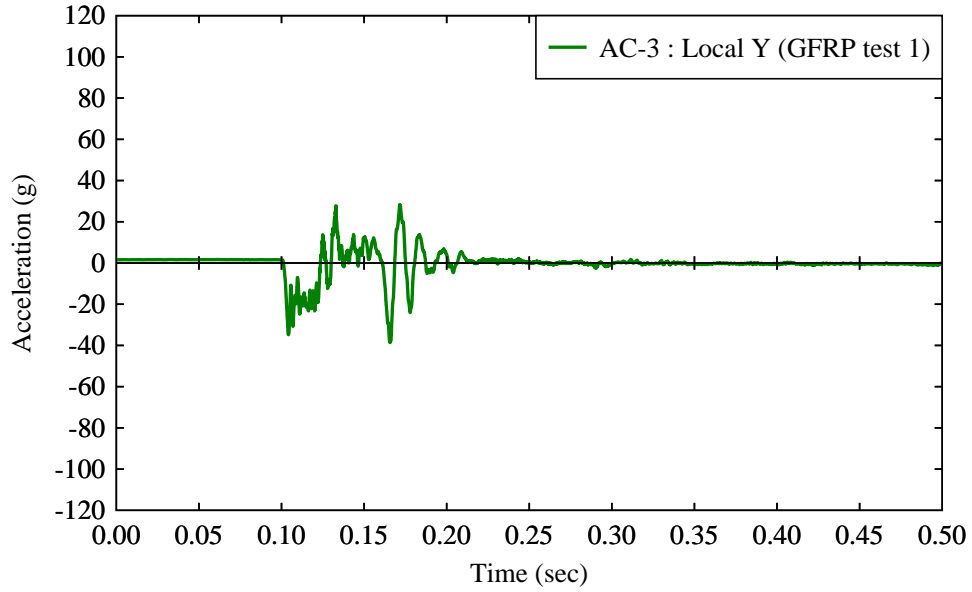


Figure 8-42 Raw front nose acceleration data (AC-3) for GFRP COR test 1 (in the impact direction, local Y direction of accelerometer)

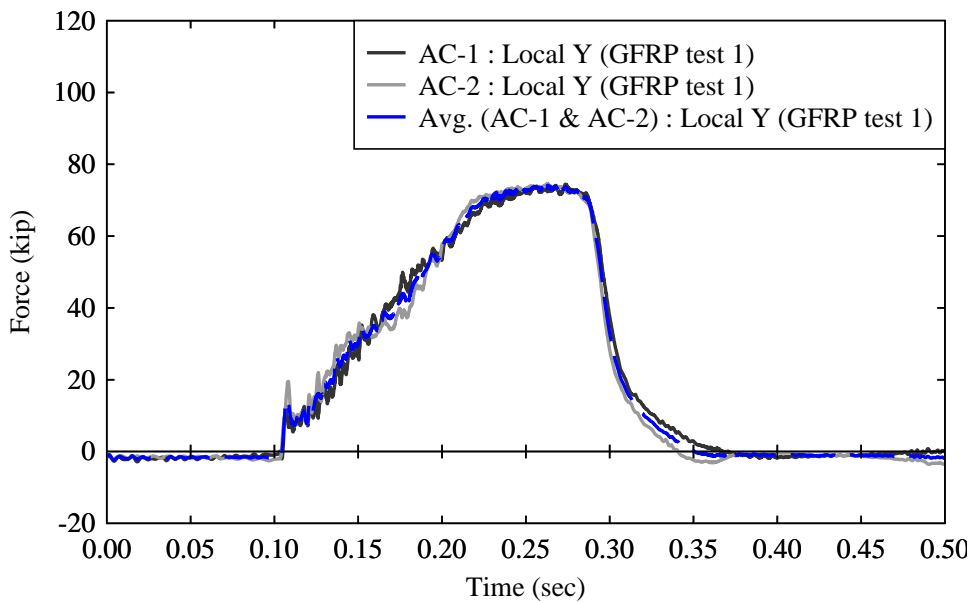


Figure 8-43 Computed impact forces from back block for GFRP COR test 1

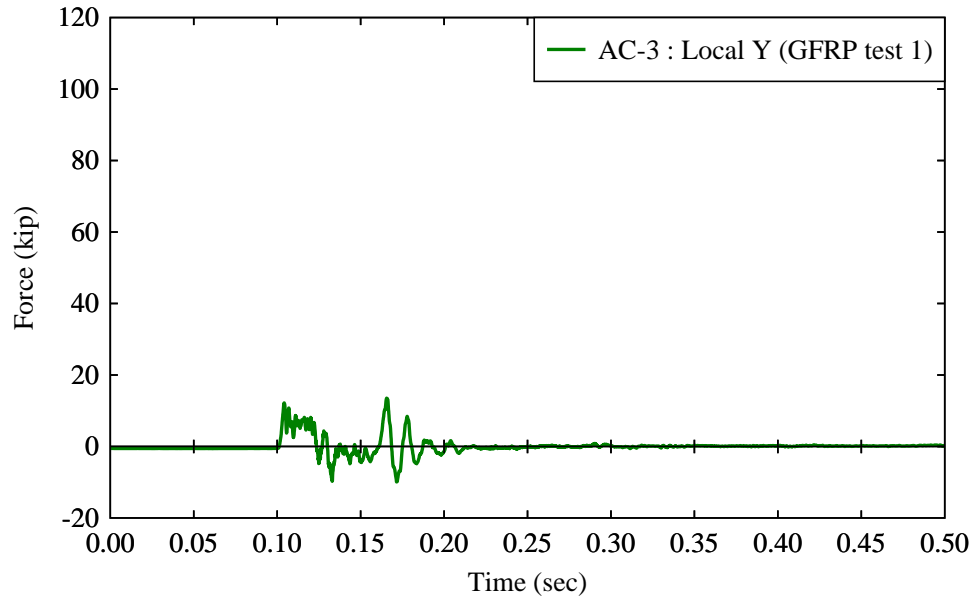


Figure 8-44 Computed impact forces from front nose for GFRP COR test 1

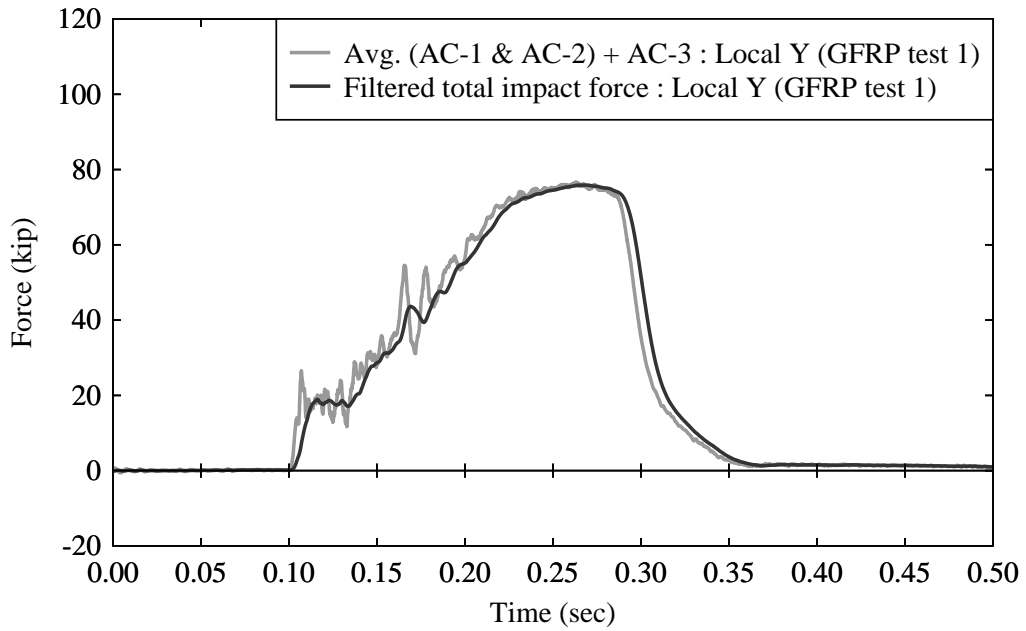


Figure 8-45 Raw and filtered total computed impact force for GFRP COR test 1

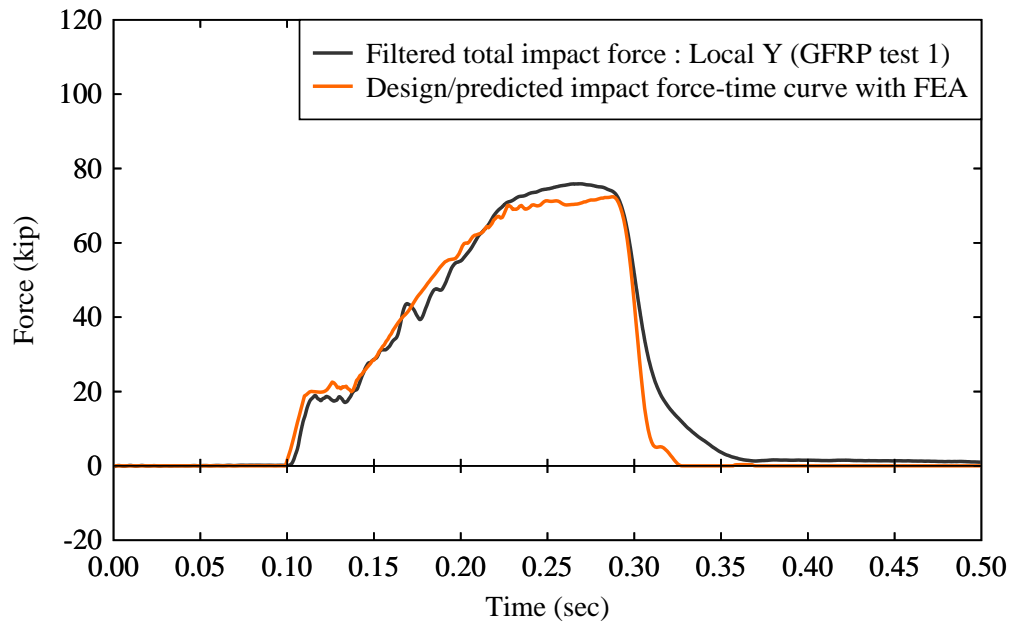


Figure 8-46 Filtered total experimental impact force for GFRP COR test 1 compared to FEA prediction

Laser displacement data captured during GFRP COR test 1 are provided in Figure 8-47, where it is shown that the maximum displacement occurred at the center of the rail (LDS-4) with a magnitude of approximately 0.09 in., when the peak impact force was applied. After completion of the impact, a very small (0.01 in. – 0.02 in.) residual displacement at the deck elevation remained, indicating that negligible sliding of the specimen occurred.

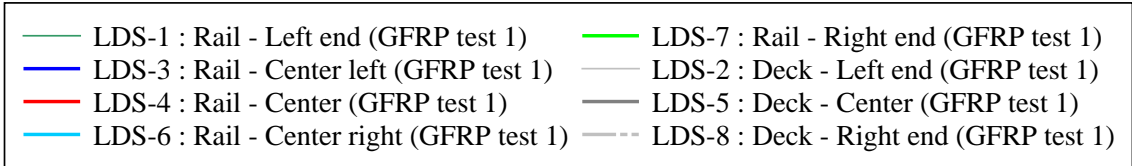
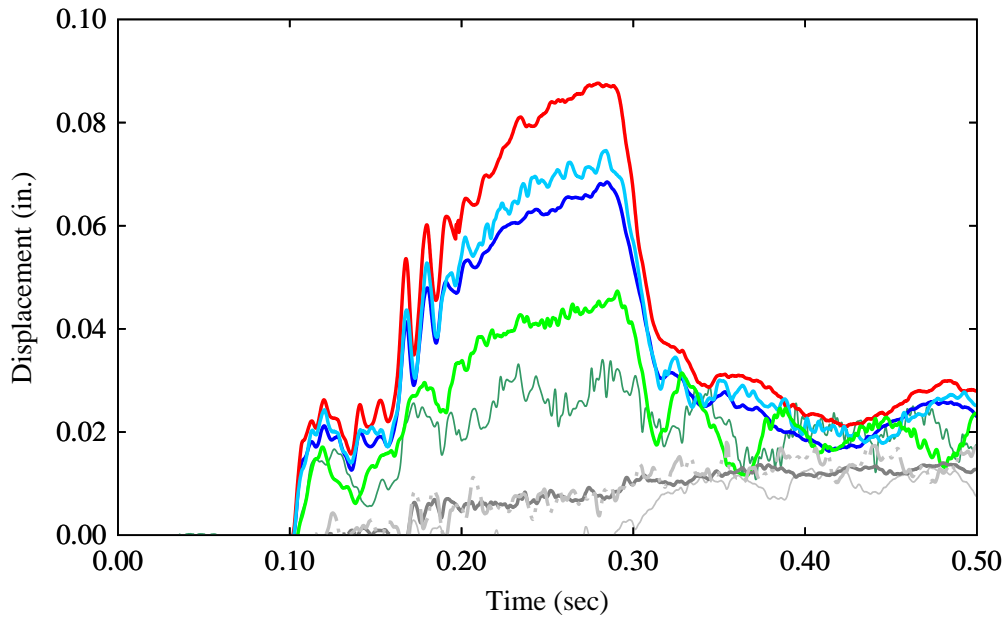


Figure 8-47 Laser displacement sensor data for GFRP COR test 1

Readings from external concrete strain gages are provided in Figures 8-48 through 8-51. External gage readings for the top front face of the rail are provided in Figure 8-48. Strain readings for the bottom (i.e., lower half and toe) of the rail front face are provided in Figure 8-49 and 8-50, and readings for the back face of the rail are provided in Figure 8-51. Although some strain levels on the front face reached the approximate tensile rupture strain for 3400-psi strength concrete, no discernible cracking was found in the rail front face or the deck after visual inspection. However, as mentioned before, a vertical crack was observed on the back face along the centerline of the rail and correspondingly the strain level in CSG-16 (approximately 10000 microstrain) was found to be much larger than 132 microstrain (the approximate tensile rupture strain).

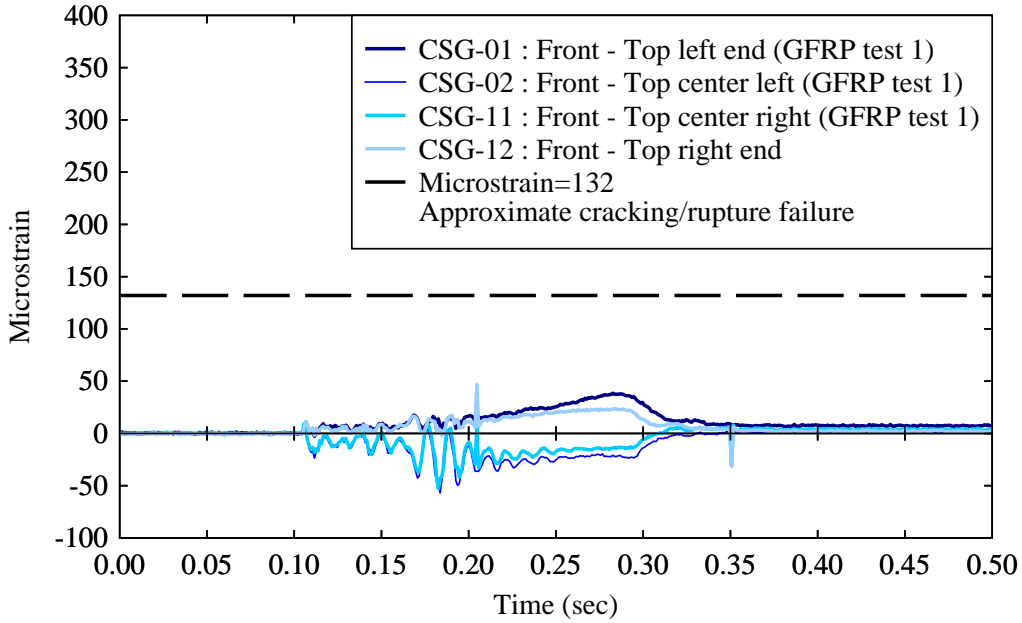


Figure 8-48 External concrete strain gage data for locations on the top front face of the rail during GFRP COR test 1

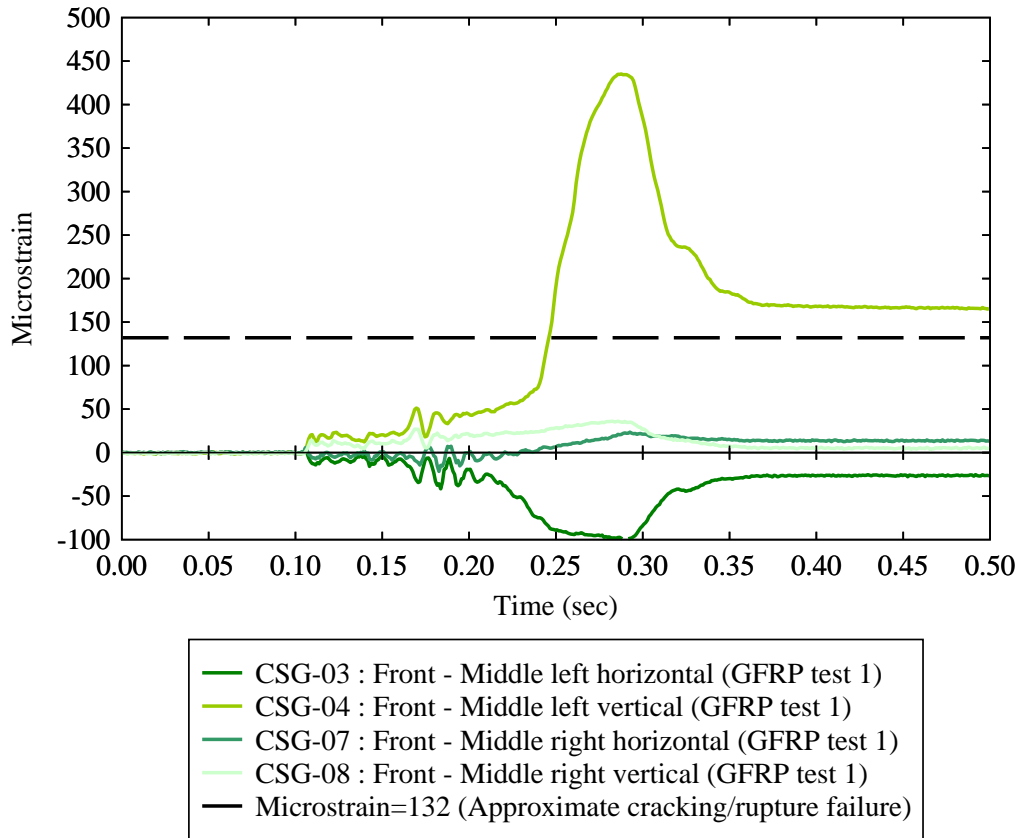


Figure 8-49 External concrete strain gage data for locations on the lower front face of the rail during GFRP COR test 1

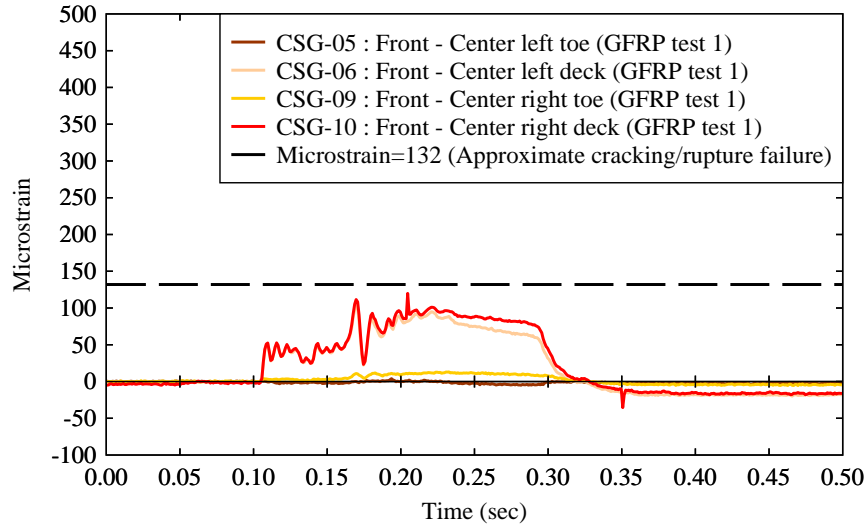


Figure 8-50 External concrete strain gage data for locations at the toe of the rail and deck during GFRP COR test 1

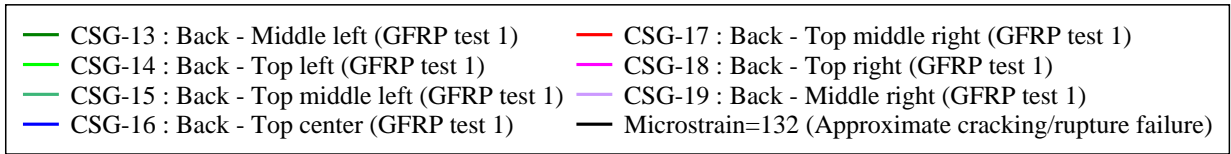
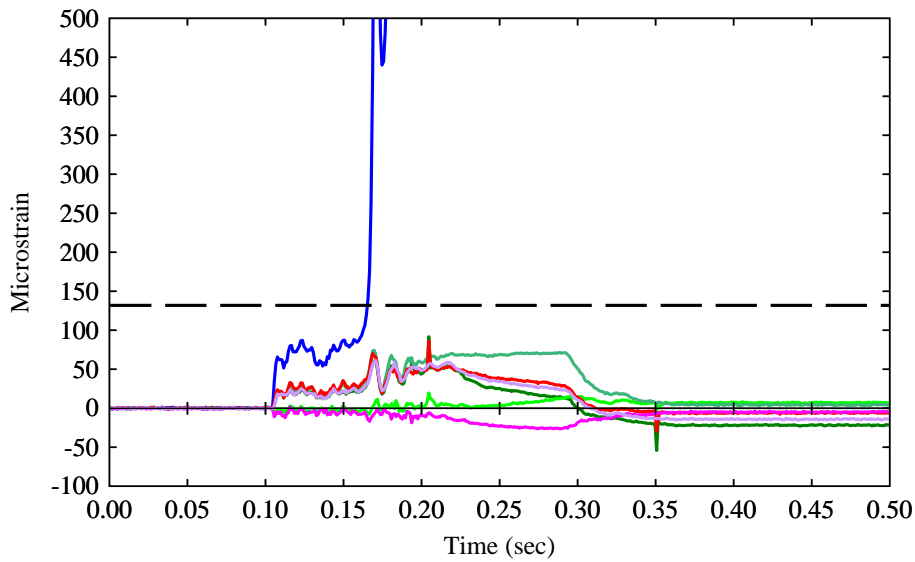
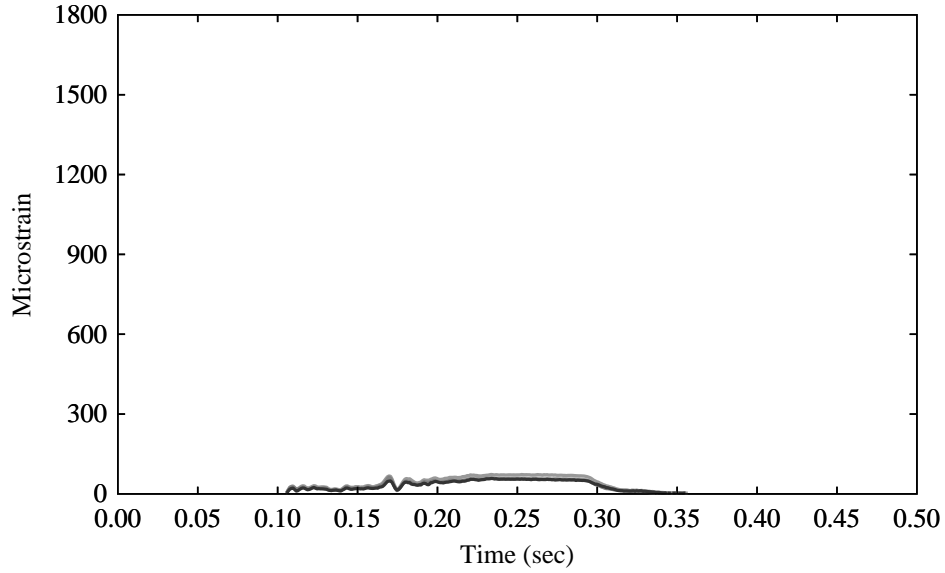


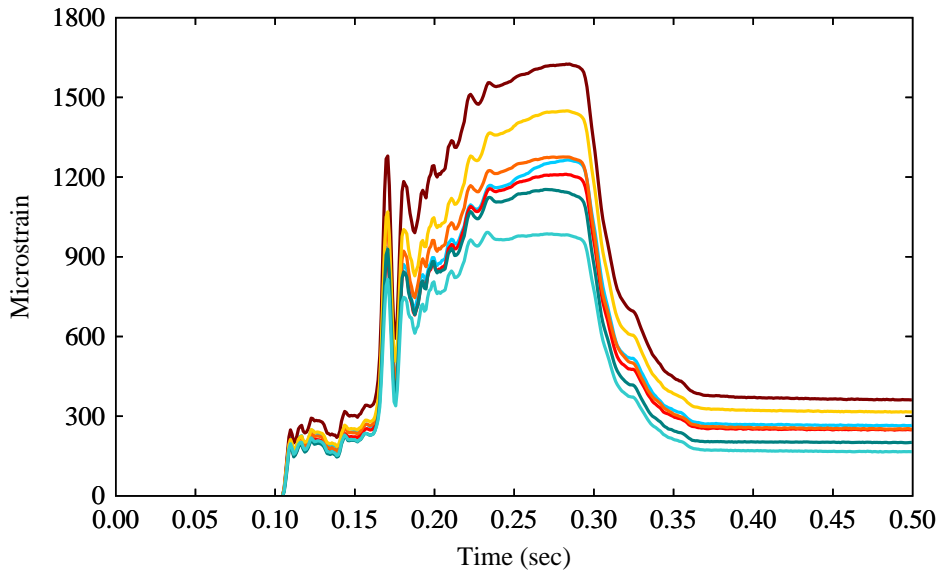
Figure 8-51 External concrete strain gage data for locations on the back face of the rail during GFRP COR test 1

Readings from internal rebar strain gages are provided in Figure 8-52. Specific locations of the deck and connection (G401) rebar gages are provided in Appendix H. Maximum strain levels in the deck and rail steel reinforcement are well below yielding strains for GFRP bars (as indicated in Table 7-1) indicating that the test specimen successfully resisted the pendulum impact with minimal damage.



- RSG-01 : Deck rebar - Left (GFRP test 1)
- RSG-02 : Deck rebar - Left (GFRP test 1)
- RSG-03 : Deck rebar - Right (GFRP test 1)
- RSG-04 : Deck rebar - Right (GFRP test 1)

(a)



- RSG-05 : G401 bar - Left (GFRP test 1)
- RSG-06 : G401 bar - Left (GFRP test 1)
- RSG-07 : G401 bar - Center left (GFRP test 1)
- RSG-08 : G401 bar - Center left (GFRP test 1)
- RSG-09 : G401 bar - Center right (GFRP test 1)
- RSG-10 : G401 bar - Center right (GFRP test 1)
- RSG-11 : G401 bar - Right (GFRP test 1)
- RSG-12 : G401 bar - Right (GFRP test 1)

(b)

Figure 8-52 Internal rebar strain gage data during GFRP COR test 1:
 (a) Deck rebar; (b) Rail rebar

8.4 Comparison of GFRP and R/C COR test specimen results

Selected data from testing of both COR specimen types are compared, to evaluate the performance of the proposed GFRP rail and to establish whether the GFRP rail system behaved similar to the traditional R/C FDOT rail under comparable impact loads.

As discussed, the following specimen configurations were pendulum impact tested:

- Fully-instrumented GFRP COR test specimen 1
- Fully-instrumented R/C COR test specimen 1
- Fully-instrumented R/C COR test specimen 2

Because some instrumentation components used in testing were damaged, data from these components could not be used for comparison.

8.4.1 Comparison of COR acceleration data and pendulum impact forces

For each of the three COR tests, accelerometers located on the pendulum impactor were used to measure deceleration of the impactor over the duration of impact. Acceleration data were subsequently used to indirectly measure the impact force applied to each test specimen. As shown in Figure 8-53, a similar force-time curve was achieved with each of the three tests and each test was found to adequately follow the designed force-time curve—which was designed to produce impact forces similar to the transverse component of a TL-4 vehicle impact test.

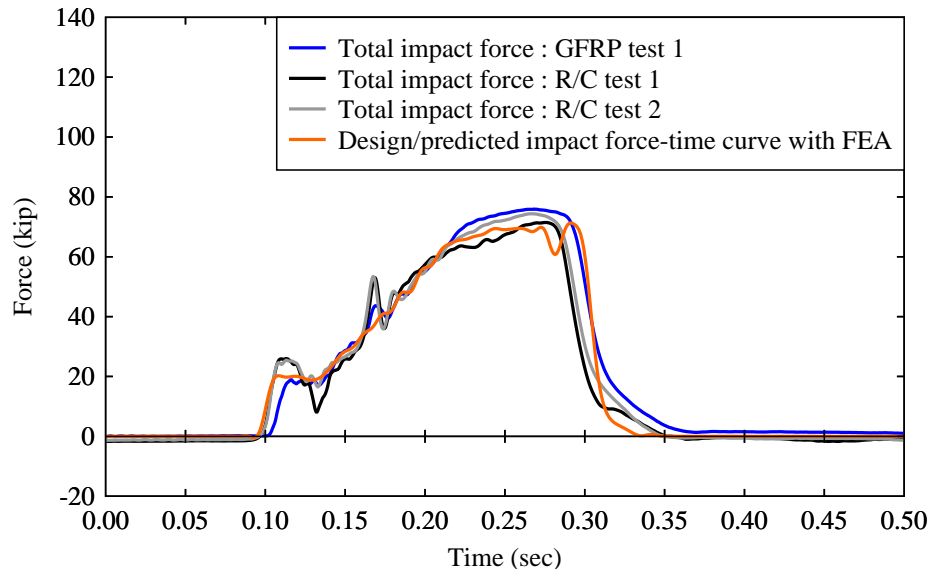


Figure 8-53 Total impact force for each traffic rail impact test

8.4.2 Comparison of COR laser displacement data

For GFRP COR test 1 and R/C COR tests 1, laser displacement sensors were used to capture transverse deflections at various locations on the back face of the rail. As previously discussed, displacements recorded during R/C test 2 were unusable due to support-stand vibrations. As opposed to comparing all LDS data from the two available tests, only the largest

observed displacements from LDS-4, located behind the center of the rail shown in Figure 7-18b were compared in Figure 8-54. The maximum displacement for the GFRP test specimen was 0.09 in and for the R/C test specimen was 0.07 in. The slightly larger displacement in the GFRP test specimen than the R/C test specimen can be attributed to the lower modulus of elasticity of the GFRP bars. However, the final or the residual displacement in both the specimens after impact was similar (about 0.03 in.) suggesting that the proposed GFRP rail was structurally adequate.

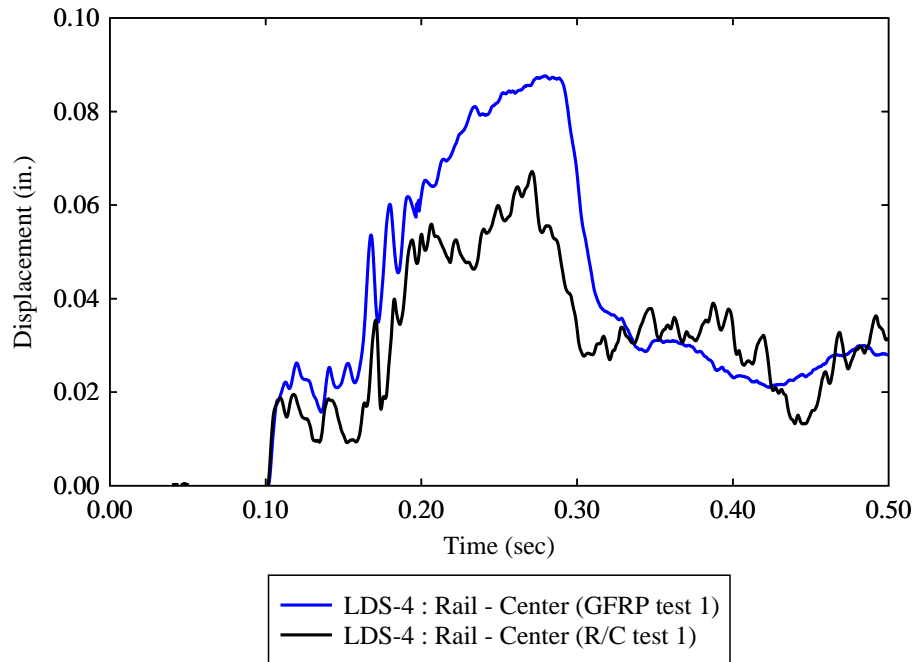


Figure 8-54 Comparison of captured displacements

8.4.3 Comparison of COR external concrete strain gage data

For the three COR tests (GFRP test 1, R/C test 1, R/C test 2), external concrete strain measurements in the rail and deck were taken at locations along the front and back sides of the test specimen. Recorded external strain data from a select number of gage locations are compared in Figure 8-55 and Figure 8-56.

Gage CSG-4 of the GFRP specimen was found to have the largest strain level on the front face. However, no visible crack was observed at the location of CSG-4. Further, gage CSG-8, the mirror gage of CSG-4, was found to have minimal strain level. This indicated that the large measured strain at CSG-4 was probably due to local imperfection on the front face of the specimen.

Gages on the deck near the toe of the rail (CSG-6 and CSG-10) were found to capture the largest strain levels for the front (impact) side of all the specimens. Because these two gages were located at mirrored distances from the centerline of the test specimen and were found to have similar magnitude readings over the impact duration, CSG-6 and CSG-10 data from each test were averaged and are compared as shown in Figure 8-55. As shown, similar strain levels were found for each of the three impact tests.

For the back side of the test specimen, strain levels from gage CSG-16 were found to be largest in magnitude (in each of the three tests) because this gage was positioned at the centerline of the test specimen (directly behind the impact location). Therefore, strain levels on the back side

of the specimen at gage CSG-16 are compared in Figure 8-56. The maximum transient strain level for GFRP test 1 at gage CSG-16 was found to be much larger in magnitude than the two standard R/C tests and was out of range of the strain gauge measurement. This finding was consistent with the fact that one surface crack was found on the back face of the GFRP test specimens after impact testing. However, readings for all other strain gages were similar for the three COR specimens, indicating the proposed GFRP COR specimen performed in a manner similar to the conventional R/C COR specimens.

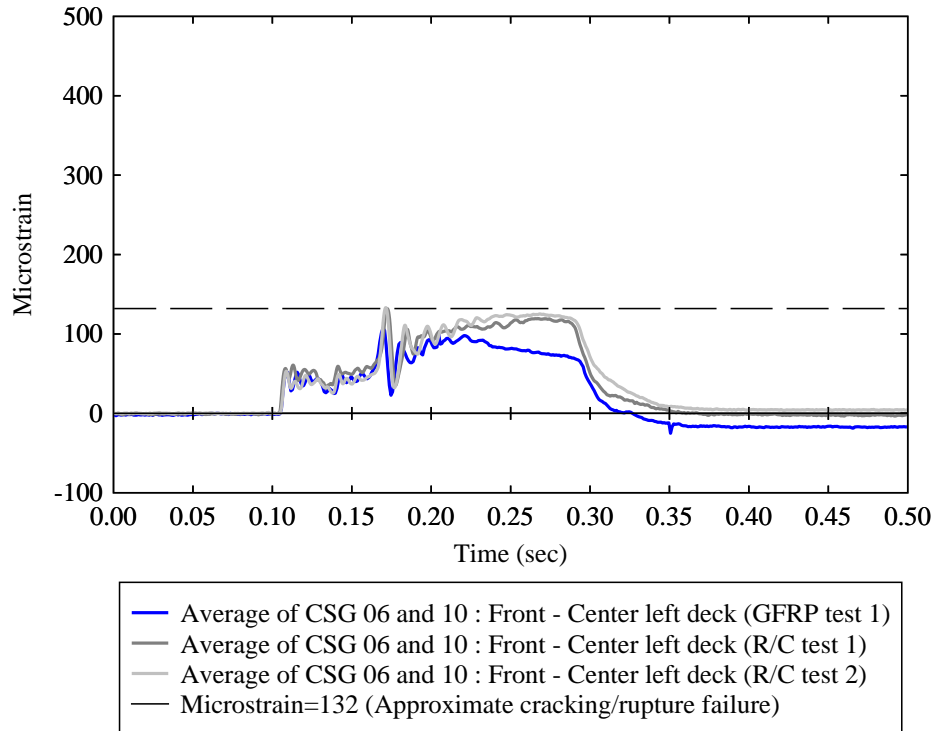


Figure 8-55 Comparison of external concrete strain gages on the deck near the rail toe (on the front side of the impact specimen)

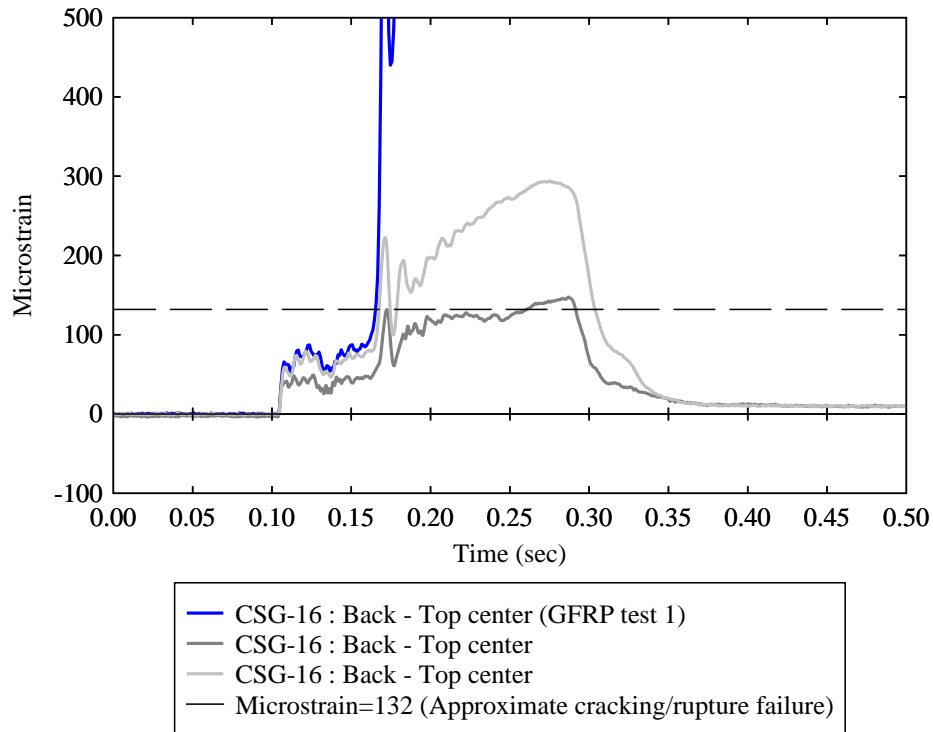


Figure 8-56 Comparison of external concrete strain gages located at the center of the specimen (on back side of the impact specimen)

8.4.4 Comparison of COR internal steel rebar strain gage data

Using the three available test data sets, selected rebar strain gage measurements were compared. For the deck reinforcement, the largest observed strains were compared in Figure 8-57, where it is shown that the strains in GFRP test were similar to R/C COR test 2, but less than in R/C COR test 1. For the rail reinforcement, the bars in GFRP specimen were found to have higher strains than bars in the two R/C specimens. For example, as shown in Figure 8-58, the largest strain in a GFRP specimen bar was about 1600 and in an R/C specimen bar was about 300. The larger strain in GFRP bars is attributed to the lower elastic modulus of GFRP bars compared to steel bars. However, the maximum strains in the reinforcement for all of the three tests were well below the yield or rupture strain of steel or GFRP rebar types, respectively. The yield strain for steel rebar is approximately 2000 microstrain and the rupture strain for GFRP bars is shown in Table 7-1. Comparisons of strain levels between each test (per external or internal gages) show that there was some variability between tests, even when comparing the two R/C COR tests.

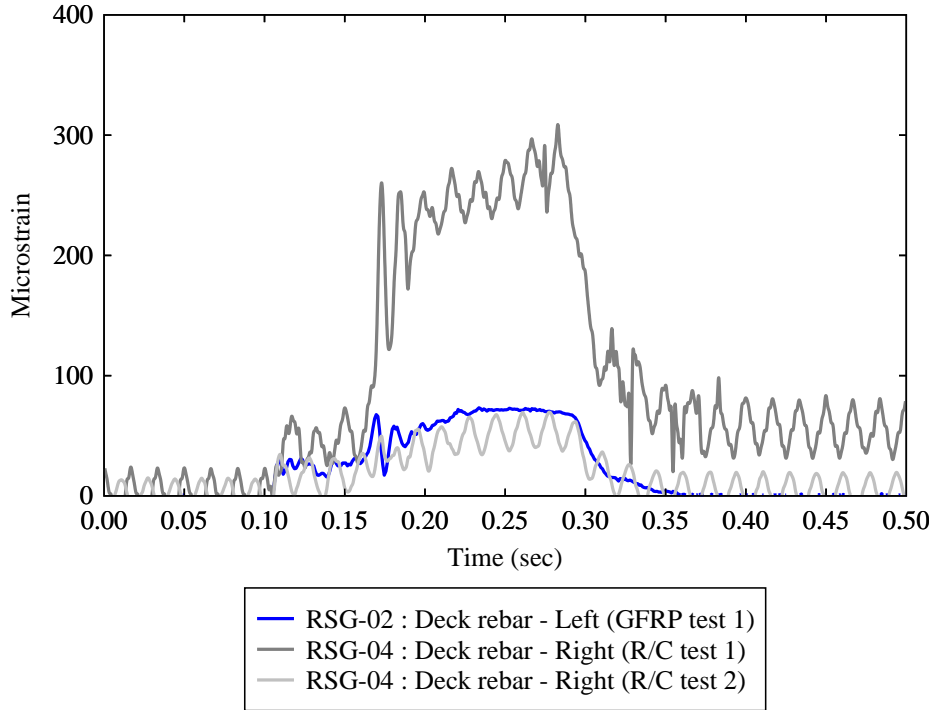


Figure 8-57 Comparison of internal strain gages located on the top deck rebar

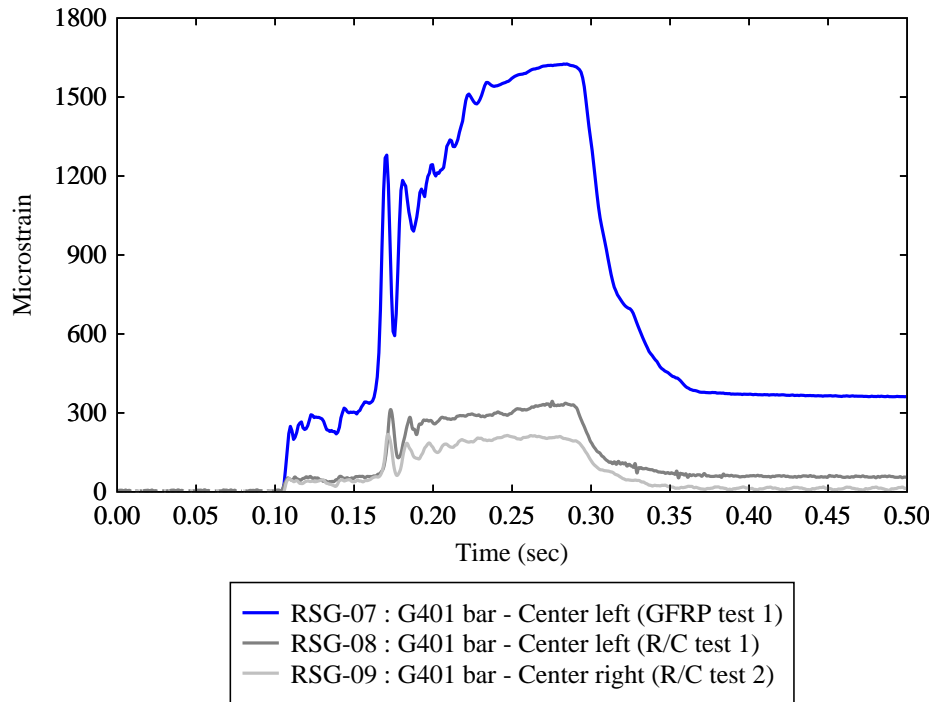


Figure 8-58 Comparison of internal strain gages located on the rail connection rebar

CHAPTER 9 FULL-SCALE END OF RAIL (EOR) IMPACT TEST RESULTS

9.1 Introduction

An end-of-rail (EOR) test specimen configuration (Figure 9-1) was included in the impact test matrix to investigate the relative performance of GFRP and R/C rails under end impact loading conditions. The EOR specimen configuration was shorter in length (8-ft) than the center-of-rail (COR) specimen configuration discussed in the previous chapter. Additionally, each EOR specimen was only supported at one end (i.e., only one end-support buttress was used). The other end of the rail was free (i.e., without an end-support buttress), with the impact load applied near the free end. This test configuration was termed an end-of-rail (EOR) impact configuration because it was used to evaluate the rail strength near a termination point of a rail (i.e., where a rail segment ends, which typically occurs at a construction joint or at the end of a bridge span).

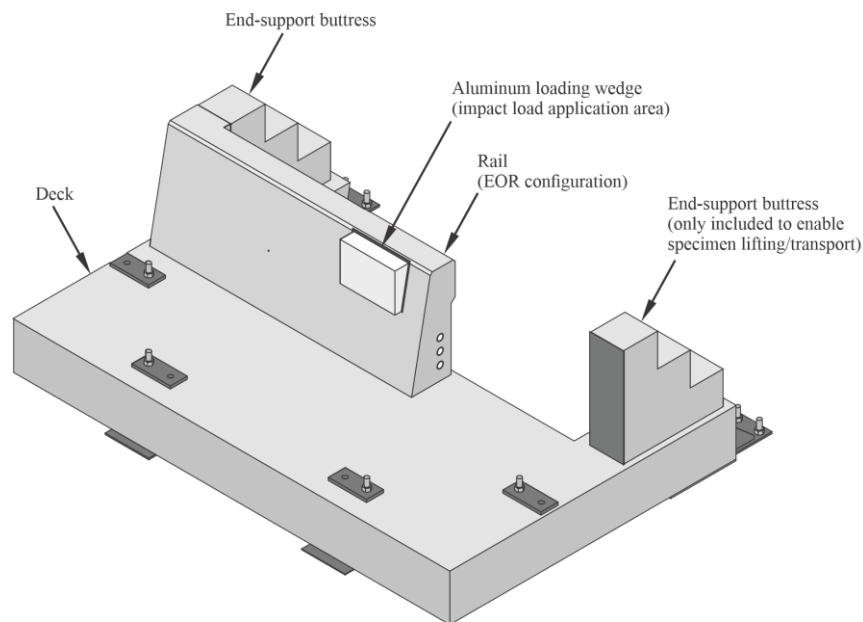


Figure 9-1 Main components of EOR specimen

In comparison to an interior impact location (i.e., a COR impact condition, where the impact occurs at an interior location along a rail), if an impact occurs near the end of a rail segment, the rail capacity is reduced because the impact occurs near an unsupported end and the failure pattern is expected to follow the yield line failure pattern detailed in Section 13 of *AASHTO LRFD Bridge Design* (2017). Therefore, this additional configuration was employed to further investigate the capacity of the proposed GFRP rail. This test was only added to the test matrix after confirming that the proposed GFRP rail could withstand impact at an interior location based on the COR configuration test results. It was expected that the EOR impact tests would produce more damage in the rail (i.e., more concrete cracking) and higher deflection levels than the COR impact tests.

In this chapter, results from three full-scale rail impact tests are discussed, where two GFRP EOR specimens and one R/C EOR specimen were tested (see Appendices D and E for EOR specimen construction drawings). Results for the EOR impact tests are organized by the two rail

types (i.e., R/C and GFRP rail) and are followed with a comparison of the EOR test results. A summary of the overall EOR test program is provided in Table 9-1. The instrumentation plan for the EOR configuration was similar to the COR test, with some gage locations changed (due to the shorter rail length and due to the different expected cracking pattern). External instrumentation components used during EOR tests are illustrated in Figure 9-2 (with additional instrumentation plans for EOR specimens detailed in Appendix H). Hardened mechanical properties of the concrete material used to cast and form each EOR pendulum impact test specimen, such as concrete compressive strength, are provided in Appendix I.

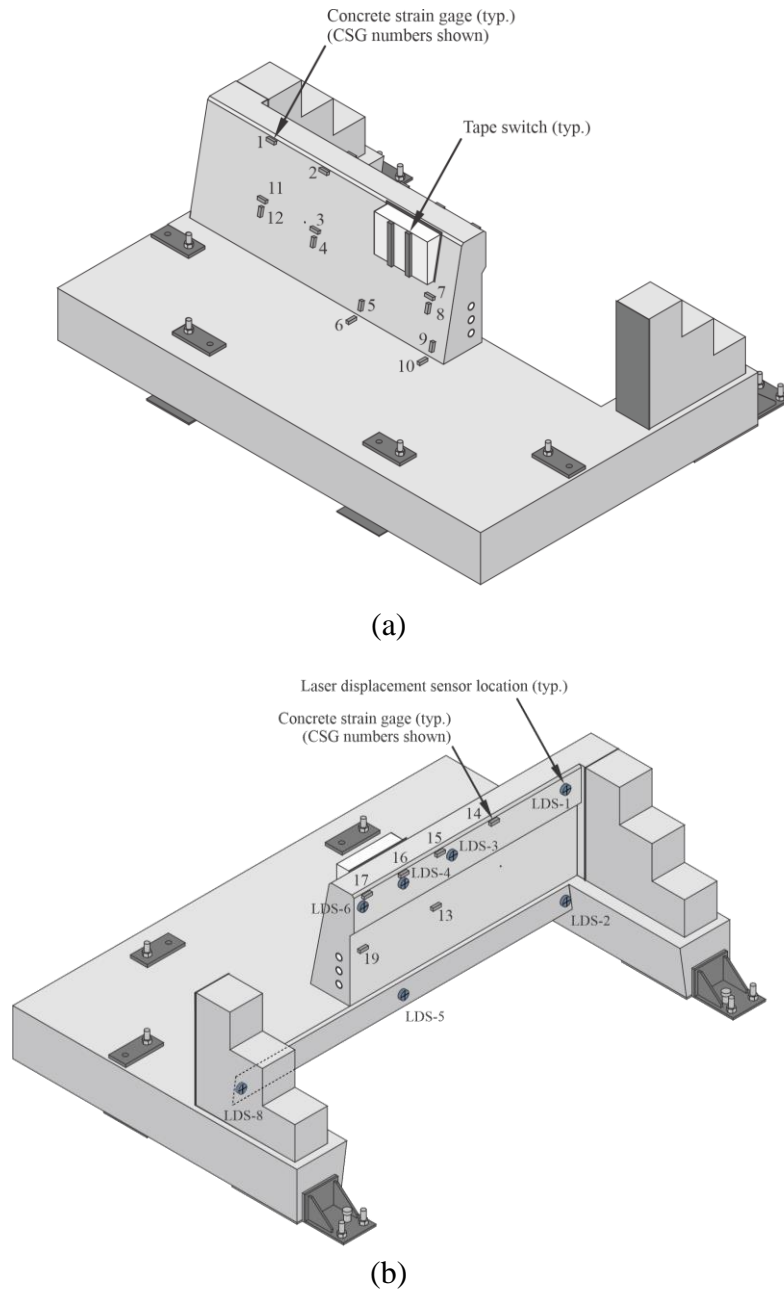


Figure 9-2 External EOR instrumentation: (a) Front concrete strain gage and tape switch sensor locations; (b) Back concrete strain gage and laser displacement sensor locations

Table 9-1 Full-scale EOR impact test summary

Impact test specimen	Test date	Drop height (ft)	Impact speed (mph) [ft/sec]	Impact energy (kip-ft)
R/C EOR 1 (R/C test 3)	4/06/2021	15	20.9 [30.8]	152.0
GFRP EOR 1 (GFRP test 2)	7/30/2021	15	21.8 [32]	164.4
GFRP EOR 2 (GFRP test 3)	11/10/2021	15	21.12 [31]	154.3

9.2 Standard (R/C) rail

9.2.1 Impact testing of R/C EOR specimen 1 (R/C test specimen 3)

On April 6, 2021, a full-scale pendulum impact test of the R/C EOR test specimen (R/C test specimen 3) was conducted. The pendulum impactor was dropped from 15 ft. Instrumentation components included with the R/C EOR test specimen were accelerometers, break beams, high-speed cameras, tape switches, laser displacement sensors, internal reinforcement strain gages, and external concrete strain gages. Additional details of the instrumentation plan used during impact testing are provided in Appendix H.

It should be noted that, concrete consolidation in certain areas of the R/C EOR specimen was relatively poor due to inadequate concrete vibration during casting (producing a poor surface condition and areas of ‘honeycombing’ near the bottom of the rail, as shown in Figure 9-3). Because cast-in-place formwork was used, the poor quality of the concrete consolidation was not known until after the formwork was removed. Despite the honeycombing, it was determined that the specimen was still suitable for testing.



(a)



(b)

Figure 9-3 Poor concrete consolidation of R/C EOR specimen 1 prior to testing:
(a) Front face of rail; (b) Bottom of the (cross-sectional) rail face at free end

Sequential images taken from high-speed camera 1 (HSC-1) over the impact duration are provided in Figure 9-4, starting with the first instant of impact and including the point in time when the maximum crush depth on the crushable front nose (i.e., maximum impact force) was reached. Additional images from high-speed camera 2 (HSC-2) are provided in Figure 9-5, where no discernable sliding of the test specimen was observed.

Photographs of the test specimen after completion of the impact test are shown in Figures 9-6 and 9-7. Diagonal cracks were found on the front and back faces of the rail. Cracks found in the test specimen were marked with a black marker to more clearly document where cracking occurred (in photographs). The largest measured crack on the front (impact) face of the R/C EOR specimen was approximately 0.016 in. wide, located near the top of the rail half-way between the end-support and the loading wedge. The largest crack on the back (non-impact) face of the rail was also approximately 0.016 in. wide, near the free end of the rail.



Figure 9-4 High-speed video frames from HSC-1 (R/C EOR test 1) showing crush deformation of aluminum honeycomb: (a) At initial impact; (b) – (c) Intermediate frames; (f) At peak impact force

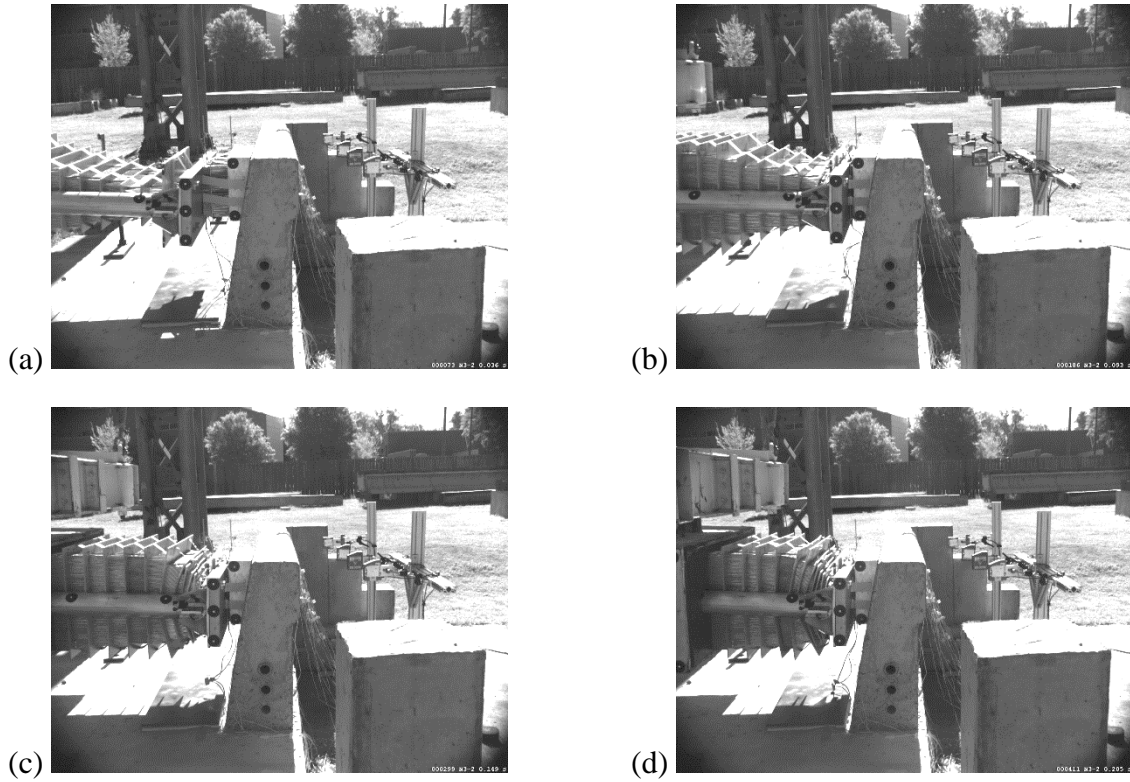


Figure 9-5 High-speed video frames from HSC-2 (R/C EOR test 1): (a) At start of impact; (b) – (c) Intermediate frames; (d) At peak impact force



Figure 9-6 R/C EOR test 1 specimen after completion of impact test



(a)



(b)

Figure 9-7 Cracking found on R/C EOR test 1 specimen: (a) On front rail face; (b) On back rail face

Break beam voltage data from R/C EOR impact test 1 are provided in Figure 9-8, and were used to quantify the impact velocity. As shown in the instrumentation plan (Appendix H), two sets of break beams were placed in front of the impact test specimen at a 1-ft spacing. For each break beam, after the impactor was released and when the impactor crossed the path of the sensor, a change in voltage was observed. The duration of time over which the impactor moved the 1-ft distance from break beam 1 to break beam 2 was used to quantify velocity just prior to impact. For R/C EOR test 1, the impact velocity was determined to be 30.8 ft/sec—compared to the design impact velocity of 31.1 ft/sec (a 1.0% difference). Tape switch data were used to determine the time at which the impact began and are shown in Figure 9-9. Note that all impact test data has been shifted such that the initiation of impact begins at 0.1 s, using the spike in tape switch voltage.

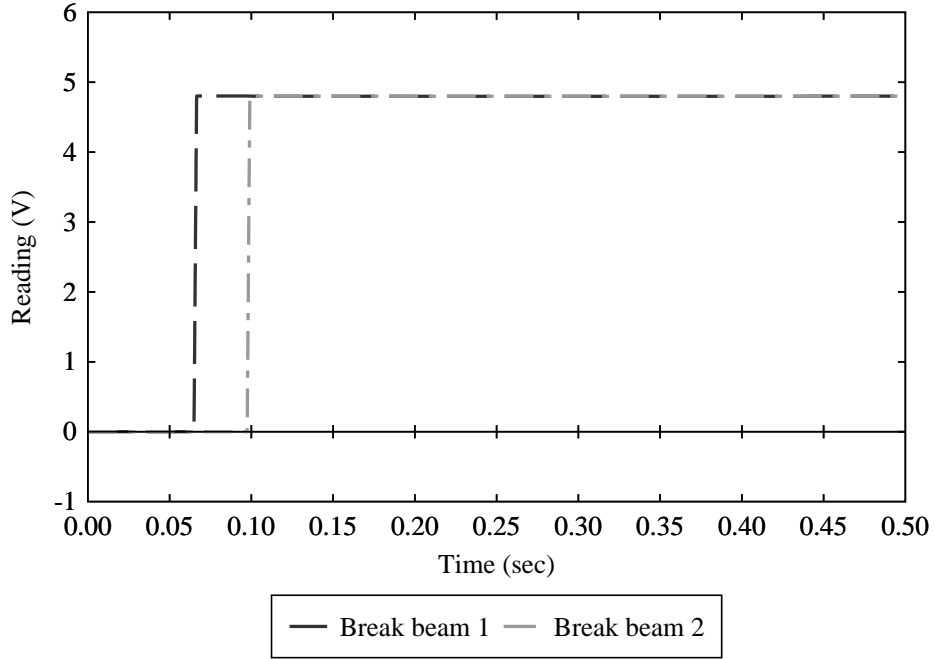


Figure 9-8 Break beam data for R/C EOR test 1

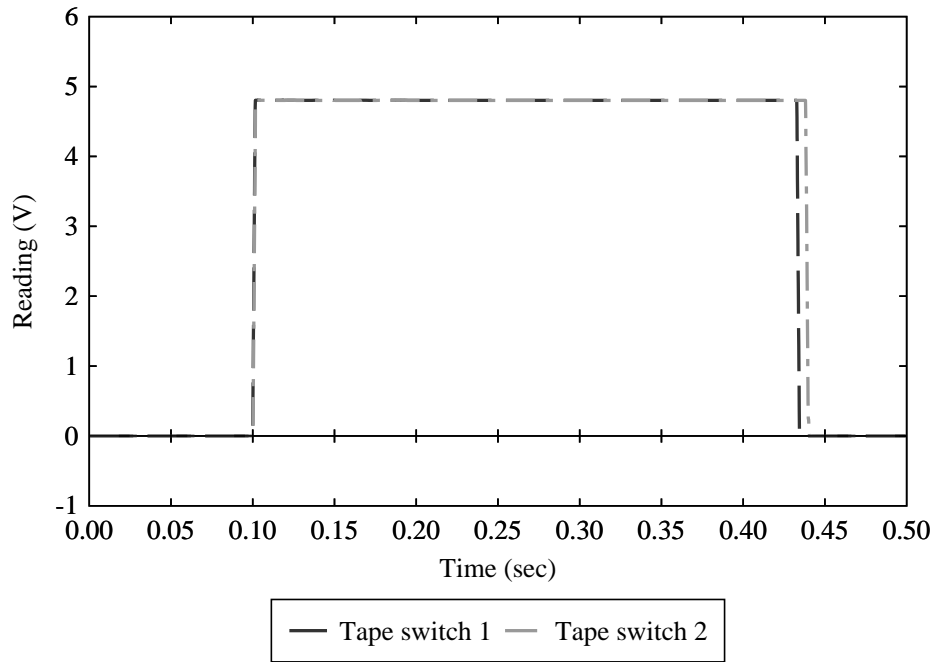


Figure 9-9 Tape switch data for R/C EOR test 1

Measured accelerations from the two accelerometers on the concrete back block (AC-1 & AC-2) in the impact direction (i.e., local Y direction of the accelerometer) are shown in Figure 9-10. Correspondingly, measured accelerations from the two accelerometers on the aluminum front nose (AC-3 & AC-4) in the impact direction (local Y direction) are shown in Figure 9-11. Computed and averaged back block impact forces (from AC-1 & AC-2) are shown

in Figure 9-12, while the computed and averaged front nose impact forces (from AC-3 & AC-4) are shown in Figure 9-13.

The total applied impact force was then computed by combining the two averages of the back block and front nose, as shown in Figure 9-14. In comparison with the designed/predicted maximum impact forces (shown in Figure 9-15, which provides the predicted impact force over time from previous FEA impact simulations), the maximum observed impact force from R/C EOR test 1 was found to be 76.9 kip (11.7% greater than the originally designed 68.8-kip peak impact force).

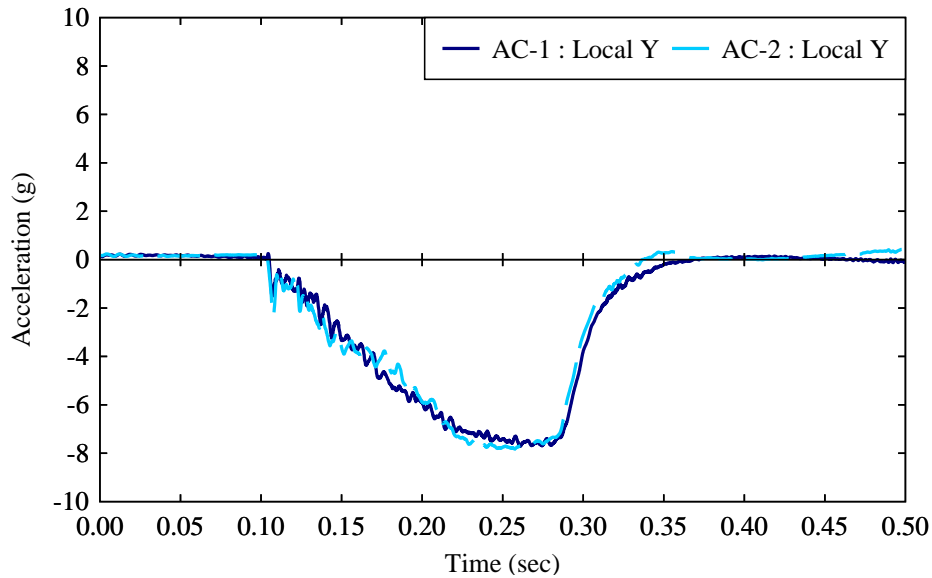


Figure 9-10 Raw concrete back block acceleration data (AC-1 & AC-2) for R/C EOR test 1 (in the impact direction, local Y direction of accelerometer)

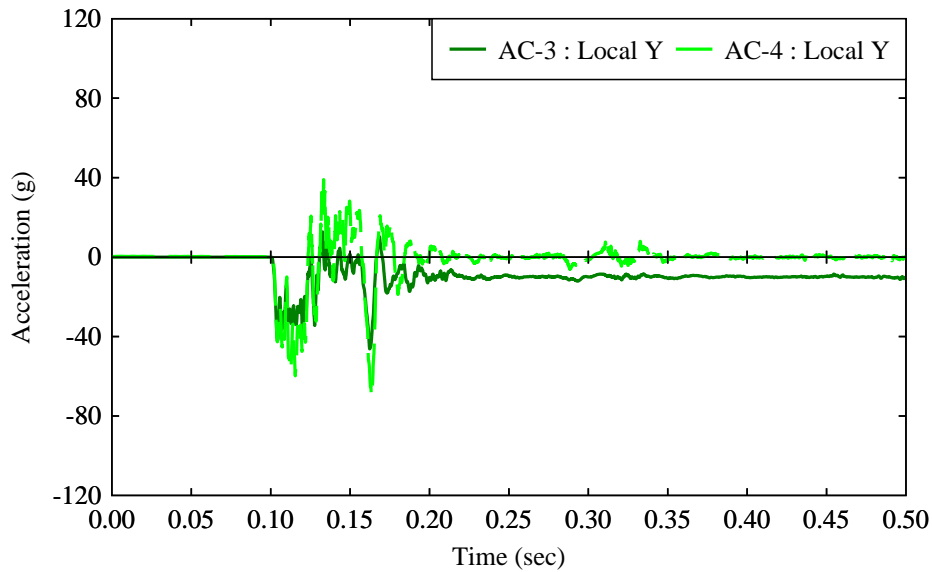


Figure 9-11 Raw front nose acceleration data (AC-3 & AC-4) for R/C COR test 1 (in the impact direction, local Y direction of accelerometer)

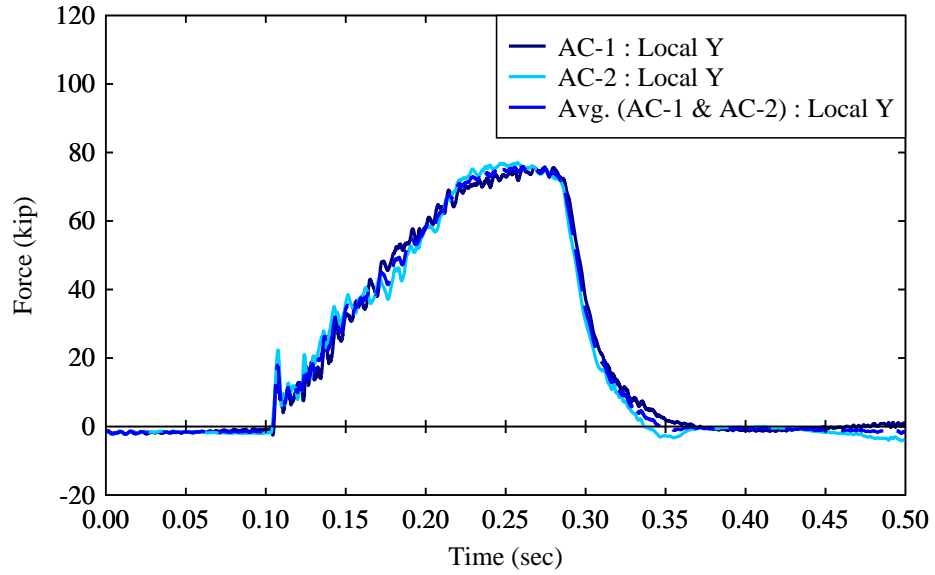


Figure 9-12 Computed impact forces from back block for R/C EOR test 1

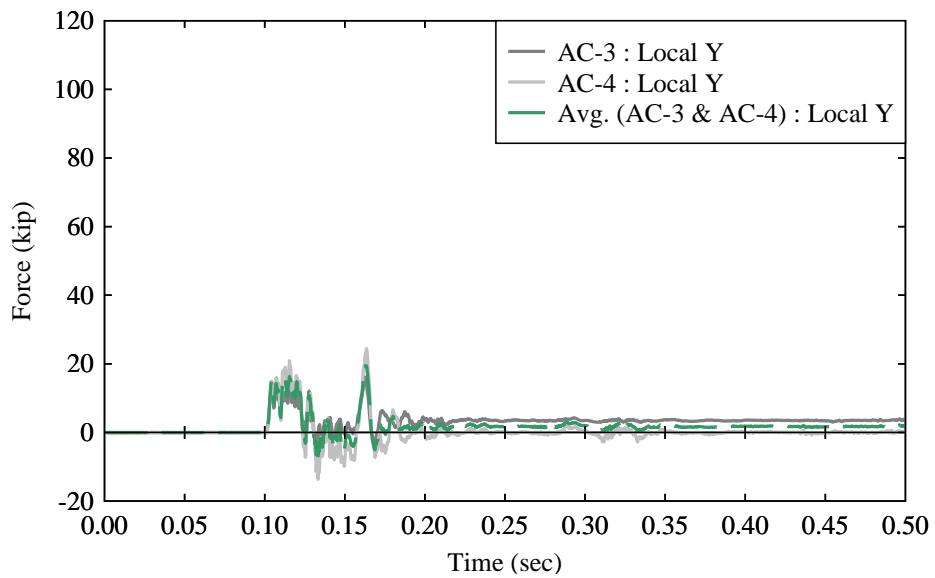


Figure 9-13 Computed impact forces from front nose for R/C EOR test 1

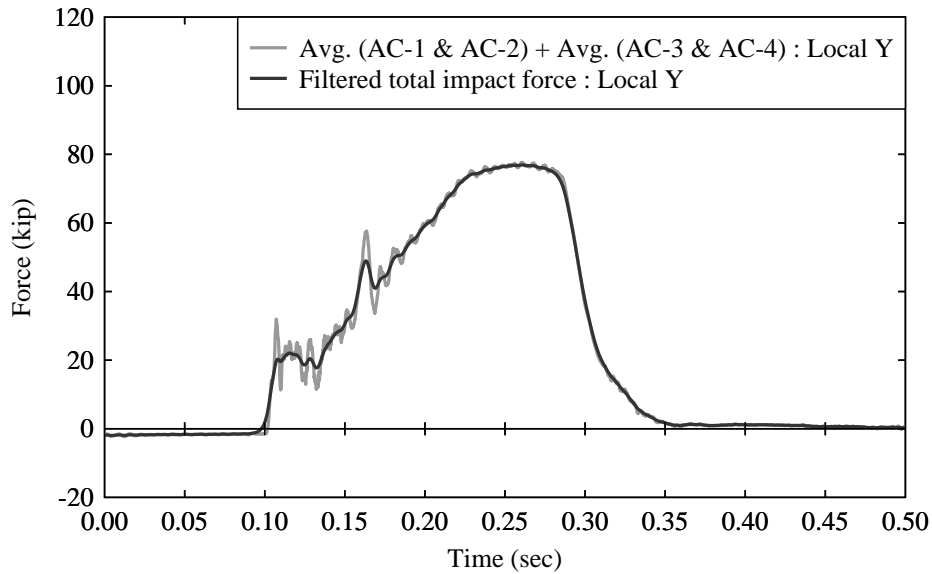


Figure 9-14 Raw and filtered total computed impact force for R/C EOR test 1

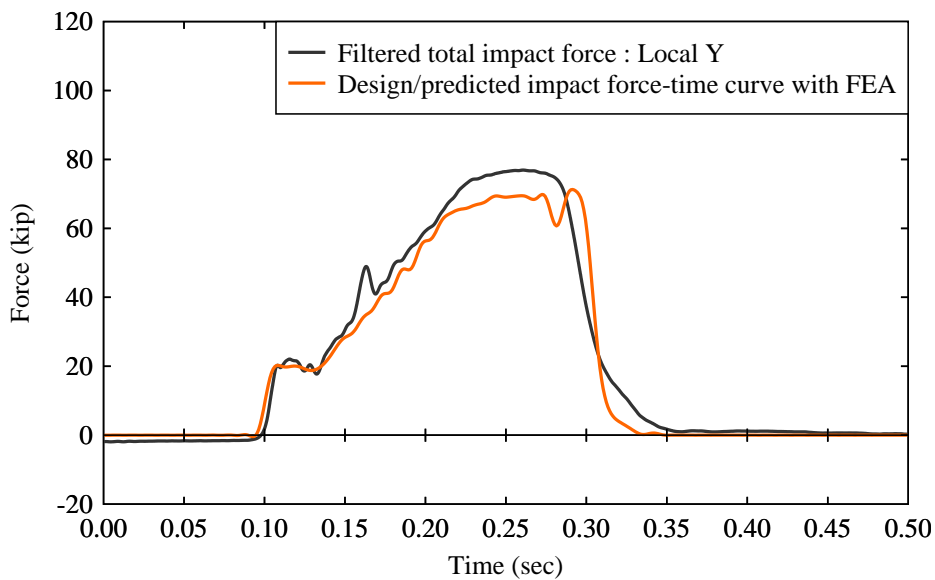


Figure 9-15 Filtered total experimental impact force for R/C EOR test 1 compared to FEA prediction

During the R/C EOR impact test, transverse deflections of the rail and any rigid sliding of the test specimen that occurred were measured with laser displacement sensors positioned behind the specimen. Further, external concrete strain measurements in the rail and deck were taken at locations along the front and back faces of the specimen. Specific locations of the laser displacement sensors (LDS) and external concrete strain gages (CSG) are depicted in Figure 9-2 (and further detailed in Appendix H).

Laser displacement data captured during R/C EOR test 1 are provided in Figure 9-16, where it is shown that the maximum displacement occurred at the free end of the rail (LDS-6) with a magnitude of 0.42 in., when the peak impact force was applied. After completion of the impact,

the maximum rail displacement reduced to approximately 0.14 in. (LDS-6), indicating that some permanent deformation occurred. Displacement sensors located along the deck of the specimen (LDS-2, LDS-5, and LDS-8) were found to record negative displacement values, indicating that there was some movement (less than 0.1 in.) in the deck—positive values indicate that the location on the specimen moved towards the sensor and negative values indicate that the location on the specimen moved further away from the sensor.

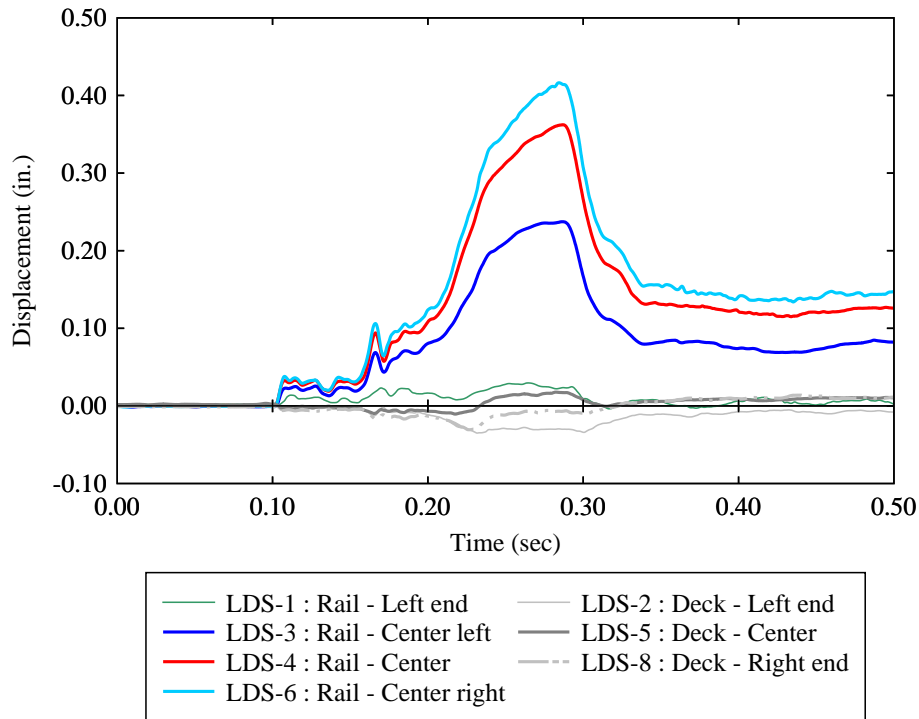


Figure 9-16 Laser displacement sensor data from R/C EOR test 1

Readings from external concrete strain gage readings for the front (impact) face of the R/C EOR test are provided in Figures 9-17 and 9-18. As previously mentioned, the surface condition of the R/C EOR specimen near the toe of the rail was relatively poor due to inadequate consolidation during casting. Consequently, a number of the concrete strain gages were shifted upwards (by about 3 in.) to ensure that the gages were properly adhered to the surface.

As previously shown in Figure 9-7, cracks were found on the front face of the rail. As a result of the cracking, a few of the concrete strain gages on the rail front face were found to reach the maximum gage limit. Once the gage limit was exceeded, readings from the gages were no longer accurate. Gage readings where the strain limit was reached – indicating that cracking occurred at the gage location – are shown in Figure 9-17. The other remaining gages with lower strain level readings located on the front face of the EOR specimen are provided in Figure 9-18.

Concrete strain readings for the back (non-impact) face of the R/C EOR are provided in Figure 9-19. Unlike the front side, no back-side gages were found to reach the maximum gage limit due to cracking, and all back-side strain readings were near or below the approximate concrete tensile rupture strain.

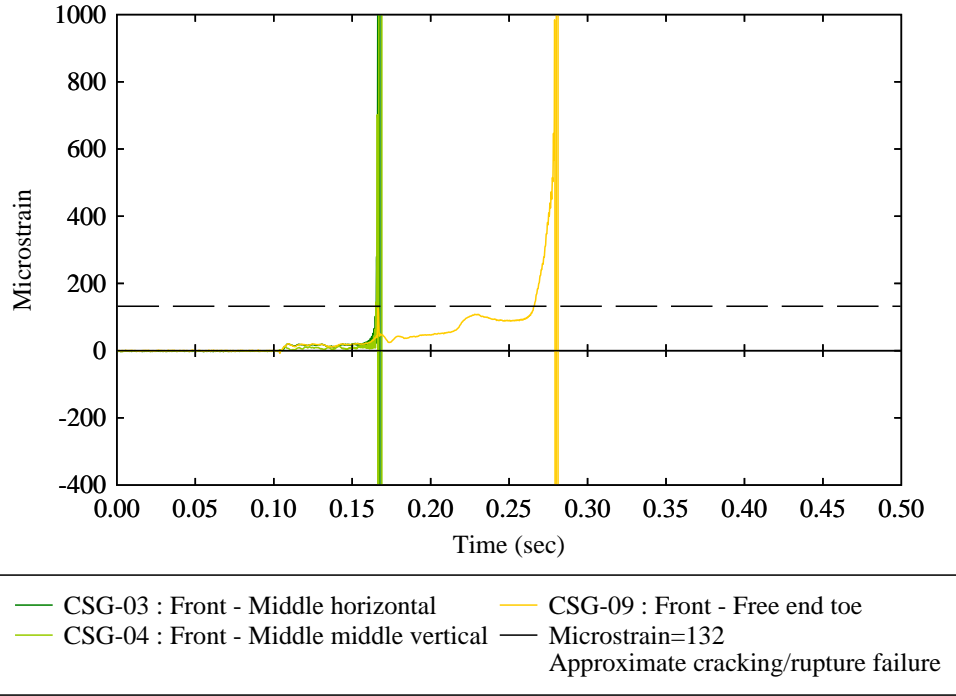


Figure 9-17 Concrete strain gage data for locations with out-of-range readings on the front face of the rail (due to cracking) for R/C EOR test 1

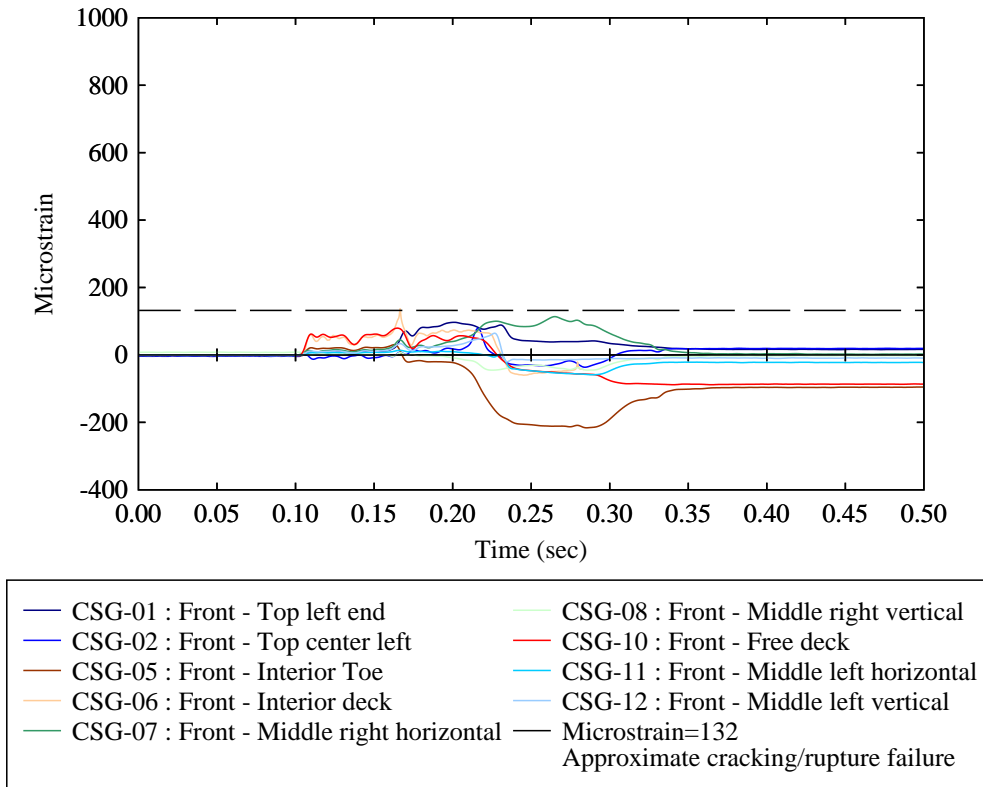


Figure 9-18 Concrete strain gage data for locations with in-range readings on the front face of the rail for R/C EOR test 1

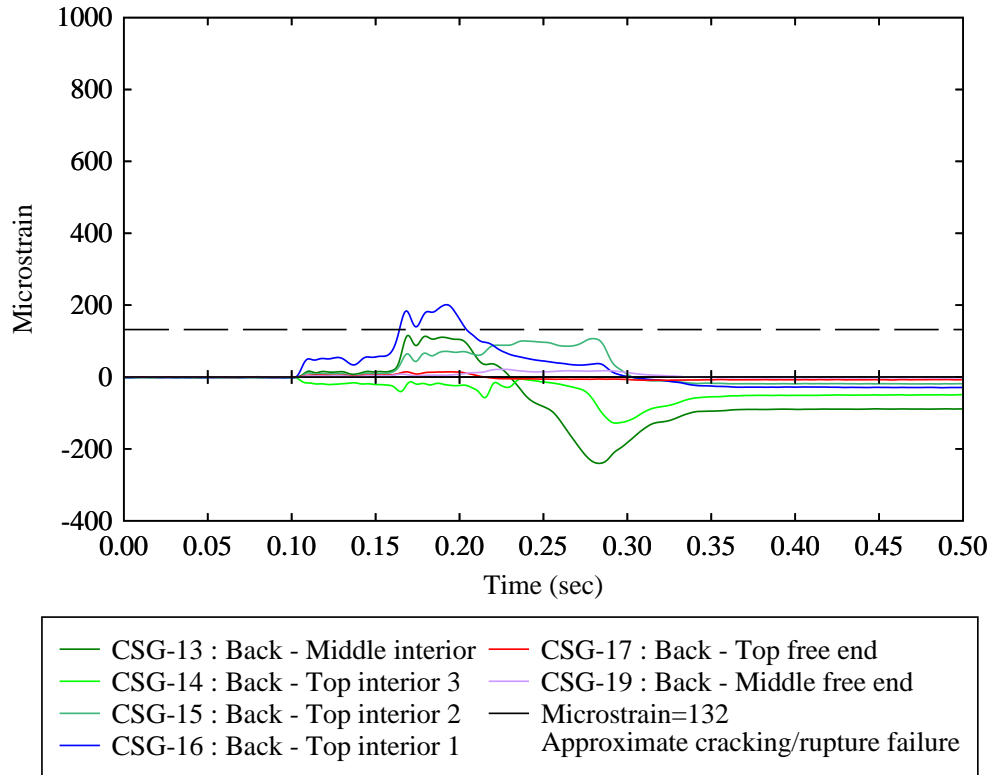
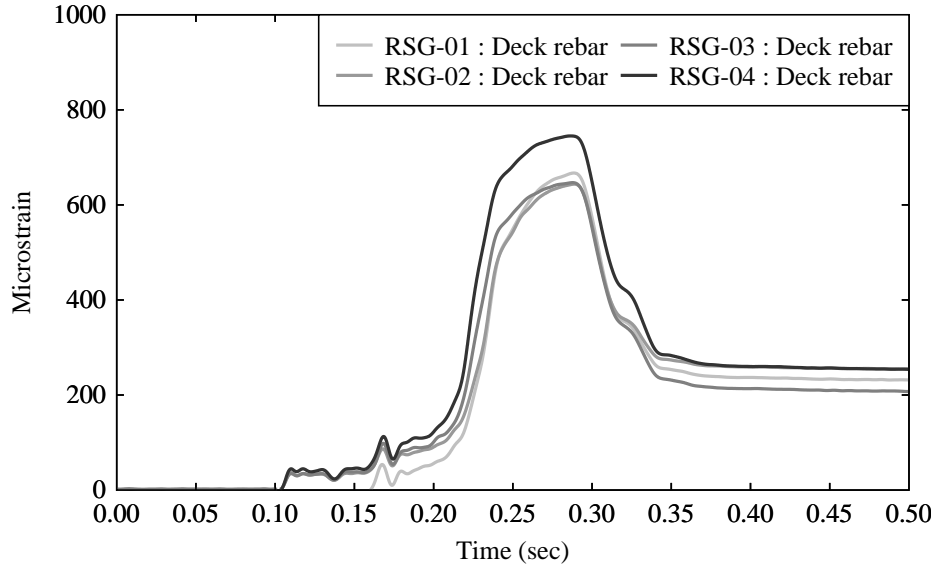
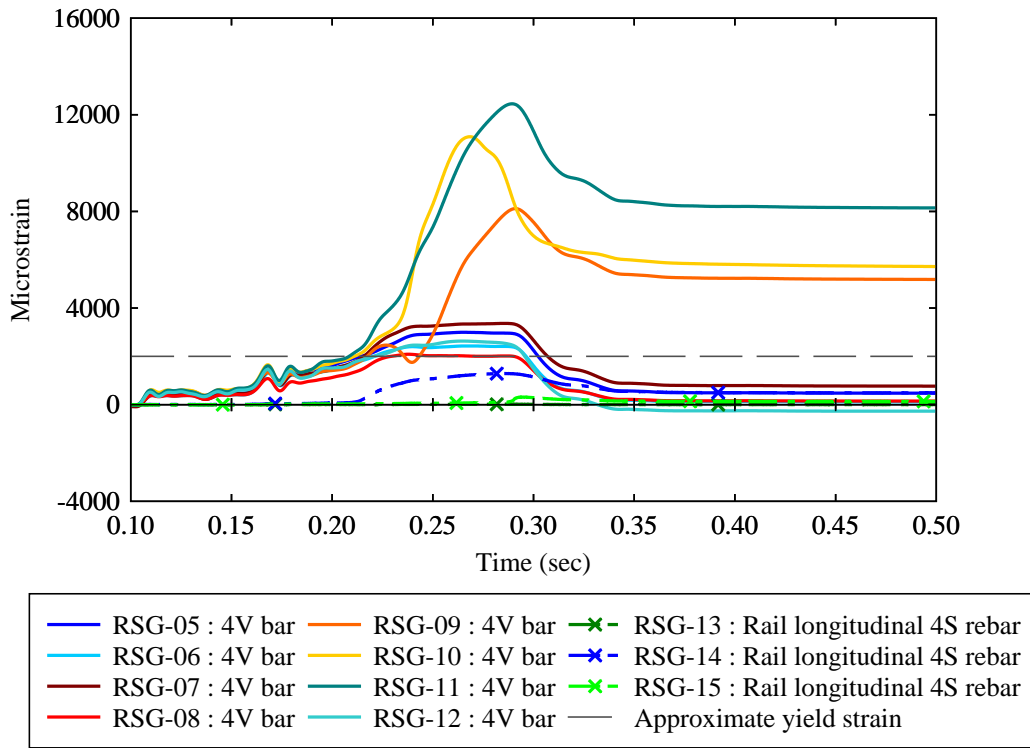


Figure 9-19 External concrete strain gage data for locations on the back face of the rail during R/C EOR test 1

Readings from internal rebar strain gages are provided in Figure 9-20. Specific locations of the deck and connection (4V) rebar gages are provided in Appendix H. Maximum strain levels in the deck rebar (Figure 9-20a) were below the steel yield strain (2000 microstrain). However, a number of gages located on the 4V connection bars (connecting the rail to the deck) reached strain levels above the rebar yield strain (Figure 9-20b), indicating that some permanent strain had occurred.



(a)



(b)

Figure 9-20 Internal rebar strain gage data during R/C EOR test 1:
(a) Deck rebar; (b) Rail rebar

9.3 GFRP rail

9.3.1 Impact testing of GFRP EOR specimen 1 (GFRP test specimen 2)

On July 30, 2021, full-scale pendulum impact testing of the GFRP EOR test 1 specimen (GFRP test specimen 2, Figure 9-21) was conducted—where the pendulum impactor was dropped from 15 ft. Instrumentation components included with the GFRP EOR test specimen were accelerometers, break beams, high-speed cameras, tape switches, laser displacement sensors, internal reinforcement strain gages, and external concrete strain gages. Additional details of the instrumentation plan used during impact testing are provided in Appendix H.



Figure 9-21 GFRP EOR specimen prepared and ready for pendulum impact testing (with instrumentation in place)

Sequential images taken from high-speed camera 1 (HSC-1) over the impact duration are provided in Figure 9-22, starting with the first instant of impact and including the point in time when the maximum crush depth on the crushable front nose (i.e., maximum impact force) was reached. Additional images from high-speed camera 2 (HSC-2) are provided in Figure 9-23. Photographs of the test specimen after completion of the impact test are shown in Figure 9-24.



Figure 9-22 High-speed video frames from HSC-1 (GFRP EOR test 1) showing crush deformation of aluminum honeycomb: (a) At initial impact; (b) – (c) Intermediate frames; (f) At peak impact force

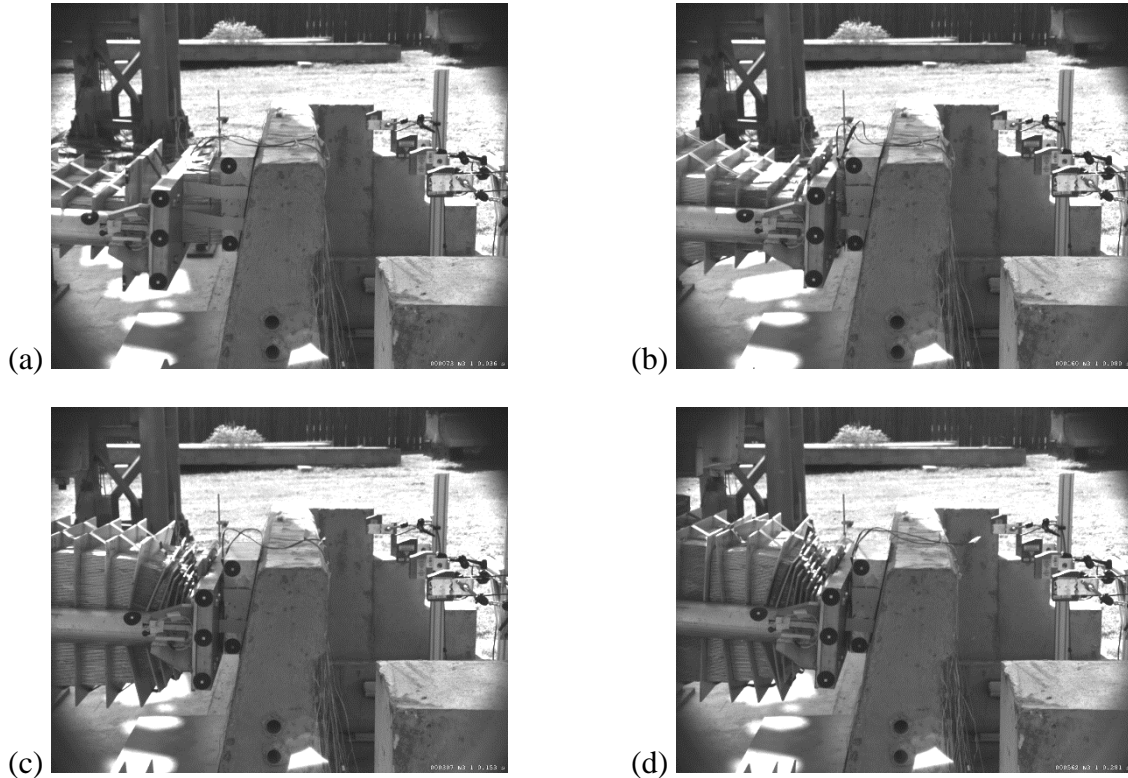


Figure 9-23 High-speed video frames from HSC-2 (GFRP EOR test 1): (a) At start of impact; (b) – (c) Intermediate frames; (d) At peak impact force

For the GFRP EOR-1 test, diagonal cracks were found on the front and back faces of the rail and were similar to the predicted failure pattern in AASHTO LRFD (2017). Cracks found in the test specimen were marked with a black marker to more clearly document where cracking occurred (in photographs). Some of the cracks on the front (impact) and the back (non-impact) faces of the GFRP EOR specimen were found to be wider than 0.10 in. (for example Figure 9-25). A significant crack (wider than 0.10 in.) was also observed in the portion of deck located beyond the end of the rail (Figure 9-26).



(a)



(b)

Figure 9-24 Cracking found on GFRP EOR-1 test specimen after impact: (a) On front rail face;
(b) On back rail face



Figure 9-25 Crack on the back face of GFRP EOR-1 specimen with width wider than 0.10 in.



Figure 9-26 Crack in deck with no rail on top (looking towards the back face)

Break beam voltage data from GFRP EOR impact test 1 are provided in Figure 9-27, and were used to quantify the impact velocity. For GFRP EOR test 1, the impact velocity was determined to be 32 ft/sec—compared to the design impact velocity of 31.1 ft/sec (a 2.9% difference). Tape switch data are shown in Figure 9-28. Note that all impact test data has been shifted such that the initiation of impact begins at 0.1 s, using the spike in tape switch voltage.

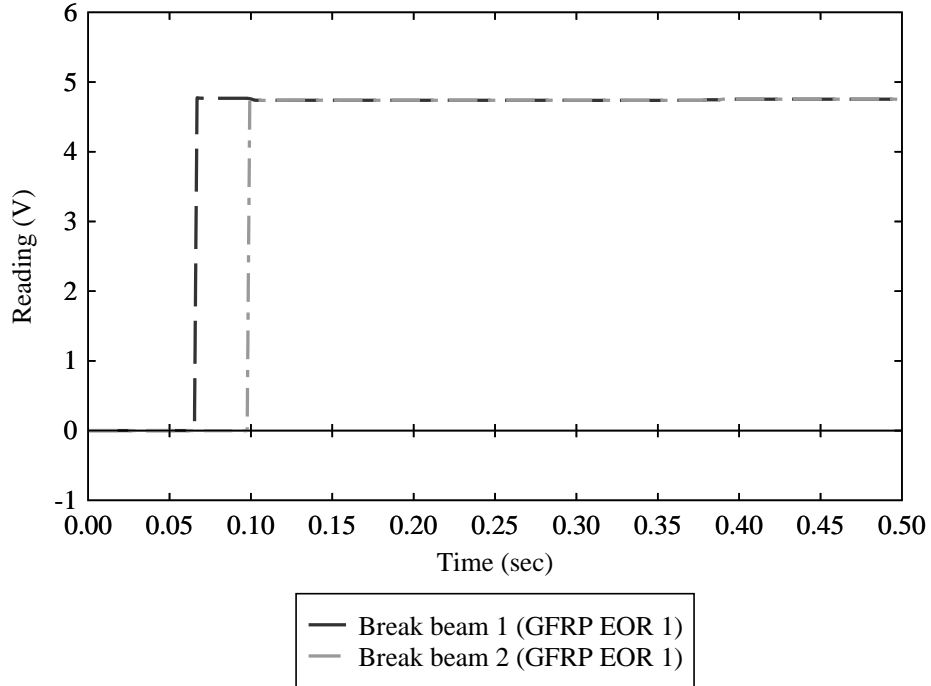


Figure 9-27 Break beam data for GFRP EOR test 1

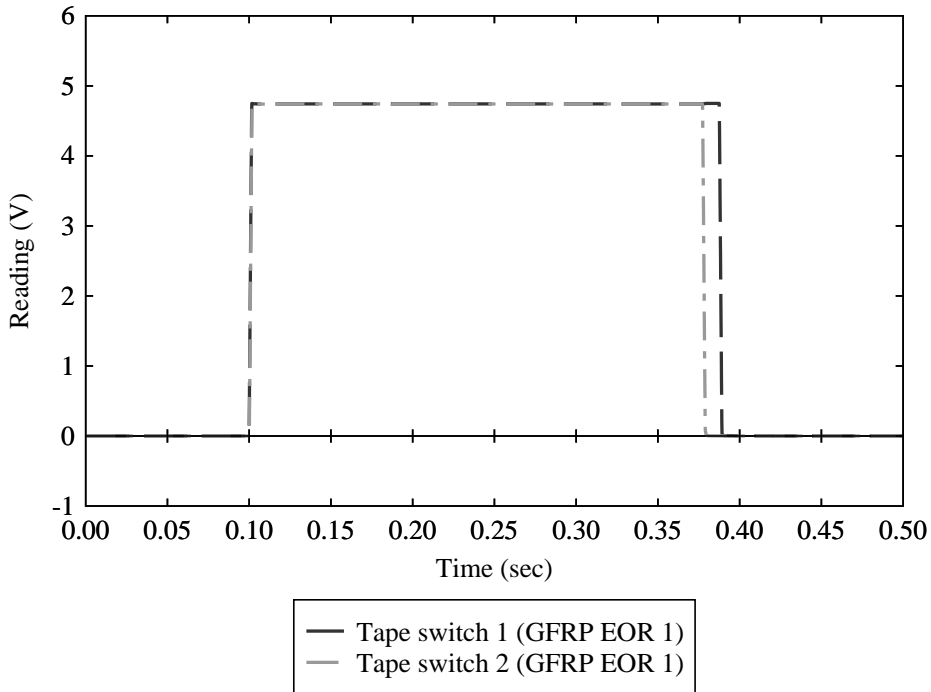


Figure 9-28 Tape switch data for GFRP EOR test 1

Measured accelerations from the two accelerometers on the concrete back block (AC-1 & AC-2) in the impact direction (i.e., local Y direction of the accelerometer) are shown in Figure 9-29. Correspondingly, measured accelerations from the two accelerometers on the

aluminum front nose (AC-3 & AC-4) in the impact direction (local Y direction) are shown in Figure 9-30. Computed and averaged back block impact forces (from AC-1 & AC-2) are shown in Figure 9-31, while the computed and averaged front nose impact forces (from AC-3 & AC-4) are shown in Figure 9-32.

The total applied impact force, computed by combining the averages of the back block and front nose, is shown in Figure 9-33. In comparison with the designed/predicted maximum impact forces shown in Figure 9-34, which provides the predicted impact force over time from previous FEA impact simulations, the maximum observed impact force from GFRP EOR test 1 was found to be 75 kip, 9% greater than the originally designed 68.8-kip peak impact force.

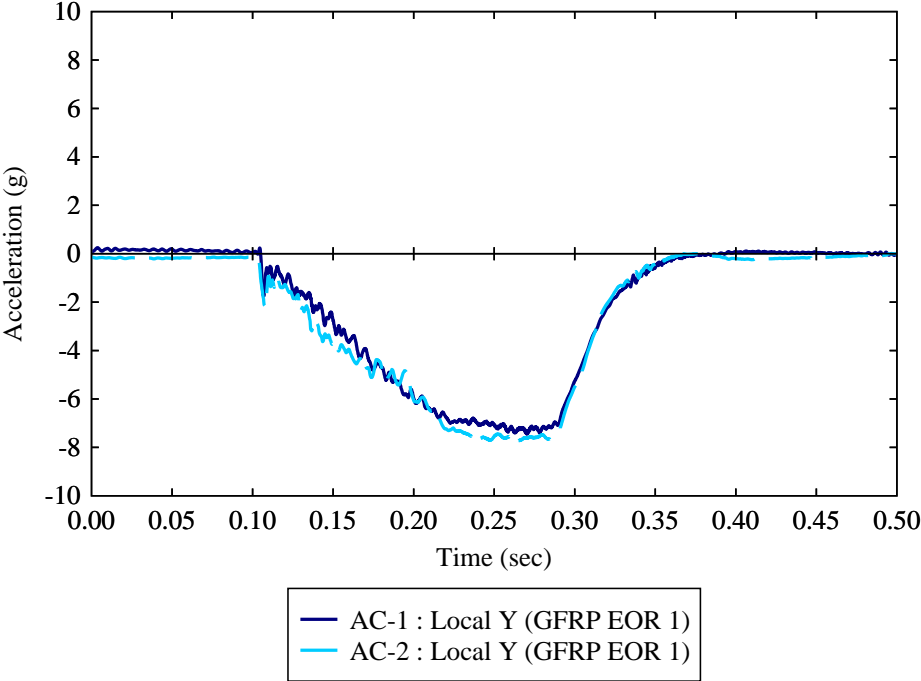


Figure 9-29 Raw concrete back block acceleration data (AC-1 & AC-2) for GFRP EOR test 1 (in the impact direction, local Y direction of accelerometer)

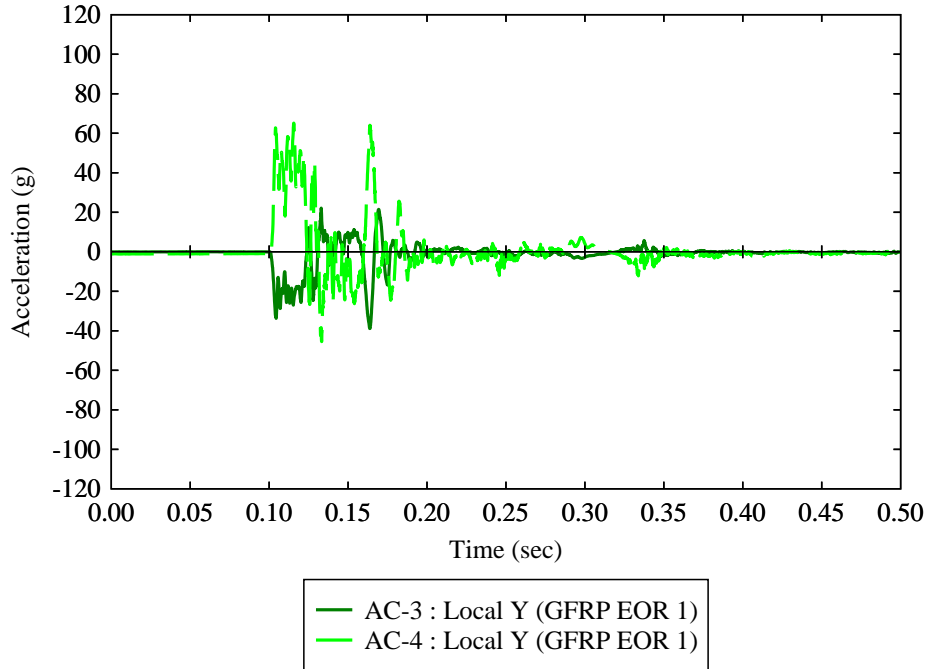


Figure 9-30 Raw front nose acceleration data (AC-3 & AC-4) for GFRP EOR test 1 (in the impact direction, local Y direction of accelerometer)

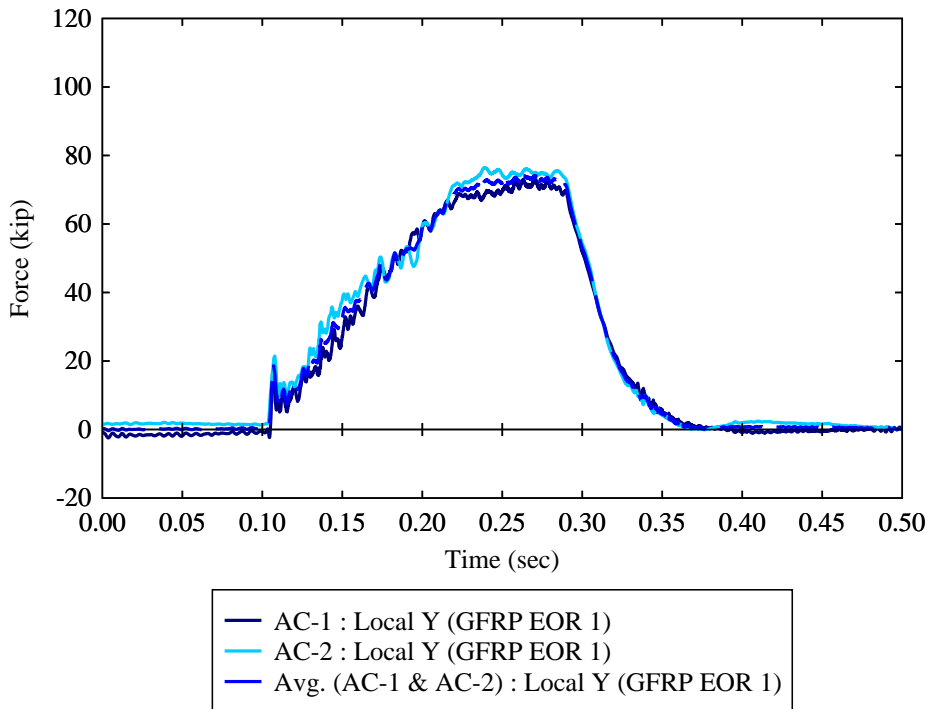


Figure 9-31 Computed impact forces from back block for GFRP EOR test 1

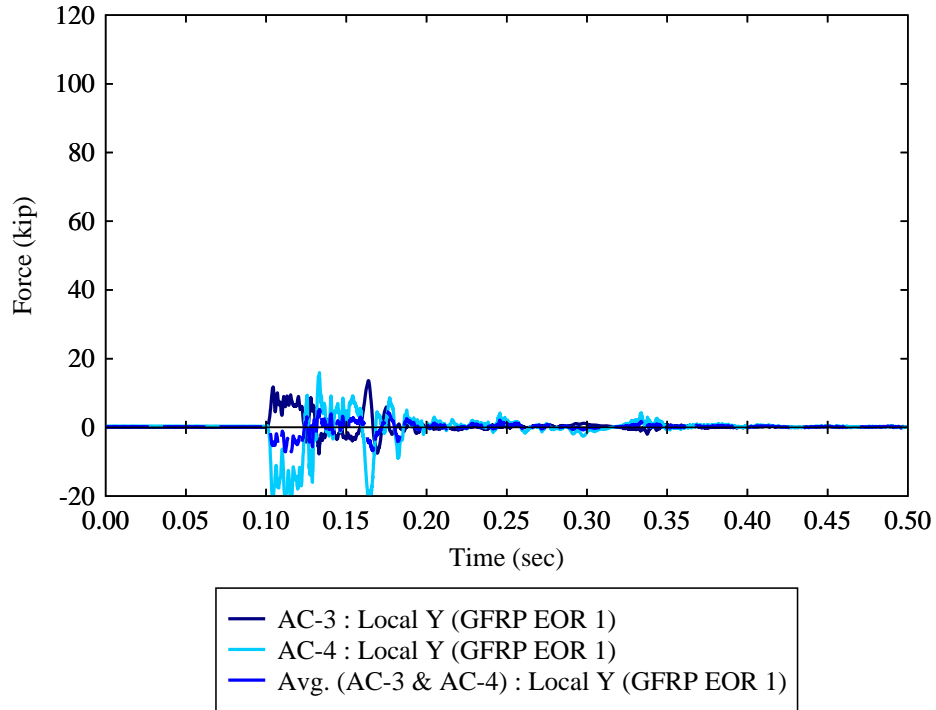


Figure 9-32 Computed impact forces from front nose for GFRP EOR test 1

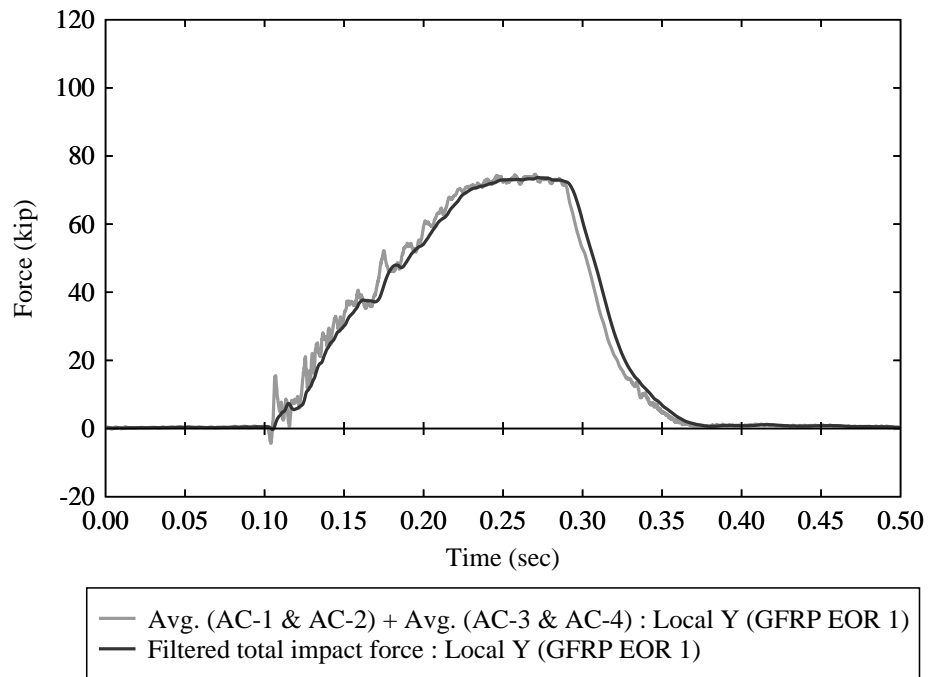


Figure 9-33 Raw and filtered total computed impact force for GFRP EOR test 1

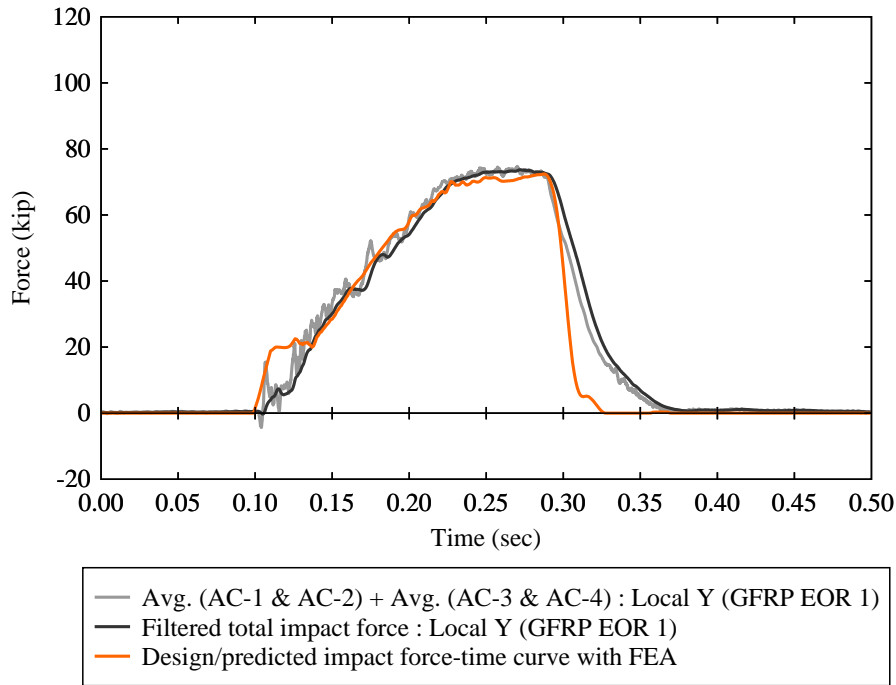


Figure 9-34 Filtered total experimental impact force for GFRP EOR test 1 compared to FEA prediction

During the GFRP EOR impact test, transverse deflections of the rail and any rigid sliding of the test specimen that occurred were measured with laser displacement sensors positioned behind the specimen. Further, external concrete strain measurements in the rail and deck were taken at locations along the front and back faces of the specimen. Specific locations of the laser displacement sensors (LDS) and external concrete strain gages (CSG) are depicted in Figure 9-2 (and further detailed in Appendix H).

Laser displacement data measured during GFRP EOR test 1 are provided in Figure 9-35, where it is shown that the maximum displacement occurred at the free end of the rail (LDS-6) with a magnitude of 1.88 in., when the peak impact force was applied. After completion of the impact, the maximum rail displacement reduced to approximately 0.84 in. (LDS-6), indicating that some permanent deformation occurred. Displacement sensors located at the ends of deck in the specimen (LDS-2 and LDS-8) were found to record almost zero displacement. On the other hand, displacement sensor LDS-5 at the center of the deck recorded a maximum displacement of 0.18 in. at peak impact force and a permanent deformation of 0.09 in. after impact. This displacement in the center of the deck corresponded to the crack formation through the deck that occurred during impact (recall Figure 9-26).

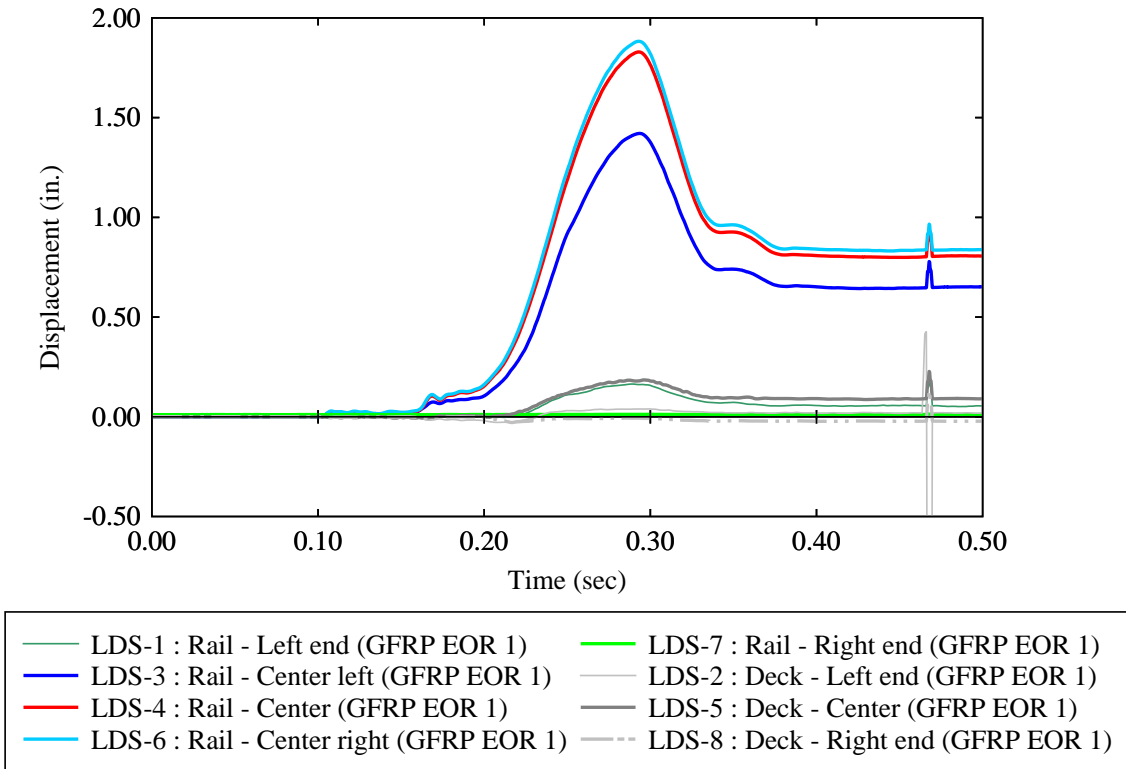


Figure 9-35 Laser displacement sensor data from GFRP EOR test 1

External strain gage readings for the front (impact) face of the GFRP EOR test are provided in Figures 9-36 and 9-37. As previously shown in Figure 9-24, diagonal cracks formed on the front face of the rail. As a result of the cracking, multiple concrete strain gages on the rail front face were found to have reached the maximum gage limit. Once the gage limit was exceeded, readings from the gages were no longer accurate. Gage readings where the strain limit was reached, indicating that cracking occurred at the gage location, are shown in Figure 9-36. The other remaining gages with lower strain level readings located on the front side of the EOR specimen are provided in Figure 9-37.

Strain readings for the back (non-impact) side of the GFRP EOR are provided in Figure 9-38. Similar to the front side, CSG-13, CSG-14 and CSG-16 were found to have reached the maximum gage limit as a result of the cracking that formed on the back side of the rail. The remaining gages were found to record strain levels near or below the approximate rupture strain.

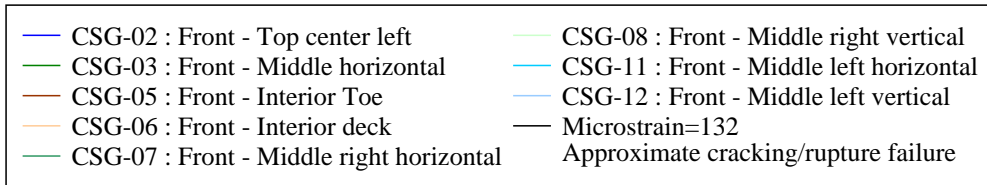
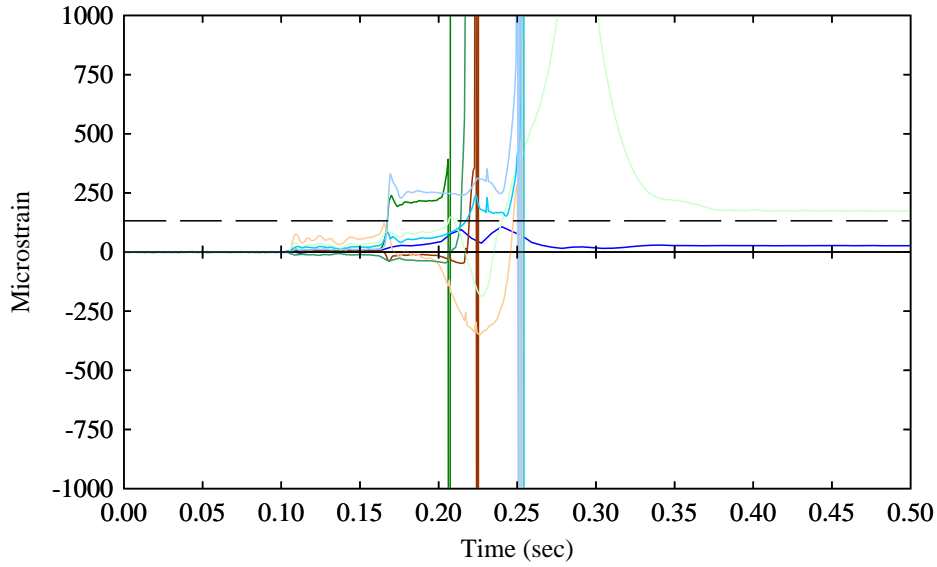


Figure 9-36 Concrete strain gage data for locations with out-of-range readings (due to cracking) for GFRP EOR test 1

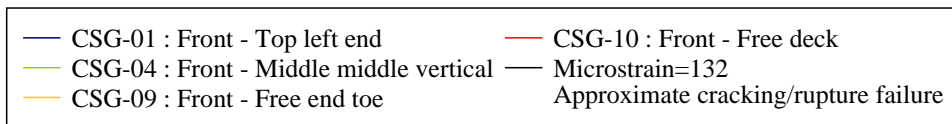
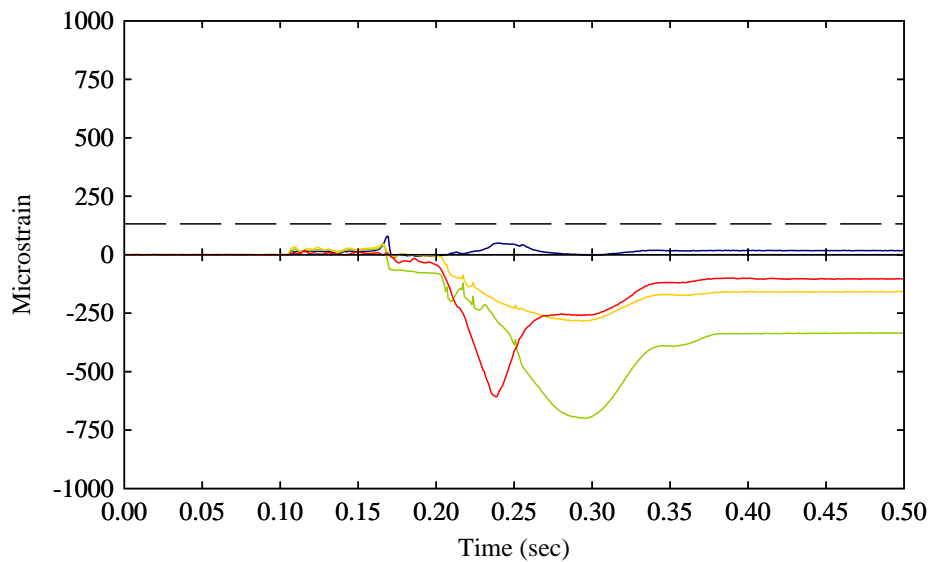


Figure 9-37 Concrete strain gage data for locations with in-range readings for GFRP EOR test 1

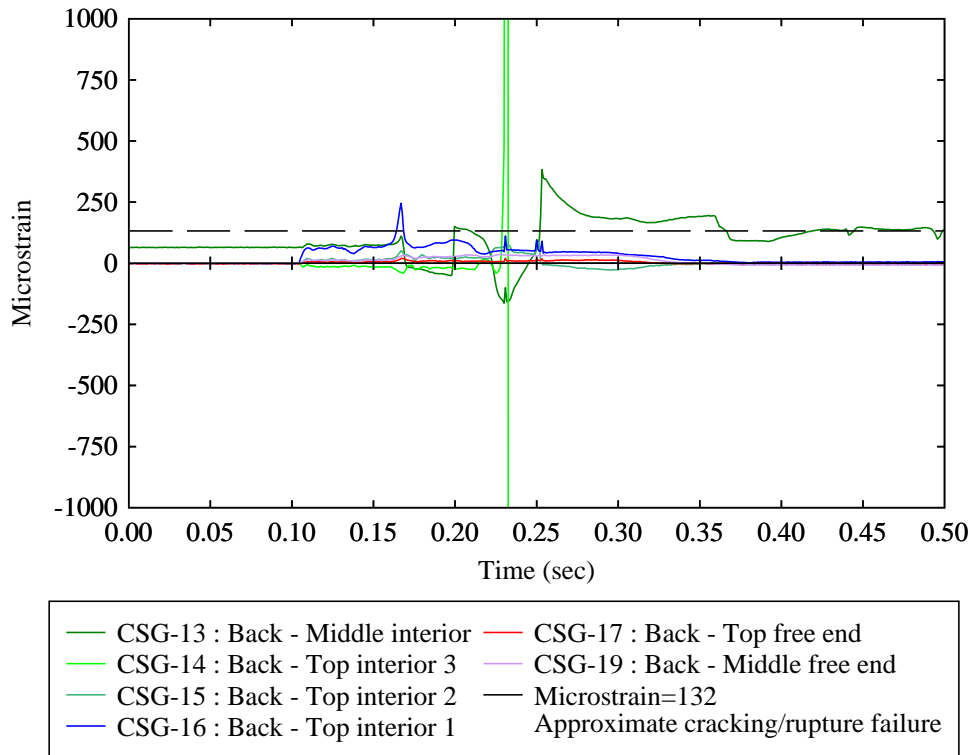
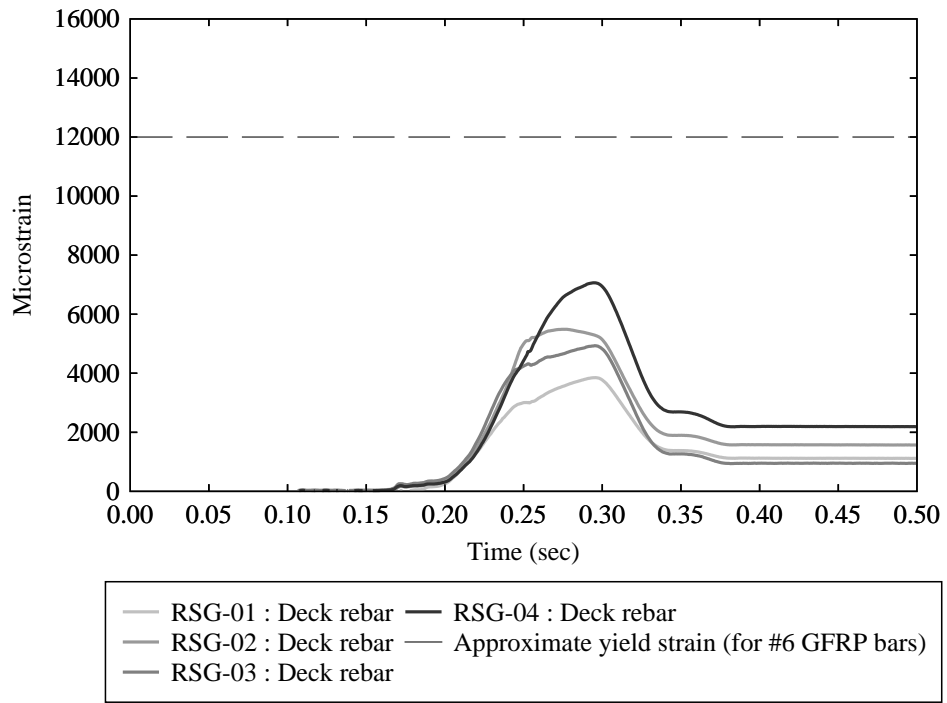


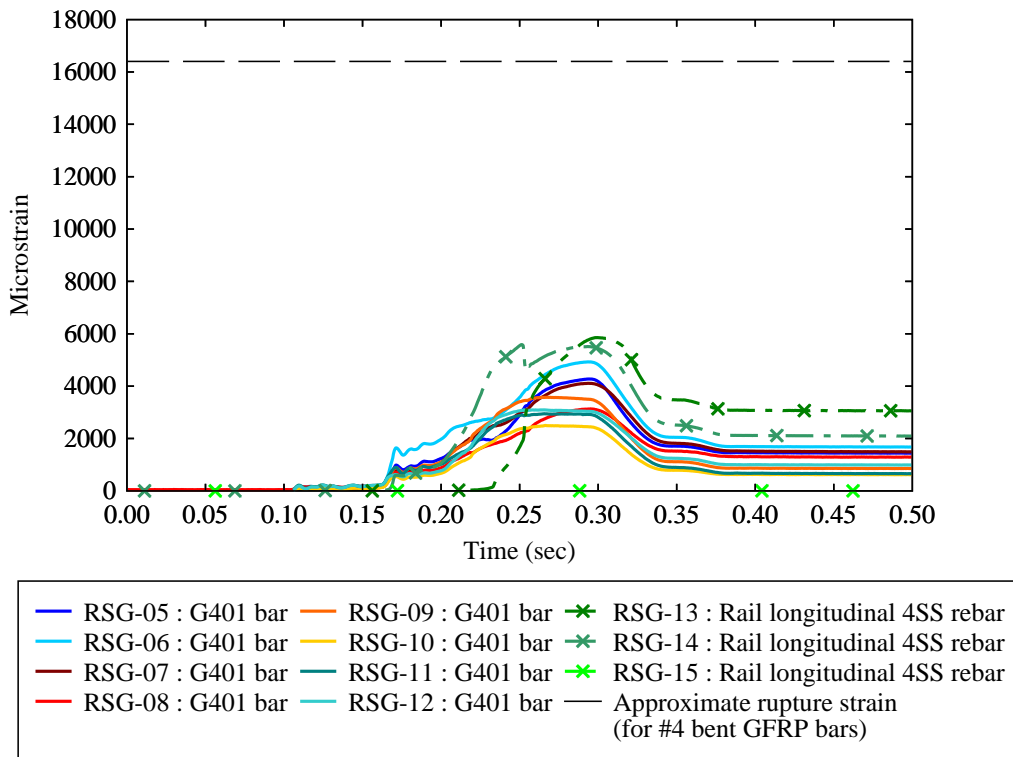
Figure 9-38 Concrete strain gage data for locations on the back (non-impact) face of the rail during GFRP EOR test 1

Readings from rebar strain gages are provided in Figure 9-39. Specific locations of the deck and connection (G401) rebar gages are provided in Appendix H. Maximum strain levels in the deck rebar (Figure 9-39a) were found to be below the ultimate strain levels of the GFRP bars. Table 4-1 provides the ultimate strains for different GFRP bars.

Given that the maximum bars strains remained well below the ultimate rupture levels, the larger than expected magnitudes of recorded rail displacements (peak transient and permanent) suggested that the full strength of the GFRP bars had not been developed during impact. This was further supported by the observed formation of a significant through-thickness crack in the deck portion of the specimen (Figure 9-26). It was hypothesized that insufficient length was available to develop the strength of the GFRP S601 deck bars in the area near the end of the rail, and that consequently, the GFRP S601 bars slipped thereby producing significant deck cracking and increased rail displacement. Following completion of impact testing, samples of GFRP bars and surrounding concrete were dissected at various locations in the deck. Two locations (Figure 9-40) provided apparent confirmation of the bond-slip hypothesis. At a location approximately 8 in. from the end of the rail (i.e., ‘near’ the EOR), indications of partial slip were apparent on the ‘lugs’ of the top layer GFRP bar (Figure 9-41a), and in the surrounding concrete. In this area, flexural moment in the deck, and tensile forces in the top layer of GFRP S601 bars were significant during impact loading. In contrast, at a more distant location (approximately 30 in. from the end of rail), where flexural moment and bar tensile force were reduced, no indication of slip was apparent (Figure 9-41b). To address the bond slip issue, an additional GFRP EOR specimen with additional GFRP deck reinforcement bars was constructed and impact tested, as described in the following section.



(a)



(b)

Figure 9-39 Internal rebar strain gage data during GFRP EOR test 1:
 (a) Deck rebar; (b) Rail rebar

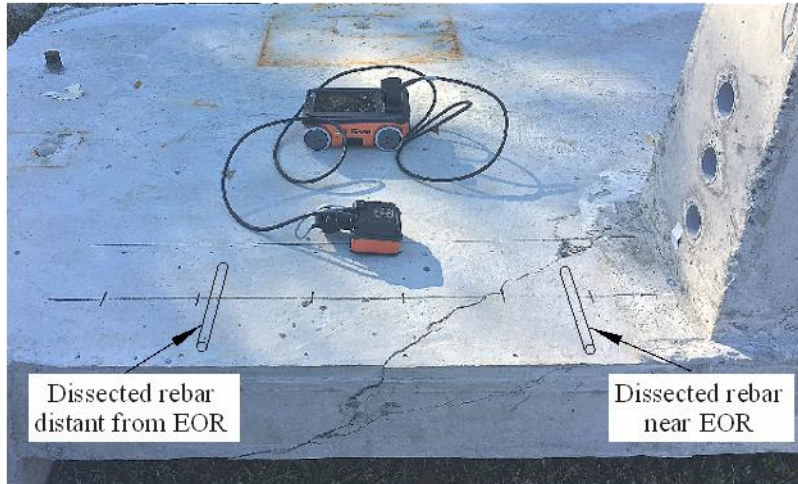
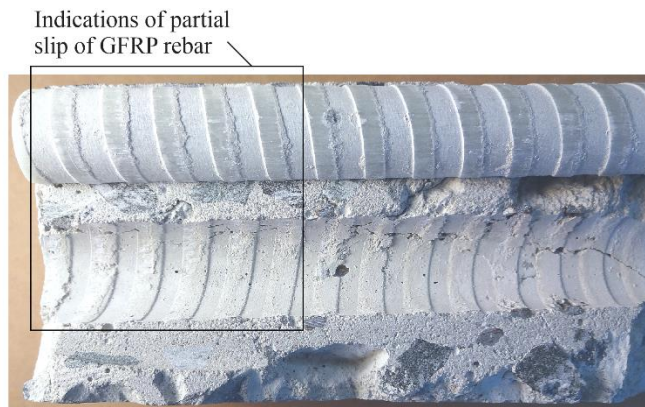
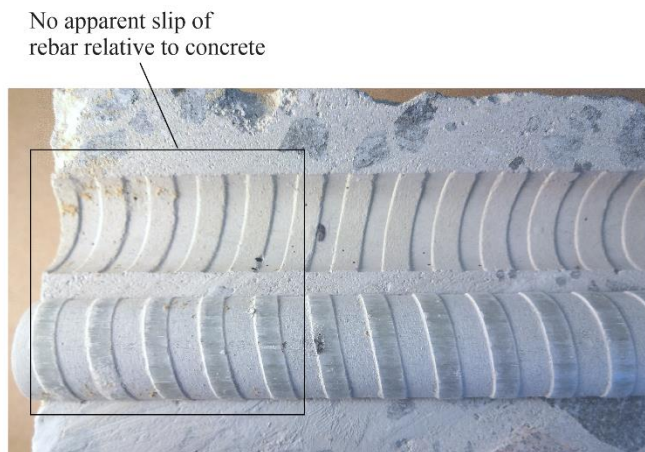


Figure 9-40 Approximate locations at which GFRP bars were dissected from GFRP EOR rail specimen 1



(a)



(b)

Figure 9-41 Dissected top layer GFRP rebars and surrounding concrete: (a) Location near end of rail (EOR); (b) Location distant from EOR

9.3.2 Impact testing of GFRP EOR specimen 2 (GFRP test specimen 3)

On November 10, 2021, full-scale pendulum impact testing of the GFRP EOR test 2 specimen (GFRP test specimen 3, Figure 9-42) was conducted. Similar to the GFRP EOR test 1, the pendulum impactor in the GFRP EOR test 2 was dropped from 15 ft. Instrumentation components for this specimen were also the same as the GFRP EOR test 1 specimen. However, the reinforcement in the EOR-2 specimen was modified based on observations from testing of the EOR test 1 specimen. Based on the hypothesis that the full strength of the GFRP S601 deck bars was not developed, and that the bars slipped relative to the concrete (resulting in larger than expected rail deflection and deck cracking), additional GFRP G403 (90-deg. hooked #4) bars were added to the EOR test 2 specimen to promote improved bond to the concrete deck (Figure 9-43). Also, to better control cracking in the rail itself, installations of G401 and G402 bars were extended through two additional positions longitudinally along the length of the rail. Finally, to ensure that adverse cracking would not occur at the supported end of the now-strengthened GFRP EOR specimen, additional steel 4V and 4P bars were added in the buttress region.



Figure 9-42 GFRP EOR test 2 specimen prepared and ready for pendulum impact testing (with instrumentation in place)

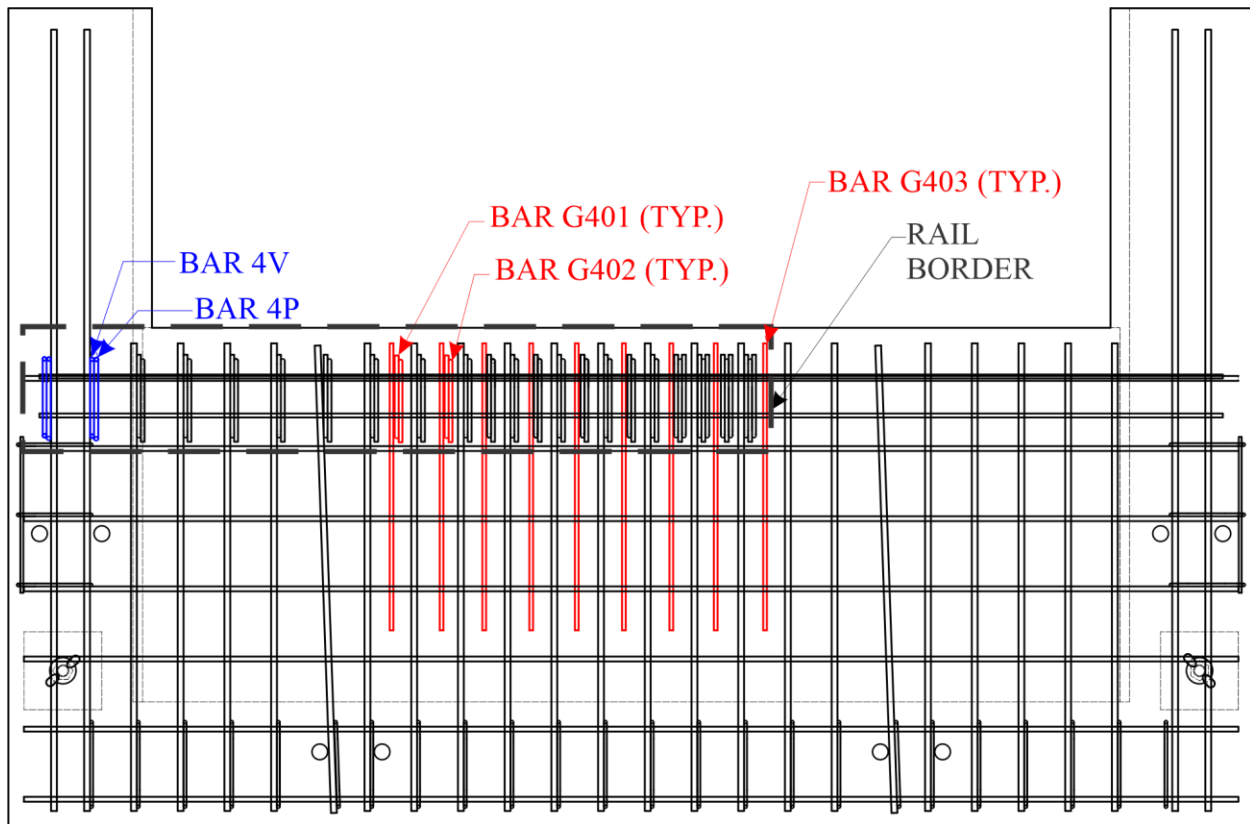


Figure 9-43 Additional rebar in GFRP EOR test 2 specimen (plan view of deck and rail reinforcement shown)

Unfortunately, during the GFRP EOR specimen 2 testing, both high-speed cameras (1 and 2) erroneously triggered prior to impact, therefore high-speed video images of the specimen during the impact were not collected. However, all remaining sensors (strain gages, accelerometers, etc.) were connected to an independent data acquisition system (separate from the high-speed cameras), and therefore data from these sensors were properly collected.

Similar to GFRP EOR-1 specimen, after impact testing, diagonal cracks were found on the front and back faces of the GFRP EOR-2 rail (Figure 9-44) as predicted by the failure pattern described in AASHTO LRFD (2017). However, the maximum crack width in the GFRP EOR-2 rail was found to be 0.035 in. as compared to the greater than 0.1 in. width found in the GFRP EOR-1 specimen. Further, the maximum crack width (0.005 in.) in the deck of the GFRP EOR-2 specimen (Figure 9-45) was also found to be much smaller than the crack width in the deck of the GFRP EOR-1 specimen (greater than 0.1 in.).

The additional GFRP rebars (G401, G402, G403) that were added to the GFRP EOR test 2 specimen (Figure 9-43) were found to be effective in improving the performance of the rail under impact loading; concrete crack widths were reduced as were rail deflections (discussed below). Additionally, the maximum crack widths in the GFRP EOR-2 specimen were of the same order of magnitude as those observed in the R/C EOR specimen.



(a)



(b)

Figure 9-44 Cracks on GFRP EOR test 2 test specimen after impact: (a) On front rail face; (b) On back rail face



Figure 9-45 Crack in deck with no rail on top (looking towards the back face)

Break beam voltage data from GFRP EOR impact test 2 are provided in Figure 9-46, and were used to quantify the impact velocity. For GFRP EOR test 2, the impact velocity was determined to be 31 ft/sec—compared to the design impact velocity of 31.1 ft/sec (a 0.3% difference). Tape switch data are shown in Figure 9-47. Note that all impact test data has been shifted such that the initiation of impact begins at 0.1 s, using the spike in tape switch voltage.

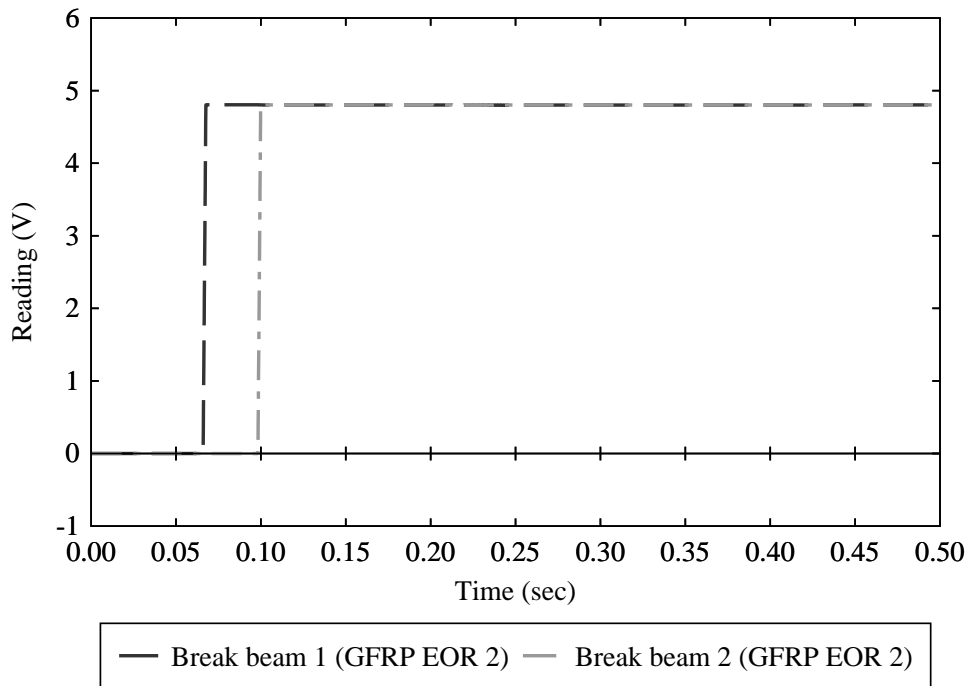


Figure 9-46 Break beam data for GFRP EOR test 2

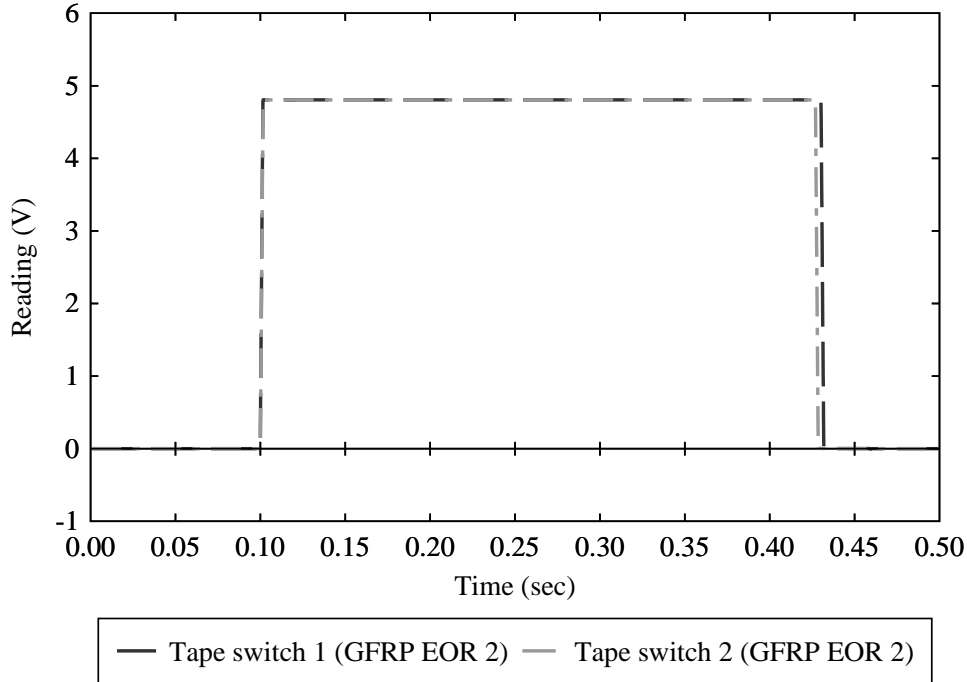


Figure 9-47 Tape switch data for GFRP EOR test 2

Measured accelerations from the two accelerometers on the concrete back block (AC-1 & AC-2) in the impact direction (i.e., local Y direction of the accelerometer) are shown in Figure 9-48. Correspondingly, measured accelerations from the two accelerometers on the aluminum front nose (AC-3 & AC-4) in the impact direction (local Y direction) are shown in Figure 9-49. Computed and averaged back block impact forces (from AC-1 & AC-2) are shown in Figure 9-50, while the computed and averaged front nose impact forces (from AC-3 & AC-4) are shown in Figure 9-51.

The total applied impact force, computed by combining the averages of the back block and front nose, is shown in Figure 9-52. In comparison with the designed/predicted maximum impact forces shown in Figure 9-53, which provides the predicted impact force over time from previous FEA impact simulations, the maximum observed impact force from GFRP EOR test 2 was found to be 74 kip, 7.6% greater than the originally designed 68.8-kip peak impact force.

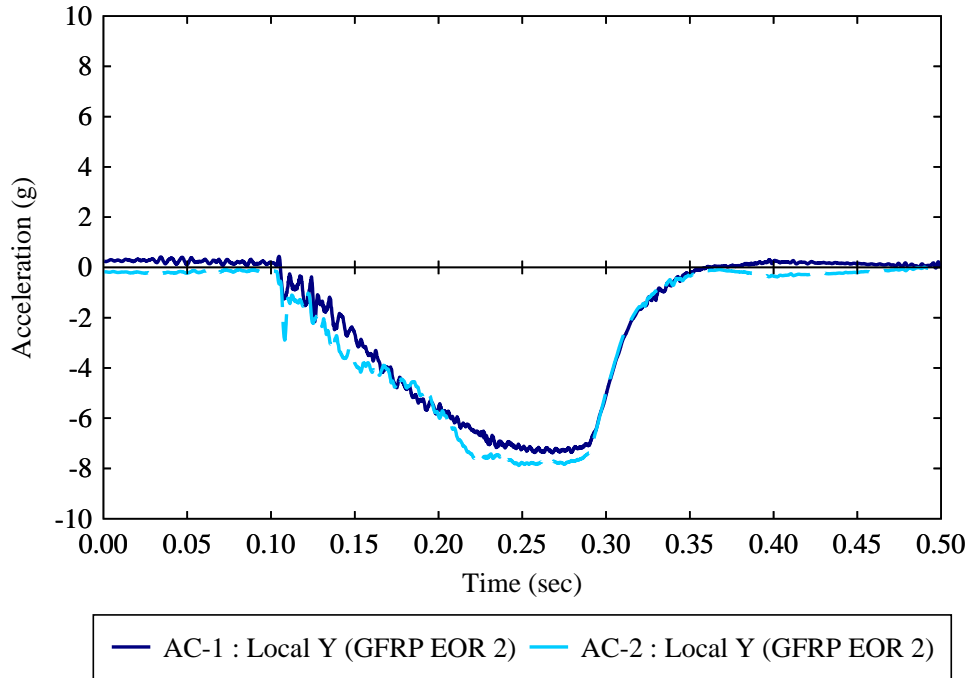


Figure 9-48 Raw concrete back block acceleration data (AC-1 & AC-2) for GFRP EOR test 2 (in the impact direction, local Y direction of accelerometer)

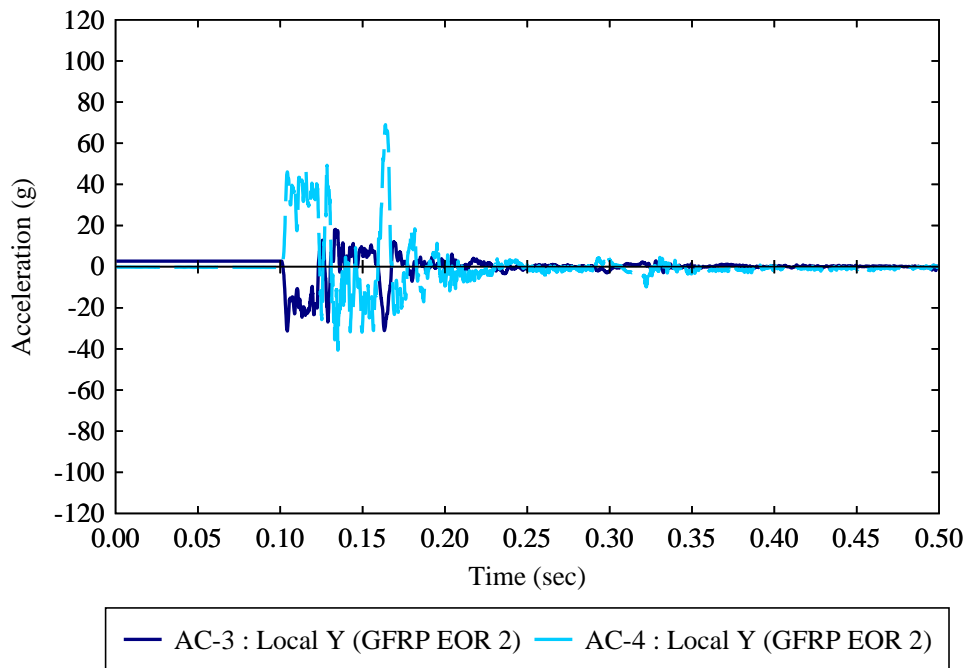


Figure 9-49 Raw front nose acceleration data (AC-3 & AC-4) for GFRP EOR test 2 (in the impact direction, local Y direction of accelerometer)

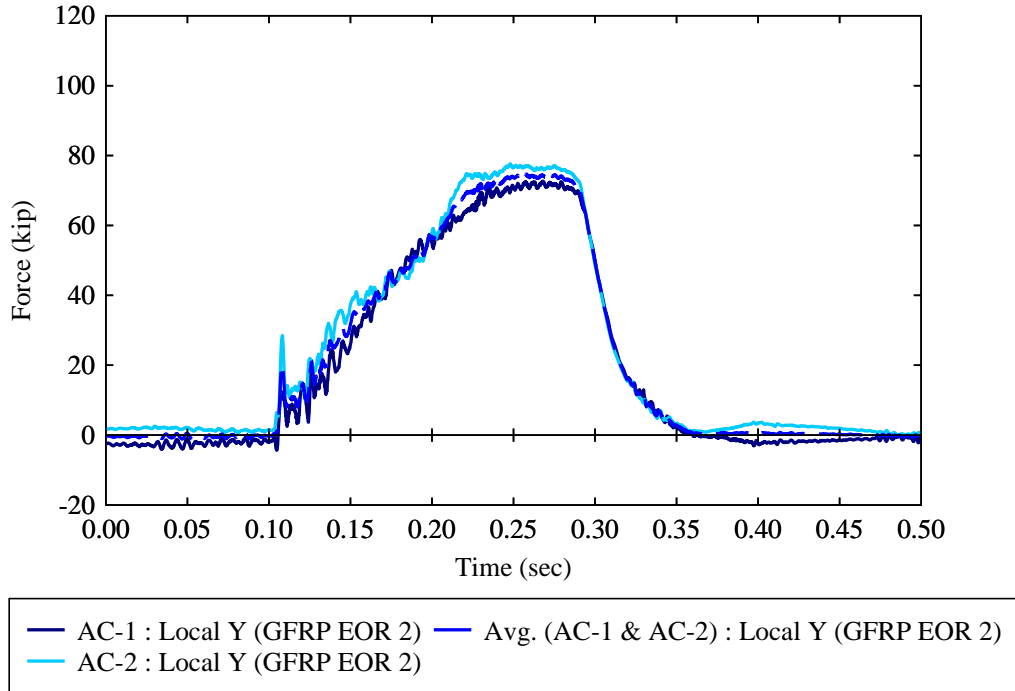


Figure 9-50 Computed impact forces from back block for GFRP EOR test 2

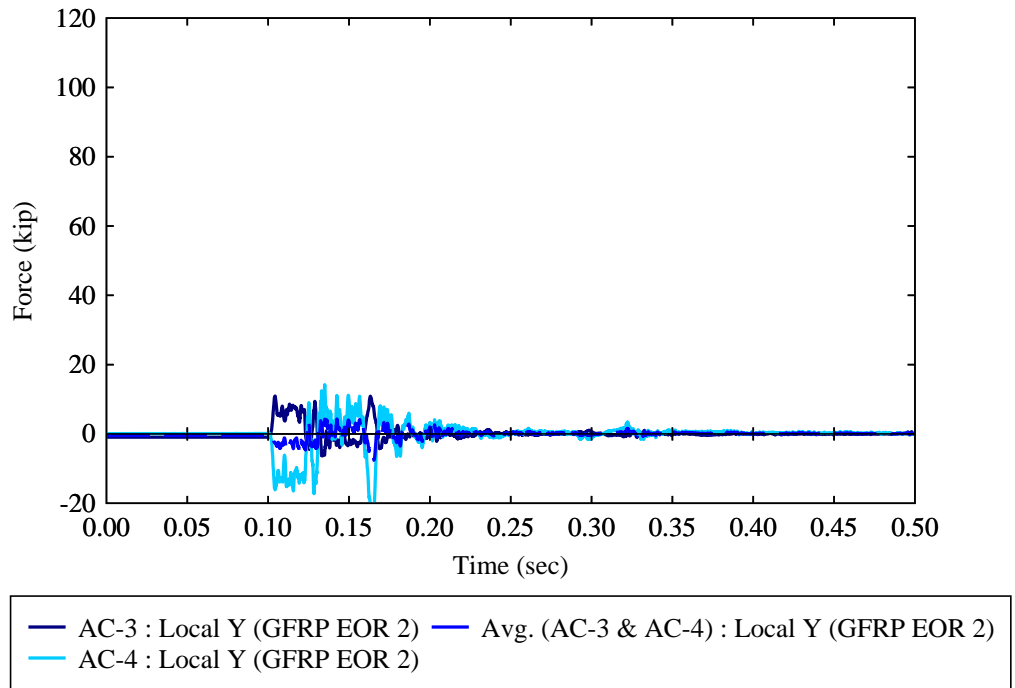


Figure 9-51 Computed impact forces from front nose for GFRP EOR test 2

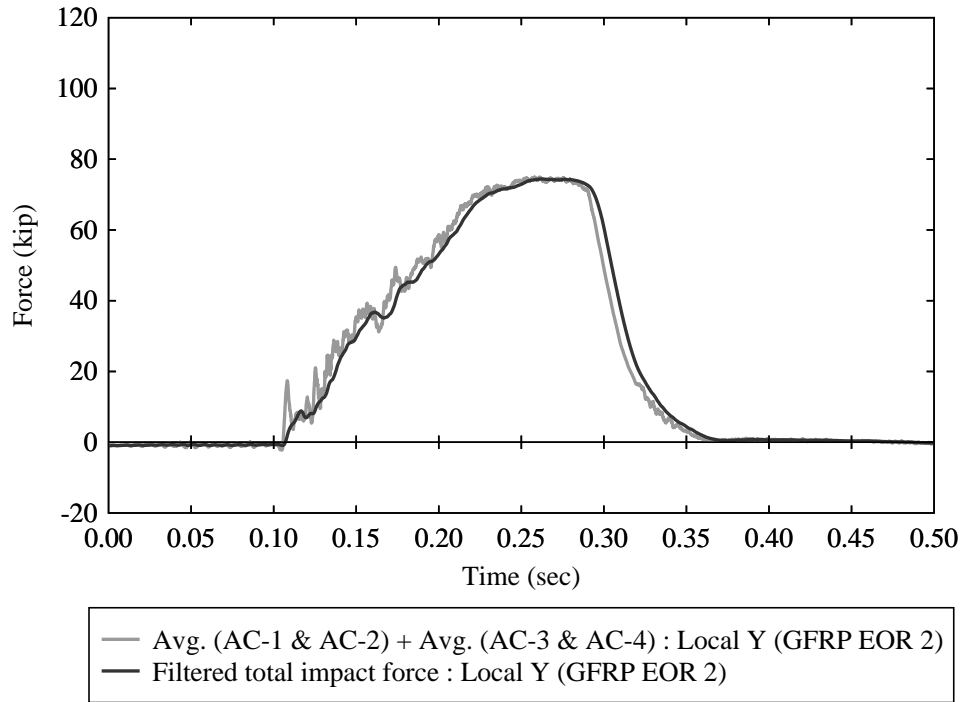


Figure 9-52 Raw and filtered total computed impact force for GFRP EOR test 2

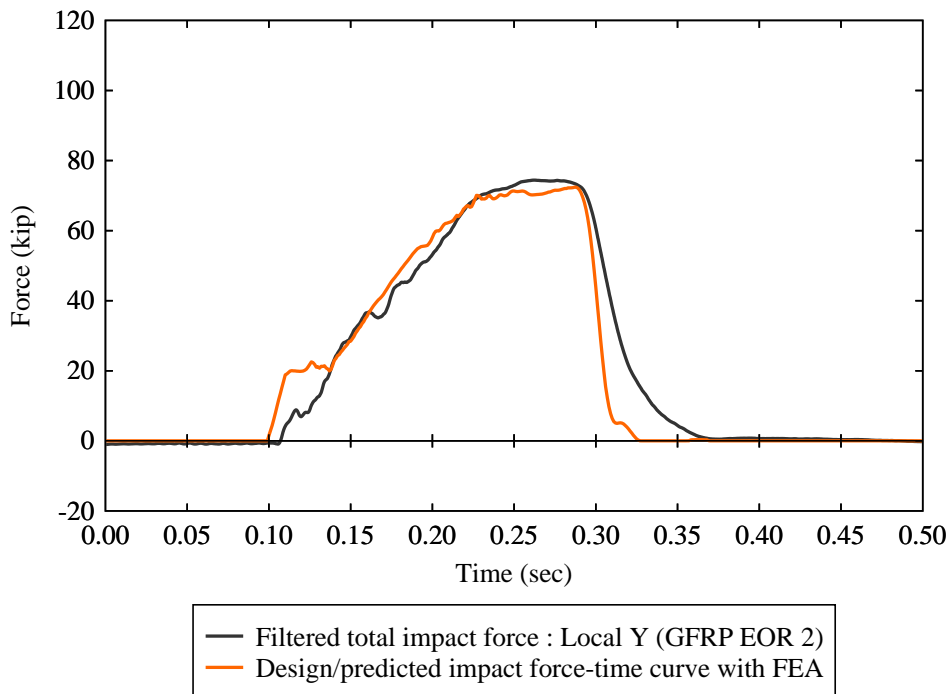


Figure 9-53 Filtered total experimental impact force for GFRP EOR test 2 compared to FEA prediction

During the GFRP EOR impact test 2, transverse deflections of the rail and any rigid sliding of the test specimen that occurred were measured with laser displacement sensors positioned behind the specimen. Further, external concrete strain measurements in the rail and deck were taken at locations along the front and back faces of the specimen. Specific locations of the laser displacement sensors (LDS) and external concrete strain gages (CSG) are depicted in Figure 9-2 (and further detailed in Appendix H).

Laser displacement data measured during GFRP EOR test 2 are provided in Figure 9-54, where it is shown that the maximum displacement occurred at the free end of the rail (LDS-4 and 6) with a magnitude of 0.67 in. when the peak impact force was applied. After completion of the impact, the maximum rail displacement reduced to approximately 0.25 in. (LDS-6). Due to the addition of reinforcement in the GFRP EOR test 2 specimen, the maximum and residual GFRP EOR test 2 displacements were about one-third of the respective maximum and residual displacements observed during the GFRP EOR test 1. Displacement sensors located at the ends of deck in the GFRP EOR test 2 specimen (LDS-2 and LDS-8) were found to record 0.01 in. and 0.07 in. of maximum displacement respectively. On the other hand, displacement sensor LDS-5 at the center of the deck recorded a maximum displacement of 0.1 in. at peak impact force and a permanent deformation of 0.07 in. after impact.

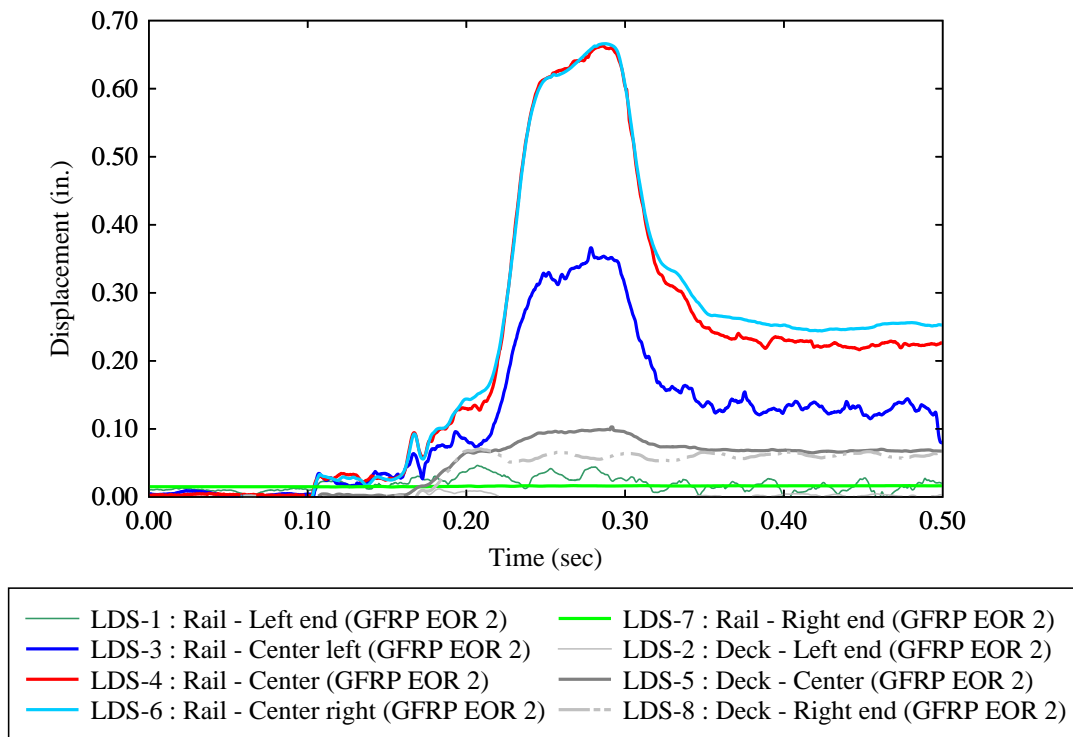


Figure 9-54 Laser displacement sensor data from GFRP EOR test 2

External strain gage readings for the front (impact) face of the GFRP EOR-2 rail test specimen are provided in Figures 9-55 and 9-56. As previously shown in Figure 9-44, diagonal cracks formed on the front face of the rail. As a result of the cracking, multiple concrete strain gages on the rail front face were found to have exceeded the maximum gage strain limit. Once the gage limit was exceeded, readings from the gages were no longer accurate. Gage readings where the strain limit was reached – indicating that cracking occurred at the gage location – are shown in

Figure 9-55. The other remaining gages with lower strain level readings located on the front side of the EOR specimen are provided in Figure 9-56.

Strain readings for the back (non-impact) side of the GFRP EOR-2 test specimen are provided in Figure 9-57. Similar to many gages on the front face of the rail, gage CSG-16 on the back face was found to exceed the maximum gage limit as a result of the cracking that formed. The remaining gages were found to record strain levels near or below the approximate rupture strain.

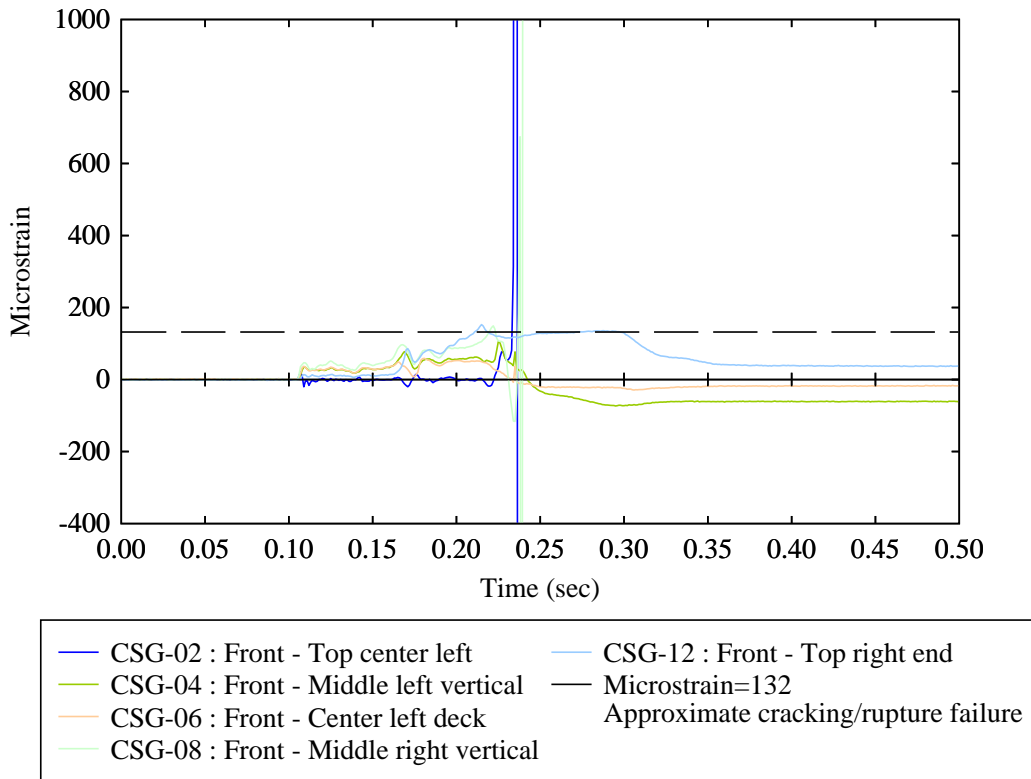


Figure 9-55 Concrete strain gage data for locations with out-of-range readings (due to cracking) for GFRP EOR test 2

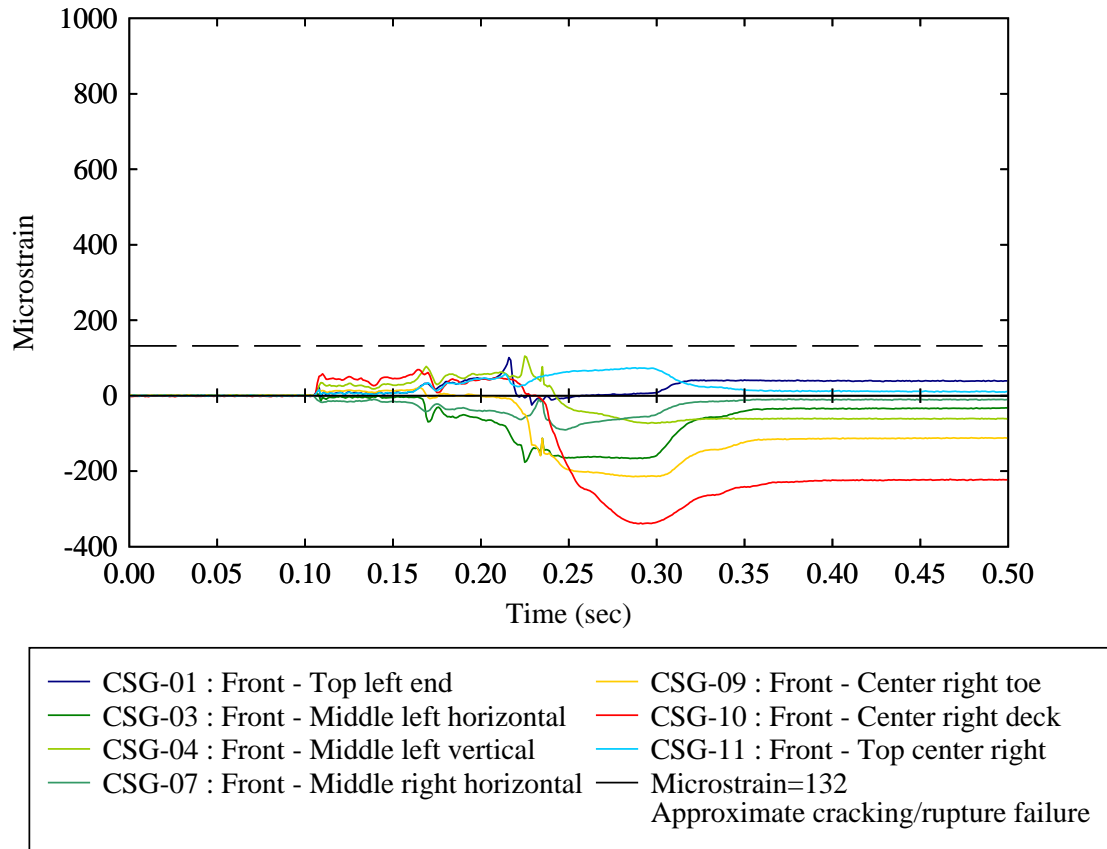


Figure 9-56 Concrete strain gage data for locations with in-range readings for GFRP EOR test 2

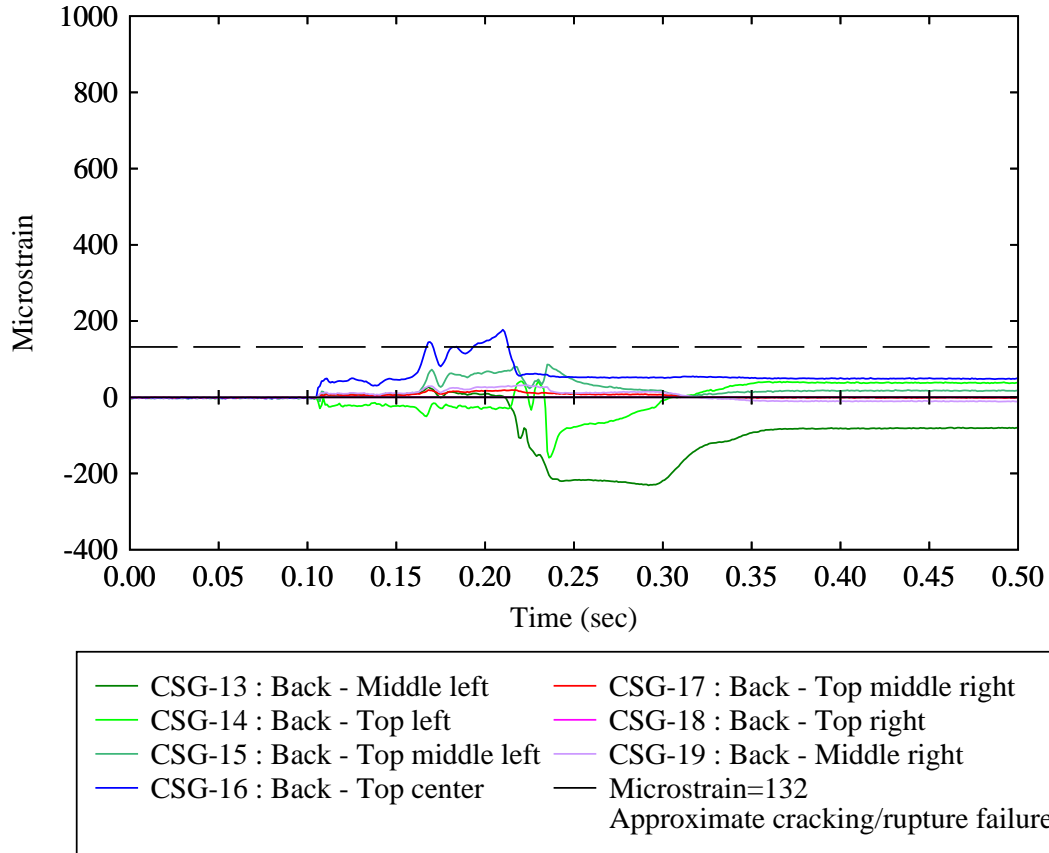
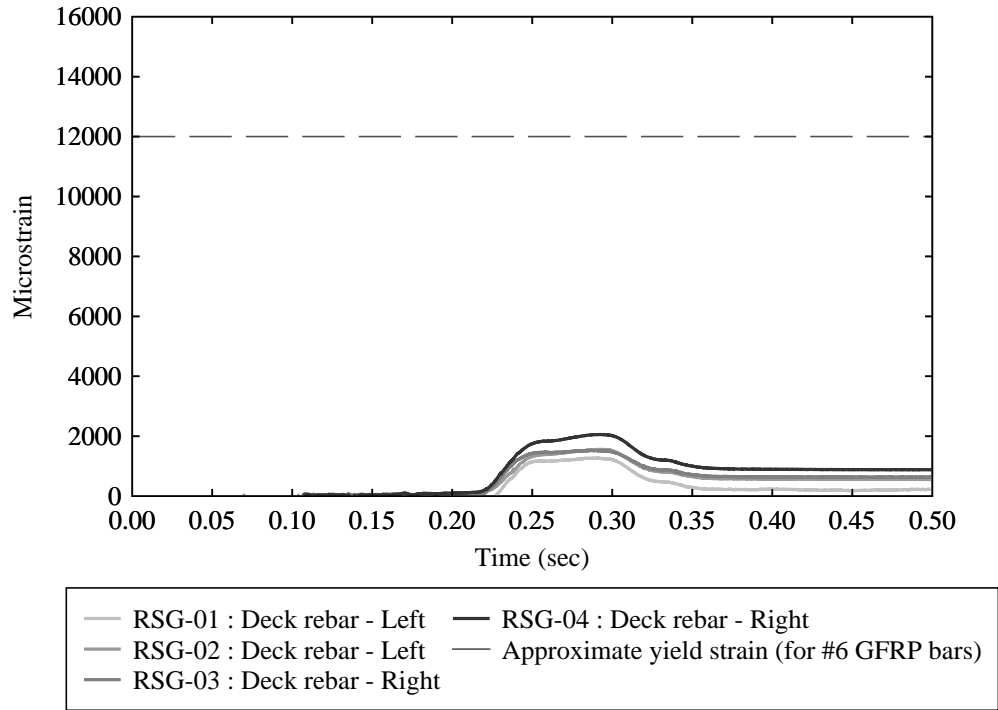
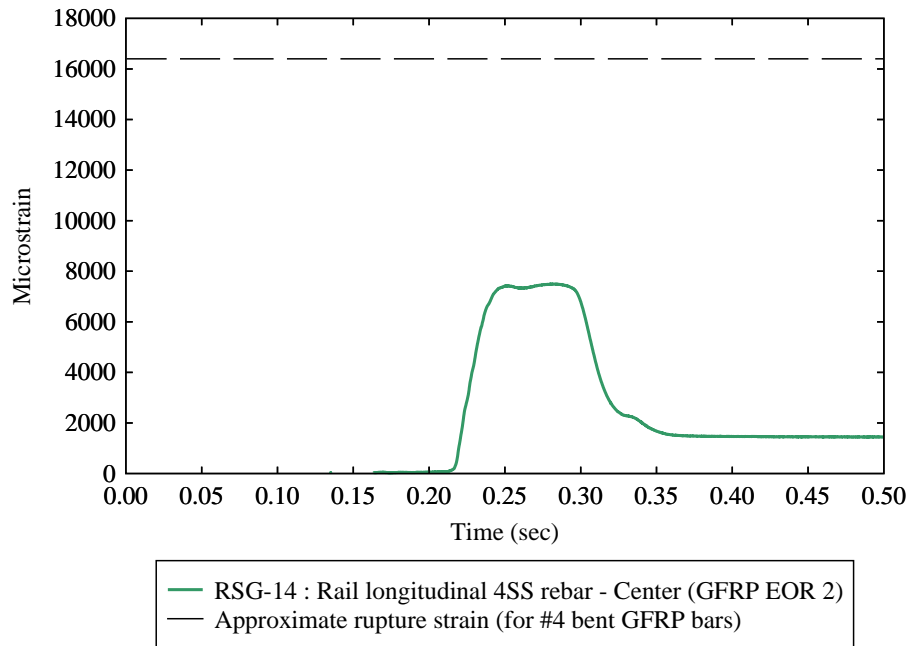


Figure 9-57 Concrete strain gage data for locations on the back (non-impact) face of the rail during GFRP EOR test 2

Readings from rebar strain gages are provided in Figure 9-58. The readings for RSG 5 to 13 and RSG 15 were not collected due to damage caused to the sensors during construction of the specimen. Specific locations of the deck and connection (G401) rebar gages are provided in Appendix H. As can be seen from the Figure 9-58, maximum strain levels in the GFRP rebars were found to be below the ultimate rupture strain levels for respective GFRP bars. The Table 4-1 provides the ultimate strains for different GFRP bars.



(a)



(b)

Figure 9-58 Internal rebar strain gage data during GFRP EOR test 2:
 (a) Deck rebar; (b) Rail rebar

9.4 Comparison of GFRP and R/C EOR test specimen results

Selected data from testing of R/C and GFRP EOR specimens are compared in this section to evaluate the performance of the proposed GFRP rail relative to the traditional R/C FDOT rail.

9.4.1 Overview

As discussed above, the following EOR specimen configurations were pendulum impact tested:

- Fully-instrumented GFRP EOR test specimens 1 and 2
- Fully-instrumented R/C EOR test specimen 1

Some differences were found when comparing test results of the GFRP EOR 2 and R/C EOR 2 specimens, however, the GFRP EOR specimen 2 performed adequately, withstanding the designed impact condition with manageable cracking (i.e., with crack widths that could, if necessary, be repaired/injected).

9.4.2 Comparison of EOR acceleration data and pendulum impact forces

For each of the three EOR tests (R/C EOR, GFRP EOR-1, GFRP EOR-2), accelerometers located on the pendulum impactor were used to measure deceleration of the impactor over the duration of impact. Acceleration data were subsequently used to compute the impact force applied to each test specimen. As shown in Figure 9-59, a similar force-time curve was achieved with each of the three tests and each test was found to adequately follow the designed force-time curve—which was intended to produce impact forces similar to the transverse component of a TL-4 vehicle impact test.

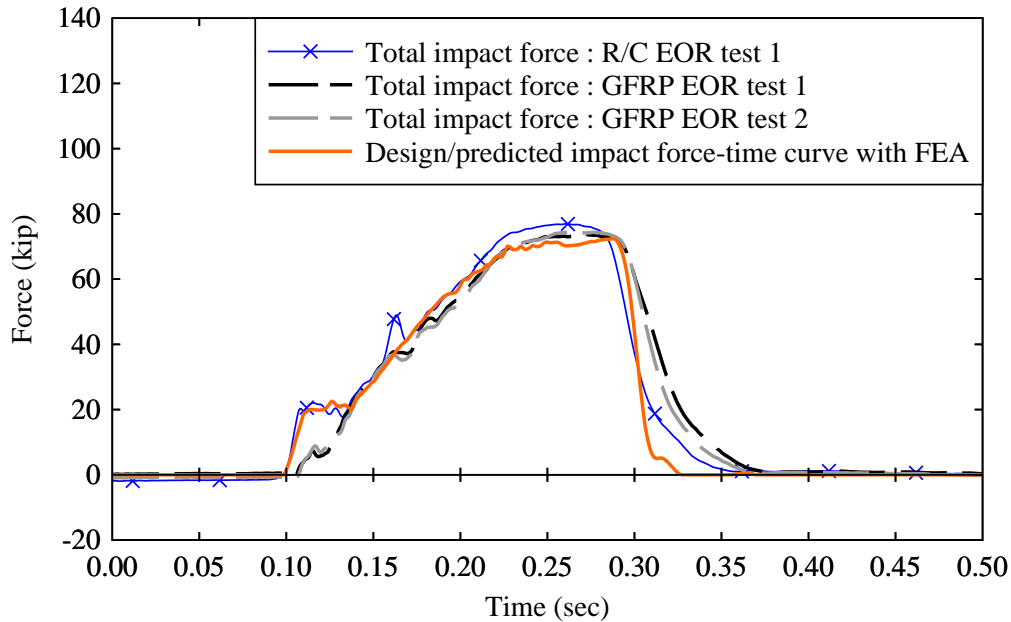


Figure 9-59 Total impact force for each traffic rail impact test

9.4.3 Comparison of EOR laser displacement data

For GFRP EOR test 1 and 2, and R/C EOR test 1, laser displacement sensors were used to measure transverse deflections at various locations on the back face of the rail. As opposed to comparing all LDS data from the three available tests, only the data with maximum displacement (LDS-4) are compared between the three EOR specimen types in Figure 9-60 (refer to Figure 9-2 for specific gage locations). Transient maximum deflection and permanent residual deflection for GFRP EOR-1 were much larger than for the other test specimens. As noted previously, this result was attributed to a probable loss of bond between GFRP bars in the deck and the surrounding concrete. In contrast, after introducing additional hooked end GFRP bars, the deflections (maximum and permanent) for the GFRP EOR-2 specimen were in much better agreement with those of the R/C EOR specimen. As expected, due to the much lower material modulus of GFRP bar relative to steel, the GFRP EOR-2 deflections were larger than the R/C EOR rail. However, the deflection levels recorded for GFRP EOR-2 would not appear to pose any issues with regard to rail serviceability.

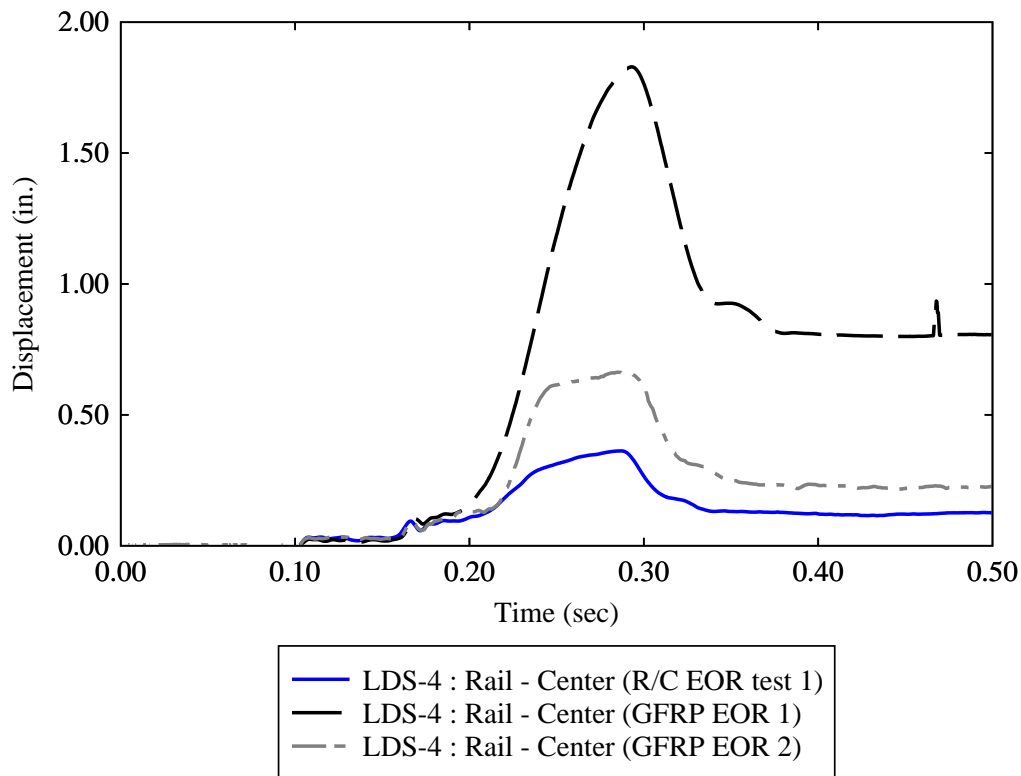


Figure 9-60 Comparison of displacements

9.4.4 Comparison of EOR external concrete strain gage data and cracking patterns

Comparing external strain gage data between the EOR specimens is challenging for a number of reasons. Primarily, gage readings for some critical locations on the GFRP EOR specimen were found to reach maximum strain limits of the gages, limiting the available concrete strain data. Additionally, due to the greater extent of crack formation in the GFRP EOR 1

specimen, a larger number of gages attached to this specimen exceeded the maximum strain limits than did gages that were attached the GFRP EOR specimen 2 and R/C EOR specimen. Nevertheless, overall crack patterns were found to be comparable between the GFRP EOR-2 specimen and R/C EOR-1 specimen (see Figures 9-61 and 9-62).



(a)



(b)



(c)

Figure 9-61 Comparison of crack pattern on the front (impact) face of EOR rail specimens: (a) GFRP EOR specimen 1; (b) GFRP EOR specimen 2; (c) R/C EOR specimen



(a)



(b)



(c)

Figure 9-62 Comparison of crack pattern on the back (non-impact) face of EOR rail specimens:
(a) GFRP EOR specimen 1; (b) GFRP EOR specimen 2; (c) R/C EOR specimen

9.4.5 Comparison of EOR internal steel rebar strain gage data

As shown in Figures 9-20a, 9-39a, and 9-58a, the deck rebars did not yield (steel) or rupture (GFRP) in any of the EOR specimens. Further, from Figures 9-20b, 9-39b, and 9-58b, the longitudinal rail rebars were also not found to yield or rupture. However, all 4V bars were found to have reached yield strain in the R/C EOR specimen. In comparison, no G401 rebars were found to reach rupture strain in GFRP EOR specimens. This can be attributed to the lower yield strain of steel ($\epsilon_y = 60/29000 = 0.002$) compared to the rupture strain of GFRP bars (recall Table 4-1). Since the strain levels in rebars of both GFRP specimens were similar, the larger deflections and wider cracks in the GFRP EOR-1 specimen were attributed to probable slip between deck rebars and concrete. However, the performance of GFRP EOR-2 specimen, with modified rebar configuration, exhibited much improved rail performance.

CHAPTER 10 SUMMARY AND CONCLUSIONS

In the present study, GFRP bars were investigated as an alternative to mild steel rebars in traffic rails on bridge structures. GFRP rebars are corrosion resistant and thus their use could reduce corrosion related damage in bridge rails exposed to aggressive marine environments. The primary objective of this study was to evaluate, using pendulum impact testing, the structural performance of a GFRP-reinforced alternative to the conventional steel-reinforced concrete (R/C) FDOT 36-in. single slope traffic rail (SSTR).

Design of the GFRP-reinforced alternative rail was based primarily on the existing steel-reinforced rebar configuration. However, due to the 'linear-elastic to rupture' nature of GFRP material behavior, yield line analysis, as recommended in AASHTO LRFD, was not applicable. Alternative methods were thus used to evaluate GFRP system capacity. In particular, advanced finite element impact simulation techniques were used to estimate system performance under pendulum impact loading conditions, and to guide modification in GFRP rebar layout.

To facilitate direct comparisons between the GFRP-reinforced concrete traffic rail and the conventional steel-reinforced rail, test specimens of each configuration were pendulum impact tested. Pendulum impact test protocols used during the physical testing phase of this project delivered impact force and impact energy that corresponded to the transverse (perpendicular to rail) components of a test level 4 (TL-4) truck impact, as described by AASHTO MASH. Specifically, the pendulum impactor used during testing imparted the transverse components of force and energy from a 10000S single unit truck (SUT) impact under TL-4 conditions.

Steel-reinforced (conventional) and GFRP-reinforced (alternative) concrete bridge rails were tested in two configurations: center-of-rail (COR), and end-of-rail (EOR). Center-of-rail tests were intended to represent vehicle impacts at central (interior) locations along a bridge rail. At such locations, significant length of rail extends in both directions away from the impact zone, and serves to partially support the impacted region against transverse deflection. In contrast, end-of-rail impacts were intended to represent conditions at locations where the rail would be discontinuous (e.g., at a rail transition point or at a construction joint). At these end-locations, only rail length extending in one direction away from the impact zone is available to contribute to resisting transverse load. Consequently, transverse deflections and damage indicators (e.g., crack widths) are expected to be larger for the more severe end-of-rail test conditions.

Pendulum impact testing of the R/C COR specimen produced a maximum deflection of approximately 0.07 in., and no discernible cracking. Corresponding testing of a GFRP COR specimen produced a maximum deflection of approximately 0.09 in., and a single crack with a width of less than 0.004 in. For central (interior) impact locations, performance of the GFRP system was thus comparable to that of the traditional R/C system.

For the more structurally demanding end-of-rail condition, pendulum impact testing of the R/C EOR specimen produced a maximum deflection of 0.42 in. and a maximum crack width of 0.016 in. Corresponding testing of two GFRP EOR specimens produced varying results. Testing of GFRP EOR specimen 1 produced significant deflection (approximately 1.9 in.) and significant cracking (>0.1 in. crack width). However, the test results suggested that during impact, bond-slip occurred between transverse deck bars and the surrounding concrete. Therefore, in GFRP EOR specimen 2, a modified rebar layout was used in which additional 90-deg. hooked bars were introduced in the deck. Pendulum impact testing of the GFRP EOR specimen 2 produced a maximum deflection of 0.67 in., residual deflection of 0.25 in., and a maximum crack width of

0.035 in. Deflections and crack widths for the GFRP rail were larger than for the R/C rail, however, the observed levels were considered acceptable given that GFRP rebar is not susceptible to corrosion.

For the center-of-rail test specimens, the traditional steel rebar layout and the GFRP rebar layout were very similar in terms of bar sizes, bar lengths, and bar spacings. However, for the end-of-rail specimens, pre-test finite element impact simulations indicated that, due to the non-ductile nature of GFRP rebar, additional transverse bars (relative to bars present in the R/C EOR specimen) were necessary to avoid a failure mode involving progressive rupturing of multiple GFRP bars. These additional bars were organized into bundles in the end region of the specimen and did prevent bar rupture during testing. However, it is noted that for end regions, a larger number (quantity) of GFRP rebars would be required in construction than would traditional mild steel rebars.

Based on pendulum impact test results obtained for traditional R/C rail specimens and alternative GFRP-reinforced rail specimens, the tested GFRP rails (COR and EOR 2) performed in manner comparable to conventional R/C rails. Deflections for GFRP rails were acceptably small, and observed cracking was manageable (i.e., cracks could, if necessary, be injected and repaired). It is therefore concluded that the tested GFRP rails may be considered for future implementation by FDOT.

REFERENCES

- AASHTO (2016). *Manual for Assessing Safety Hardware (MASH): 2nd Edition*, American Association of State Highway and Transportation Officials, Washington, D.C.
- AASHTO (2017). *LRFD Bridge Design Specifications: 8th Edition*, American Association of State Highway and Transportation Officials, Washington, D.C.
- AASHTO (2018). *LRFD Bridge Design Specifications for GFRP-Reinforced Concrete: 2nd Edition*, American Association of State Highway and Transportation Officials, Washington, D.C.
- American Concrete Institute (ACI) Committee 440 (2015). *Guide for the Design and Construction of Concrete Reinforced with FRP bars*, 440.1R-15. Farmington Hills, MI, USA
- Ahmed, E.A., Dulude, C., and Benmokrane, B. (2013). *Concrete bridge barriers reinforced with glass fibre-reinforced polymer: static tests and pendulum impacts*. Department of Civil Engineering at the University of Sherbrooke, Sherbrooke, Quebec, Canada.
- AISC (2017). *Steel Construction Manual, 15th edition*, American Institute of Steel Construction, Chicago, IL.
- Ashour, A.F., and Habeeb, M.N. (2015). *Continuous concrete beams reinforced with CFRP bars*. School of Engineering, Design and Technology, University of Bradford, West Uprkshire, UK.
- Canadian Standard Association (CSA) (2014). *Canadian Highway Bridge Design Code*. CAN/CSA S6-14, Rexdale, Ontario, Canada.
- Consolazio, G. R., Hamilton, H. R., and Honig, J. M. (2021). *Fiber-reinforced concrete traffic railings for impact loading*. Structures Research Report No. 2021/34538-34539, University of Florida, Gainesville, FL.
- Consolazio, G. R., Hamilton, H. R., and Pérez, S. (2022). *Flexural Capacity of Concrete Elements with Unbonded and Bonded Prestressing*. Structures Research Report No. 2022/P0071623-P0071624, University of Florida, Gainesville, FL.
- D'Antino, T., and Pisani, M.A. (2018). *Influence of sustained stress on the durability of glass FRP reinforcing bars*. Milan, Italy.
- El-Salakawy, E., Brière, F., Masmoudi, R., Tighiouart, B., and Benmokrane, B. (2001). *Impact tests on concrete bridge barriers reinforced with composite bars*. Final Technical Report, Ministry of Transportation of Quebec (MTQ), Sherbrooke, Quebec, Canada.
- FDOT (2019). *Standard Plans Index No. 521-427: Traffic Railing – 36" Single-Slope*, Florida Department of Transportation, Tallahassee, FL.

- FDOT (2020a). Structures Design Guidelines (SDG), Florida Department of Transportation, Tallahassee, FL.
- FDOT (2020b). Standard Specifications for Road and Bridge Construction, Florida Department of Transportation, Tallahassee, FL.
- Goldston, M., Remennikov, A., and Neaz Sheikh, M. (2016). *Experimental investigation of the behaviour of concrete beams reinforced with GFRP bars under static and impact loading*. University of Wollongong, Australia.
- Kocaoz, S., Nanni, A., and Samaranyake, V.A. (2004). *Tensile characterization of glass FRP bars*. University of Missouri, Rolla, MO, USA.
- LSTC, *LS-DYNA Keyword User's Manual*, Livermore Software Technology Corporation, Livermore, CA, 2019.
- Murray, Y.D., *User's Manual for LS-DYNA Concrete Material Model 159*, Report No. FHWA-HRT-05-062, May 2007.
- Murray, Y.D., Abu-Odeh, A., Bligh, R., *Evaluation of Concrete Material Model 159*, Report No. FHWA-HRT-05-063, May 2007.
- Rocchetti, P. (2017). *RC Traffic Railing Designs with GFRP Reinforcement*. University of Miami (UM), Coral Gables, FL.
- Sheikh, N., Bligh, R., and Menges, W. (2011). *Determination of minimum height and lateral design load for MASH test level 4 bridge rails*, Test Report No. 9-1002-5, Texas Transportation Institute (TTI), College Station, TX.
- Sennah, K., and Mostafa, A. (2018). *Performance of a developed TL-5 concrete bridge barrier reinforced with GFRP hooked bars: vehicle crash testing*. University of Toronto, ON, Canada.
- Young, W.C. and Buynas, R.G., *Roark's Formulas for Stress and Strain: 7th Edition*. McGraw-Hill Companies, Inc. 2002.

**APPENDIX A:
CALCULATION OF IMPACT TEST DESIGN**

Presented in this appendix is a calculation worksheet that was used to calculate energy required by a MASH TL-4 vehicular impact test for a pendulum impact test. The worksheet, originally developed in BDV31-977-72 (Consolazio et al., 2021), was adapted in the present study to calculate the size of each aluminum cartridge of the impactor front nose, so as to represent the desired force-displacement curve.

Impact test protocol calculations and initial cartridge design:

Per MASH 2016 :

TABLE 1-1. Test Levels

Test Level	Test Vehicle Designation* and Type	Test Conditions	
		Speed mph (km/h)	Angle (degrees)
1	1100C (Passenger Car) 2270P (Pickup Truck)	31 (50) 31 (50)	25 25
2	1100C (Passenger Car) 2270P (Pickup Truck)	44 (70) 44 (70)	25 25
3	1100C (Passenger Car) 2270P (Pickup Truck)	62 (100) 62 (100)	25 25
4	1100C (Passenger Car) 2270P (Pickup Truck) 10000S (Single-Unit Truck)	62 (100) 62 (100) 56 (90)	25 25 15
5	1100C (Passenger Car) 2270P (Pickup Truck) 36000V (Tractor-Van Trailer)	62 (100) 62 (100) 50 (80)	25 25 15
6	1100C (Passenger Car) 2270P (Pickup Truck) 36000T (Tractor-Tank Trailer)	62 (100) 62 (100) 50 (80)	25 25 15

* See Chapter 2 for detailed description of each vehicle designation.

Using MASH TL-4 Single-Unit Truck SUT test conditions:

Velocity := 56mph

ImpactAngle := 15deg

DirectImpactVelocityComponent := Velocity · sin ImpactAngle = 14.5 · mph

MassSUT := 10000kg **Mass of the Single Unit Truck SUT per MASH**

ReqImpactEnergy := $\frac{1}{2} \cdot \text{MassSUT} \cdot \text{Velocity} \cdot \sin \text{ImpactAngle}^2 = 154.8 \cdot \text{kip} \cdot \text{ft}$

Assumed preliminary pendulum impact test conditions:

PendulumDropHeight := 15.5ft **Assumed drop height**

PendulumImpactorMass := $\frac{10000 \text{ lbf}}{g} = 4536 \cdot \text{kg}$ **Assumed impactor mass close to max capacity of pendulum**

PendulumImpactEnergy := PendulumImpactorMass · g · PendulumDropHeight = 155.0 · kip · ft **Pendulum impact energy**

PendulumImpactVelocity := $\sqrt{2 \cdot g \cdot \text{PendulumDropHeight}} = 21.53 \cdot \text{mph}$ **Impact velocity computed using:** $m \cdot g \cdot h = \frac{1}{2} \cdot m \cdot v^2$

MASH TL-4 perpendicular component :

ReqImpactEnergy = 154.8 · kip · ft

MassSUT = 22046 · lb

DirectImpactVelocityComponent = 14.5 · mph

Pendulum impact:

PendulumImpactEnergy = 155.0 · kip · ft

PendulumImpactorMass = 10000 lb

PendulumImpactVelocity = 21.5 · mph

PendulumDropHeight = 15.5 ft

Per AASHTO LRFD Bridge Design, assume that the impactor applies a force with a 3.5 ft width:

ImpactorNoseWidth := 3.5ft = 42·in

Table A13.2-1—Design Forces for Traffic Railings

Design Forces and Designations	Railing Test Levels					
	TL-1	TL-2	TL-3	TL-4	TL-5	TL-6
F_t Transverse (kips)	13.5	27.0	54.0	54.0	124.0	175.0
F_t Longitudinal (kips)	4.5	9.0	18.0	18.0	41.0	58.0
F_v Vertical (kips) Down	4.5	4.5	4.5	18.0	80.0	80.0
L_t and L_l (ft)	4.0	4.0	4.0	3.5	8.0	8.0
L_v (ft)	18.0	18.0	18.0	18.0	40.0	40.0
H_r (min) (in.)	18.0	20.0	24.0	32.0	42.0	56.0
Minimum H Height of Rail (in.)	27.0	27.0	27.0	32.0	42.0	90.0

Yield line analysis as prescribed for design of a railing in AASHTO LRFD Bridge Design):

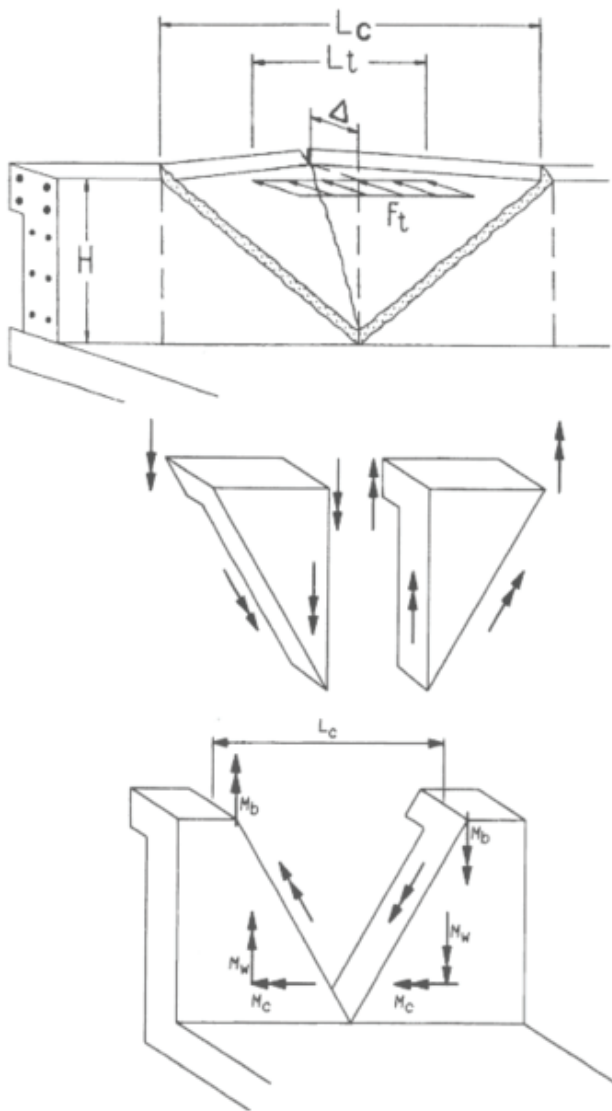


Figure CA13.3.1-1—Yield Line Analysis of Concrete Parapet Walls for Impact within Wall Segment

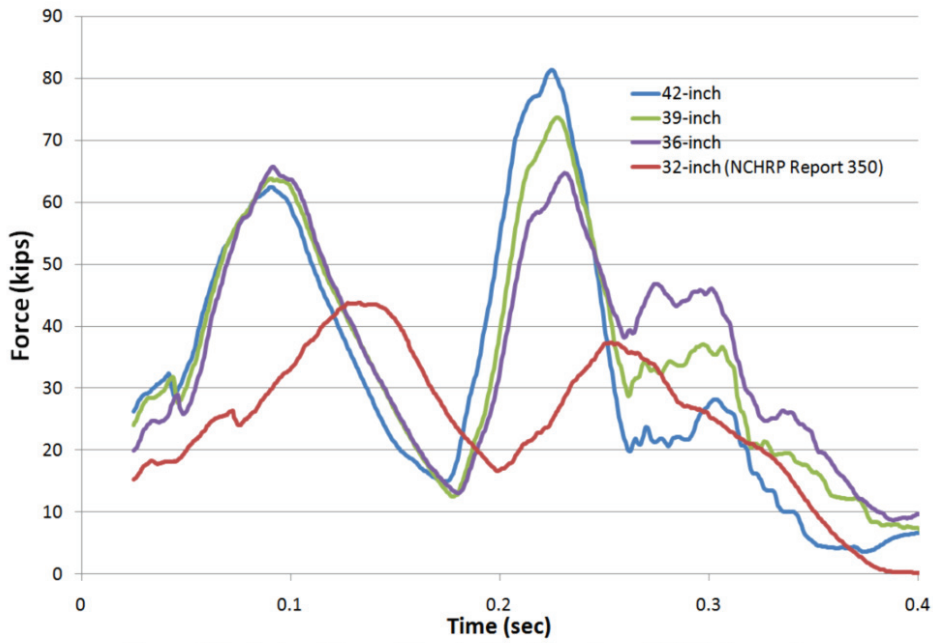
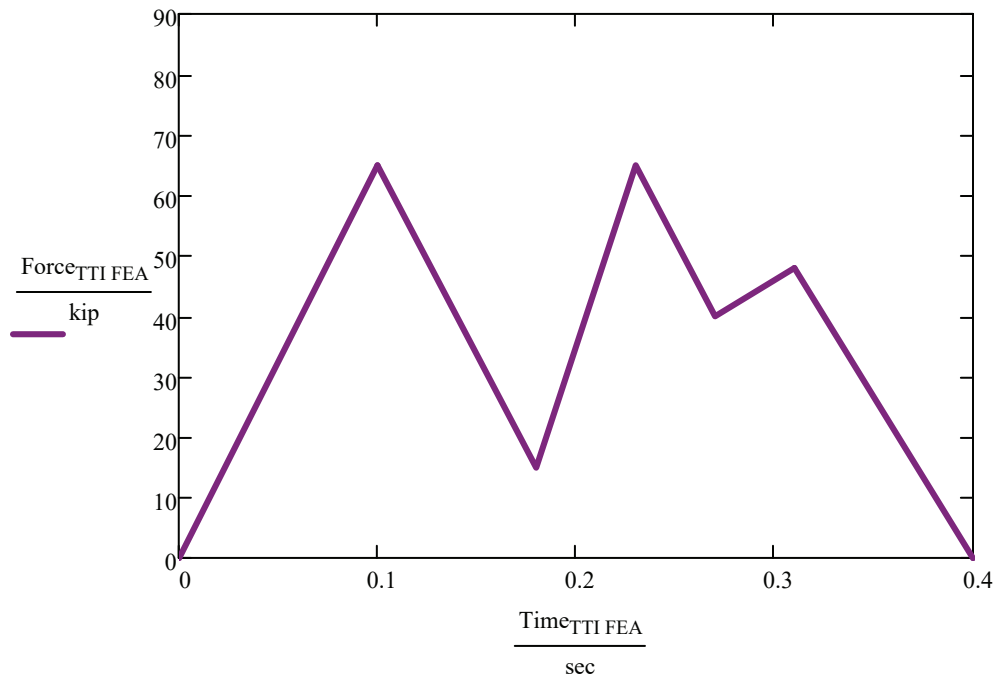


Figure 2.5. Lateral Impact Loads Resulting from Vehicle Impact with Various Rail Heights.

Attempt to design the purple force-time curve shown in the Figure above (impact force on 36-in SSTR per TTI FEA :

$$\text{Force}_{\text{TTI FEA}} := 0 \ 65 \ 15 \ 65 \ 40 \ 48 \ 0 \ \text{kip}$$

$$\text{Time}_{\text{TTI FEA}} := 0 \ 0.1 \ 0.18 \ 0.23 \ 0.27 \ 0.31 \ 0.4 \ \text{sec}$$



ORIGIN \equiv 1

Design Parameters:

TotalCartridgeThickness := 4in *Thickness after pre-crushing to be ordered from Plascore*

UsableThicknessPercentage := 75% *Assumed that the crush strength is constant until reaching a crushed thickness that is 75% of total thickness based on previous project test data and aluminum honeycomb data sheets*

UsableCartridgeThickness := UsableThicknessPercentage · TotalCartridgeThickness = 3·in

V_1 := PendulumImpactVelocity = 21.5·mph *Initial impact velocity*

TotalMass := PendulumImpactorMass = 10000 lb

ImpactHeadMass := 350lb

SystemMass := TotalMass – ImpactHeadMass = 9650 lb

CrushStrength := 130psi *Design Strength of aluminum honeycomb cartridges (iterated)*

Preliminary design: only design for first spike in the force-time curve

PrelimImpactTime := 0 0.1 0.1001 ^T·sec *Target time of pendulum impact*

PrelimImpactForce := 0 65 0 ^T·kip *Target force of pendulum impact*

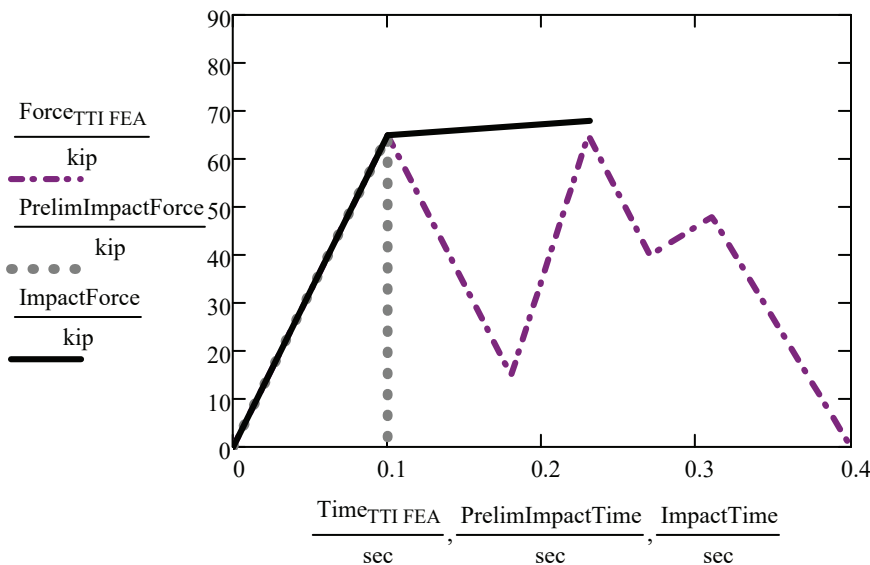
After iteration, design for more severe condition to keep force constant once 65-kip force is achieved (but with a slight linear increase to ensure sequential cartridge crush . Continue force-time curve until all remaining kinetic energy is 0 i.e., add additional cartridges to produce a similar black curve below, which was determined through iteration . Note that it is difficult to reproduce TTI-FEA purple curve below using a pendulum impactor, due to the decrease in force after the first peak.

ImpactTime := 0 0.1 0.231 ^T·sec *Target time of pendulum impact*

ImpactForce := 0 65 68 ^T·kip *Target force of pendulum impact*

CartridgeTime := ImpactTime *Time for force-time curve of cartridges*

CartridgeForce := ImpactForce *Force for force-time curve of cartridges*



For cartridge 1 $i := 1$

$$t_1 := 0 \cdot \text{sec}$$

$$KE_i := \frac{1}{2} \cdot \text{ImpactHeadMass} \cdot (V_1)^2 \quad KE_i = 5.42 \cdot \text{kip} \cdot \text{ft}$$

$$\text{FrontCartridgeThickness} := 5.36 \text{in} \cdot 75\% = 4.02 \text{in} \quad \text{Front cartridge cartridge 1 is thickened based on FEA result}$$

$$F_{cr_i} := KE_i \div \text{FrontCartridgeThickness} \quad F_{cr_i} = 16.19 \cdot \text{kip}$$

$$A_i := F_{cr_i} \div \text{CrushStrength}$$

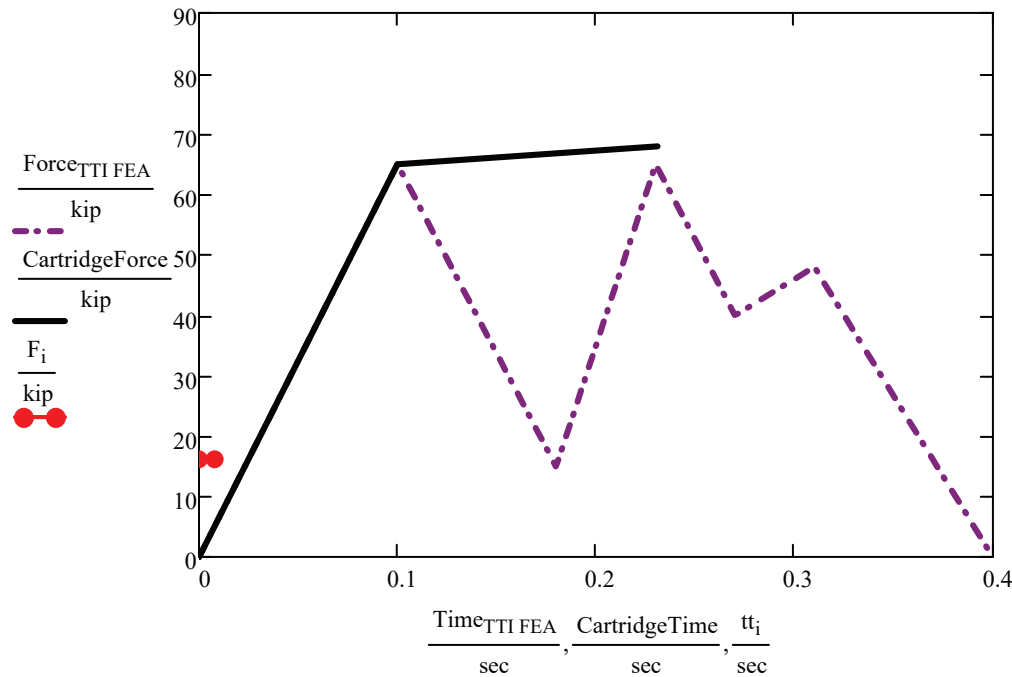
$$V_{i+1} := V_i$$

$$KE_{i+1} := \frac{1}{2} \cdot \text{SystemMass} \cdot (V_{i+1})^2$$

$$t_{i+1} := \frac{\text{UsableCartridgeThickness}}{(V_i + V_{i+1}) \div 2} + t_i$$

$$tt_i := (t_i \quad t_{i+1})^T \quad tt_i^T = 0 \quad 0.008 \quad \text{s}$$

$$F_i := (F_{cr_i} \quad F_{cr_i})^T \quad F_i^T = 16.194 \quad 16.194 \quad \cdot \text{kip}$$



For cartridge 2 $i := 2$

$F_{cr_i} := 7.7 \text{ kip}$ *Design cartridge force, iterated based on estimated average below*

$A_i := F_{cr_i} \div \text{CrushStrength}$

$KE_{i+1} := KE_i - F_{cr_i} \cdot \text{UsableCartridgeThickness}$ $KE_i = 149.57 \cdot \text{kip} \cdot \text{ft}$ $KE_{i+1} = 147.65 \cdot \text{kip} \cdot \text{ft}$

$V_{i+1} := \sqrt{2 \cdot KE_{i+1} \div \text{SystemMass}}$

$t_{i+1} := \frac{\text{UsableCartridgeThickness}}{(V_i + V_{i+1}) \div 2} + t_i$

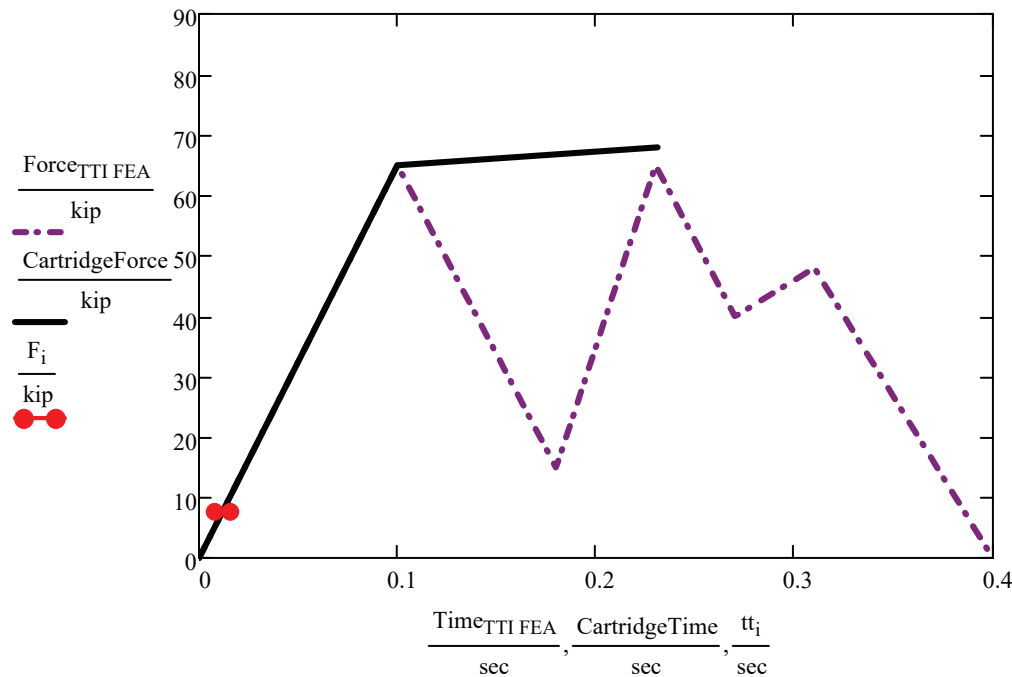
$\text{CrushForceEst1} := \text{interp}(\text{CartridgeTime}, \text{CartridgeForce}, t_i) = 5.1 \cdot \text{kip}$

$\text{CrushForceEst2} := \text{interp}(\text{CartridgeTime}, \text{CartridgeForce}, t_{i+1}) = 10.3 \cdot \text{kip}$

$\text{CrushForceEstAvg} := \frac{1}{2} \cdot \text{CrushForceEst1} + \text{CrushForceEst2} = 7.7 \cdot \text{kip}$

$tt_i := (t_i \ t_{i+1})^T$ $tt_i^T = 0.008 \ 0.016 \ \text{s}$

$F_i := (F_{cr_i} \ F_{cr_i})^T$ $F_i^T = 7.7 \ 7.7 \ \cdot \text{kip}$



For cartridge 3 $i := 3$

$F_{cr,i} := 12.9 \text{ kip}$ *Design cartridge force, iterated based on estimated average below*

$A_i := F_{cr,i} \div \text{CrushStrength}$

$KE_{i+1} := KE_i - F_{cr,i} \cdot \text{UsableCartridgeThickness}$

$V_{i+1} := \sqrt{2 \cdot KE_{i+1} \div \text{SystemMass}}$

$t_{i+1} := \frac{\text{UsableCartridgeThickness}}{(V_i + V_{i+1}) \div 2} + t_i$

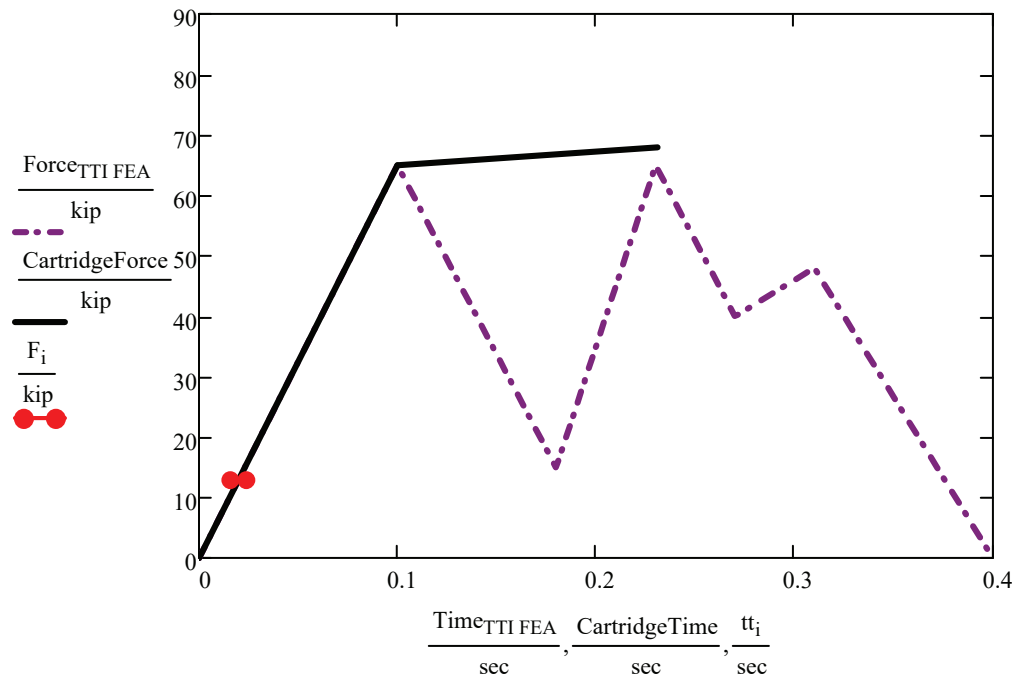
$\text{CrushForceEst1} := \text{linterp}(\text{CartridgeTime}, \text{CartridgeForce}, t_i) = 10.3 \cdot \text{kip}$

$\text{CrushForceEst2} := \text{linterp}(\text{CartridgeTime}, \text{CartridgeForce}, t_{i+1}) = 15.5 \cdot \text{kip}$

$\text{CrushForceEstAvg} := \frac{1}{2} \cdot \text{CrushForceEst1} + \text{CrushForceEst2} = 12.9 \cdot \text{kip}$

$tt_i := (t_i \ t_{i+1})^T$

$F_i := (F_{cr,i} \ F_{cr,i})^T$



For cartridge 4 $i := 4$

$F_{cr_i} := 18.2 \text{ kip}$ *Design cartridge force, iterated based on estimated average below*

$A_i := F_{cr_i} \div \text{CrushStrength}$

$KE_{i+1} := KE_i - F_{cr_i} \cdot \text{UsableCartridgeThickness}$

$V_{i+1} := \sqrt{2 \cdot KE_{i+1} \div \text{SystemMass}}$

$t_{i+1} := \frac{\text{UsableCartridgeThickness}}{(V_i + V_{i+1}) \div 2} + t_i$

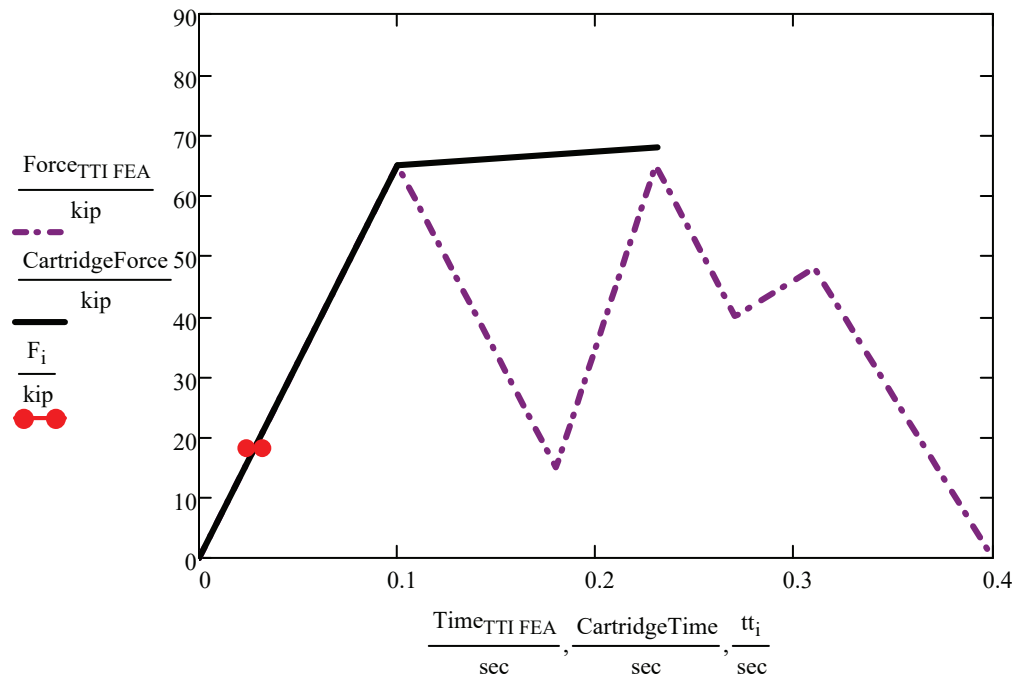
$\text{CrushForceEst1} := \text{interp}(\text{CartridgeTime}, \text{CartridgeForce}, t_i) = 15.5 \cdot \text{kip}$

$\text{CrushForceEst2} := \text{interp}(\text{CartridgeTime}, \text{CartridgeForce}, t_{i+1}) = 20.8 \cdot \text{kip}$

$\text{CrushForceEstAvg} := \frac{1}{2} \cdot \text{CrushForceEst1} + \text{CrushForceEst2} = 18.2 \cdot \text{kip}$

$tt_i := (t_i \ t_{i+1})^T$

$F_i := (F_{cr_i} \ F_{cr_i})^T$



For cartridge 5 $i := 5$

$F_{cr_i} := 23.5 \text{ kip}$ *Design cartridge force, iterated based on estimated average below*

$A_i := F_{cr_i} \div \text{CrushStrength}$

$KE_{i+1} := KE_i - F_{cr_i} \cdot \text{UsableCartridgeThickness}$

$V_{i+1} := \sqrt{2 \cdot KE_{i+1} \div \text{SystemMass}}$

$t_{i+1} := \frac{\text{UsableCartridgeThickness}}{(V_i + V_{i+1}) \div 2} + t_i$

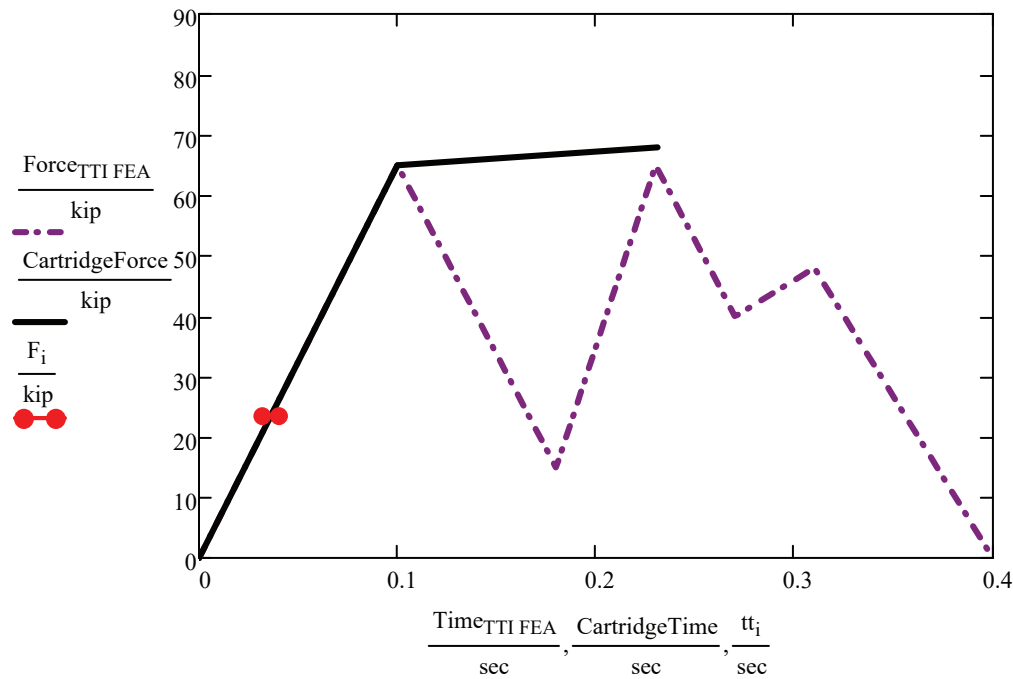
$\text{CrushForceEst1} := \text{interp}(\text{CartridgeTime}, \text{CartridgeForce}, t_i) = 20.8 \cdot \text{kip}$

$\text{CrushForceEst2} := \text{interp}(\text{CartridgeTime}, \text{CartridgeForce}, t_{i+1}) = 26.2 \cdot \text{kip}$

$\text{CrushForceEstAvg} := \frac{1}{2} \cdot \text{CrushForceEst1} + \text{CrushForceEst2} = 23.5 \cdot \text{kip}$

$tt_i := (t_i \ t_{i+1})^T$

$F_i := (F_{cr_i} \ F_{cr_i})^T$



For cartridge 6 $i := 6$

$F_{cr_i} := 28.9 \text{ kip}$ *Design cartridge force, iterated based on estimated average below*

$A_i := F_{cr_i} \div \text{CrushStrength}$

$KE_{i+1} := KE_i - F_{cr_i} \cdot \text{UsableCartridgeThickness}$

$V_{i+1} := \sqrt{2 \cdot KE_{i+1} \div \text{SystemMass}}$

$t_{i+1} := \frac{\text{UsableCartridgeThickness}}{(V_i + V_{i+1}) \div 2} + t_i$

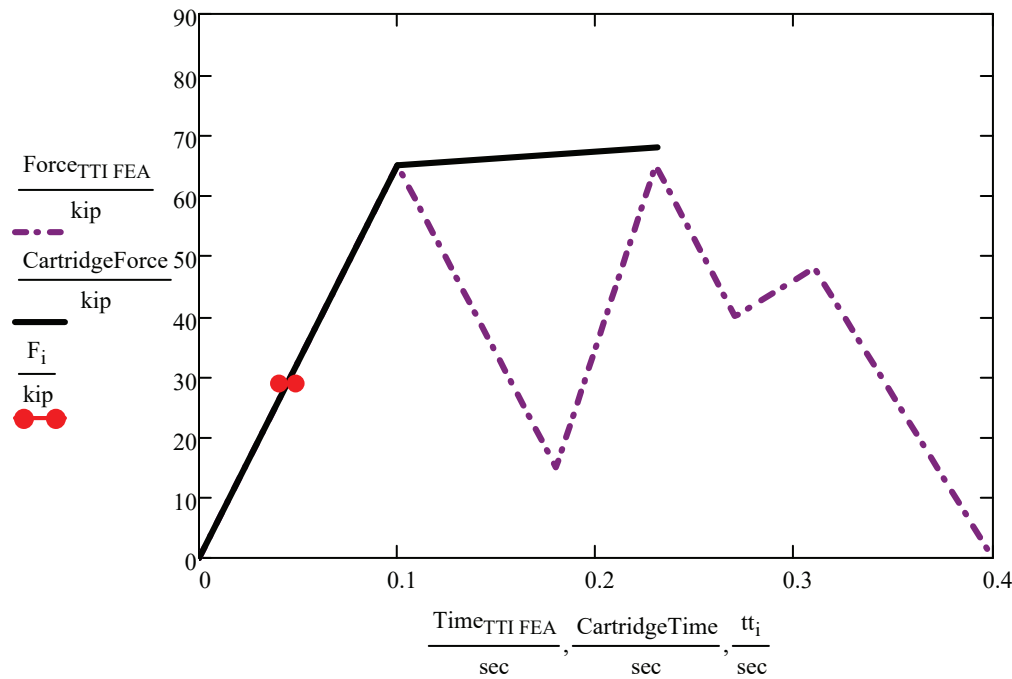
$\text{CrushForceEst1} := \text{interp}(\text{CartridgeTime}, \text{CartridgeForce}, t_i) = 26.2 \cdot \text{kip}$

$\text{CrushForceEst2} := \text{interp}(\text{CartridgeTime}, \text{CartridgeForce}, t_{i+1}) = 31.7 \cdot \text{kip}$

$\text{CrushForceEstAvg} := \frac{1}{2} \cdot \text{CrushForceEst1} + \text{CrushForceEst2} = 28.9 \cdot \text{kip}$

$tt_i := (t_i \ t_{i+1})^T$

$F_i := (F_{cr_i} \ F_{cr_i})^T$



For cartridge 7 $i := 7$

$F_{cr_i} := 34.5 \text{ kip}$ *Design cartridge force, iterated based on estimated average below*

$A_i := F_{cr_i} \div \text{CrushStrength}$

$KE_{i+1} := KE_i - F_{cr_i} \cdot \text{UsableCartridgeThickness}$

$V_{i+1} := \sqrt{2 \cdot KE_{i+1} \div \text{SystemMass}}$

$t_{i+1} := \frac{\text{UsableCartridgeThickness}}{(V_i + V_{i+1}) \div 2} + t_i$

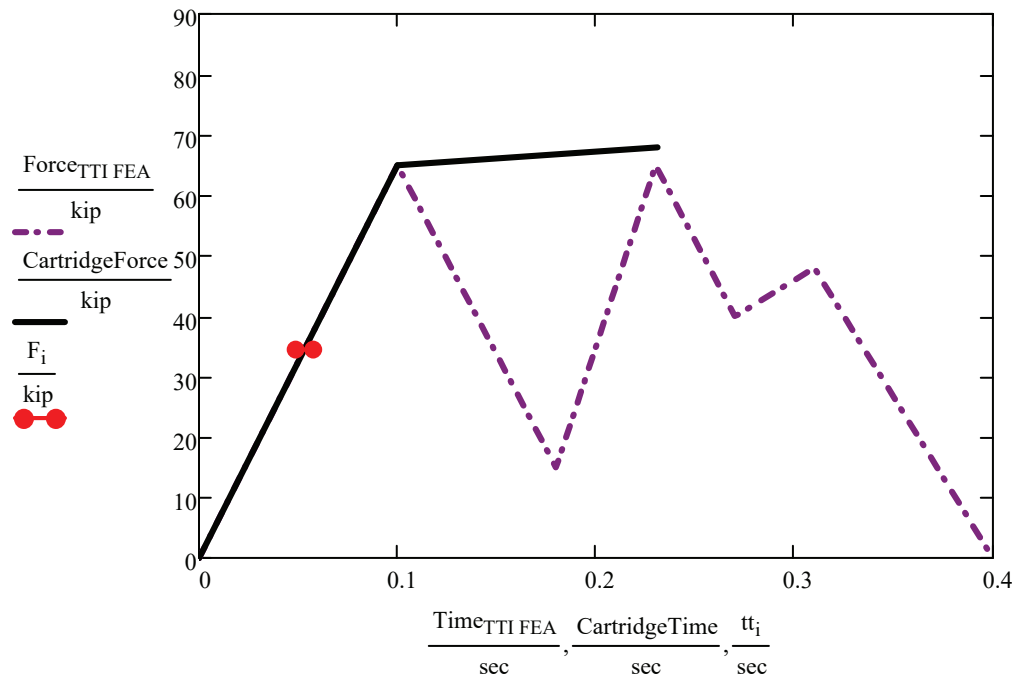
$\text{CrushForceEst1} := \text{interp}(\text{CartridgeTime}, \text{CartridgeForce}, t_i) = 31.7 \cdot \text{kip}$

$\text{CrushForceEst2} := \text{interp}(\text{CartridgeTime}, \text{CartridgeForce}, t_{i+1}) = 37.4 \cdot \text{kip}$

$\text{CrushForceEstAvg} := \frac{1}{2} \cdot \text{CrushForceEst1} + \text{CrushForceEst2} = 34.5 \cdot \text{kip}$

$tt_i := (t_i \ t_{i+1})^T$

$F_i := (F_{cr_i} \ F_{cr_i})^T$



For cartridge 8 $i := 8$

$F_{cr_i} := 40.3 \text{ kip}$ *Design cartridge force, iterated based on estimated average below*

$A_i := F_{cr_i} \div \text{CrushStrength}$

$KE_{i+1} := KE_i - F_{cr_i} \cdot \text{UsableCartridgeThickness}$

$V_{i+1} := \sqrt{2 \cdot KE_{i+1} \div \text{SystemMass}}$

$t_{i+1} := \frac{\text{UsableCartridgeThickness}}{(V_i + V_{i+1}) \div 2} + t_i$

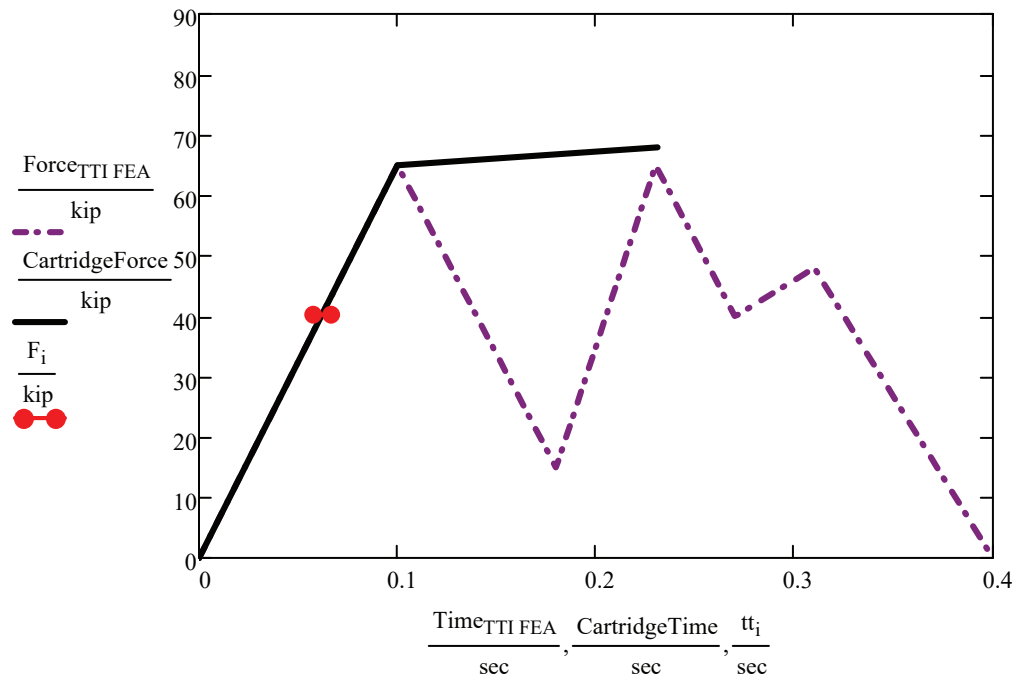
$\text{CrushForceEst1} := \text{interp}(\text{CartridgeTime}, \text{CartridgeForce}, t_i) = 37.4 \cdot \text{kip}$

$\text{CrushForceEst2} := \text{interp}(\text{CartridgeTime}, \text{CartridgeForce}, t_{i+1}) = 43.3 \cdot \text{kip}$

$\text{CrushForceEstAvg} := \frac{1}{2} \cdot \text{CrushForceEst1} + \text{CrushForceEst2} = 40.3 \cdot \text{kip}$

$tt_i := (t_i \ t_{i+1})^T$

$F_i := (F_{cr_i} \ F_{cr_i})^T$



For cartridge 9 $i := 9$

$F_{cr,i} := 46.4 \text{ kip}$ *Design cartridge force, iterated based on estimated average below*

$A_i := F_{cr,i} \div \text{CrushStrength}$

$KE_{i+1} := KE_i - F_{cr,i} \cdot \text{UsableCartridgeThickness}$

$V_{i+1} := \sqrt{2 \cdot KE_{i+1} \div \text{SystemMass}}$

$t_{i+1} := \frac{\text{UsableCartridgeThickness}}{(V_i + V_{i+1}) \div 2} + t_i$

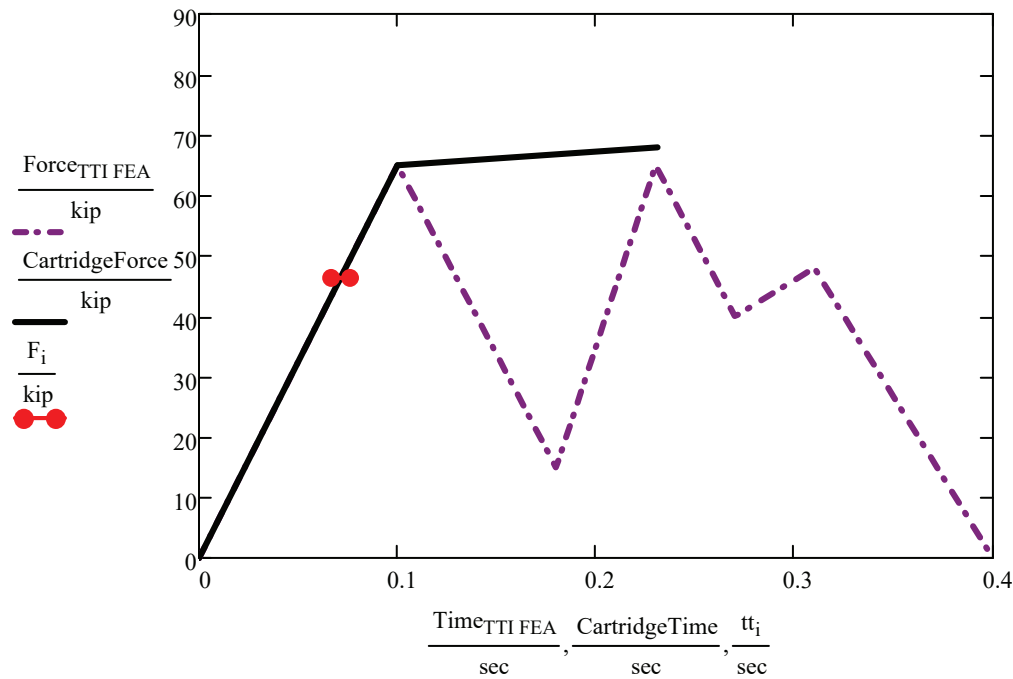
$\text{CrushForceEst1} := \text{interp}(\text{CartridgeTime}, \text{CartridgeForce}, t_i) = 43.3 \cdot \text{kip}$

$\text{CrushForceEst2} := \text{interp}(\text{CartridgeTime}, \text{CartridgeForce}, t_{i+1}) = 49.5 \cdot \text{kip}$

$\text{CrushForceEstAvg} := \frac{1}{2} \cdot \text{CrushForceEst1} + \text{CrushForceEst2} = 46.4 \cdot \text{kip}$

$tt_i := (t_i \ t_{i+1})^T$

$F_i := (F_{cr,i} \ F_{cr,i})^T$



For cartridge 10 $i := 10$

$F_{cr_i} := 52.8 \text{ kip}$ *Design cartridge force, iterated based on estimated average below*

$A_i := F_{cr_i} \div \text{CrushStrength}$

$KE_{i+1} := KE_i - F_{cr_i} \cdot \text{UsableCartridgeThickness}$

$V_{i+1} := \sqrt{2 \cdot KE_{i+1} \div \text{SystemMass}}$

$t_{i+1} := \frac{\text{UsableCartridgeThickness}}{(V_i + V_{i+1}) \div 2} + t_i$

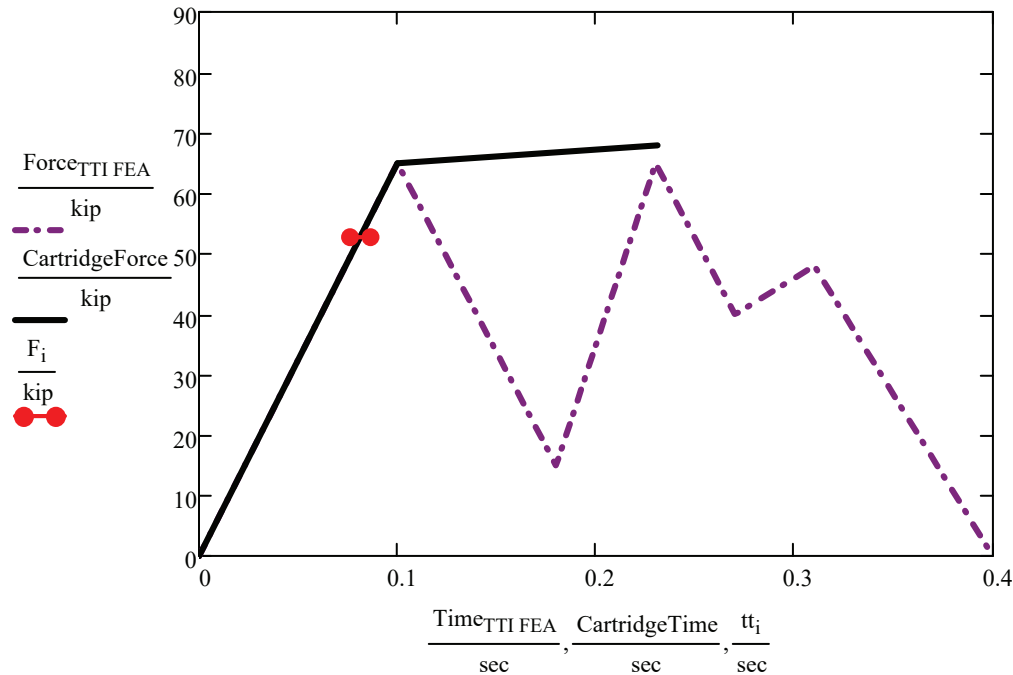
$\text{CrushForceEst1} := \text{linterp}(\text{CartridgeTime}, \text{CartridgeForce}, t_i) = 49.5 \cdot \text{kip}$

$\text{CrushForceEst2} := \text{linterp}(\text{CartridgeTime}, \text{CartridgeForce}, t_{i+1}) = 56.2 \cdot \text{kip}$

$\text{CrushForceEstAvg} := \frac{1}{2} \cdot \text{CrushForceEst1} + \text{CrushForceEst2} = 52.8 \cdot \text{kip}$

$tt_i := (t_i \ t_{i+1})^T$

$F_i := (F_{cr_i} \ F_{cr_i})^T$



For cartridge 11 $i := 11$

$F_{cr_i} := 59.8 \text{ kip}$ *Design cartridge force, iterated based on estimated average below*

$A_i := F_{cr_i} \div \text{CrushStrength}$

$KE_{i+1} := KE_i - F_{cr_i} \cdot \text{UsableCartridgeThickness}$

$V_{i+1} := \sqrt{2 \cdot KE_{i+1} \div \text{SystemMass}}$

$t_{i+1} := \frac{\text{UsableCartridgeThickness}}{(V_i + V_{i+1}) \div 2} + t_i$

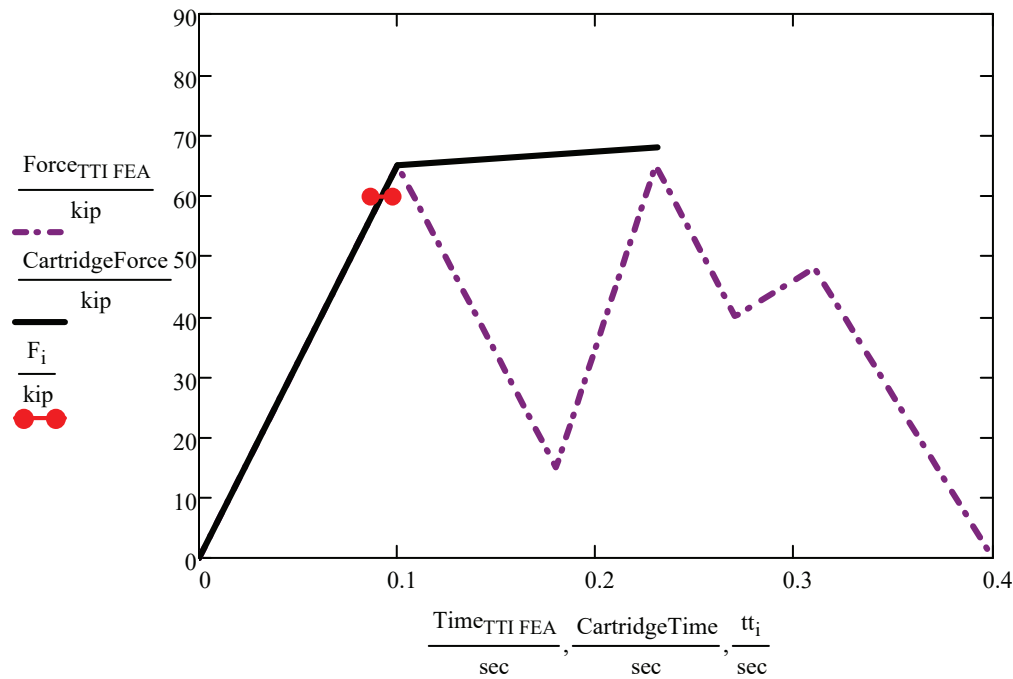
$\text{CrushForceEst1} := \text{interp}(\text{CartridgeTime}, \text{CartridgeForce}, t_i) = 56.2 \cdot \text{kip}$

$\text{CrushForceEst2} := \text{interp}(\text{CartridgeTime}, \text{CartridgeForce}, t_{i+1}) = 63.4 \cdot \text{kip}$

$\text{CrushForceEstAvg} := \frac{1}{2} \cdot \text{CrushForceEst1} + \text{CrushForceEst2} = 59.8 \cdot \text{kip}$

$tt_i := (t_i \ t_{i+1})^T$

$F_i := (F_{cr_i} \ F_{cr_i})^T$



For remaining cartridges, selected values for F_{cr} such that an average force for remaining cartridges was equal to peak FEA force of

For cartridge 12 $i := 12$

$$F_{cr_i} := 61.35 \text{ kip}$$

$$A_i := F_{cr_i} \div \text{CrushStrength}$$

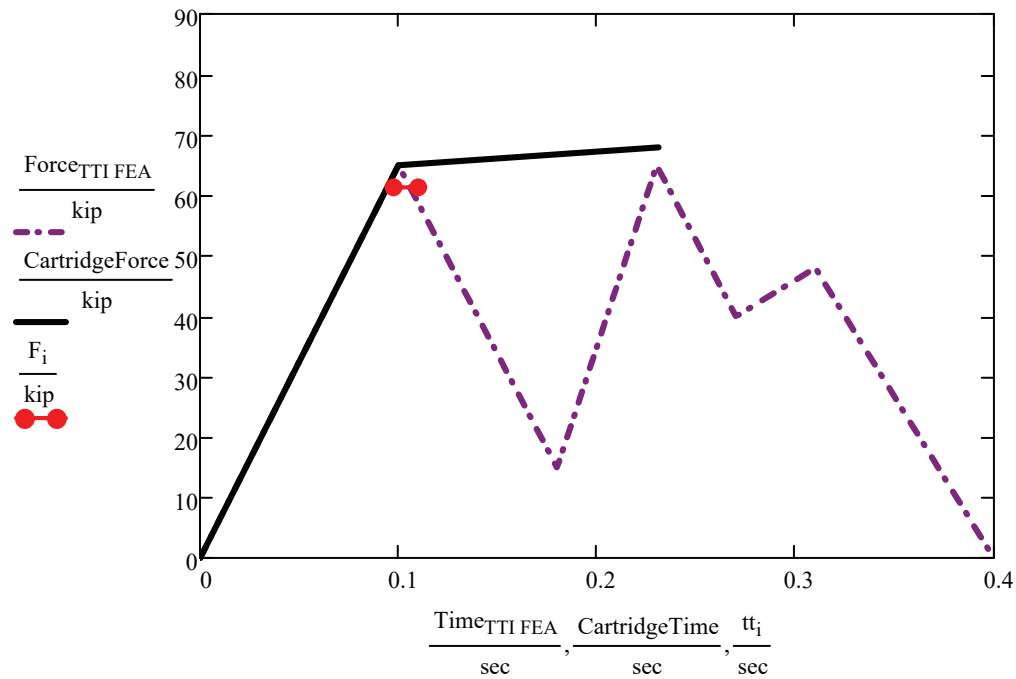
$$KE_{i+1} := KE_i - F_{cr_i} \cdot \text{UsableCartridgeThickness}$$

$$V_{i+1} := \sqrt{2 \cdot KE_{i+1} \div \text{SystemMass}}$$

$$t_{i+1} := \frac{\text{UsableCartridgeThickness}}{(V_i + V_{i+1}) \div 2} + t_i$$

$$tt_i := (t_i \ t_{i+1})^T$$

$$F_i := (F_{cr_i} \ F_{cr_i})^T$$



Continue curve with a slight linearly increasing curve (so that force is not constant, to ensure sequential cartridge crush until remaining kinetic energy 0

For cartridge 13 $i := 13$

$$F_{cr_i} := 63.2 \text{ kip}$$

$$A_i := F_{cr_i} \div \text{CrushStrength}$$

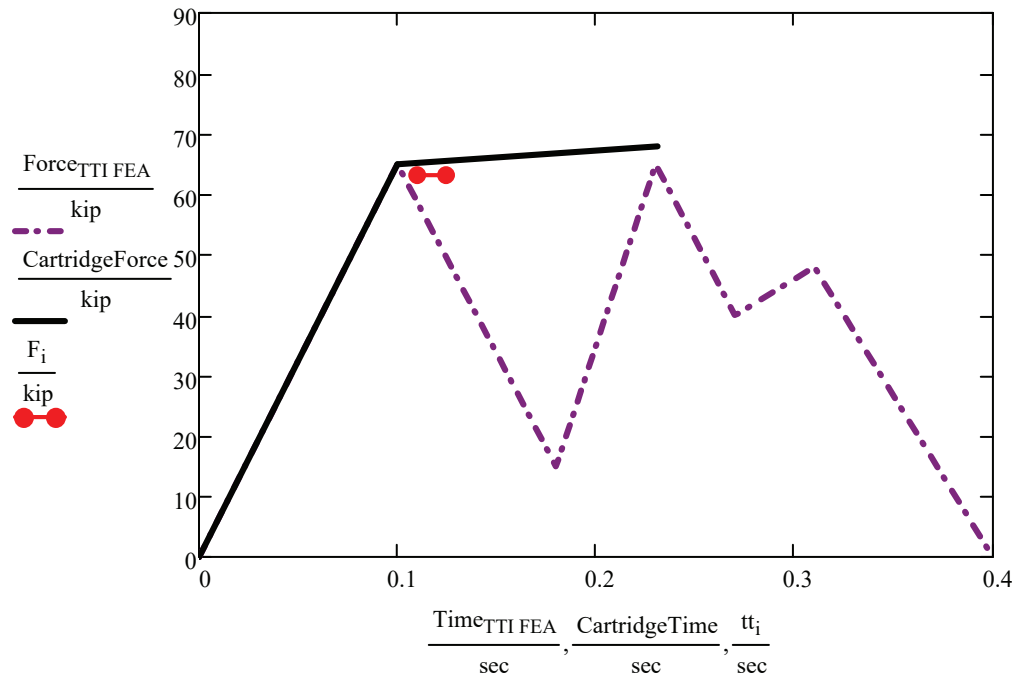
$$KE_{i+1} := KE_i - F_{cr_i} \cdot \text{UsableCartridgeThickness} \quad KE_{i+1} = 37.2 \cdot \text{kip} \cdot \text{ft}$$

$$V_{i+1} := \sqrt{2 \cdot KE_{i+1} \div \text{SystemMass}}$$

$$t_{i+1} := \frac{\text{UsableCartridgeThickness}}{(V_i + V_{i+1}) \div 2} + t_i$$

$$tt_i := (t_i \quad t_{i+1})^T$$

$$F_i := (F_{cr_i} \quad F_{cr_i})^T$$



For cartridge 14 $i := 14$

$$F_{cr_i} := 65.05 \text{ kip}$$

$$A_i := F_{cr_i} \div \text{CrushStrength}$$

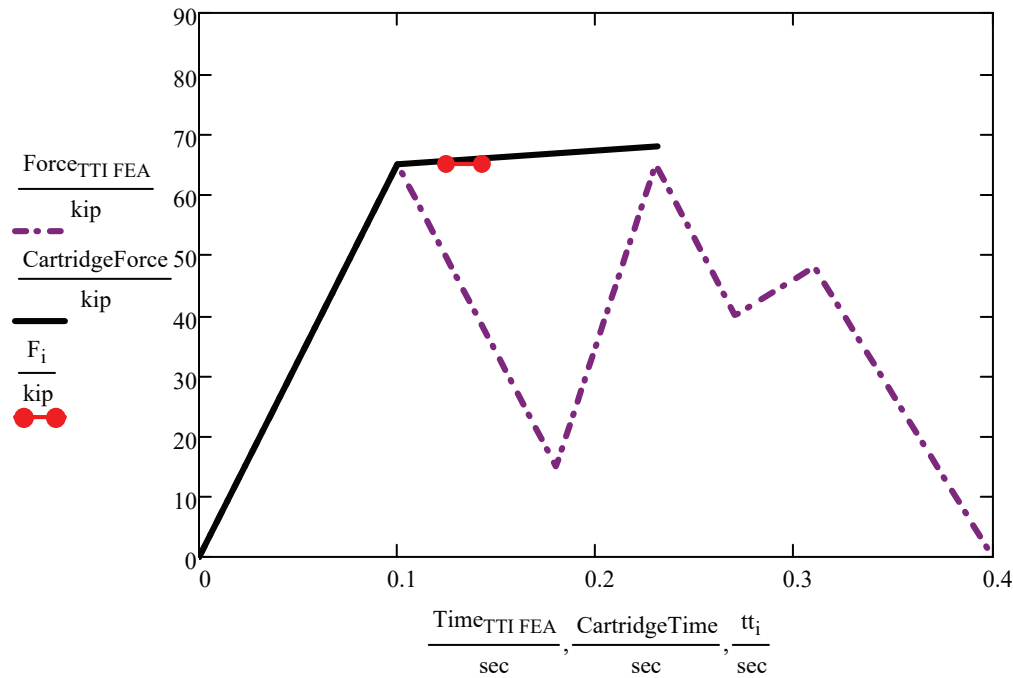
$$KE_{i+1} := KE_i - F_{cr_i} \cdot \text{UsableCartridgeThickness} \quad KE_{i+1} = 20.9 \cdot \text{kip} \cdot \text{ft}$$

$$V_{i+1} := \sqrt{2 \cdot KE_{i+1} \div \text{SystemMass}}$$

$$t_{i+1} := \frac{\text{UsableCartridgeThickness}}{(V_i + V_{i+1}) \div 2} + t_i$$

$$tt_i := (t_i \quad t_{i+1})^T$$

$$F_i := (F_{cr_i} \quad F_{cr_i})^T$$



For cartridge 15 $i := 15$

$$F_{cr_i} := 66.9 \text{ kip}$$

$$A_i := F_{cr_i} \div \text{CrushStrength}$$

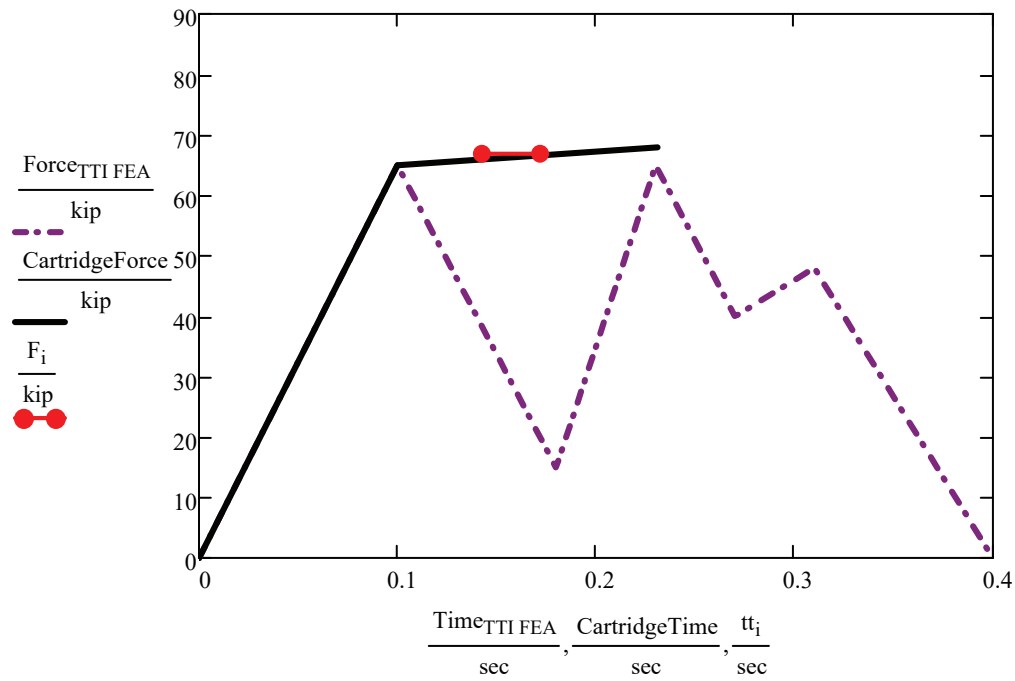
$$KE_{i+1} := KE_i - F_{cr_i} \cdot \text{UsableCartridgeThickness} \quad KE_{i+1} = 4.2 \cdot \text{kip} \cdot \text{ft}$$

$$V_{i+1} := \sqrt{2 \cdot KE_{i+1} \div \text{SystemMass}}$$

$$t_{i+1} := \frac{\text{UsableCartridgeThickness}}{(V_i + V_{i+1}) \div 2} + t_i$$

$$tt_i := (t_i \quad t_{i+1})^T$$

$$F_i := (F_{cr_i} \quad F_{cr_i})^T$$



For cartridge 16 $i := 16$

$$F_{cr_i} := 68.75 \text{ kip}$$

$$\text{FinalCartridgeCrushDepth} := 0.733 \text{ in}$$

$$A_i := F_{cr_i} \div \text{CrushStrength}$$

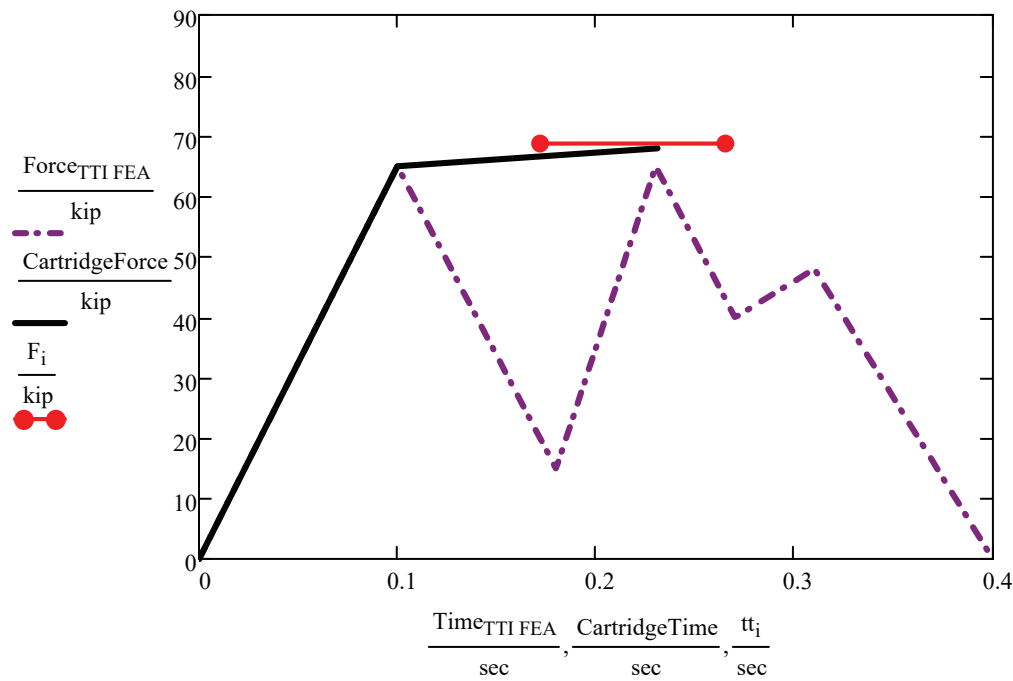
$$KE_{i+1} := KE_i - F_{cr_i} \cdot \text{FinalCartridgeCrushDepth} \quad KE_{i+1} = 0 \cdot \text{kip} \cdot \text{ft}$$

$$V_{i+1} := \sqrt{2 \cdot KE_{i+1} \div \text{SystemMass}}$$

$$t_{i+1} := \frac{\text{UsableCartridgeThickness}}{(V_i + V_{i+1}) \div 2} + t_i$$

$$tt_i := (t_i \ t_{i+1})^T$$

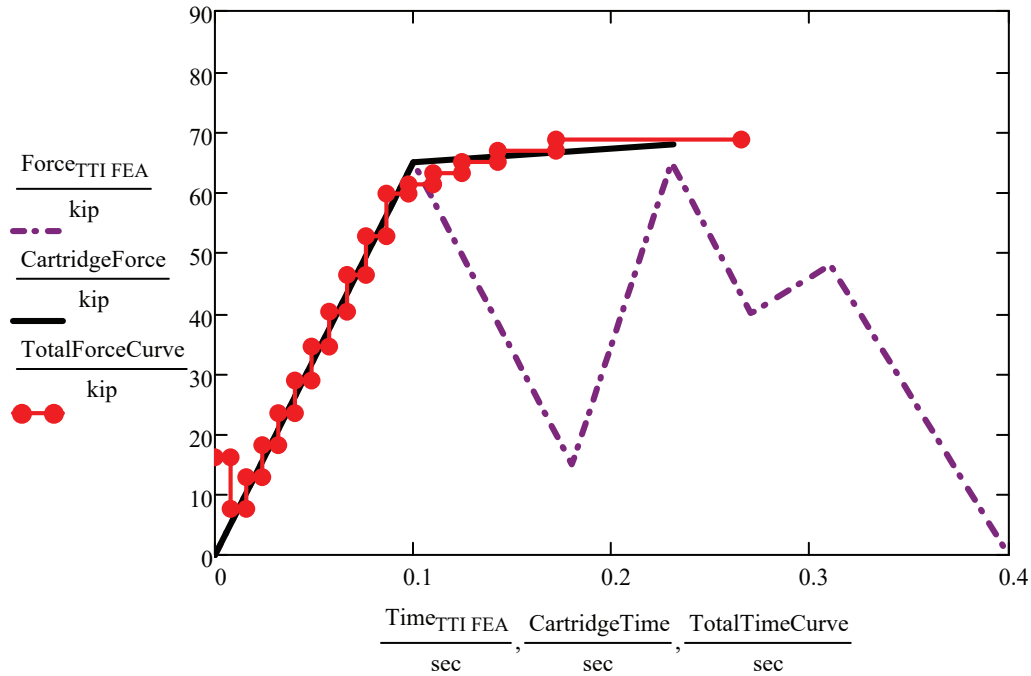
$$F_i := (F_{cr_i} \ F_{cr_i})^T$$



NumOfCartridges := i = 16

TotalForceCurve := stack(F₁, F₂, F₃, F₄, F₅, F₆, F₇, F₈, F₉, F₁₀, F₁₁, F₁₂, F₁₃, F₁₄, F₁₅, F₁₆)

TotalTimeCurve := stack(tt₁, tt₂, tt₃, tt₄, tt₅, tt₆, tt₇, tt₈, tt₉, tt₁₀, tt₁₁, tt₁₂, tt₁₃, tt₁₄, tt₁₅, tt₁₆)



KE^T = 5.4 149.6 147.6 144.4 139.9 134 126.8 118.1 108.1 96.5 83.3 68.3 53 37.2 20.9 4.2 0)·kip·ft

KE₁₊₁₆ = 0·kip·ft *Remaining kinetic energy after the last cartridge is crushed is equal to zero*

Crush force for each cartridge:

F_{cr}^T = 16.19 7.7 12.9 18.2 23.5 28.9 34.5 40.3 46.4 52.8 59.8 61.35 63.2 65.05 66.9 68.75)·kip

Started second linear increase at cartridge number 12: F_{cr12} = 61.35·kip F_{cr16} = 68.75·kip

AverageForceOfLinearIncrease := $\frac{F_{cr12} + F_{cr16}}{2} = 65.05 \cdot \text{kip}$ *which is equal to peak force of*

Determine cartridge sizes

CrushStrength = 130 psi

Assumed strength of aluminum honeycomb

TotalLengthOfCartridges := TotalCartridgeThickness · NumOfCartridges = 5.33·ft

For cartridges 1-16 i := 1..16

$$A_i := \frac{F_{cr_i}}{\text{CrushStrength}}$$

$A^T = 124.6 \ 59.2 \ 99.2 \ 140 \ 180.8 \ 222.3 \ 265.4 \ 310 \ 356.9 \ 406.2 \ 460 \ 471.9 \ 486.2 \ 500.4 \ 514.6 \ 528.8) \cdot \text{in}^2$

If perfectly square cartridges were used:

$\sqrt{A^T} = 11.16 \ 7.70 \ 9.96 \ 11.83 \ 13.45 \ 14.91 \ 16.29 \ 17.61 \ 18.89 \ 20.15 \ 21.45 \ 21.72 \ 22.05 \ 22.37 \ 22.69 \ 23.00) \cdot \text{in}$

Instead, determine dimensions based on aluminum honeycomb sheet order size to reduce the number of required cuts on a sheet :

SheetLength := 96in

SheetWidth := 48in

CartridgeWidth := SheetWidth ÷ 2 = 24·in

Cartridge lengths based on the 48-in. width:

$\frac{A^T}{\text{CartridgeWidth}} = 5.19 \ 2.47 \ 4.13 \ 5.83 \ 7.53 \ 9.26 \ 11.06 \ 12.92 \ 14.87 \ 16.92 \ 19.17 \ 19.66 \ 20.26 \ 20.85 \ 21.44 \ 22.04) \cdot \text{in}$

Note that the first cartridge will be based on the kinetic energy of the impact head, so dimensions may need to change. Also, note that the second cartridge has a dimension that is below the 3-in. thickness dimension of a cartridge which has potential to shear, so consider smaller width dimension for the first few cartridges.

$$\text{Cartridge1Width} := 12\text{in}$$

$$\text{Cartridge1Length} := A_1 \div \text{Cartridge1Width} = 10.38\text{in}$$

$$\text{Cartridge2Width} := 12\text{in}$$

$$\text{Cartridge2Length} := A_2 \div \text{Cartridge2Width} = 4.94\text{in}$$

Because $\text{Cartridge1Width} + \text{Cartridge2Width} = 24\text{in} < \text{SheetWidth} \div 2 = 24\text{in}$ **→ only consider cartridge 1 length for calculation of total required sheets**

$$\text{TotalReqLength} := \text{Cartridge1Length} + \sum_{j=3}^{16} \frac{A_j}{\text{CartridgeWidth}} = 216.33\text{in}$$

$$\text{NumOfRequiredSheets} := \frac{\text{TotalReqLength}}{\text{SheetLength} \cdot 2} = 1.13$$

More than one sheet required per impact test

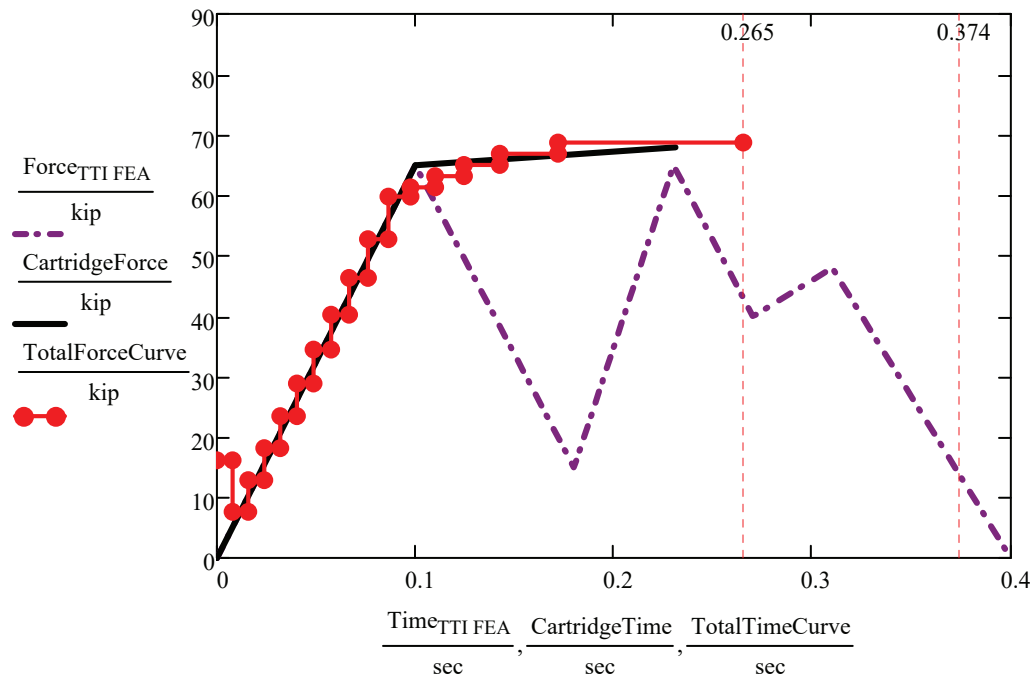
$$\text{RemainingLength} := 4 \cdot \text{SheetLength} - \text{TotalReqLength} = 167.67\text{in}$$

Double check by area:

$$\text{TotalRequiredArea} := \sum_{j=1}^{16} A_j = 5126\text{in}^2$$

$$\text{NumOfRequiredSheetsByArea} := \frac{\text{TotalRequiredArea}}{\text{SheetLength} \cdot \text{SheetWidth}} = 1.11$$

The kinetic energy of the designed pendulum impact test is equal to the kinetic energy of a SUT TL-4 impact. But impulse area under the force-time curve for the pendulum impact test may also be compared to TTI's FEA results. Comparison of impulse:



For the pendulum test:

$$\text{PendulumTestForce } t := \text{linterp } \text{CartridgeTime}, \text{CartridgeForce}, t$$

$$\text{PendulumEndTime} := 0.265\text{sec}$$

$$\text{PendulumTestImpulse} := \int_0^{\text{PendulumEndTime}} \text{PendulumTestForce } t \, dt = 14.29 \cdot \text{kip} \cdot \text{sec}$$

Determine time in FEA curve when the impulse is equal to pendulum test:

$$\text{ForcePerTTI-FEA } t := \text{linterp}(\text{Time}_{\text{TTI-FEA}}, \text{Force}_{\text{TTI-FEA}}, t)$$

$$\text{EquivalentFEATime} := 0.374\text{sec}$$

$$\text{ImpulsePerTTI-FEA}_1 := \int_0^{\text{EquivalentFEATime}} \text{ForcePerTTI-FEA } t \, dt = 14.29 \cdot \text{kip} \cdot \text{sec} \quad \text{approximately equal to pendulum test}$$

For the entire FEA force-time curve:

$$\text{FEATotalTime} := 0.4\text{sec}$$

$$\text{ImpulsePerTTI-FEA}_2 := \int_0^{\text{FEATotalTime}} \text{ForcePerTTI-FEA } t \, dt = 14.47 \cdot \text{kip} \cdot \text{sec}$$

$$\text{PercentOfImpulseRemaining} := \frac{\text{ImpulsePerTTI-FEA}_2 - \text{PendulumTestImpulse}}{\text{ImpulsePerTTI-FEA}_2} = 1.3\% \quad \text{Impulse from pendulum test is approximately 98.7\% of FEA impulse}$$

APPENDIX B: MATERIAL KEYWORDS FOR FINITE ELEMENT MODELING

Material cards used in the LS-DYNA finite element models are documented in this appendix. Note that all finite element models analyzed in this study employed units of kip, in., and seconds. Concrete components were modeled using the `MAT_CSCM` material model. Depending on the compressive strength of the concrete components being modeled, material models for either 3400 psi compressive strength (rail) or 4500 psi compressive strength (deck) were used.

*MAT_CSCM_TITLE

Concrete (3400 psi) (for rail)

mid	ro	nplot	incre	irate	erode	recov	itretrc
<varies>	2.24800E-7	1	0.0	0	1.05	0.0	0
pred							
0.0							
g	k	alpha	theta	lamda	beta	nh	ch
1531.0	1677.0	1.955	0.2765	1.524	0.133	1.0	0.0
alpha1	theta1	lamda1	beta1	alpha2	theta2	lamda2	beta2
0.7473	0.008997	0.17	0.525	0.66	0.011	0.16	0.525
r	xd	w	d1	d2			
5.0	12.76	0.05	0.001724	1.66000E-5			
b	gfc	d	gft	gfs	pwrc	pwrt	pmod
100.0	0.042	0.1	4.18100E-4	4.18100E-4	5.0	1.0	0.0
eta0c	nc	etaot	nt	overc	overt	srate	rep0w
1.07100E-4	0.78	5.67500E-5	0.48	2.819	2.819	1.0	1.0

*MAT_CSCM_TITLE

Concrete (4500 psi) (for deck)

mid	ro	nplot	incre	irate	erode	recov	itretrc
<varies>	2.24800E-7	1	0.0	0	1.05	0.0	0
pred							
0.0							
g	k	alpha	theta	lamda	beta	nh	ch
1681.0	1841.0	2.123	0.2998	1.524	0.133	1.0	0.0
alpha1	theta1	lamda1	beta1	alpha2	theta2	lamda2	beta2
0.7473	0.007749	0.17	0.4795	0.66	0.009341	0.16	0.4795
r	xd	w	d1	d2			
5.0	13.2	0.05	0.001724	1.66000E-5			
b	gfc	d	gft	gfs	pwrc	pwrt	pmod
100.0	0.051	0.1	5.08700E-4	5.08700E-4	5.0	1.0	0.0
eta0c	nc	etaot	nt	overc	overt	srate	rep0w
0.0	0.0	6.26800E-5	0.48	3.172	3.172	1.0	1.0

Steel rebar behavior was modeled using the `MAT_PIECEWISE_LINEAR_PLASTICITY` material model, and was based on a grade 60 steel stress-strain curve (i.e., yield stress $\sigma_y = 60$ ksi).

*MAT_PIECEWISE_LINEAR_PLASTICITY_TITLE

Steel rebar

mid	ro	e	pr	sigy	etan	fail	tdel
<varies>	7.34000E-7	29000.0	0.33	60.0	0.0	0.1	0.0
c	p	lcss	lcsr	vp			
40.5	5.0	21831	0	0.0			
eps1	eps2	eps3	eps4	eps5	eps6	eps7	eps8
0.0	0.0	0.0	0.0	0.0	0.0	0.0	0.0
es1	es2	es3	es4	es5	es6	es7	es8
0.0	0.0	0.0	0.0	0.0	0.0	0.0	0.0

```

*DEFINE_CURVE_TITLE
Steel rebar (grade 60) stress-strain curve with hardening
  lcid      sidr      sfa      sfo      offa      offo      dattyp      lcint
<varies>      0          1.0        0.0        0.0        0.0        0.0        0.0
  a1      o1
0.0            60.0
0.00766       61.0
0.0153        67.9
0.0230        76.4
0.0306        82.6
0.0383        87.2
0.0459        90.7
0.0536        93.5
0.0613        95.6
0.0689        96.9
0.0766        97.8
0.0842        98.4
0.0919        99.0

```

GFRP rebar behavior was modeled using the MAT_PLASTIC_KINEMATIC material model. Although GFRP rebar does not exhibit plasticity or yielding, this particular material model was employed based on the fact that it permits the specification a material failure strain. For each GFRP material model, the specified failure strain was set at a value less than 1% larger than the material rupture strain (σ_y / E), thus producing essentially ‘linear-elastic to rupture’ material behavior. Since material properties vary across different sizes of GFRP rebar, separate material models were defined for each size of rebar.

```

*MAT_PLASTIC_KINEMATIC_TITLE
No.4 GFRP rebar
  mid      ro      e      pr      sigy      etan      beta
<varies>    2.08E-7  6700.0  0.22    77.0      0.0      0.0
  src      srp      fs      vp
0.0         0.0      0.0115  0.0

```

```

*MAT_PLASTIC_KINEMATIC_TITLE
No.5 GFRP rebar
  mid      ro      e      pr      sigy      etan      beta
<varies>    2.018E-7  6700.0  0.22    73.5      0.0      0.0
  src      srp      fs      vp
0.0         0.0      0.0110  0.0

```

```

*MAT_PLASTIC_KINEMATIC_TITLE
No.6 GFRP rebar
  mid      ro      e      pr      sigy      etan      beta
<varies>    1.992E-7  6700.0  0.22    70.0      0.0      0.0
  src      srp      fs      vp
0.0         0.0      0.0104  0.0

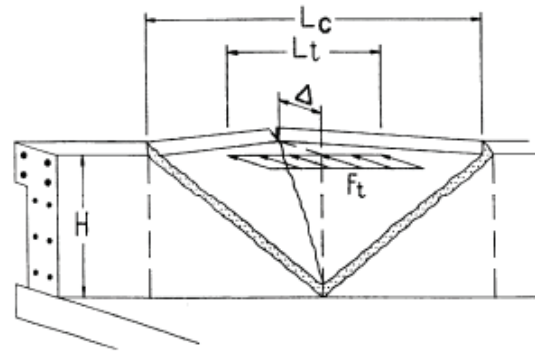
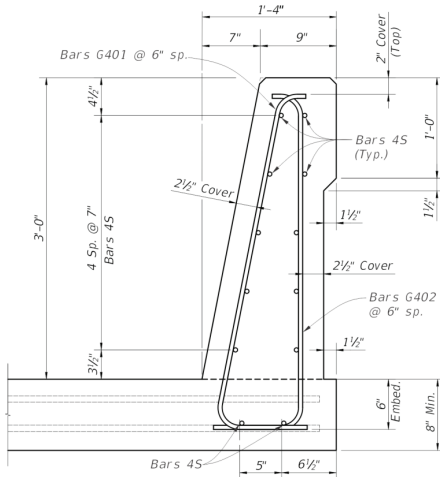
```

**APPENDIX C:
CALCULATION OF 36" SINGLE SLOPE BRIDGE RAIL**

Presented in this appendix are design calculations for GFRP reinforced rail using current design specifications – AASHTO GFRP (2018) and ACI 440 (2015), and steel reinforced rail using AASHTO GFRP (2017). Design requirements for development length and minimum spacing using the proposed GFRP reinforcement layout are verified. Approximated 36" SSTR sectional moment capacity and failure modes calculations are documented.

GRFP Reinforcement Verification (Longitudinal bars 4S)

This MathCAD worksheet is intended to check the proposed GFRP longitudinal rebar layout using existing design specifications. The straight longitudinal bars are based on current FDOT standard plan for 36" single slope traffic railing 521-427. They are designed to provide flexural and shear resistance against transverse impact force. Due to the complex two directional bending reaction under impact, the verification references to the shear and moment results estimated using Roark's equations. The design aids referenced in this calculation is AASHTO GFRP 20 18 edition.



GFRP Properties

GFRP rebar properties used are design values obtained from Owens Corning Aslan product datasheet.

PHYSICAL & MECHANICAL PROPERTIES

Nominal Diameter		Nominal Area		f'_u , Guaranteed Tensile Strength		Ultimate Tensile Load		E_f , Tensile Modulus of Elasticity		Ultimate Strain	
Size	mm	in	mm ²	in ²	MPa	ksi	kN	kips	GPa	psi 10 ⁶	%
2	6	1/4	31.67	0.049	896	130	28.34	6.37	46	6.7	1.94%
3	10	3/8	71.26	0.110	827	120	58.72	13.20	46	6.7	1.79%
4	13	1/2	126.7	0.196	758	110	95.90	21.56	46	6.7	1.64%
5	16	5/8	197.9	0.307	724	105	143.41	32.24	46	6.7	1.57%
6	19	3/4	285.0	0.442	690	100	196.60	44.20	46	6.7	1.49%
7	22	7/8	387.9	0.601	655	95	254.00	57.10	46	6.7	1.42%
8	25	1	506.7	0.785	620	90	314.27	70.65	46	6.7	1.34%
9	29	1-1/8	641.3	0.994	586	85	375.83	84.49	46	6.7	1.27%
10	32	1-1/4	791.7	1.227	551	80	436.60	98.16	46	6.7	1.19%
11*	35	1-3/8	958.1	1.485	482	70	462.40	104*	46	6.7	1.04%
12*	38	1-1/2	1160	1.800	448	65	520.40	117*	46	6.7	0.97%
13*	41	1-5/8	1338	2.074	413	60	553.50	124*	46	6.7	0.90%

*Tensile properties of #11, #12 & #13 bar are NOT guaranteed due to the inability to achieve a valid bar break per ASTM D7205.

We reserve the right to make improvements in the product and/or process which may result in benefits or changes to some physical-mechanical characteristics. The data contained herein is considered representative of current production and is believed to be reliable and to represent the best available characterization of the product as of July 2011. Tensile tests per ASTM D7205.

Use GFRP #4 bars

$$d_b = 0.5 \text{ in}$$

Nominal bar diameter

$$A_b = 0.196 \text{ in}^2$$

Nominal bar area

$$f_{tu} = 110 \text{ ksi}$$

Guaranteed tensile strength

$$E_f = 6.7 \cdot 10^6 \text{ psi}$$

Tensile modulus of elasticity

$$\epsilon_{fu} = 1.64\%$$

Ultimate strain

$$n = 10$$

Number of longitudinal bars in the rail

$$A_f = n \cdot A_b = 1.96 \cdot \text{in}^2 \quad \text{Longitudinal reinforcement area}$$

Rail Concrete Properties

$$f_c = 3400 \text{psi} \quad \text{Specified compressive strength of rail concrete}$$

$$\epsilon_{cu} = 0.003 \quad \text{Concrete ultimate strain}$$

$$\beta_1 = \begin{cases} 0.85 & \text{if } f_c \leq 4000 \text{psi} \\ 0.85 - \frac{f_c - 4000 \text{psi}}{1000 \text{psi}} \cdot 0.05 & \text{if } 4000 \text{psi} < f_c < 6000 \text{psi} \\ 0.65 & \text{otherwise} \end{cases}$$

$$A_{\text{barrier}} = 414.6 \text{in}^2 \quad \text{Cross sectional area of the rail}$$

$$\rho_f = \frac{A_f}{A_{\text{barrier}}} = 0.005 \quad \text{Reinforcement ratio (longitudinal bars over rail cross section)}$$

Tensile Strength Calculation

AASHTO GFRP 2.4.2, 2.6.3

$$C_E = 0.7 \quad \text{Environmental reduction factor AASHTO table 2.4.2.1-1}$$

$$f_{fd} = C_E \cdot f_{fu} = 77 \cdot \text{ksi} \quad \text{Design tensile strength; Effective strength when tension controls}$$

$$\epsilon_{fd} = C_E \cdot \epsilon_{fu} = 0.011 \quad \text{Design tensile strain}$$

$$f_f = \min \left[\sqrt{\frac{(E_f \cdot \epsilon_{cu})^2}{4} + \frac{0.85 \cdot \beta_1 \cdot f_c}{\rho_f} \cdot E_f \cdot \epsilon_{cu}} - 0.5 \cdot E_f \cdot \epsilon_{cu}, f_{fd} \right] = 77 \cdot \text{ksi} \quad \text{Effective strength when compression controls 2.6.3.1-1}$$

Development Length Calculation

AASHTO GFRP 2.9.7.4

$$f_{fr} = \min(f_f, f_{fd}) = 77 \cdot \text{ksi} \quad \text{Required GFRP reinforcing bar stress 2.7.3.7-2}$$

$$\alpha \theta = 1 \quad \text{Bar location modification factor.} \\ 1 \text{ for most cases.} \\ 1.5 \text{ for bars with more than 12 in. of concrete cast below.}$$

$$C = \min \left(\frac{1}{2} \cdot 6 \text{in}, 2.5 \text{in} + \frac{1}{2} \cdot d_b \right) = 2.75 \cdot \text{in} \quad \text{Lesser of the cover to the center of the bar or one-half of the center-to-center spacing of the bars being developed, in}$$

$$C_{db} = \min \left(3.5, \frac{C}{d_b} \right) = 3.5 \quad C / d_b$$

$$L_d = \frac{31.6 \alpha \cdot \frac{f_{fr}}{\sqrt{f_c \cdot \text{ksi}}} - 340}{13.6 + C_{db}} \cdot d_b = 28.64 \cdot \text{in} \quad \text{Development length in the rail}$$

Maximum Reinforcement Spacing

AASHTO GFRP 2.6.7

f_{ts} is calculated tensile stress in GFRP reinforcement at the service limit state.

Service limit state not applicable in the extreme event condition.

Minimum Transverse Reinforcement

AASHTO GFRP 2.7.2.4

$A_{fv} = 2 \cdot A_b = 0.392 \cdot \text{in}^2$	Area of transverse reinforcement within $s = 6\text{in}$.
$b_v = 14.5\text{in}$	Effective web width
$f_{fv} = 77\text{ksi}$	Design tensile strength of transverse rebar see transverse calculation sheet
$s = 6\text{in}$	Transverse reinforcement spacing

$$\text{CheckMinTransReinf} = \text{if} \left(A_{fv} \div \text{in}^2 \geq 0.05 \cdot \frac{b_v \div \text{in} \cdot s \div \text{in}}{f_{fv} \div \text{ksi}}, \text{"OK"}, \text{"Need more reinforcement"} \right) = \text{"OK"}$$

Shrinkage and Temperature Reinforcement

AASHTO GFRP 2.9.6

When the impact load is applied, the longitudinal bars can be treated as shrinkage and temperature reinforcement.

$n_{\text{each.side}} = 10$	Longitudinal bars at each side
$\rho_{f.\text{each.face}} = \frac{n_{\text{each.side}} \cdot A_b}{A_{\text{barrier}}} = 0.00473$	Ratio of shrinkage and temperature longitudinally in the rail
$\rho_{f.\text{st.max}} = 0.0036$	Required maximum reinforcement for shrinkage and temperature

$$\text{CheckShrinkTempReinf} = \text{if} (\rho_{f.\text{each.face}} \geq \rho_{f.\text{st.max}}, \text{"OK"}, \text{"Not enough"}) = \text{"OK"}$$

Limit State Calculation

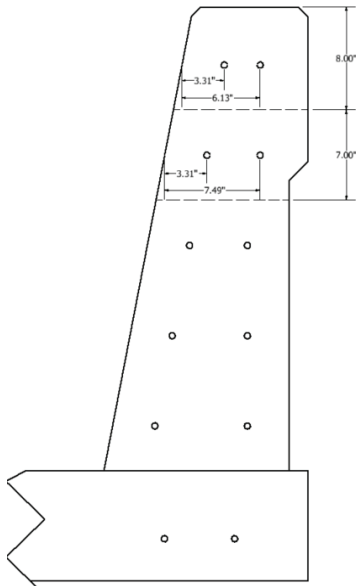
AASHTO GFRP 2.6.3.2, ACI 440.1R-15

A general equation $\phi \cdot M_n = \phi \cdot A_s \cdot f_y \cdot \left(d - \frac{a}{2} \right)$ is used to calculate moment capacity provided by each bar

$\phi = 1.0$ Extreme event resistance factor AASHTO GFRP 2.5.6

The flexural resistance of a GFRP reinforced member is dependent on whether the failure is controlled by crushing of the concrete or rupture of GFRP bars.

$A_s = 4 \cdot A_b = 0.784 \cdot \text{in}^2$ Both layers of longitudinal bars are in tension



Using ACI method:

Calculate the reinforcement ratio at the balanced failure condition:

$$\rho_{fb} = 0.85 \cdot \beta_1 \cdot \frac{f_c}{f_{fd}} \cdot \frac{E_f \cdot \epsilon_{cu}}{E_f \cdot \epsilon_{cu} + f_{fd}} = 0.0066 \quad \text{ACI 7.2.1b}$$

Calculate the reinforcement ratio in the top section:

$$A_{top} = 10\text{in} \cdot 15\text{in} = 150 \cdot \text{in}^2 \quad \text{Area of the top portion}$$

$$\rho_f = \frac{4 \cdot A_b}{A_{top}} = 0.0052$$

$$\text{LimitState} = \begin{cases} \text{"tension control"} & \text{if } \rho_f < \rho_{fb} \\ \text{"compression control"} & \text{if } \rho_f > \rho_{fb} \end{cases}$$

$$\text{LimitState} = \text{"tension control"}$$

Using AASHTO method:

$$d_1 = 3.31\text{in} \quad d_2 = \frac{6.13\text{in} + 7.49\text{in}}{2} = 6.81 \cdot \text{in}$$

Depth of two layers of rebar

$$b_{rec} = 15\text{in} \quad \text{Height of the top portion of the rail}$$

$$d_{rec} = 9.5\text{in}$$

By balancing two layers of rebars:

$$0.85f_c \cdot b_{rec} \cdot c \cdot \beta_1 = 2A_b \cdot f_1 + 2A_c \cdot f_f$$

Using similar triangle:

$$\frac{f_1}{f_f} = \frac{d_1 - c}{d_2 - c}$$

Then:

$$c = \frac{2A_b \cdot \frac{(d_1 - c) \cdot f_f}{d_2 - c} + 2 \cdot A_b \cdot f_f}{0.85f_c \cdot b_{rec} \cdot \beta_1}$$

Guess:

$$c = 1.133\text{in}$$

$$\frac{2A_b \cdot \frac{(d_1 - c) \cdot f_f}{d_2 - c} + 2 \cdot A_b \cdot f_f}{0.85f_c \cdot b_{rec} \cdot \beta_1} = 1.133 \cdot \text{in}$$

$$\epsilon_{ft1} = \frac{d_1 - c}{c} \cdot \epsilon_{cu} = 0.006 \quad \text{GFRP bar strain in layer 1}$$

$$\epsilon_{ft2} = \frac{d_2 - c}{c} \cdot \epsilon_{cu} = 0.015 \quad \text{GFRP bar strain in layer 2}$$

$$\epsilon_{fd} = 0.0115$$

$$\text{LimitState}(\varepsilon_{ft}) = \begin{cases} \text{"tension control"} & \text{if } \varepsilon_{ft} > \varepsilon_{fd} \\ \text{"compression control"} & \text{if } \varepsilon_{ft} < \varepsilon_{fd} \end{cases}$$

$$\text{LimitState}(\varepsilon_{ft1}) = \text{"compression control"}$$

$$\text{LimitState}(\varepsilon_{ft2}) = \text{"tension control"}$$

The limite state calculation matches the prediction of beams in FEA analysis.

Minimum Reinforcement Calculation

AASHTO GFRP 2.6.3.3

The requirement of minimum reinforcement provisions are intended to reduce the probability of brittle failure upon concrete cracking.

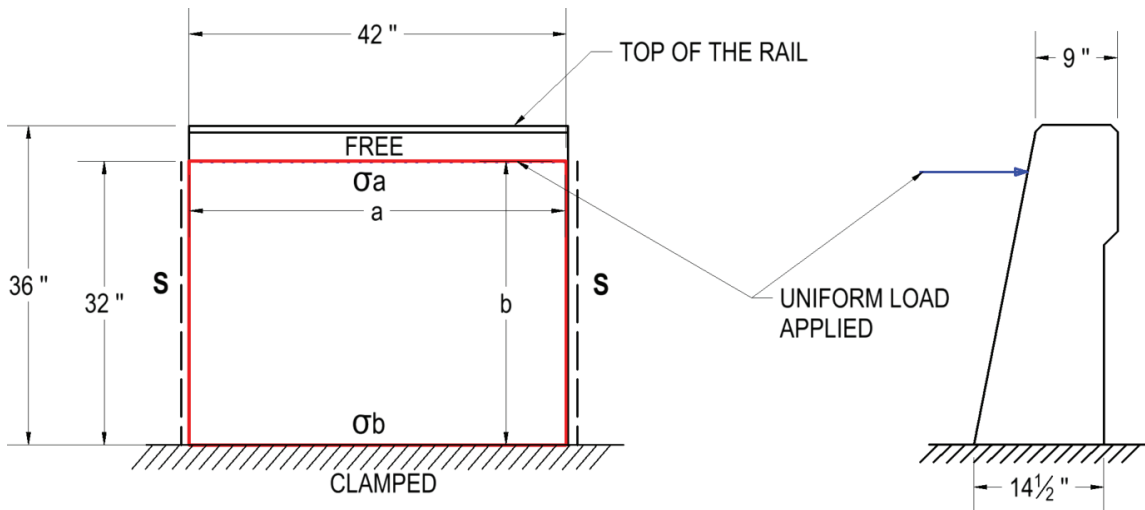
$$f_r = 0.24 \cdot \sqrt{f_c} \cdot \text{ksi} = 0.443 \cdot \text{ksi} \quad \text{Rail concrete modulus of rupture}$$

For simplified sectional modulus calculation, assume the cross section is rectangular, where:

$$h = 15 \text{ in} \quad b = 10 \text{ in} \quad \text{Use the top portion of the rail. } h: \text{ height; } b: \text{ average thickness}$$

$$S_r = \frac{1}{6} \cdot b^2 \cdot h = 250 \cdot \text{in}^3$$

Assume load results in a simply supported moment reaction, using Roarks formula to estimate resultant moment and shear:



$$L_t = 3.5 \text{ ft} \quad \text{Longitudinal length of distribution of impact force } F_t \text{ along the railing}$$

$$F_{tr} = 68 \text{ kip} \quad \text{Transverse vehicle impact force adjusted based on TTI research}$$

$$M_{\text{impact}} = 13.7 \text{ kip} \cdot \text{ft} \quad \text{Impact flexural moment about rail vertical axis}$$

$$c_b = \frac{\varepsilon_{cu}}{\varepsilon_{cu} + \varepsilon_{fd}} \cdot d_2 = 1.411 \cdot \text{in} \quad \text{Neutral axis depth at balanced condition}$$

$$\phi M = \phi \cdot (2A_b) \cdot f_{fd} \cdot \left(d_2 - \frac{\beta_1 \cdot c_b}{2} \right) + \phi \cdot (2A_b) \cdot f_{fd} \cdot \left(\frac{d_1 - c_b}{d_2 - c_b} \right) \cdot \left(d_1 - \frac{\beta_1 \cdot c_b}{2} \right) = 18 \cdot \text{kip} \cdot \text{ft}$$

$$\text{CheckMinFlexReinf} = \text{if}(\phi M \geq \min(1.33 \cdot M_{\text{impact}}, 1.6 f_r \cdot S_r), \text{"OK"}, \text{"Need more reinforcement"}) = \text{"OK"}$$

Shear Reinforcement Verification Simplified Method

AASHTO GFRP 2.7.3.4

$$V_{\text{impact}} = 9.2 \text{ kip} \quad \text{Transverse impact induced maximum shear, estimated using Roark's formula}$$

$$E_f = 6.7 \times 10^6 \text{ psi} \quad E_c = 57000 \sqrt{f'_c \cdot \text{psi}} = 3.324 \times 10^6 \text{ psi}$$

$$n_f = \frac{E_f}{E_c} = 2.016 \quad \rho_f = 0.0052$$

$$k = \sqrt{2 \cdot \rho_f \cdot n_f + (\rho_f \cdot n_f)^2} - \rho_f \cdot n_f = 0.135 \quad \text{AASHTO GFRP 2.5.3-4}$$

$$\beta\theta = 5 \cdot k = 45 \text{ deg} \quad \text{AASHTO GFRP 2.7.3.6.1}$$

For simplified sectional modulus calculation, assume the whole cross section is rectangular, where:

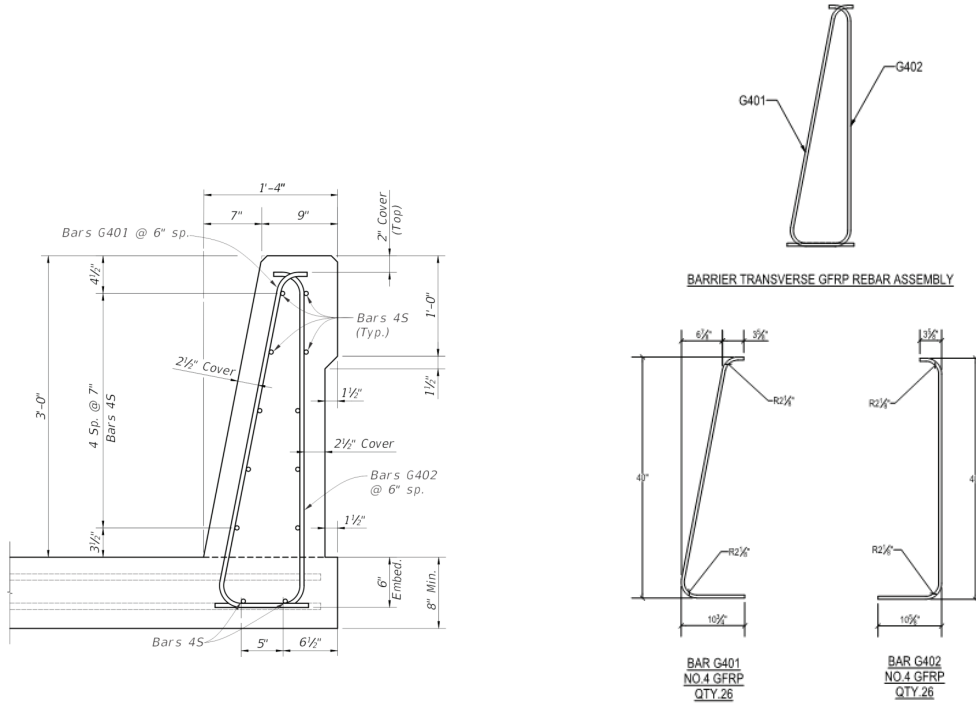
$$h = 36 \text{ in} \quad b = \frac{9 \text{ in} + 14.5 \text{ in}}{2} = 11.75 \cdot \text{in}$$

$$V_c = 0.0316 \cdot \beta \cdot \sqrt{f'_c \cdot \text{ksi}} \cdot b \cdot h = 16.6 \cdot \text{kip} \quad \text{AASHTO GFRP 2.7.3.4-1}$$

CheckMinShearReinf = if($0.75V_c \geq V_{\text{impact}}$, "OK", "Need more reinforcement") = "OK"

GRFP Reinforcement Verification Transverse bars G401, G402

This MathCAD worksheet is intended to check the proposed GFRP rebar layout using existing design specifications and guidelines. Due to the complex two directional bending reaction under impact, the verification references to the shear and moment results estimated using Roark's equations. The design aids referenced in this calculation is AASHTO GFRP 2018 edition.



GFRP Properties

GFRP rebar properties used are design values obtained from Owens Corning Aslan product datasheet.

PHYSICAL & MECHANICAL PROPERTIES

Nominal Diameter		Nominal Area		f _{tu} Guaranteed Tensile Strength		Ultimate Tensile Load		E, Tensile Modulus of Elasticity		Ultimate Strain	
Size	mm	in	mm ²	in ²	MPa	ksi	kN	kips	GPa	psi 10 ⁶	%
2	6	1/4	31.67	0.049	896	130	28.34	6.37	46	6.7	1.94%
3	10	3/8	71.26	0.110	827	120	58.72	13.20	46	6.7	1.79%
4	13	1/2	126.7	0.196	758	110	95.90	21.56	46	6.7	1.64%
5	16	5/8	197.9	0.307	724	105	143.41	32.24	46	6.7	1.57%
6	19	3/4	285.0	0.442	690	100	196.60	44.20	46	6.7	1.49%
7	22	7/8	387.9	0.601	655	95	254.00	57.10	46	6.7	1.42%
8	25	1	506.7	0.785	620	90	314.27	70.65	46	6.7	1.34%
9	29	1-1/8	641.3	0.994	586	85	375.83	84.49	46	6.7	1.27%
10	32	1-1/4	791.7	1.227	551	80	436.60	98.16	46	6.7	1.19%
11*	35	1-3/8	958.1	1.485	482	70	462.40	104*	46	6.7	1.04%
12*	38	1-1/2	1160	1.800	448	65	520.40	117*	46	6.7	0.97%
13*	41	1-5/8	1338	2.074	413	60	553.50	124*	46	6.7	0.90%

*Tensile properties of #11, #12 & #13 bar are NOT guaranteed due to the inability to achieve a valid bar break per ASTM D7205. We reserve the right to make improvements in the product and/or process which may result in benefits or changes to some physical-mechanical characteristics. The data contained herein is considered representative of current production and is believed to be reliable and to represent the best available characterization of the product as of July 2011. Tensile tests per ASTM D7205.

Use GFRP #4 bars

$$d_b = 0.5 \text{ in}$$

Nominal bar diameter

$$A_b = 0.196 \text{ in}^2$$

Nominal bar area

$f_{fu} = 110\text{ksi}$	Guaranteed tensile strength
$E_f = 6.7 \cdot 10^6 \text{psi}$	Tensile modulus of elasticity
$\epsilon_{fu} = 1.64\%$	Ultimate strain
$s = 6\text{in}$	Transverse bar spacing
$n = 4$	Number of bars per linear foot
$A_f = n \cdot A_b = 0.784 \cdot \text{in}^2$	Area of reinforcement

Rail Concrete Properties

$f_c = 3400\text{psi}$	Specified compressive strength of rail concrete
$\epsilon_{cu} = 0.003$	Concrete ultimate strain

$$\beta_1 = \begin{cases} 0.85 & \text{if } f_c \leq 4000\text{psi} \\ 0.85 - \frac{f_c - 4000\text{psi}}{1000\text{psi}} \cdot 0.05 & \text{if } 4000\text{psi} < f_c < 6000\text{psi} \\ 0.65 & \text{otherwise} \end{cases}$$

$$d_{\text{barrier}} = \left(\frac{9 + 11}{2} \cdot \frac{12}{36} + \frac{11 + 14.5}{2} \cdot \frac{24}{36} \right) \text{in} = 11.83 \cdot \text{in}$$

$$A_{\text{barrier}} = 12\text{in} \cdot d_{\text{barrier}} = 142 \cdot \text{in}^2 \quad \text{Cross sectional area of the base of the rail per ft}$$

$$\rho_f = \frac{A_f}{A_{\text{barrier}}} = 0.0055 \quad \text{Reinforcement ratio vertical bars}$$

Tensile Strength Calculation

AASHTO GFRP 2.4.2, 2.6.3

$$C_E = 0.7 \quad \text{Environmental reduction factor AASHTO table 2.4.2.1-1}$$

$$f_{fd} = C_E \cdot f_{fu} = 77 \cdot \text{ksi} \quad \text{Design tensile strength; Effective strength when tension controls}$$

$$\epsilon_{fd} = C_E \cdot \epsilon_{fu} = 0.011 \quad \text{Design tensile strain}$$

$$f_f = \sqrt{\frac{(E_f \cdot \epsilon_{cu})^2}{4} + \frac{0.85 \cdot \beta_1 \cdot f_c}{\rho_f} \cdot E_f \cdot \epsilon_{cu} - 0.5 \cdot E_f \cdot \epsilon_{cu}} = 85.05 \cdot \text{ksi} \quad \text{Effective strength when compression controls 2.6.3.1-1}$$

Development Length Calculation

AASHTO GFRP 2.9.7.4

$$f_{fr} = \min(f_f, f_{fd}) = 77 \cdot \text{ksi} \quad \text{Required GFRP reinforcing bar stress 2.7.3.7-2}$$

$$\alpha \theta = 1 \quad \text{Bar location modification factor.} \\ \text{1 for most cases.} \\ \text{1.5 for bars with more than 12 in. of concrete cast below.}$$

$$C = \min\left(\frac{1}{2} \cdot 6\text{in}, 2.5\text{in} + \frac{1}{2} \cdot d_b\right) = 2.75 \cdot \text{in} \quad \text{Lesser of the cover to the center of the bar or one-half of the center-to-center spacing of the bars being developed, in}$$

$$C_{db} = \min\left(3.5, \frac{C}{d_b}\right) = 3.5 \quad C / d_b$$

$$L_d = \frac{31.6\alpha \cdot \frac{f_{fd}}{\sqrt{f_c \cdot \text{ksi}}} - 340}{13.6 + C_{db}} \cdot d_b = 28.64 \cdot \text{in} \quad \text{Development length in the rail}$$

$$L_{G401.rail} = 32.5 \text{in} \quad L_{G402.rail} = 31.25 \text{in} \quad \text{Embedded bend bar length in deck}$$

$$\text{CheckMinHookLength} = \text{if}(L_d < \min(L_{G401.rail}, L_{G402.rail}), \text{"OK"}, \text{"Need longer bars"}) = \text{"OK"}$$

Bent Bar Hook Length Calculation

AASHTO GFRP 2.9.7.4.3

$$f_{c.deck} = 4500 \text{psi} \quad \text{Deck concrete design compressive strength}$$

$$L_{dh} = \begin{cases} 63.2 \cdot \frac{d_b}{\sqrt{f_{c.deck} \div \text{ksi}}} & \text{if } f_{fd} \leq 75 \text{ksi} \\ \frac{f_{fd} \div \text{ksi}}{1.2} \cdot \frac{d_b}{\sqrt{f_{c.deck} \div \text{ksi}}} & \text{if } 75 \text{ksi} < f_{fd} < 150 \text{ksi} \\ 126.4 \cdot \frac{d_b}{\sqrt{f_{c.deck} \div \text{ksi}}} & \text{if } f_{fd} \geq 150 \text{ksi} \end{cases}$$

$$L_{dh} = 15.12 \cdot \text{in} \quad \text{Bar bend hook length in the deck}$$

$$L_{G401.emb} = 15.625 \text{in} \quad L_{G402.emb} = 15.5 \text{in} \quad \text{Embedded bend bar length in deck}$$

$$\text{CheckMinHookLength} = \text{if}(L_{dh} < \min(L_{G401.emb}, L_{G402.emb}), \text{"OK"}, \text{"Need longer bars"}) = \text{"OK"}$$

Shrinkage and Temperature Reinforcement

AASHTO GFRP 2.9.6

When the impact load is applied, the longitudinal bars can be treated as shrinkage and temperature reinforcement.

$$n_{\text{each.side}} = 4 \quad \text{Longitudinal bars at each side}$$

$$A_{\text{concrete}} = 12 \text{in} \cdot \left(\frac{9 + 11}{2} \cdot \frac{12}{36} + \frac{11 + 14.5}{2} \cdot \frac{24}{36} \right) \text{in} = 142 \cdot \text{in}^2 \quad \text{Rail cross sectional area per 12"}$$

$$\rho_{f.\text{each.face}} = \frac{n_{\text{each.side}} \cdot A_b}{A_{\text{concrete}}} = 0.00552 \quad \text{Ratio of shrinkage and temperature longitudinally in each side of the rail}$$

$$\rho_{f.st.\text{max}} = 0.0036 \quad \text{Required maximum reinforcement for shrinkage and temperature}$$

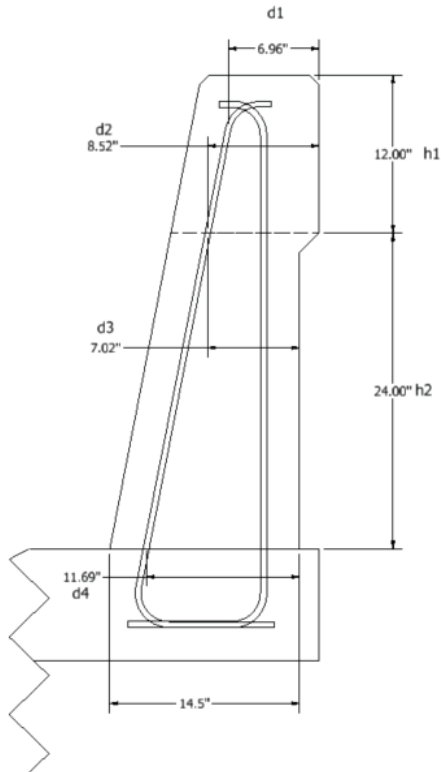
$$\text{CheckShrinkTempReinf} = \text{if}(\rho_{f.\text{each.face}} \geq \rho_{f.st.\text{max}}, \text{"OK"}, \text{"Not enough"}) = \text{"OK"}$$

Limit State Calculation

AASHTO GFRP 2.6.3.2, ACI 440.1R-15

Flexural resistance calculation:

Barrier is divided to two sections due to thickness changes.



Using ACI method:

Calculate the reinforcement ratio at the balanced failure condition:

$$\rho_{fb} = 0.85 \cdot \beta_1 \cdot \frac{f_c}{f_{fd}} \cdot \frac{E_f \cdot \epsilon_{cu}}{E_f \cdot \epsilon_{cu} + f_{fd}} = 0.0066 \quad \text{ACI 7.2.1b}$$

Calculate the reinforcement ratio in a 12" strip section with 4 tension bars :

$$A_{\text{barrier}} = 142 \cdot \text{in}^2$$

$$\rho_f = \frac{4 \cdot A_b}{A_{\text{barrier}}} = 0.0055$$

$$\text{LimitState} = \begin{cases} \text{"tension control"} & \text{if } \rho_f < \rho_{fb} \\ \text{"compression control"} & \text{if } \rho_f > \rho_{fb} \end{cases}$$

LimitState = "tension control"

Using AASHTO method:

$$d_1 = 2.86 \text{in}$$

$$d_2 = 11.69 \text{in}$$

Depth of two layers of rebar

$$b_{\text{rec}} = 12 \text{in}$$

By balancing two layers of rebars:

$$c = \frac{2A_b \cdot \frac{(d_1 - c) \cdot f_f}{d_2 - c} + 2 \cdot A_b \cdot f_f}{0.85f_c \cdot b_{rec} \cdot \beta_1}$$

Guess:

$$c = 1.301 \text{ in}$$

$$\frac{2A_b \cdot \frac{(d_1 - c) \cdot f_f}{d_2 - c} + 2 \cdot A_b \cdot f_f}{0.85f_c \cdot b_{rec} \cdot \beta_1} = 1.301 \cdot \text{in}$$

$$\epsilon_{ft1} = \frac{d_1 - c}{c} \cdot \epsilon_{cu} = 0.004$$

$$\epsilon_{ft2} = \frac{d_2 - c}{c} \cdot \epsilon_{cu} = 0.024$$

$$\epsilon_{fd} = 0.0115$$

$$\text{LimitState}(\epsilon_{ft}) = \begin{cases} \text{"tension control"} & \text{if } \epsilon_{ft} > \epsilon_{fd} \\ \text{"compression control"} & \text{if } \epsilon_{ft} < \epsilon_{fd} \end{cases}$$

$$\text{LimitState}(\epsilon_{ft1}) = \text{"compression control"}$$

$$\text{LimitState}(\epsilon_{ft2}) = \text{"tension control"}$$

Minimum Reinforcement Calculation

AASHTO GFRP 2.6.3.3

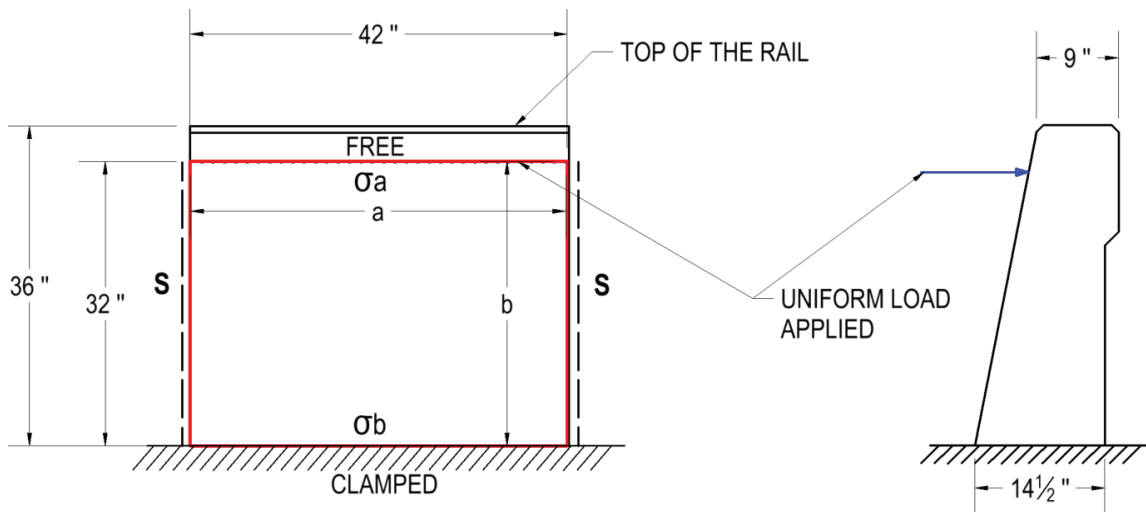
The requirement of minimum reinforcement provisions are intended to reduce the probability of brittle failure upon concrete cracking. AASHTO GFRP 2.6.3.3.

$$f_r = 0.24 \sqrt{f_c} \cdot \text{ksi} = 0.443 \cdot \text{ksi} \quad \text{Rail concrete modulus of rupture}$$

$$h = 12 \text{ in} \quad b = 14.5 \text{ in}$$

$$S_r = \frac{1}{6} \cdot b^2 \cdot h = 420.5 \cdot \text{in}^3$$

Assume load results in a simply supported moment reaction, using Roarks formula to estimate resultant moment and shear:



$L_t = 3.5\text{ft}$ Longitudinal length of distribution of impact force F_t along the railing
 $F_{tr} = 68\text{kip}$ Transverse vehicle impact force adjusted based on TTI research
 $H_e = 32\text{in}$ Effective height AASHTO LRFD
 $M_{\text{impact}} = 11.2\text{kip}\cdot\text{ft}$ Impact flexural moment about rail horizontal axis
 $\phi\theta = 1.0$ Extreme event resistance factor AASHTO GFRP2.5.6

$$c_b = \frac{\epsilon_{cu}}{\epsilon_{cu} + \epsilon_{fd}} \cdot d_2 = 2.422 \cdot \text{in}$$

$$\phi M = \phi \cdot (2A_b) \cdot f_{fd} \cdot \left(d_2 - \frac{\beta_1 \cdot c_b}{2} \right) + \phi \cdot (2A_b) \cdot f_{fd} \cdot \left(\frac{d_1 - c_b}{d_2 - c_b} \right) \cdot \left(d_1 - \frac{\beta_1 \cdot c_b}{2} \right) = 27 \cdot \text{kip}\cdot\text{ft}$$

CheckMinFlexReinf = if($\phi M \geq \min(1.33 \cdot M_{\text{impact}}, 1.6 f_r S_r)$, "OK", "Need more reinforcement") = "OK"

Shear Reinforcement Verification Simplified Method

AASHTO GFRP 2.7.3.4

$V_{\text{impact}} = 1.0\text{kip}$ Transverse impact induced maximum shear, estimated using Roark's formula

$$E_f = 6.7 \times 10^6 \text{psi} \quad E_c = 57000 \sqrt{f'_c} \cdot \text{psi} = 3.324 \times 10^6 \text{psi}$$

$$n_f = \frac{E_f}{E_c} = 2.016 \quad \rho_f = 0.006$$

$$k = \sqrt{2 \cdot \rho_f \cdot n_f + (\rho_f \cdot n_f)^2} - \rho_f \cdot n_f = 0.138 \quad \text{AASHTO GFRP2.5.3-4}$$

$$\beta\theta = 5 \cdot k = 45\text{deg} \quad \text{AASHTO GFRP2.7.3.6.1}$$

For simplified sectional modulus calculation, assume the cross section is rectangular, where:

$$h = 12\text{in} \quad b = \frac{9\text{in} + 14.5\text{in}}{2} = 11.75 \cdot \text{in}$$

$$V_c = 0.0316 \cdot \beta \cdot \sqrt{f'_c} \cdot \text{ksi} \cdot b \cdot h = 5.7 \cdot \text{kip} \quad \text{AASHTO GFRP2.7.3.4-1}$$

CheckMinShearReinf = if($0.75 V_c \geq V_{\text{impact}}$, "OK", "Need more reinforcement") = "OK"

Steel Reinforced Rail Calculation Longitudinal bars 4S

This MathCAD worksheet is intended to calculate the steel section capacity for FEA beam verification and comparison.

$d_b = 0.5\text{in}$	Nominal bar diameter
$A_b = 0.2\text{in}^2$	Nominal bar area
$f_y = 60\text{ksi}$	Guaranteed tensile strength
$E_f = 2.9 \cdot 10^9\text{psi}$	Tensile modulus of elasticity
$\epsilon_{fu} = 20\%$	Ultimate strain
$n = 10$	Number of longitudinal bars in the rail
$A_f = n \cdot A_b = 2 \cdot \text{in}^2$	Longitudinal reinforcement area

Rail Concrete Properties

$f_c = 3400\text{psi}$	Specified compressive strength of rail concrete
$\epsilon_{cu} = 0.003$	Concrete ultimate strain

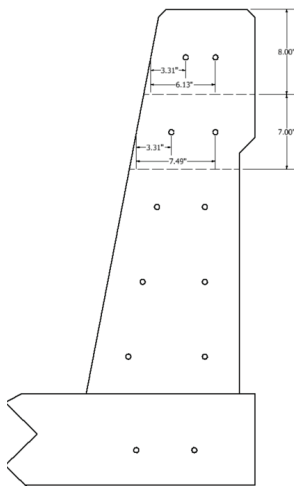
$$\beta_1 = \begin{cases} 0.85 & \text{if } f_c \leq 4000\text{psi} \\ 0.85 - \frac{f_c - 4000\text{psi}}{1000\text{psi}} \cdot 0.05 & \text{if } 4000\text{psi} < f_c < 6000\text{psi} \\ 0.65 & \text{otherwise} \end{cases}$$

$A_{\text{barrier}} = 414.6\text{in}^2$	Cross sectional area of the rail
$\rho_f = \frac{A_f}{A_{\text{barrier}}} = 0.005$	Reinforcement ratio (longitudinal bars over rail cross section)

A general equation $\phi \cdot M_n = \phi \cdot A_s \cdot f_y \cdot \left(d - \frac{a}{2} \right)$ is used to calculate moment capacity provided by each bar

$\phi\theta = 1.0$ Extreme event resistance factor

$A_s = A_b = 0.2 \cdot \text{in}^2$ Both layers of longitudinal bars are in tension



$$d_1 = 3.31 \text{ in} \qquad d_2 = \frac{6.13 \text{ in} + 7.49 \text{ in}}{2} = 6.81 \text{ in}$$

Depth of two layers of rebar

$$b_{\text{rec}} = 15 \text{ in} \qquad \text{Height of the top portion of the rail}$$

$$d_{\text{rec}} = 9.5 \text{ in}$$

$$a = \frac{4A_s \cdot f_y}{0.85 \cdot f'_c \cdot b_{\text{rec}}} = 1.107 \text{ in}$$

Limit state check:

$$\epsilon_{fd} = 0.00207 \qquad \beta_1 = 0.85 \qquad \epsilon_{cu} = 0.003$$

$$\text{LimitState}(\epsilon_{ft}) = \begin{cases} \text{"steel yield"} & \text{if } \epsilon_{ft} > \epsilon_{fd} \\ \text{"steel not yield"} & \text{if } \epsilon_{ft} < \epsilon_{fd} \end{cases}$$

$$c = \left(\frac{a}{\beta_1} \right) = 1.303 \text{ in}$$

$$\epsilon_{ft1} = \frac{d_1 - c}{c} \cdot \epsilon_{cu} = 0.00462 \qquad \text{LimitState}(\epsilon_{ft1}) = \text{"steel yield"}$$

$$\epsilon_{ft2} = \frac{d_2 - c}{c} \cdot \epsilon_{cu} = 0.01268 \qquad \text{LimitState}(\epsilon_{ft2}) = \text{"steel yield"}$$

$$\phi M_n = \phi \cdot 2A_s \cdot f_y \cdot \left(d_2 - \frac{a}{2} \right) + \phi \cdot 2A_s \cdot f_y \cdot \left(d_1 - \frac{a}{2} \right) = 18.03 \cdot \text{kip} \cdot \text{ft}$$

Steel Section Capacity Transverse bars 4P, 4V

This MathCAD worksheet is intended to calculate the steel section capacity for FEA beam verification and comparison.

$d_b = 0.5\text{in}$	Nominal bar diameter
$A_b = 0.2\text{in}^2$	Nominal bar area
$f_y = 60\text{ksi}$	Guaranteed tensile strength
$E_f = 2.9 \cdot 10^9 \text{psi}$	Tensile modulus of elasticity
$\epsilon_{fu} = 20\%$	Ultimate strain
$n = 10$	Number of longitudinal bars in the rail
$A_f = n \cdot A_b = 2 \cdot \text{in}^2$	Longitudinal reinforcement area

Rail Concrete Properties

$f_c = 3400\text{psi}$	Specified compressive strength of rail concrete
$\epsilon_{cu} = 0.003$	Concrete ultimate strain

$$\beta_1 = \begin{cases} 0.85 & \text{if } f_c \leq 4000\text{psi} \\ 0.85 - \frac{f_c - 4000\text{psi}}{1000\text{psi}} \cdot 0.05 & \text{if } 4000\text{psi} < f_c < 6000\text{psi} \\ 0.65 & \text{otherwise} \end{cases}$$

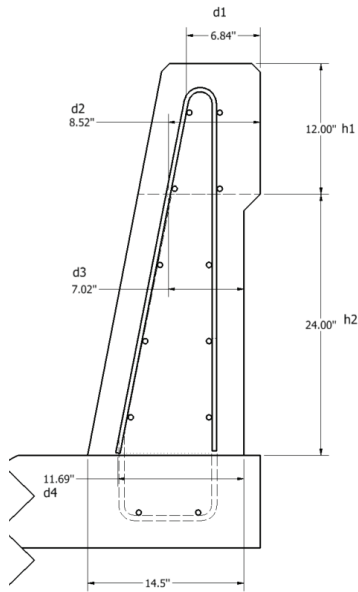
$A_{\text{barrier}} = 414.6\text{in}^2$	Cross sectional area of the rail
$\rho_f = \frac{A_f}{A_{\text{barrier}}} = 0.005$	Reinforcement ratio (longitudinal bars over rail cross section)

A general equation $\phi \cdot M_n = \phi \cdot A_s \cdot f_y \cdot \left(d - \frac{a}{2} \right)$ is used to calculate moment capacity provided by each bar

$\phi_{\theta} = 1.0$ Extreme event resistance factor AASHTO GFRP 2.5.6

The flexural resistance of a GFRP reinforced member is dependent on whether the failure is controlled by crushing of the concrete or rupture of GFRP bars.

$A_s = A_b = 0.2 \cdot \text{in}^2$ Both layers of longitudinal bars are in tension



Limit State Calculation

AASHTO GFRP 2.6.3.2, ACI 440.1R-15

Flexural resistance calculation:

Barrier is divided to two sections due to thickness changes.

$$d_1 = 2.75 \text{ in}$$

$$d_2 = 11.69 \text{ in}$$

Depth of two layers of rebar

$$b_{\text{rec}} = 12 \text{ in}$$

$$a = \frac{4A_s \cdot f_y}{0.85 \cdot f'_c \cdot b_{\text{rec}}} = 1.384 \text{ in}$$

Limit state check:

$$\epsilon_{fd} = 0.00207 \quad \beta_1 = 0.85 \quad \epsilon_{cu} = 0.003$$

$$\text{LimitState}(\epsilon_{ft}) = \begin{cases} \text{"steel yield"} & \text{if } \epsilon_{ft} > \epsilon_{fd} \\ \text{"steel not yield"} & \text{if } \epsilon_{ft} < \epsilon_{fd} \end{cases}$$

$$c = \left(\frac{a}{\beta_1} \right) = 1.628 \text{ in}$$

$$\epsilon_{ft1} = \frac{d_1 - c}{c} \cdot \epsilon_{cu} = 0.002067 \quad \text{LimitState}(\epsilon_{ft1}) = \text{"steel not yield"}$$

$$\epsilon_{ft2} = \frac{d_2 - c}{c} \cdot \epsilon_{cu} = 0.01854 \quad \text{LimitState}(\epsilon_{ft2}) = \text{"steel yield"}$$

$$\phi M_n = \phi \theta A_s \cdot f_y \cdot \left(d_2 - \frac{a}{2} \right) + \phi \cdot 2A_s \cdot f_y \cdot \frac{\epsilon_{ft1}}{\epsilon_{fd}} \cdot \left(d_1 - \frac{a}{2} \right) = 26.1 \cdot \text{kip} \cdot \text{ft}$$

Steel Reinforced Rail Calculation (Critical Length)

A full cross sectional analysis is performed on standard steel reinforced rail to calculate the critical length of the rail based on AASHTO LRFD 2017) Chapter 13.

Longitudinal Rebar 4S)

$$A_s = 0.2 \text{ in}^2$$

Longitudinal bar diameter

$$f_y = 60 \text{ ksi}$$

Bar yield stress

$$f_c = 3400 \text{ psi}$$

Concrete strength

$$\phi = 1.0$$

(Extreme event

Zone Properties:

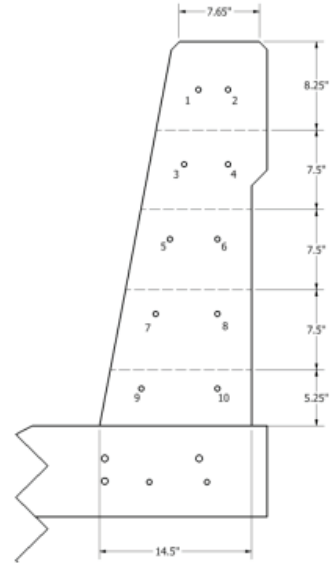
$$b_{\text{zone}_1} = 8.25 \text{ in} \quad x_{12} = 2.81 \text{ in} \quad d_{\text{bar}_1} = 6.56 \text{ in} \quad d_{\text{bar}_2} = 6.13 \text{ in}$$

$$b_{\text{zone}_2} = 7.5 \text{ in} \quad x_{34} = 4.18 \text{ in} \quad d_{\text{bar}_3} = 7.93 \text{ in} \quad d_{\text{bar}_4} = 7.49 \text{ in}$$

$$b_{\text{zone}_3} = 7.5 \text{ in} \quad x_{56} = 4.54 \text{ in} \quad d_{\text{bar}_5} = 7.79 \text{ in} \quad d_{\text{bar}_6} = 7.85 \text{ in}$$

$$b_{\text{zone}_4} = 7.5 \text{ in} \quad x_{78} = 5.9 \text{ in} \quad d_{\text{bar}_7} = 9.15 \text{ in} \quad d_{\text{bar}_8} = 9.21 \text{ in}$$

$$b_{\text{zone}_5} = 5.25 \text{ in} \quad x_{910} = 7.26 \text{ in} \quad d_{\text{bar}_9} = 10.51 \text{ in} \quad d_{\text{bar}_{10}} = 10.57 \text{ in}$$



When interior bars are in tension...

Bar Capacities:

$$a_{\text{zone}_1} = \frac{A_s \cdot f_y}{0.85 f_c \cdot b_{\text{zone}_1}} = 0.503 \cdot \text{in} \quad \phi M_{n_1} = \phi \cdot A_s \cdot f_y \cdot \left(d_{\text{bar}_1} - \frac{a_{\text{zone}_1}}{2} \right) = 6.308 \cdot \text{kip} \cdot \text{ft}$$

$$a_{\text{zone}_2} = \frac{A_s \cdot f_y}{0.85 f_c \cdot b_{\text{zone}_2}} = 0.554 \cdot \text{in} \quad \phi M_{n_2} = \phi \cdot A_s \cdot f_y \cdot \left(d_{\text{bar}_3} - \frac{a_{\text{zone}_2}}{2} \right) = 7.653 \cdot \text{kip} \cdot \text{ft}$$

$$a_{\text{zone}_3} = \frac{A_s \cdot f_y}{0.85 f_c \cdot b_{\text{zone}_3}} = 0.554 \cdot \text{in} \quad \phi M_{n_3} = \phi \cdot A_s \cdot f_y \cdot \left(d_{\text{bar}_5} - \frac{a_{\text{zone}_3}}{2} \right) = 7.513 \cdot \text{kip} \cdot \text{ft}$$

$$a_{\text{zone}_4} = \frac{A_s \cdot f_y}{0.85 f_c \cdot b_{\text{zone}_4}} = 0.554 \cdot \text{in} \quad \phi M_{n_4} = \phi \cdot A_s \cdot f_y \cdot \left(d_{\text{bar}_7} - \frac{a_{\text{zone}_4}}{2} \right) = 8.873 \cdot \text{kip} \cdot \text{ft}$$

$$a_{\text{zone}_5} = \frac{A_s \cdot f_y}{0.85 f_c \cdot b_{\text{zone}_5}} = 0.791 \cdot \text{in} \quad \phi M_{n_5} = \phi \cdot A_s \cdot f_y \cdot \left(d_{\text{bar}_9} - \frac{a_{\text{zone}_5}}{2} \right) = 10.115 \cdot \text{kip} \cdot \text{ft}$$

$$M_{\text{long.int}} = \sum_{i=1}^5 \phi M_{n_i} = 40.462 \cdot \text{kip} \cdot \text{ft}$$

When exterior bars are in tension...

Bar Capacities:

$$\phi M_{n_1} = \phi \cdot A_s \cdot f_y \cdot \left(d_{\text{bar}_2} - \frac{a_{\text{zone}_1}}{2} \right) = 5.878 \cdot \text{kip} \cdot \text{ft}$$

$$\phi M_{n_2} = \phi \cdot A_s \cdot f_y \cdot \left(d_{\text{bar}_4} - \frac{a_{\text{zone}_2}}{2} \right) = 7.213 \cdot \text{kip} \cdot \text{ft}$$

$$\phi M_{n_3} = \phi \cdot A_s \cdot f_y \cdot \left(d_{\text{bar}_6} - \frac{a_{\text{zone}_3}}{2} \right) = 7.573 \cdot \text{kip} \cdot \text{ft}$$

$$\phi M_{n_4} = \phi \cdot A_s \cdot f_y \cdot \left(d_{\text{bar}_8} - \frac{a_{\text{zone}_4}}{2} \right) = 8.933 \cdot \text{kip} \cdot \text{ft}$$

$$\phi M_{n_5} = \phi \cdot A_s \cdot f_y \cdot \left(d_{\text{bar}_{10}} - \frac{a_{\text{zone}_5}}{2} \right) = 10.175 \cdot \text{kip} \cdot \text{ft}$$

$$M_{\text{long,ext}} = \sum_{i=1}^5 \phi M_{n_i} = 39.772 \cdot \text{kip} \cdot \text{ft}$$

$$M_b = \min(M_{\text{long,int}}, M_{\text{long,ext}}) = 39.8 \cdot \text{kip} \cdot \text{ft} \quad \text{Flexural resistance of the wall about its vertical axis}$$

Transverse Rebar 4P & 4V

$$d1 = 6.84 \text{ in} \quad d2 = 8.52 \text{ in} \quad d3 = 7.02 \text{ in} \quad d4 = 11.69 \text{ in}$$

$$h1 = 12 \text{ in} \quad h2 = 24 \text{ in}$$

$$d_{\text{ave}} = \frac{d1 + d2}{2} \cdot \frac{h1}{h1 + h2} + \frac{d3 + d4}{2} \cdot \frac{h2}{h1 + h2} = 8.797 \cdot \text{in}$$

$$b = 12 \text{ in} \quad \text{unit length of the rail}$$

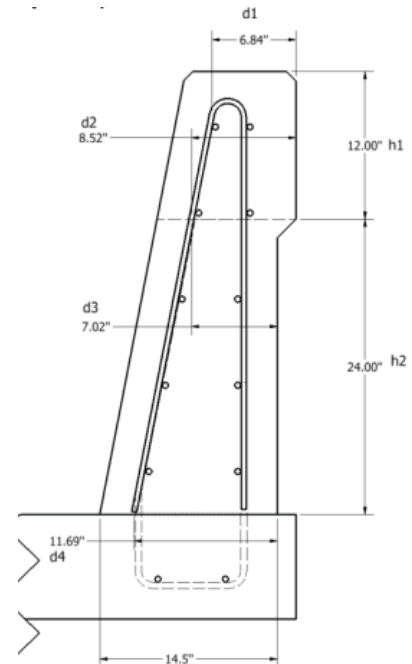
$$s = 6 \text{ in} \quad \text{bar spacing}$$

$$A_{\text{tr}} = 0.4 \text{ in}^2 \quad \text{total area}$$

$$a = \frac{A_{\text{tr}} \cdot f_y}{0.85 f'_c \cdot b} = 0.692 \cdot \text{in}$$

$$M_c = \frac{\phi \cdot A_{\text{tr}} \cdot f_y \cdot \left(d_{\text{ave}} - \frac{a}{2} \right)}{b} = 16.9 \cdot \frac{\text{kip} \cdot \text{ft}}{\text{ft}}$$

Flexural resistance of cantilevered wall



Critical Length A13.3.1

Table A13.2-1—Design Forces for Traffic Railings

Design Forces and Designations	Railing Test Levels					
	TL-1	TL-2	TL-3	TL-4	TL-5	TL-6
F_T Transverse (kips)	13.5	27.0	54.0	54.0	124.0	175.0
F_L Longitudinal (kips)	4.5	9.0	18.0	18.0	41.0	58.0
F_V Vertical (kips) Down	4.5	4.5	4.5	18.0	80.0	80.0
L_t and L_L (ft)	4.0	4.0	4.0	3.5	8.0	8.0
L_v (ft)	18.0	18.0	18.0	18.0	40.0	40.0
H_e (min) (in.)	18.0	20.0	24.0	32.0	42.0	56.0
Minimum H Height of Rail (in.)	27.0	27.0	27.0	32.0	42.0	90.0

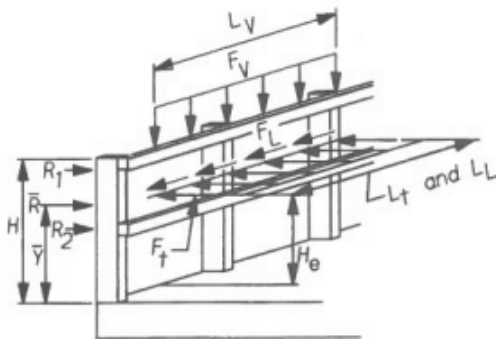


Figure A13.2-1—Metal Bridge Railing Design Forces, Vertical Location, and Horizontal Distribution Length

$$L_t = 3.5 \text{ ft}$$

Transverse force length

$$H = 36 \text{ in}$$

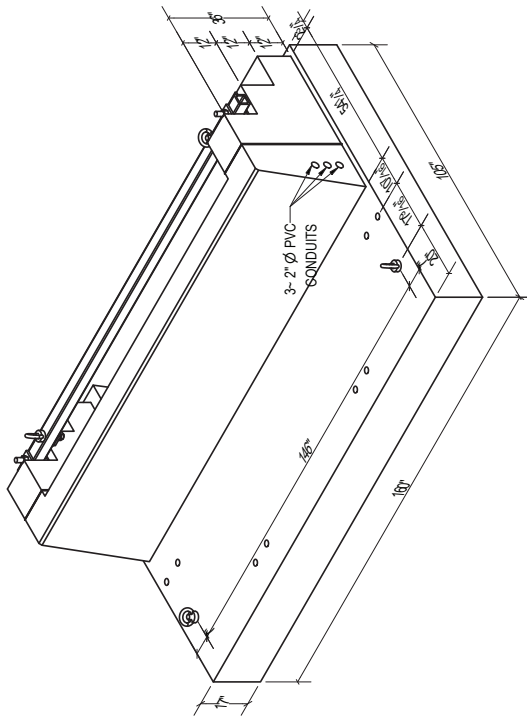
Height of the rail

$$L_c = \frac{L_t}{2} + \sqrt{\left(\frac{L_t}{2}\right)^2 + 8H \cdot \frac{M_b}{M_c}} = 9.466 \text{ ft}$$

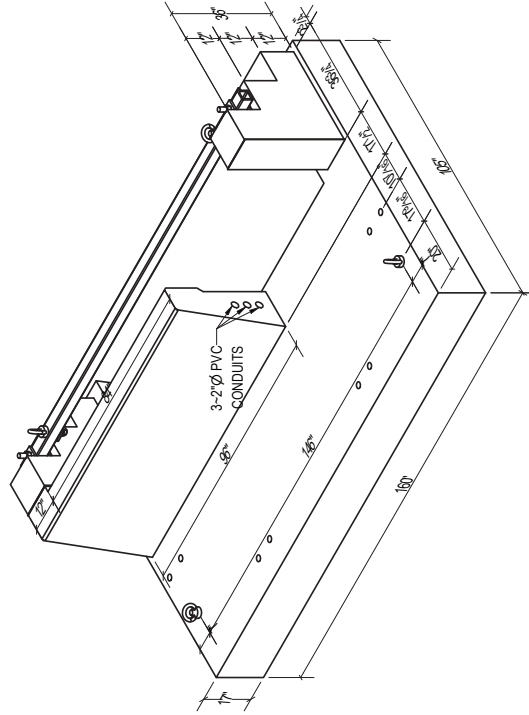
Critical wall length A13.3.1-2

**APPENDIX D:
STRUCTURAL DRAWINGS FOR GFRP-REINFORCED TEST SPECIMEN**

Presented in this appendix are structural drawings for the GFRP-reinforced test specimen developed and tested in this study, with center-of-rail (COR) and end-of-rail (EOR) variations.

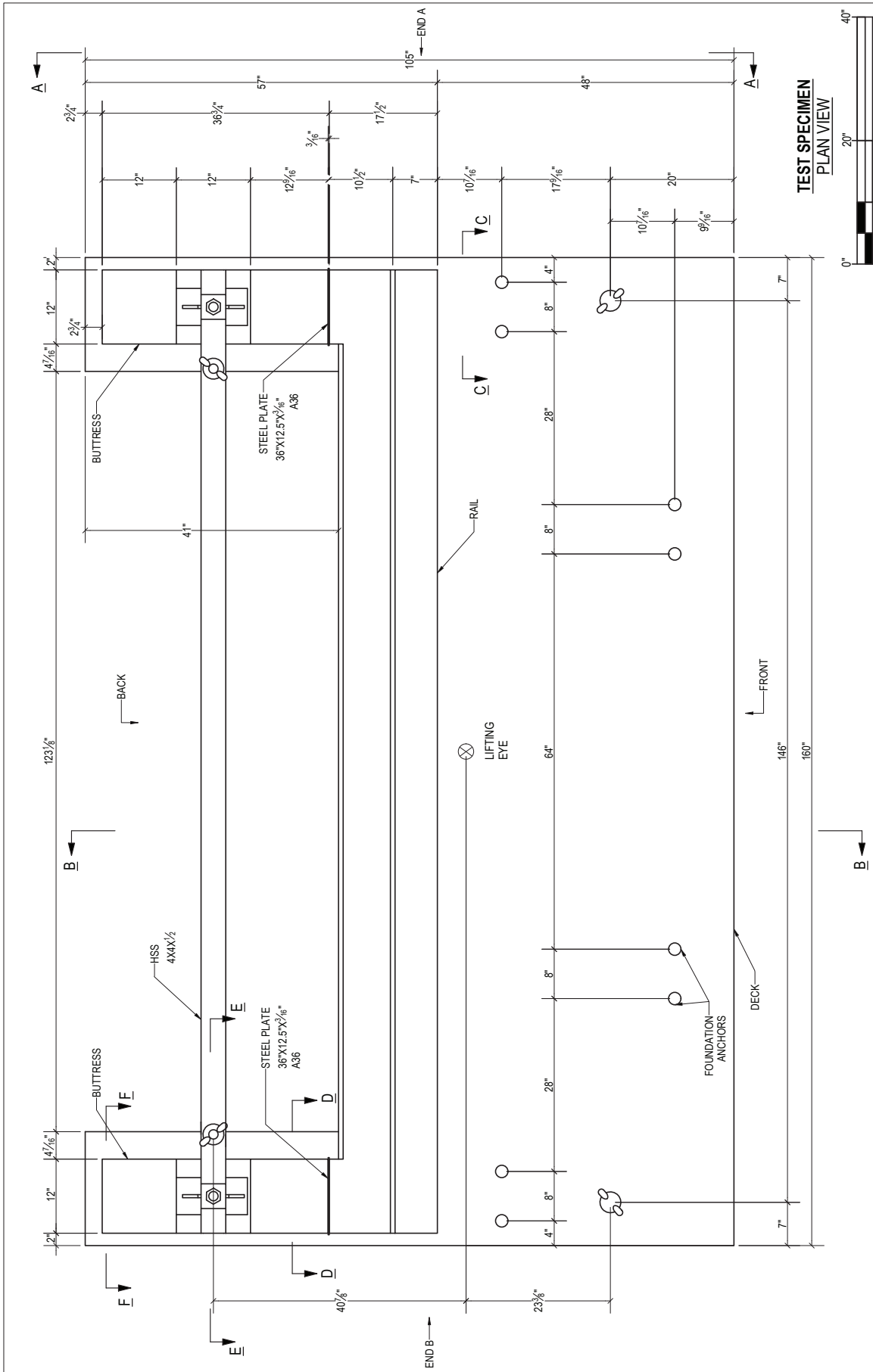


COR TEST SPECIMEN
FRONT ISOMETRIC VIEW

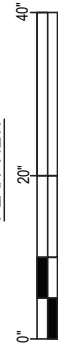


EOR TEST SPECIMEN
FRONT ISOMETRIC VIEW

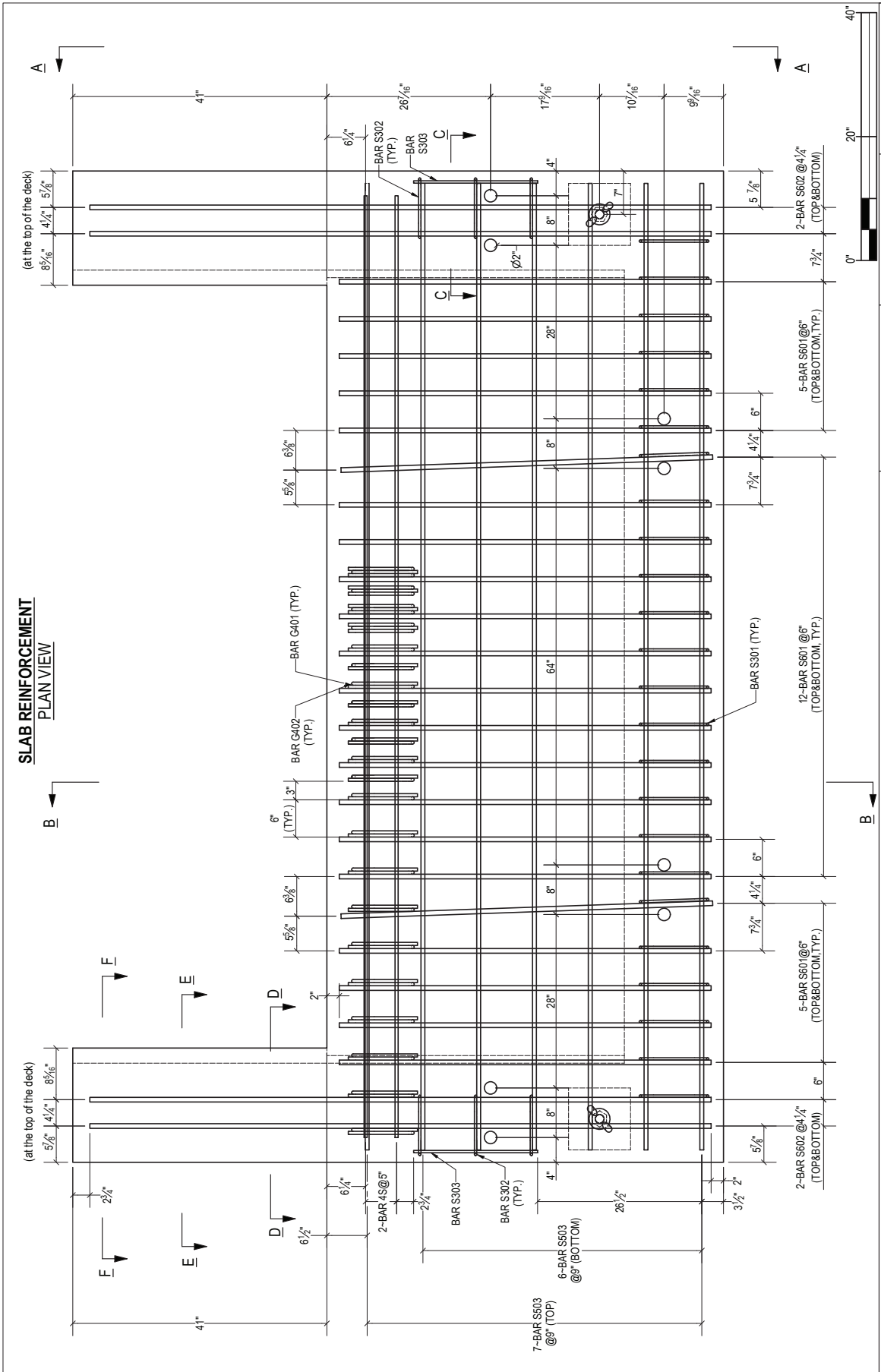
GFRP REINFORCED TEST SPECIMEN		Revision:	
TEST SPECIMEN OVERVIEW	<i>University of Florida</i>	SHEET 1 OF 24	



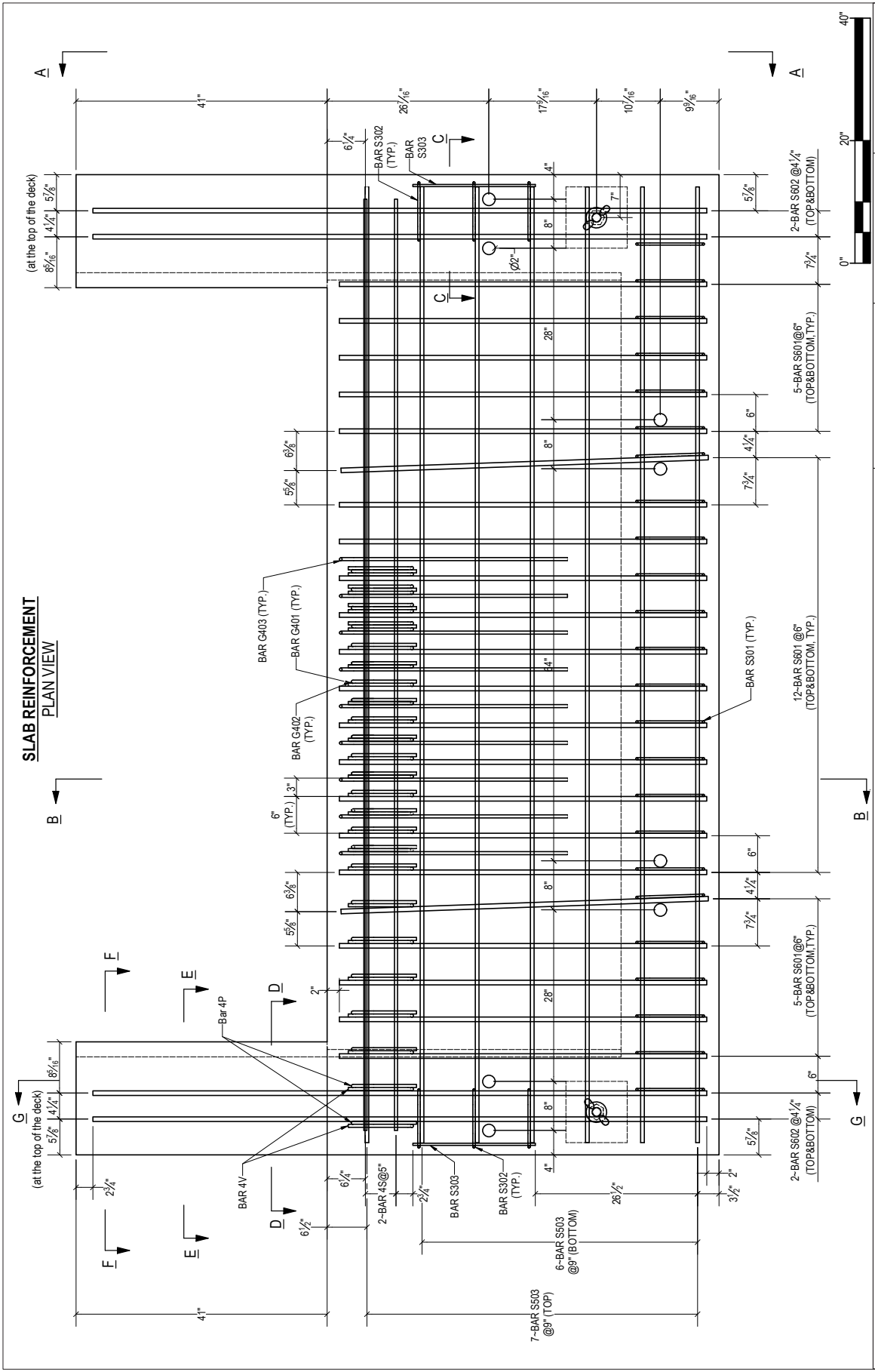
TEST SPECIMEN
PLAN VIEW



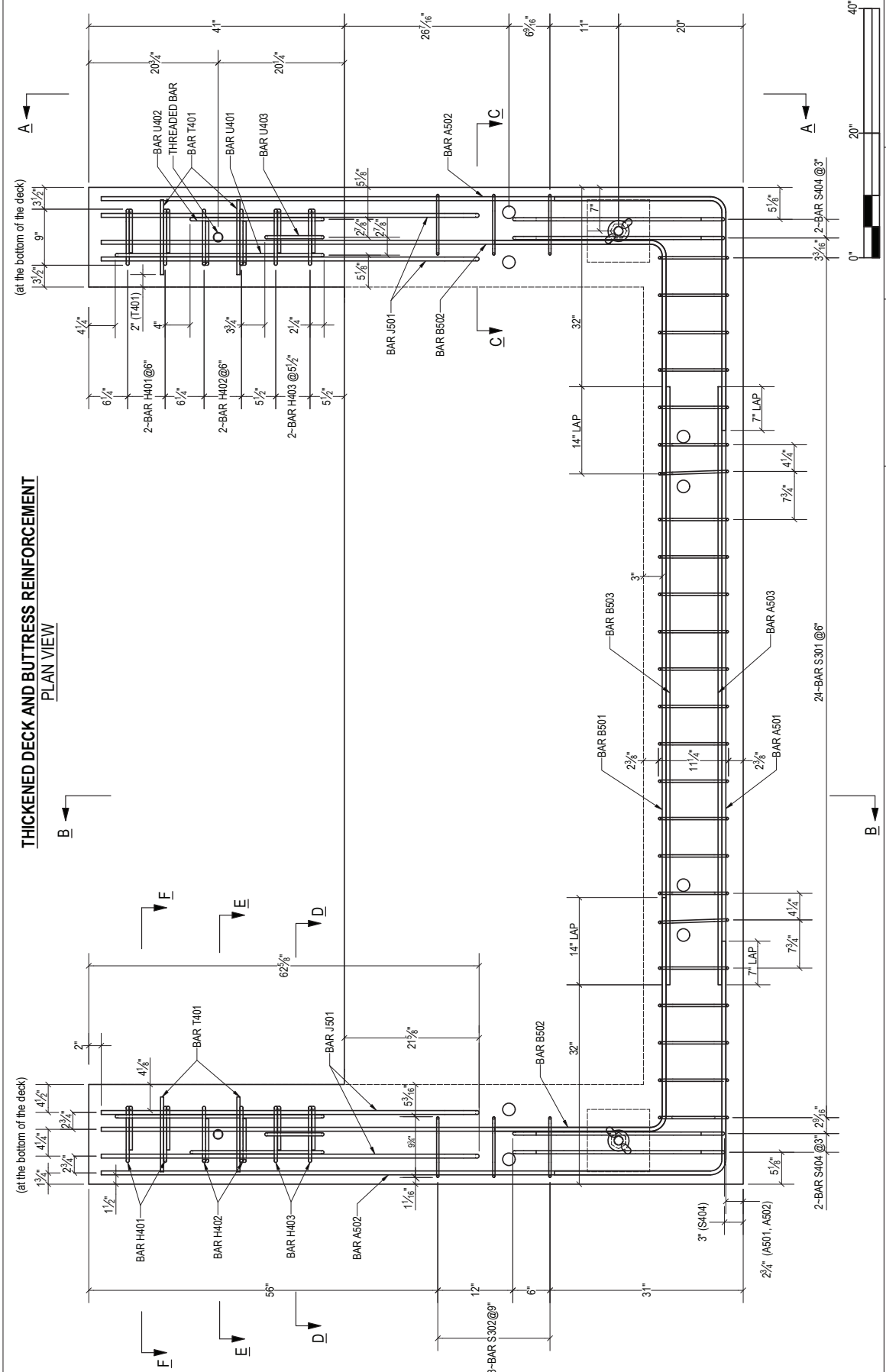
REVISION:	
OVERVIEW: COR TEST SPECIMEN	UNIVERSITY OF FLORIDA
GFRP REINFORCED TEST SPECIMEN	
SHEET 2 OF 24	



Revision:	
SLAB REINFORCEMENT: EOR TEST 1 SPECIMEN	University of Florida
GFRP REINFORCED TEST SPECIMEN	
SHEET 5 OF 24	



<i>GFRP REINFORCED TEST SPECIMEN</i>	
SLAB REINFORCEMENT: EOR TEST 2 SPECIMEN	Revision:
University of Florida	SHEET 6 OF 24



THICKENED DECK AND BUTTRESS REINFORCEMENT
PLAN VIEW

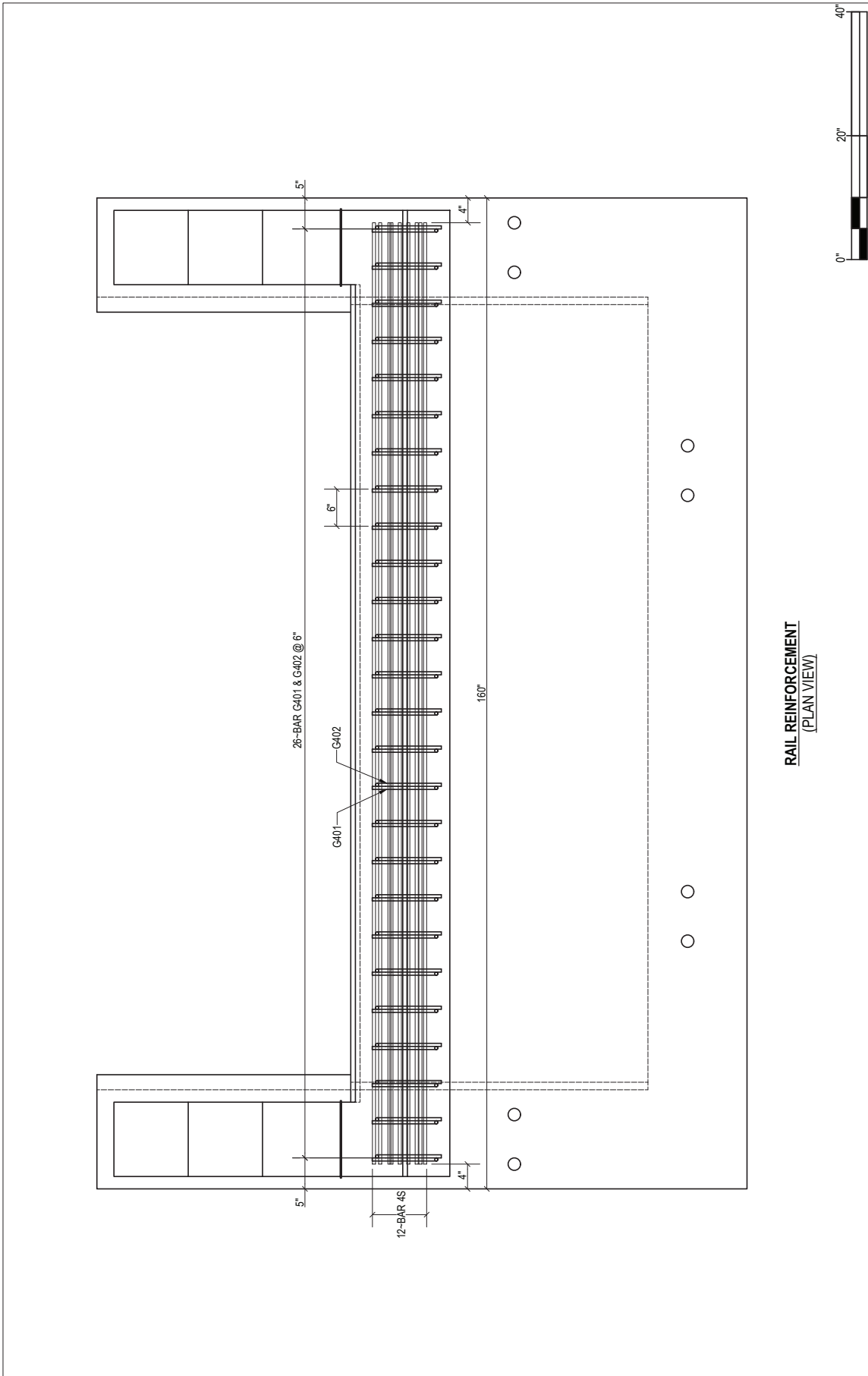
Revision:

SHEET 7 OF 24

University of Florida

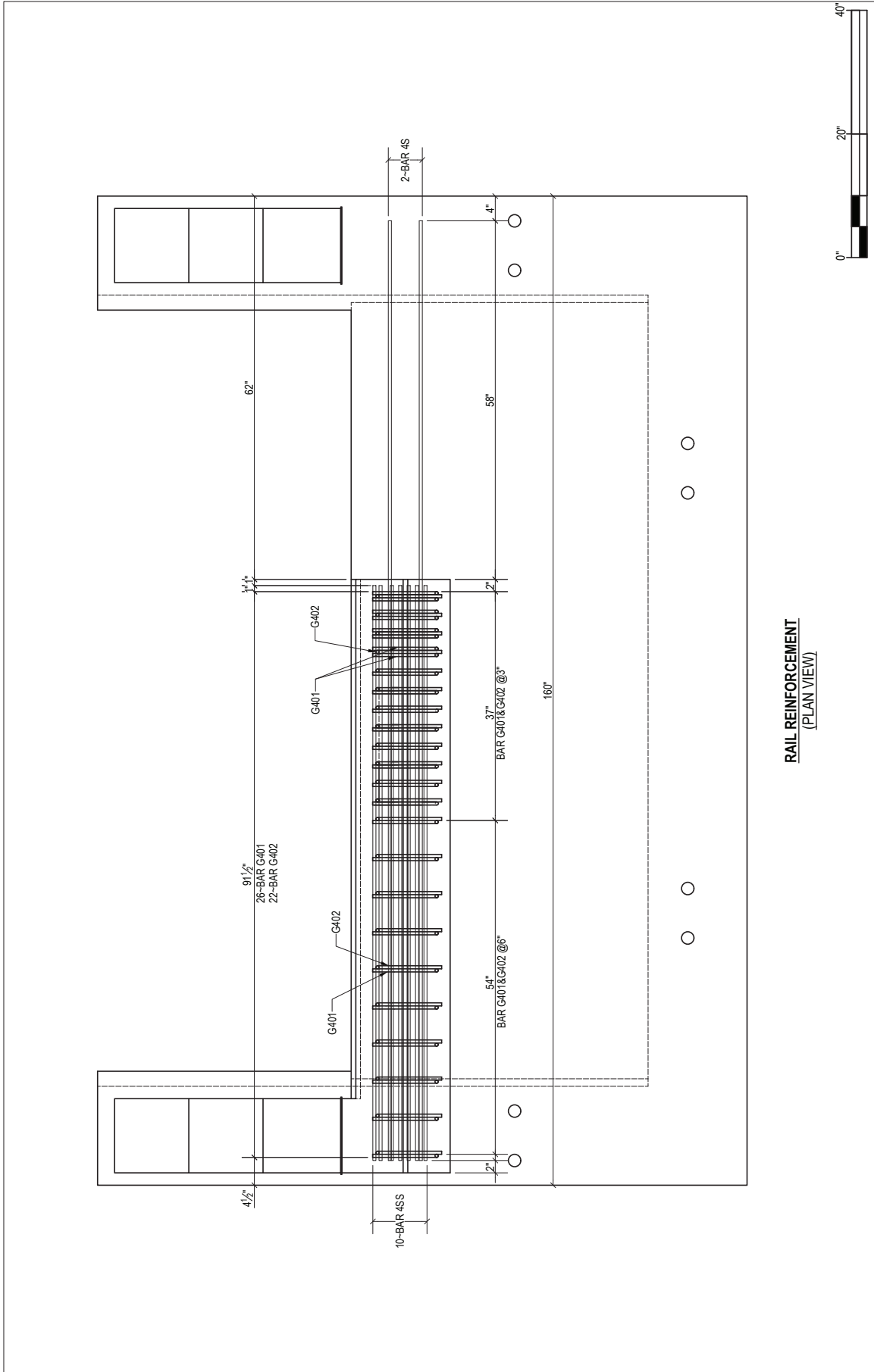
GFRP REINFORCED TEST SPECIMEN

THICKENED DECK REINFORCEMENT



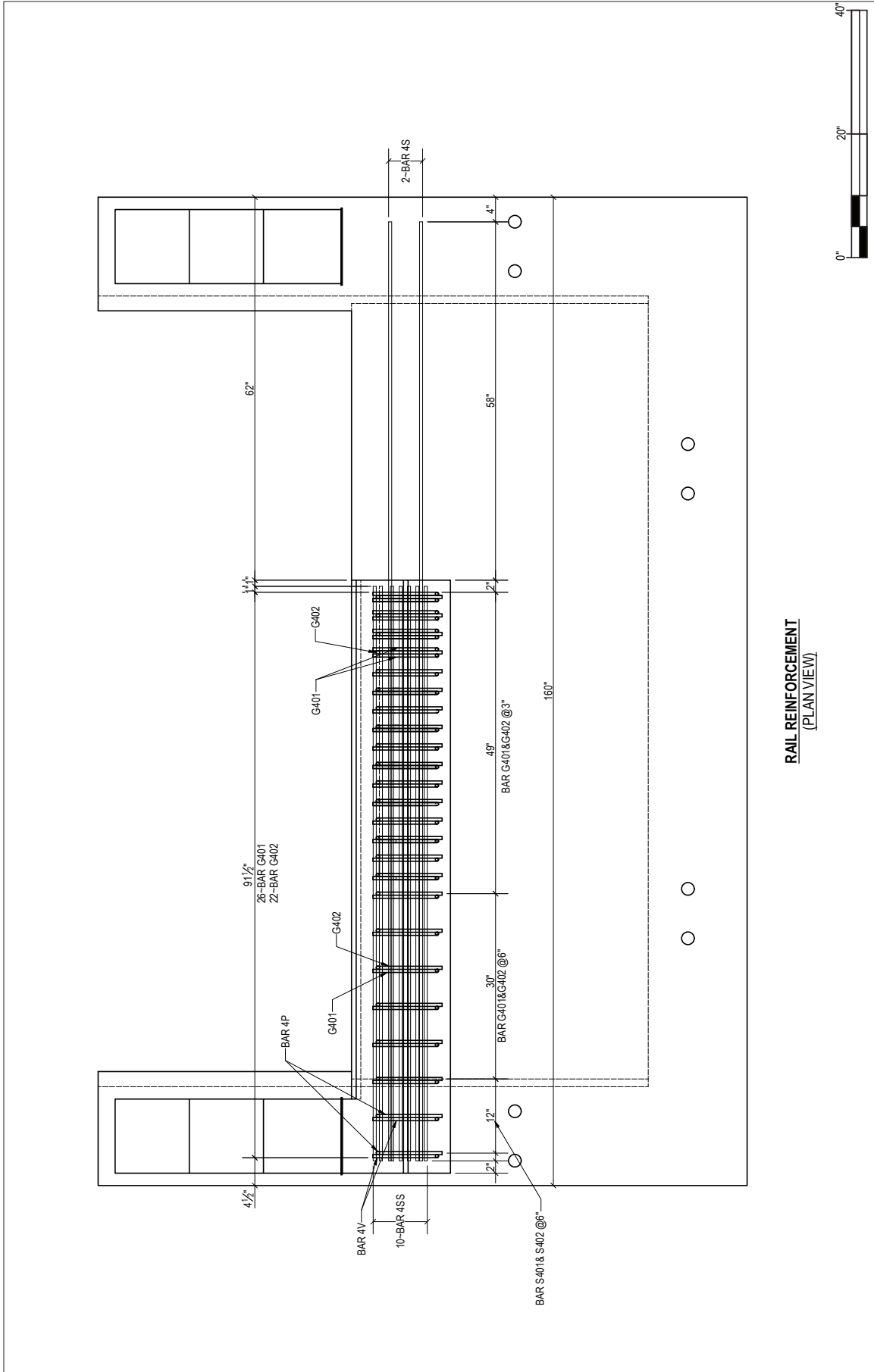
RAIL REINFORCEMENT
(PLAN VIEW)

<i>GFRP REINFORCED TEST SPECIMEN</i>		<i>Revision:</i>	
RAILING REINFORCEMENT: COR TEST SPECIMEN	<i>University of Florida</i>	<i>SHEET 8 OF 24</i>	



RAIL REINFORCEMENT
(PLAN VIEW)

GFRP REINFORCED TEST SPECIMEN		Revision:	
RAILING REINFORCEMENT: EOR TEST 1 SPECIMEN		University of Florida	SHEET 9 OF 24



RAIL REINFORCEMENT
(PLAN VIEW)

<i>GFRP REINFORCED TEST SPECIMEN</i>		<i>Revision:</i>
RAILING REINFORCEMENT: EOR TEST 2 SPECIMEN	<i>University of Florida</i>	<i>SHEET 10 OF 24</i>

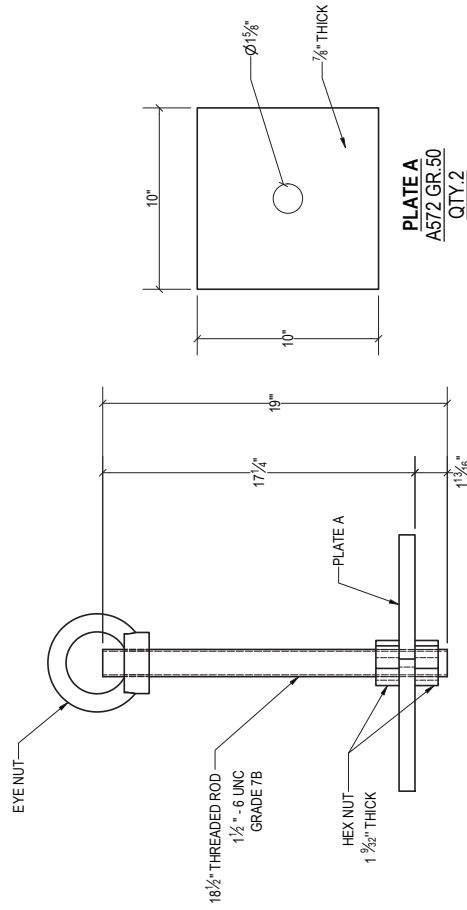
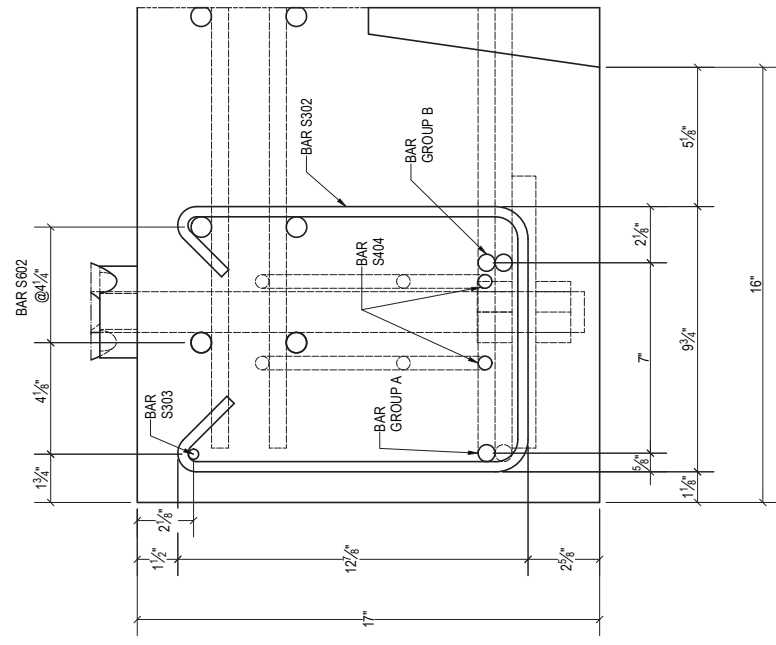
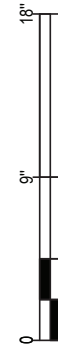
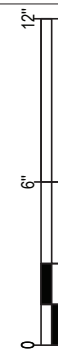


PLATE A
 A572 GR.50
 QTY. 2

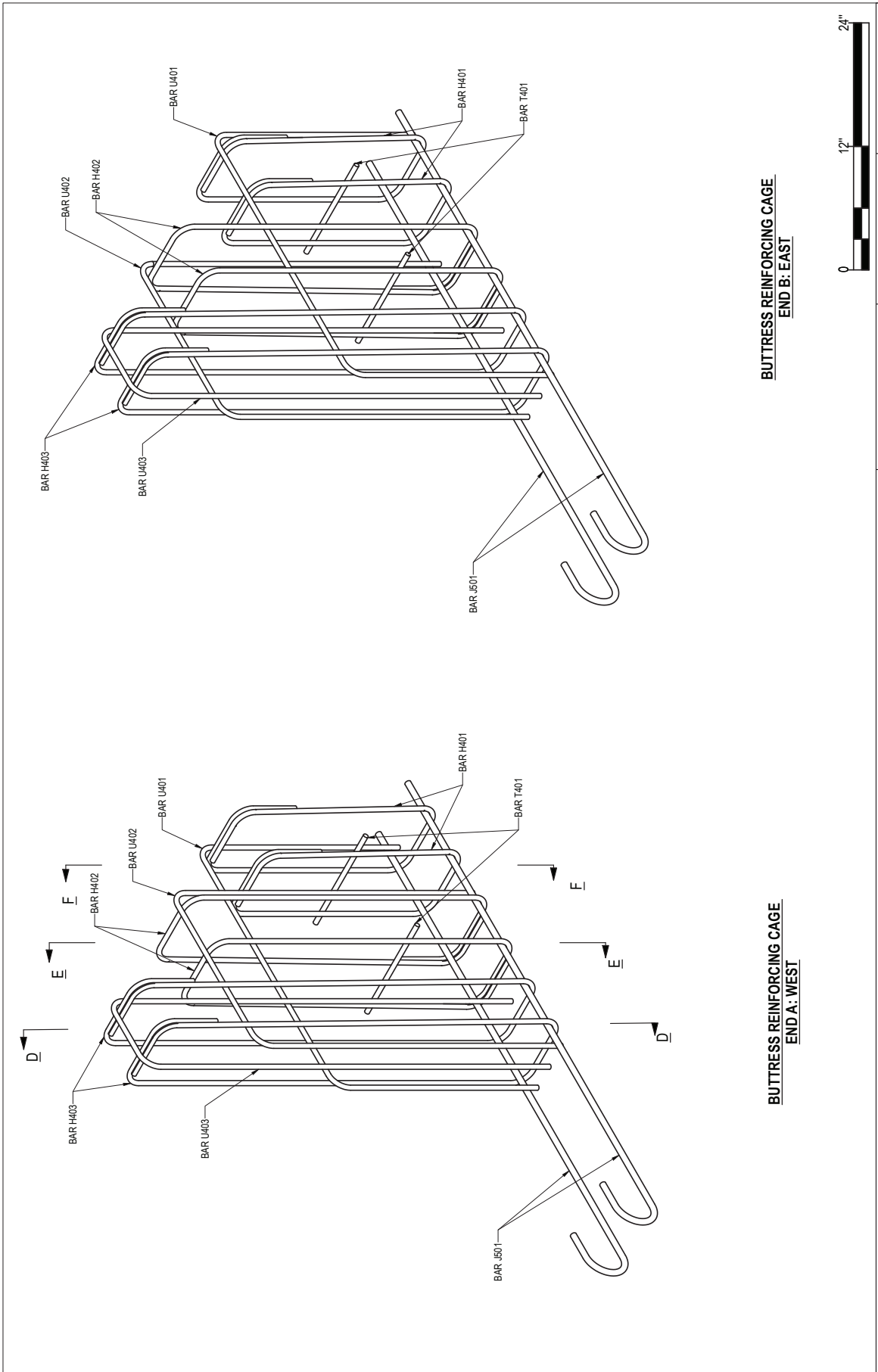
ANCHOR AND PLATE CONNECTION



THICKENED EDGE SECTION C-C



GFRP REINFORCED TEST SPECIMEN		Revision:	
ANCHOR PLATE AND SECTION C-C	University of Florida	SHEET 13 OF 24	

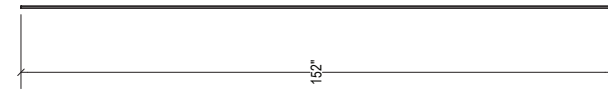


BUTTRESS REINFORCING CAGE
END B: EAST

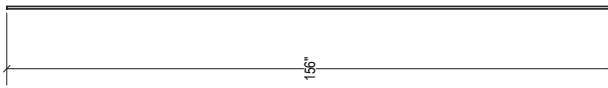
BUTTRESS REINFORCING CAGE
END A: WEST

<i>GFRP REINFORCED TEST SPECIMEN</i>		<i>Revision:</i>	
BUTTRESS REINFORCEMENT	<i>University of Florida</i>	<i>SHEET 15 OF 24</i>	

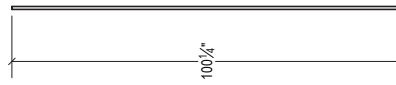
* 4SS BARS ARE FOR EOR TEST SPECIMENS ONLY. CUT FROM AVAILABLE 4S BARS. A BAND SAW OR AN ANGLE GRINDER WITH A DIAMOND BLADE IS RECOMMENDED FOR CUTTING.



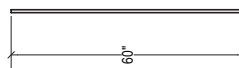
BAR 4S
NO.4 GFRP
QTY. 12 (COR)
QTY. 2 (EOR)



BAR S503
NO.5 GFRP
QTY. 13

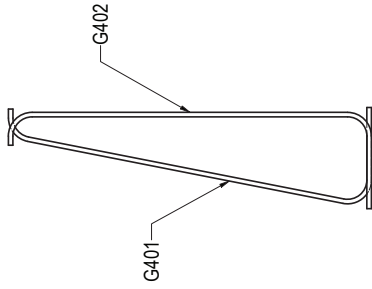
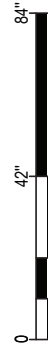


BAR S602
NO.6 GR.60
QTY. 8

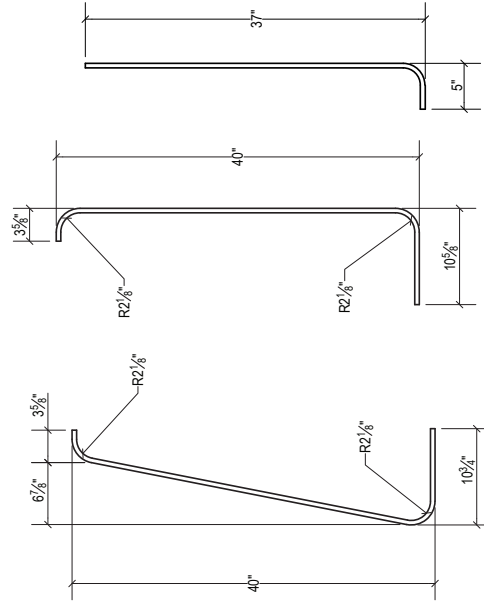


BAR S601
NO.6 GFRP
QTY. 44

BAR 4SS*
NO.4 GFRP
QTY. 10 (EOR)



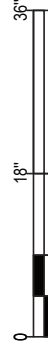
BARRIER TRANSVERSE GFRP REBAR ASSEMBLY



BAR G402
NO.4 GFRP
QTY. 26 (COR)
QTY. 22 (EOR)

BAR G401
NO.4 GFRP
QTY. 26

BAR G403
NO.4 GFRP
QTY. 0 (COR)
QTY. 9 (EOR)



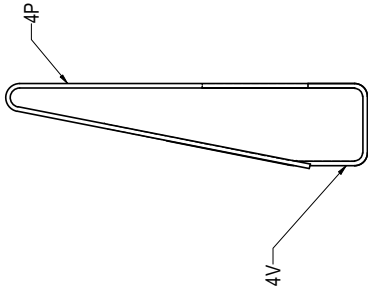
Revision:

GFRP REINFORCED TEST SPECIMEN

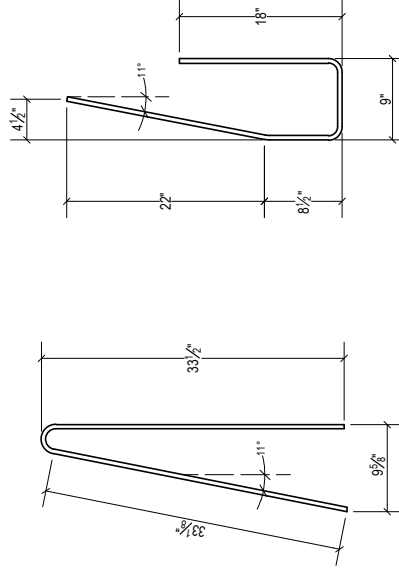
BAR LIST (PER TEST SPECIMEN) - SLAB

University of Florida

SHEET 16 OF 24



BARRIER STIRRUP 4P&4V
(FDOT STANDARD PLANS 621-427)



BAR 4P
NO 4 GR 60
QTY. 0 (COR)
QTY. 16 (EOR)

BAR 4V
NO 4 GR 60
QTY. 0 (COR)
QTY. 16 (EOR)

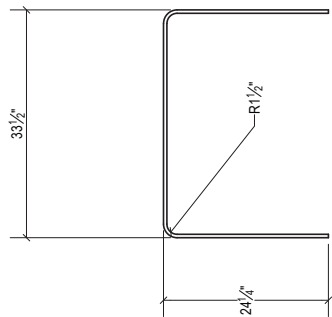
GFRP REINFORCED TEST SPECIMEN

BAR LIST (PER TEST SPECIMEN) - SLAB

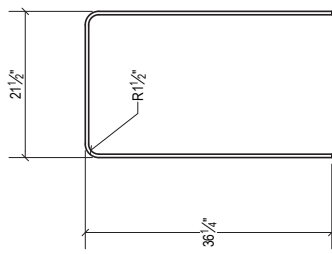
University of Florida

SHEET 17 OF 24

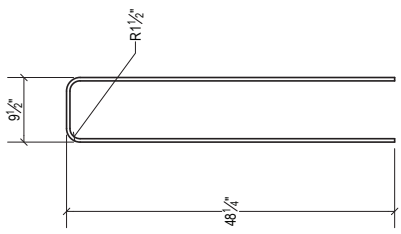
Revision:



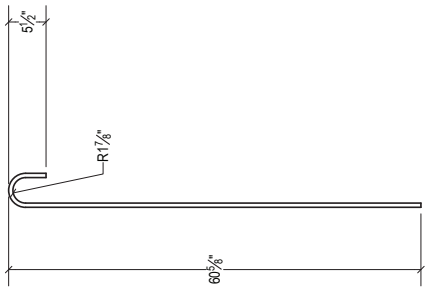
BAR U401
NO. 4 GR. 60
QTY. 2



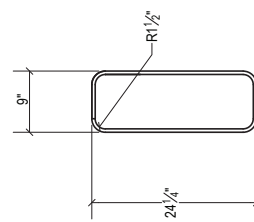
BAR U402
NO. 4 GR. 60
QTY. 2



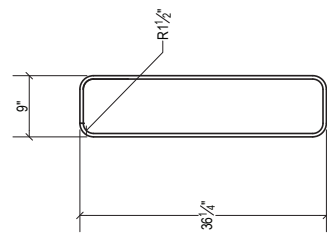
BAR U403
NO. 4 GR. 60
QTY. 2



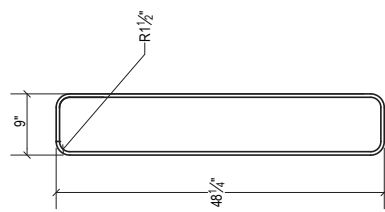
BAR U501
NO. 5 GR. 60
QTY. 4



BAR H401
NO. 4 GR. 60
QTY. 4



BAR H402
NO. 4 GR. 60
QTY. 4

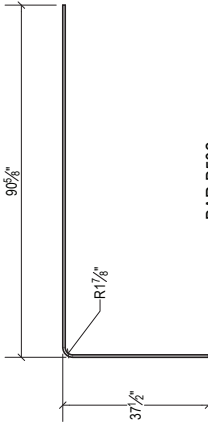


BAR H403
NO. 4 GR. 60
QTY. 4

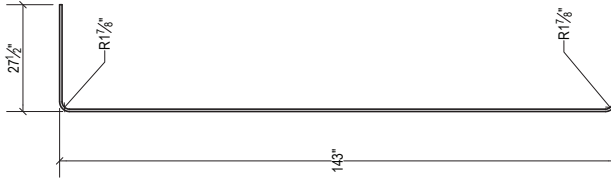
BUTTRESS REINFORCEMENT



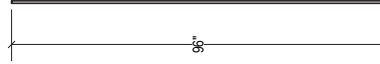
<i>GFRP REINFORCED TEST SPECIMEN</i>		<i>Revision:</i>	
BAR LIST (PER TEST SPECIMEN) - BUTTRESS	<i>University of Florida</i>	SHEET 18 OF 24	



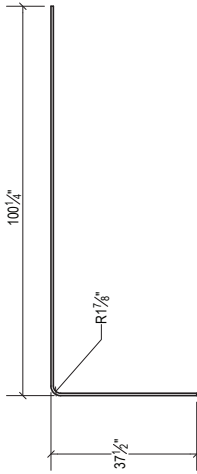
BAR B502
NO. 5 GR. 60
QTY. 2



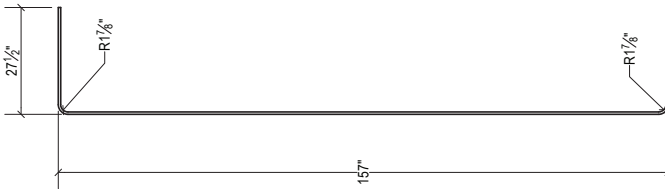
BAR B501
NO. 5 GR. 60
QTY. 1



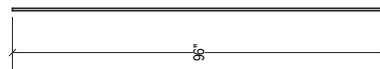
BAR B503
NO. 5 GR. 60
QTY. 1



BAR A502
NO. 5 GR. 60
QTY. 2



BAR A501
NO. 5 GR. 60
QTY. 1

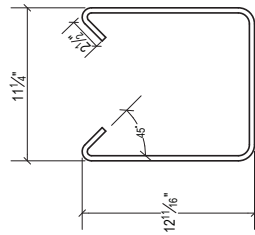


BAR A503
NO. 5 GR. 60
QTY. 1

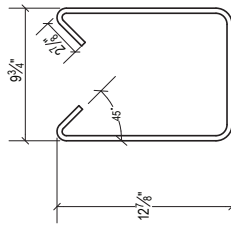
THICKENED DECK REINFORCEMENT



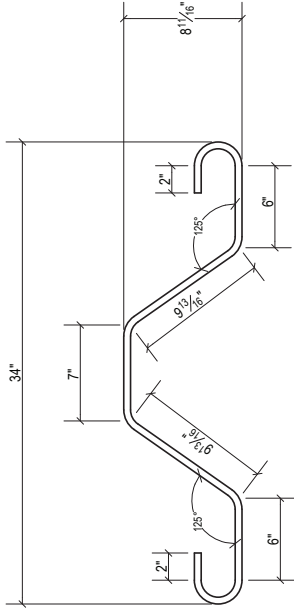
<i>GFRP REINFORCED TEST SPECIMEN</i>		<i>Revision:</i>	
BAR LIST (PER TEST SPECIMEN) - THICKENED DECK	<i>University of Florida</i>	SHEET 19 OF 24	



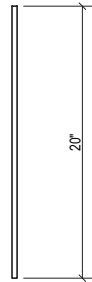
BAR S301
NO.3 GR.60
QTY. 24



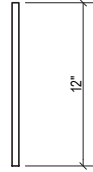
BAR S302
NO.3 GR. 60
QTY. 6



BAR S404
NO.4 GR.60
QTY. 4

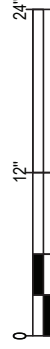


BAR S303
NO.3 GR. 60
QTY. 2

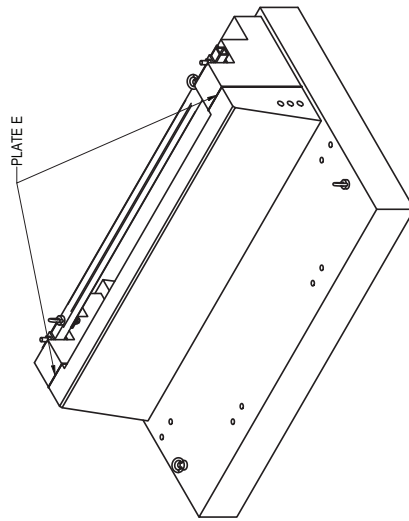


BAR T401
NO.4 GR.60
QTY. 4

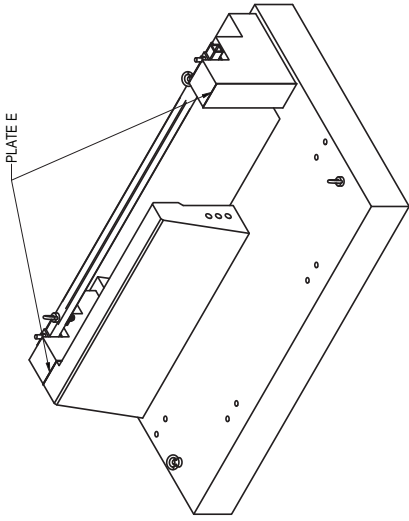
THICKENED DECK REINFORCEMENT



<i>GFRP REINFORCED TEST SPECIMEN</i>		<i>Revision:</i>	
BAR LIST (PER TEST SPECIMEN) - THICKENED DECK	University of Florida	SHEET 20 OF 24	



COR TEST SPECIMEN



EOR TEST SPECIMEN

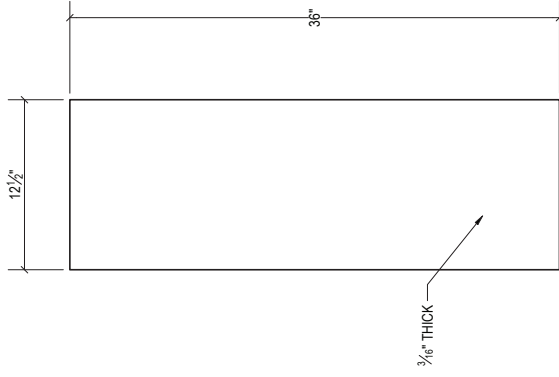
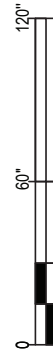


PLATE
STEEL SEPARATION PLATE
A36
QTY. 2



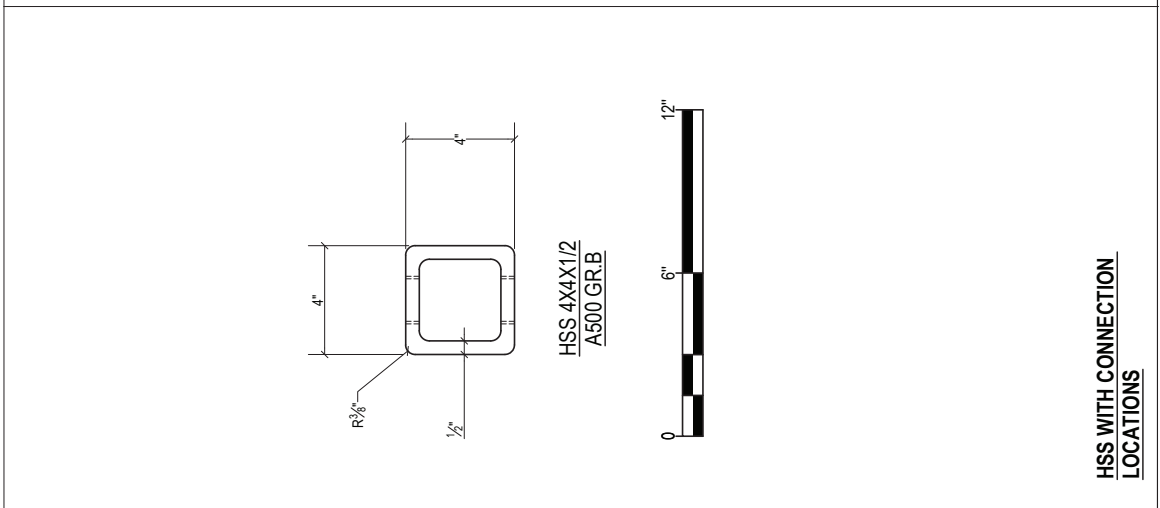
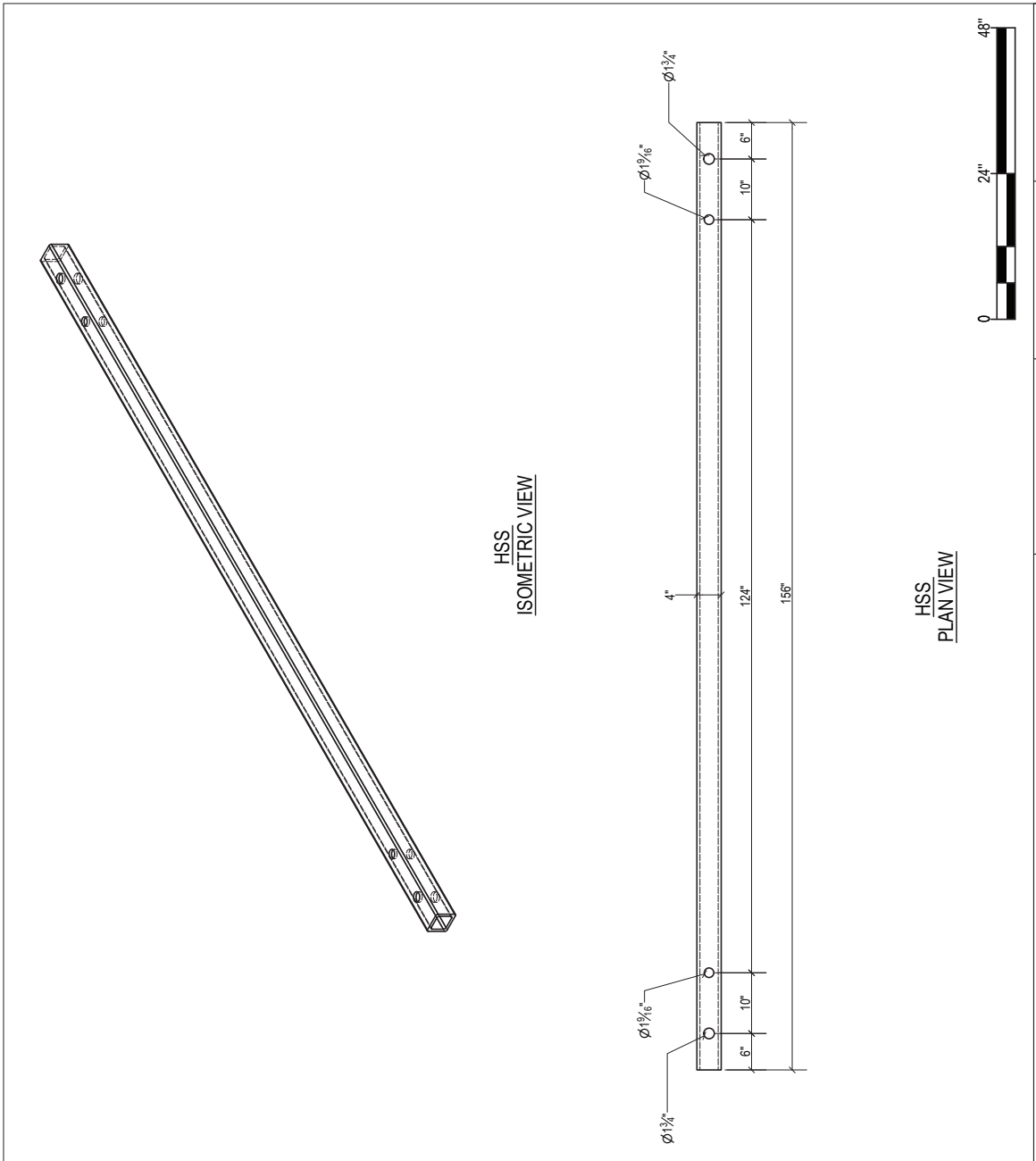
GFRP REINFORCED TEST SPECIMEN

BUTTRESS-RAIL INTERFACE

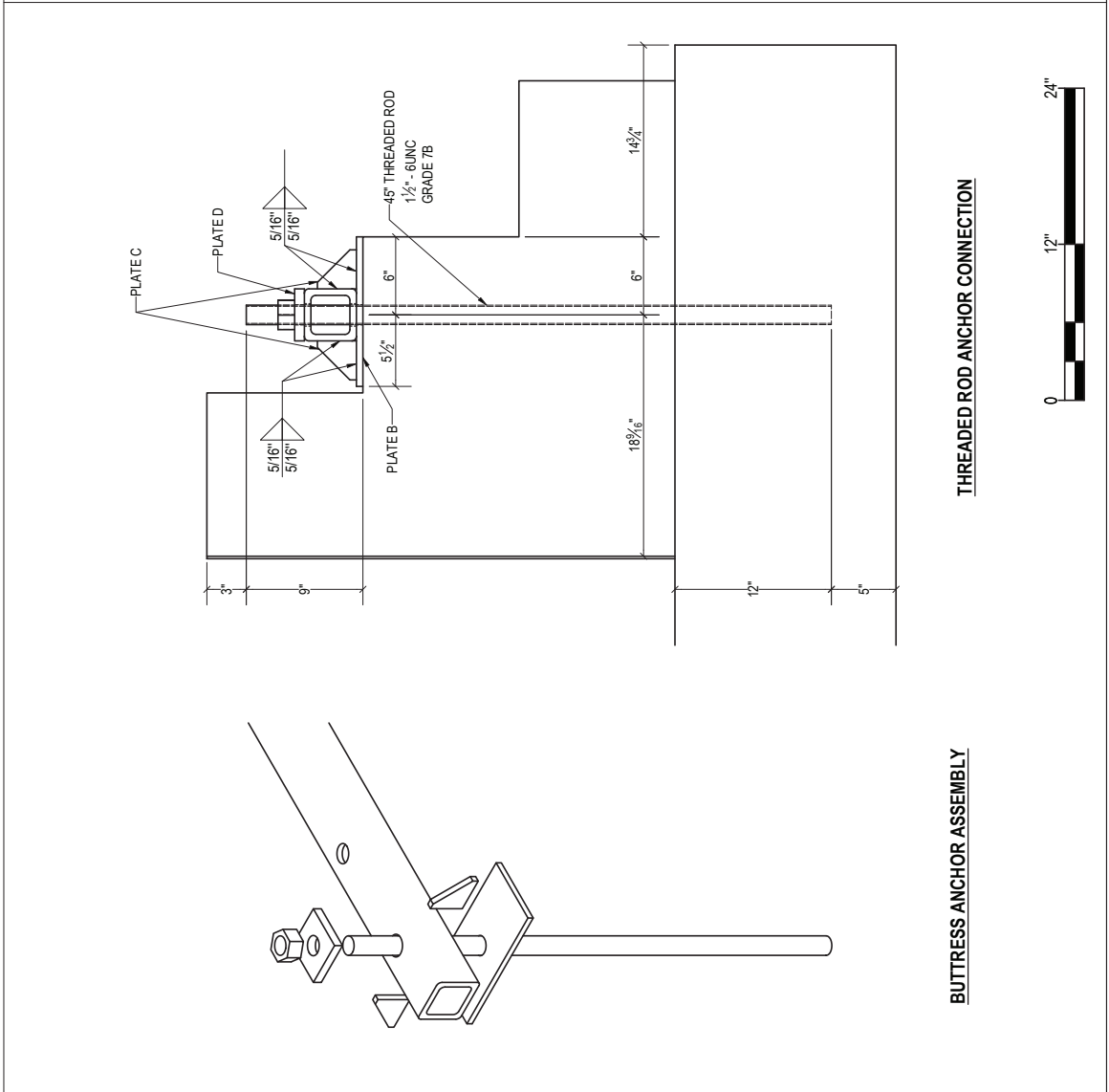
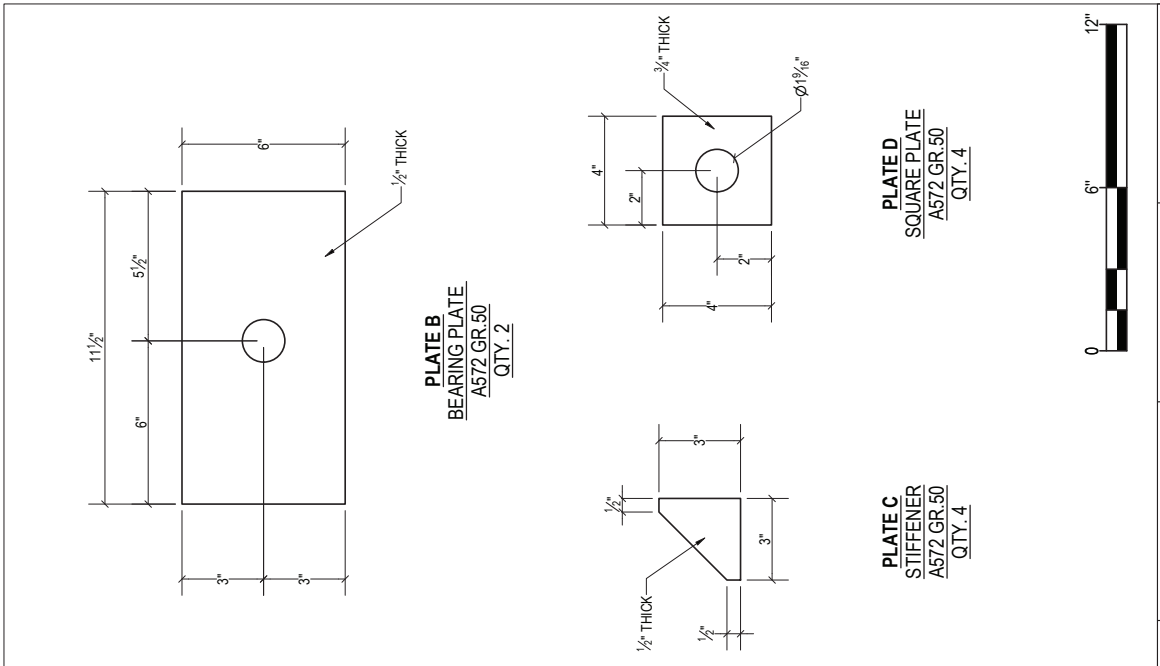
University of Florida

SHEET 21 OF 24

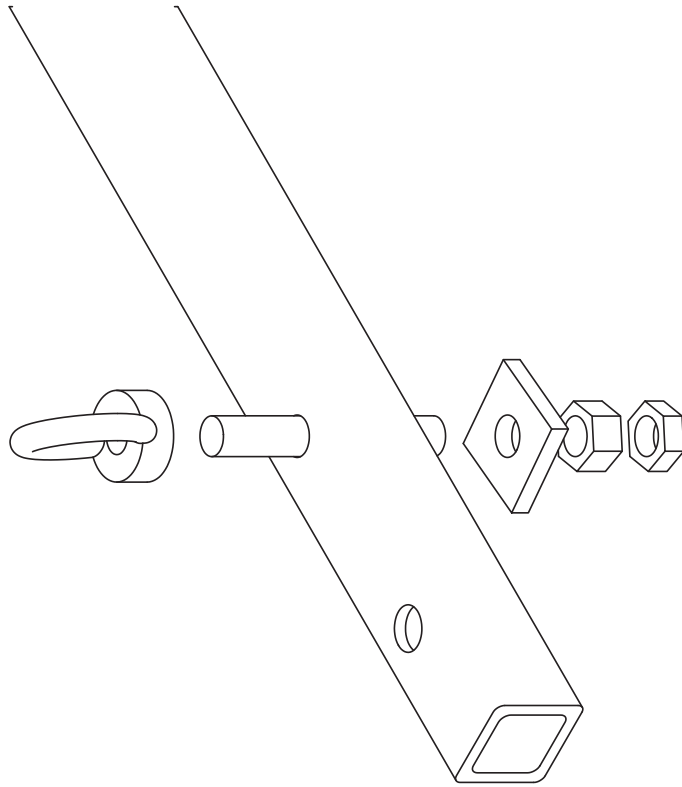
Revision:



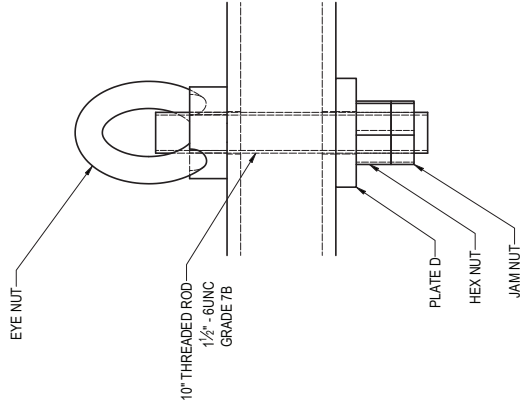
HSS DETAIL	<i>GFRP REINFORCED TEST SPECIMEN</i>	<i>Revision:</i>	
	<i>University of Florida</i>	<i>SHEET 22 OF 24</i>	



<i>GFRP REINFORCED TEST SPECIMEN</i>	
HSS-BUTTRESS CONNECTION	University of Florida
Revision:	SHEET 23 OF 24



LIFTING EYE NUT ASSEMBLY



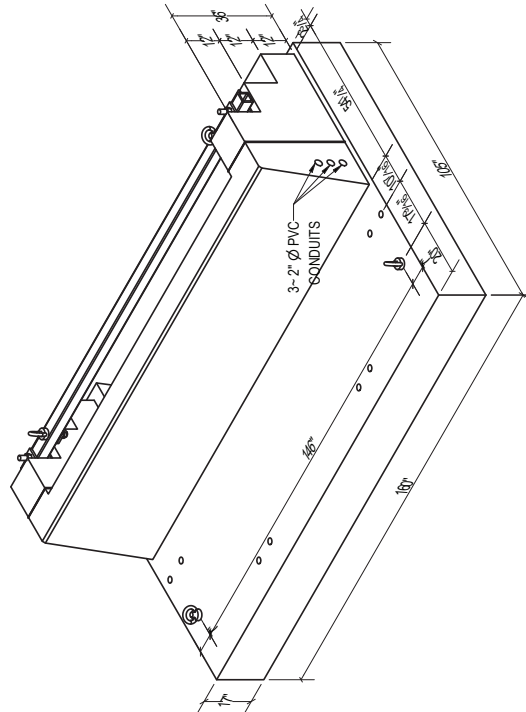
LIFTING EYE NUT CONNECTION



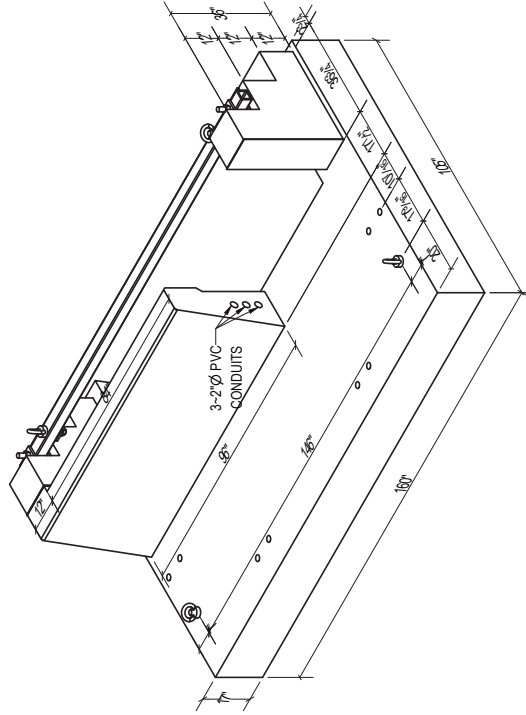
<i>GFRP REINFORCED TEST SPECIMEN</i>		<i>Revision:</i>	
HSS-LIFTING EYE BOLT CONNECTION	<i>University of Florida</i>	SHEET 24 OF 24	

**APPENDIX E:
STRUCTURAL DRAWINGS FOR STEEL-REINFORCED TEST SPECIMEN**

Presented in this appendix are structural drawings for the steel-reinforced test specimen developed and tested in this study, with center-of-rail (COR) and end-of-rail (EOR) variations.

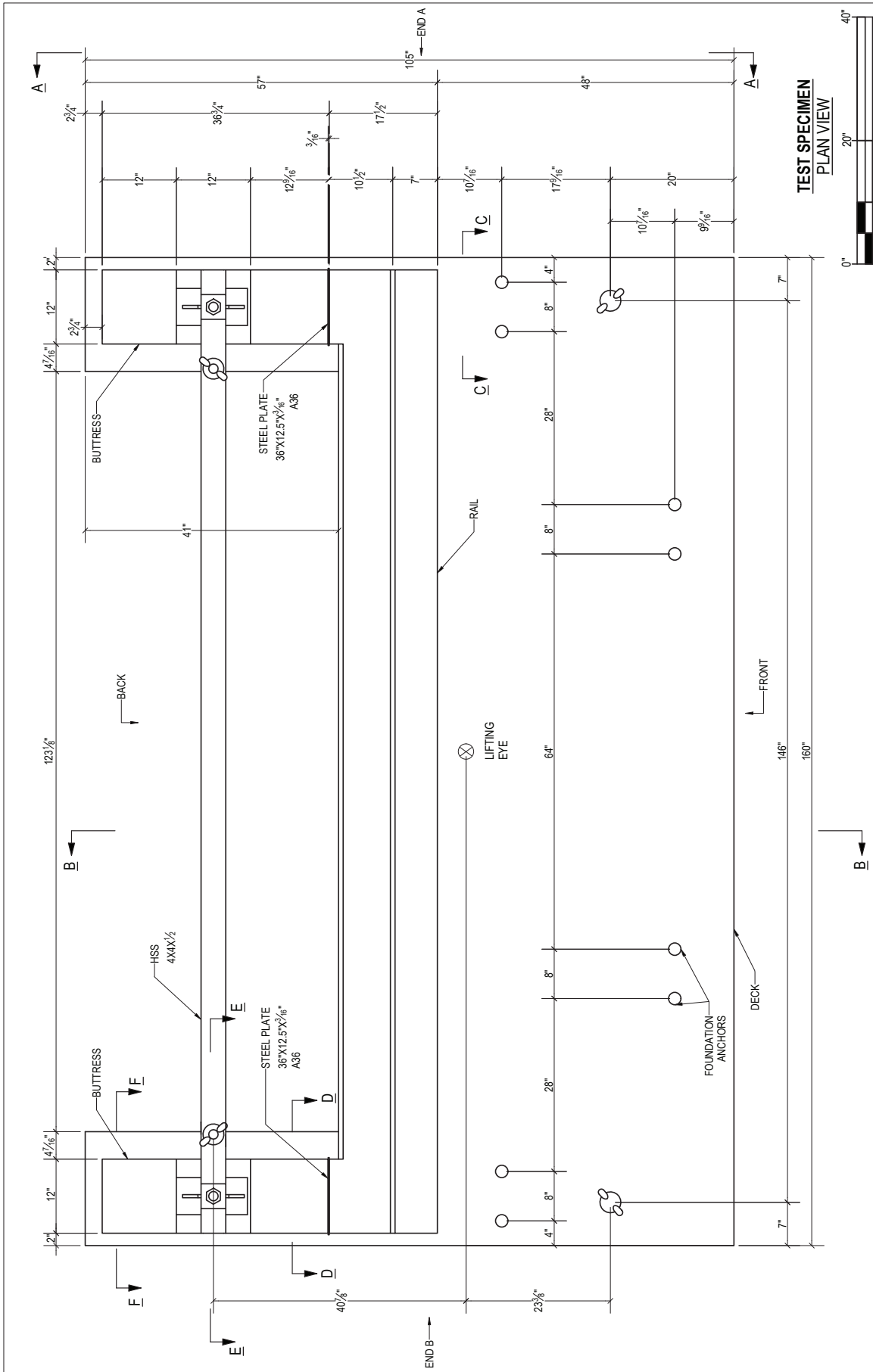


COR TEST SPECIMEN
FRONT ISOMETRIC VIEW



EOR TEST SPECIMEN
FRONT ISOMETRIC VIEW

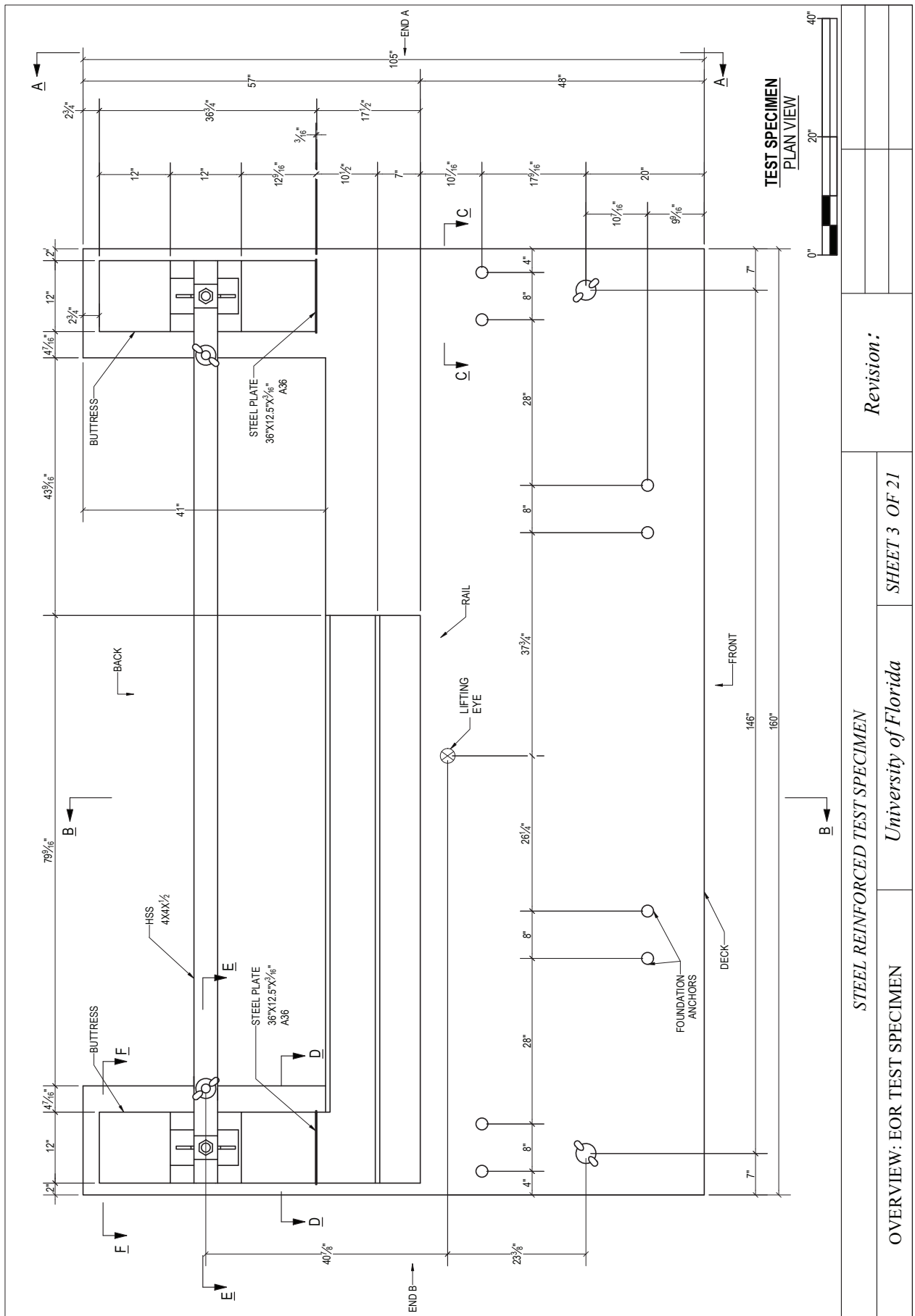
<i>STEEL REINFORCED TEST SPECIMEN</i>		<i>Revision:</i>	
TEST SPECIMEN OVERVIEW	<i>University of Florida</i>	SHEET 1 OF 21	



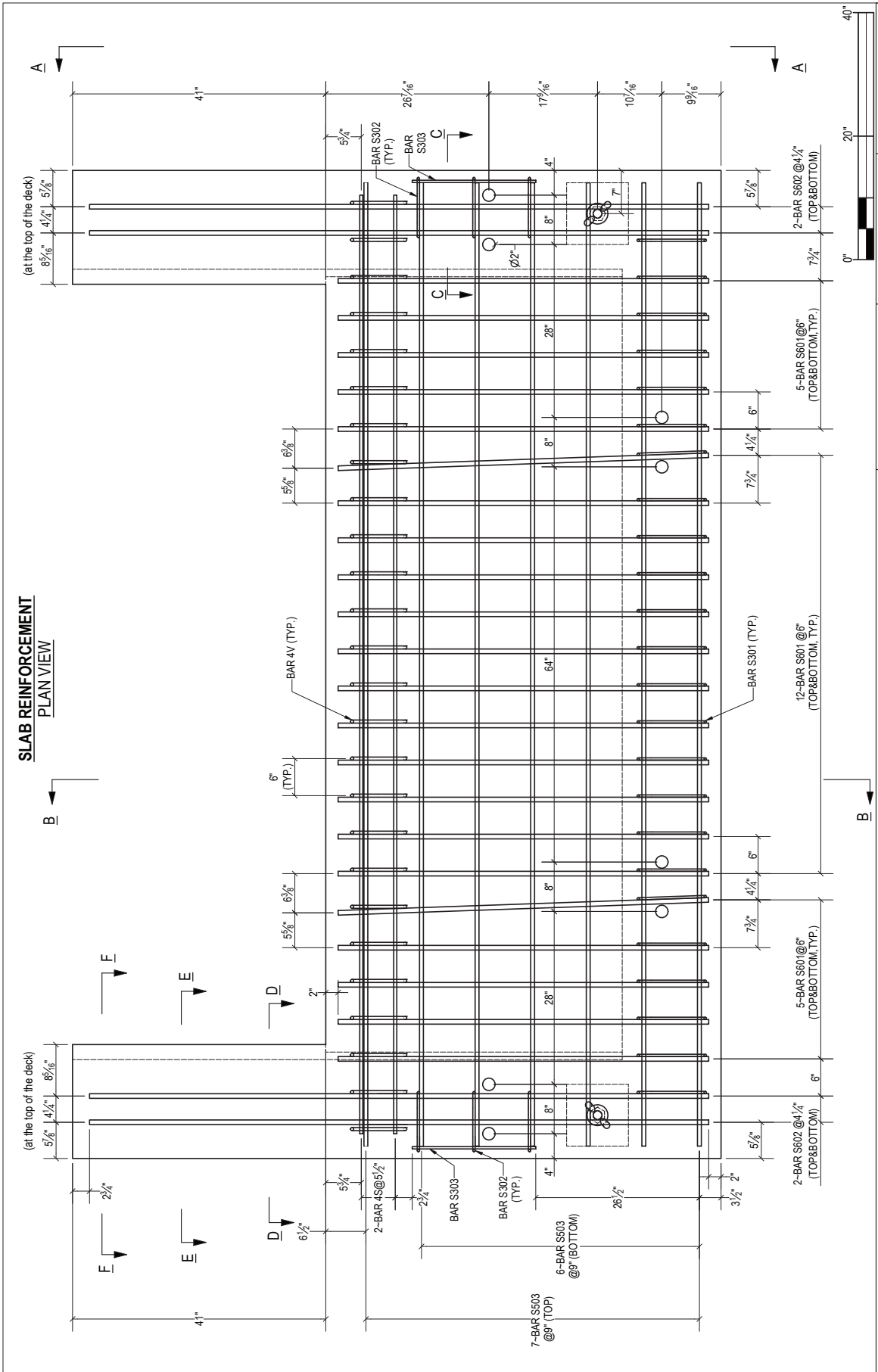
TEST SPECIMEN
PLAN VIEW



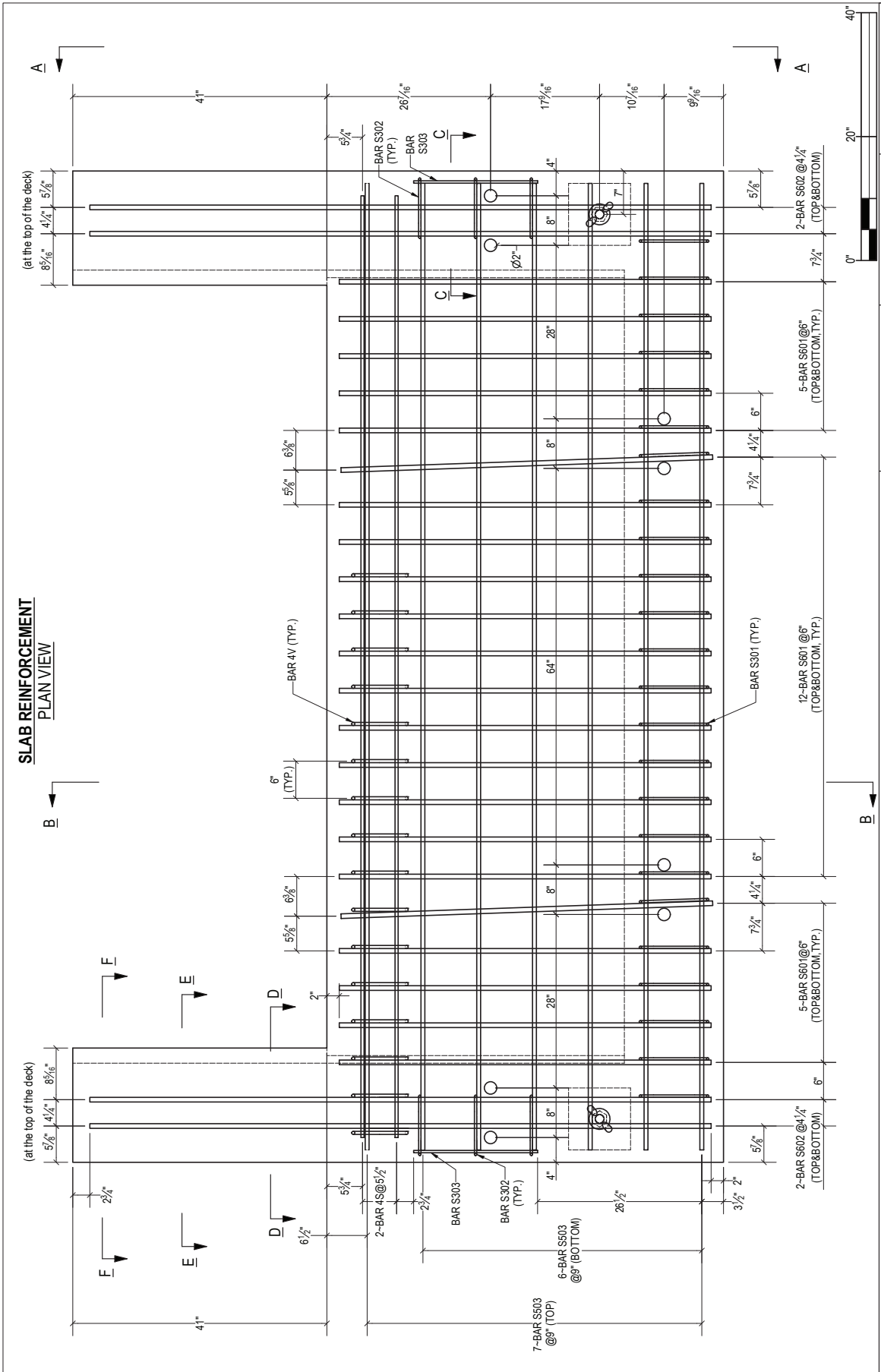
STEEL REINFORCED TEST SPECIMEN		<i>Revision:</i>
OVERVIEW: COR TEST SPECIMEN	University of Florida	SHEET 2 OF 21



STEEL REINFORCED TEST SPECIMEN		Revision:	
OVERVIEW: EOR TEST SPECIMEN	University of Florida	SHEET 3 OF 21	

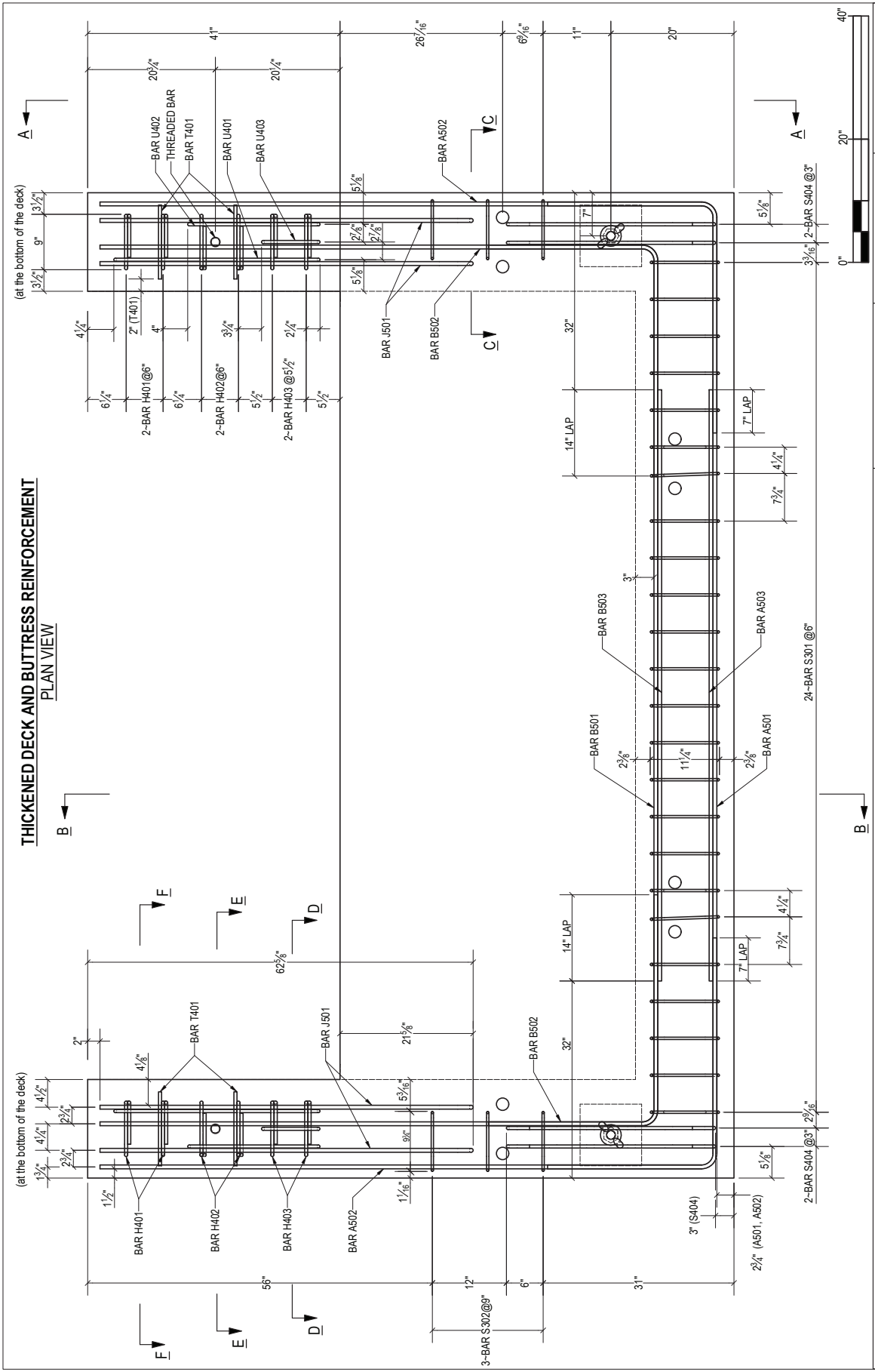


<i>STEEL REINFORCED TEST SPECIMEN</i>		<i>Revision:</i>	
SLAB REINFORCEMENT: COR TEST SPECIMEN	<i>University of Florida</i>	<i>SHEET 4 OF 21</i>	

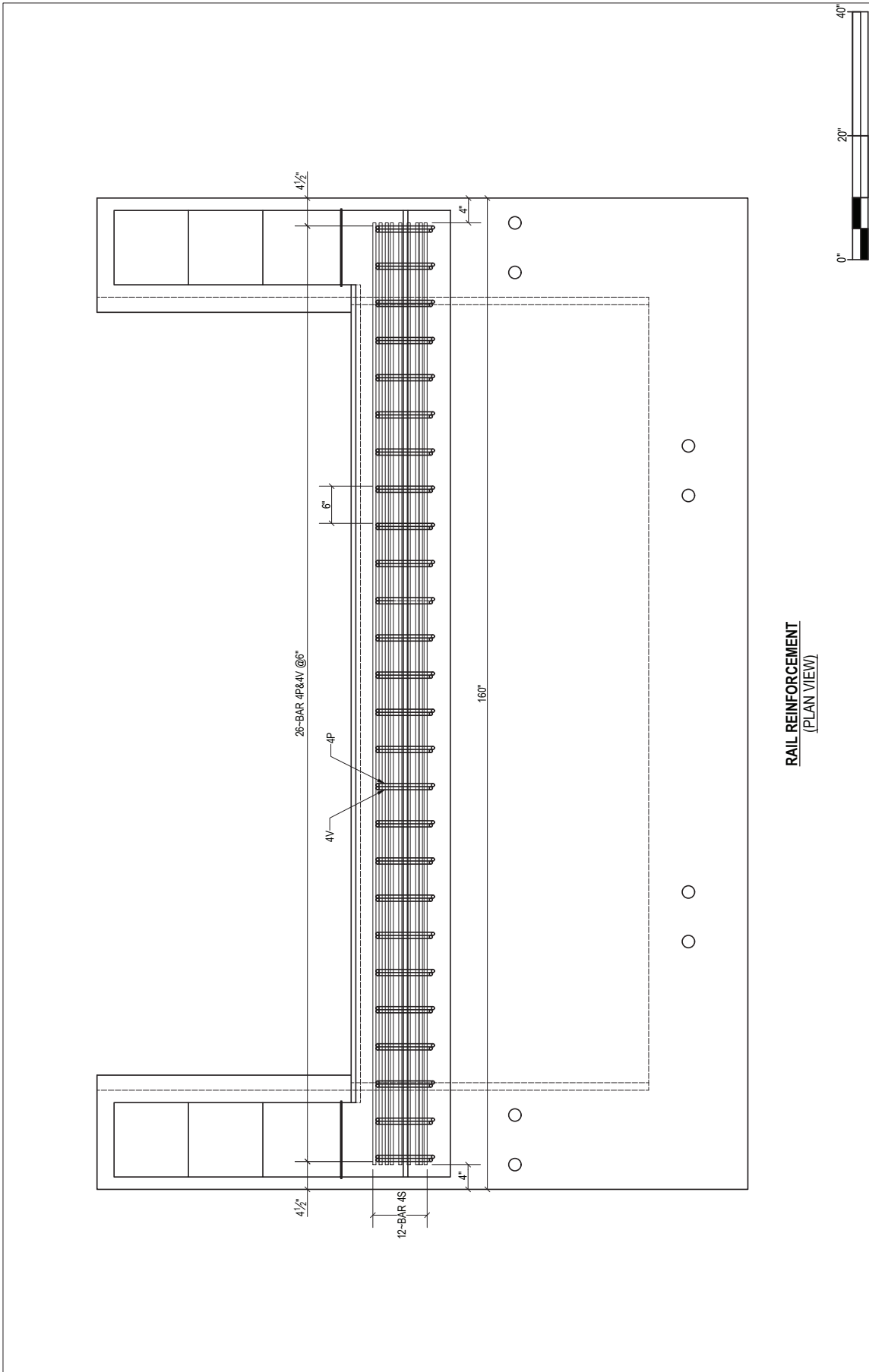


**SLAB REINFORCEMENT
PLAN VIEW**

STEEL REINFORCED TEST SPECIMEN		Revision:	
SLAB REINFORCEMENT: EOR TEST SPECIMEN	<i>University of Florida</i>	SHEET 5 OF 21	

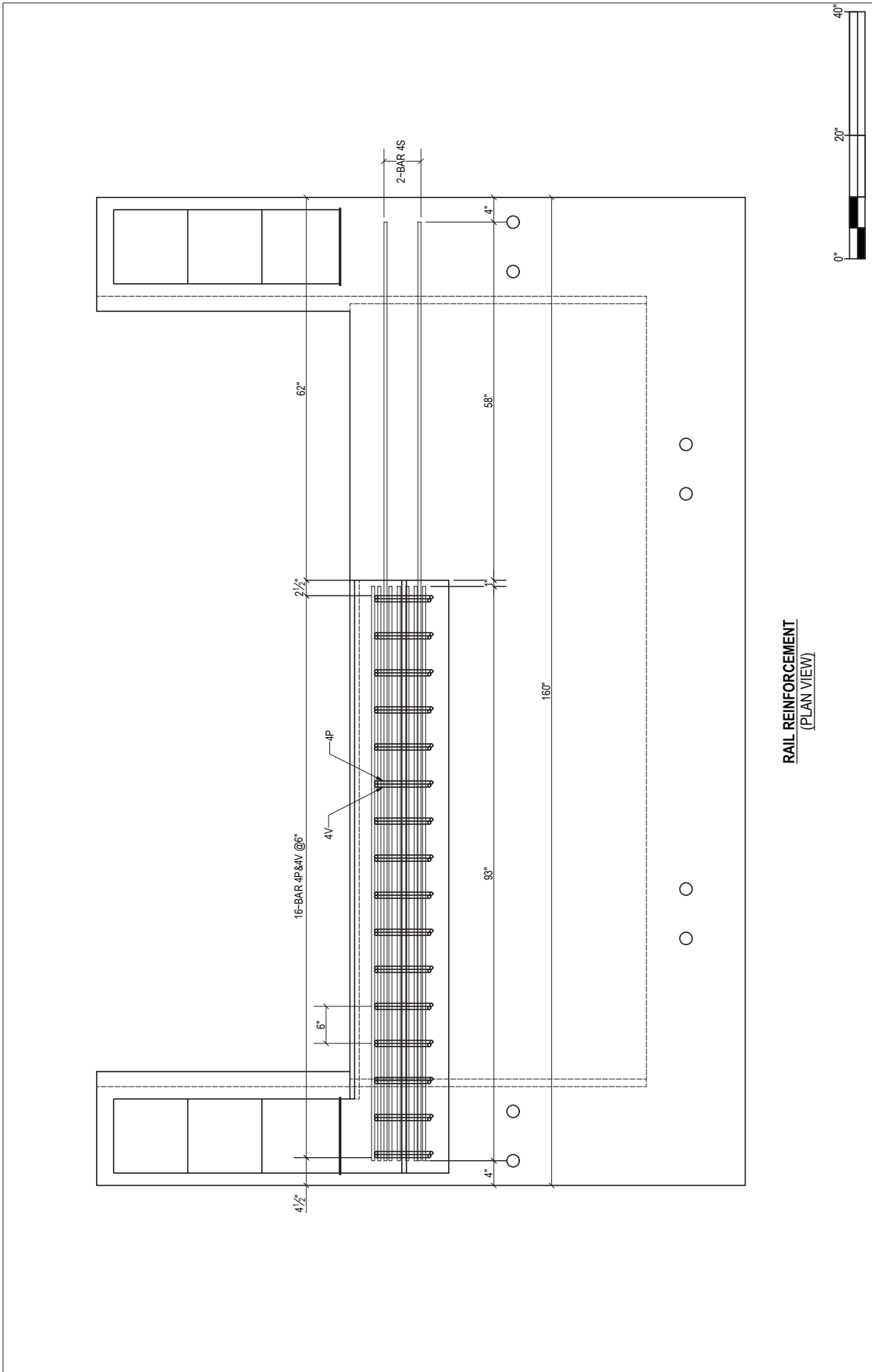


STEEL REINFORCED TEST SPECIMEN		Revision:
THICKENED DECK REINFORCEMENT	<i>University of Florida</i>	SHEET 6 OF 21



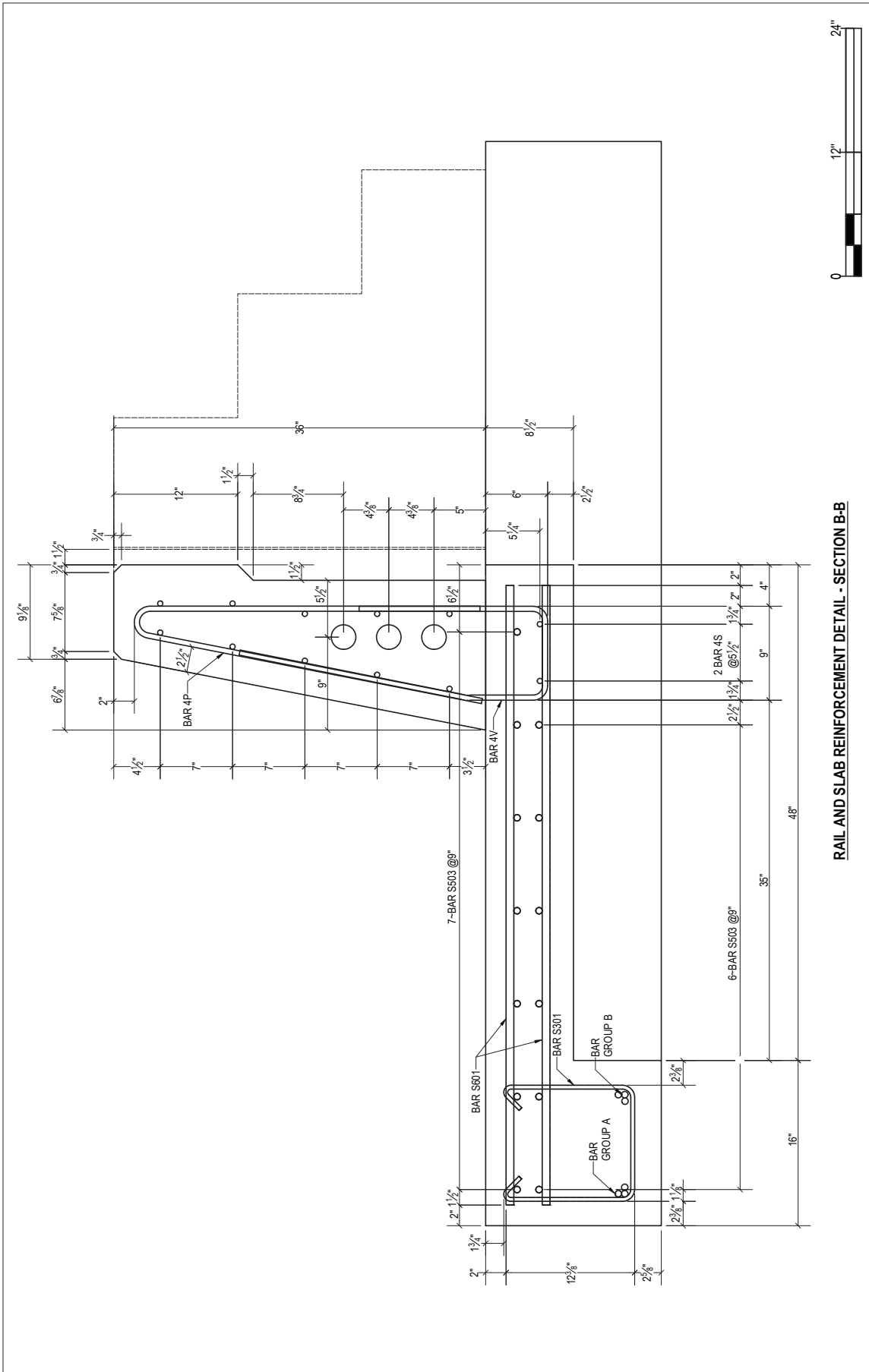
RAIL REINFORCEMENT
(PLAN VIEW)

<i>STEEL REINFORCED TEST SPECIMEN</i>		<i>Revision:</i>	
RAILING REINFORCEMENT: COR TEST SPECIMEN	<i>University of Florida</i>	SHEET 7 OF 21	



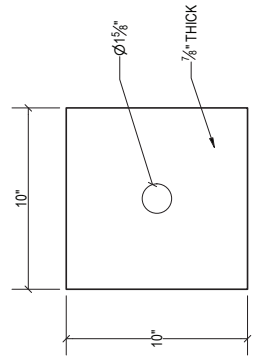
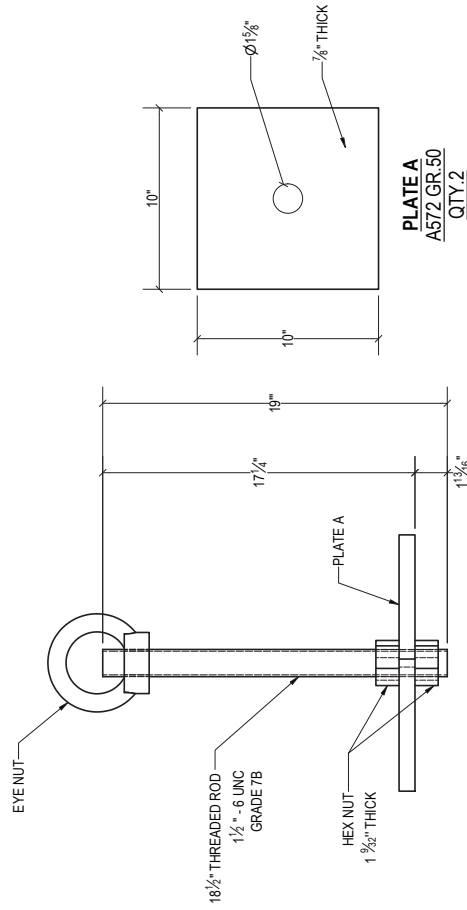
RAIL REINFORCEMENT
(PLAN VIEW)

<i>STEEL REINFORCED TEST SPECIMEN</i>		<i>Revision:</i>	
RAILING REINFORCEMENT: EOR TEST SPECIMEN	<i>University of Florida</i>	SHEET 8 OF 21	

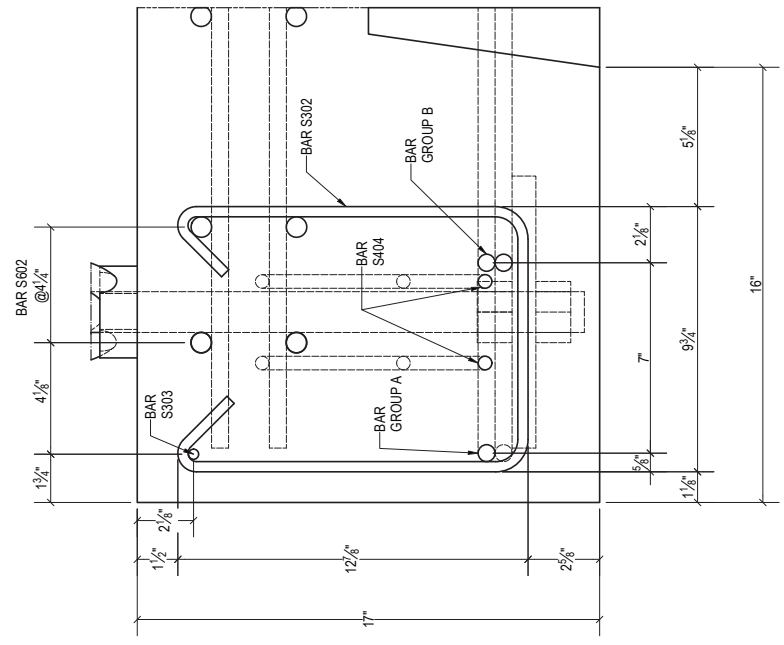
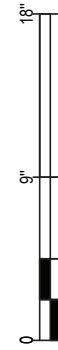


RAIL AND SLAB REINFORCEMENT DETAIL - SECTION BB

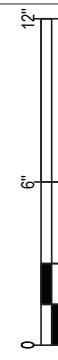
STEEL REINFORCED TEST SPECIMEN		Revision:	
SECTION B-B	University of Florida	SHEET 10 OF 21	



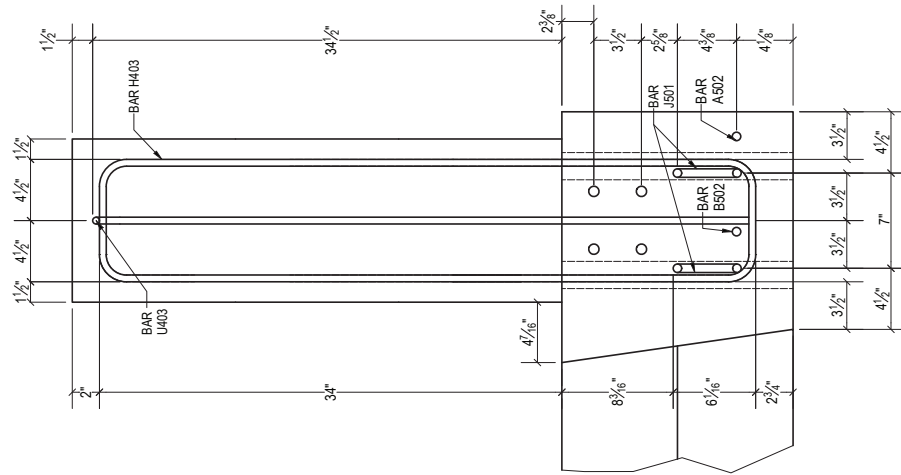
ANCHOR AND PLATE CONNECTION



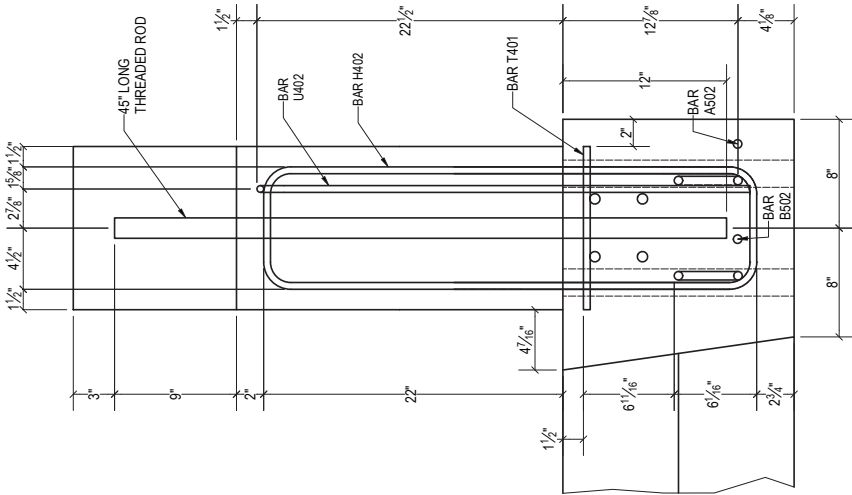
THICKENED EDGE SECTION C-C



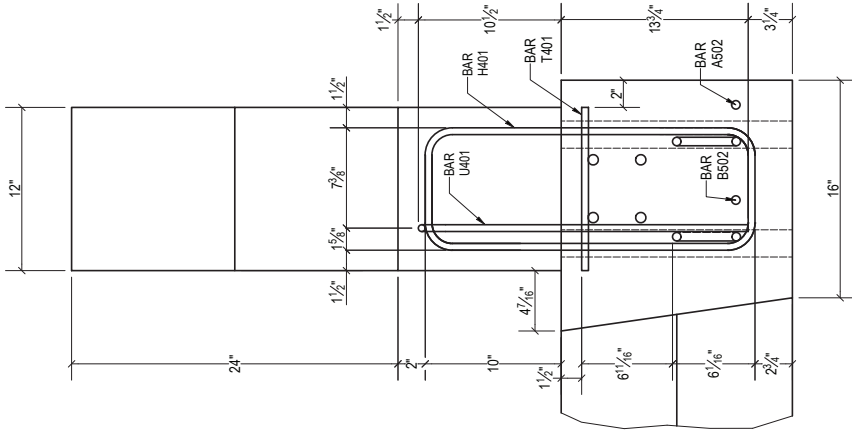
STEEL REINFORCED TEST SPECIMEN		Revision:	
ANCHOR PLATE AND SECTION C-C	University of Florida		
		SHEET 11 OF 21	



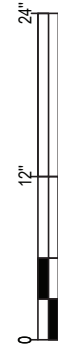
BUTTRESS REINFORCEMENT
SECTION D-D



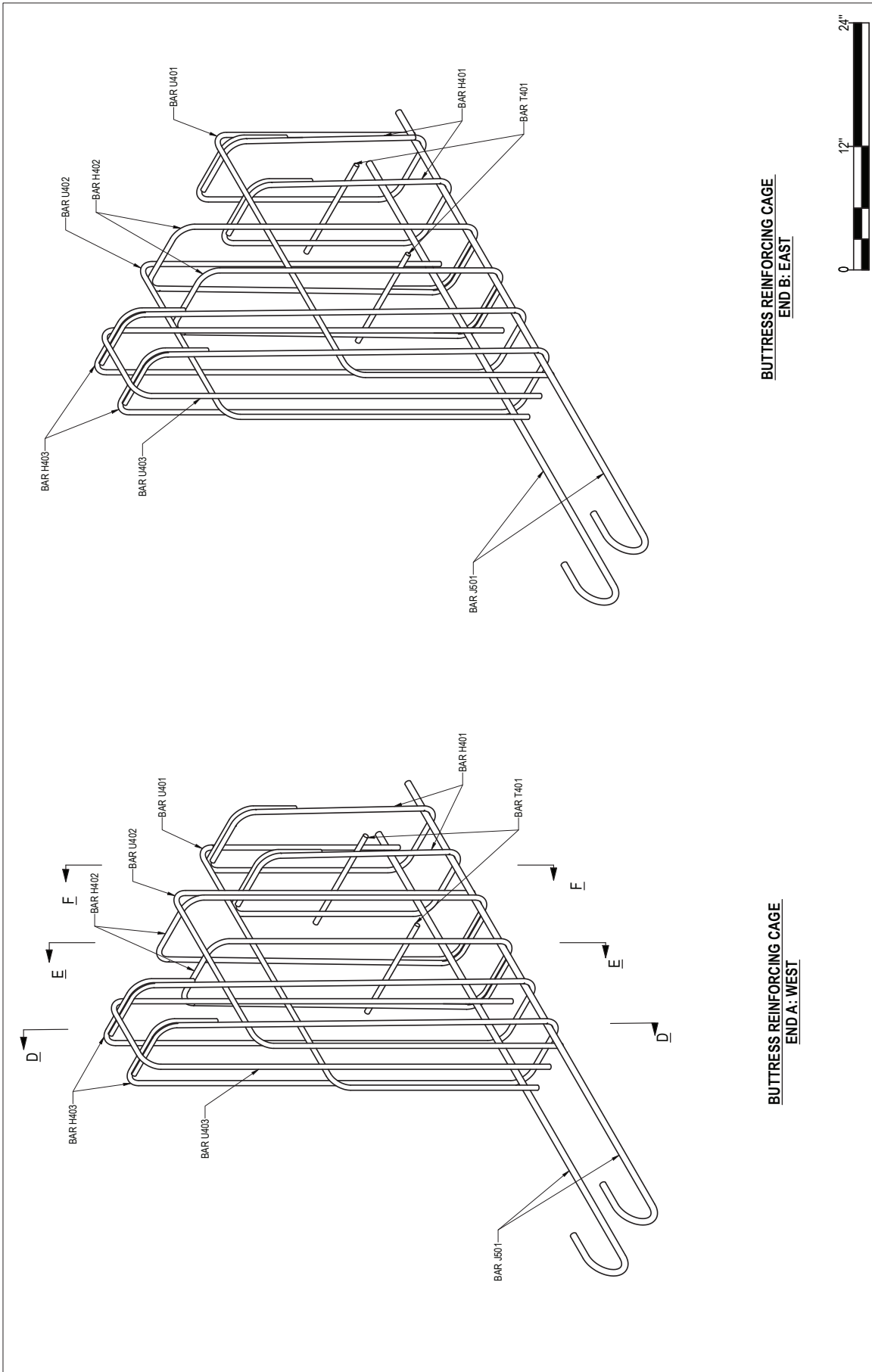
BUTTRESS REINFORCEMENT
SECTION E-E



BUTTRESS REINFORCEMENT
SECTION F-F



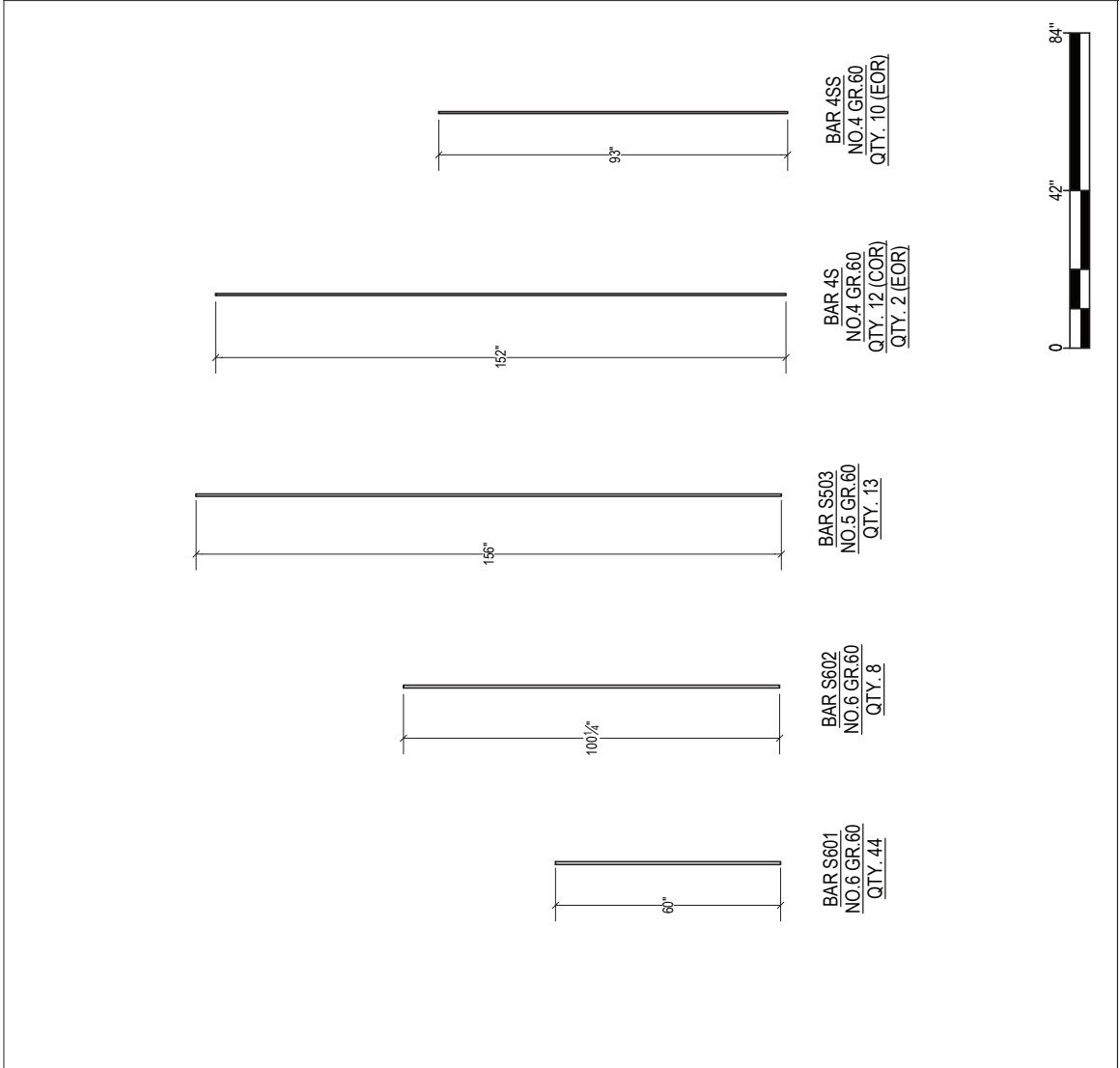
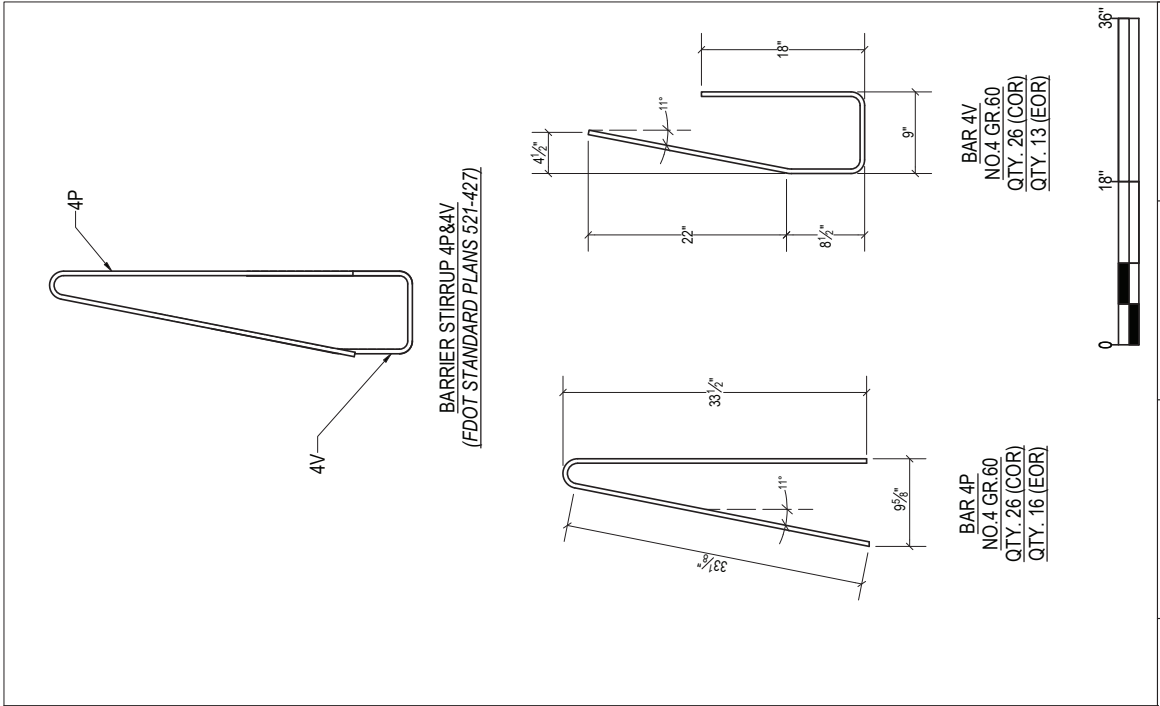
<i>STEEL REINFORCED TEST SPECIMEN</i>		<i>Revision:</i>
SECTION D, E, F: BUTTRESS REINFORCEMENT	<i>University of Florida</i>	SHEET 12 OF 21



BUTTRESS REINFORCING CAGE
END B: EAST

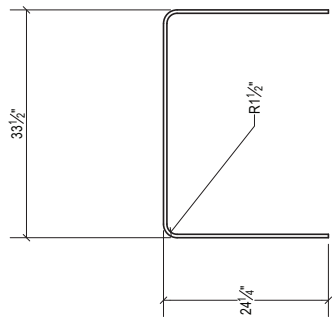
BUTTRESS REINFORCING CAGE
END A: WEST

<i>STEEL REINFORCED TEST SPECIMEN</i>		<i>Revision:</i>	
BUTTRESS REINFORCEMENT	<i>University of Florida</i>	<i>SHEET 13 OF 21</i>	

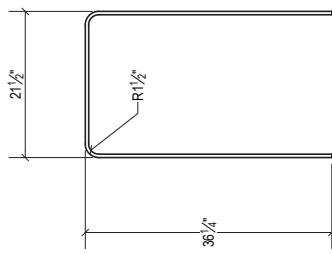


Revision:	

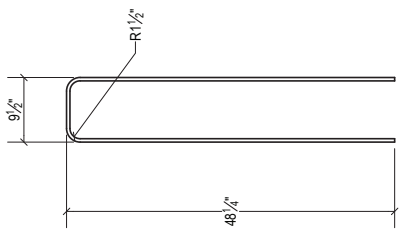
STEEL REINFORCED TEST SPECIMEN	
BAR LIST (PER TEST SPECIMEN) - SLAB	SHEET 14 OF 21
University of Florida	



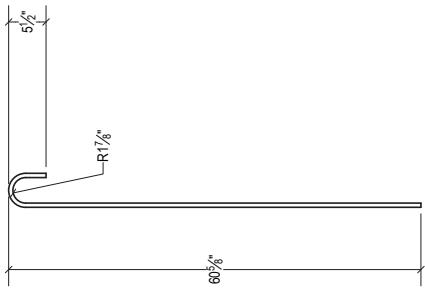
BAR U401
NO. 4 GR. 60
QTY. 2



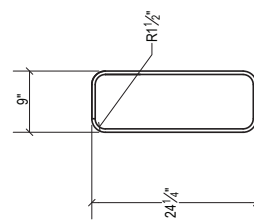
BAR U402
NO. 4 GR. 60
QTY. 2



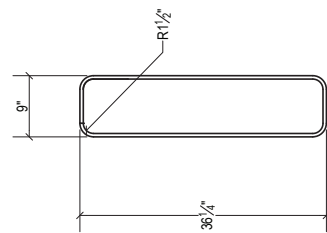
BAR U403
NO. 4 GR. 60
QTY. 2



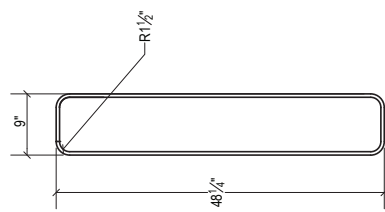
BAR U501
NO. 5 GR. 60
QTY. 4



BAR H401
NO. 4 GR. 60
QTY. 4



BAR H402
NO. 4 GR. 60
QTY. 4

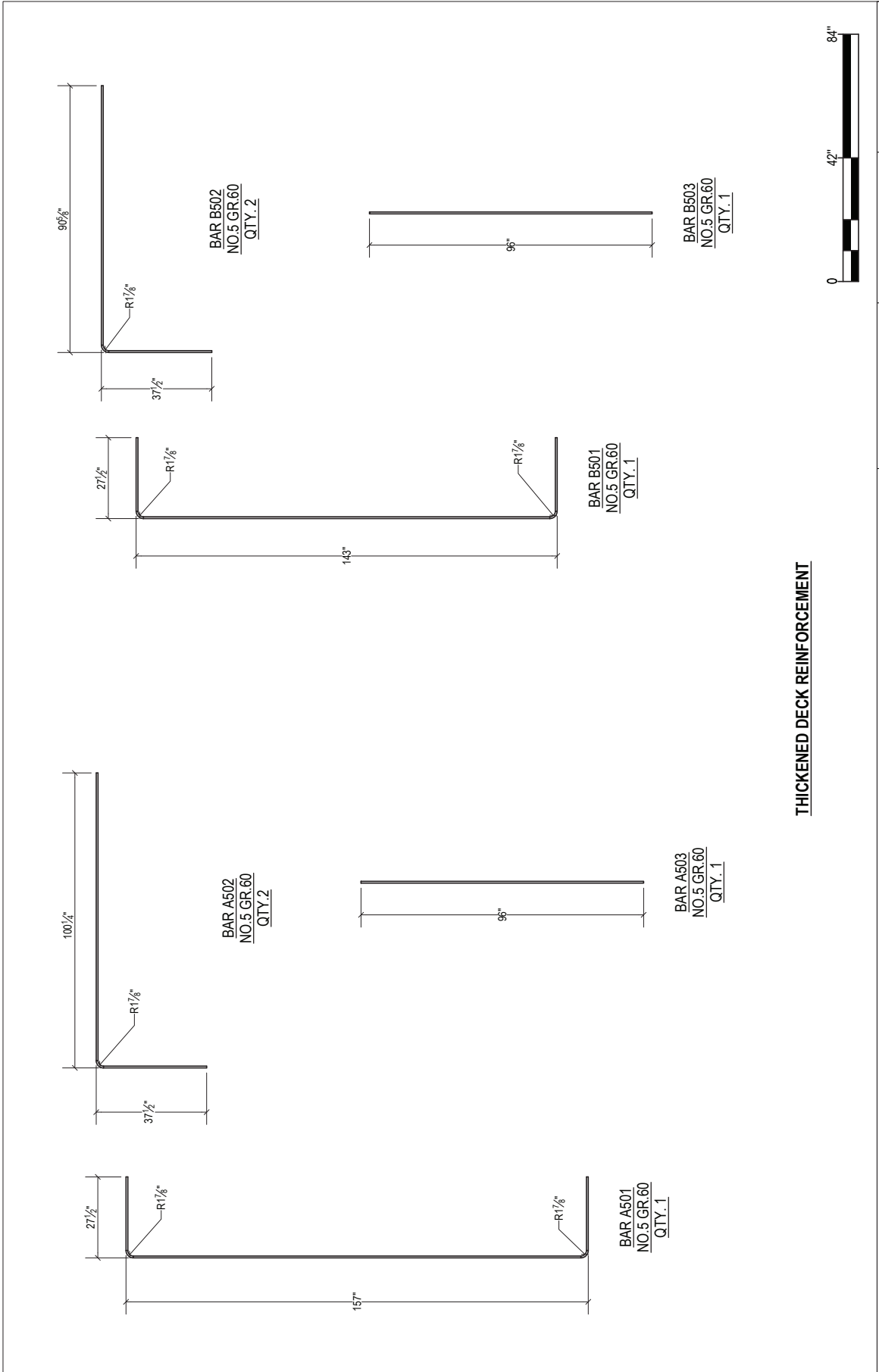


BAR H403
NO. 4 GR. 60
QTY. 4

BUTTRESS REINFORCEMENT

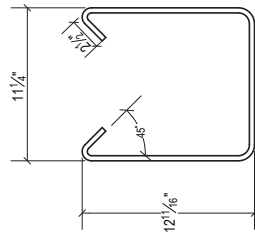


<i>STEEL REINFORCED TEST SPECIMEN</i>		<i>Revision:</i>
BAR LIST (PER TEST SPECIMEN) - BUTTRESS	<i>University of Florida</i>	<i>SHEET 15 OF 21</i>

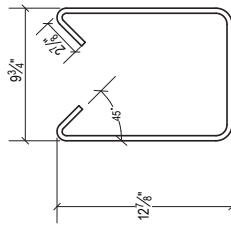


THICKENED DECK REINFORCEMENT

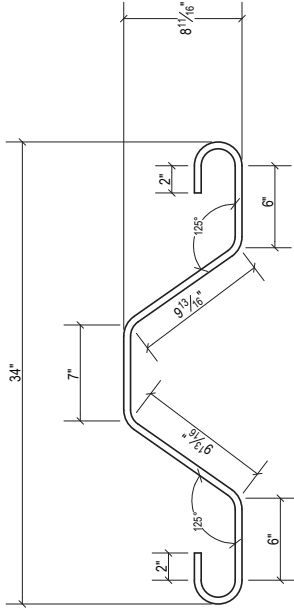
<i>STEEL REINFORCED TEST SPECIMEN</i>		<i>Revision:</i>	
BAR LIST (PER TEST SPECIMEN)	<i>University of Florida</i>	<i>SHEET 16 OF 21</i>	
- THICKENED DECK			



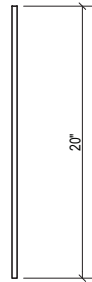
BAR S301
NO.3 GR.60
QTY. 24



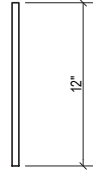
BAR S302
NO.3 GR.60
QTY. 6



BAR S404
NO.4 GR.60
QTY. 4

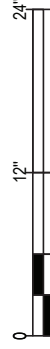


BAR S303
NO.3 GR.60
QTY. 2

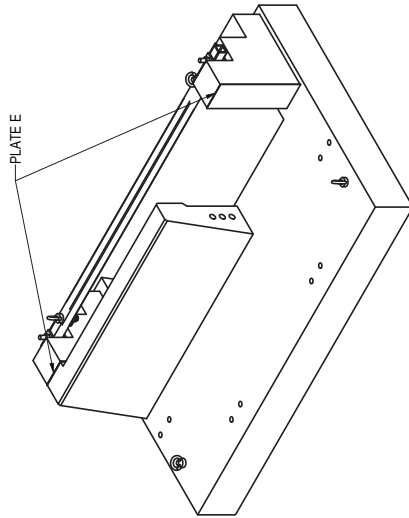
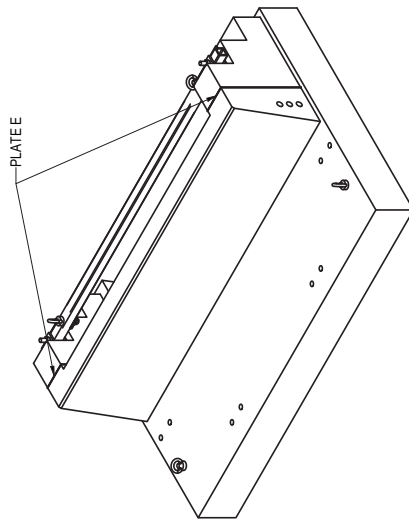


BAR T401
NO.4 GR.60
QTY. 4

THICKENED DECK REINFORCEMENT



<i>STEEL REINFORCED TEST SPECIMEN</i>		<i>Revision:</i>	
BAR LIST (PER TEST SPECIMEN)	University of Florida	SHEET 17 OF 21	
- THICKENED DECK			



EOR TEST SPECIMEN

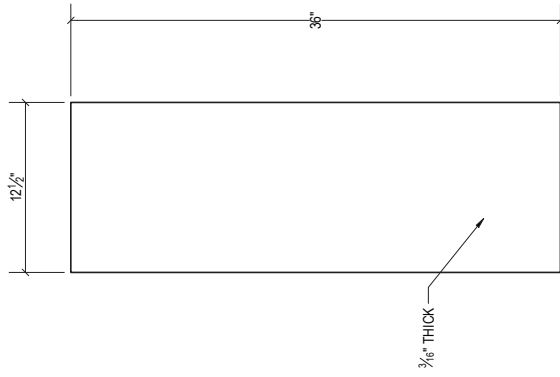
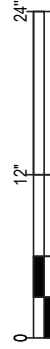
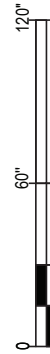


PLATE E
STEEL SEPARATION PLATE
A36
QTY. 2



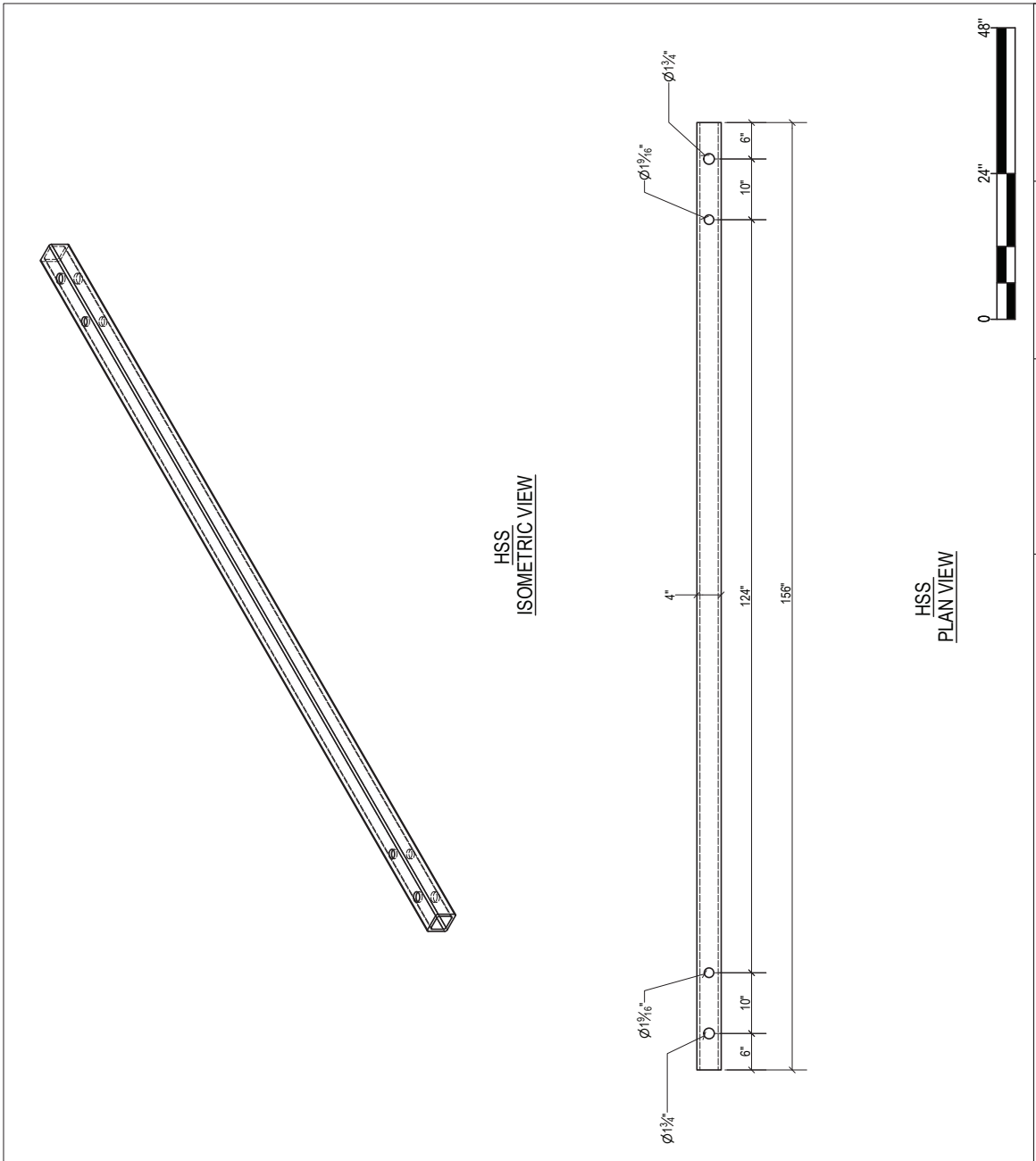
STEEL REINFORCED TEST SPECIMEN

BUTTRESS-RAIL INTERFACE

University of Florida

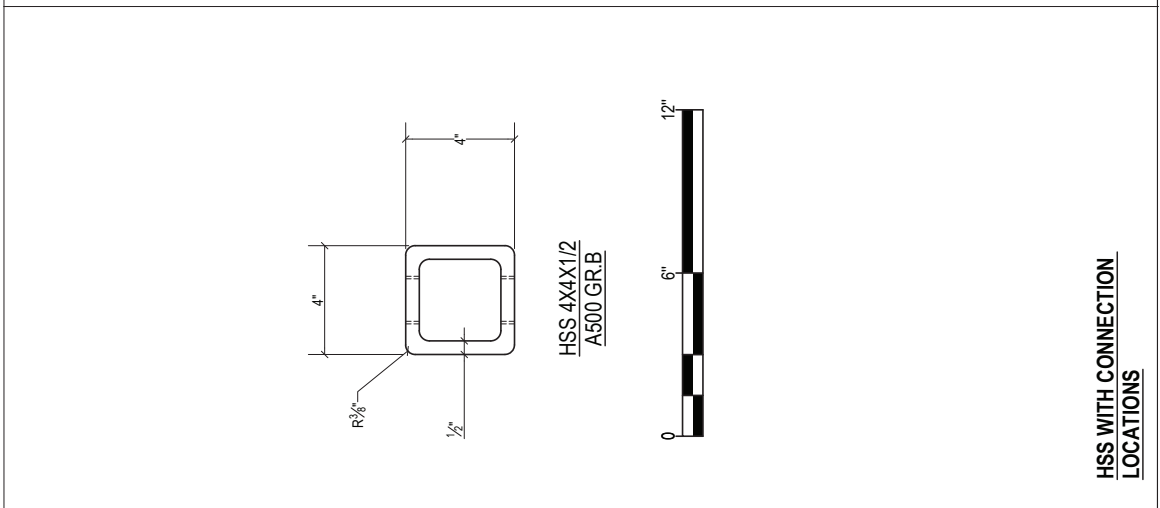
SHEET 18 OF 21

Revision:



HSS
ISOMETRIC VIEW

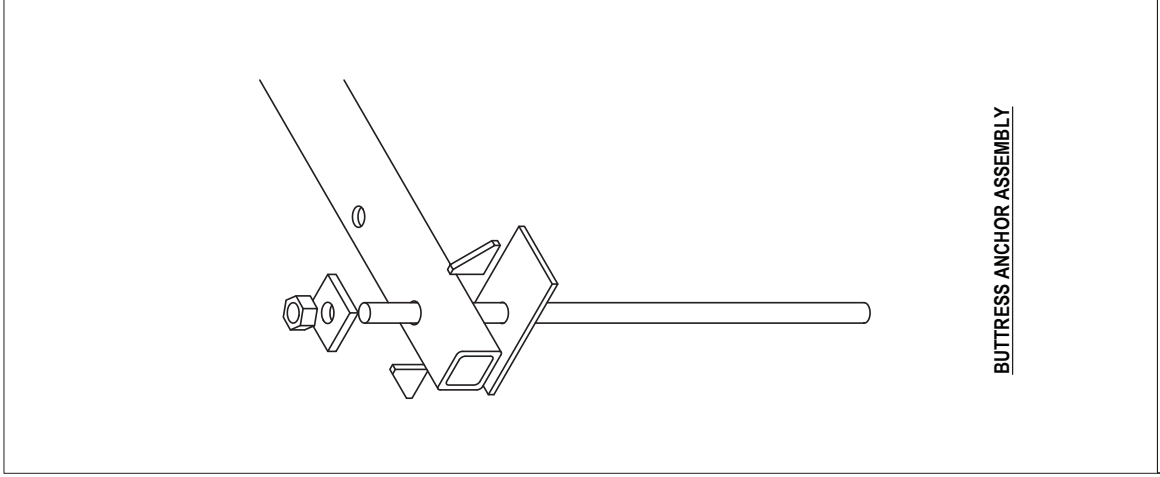
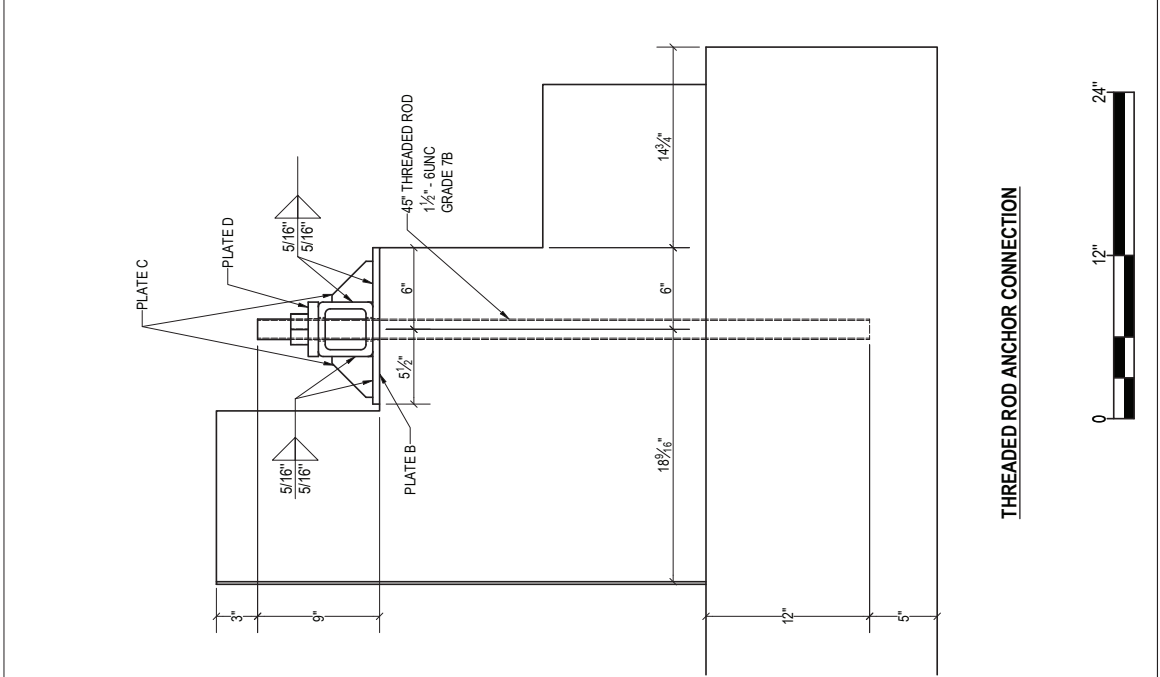
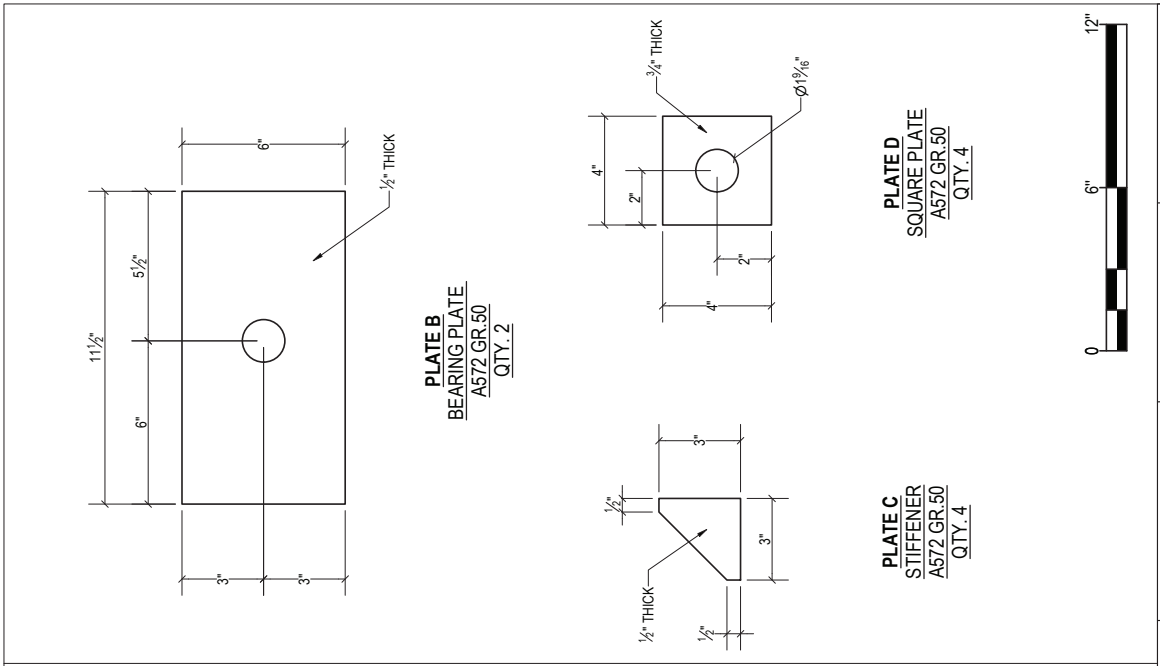
HSS
PLAN VIEW



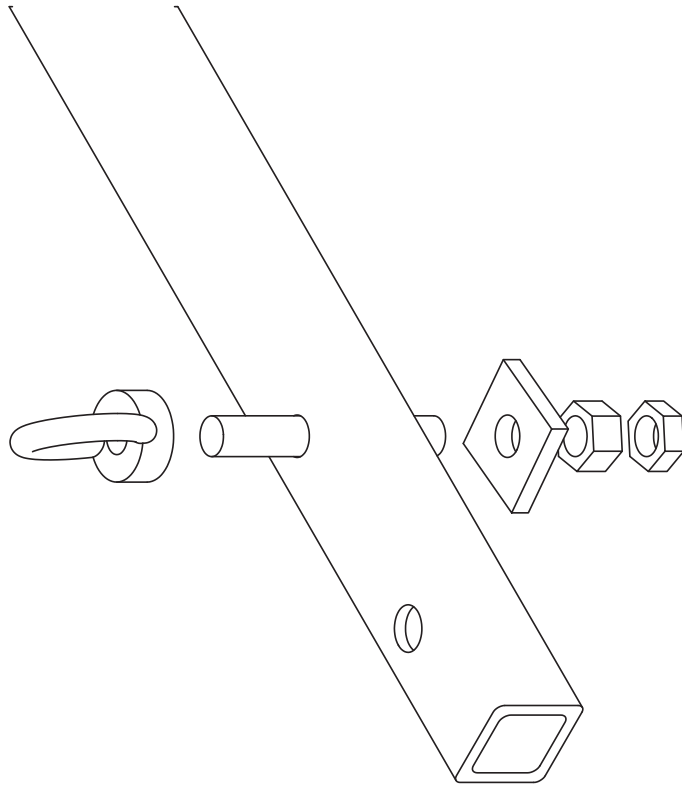
HSS 4X4X1/2
A500 GR.B

HSS WITH CONNECTION
LOCATIONS

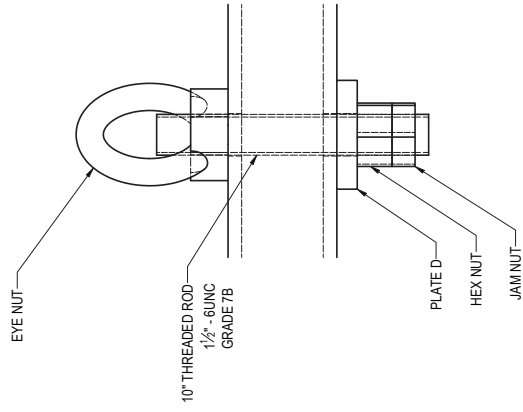
STEEL REINFORCED TEST SPECIMEN		Revision:	
HSS DETAIL	University of Florida	SHEET 19 OF 21	



<i>STEEL REINFORCED TEST SPECIMEN</i>		<i>Revision:</i>	
HSS-BUTTRESS CONNECTION	University of Florida	SHEET 20 OF 21	



LIFTING EYE NUT ASSEMBLY



LIFTING EYE NUT CONNECTION



<i>STEEL REINFORCED TEST SPECIMEN</i>		<i>Revision:</i>	
HSS-LIFTING EYE BOLT CONNECTION	<i>University of Florida</i>	SHEET 21 OF 21	

APPENDIX F: CONCRETE MIXTURE DESIGNS AND DELIVERED MIXTURES

The original concrete mix designs and on site adjustment procedures were developed in BDV31-977-72 for steel R/C test specimens. They were adapted for GFRP reinforced test specimens and end impact specimens in this project. Coordinated with BDV31-977-72, concrete mixtures used for test specimens described in this report, including original designs, delivery details and adjustments, are documented in the following order:

- Deck concrete mixture design
 - Steel R/C test specimens
 - Deck concrete delivery slip (steel-COR1)
 - Deck concrete adjustment sheet (steel-COR1)
 - Deck concrete delivery slip (steel-COR2)
 - Deck concrete adjustment sheet (steel-COR2)
 - Deck concrete delivery slip (steel-EOR)
 - Deck concrete adjustment sheet (steel-EOR)
 - GFRP R/C test specimens
 - Deck concrete delivery slip (GFRP-COR1)
 - Deck concrete adjustment sheet (GFRP-COR1)
 - Deck concrete delivery slip (GFRP-EOR1)
 - Deck concrete adjustment sheet (GFRP-EOR1)
 - Deck concrete delivery slip (GFRP-EOR2)
 - Deck concrete adjustment sheet (GFRP-EOR2)

- Rail concrete mixture design
 - Steel R/C test specimens
 - Rail concrete delivery slip (steel-COR1)
 - Rail concrete adjustment sheet (steel-COR1)
 - Rail concrete delivery slip (steel-COR2)
 - Rail concrete adjustment sheet (steel-COR2)
 - Rail concrete delivery slip (steel-EOR)
 - Rail concrete adjustment sheet (steel-EOR)
 - GFRP R/C test specimens
 - Rail concrete delivery slip (GFRP-COR1)
 - Rail concrete adjustment sheet (GFRP-COR1)
 - Rail concrete delivery slip (GFRP-EOR1)
 - Rail concrete adjustment sheet (GFRP-EOR2)
 - Rail concrete delivery slip (GFRP-EOR2)
 - Rail concrete adjustment sheet (GFRP-EOR2)

Producer: Smyrna Ready Mix

Class II Bridge Deck (4500 PSI) / Increased Slump

Effective Date: 3/6/2019

Aggregate Correction Factor: 0.2

Environment: Extremely Aggressive

Hot Weather

Source of Materials

Product	Quantity	Production Facility
921: Cement - Type II (MH)	489 Pound(s)	CMT29 - Suwannee American Cement - Branford, FL
929: Fly Ash - Class F	122 Pound(s)	FA45 - Boral - Bucks, AL (Barry)
901: C12 - #67 Stone	1900 Pound(s)	GA553 - JUNCTION CITY MINING
902: F01 - Silica Sand (Concrete)	1255 Pound(s)	50471 - A MINING GROUP, LLC
MasterAir AE 90 (MB-AE 90) [924-000-014 - Admixture for Concrete - Air Entraining]	.6 FL OZ	BASF Construction Chemicals, LLC
MasterSet DELVO (Delvo) [924-003-021 - Admixture for Concrete Type D]	30.6 FL OZ	BASF Construction Chemicals, LLC
MasterGlenium 7920 [924-005-093 - Admixture for Concrete Type F]	12.2 FL OZ	BASF Construction Chemicals, LLC
Water	32.5 GAL	
Water	271 LB	

Calculated Values**Producer Data**

Theoretical Unit Weight	149.5	PCF
Theoretical Yield	27.01	CF
Water Contributed from Admixture(s)	0.0	LB

Mix Design Limits*

Slump = 5 +/- 1.5 in

Water to Cementitious Materials Ratio <= 0.44

**See Contract Documents for Limits not displayed*

Special Use Instructions: Extended Transit Time: 2 Hours 30 Minutes

RC-1 COR deck concrete
2020-06-29: SRM Class II deck truck delivery mixture

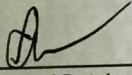
Financial Project No.: _____
 Plant No.: 55-503
 Concrete Supplier: Smyrna Ready Mix
 Phone Number: 850-575-3888
 Address: 5379 Capitol Circle
Tallahassee, FL 32305

Serial No.: 4033679
 Date: 6/29/2020
 Deliver To: Jeff Honing
 Phone No.: 561-632-4076
 Address: 2007 E. Paul Dirac DR

Truck No. 1680	DOT Class Class II 4500 Deck	DOT Mix No. 03-2177-02	Cubic Yards This Load 4				
Allowable Jobsite water 20	Time Loaded 9:27	Mixing Revolutions	Cubic Yards Total Today 4				
Cement <u>Argos</u> Source	<u>IL</u> Type	1900 Amount	Fly Ash or Slag	<u>Boral</u> Source	<u>Class F</u> Type	490 Amount	
Coarse Agg. <u>GA553</u> Pit No.	1.1 % Moisture	7800 Amount	Air Entraining	<u>BASF</u> Source	<u>AE 90</u> Brand	4 Amount	
Fine Agg. <u>50-382</u> Pit No.	3.7 % Moisture	4900 Amount	Admixture	<u>BASF</u> Source	<u>Retarder</u> Brand	<u>D</u> Type	60 Amount
Batch Water (gals or lbs)		76 Amount	Admixture	<u>BASF</u> Source	<u>7920</u> Brand	<u>G</u> Type	73 Amount
			Admixture	<u>BASF</u> Source	<u>SRA 020</u> Brand	<u>S</u> Type	0 Amount

Issuance of this ticket constitutes certification that the concrete batched was produced and information recorded in compliance with Department specification requirements for Structural Concrete.

2000848
 CTQP Technician Identification Number


 Signature of Batch Plant Operator

Arrival Time At Jobsite:		Number of Revolutions Upon Arrival At Job Site	
Water Added At Job Site (gals or lbs)		Additional Mixing Revolutions With Added Water	
Time Concrete Completely Discharged		Total Number of Revolutions	
Initial Slump	Initial Air	Initial Concrete Temperature	Initial W/C Ratio
Acceptance Slump	Acceptance Air	Acceptance Concrete Temperature	Acceptance W/C Ratio

Issuance of this ticket constitutes certification that the maximum specified water cementitious ratio was not exceeded and the batch was delivered and placed in compliance with Department specification requirements.

RC COR-1 deck concrete 2020-06-29: SRM Class II deck design vs truck delivery mixture

Batch size (cy)	4
Batch size (ft ³)	108

	Natural moisture (%)	Absorption (%)	Difference (%)
#67 stone - Coarse aggregate	1.10%	0.53%	0.57%
Sand - Fine aggregate	3.70%	0.40%	3.30%

Product	Quantity Units	SG	Volume/cy (ft ³ /cy)
Cement - Type 1L	489 lb/cy	3.15	2.49
Fly ash - Class F	122 lb/cy	2.37	0.82
#67 stone - Coarse aggregate	1900 lb/cy	2.80	10.87
Sand - Fine aggregate	1255 lb/cy	2.63	7.65
Water	271 lb/cy	1.00	4.34
Air	32.5 gallons/cy		
Fiber - Sika hooked-end (1% volume)	3.5% - 0 lb/cy		0.95
AE 90 - Air entraining Admixture	0.6 fl oz/cy	7.85	0.00
MasterSet DELVO - Retarding Admixture	30.6 fl oz/cy	-	-
MasterGlenium 7920 - High-range WRDA	12.2 fl oz/cy	-	-

Mix info	
Total volume	27.1 ft ³
Total mass	4037.00 lb/cy
Unit weight	148.84 lb/ft ³
Total cm/cy	611.00 lb/cy
w/c	0.554
w/cm	0.444
% fly ash	19.97%
sand/agg	0.398

Adjustments for moisture	
Aggregate weight adjustments for natural moisture	
#67 stone - Coarse aggregate	1920.9 lb/cy
Sand - Fine aggregate	1301.4 lb/cy
Water weight adjustment based on absorption and natural moisture	
Water from #67 stone - Coarse aggregate	10.7 lb/cy
Water from Sand - Fine aggregate	41.4 lb/cy
Water adjustment	-52.2 lb/cy
Water (adjusted mix quantity)	-6.3 gallons/cy
	218.8 lb/cy
	26.3 gallons/cy

Total content added to the truck (from delivery ticket)	Units	Design quantities (with moisture adjustments)	Difference
Cement - Type 1L	1900.0 lb	1956.0 lb	-56.0 lb
Fly ash - Class F	490.0 lb	488.0 lb	2.0 lb
#67 stone - Coarse aggregate	7800.0 lb	7683.6 lb	116.4 lb
Sand - Fine aggregate	4900.0 lb	5205.7 lb	-305.7 lb
Water	633.3 lb	875.4 lb	-242.1 lb
	76.0 gallons	105.0 gallons	-29.0 gallons
WR Grace Darex AEA - Air entraining Admixture	4.0 fl oz	2.4 fl oz	1.6 fl oz
MasterSet DELVO - Retarding Admixture	60.0 fl oz	122.4 fl oz	-62.4 fl oz
MasterGlenium 7920 - High-range WRDA	73.0 fl oz	48.8 fl oz	24.2 fl oz

<--- Total number of gallons that may be added to the truck (if negative)

Mix Design based on truck delivery quantities		% Difference from design	
Product	Quantity Units	SG	Volume/cy (ft ³ /cy)
Cement - Type 1L	475.0 lb/cy	3.15	2.42
Fly ash - Class F	122.5 lb/cy	2.37	0.83
#67 stone - Coarse aggregate	1928.6 lb/cy	2.80	11.04
Sand - Fine aggregate	1179.7 lb/cy	2.63	7.19
Water	259.0 lb/cy	1.00	4.15
Air	31.1 gallons/cy		
Fiber - Sika hooked-end (1% volume)	3.5% - 0.0 lb/cy		0.95
WR Grace Darex AEA - Air entraining Admixture	0.0 fl oz/cy	7.85	0.00
MasterSet DELVO - Retarding Admixture	15.0 fl oz/cy	-	66.7%
MasterGlenium 7920 - High-range WRDA	18.3 fl oz/cy	-	-51.0%
			49.6%

Mix info based on truck delivery	
Total volume	26.57 ft ³
Total mass	3964.73 lb/cy
Unit weight	149.24 lb/ft ³
Total cm/cy	597.50 lb/cy
w/c	0.55
w/cm	0.43
% fly ash	20.50%
sand/agg	0.38

RC COR-2 deck concrete
2020-08-31: SRM Class II deck truck delivery mixture

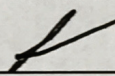
Financial Project No.: _____
Plant No.: 55-503
Concrete Supplier: Smyrna Ready Mix
Phone Number: 850-575-3888
Address: 5379 Capitol Circle
Tallahassee, FL 32305

Serial No.: 4034906
Date: 8/31/2020
Deliver To: University Of Florida
Phone No.: 850-921-7111
Address: 2007 Paul Dirac

Truck No. 4038	DOT Class Class II 4500 DECK	DOT Mix No. 03-2177-04	Cubic Yards This Load 4					
Allowable Jobsite water 30	Time Loaded 9:15	Mixing Revolutions	Cubic Yards Total Today 4					
Cement	<u>Argos</u> Source	<u>IL</u> Type	<u>1950</u> Amount	Fly Ash or Slag	<u>Boral</u> Source	<u>Class F</u> Type	<u>500</u> Amount	
Coarse Agg.	<u>GA553</u> Pit No.	<u>1.1</u> % Moisture	<u>7800</u> Amount	Air Entraining	<u>BASF</u> Source	<u>AE 90</u> Brand	<u>---</u> Type	<u>4</u> Amount
Fine Agg.	<u>50-382</u> Pit No.	<u>3.7</u> % Moisture	<u>5080</u> Amount	Admixture	<u>BASF</u> Source	<u>Retarder</u> Brand	<u>D</u> Type	<u>72</u> Amount
Batch Water (gals or lbs)			<u>68</u> Amount	Admixture	<u>BASF</u> Source	<u>7920</u> Brand	<u>G</u> Type	<u>60</u> Amount
				Admixture	<u>BASF</u> Source	<u>SRA 020</u> Brand	<u>S</u> Type	<u>0</u> Amount

Issuance of this ticket constitutes certification that the concrete batched was produced and information recorded in compliance with Department specification requirements for Structural Concrete.

E351810854210
CTQP Technician Identification Number


Signature of Batcher Plant Operator

Arrival Time At Jobsite:		Number of Revolutions Upon Arrival At Job Site	
Water Added At Job Site (gals or lbs)		Additional Mixing Revolutions With Added Water	
Time Concrete Completely Discharged		Total Number of Revolutions	
Initial Slump	Initial Air	Initial Concrete Temperature	Initial W/C Ratio
Acceptance Slump	Acceptance Air	Acceptance Concrete Temperature	Acceptance W/C Ratio

Issuance of this ticket constitutes certification that the maximum specified water cementitious ratio was not exceeded and the batch was delivered and placed in compliance with Department specification requirements.

RC COR-2 deck concrete 2020-08-31: SRM Class II deck design vs truck delivery mixture

Batch size (cy)	4
Batch size (ft ³)	108

	Natural moisture (%)	Absorption (%)	Difference (%)
#67 stone - Coarse aggregate	1.10%	0.53%	0.57%
Sand - Fine aggregate	3.70%	0.40%	3.30%

Product	Quantity Units	SG	Volume/cy (ft ³ /cy)
Cement - Type 1L	489 lb/cy	3.15	2.49
Fly ash - Class F	122 lb/cy	2.37	0.82
#67 stone - Coarse aggregate	1900 lb/cy	2.80	10.87
Sand - Fine aggregate	1255 lb/cy	2.63	7.65
Water	271 lb/cy	1.00	4.34
Air	32.5 gallons/cy		
Fiber - Sika hooked-end (1% volume)	3.5% -		0.95
AE 90 - Air entraining Admixture	0 lb/cy	7.85	0.00
MasterSet DELVO - Retarding Admixture	0.6 fl oz/cy	-	
MasterGlenium 7920 - High-range WRDA	30.6 fl oz/cy	-	
	12.2 fl oz/cy	-	

Mix info	
Total volume	27.1 ft ³
Total mass	4037.00 lb/cy
Unit weight	148.84 lb/ft ³
Total cm/cy	611.00 lb/cy
w/c	0.554
w/cm	0.444
% fly ash	19.97%
sand/agg	0.398

Adjustments for moisture	
Aggregate weight adjustments for natural moisture	
#67 stone - Coarse aggregate	1920.9 lb/cy
Sand - Fine aggregate	1301.4 lb/cy
Water weight adjustment based on absorption and natural moisture	
Water from #67 stone - Coarse aggregate	10.7 lb/cy
Water from Sand - Fine aggregate	41.4 lb/cy
Water adjustment	-52.2 lb/cy
Water (adjusted mix quantity)	-6.3 gallons/cy
	218.8 lb/cy
	26.3 gallons/cy

Total content added to the truck (from delivery ticket)	Units	Design quantities (with moisture adjustments)	Difference
Cement - Type 1L	1950.0 lb	1956.0 lb	-6.0 lb
Fly ash - Class F	500.0 lb	488.0 lb	12.0 lb
#67 stone - Coarse aggregate	7800.0 lb	7683.6 lb	116.4 lb
Sand - Fine aggregate	5080.0 lb	5205.7 lb	-125.7 lb
Water	566.7 lb	875.4 lb	-308.7 lb
	68.0 gallons	105.0 gallons	-37.0 gallons
WR Grace Darex AEA - Air entraining Admixture	4.0 fl oz	2.4 fl oz	1.6 fl oz
MasterSet DELVO - Retarding Admixture	60.0 fl oz	122.4 fl oz	-62.4 fl oz
MasterGlenium 7920 - High-range WRDA	72.0 fl oz	48.8 fl oz	23.2 fl oz

<--- Total number of gallons that may be added to the truck (if negative)

Mix Design based on truck delivery quantities	Quantity Units	SG	Volume/cy (ft ³ /cy)	% Difference from design
Product				
Cement - Type 1L	487.5 lb/cy	3.15	2.48	-0.3%
Fly ash - Class F	125.0 lb/cy	2.37	0.85	2.5%
#67 stone - Coarse aggregate	1928.6 lb/cy	2.80	11.04	1.5%
Sand - Fine aggregate	1223.0 lb/cy	2.63	7.45	-2.5%
Water	259.0 lb/cy	1.00	4.15	-4.4%
Air	31.1 gallons/cy			-4.4%
Fiber - Sika hooked-end (1% volume)	3.5% -		0.95	0.0%
	0.0 lb/cy	7.85	0.00	0.0%
WR Grace Darex AEA - Air entraining Admixture	1.0 fl oz/cy	-		66.7%
MasterSet DELVO - Retarding Admixture	15.0 fl oz/cy	-		-51.0%
MasterGlenium 7920 - High-range WRDA	18.0 fl oz/cy	-		47.5%

Mix info based on truck delivery	
Total volume	26.91 ft ³
Total mass	4023.06 lb/cy
Unit weight	149.49 lb/ft ³
Total cm/cy	612.50 lb/cy
w/c	0.53
w/cm	0.42
% fly ash	20.41%
sand/agg	0.39

GFRP RC COR-1 deck concrete
 2021-04-13: SRM Class II deck design vs truck delivery mixture

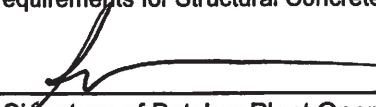
Financial Project No.: _____
 Plant No.: 55-503
 Concrete Supplier: Smyrna Ready Mix
 Phone Number: 850-575-3888
 Address: 5379 Capitol Circle
Tallahassee, FL 32305

Serial No.: 4039431
 Date: 4/13/2021
 Deliver To: FDOT
 Phone No.: 352-888-1099
 Address: 2007 East Paul Dirac

Truck No. 4136	DOT Class CLAS II 4500	DOT Mix No. <u>03-2177-02</u>	Cubic Yards This Load 4				
Allowable Jobsite water 30	Time Loaded 10:46	Mixing Revolutions	Cubic Yards Total Today 4				
Cement	<u>Argos</u> Source	<u>IL</u> Type	1956 Amount	Fly Ash or Slag	<u>Boral</u> Source	<u>Class F</u> Type	488 Amount
Coarse Agg.	<u>GA553</u> Pit No.	1.1 % Moisture	7691 Amount	Air Entraining	<u>BASF</u> Source	<u>AE 90</u> Brand	4 Amount
Fine Agg.	<u>50-382</u> Pit No.	3.7 % Moisture	5171 Amount	Admixture	<u>BASF</u> Source	<u>Retarder</u> Brand	0 Amount
Batch Water (gals or lbs)			50 Amount	Admixture	<u>BASF</u> Source	<u>7920</u> Brand	61 Amount
				Admixture	<u>BASF</u> Source	<u>SRA 020</u> Brand	0 Amount

Issuance of this ticket constitutes certification that the concrete batched was produced and information recorded in compliance with Department specification requirements for Structural Concrete.

E351810854210
 CTQP Technician Identification Number


 Signature of Batcher Plant Operator

Arrival Time At Jobsite:		Number of Revolutions Upon Arrival At Job Site	
Water Added At Job Site (gals or lbs)		Additional Mixing Revolutions With Added Water	
Time Concrete Completely Discharged		Total Number of Revolutions	
Initial Slump	Initial Air	Initial Concrete Temperature	Initial W/C Ratio
Acceptance Slump	Acceptance Air	Acceptance Concrete Temperature	Acceptance W/C Ratio

Issuance of this ticket constitutes certification that the maximum specified water cementitious ratio was not exceeded and the batch was delivered and placed in compliance with Department specification requirements.

GFRP RC COR-1 deck concrete 2021-04-13: SRM Class II deck design vs truck delivery mixture

Batch size (cy)	4
Batch size (ft³)	108

	Natural moisture (%)	Absorption (%)	Difference (%)
#67 stone - Coarse aggregate	1.10%	0.53%	0.57%
Sand - Fine aggregate	3.70%	0.40%	3.30%

Product	Quantity	Units	SG	Volume/cy (ft³/cy)
Cement - Type 1L	489	lb/cy	3.15	2.49
Fly ash - Class F	122	lb/cy	2.37	0.82
#67 stone - Coarse aggregate	1900	lb/cy	2.80	10.87
Sand - Fine aggregate	1255	lb/cy	2.63	7.65
Water	271	lb/cy	1.00	4.34
Air	32.5	gallons/cy		
Fiber - Sika hooked-end (1% volume)	3.5%	-		
AE 90 - Air entraining Admixture	0	lb/cy	7.85	0.95
MasterSet DELVO - Retarding Admixture	0.6	fl oz/cy	-	0.00
MasterGlenium 7920 - High-range WRDA	30.6	fl oz/cy	-	-
	12.2	fl oz/cy	-	-

Product	Quantity	Units	Volume/cy (ft³/cy)
#67 stone - Coarse aggregate	1920.9	lb/cy	
Sand - Fine aggregate	1301.4	lb/cy	
Water from #67 stone - Coarse aggregate	10.7	lb/cy	
Water from Sand - Fine aggregate	41.4	lb/cy	
Water adjustment	-52.2	lb/cy	
Water (adjusted mix quantity)	218.8	lb/cy	
	26.3	gallons/cy	

Product	Quantity	Units	Design quantities (with moisture adjustments)	Difference	% difference
Cement - Type 1L	1956.0	lb	1956.0 lb	0.0 lb	0.0
Fly ash - Class F	488.0	lb	488.0 lb	0.0 lb	0.0
#67 stone - Coarse aggregate	7691.0	lb	7683.6 lb	7.4 lb	0.1
Sand - Fine aggregate	5171.0	lb	5205.7 lb	-34.7 lb	-0.7
Water	416.7	lb	875.4 lb	-458.7 lb	-52.4
			105.0 gallons	-55.0 gallons	
WR Grace Dairex AEA - Air entraining Admixture	4.0	fl oz	2.4 fl oz	1.6 fl oz	66.7
MasterSet DELVO - Retarding Admixture	61.0	fl oz	122.4 fl oz	-61.4 fl oz	-50.2
MasterGlenium 7920 - High-range WRDA	0.0	fl oz	48.8 fl oz	-48.8 fl oz	-100.0

Product	Quantity	Units	SG	Volume/cy (ft³/cy)	% Difference from design
Cement - Type 1L	489	lb/cy	3.15	2.49	0.0%
Fly ash - Class F	122	lb/cy	2.37	0.82	0.0%
#67 stone - Coarse aggregate	1901.6	lb/cy	2.80	10.88	0.1%
Sand - Fine aggregate	1244.9	lb/cy	2.63	7.59	-0.8%
Water	259.0	lb/cy	1.00	4.15	-4.4%
Air	31.1	gallons/cy			-4.4%
Fiber - Sika hooked-end (1% volume)	3.5%	-			0.0%
WR Grace Dairex AEA - Air entraining Admixture	1.0	fl oz/cy	7.85	0.95	66.7%
MasterSet DELVO - Retarding Admixture	15.3	fl oz/cy	-	-	-50.2%
MasterGlenium 7920 - High-range WRDA	0.0	fl oz/cy	-	-	-100.0%

Mix info	Total volume	27.1 ft³
Total mass	4037.00	lb/cy
Unit weight	148.84	lb/ft³
Total cm/cy	611.00	lb/cy
w/c	0.554	
% fly ash	19.97%	
sand/agg	0.398	

Fiber dosage	Sika hooked-end steel fiber
Fiber type	SG
Dosage by volume	1%
Unit weight	489.84 lb/ft³
Fiber dosage	132.26 lb/cy
FRC batch size	1.86 cy
FRC batch size	50.3 ft³
Total fiber quantity	246.4 lb
Number of buckets	10 buckets
Fiber wt per bucket	24.6 lb/bucket

Initial slump	5.0 in
Water added	4.0 gallons
Final slump	6.0 in

← Total number of gallons that may be added to the truck (if negative)

Mix info based on truck delivery	Total volume	26.88 ft³
Total mass	4016.52	lb/cy
Unit weight	149.44	lb/ft³
Total cm/cy	611.00	lb/cy
w/c	0.53	
% fly ash	0.42	
sand/agg	0.40	

GFRP RC EOR-1 deck concrete
 2021-06-02: SRM Class II deck design vs truck delivery mixture

Financial Project No.: _____
 Plant No.: 55-503
 Concrete Supplier: Smyrna Ready Mix
 Phone Number: 850-575-3888
 Address: 5379 Capitol Circle
Tallahassee, FI 32305

Serial No.: 4040494
 Date: 6/2/2021
 Deliver To: FDOT
 Phone No.: 352-888-1099
 Address: 2007 E Paul Dirac

Truck No. 4034	DOT Class ClassII 4500 Deck	DOT Mix No. 03-2275-01	Cubic Yards This Load 4
Allowable Jobsite water 12	Time Loaded 12:00	Mixing Revolutions	Cubic Yards Total Today 4
Cement ASH GROVE	I/II 2010	Fly Ash or Slag	Boral 520
Source	Type	Amount	Source
Coarse Agg. GA553	1.2	8000	Air Entraining BASF AE 90 4
Pit No.	% Moisture	Amount	Source
Fine Agg. 50-471	3	5160	Admixture BASF Retarder D 160
Pit No.	% Moisture	Amount	Source
Batch Water (gals or lbs)	88	Admixture BASF 7920 G 60	Source
Amount		Source	Brand
		Admixture BASF SRA 020 S 0	Source
		Source	Brand

Issuance of this ticket constitutes certification that the concrete batched was produced and information recorded in compliance with Department specification requirements for Structural Concrete.

B65055259
 CTQP Technician Identification Number


 Signature of Batcher Plant Operator

Arrival Time At Jobsite:	Number of Revolutions Upon Arrival At Job Site		
Water Added At Job Site (gals or lbs)	Additional Mixing Revolutions With Added Water		
Time Concrete Completely Discharged	Total Number of Revolutions		
Initial Slump	Initial Air	Initial Concrete Temperature	Initial W/C Ratio
Acceptance Slump	Acceptance Air	Acceptance Concrete Temperature	Acceptance W/C Ratio

Issuance of this ticket constitutes certification that the maximum specified water cementitious ratio was not exceeded and the batch was delivered and placed in compliance with Department specification requirements.

GFRP RC EOR-1 deck concrete 2021-06-02: SRM Class II deck design vs truck delivery mixture

Batch size (cy)	4
Batch size (ft³)	108

	Natural moisture (%)	Absorption (%)	Difference (%)
#67 stone - Coarse aggregate	1.20%	0.53%	0.67%
Sand - Fine aggregate	3.00%	0.40%	2.60%

Mix Design	Product	Quantity	Units	SG	Volume/cy (ft³/cy)
Cement - Type 1L	Cement - Type 1L	489	lb/cy	3.15	2.49
	Fly ash - Class F	122	lb/cy	2.37	0.82
#67 stone - Coarse aggregate	#67 stone - Coarse aggregate	1900	lb/cy	2.80	10.87
	Sand - Fine aggregate	1255	lb/cy	2.63	7.65
Water	Water	271	lb/cy	1.00	4.34
		32.5	gallons/cy		
Air	Air	3.5%	-		0.95
	Fiber - Sika hooked-end (1% volume)	0	lb/cy	7.85	0.00
AE 90 - Air entraining Admixture	AE 90 - Air entraining Admixture	0.6	fl oz/cy	-	
	MasterSet DELVO - Retarding Admixture	30.6	fl oz/cy	-	
	MasterGlenium 7920 - High-range WRDA	12.2	fl oz/cy	-	

Adjustments for moisture	
Aggregate weight adjustments for natural moisture	
#67 stone - Coarse aggregate	1922.8 lb/cy
Sand - Fine aggregate	1292.7 lb/cy
Water weight adjustment based on absorption and natural moisture	
Water from #67 stone - Coarse aggregate	12.6 lb/cy
Water from Sand - Fine aggregate	32.6 lb/cy
Water adjustment	-45.3 lb/cy
Water (adjusted mix quantity)	-5.4 gallons/cy
	225.7 lb/cy
	27.1 gallons/cy

Total content added to the truck (from delivery ticket)	Units	Design quantities (with moisture adjustments)	Difference	% diff
Cement - Type 1L	2010.0 lb	1956.0 lb	54.0 lb	2.76
Fly ash - Class F	520.0 lb	488.0 lb	32.0 lb	6.56
#67 stone - Coarse aggregate	8000.0 lb	7691.2 lb	308.8 lb	4.01
Sand - Fine aggregate	5160.0 lb	5170.6 lb	-10.6 lb	-0.21
Water	733.3 lb	902.9 lb	-169.6 lb	-18.78
	88.0 gallons	108.4 gallons	-20.4 gallons	
WR Grace Darex AEA - Air entraining Admixture	4.0 fl oz	2.4 fl oz	1.6 fl oz	66.67
MasterSet DELVO - Retarding Admixture	160.0 fl oz	122.4 fl oz	37.6 fl oz	30.72
MasterGlenium 7920 - High-range WRDA	60.0 fl oz	48.8 fl oz	11.2 fl oz	22.95

Initial slum	2.0 in
Water add	22.0 gallons
Final slum	7.5 in

←--- Total number of gallons that may be added to the truck (if negative)

Mix info based on truck delivery	
Total volume	27.47 ft³
Total mass	4118.80 lb/cy
Unit weight	149.96 lb/ft³
Total cm/cy	632.50 lb/cy
w/c	0.52
w/cm	0.41
% fly ash	20.55%
sand/agg	0.39

Mix Design based on truck delivery quantities	Product	Quantity	Units	SG	Volume/cy (ft³/cy)	% Difference from design
Cement - Type 1L	Cement - Type 1L	502.5	lb/cy	3.15	2.56	2.8%
	Fly ash - Class F	130.0	lb/cy	2.37	0.88	6.6%
#67 stone - Coarse aggregate	#67 stone - Coarse aggregate	1976.0	lb/cy	2.80	11.31	4.0%
	Sand - Fine aggregate	1251.3	lb/cy	2.63	7.62	-0.3%
Water	Water	259.0	lb/cy	1.00	4.15	-4.4%
		31.1	gallons/cy			
Air	Air	3.5%	-		0.95	0.0%
	Fiber - Sika hooked-end (1% volume)	0.0	lb/cy	7.85	0.00	66.7%
AE 90 - Air entraining Admixture	AE 90 - Air entraining Admixture	1.0	fl oz/cy	-		30.7%
	MasterSet DELVO - Retarding Admixture	40.0	fl oz/cy	-		
	MasterGlenium 7920 - High-range WRDA	15.0	fl oz/cy	-		23.0%

Fiber dosage	
Fiber type	Sika hooked-end steel fiber
SG	7.85
Dosage by volume	1%
Unit weight	489.84 lb/ft³
Fiber dosage	132.26 lb/cy
FRC batch size	1.86 cy
FRC batch size	50.3 ft³
Total fiber quantity	246.4 lb
Number of buckets	10 buckets
Fiber wt per bucket	24.6 lb/bucket

Mix info	
Total volume	27.1 ft³
Total mass	4037.00 lb/cy
Unit weight	148.84 lb/ft³
Total cm/cy	611.00 lb/cy
w/c	0.554
w/cm	0.444
% fly ash	19.97%
sand/agg	0.398

GFRP RC EOR-2 deck concrete
 2021-09-08: SRM Class II deck design vs truck delivery mixture

Financial Project No.: _____
 Plant No.: 55-503
 Concrete Supplier: Smyrna Ready Mix
 Phone Number: 850-575-3888
 Address: 5379 Capitol Circle
Tallahassee, FI 32305

Serial No.: 4042550
 Date: 9/8/2021
 Deliver To: FDOT
 Phone No.: 352-888-1099
 Address: 2007 East Paul Dirac

Truck No. 4237	DOT Class CLASS II 4500 Deck	DOT Mix No. 03-2275-01	Cubic Yards This Load 4			
Allowable Jobsite water 12	Time Loaded 10:25	Mixing Revolutions	Cubic Yards Total Today 4			
Cement <u>ASH GROVE</u> I/II 1950	Source Type Amount	Fly Ash or Slag	Boral	Class F	560	
Coarse Agg. <u>GA553</u> 1.2 7720	Pit No. % Moisture Amount	Air Entraining <u>BASF</u> <u>AE 90</u> --- 4	Source Brand Type Amount			
Fine Agg. <u>50-471</u> 3 5160	Pit No. % Moisture Amount	Admixture <u>BASF</u> <u>Retarder</u> <u>D</u> 157	Source Brand Type Amount			
Batch Water (gals or lbs) 88	Amount	Admixture <u>BASF</u> <u>7920</u> <u>G</u> 60	Source Brand Type Amount			
		Admixture <u>BASF</u> <u>SRA 020</u> <u>S</u> 0	Source Brand Type Amount			

Issuance of this ticket constitutes certification that the concrete batched was produced and information recorded in compliance with Department specification requirements for Structural Concrete.

B65055259
 CTQP Technician Identification Number


 Signature of Batch Plant Operator

Arrival Time At Jobsite:	Number of Revolutions Upon Arrival At Job Site		
Water Added At Job Site (gals or lbs)	Additional Mixing Revolutions With Added Water		
Time Concrete Completely Discharged	Total Number of Revolutions		
Initial Slump	Initial Air	Initial Concrete Temperature	Initial W/C Ratio
Acceptance Slump	Acceptance Air	Acceptance Concrete Temperature	Acceptance W/C Ratio

Issuance of this ticket constitutes certification that the maximum specified water cementitious ratio was not exceeded and the batch was delivered and placed in compliance with Department specification requirements.

GRP RC EOR-2 deck concrete
2021-09-08: SRM Class II deck design vs truck delivery mixture

Batch size (cy)	4
Batch size (ft^3)	108

	Natural moisture (%)	Absorption (%)	Difference (%)
#67 stone - Coarse aggregate	1.20%	0.53%	0.67%
Sand - Fine aggregate	3.00%	0.40%	2.60%

Mix Design	Product	Quantity	Units	Volume/cy (ft^3/cy)	SG
	Cement - Type 1L	489	lb/cy	3.15	3.15
	Fly ash - Class F	122	lb/cy	0.82	2.37
	#67 stone - Coarse aggregate	1900	lb/cy	10.87	2.80
	Sand - Fine aggregate	1255	lb/cy	7.65	2.63
	Water	271	lb/cy	4.34	1.00
	Air	32.5	gallons/cy		
	Fiber - Sika hooked-end (1% volume)	0	lb/cy	0.95	7.85
	AE 90 - Air entraining Admixture	0.6	fl oz/cy		
	MasterSet DELVO - Retarding Admixture	30.6	fl oz/cy		
	MasterGlenium 7920 - High-range WRDA	12.2	fl oz/cy		

Adjustments for moisture	
Aggregate weight adjustments for natural moisture	
#67 stone - Coarse aggregate	1922.8 lb/cy
Sand - Fine aggregate	1292.7 lb/cy
Water weight adjustment based on absorption and natural moisture	
Water from #67 stone - Coarse aggregate	12.6 lb/cy
Water from Sand - Fine aggregate	32.6 lb/cy
Water adjustment	-45.3 lb/cy
Water (adjusted mix quantity)	225.7 lb/cy
	27.1 gallons/cy

Total content added to the truck (from delivery ticket)	Units	Design quantities (with moisture adjustments)	Difference	% diff
Cement - Type 1L	1950.0 lb	1956.0 lb	-6.0 lb	-0.31
Fly ash - Class F	560.0 lb	488.0 lb	72.0 lb	14.75
#67 stone - Coarse aggregate	7720.0 lb	7691.2 lb	28.8 lb	0.37
Sand - Fine aggregate	5160.0 lb	5170.6 lb	-10.6 lb	-0.21
Water	733.3 lb	902.9 lb	-169.6 lb	-18.78
	88.0 gallons	108.4 gallons	-20.4 gallons	
WR Grace Darex AEA - Air entraining Admixture	4.0 fl oz	2.4 fl oz	1.6 fl oz	66.67
MasterSet DELVO - Retarding Admixture	157.0 fl oz	122.4 fl oz	34.6 fl oz	28.27
MasterGlenium 7920 - High-range WRDA	60.0 fl oz	48.8 fl oz	11.2 fl oz	22.95

Initial slump	6.5 in
Water added	0.0 gallons
Final slump	6.5 in

<--- Total number of gallons that may be added to the truck (if negative)

Mix Design based on truck delivery quantities	Product	Quantity	Units	Volume/cy (ft^3/cy)	SG	% Difference from design
	Cement - Type 1L	487.5	lb/cy	3.15	3.15	-0.3%
	Fly ash - Class F	140.0	lb/cy	0.95	2.37	14.8%
	#67 stone - Coarse aggregate	1906.8	lb/cy	10.91	2.80	0.4%
	Sand - Fine aggregate	1251.3	lb/cy	7.62	2.63	-0.3%
	Water	259.0	lb/cy	4.15	1.00	-4.4%
	Air	31.1	gallons/cy			-4.4%
	Fiber - Sika hooked-end (1% volume)	0.0	lb/cy	0.95	7.85	0.0%
	WR Grace Darex AEA - Air entraining Admixture	1.0	fl oz/cy			66.7%
	MasterSet DELVO - Retarding Admixture	39.3	fl oz/cy			28.3%
	MasterGlenium 7920 - High-range WRDA	15.0	fl oz/cy			23.0%

Mix info based on truck delivery	
Total volume	27.06 ft^3
Total mass	4044.64 lb/cy
Unit weight	149.46 lb/ft^3
Total cm/cy	627.50 lb/cy
w/c	0.53
w/cm	0.41
% fly ash	22.31%
sand/agg	0.40

Mix info	
Total volume	27.1 ft^3
Total mass	4037.00 lb/cy
Unit weight	148.84 lb/ft^3
Total cm/cy	611.00 lb/cy
w/c	0.554
w/cm	0.444
% fly ash	19.97%
sand/agg	0.398

Fiber dosage	
Fiber type	Sika hooked-end steel fiber
SG	7.85
Dosage by volume	1%
Unit weight	489.84 lb/ft^3
Fiber dosage	132.26 lb/cy
FRC batch size	1.86 cy
FRC batch size	50.3 ft^3
Total fiber quantity	246.4 lb
Number of buckets	10 buckets
Fiber wt per bucket	24.6 lb/bucket

Producer: Smyrna Ready Mix

Class II (3400 PSI) / Increased Slump

Effective Date: 3/7/2019

Aggregate Correction Factor: 0.2

Environment: Extremely Aggressive

Hot Weather

Source of Materials

Product	Quantity	Production Facility
921: Cement - Type II (MH)	416 Pound(s)	CMT29 - Suwannee American Cement - Branford, FL
929: Fly Ash - Class F	104 Pound(s)	FA45 - Boral - Bucks, AL (Barry)
901: C12 - #67 Stone	1900 Pound(s)	GA553 - JUNCTION CITY MINING
902: F01 - Silica Sand (Concrete)	1319 Pound(s)	50471 - A MINING GROUP, LLC
MasterAir AE 90 (MB-AE 90) [924-000-014 - Admixture for Concrete - Air Entraining]	.5 FL OZ	BASF Construction Chemicals, LLC
MasterSet DELVO (Delvo) [924-003-021 - Admixture for Concrete Type D]	26 FL OZ	BASF Construction Chemicals, LLC
MasterGlenium 7920 [924-005-093 - Admixture for Concrete Type F]	13 FL OZ	BASF Construction Chemicals, LLC
Water	33.2 GAL	
Water	277 LB	

Calculated Values

Producer Data

Theoretical Unit Weight	148.7	PCF
Theoretical Yield	27.01	CF
Water Contributed from Admixture(s)	0.0	LB

Mix Design Limits*

Slump = 5 +/- 1.5 in

Water to Cementitious Materials Ratio <= 0.53

**See Contract Documents for Limits not displayed*

Special Use Instructions: Extended Transit Time: 2 Hours 30 Minutes

RC-1 railing concrete
2020-07-16: SRM Class II railing truck delivery mixture

Financial Project No.: _____
 Plant No.: 50-466
 Concrete Supplier: Smyrna Ready Mix
 Phone Number: 850-575-3888
 Address: 1800 Brickyard Rd. E
Midway, Fl. 32343

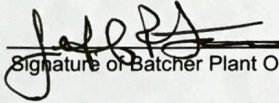
Serial No.: 2005448
 Date: 7/16/2020
 Deliver To: UNIVERSITY OF FLORIDA
 Phone No.: _____
 Address: 2007 E. PAUL DIRAC DR

Truck No.	DOT Class		DOT Mix No.	Cubic Yards This Load		
4044	CLASS II 3400 GRANITE		34090	3		
Allowable Jobsite water	Time Loaded		Mixing Revolutions	Cubic Yards Total Today		
6	8:38		81	3		
Cement	SAC	I/II	Fly Ash or Slag		Boral	Class F
	Source	Type	Amount		Source	Type
			1295			305
Coarse Agg.	GA553	1.2	5790	Air Entraining	BASF	AE 90
	Pit No.	% Moisture	Amount		Source	Brand
						Type
						Amount
						3
Fine Agg.	50-471	3.2	4180	Admixture	BASF	Retarder
	Pit No.	% Moisture	Amount		Source	Brand
						Type
						Amount
						48
Batch Water (gals or lbs)			70	Admixture	BASF	7920
			Amount		Source	Brand
						Type
						Amount
						32

Issuance of this ticket constitutes certification that the concrete batched was produced and information recorded in compliance with Department specification requirements for Structural Concrete.

F-500-436-56-062-0

CTQP Technician Identification Number


 Signature of Batcher Plant Operator

Arrival Time At Jobsite:		Number of Revolutions Upon Arrival At Job Site	
Water Added At Job Site (gals or lbs)		Additional Mixing Revolutions With Added Water	
Time Concrete Completely Discharged		Total Number of Revolutions	
Initial Slump	Initial Air	Initial Concrete Temperature	Initial W/C Ratio
Acceptance Slump	Acceptance Air	Acceptance Concrete Temperature	Acceptance W/C Ratio

Issuance of this ticket constitutes certification that the maximum specified water cementitious ratio was not exceeded and the batch was delivered and placed in compliance with Department specification requirements.

CTQP Technician Identification Number

Signature of Contractor's Representative

RC COR-1 railing concrete 2020-07-16: SRM Class II railing design vs truck delivery mixture

Batch size (cy)	3
Batch size (ft ³)	81

	Natural moisture (%)	Absorption (%)	Difference (%)
#67 stone - Coarse aggregate	1.20%	0.53%	0.67%
Sand - Fine aggregate	3.20%	0.40%	2.80%

Mix Design	Quantity	Units	SG	Volume/cy (ft ³ /cy)
Cement - Type II	416	lb/cy	3.15	2.12
Fly ash - Class F	104	lb/cy	2.37	0.70
#67 stone - Coarse aggregate	1900	lb/cy	2.80	10.87
Sand - Fine aggregate	1319	lb/cy	2.63	8.04
Water	277	lb/cy	1.00	4.44
Air	33.2	gallons/cy		0.81
Fiber - Sika hooked-end (1% volume)	3.0%	lb/cy	7.85	0.00
AE 90 - Air entraining Admixture	0.5	fl oz/cy	-	-
MasterSet DELVO - Retarding Admixture	26	fl oz/cy	-	-
MasterGlenium 7920 - High-range WRDA	13	fl oz/cy	-	-

Mix info	
Total volume	27.0 ft³
Total mass	4016.00 lb/cy
Unit weight	148.85 lb/ft ³
Total cm/cy	520.00 lb/cy
w/c	0.666
w/cm	0.533
% fly ash	20.00%
sand/agg	0.410

Adjustments for moisture	Quantity	Units
Aggregate weight adjustments for natural moisture		
#67 stone - Coarse aggregate	1922.8	lb/cy
Sand - Fine aggregate	1361.2	lb/cy
Water weight adjustment based on absorption and natural moisture		
Water from #67 stone - Coarse aggregate	12.6	lb/cy
Water from Sand - Fine aggregate	36.9	lb/cy
Water adjustment	-49.6	lb/cy
Water (adjusted mix quantity)	-5.9	gallons/cy
Water (adjusted mix quantity)	227.4	lb/cy
Water (adjusted mix quantity)	27.3	gallons/cy

Total content added to the truck (from delivery ticket)	Units	Design quantities (with moisture adjustments)	Difference
Cement - Type II	1295.0	1248.0 lb	47.0 lb
Fly ash - Class F	305.0	312.0 lb	-7.0 lb
#67 stone - Coarse aggregate	5790.0	5768.4 lb	21.6 lb
Sand - Fine aggregate	4180.0	4083.6 lb	96.4 lb
Water	583.3	682.3 lb	-99.0 lb
WR Grace Darex AEA - Air entraining Admixture	70.0	81.9 gallons	-11.9 gallons
MasterSet DELVO - Retarding Admixture	3.0	1.5 fl oz	1.5 fl oz
MasterGlenium 7920 - High-range WRDA	32.0	78.0 fl oz	-46.0 fl oz
	48.0	39 fl oz	9 fl oz

<--- Total number of gallons that may be added to the truck (if negative)

Mix Design based on truck delivery quantities	Quantity	Units	SG	Volume/cy (ft ³ /cy)	% Difference from design
Cement - Type II	431.7	lb/cy	3.15	2.20	3.8%
Fly ash - Class F	101.7	lb/cy	2.37	0.69	-2.2%
#67 stone - Coarse aggregate	1906.8	lb/cy	2.80	10.91	0.4%
Sand - Fine aggregate	1348.7	lb/cy	2.63	8.22	2.3%
Water	259.0	lb/cy	1.00	4.15	-6.5%
Air	31.1	gallons/cy		0.95	-6.5%
Fiber - Sika hooked-end (1% volume)	3.5%	lb/cy	7.85	0.27	16.7%
WR Grace Darex AEA - Air entraining Admixture	1.0	fl oz/cy	-	-	100.0%
MasterSet DELVO - Retarding Admixture	10.7	fl oz/cy	-	-	-59.0%
MasterGlenium 7920 - High-range WRDA	16.0	fl oz/cy	-	-	23.1%

Mix info based on truck delivery	
Total volume	27.38 ft³
Total mass	4180.18 lb/cy
Unit weight	152.67 lb/ft ³
Total cm/cy	533.33 lb/cy
w/c	0.60
w/cm	0.49
% fly ash	19.06%
sand/agg	0.41

RC-2 railing concrete
 2020-09-15: SRM Class II railing truck delivery mixture

Financial Project No.: _____
 Plant No.: 55-503
 Concrete Supplier: Smyrna Ready Mix
 Phone Number: 850-575-3888
 Address: 5379 Capitol Circle
Tallahassee, FL 32305

Serial No.: 4035230
 Date: 9/15/2020
 Deliver To: FDOT
 Phone No.: 561-632-4076
 Address: 2007 Paul Dirac

Truck No.	DOT Class		DOT Mix No.	Cubic Yards This Load			
4006	CLASS II 3400		03-2176-02	3			
Allowable Jobsite water	Time Loaded		Mixing Revolutions	Cubic Yards Total Today			
30	8:55			3			
Cement	<u>Argos</u>	<u>IL</u>	1260	Fly Ash or Slag	<u>Boral</u>	<u>Class F</u>	310
	Source	Type	Amount		Source	Type	Amount
Coarse Agg.	<u>GA553</u>	1.1	5760	Air Entraining	<u>BASF</u>	<u>AE 90</u>	3
	Pit No.	% Moisture	Amount		Source	Brand	Type
Fine Agg.	<u>50-382</u>	3.7	4110	Admixture	<u>BASF</u>	<u>Retarder</u>	23
	Pit No.	% Moisture	Amount		Source	Brand	Type
Batch Water (gals or lbs)			40	Admixture	<u>BASF</u>	<u>7920</u>	42
			Amount		Source	Brand	Type
				Admixture	<u>BASF</u>	<u>Delvo</u>	48
					Source	Brand	Type

Issuance of this ticket constitutes certification that the concrete batched was produced and information recorded in compliance with Department specification requirements for Structural Concrete.

E351810854210

CTQP Technician Identification Number


 Signature of Batcher Plant Operator

Arrival Time At Jobsite:		Number of Revolutions Upon Arrival At Job Site	
Water Added At Job Site (gals or lbs)		Additional Mixing Revolutions With Added Water	
Time Concrete Completely Discharged		Total Number of Revolutions	
Initial Slump	Initial Air	Initial Concrete Temperature	Initial W/C Ratio
Acceptance Slump	Acceptance Air	Acceptance Concrete Temperature	Acceptance W/C Ratio

Issuance of this ticket constitutes certification that the maximum specified water cementitious ratio was not exceeded and the batch was delivered and placed in compliance with Department specification requirements.

RC COR-2 railing concrete 2020-09-15: SRM Class II railing design vs truck delivery mixture

Batch size (cy)	3
Batch size (ft ³)	81

	Natural moisture (%)	Absorption (%)	Difference (%)
#67 stone - Coarse aggregate	1.10%	0.53%	0.57%
Sand - Fine aggregate	3.70%	0.40%	3.30%

Mix Design	Quantity	Units	SG	Volume/cy (ft ³ /cy)
Cement - Type II	416	lb/cy	3.15	2.12
Fly ash - Class F	104	lb/cy	2.37	0.70
#67 stone - Coarse aggregate	1900	lb/cy	2.80	10.87
Sand - Fine aggregate	1319	lb/cy	2.63	8.04
Water	277	lb/cy	1.00	4.44
Air	33.2	gallons/cy		0.81
Fiber - Sika hooked-end (1% volume)	3.0%	-	7.85	0.00
AE 90 - Air entraining Admixture	0.5	fl oz/cy	-	-
MasterSet DELVO - Retarding Admixture	26	fl oz/cy	-	-
MasterGlenium 7920 - High-range WRDA	13	fl oz/cy	-	-

Mix info	
Total volume	27.0 ft³
Total mass	4016.00 lb/cy
Unit weight	148.85 lb/ft ³
Total cm/cy	520.00 lb/cy
w/c	0.666
w/cm	0.533
% fly ash	20.00%
sand/agg	0.410

Adjustments for moisture	Aggregate weight adjustments for natural moisture
#67 stone - Coarse aggregate	1920.9 lb/cy
Sand - Fine aggregate	1367.8 lb/cy
Water weight adjustment based on absorption and natural moisture	
Water from #67 stone - Coarse aggregate	10.7 lb/cy
Water from Sand - Fine aggregate	43.5 lb/cy
Water adjustment	-54.3 lb/cy
Water (adjusted mix quantity)	-6.5 gallons/cy
	222.7 lb/cy
	26.7 gallons/cy

Total content added to the truck (from delivery ticket)	Units	Design quantities (with moisture adjustments)	Difference
Cement - Type II	1260.0 lb	1248.0 lb	12.0 lb
Fly ash - Class F	310.0 lb	312.0 lb	-2.0 lb
#67 stone - Coarse aggregate	5760.0 lb	5762.7 lb	-2.7 lb
Sand - Fine aggregate	4110.0 lb	4103.4 lb	6.6 lb
Water	333.3 lb	668.2 lb	-334.9 lb
WR Grace Darex AEA - Air entraining Admixture	40.0 gallons	80.2 gallons	-40.2 gallons
MasterSet DELVO - Retarding Admixture	3.0 fl oz	1.5 fl oz	1.5 fl oz
MasterGlenium 7920 - High-range WRDA	48.0 fl oz	78.0 fl oz	-30.0 fl oz
	42.0 fl oz	39 fl oz	3 fl oz

<--- Total number of gallons that may be added to the truck (if negative)

Mix Design based on truck delivery quantities	Quantity	Units	SG	Volume/cy (ft ³ /cy)	% Difference from design
Cement - Type 1L	420.0	lb/cy	3.15	2.14	1.0%
Fly ash - Class F	103.3	lb/cy	2.37	0.70	-0.6%
#67 stone - Coarse aggregate	1898.9	lb/cy	2.80	10.87	-0.1%
Sand - Fine aggregate	1319.3	lb/cy	2.63	8.04	0.0%
Water	259.0	lb/cy	1.00	4.15	-6.5%
Air	31.1	gallons/cy		0.95	-6.5%
Fiber - Sika hooked-end (1% volume)	3.5%	-	7.85	0.27	16.7%
WR Grace Darex AEA - Air entraining Admixture	132.3	lb/cy	-	-	#DIV/0!
MasterSet DELVO - Retarding Admixture	1.0	fl oz/cy	-	-	100.0%
MasterGlenium 7920 - High-range WRDA	16.0	fl oz/cy	-	-	-38.5%
	14.0	fl oz/cy	-	-	7.7%

Mix info based on truck delivery	
Total volume	27.11 ft³
Total mass	4132.78 lb/cy
Unit weight	152.45 lb/ft ³
Total cm/cy	523.33 lb/cy
w/c	0.62
w/cm	0.49
% fly ash	19.75%
sand/agg	0.41

GFRP RC COR-I railing concrete
 2021-05-04: SRM Class II railing truck delivery mixture

Financial Project No.: _____
 Plant No.: 55-503
 Concrete Supplier: Smyrna Ready Mix
 Phone Number: 850-575-3888
 Address: 5379 Capitol Circle
Tallahassee, Fl 32305

Serial No.: 4039829
 Date: 5/4/2021
 Deliver To: FDOT
 Phone No.: _____
 Address: 2007 E Paul Dirac

Truck No. 4136	DOT Class II 3400	DOT Mix No. 03-2176-02	Cubic Yards This Load 3			
Allowable Jobsite water 10	Time Loaded 8:35	Mixing Revolutions	Cubic Yards Total Today 3			
Cement <u>ASH GROVE</u>	I/II	1380	Fly Ash or Slag	Boral	Class F	390
Source	Type	Amount	Source	Type	Amount	
Coarse Agg. <u>GA553</u>	1.2	5840	Air Entraining <u>BASF</u>	<u>AE 90</u>	---	6
Pit No.	% Moisture	Amount	Source	Brand	Type	Amount
Fine Agg. <u>50-471</u>	3	4160	Admixture <u>BASF</u>	<u>Retarder</u>	<u>D</u>	20
Pit No.	% Moisture	Amount	Source	Brand	Type	Amount
Batch Water (gals or lbs)		60	Admixture <u>BASF</u>	<u>7920</u>	<u>G</u>	39
	Amount		Source	Brand	Type	Amount
			Admixture <u>BASF</u>	<u>SRA 020</u>	<u>S</u>	0
			Source	Brand	Type	Amount

Issuance of this ticket constitutes certification that the concrete batched was produced and information recorded in compliance with Department specification requirements for Structural Concrete.

B65055259
 CTQP Technician Identification Number


 Signature of Batcher Plant Operator

Arrival Time At Jobsite:		Number of Revolutions Upon Arrival At Job Site	
Water Added At Job Site (gals or lbs)		Additional Mixing Revolutions With Added Water	
Time Concrete Completely Discharged		Total Number of Revolutions	
Initial Slump	Initial Air	Initial Concrete Temperature	Initial W/C Ratio
Acceptance Slump	Acceptance Air	Acceptance Concrete Temperature	Acceptance W/C Ratio

Issuance of this ticket constitutes certification that the maximum specified water cementitious ratio was not exceeded and the batch was delivered and placed in compliance with Department specification requirements.

GFRP RC COR-1 railing concrete
2021-05-04: SRM Class II railing truck delivery mixture

Batch size (cy)	3
Batch size (ft³)	81

	Natural moisture (%)	Absorption (%)	Difference (%)
#67 stone - Coarse aggregate	1.10%	0.53%	0.57%
Sand - Fine aggregate	3.70%	0.40%	3.30%

Product	Quantity	Units	SG	Volume/cy (ft³/cy)
Cement - Type II		lb/cy	3.15	2.12
Fly ash - Class F		lb/cy	2.37	0.70
#67 stone - Coarse aggregate		lb/cy	2.80	10.87
Sand - Fine aggregate		lb/cy	2.63	8.04
Water		lb/cy	1.00	4.44
		33.2 gallons/cy		
Air		-	7.85	0.81
Fiber - Sika hooked-end (1% volume)		lb/cy	-	0.00
AE 90 - Air entraining Admixture		fl oz/cy	-	-
MasterSet DELVO - Retarding Admixture		fl oz/cy	-	-
MasterGlenium 7920 - High-range WRDA		fl oz/cy	-	-

Mix info	
Total volume	27.0 ft³
Total mass	4016.00 lb/cy
Unit weight	148.85 lb/ft³
Total cm/cy	520.00 lb/cy
w/c	0.666
w/cm	0.533
% fly ash	20.00%
sand/agg	0.410

Adjustments for moisture	
Aggregate weight adjustments for natural moisture	
#67 stone - Coarse aggregate	lb/cy
Sand - Fine aggregate	lb/cy
Water weight adjustment based on absorption and natural moisture	
Water from #67 stone - Coarse aggregate	10.7 lb/cy
Water from Sand - Fine aggregate	43.5 lb/cy
Water adjustment	-54.3 lb/cy
	-6.5 gallons/cy
Water (adjusted mix quantity)	lb/cy
	gallons/cy

Total content added to the truck (from delivery ticket)	Design quantities (with moisture adjustments)	Difference	% difference
Cement - Type II	1248.0 lb	132.0 lb	10.6
Fly ash - Class F	312.0 lb	78.0 lb	25.0
#67 stone - Coarse aggregate	5762.7 lb	77.3 lb	1.3
Sand - Fine aggregate	4103.4 lb	56.6 lb	1.4
Water	668.2 lb	-168.2 lb	-25.2
	80.2 gallons		
WR Grace Darex AEA - Air entraining Admixture	1.5 fl oz	4.5 fl oz	300.0
MasterSet DELVO - Retarding Admixture	78.0 fl oz	-58.0 fl oz	-74.4
MasterGlenium 7920 - High-range WRDA	39 fl oz	0 fl oz	0.0

<--- Total number of gallons that may be added to the truck (if negative)

Initial slump	5.0 in
Water added	3.0 gallons
Final slump	6.5 in

Mix Design based on truck delivery quantities			
Product	Quantity	Units	% Difference from design
Cement - Type II	460.0	lb/cy	2.34
Fly ash - Class F	130.0	lb/cy	0.88
#67 stone - Coarse aggregate	1925.3	lb/cy	11.02
Sand - Fine aggregate	1335.4	lb/cy	8.14
Water	259.0	lb/cy	-6.5%
	31.1	gallons/cy	-6.5%
Air	3.5%	-	0.95
Fiber - Sika hooked-end (1% volume)	132.3	lb/cy	0.27
WR Grace Darex AEA - Air entraining Admixture	2.0	fl oz/cy	300.0%
MasterSet DELVO - Retarding Admixture	6.7	fl oz/cy	-74.4%
MasterGlenium 7920 - High-range WRDA	13.0	fl oz/cy	0.0%

Mix info based on truck delivery	
Total volume	27.74 ft³
Total mass	4241.87 lb/cy
Unit weight	152.91 lb/ft³
Total cm/cy	590.00 lb/cy
w/c	0.56
w/cm	0.44
% fly ash	22.03%
sand/agg	0.41

GFRP RC EOR-1 railing concrete
 2021-06-29: SRM Class II railing truck delivery mixture

Financial Project No.: _____
 Plant No.: 55-503
 Concrete Supplier: Smyrna Ready Mix
 Phone Number: 850-575-3888
 Address: 5379 Capitol Circle
Tallahassee, FL 32305

Serial No.: 4041005
 Date: 6/29/2021
 Deliver To: FDOT
 Phone No.: 352-888-1099
 Address: 2007 East Paul Dirac

Truck No.	DOT Class		DOT Mix No.	Cubic Yards This Load			
4041	CLASS II 3400		03-2176-02	3			
Allowable Jobsite water	Time Loaded	12:55	Mixing Revolutions	Cubic Yards Total Today			
12				3			
Cement	<u>ASH GROVE</u>	I/II	1280	Fly Ash or Slag	Boral	Class F	340
	Source	Type	Amount		Source	Type	Amount
Coarse Agg.	<u>GA553</u>	1.2	5880	Air Entraining	<u>BASF</u>	<u>AE 90</u>	5
	Pit No.	% Moisture	Amount		Source	Brand	Type
Fine Agg.	<u>50-471</u>	3	4080	Admixture	<u>BASF</u>	<u>Retarder</u>	81
	Pit No.	% Moisture	Amount		Source	Brand	Type
Batch Water (gals or lbs)			65	Admixture	<u>BASF</u>	<u>7920</u>	42
			Amount		Source	Brand	Type
				Admixture	<u>BASF</u>	<u>SRA 020</u>	0
					Source	Brand	Type

Issuance of this ticket constitutes certification that the concrete batched was produced and information recorded in compliance with Department specification requirements for Structural Concrete.

B65055259
 CTQP Technician Identification Number


 Signature of Batch Plant Operator

Arrival Time At Jobsite:		Number of Revolutions Upon Arrival At Job Site	
Water Added At Job Site (gals or lbs)		Additional Mixing Revolutions With Added Water	
Time Concrete Completely Discharged		Total Number of Revolutions	
Initial Slump	Initial Air	Initial Concrete Temperature	Initial W/C Ratio
Acceptance Slump	Acceptance Air	Acceptance Concrete Temperature	Acceptance W/C Ratio

Issuance of this ticket constitutes certification that the maximum specified water cementitious ratio was not exceeded and the batch was delivered and placed in compliance with Department specification requirements.

GFRP RC EOR-1 railing concrete
2021-06-29: SRM Class II railing truck delivery mixture

Batch size (cy)	3
Batch size (ft^3)	81

	Natural moisture (%)	Absorption (%)	Difference (%)
#67 stone - Coarse aggregate	1.20%	0.53%	0.67%
Sand - Fine aggregate	3.00%	0.40%	2.60%

Mix Design	Product	Quantity	Units	Volume/cy (ft^3/cy)	SG
	Cement - Type II	416	lb/cy	3.15	3.15
	Fly ash - Class F	104	lb/cy	2.37	2.37
	#67 stone - Coarse aggregate	1900	lb/cy	10.87	2.80
	Sand - Fine aggregate	1319	lb/cy	8.04	2.63
	Water	277	lb/cy	4.44	1.00
		33.2	gallons/cy		
	Air	3.0%	-	0.81	
	Fiber - Sika hooked-end (1% volume)	0	lb/cy	7.85	0.00
	AE 90 - Air entraining Admixture	0.5	fl oz/cy	-	-
	MasterSet DELVO - Retarding Admixture	26	fl oz/cy	-	-
	MasterGlenium 7920 - High-range WRDA	13	fl oz/cy	-	-

Mix info	27.0 ft^3
Total volume	4016.00 lb/cy
Total mass	148.85 lb/ft^3
Unit weight	520.00 lb/cy
Total cm/cy	0.666
w/c	0.533
% fly ash	20.00%
sand/agg	0.410

Adjustments for moisture	Units
Aggregate weight adjustments for natural moisture	
#67 stone - Coarse aggregate	1922.8 lb/cy
Sand - Fine aggregate	1358.6 lb/cy
Water weight adjustment based on absorption and natural moisture	
Water from #67 stone - Coarse aggregate	12.6 lb/cy
Water from Sand - Fine aggregate	34.3 lb/cy
Water adjustment	-46.9 lb/cy
	-5.6 gallons/cy
Water (adjusted mix quantity)	230.1 lb/cy
	27.6 gallons/cy

Total content added to the truck (from delivery ticket)	Units	Design quantities (with moisture adjustments)	Difference	% diff
Cement - Type II	1280.0 lb	1248.0 lb	32.0 lb	2.564102564
Fly ash - Class F	340.0 lb	312.0 lb	28.0 lb	8.974358974
#67 stone - Coarse aggregate	5880.0 lb	5768.4 lb	111.6 lb	1.934678594
Sand - Fine aggregate	4080.0 lb	4075.7 lb	4.3 lb	0.105257734
Water	541.7 lb	690.2 lb	-148.5 lb	-21.5205142
	65.0 gallons	82.8 gallons	-17.8 gallons	
WR Grace Darex AEA - Air entraining Admixture	5.0 fl oz	1.5 fl oz	3.5 fl oz	233.3333333
MasterSet DELVO - Retarding Admixture	81.0 fl oz	78.0 fl oz	3.0 fl oz	3.846153846
MasterGlenium 7920 - High-range WRDA	42.0 fl oz	39 fl oz	3 fl oz	7.692307692

Initial slump	5.0 in
Water added	5.0 gallons
Final slump	7.8 in

<--- Total number of gallons that may be added to the truck (if negative)
 233.3333333
 3.846153846
 7.692307692

Mix Design based on truck delivery quantities	Product	Quantity	Units	Volume/cy (ft^3/cy)	SG	% Difference from design
	Cement - Type 1L	426.7	lb/cy	2.17	3.15	2.6%
	Fly ash - Class F	113.3	lb/cy	0.77	2.37	9.0%
	#67 stone - Coarse aggregate	1936.5	lb/cy	11.08	2.80	1.9%
	Sand - Fine aggregate	1319.2	lb/cy	8.04	2.63	0.0%
	Water	259.0	lb/cy	4.15	1.00	-6.5%
		31.1	gallons/cy			-6.5%
	Air	3.5%	-	0.95	7.85	16.7%
	Fiber - Sika hooked-end (1% volume)	132.3	lb/cy	0.27		#DIV/0!
	WR Grace Darex AEA - Air entraining Admixture	1.7	fl oz/cy			233.3%
	MasterSet DELVO - Retarding Admixture	27.0	fl oz/cy			3.8%
	MasterGlenium 7920 - High-range WRDA	14.0	fl oz/cy			7.7%

Mix info based on truck delivery	27.42 ft^3
Total mass	4186.94 lb/cy
Unit weight	152.67 lb/ft^3
Total cm/cy	540.00 lb/cy
w/c	0.61
% fly ash	20.99%
sand/agg	0.41

GFRP RC EOR-2 railing concrete
 2021-10-11: SRM Class II railing truck delivery mixture

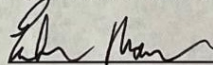
Financial Project No.: _____
 Plant No.: 55-503
 Concrete Supplier: Smyrna Ready Mix
 Phone Number: 850-575-3888
 Address: 5379 Capitol Circle
Tallahassee, FL 32305

Serial No.: 4043266
 Date: 10/11/2021
 Deliver To: FDOT
 Phone No.: 352-888-1099
 Address: 2007 East Paul Dirac

Truck No.	DOT Class	DOT Mix No.	03-2272-01				Cubic Yards This Load
4227	CLASS II 3400						3
Allowable Jobsite water	Time Loaded	Mixing Revolutions					Cubic Yards Total Today
12	12:49						3
Cement	ASH GROVE	I/II	1300	Fly Ash or Slag	Boral	Class F	260
	Source	Type	Amount		Source	Type	Amount
Coarse Agg.	GA553	1.2	5920	Air Entraining	BASF	AE 90	5
	Pit No.	% Moisture	Amount		Source	Brand	Type
							Amount
Fine Agg.	50-471	3	4000	Admixture	BASF	Retarder	D
	Pit No.	% Moisture	Amount		Source	Brand	Type
							Amount
Batch Water (gals or lbs)			61	Admixture	BASF	7920	G
			Amount		Source	Brand	Type
							Amount
				Admixture	BASF	SRA 020	S
					Source	Brand	Type
							Amount

Issuance of this ticket constitutes certification that the concrete batched was produced and information recorded in compliance with Department specification requirements for Structural Concrete.

B65055259
 CTQP Technician Identification Number


 Signature of Batcher Plant Operator

Arrival Time At Jobsite:		Number of Revolutions Upon Arrival At Job Site	
Water Added At Job Site (gals or lbs)		Additional Mixing Revolutions With Added Water	
Time Concrete Completely Discharged		Total Number of Revolutions	
Initial Slump	Initial Air	Initial Concrete Temperature	Initial W/C Ratio
Acceptance Slump	Acceptance Air	Acceptance Concrete Temperature	Acceptance W/C Ratio

Issuance of this ticket constitutes certification that the maximum specified water cementitious ratio was not exceeded and the batch was delivered and placed in compliance with Department specification requirements.

**GFRP RC EOR-2 railing concrete
2021-10-11: SRM Class II railing truck delivery mixture**

Batch size (cy)	3
Batch size (ft^3)	81

	Natural moisture (%)	Absorption (%)	Difference (%)
#67 stone - Coarse aggregate	1.20%	0.53%	0.67%
Sand - Fine aggregate	3.00%	0.40%	2.60%

Mix Design	Product	Quantity	Units	SG	Volume/cy (ft^3/cy)
	Cement - Type II		lb/cy	3.15	2.12
	Fly ash - Class F		lb/cy	2.37	0.70
	#67 stone - Coarse aggregate		lb/cy	2.80	10.87
	Sand - Fine aggregate		lb/cy	2.63	8.04
	Water		lb/cy	1.00	4.44
			33.2 gallons/cy		
	Air		3.0% -		0.81
	Fiber - Sika hooked-end (1% volume)		0 lb/cy	7.85	0.00
	AE 90 - Air entraining Admixture		0.5 fl oz/cy		
	MasterSet DELVO - Retarding Admixture		26 fl oz/cy		
	MasterGlenium 7920 - High-range WRDA		13 fl oz/cy		

Mix info	27.0 ft^3
Total volume	4016.00 lb/cy
Total mass	148.85 lb/ft^3
Unit weight	520.00 lb/cy
Total cm/cy	0.666
w/c	0.533
% fly ash	20.00%
sand/agg	0.410

Adjustments for moisture	Aggregate weight adjustments for natural moisture
#67 stone - Coarse aggregate	lb/cy
Sand - Fine aggregate	lb/cy
Water weight adjustment based on absorption and natural moisture	
Water from #67 stone - Coarse aggregate	12.6 lb/cy
Water from Sand - Fine aggregate	34.3 lb/cy
Water adjustment	-46.9 lb/cy
	-5.6 gallons/cy
Water (adjusted mix quantity)	lb/cy
	gallons/cy

Total content added to the truck (from delivery ticket)	Units	Design quantities (with moisture adjustments)	Difference	% diff
Cement - Type II	1300.0 lb	1248.0 lb	52.0 lb	4.16666667
Fly ash - Class F	260.0 lb	312.0 lb	-52.0 lb	-16.6666667
#67 stone - Coarse aggregate	5920.0 lb	5768.4 lb	151.6 lb	2.62811781
Sand - Fine aggregate	4000.0 lb	4075.7 lb	-75.7 lb	-1.85759046
Water	508.3 lb	690.2 lb	-181.9 lb	-26.350021
	61.0 gallons	82.8 gallons	-21.8 gallons	<--- Total number of gallons that may be added to the truck (if negative)
WR Grace Darex AEA - Air entraining Admixture	5.0 fl oz	1.5 fl oz	3.5 fl oz	233.3333333
MasterSet DELVO - Retarding Admixture	15.0 fl oz	78.0 fl oz	-63.0 fl oz	-80.7692308
MasterGlenium 7920 - High-range WRDA	39.0 fl oz	39 fl oz	0 fl oz	0

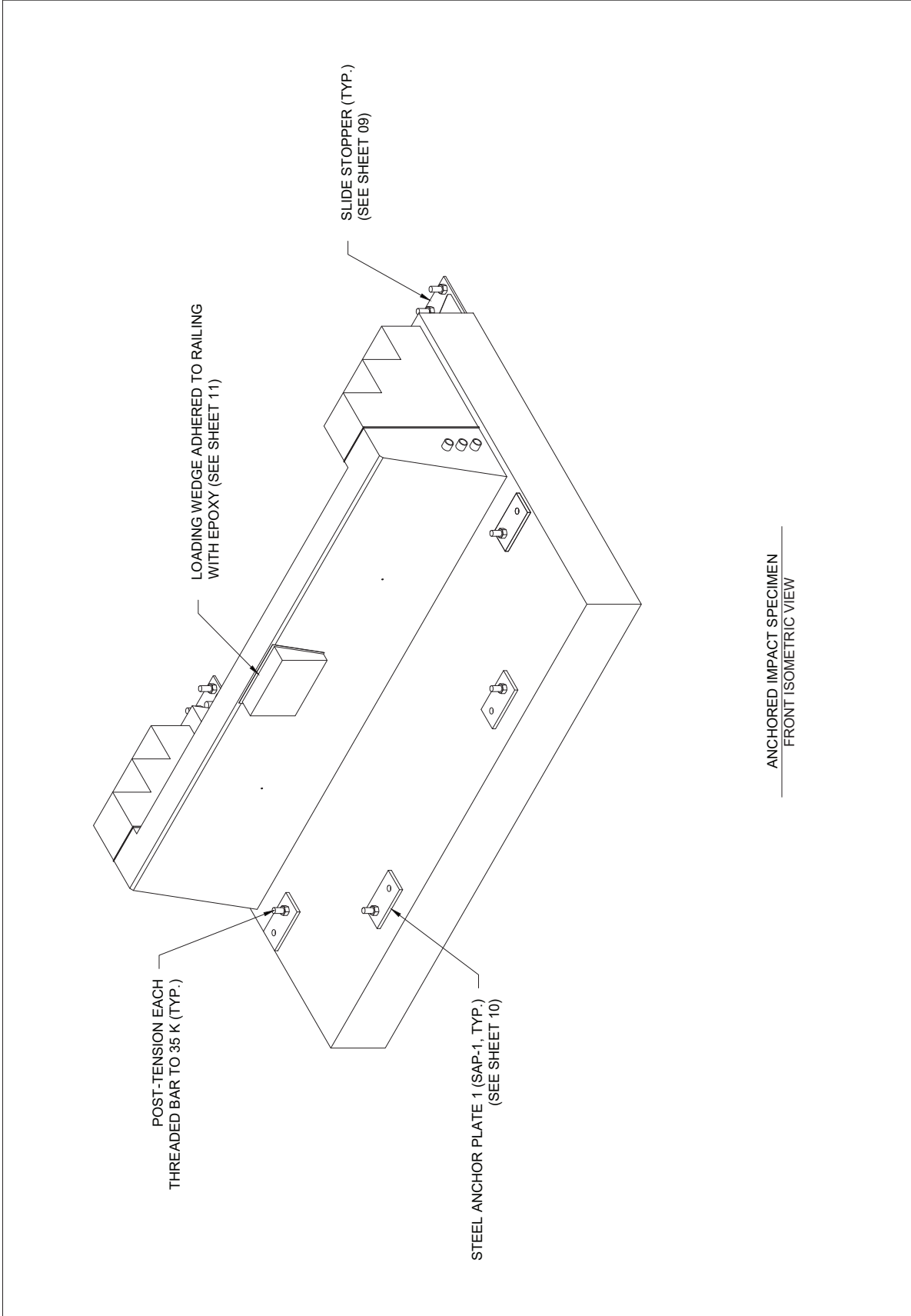
Initial slump	5.0 in
Water added	0.0 gallons
Final slump	5.0 in

Mix Design based on truck delivery quantities	Product	Quantity	Units	SG	Volume/cy (ft^3/cy)	% Difference from design
	Cement - Type 1L		433.3 lb/cy	3.15	2.20	4.2%
	Fly ash - Class F		86.7 lb/cy	2.37	0.59	-16.7%
	#67 stone - Coarse aggregate		1949.7 lb/cy	2.80	11.16	2.6%
	Sand - Fine aggregate		1293.3 lb/cy	2.63	7.88	-1.9%
	Water		259.0 lb/cy	1.00	4.15	-6.5%
			31.1 gallons/cy			-6.5%
	Air		3.5% -		0.95	16.7%
	Fiber - Sika hooked-end (1% volume)		132.3 lb/cy	7.85	0.27	#DIV/0!
	WR Grace Darex AEA - Air entraining Admixture		1.7 fl oz/cy			233.3%
	MasterSet DELVO - Retarding Admixture		5.0 fl oz/cy			-80.8%
	MasterGlenium 7920 - High-range WRDA		13.0 fl oz/cy			0.0%

Mix info based on truck delivery	27.20 ft^3
Total mass	4154.25 lb/cy
Unit weight	152.75 lb/ft^3
Total cm/cy	520.00 lb/cy
w/c	0.60
% fly ash	0.50
sand/agg	16.67%
	0.40

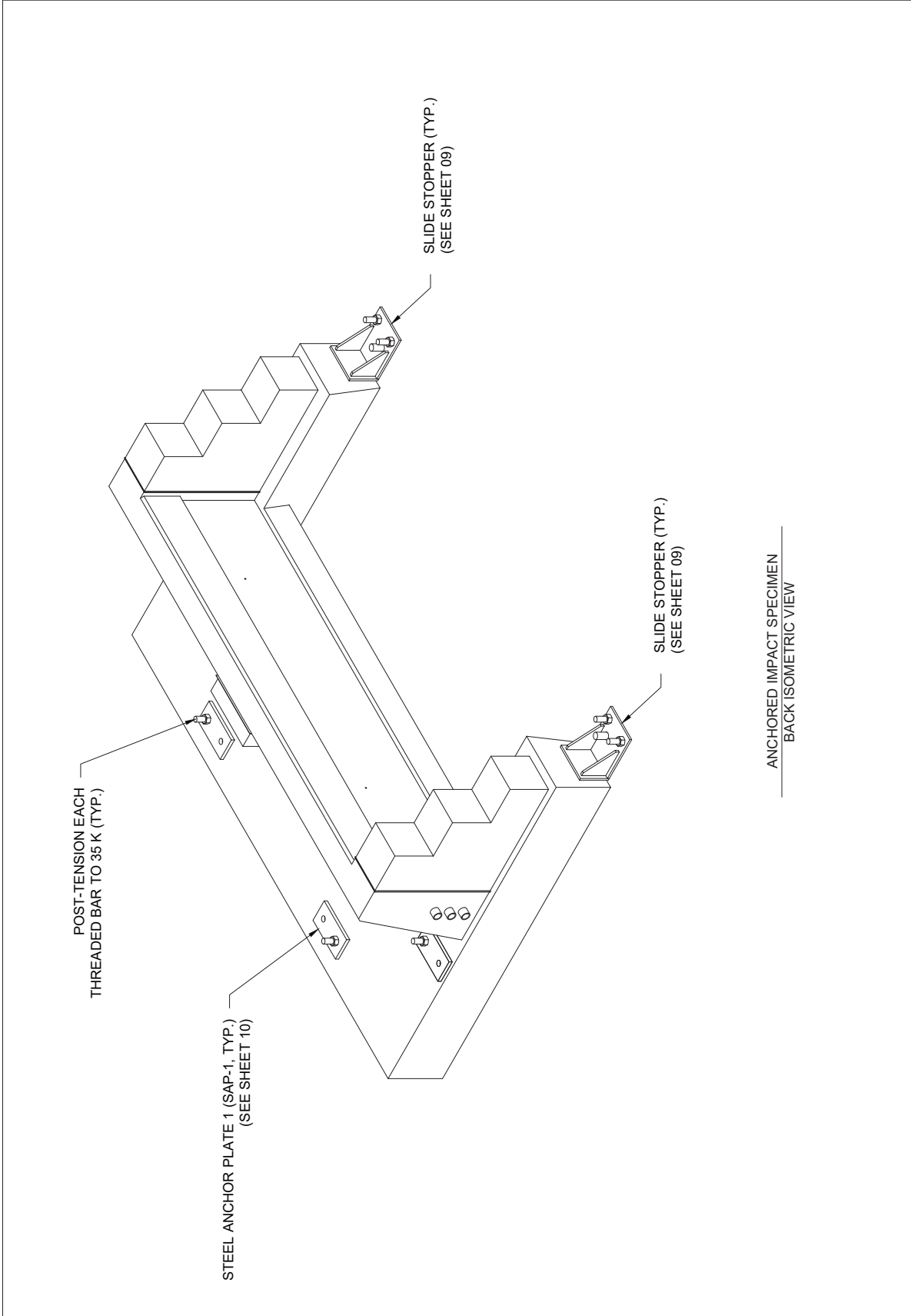
APPENDIX G: ANCHORAGE SEQUENCE

Presented in this appendix are the anchoring sequence plan for test specimens developed in BDV31-977-72. The center-of-rail plan is shown, and the end-of-rail plan is similar.

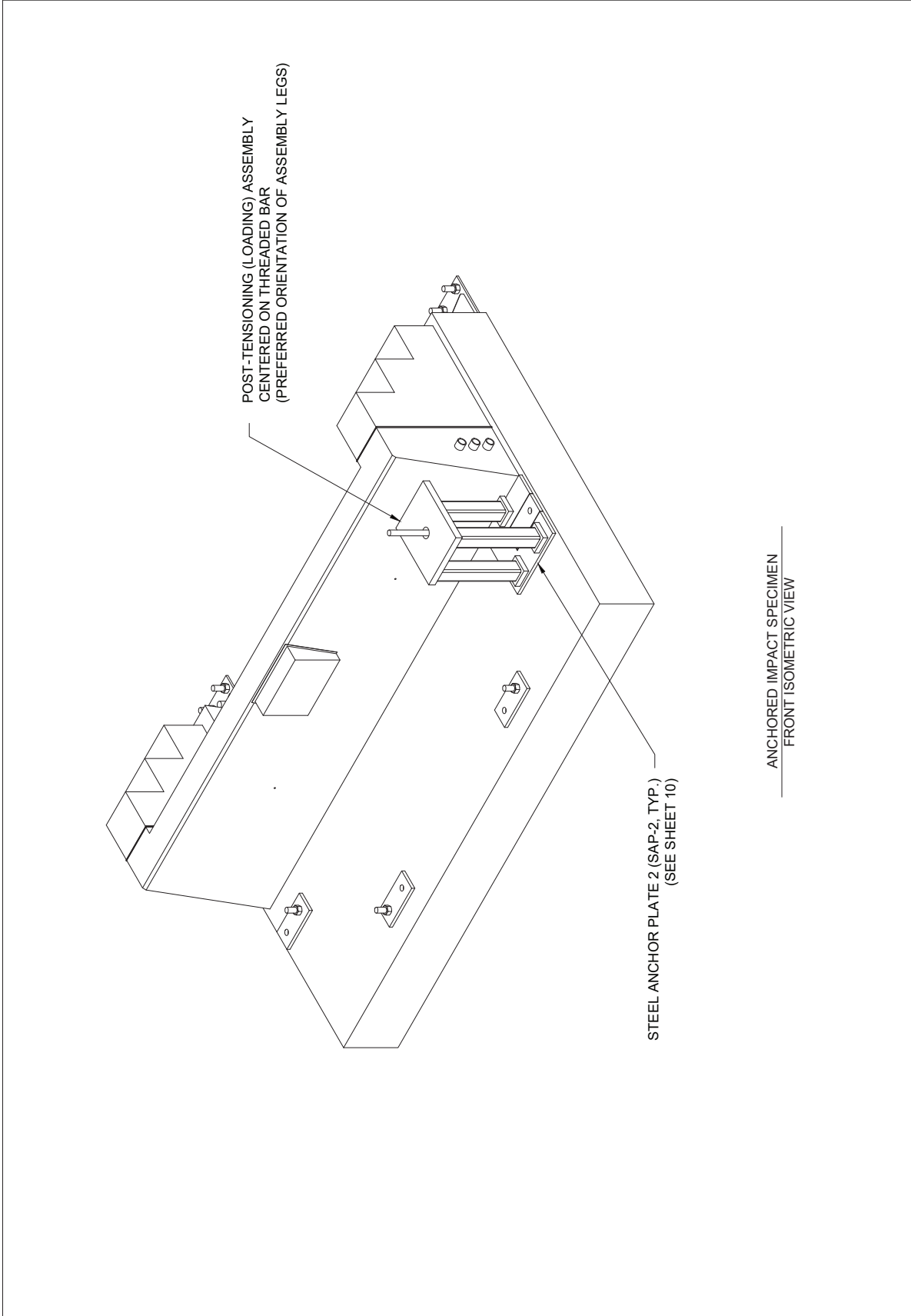


ANCHORED IMPACT SPECIMEN
FRONT ISOMETRIC VIEW

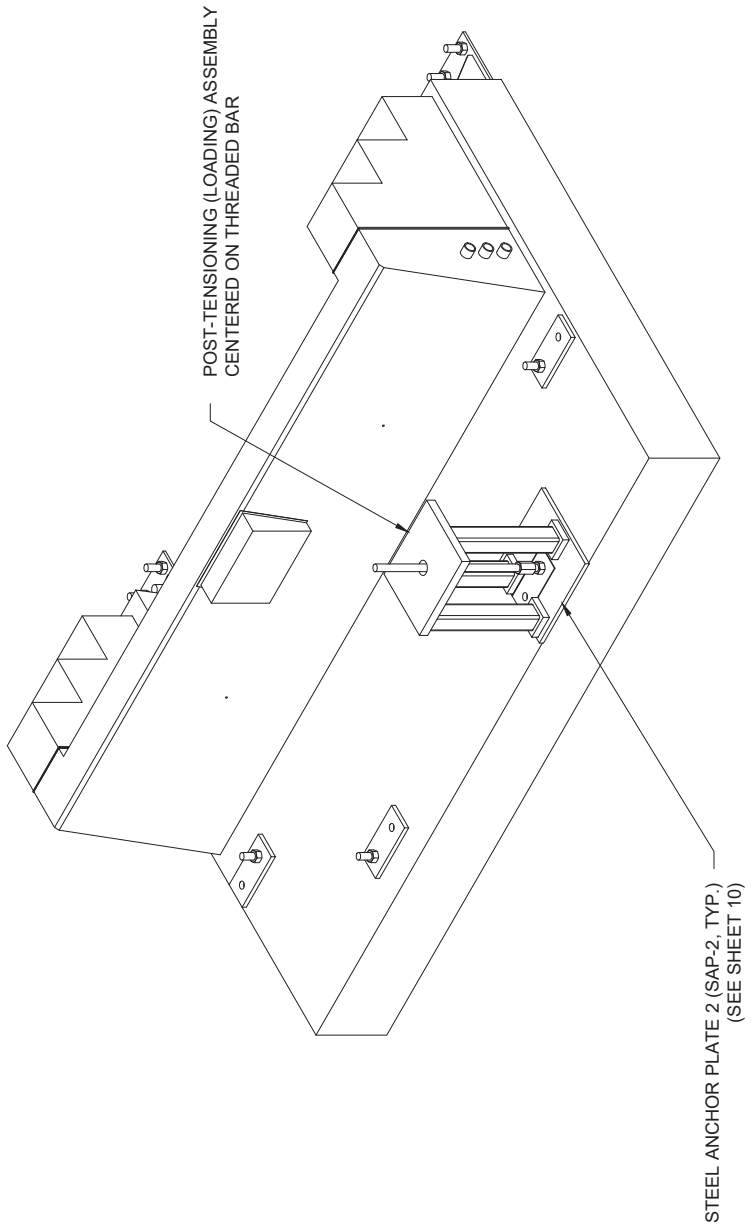
<i>Reinforced Concrete Traffic Railings for Impact Loading</i>		Revisions:
<i>Specimen Anchoring Plan</i>	2020-04-20	<i>University of Florida</i>



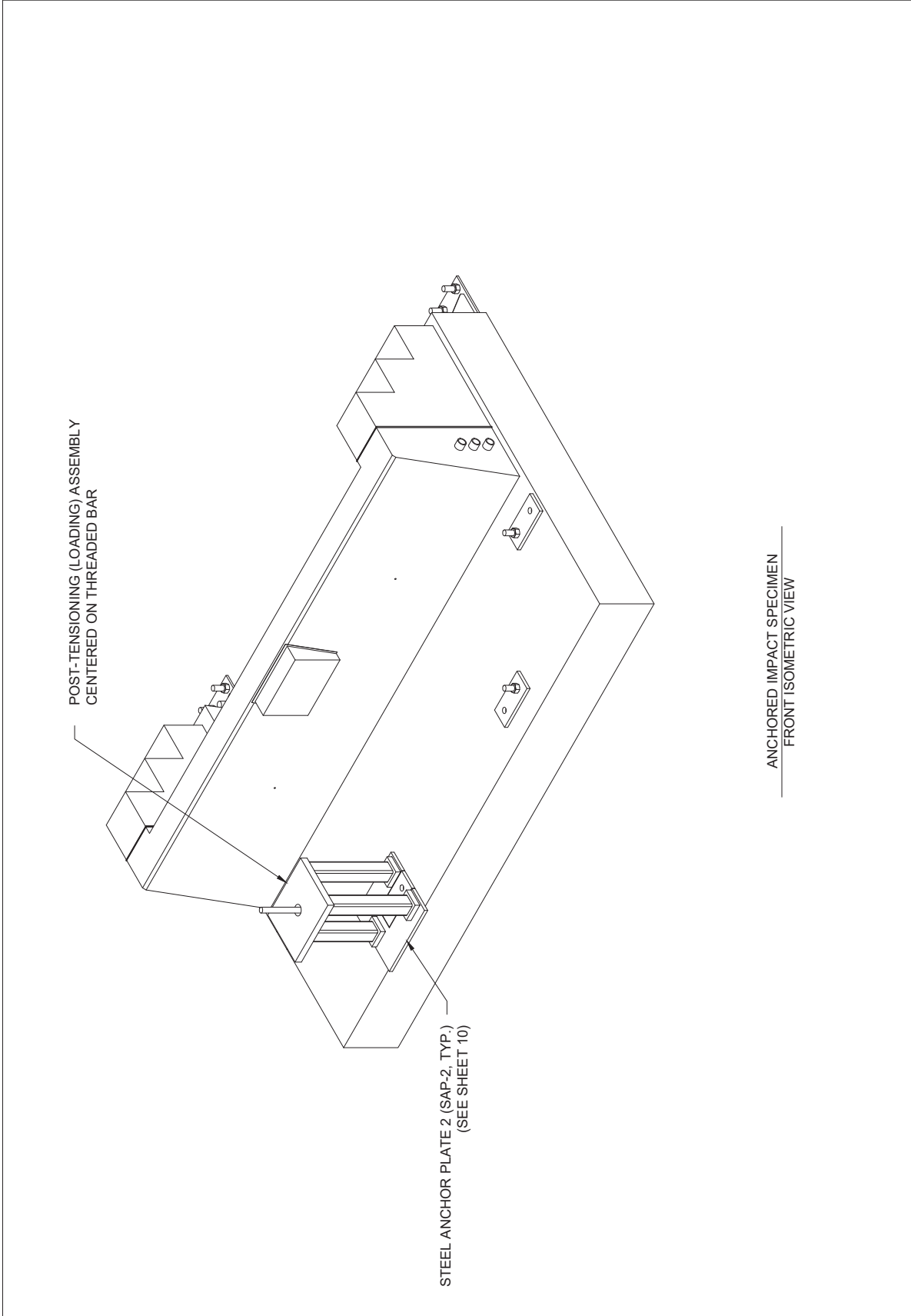
<i>Reinforced Concrete Traffic Railings for Impact Loading</i>		Revisions:	
<i>Specimen Anchoring Plan</i>	2020-04-20	<i>University of Florida</i>	



<i>Reinforced Concrete Traffic Railings for Impact Loading</i>		Revisions:	
<i>Specimen Anchoring Plan</i>	2020-04-20	<i>University of Florida</i>	

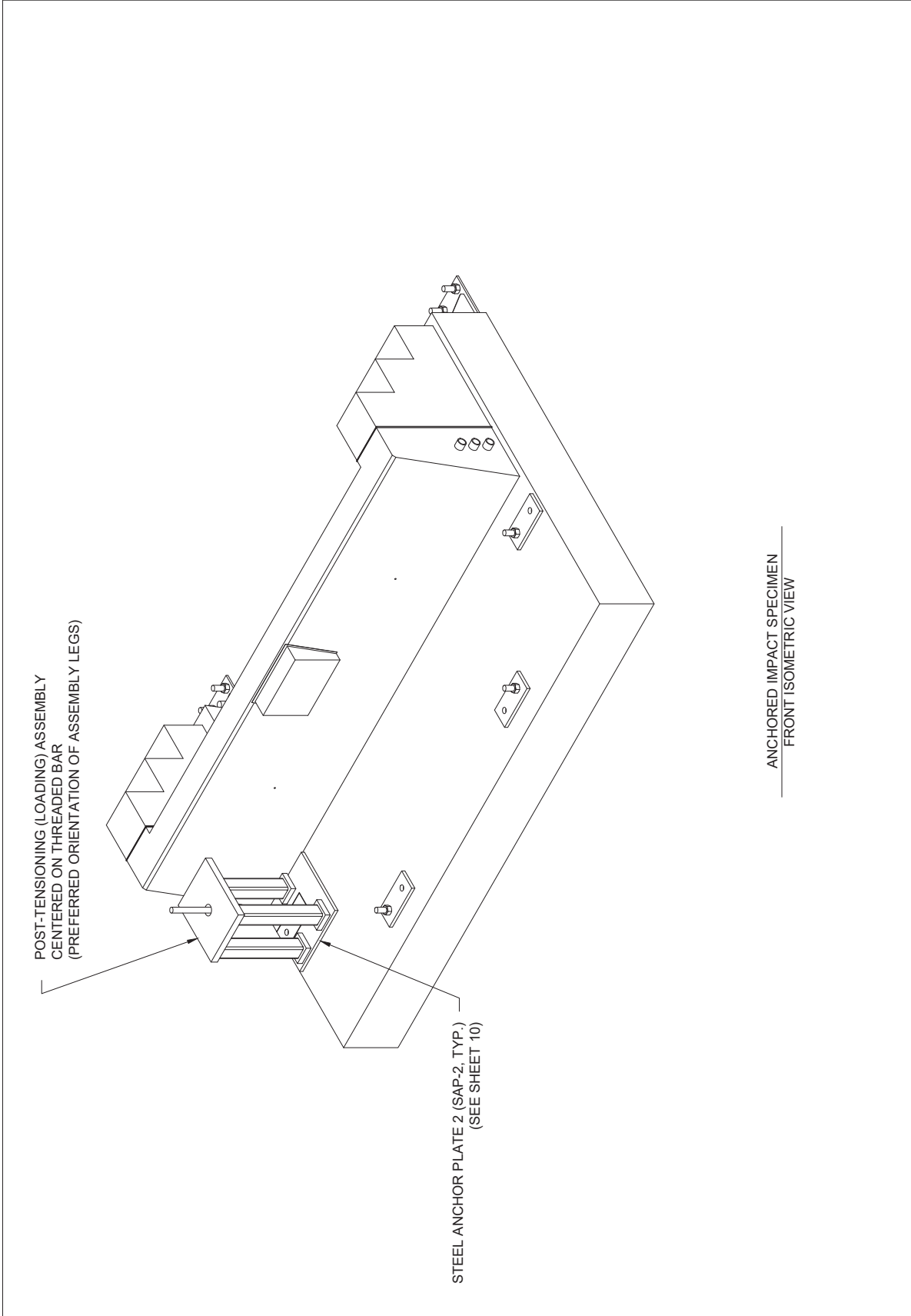


<i>Reinforced Concrete Traffic Railings for Impact Loading</i>		Revisions:	
<i>Specimen Anchoring Plan</i>	2020-04-20	<i>University of Florida</i>	

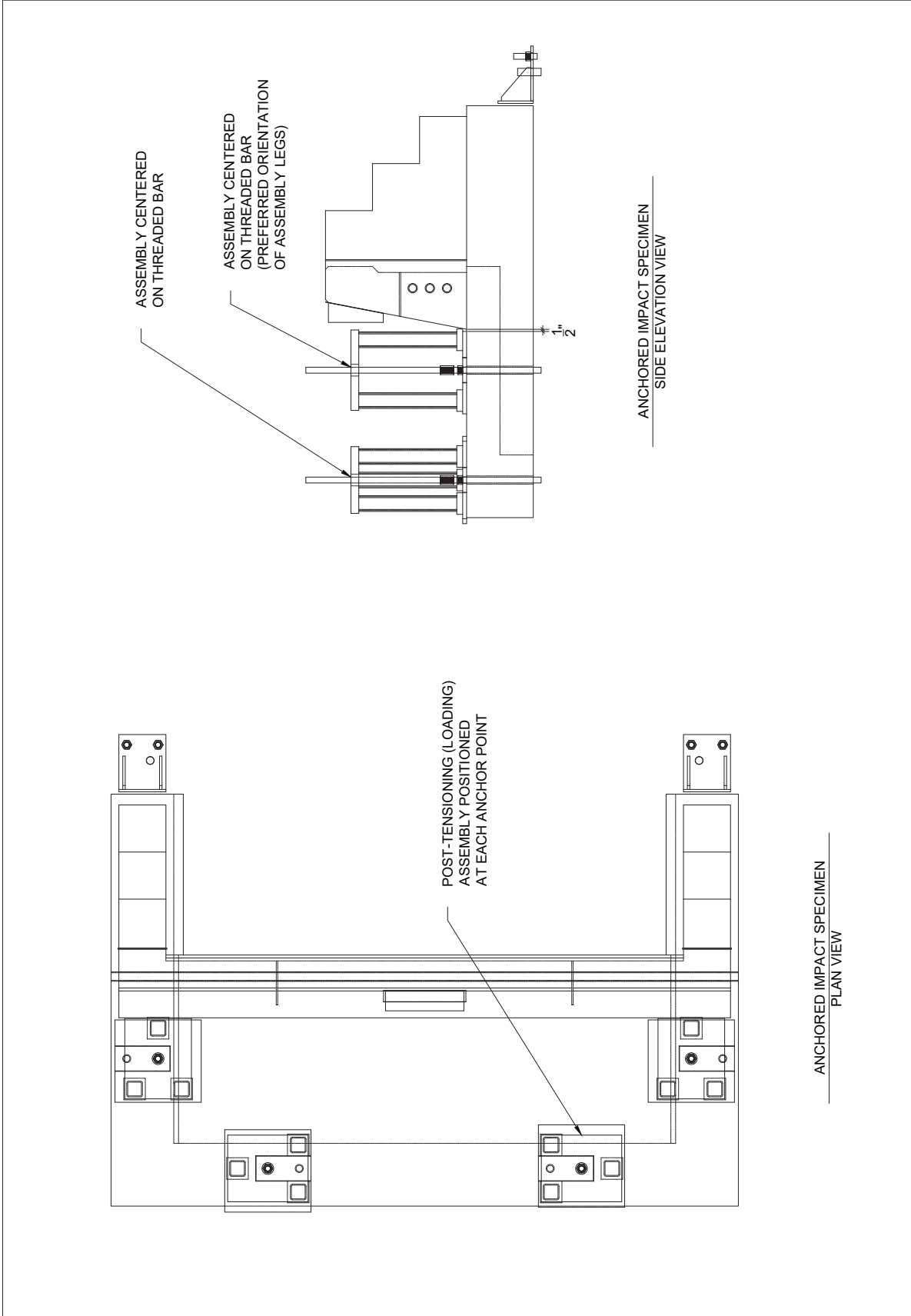


ANCHORED IMPACT SPECIMEN
FRONT ISOMETRIC VIEW

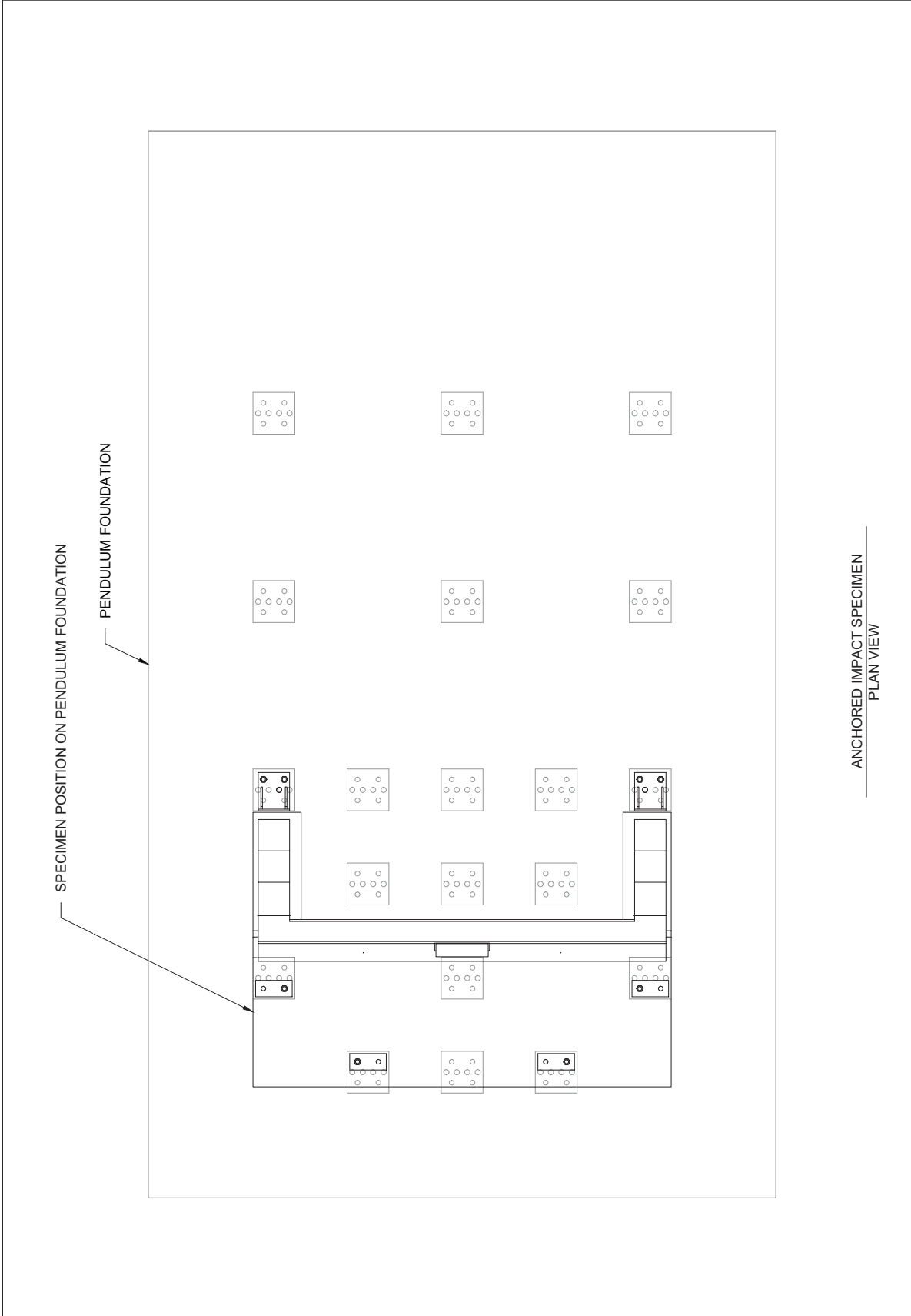
<i>Reinforced Concrete Traffic Railings for Impact Loading</i>		Revisions:
<i>Specimen Anchoring Plan</i>	2020-04-20	<i>University of Florida</i>



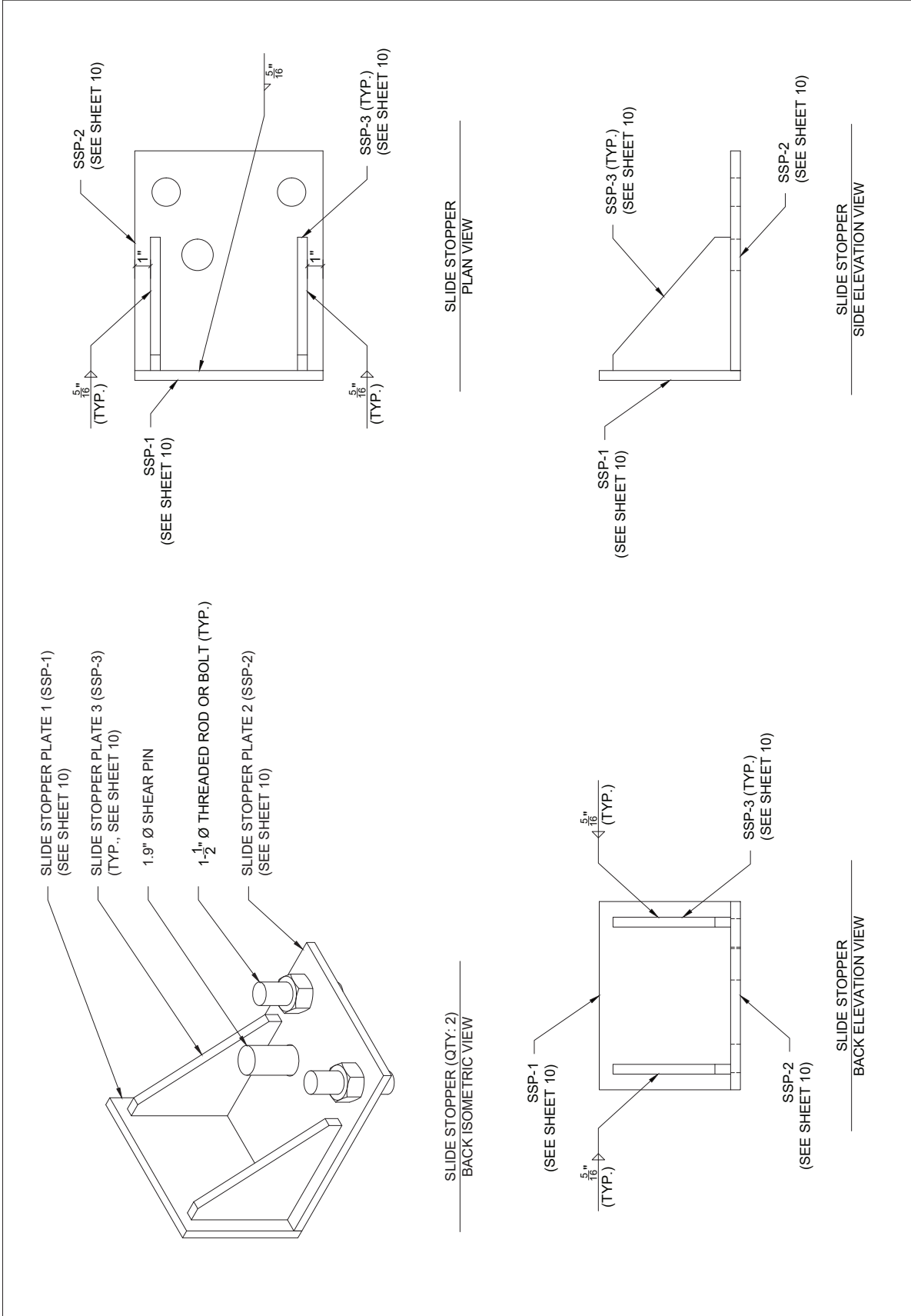
<i>Reinforced Concrete Traffic Railings for Impact Loading</i>		<i>Revisions:</i>
<i>Specimen Anchoring Plan</i>	<i>2020-04-20</i>	<i>University of Florida</i>



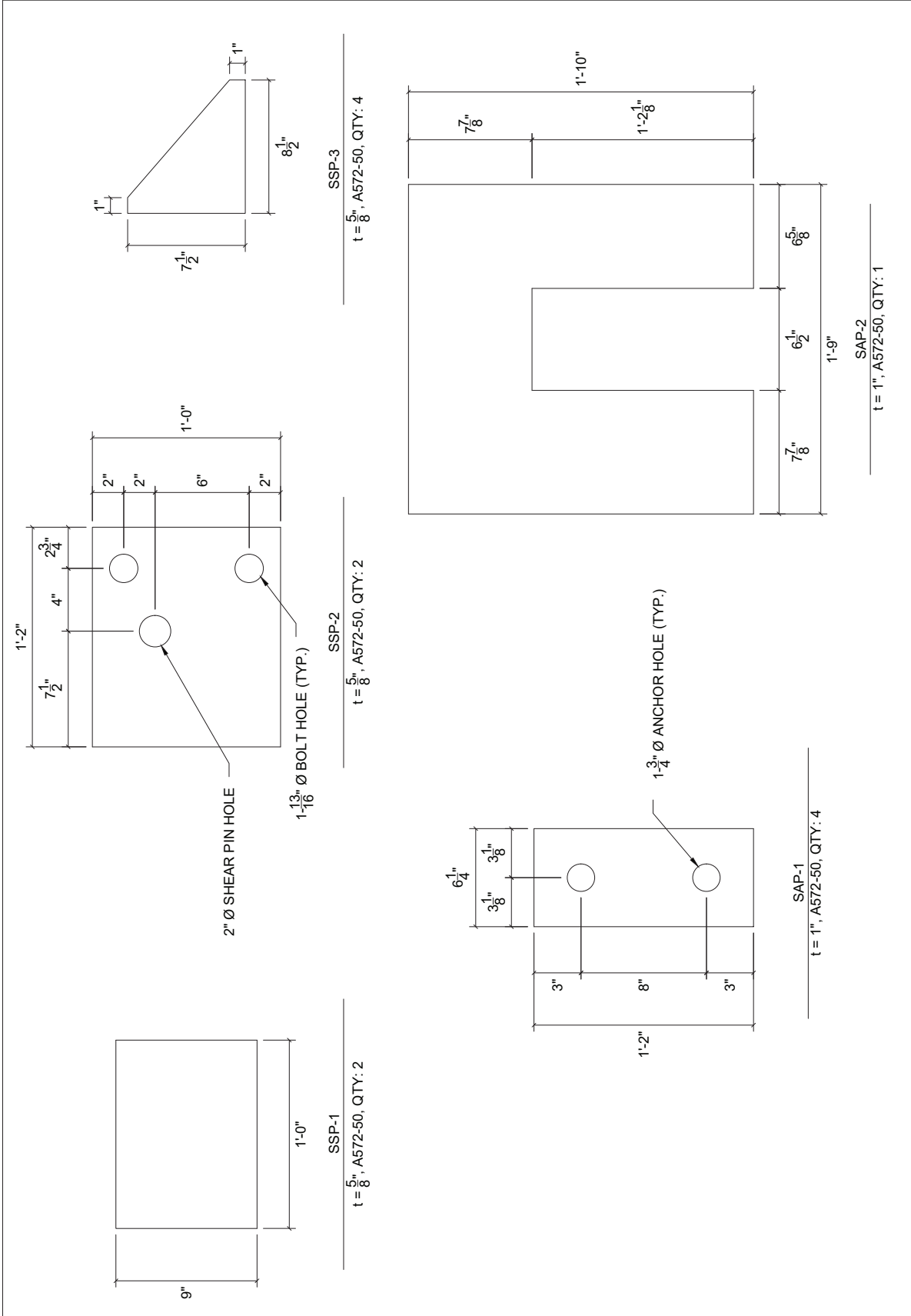
<i>Reinforced Concrete Traffic Railings for Impact Loading</i>		<i>Revisions:</i>
<i>Specimen Anchoring Plan</i>	<i>2020-04-20</i>	<i>University of Florida</i>



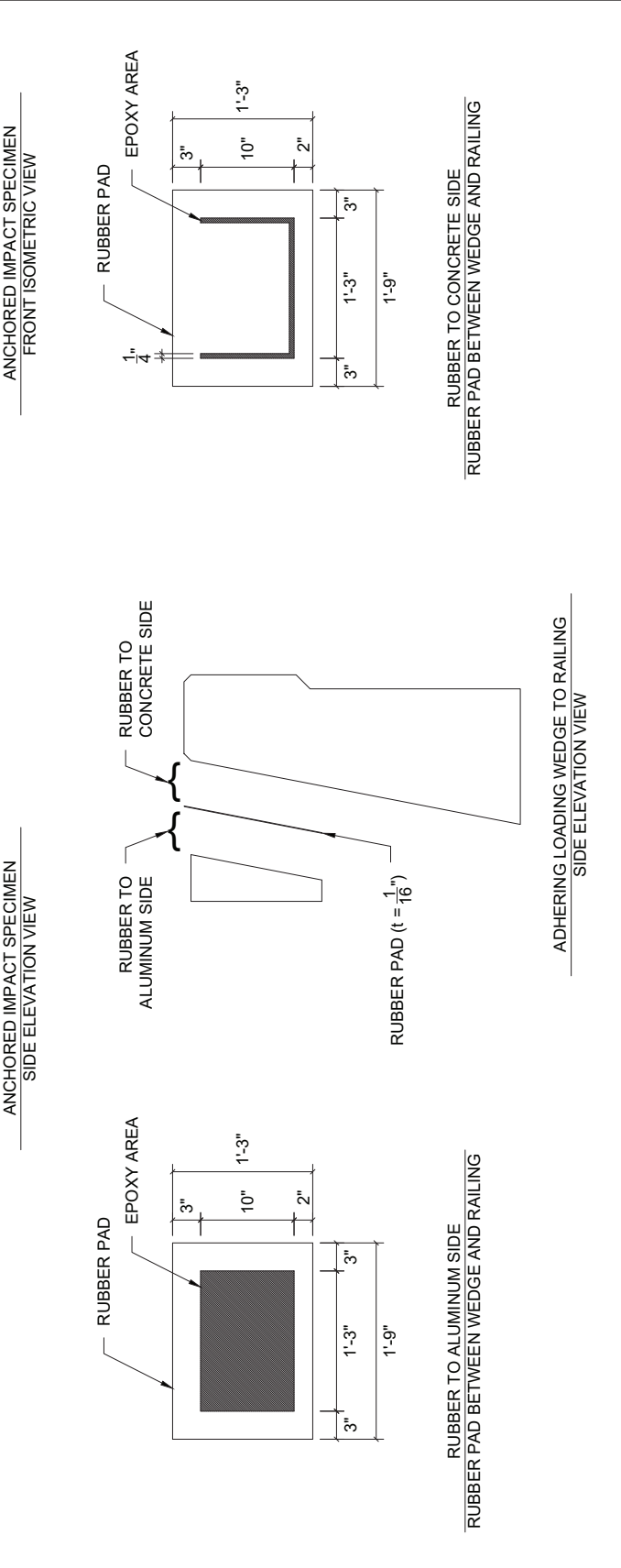
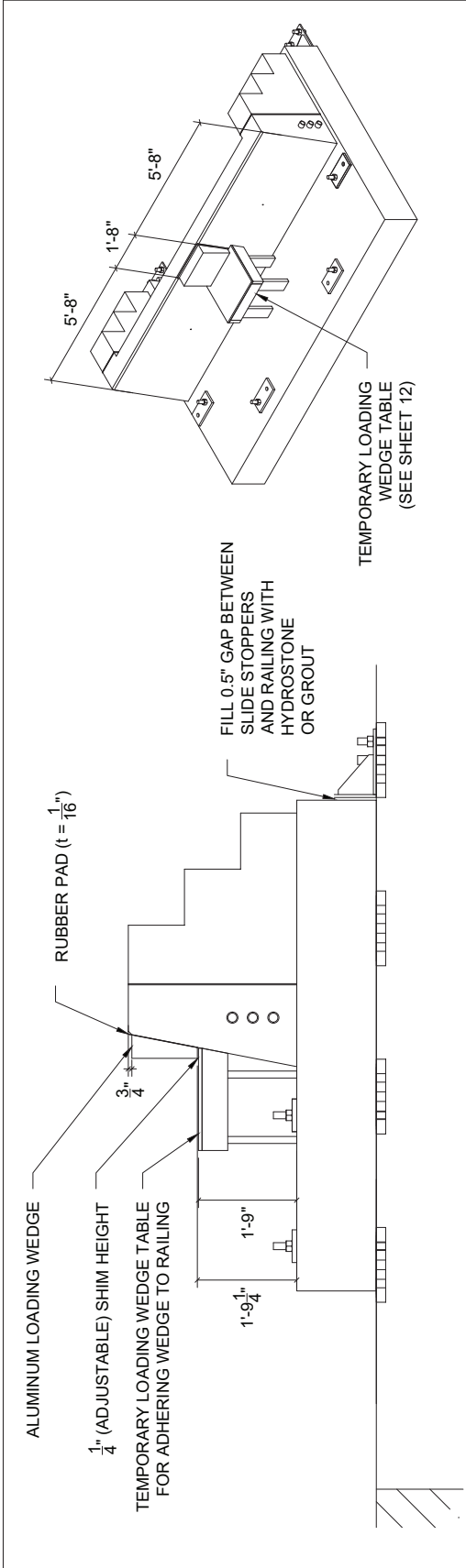
<i>Reinforced Concrete Traffic Railings for Impact Loading</i>		<i>Revisions:</i>	
<i>Specimen Anchoring Plan</i>	<i>2020-04-20</i>	<i>University of Florida</i>	



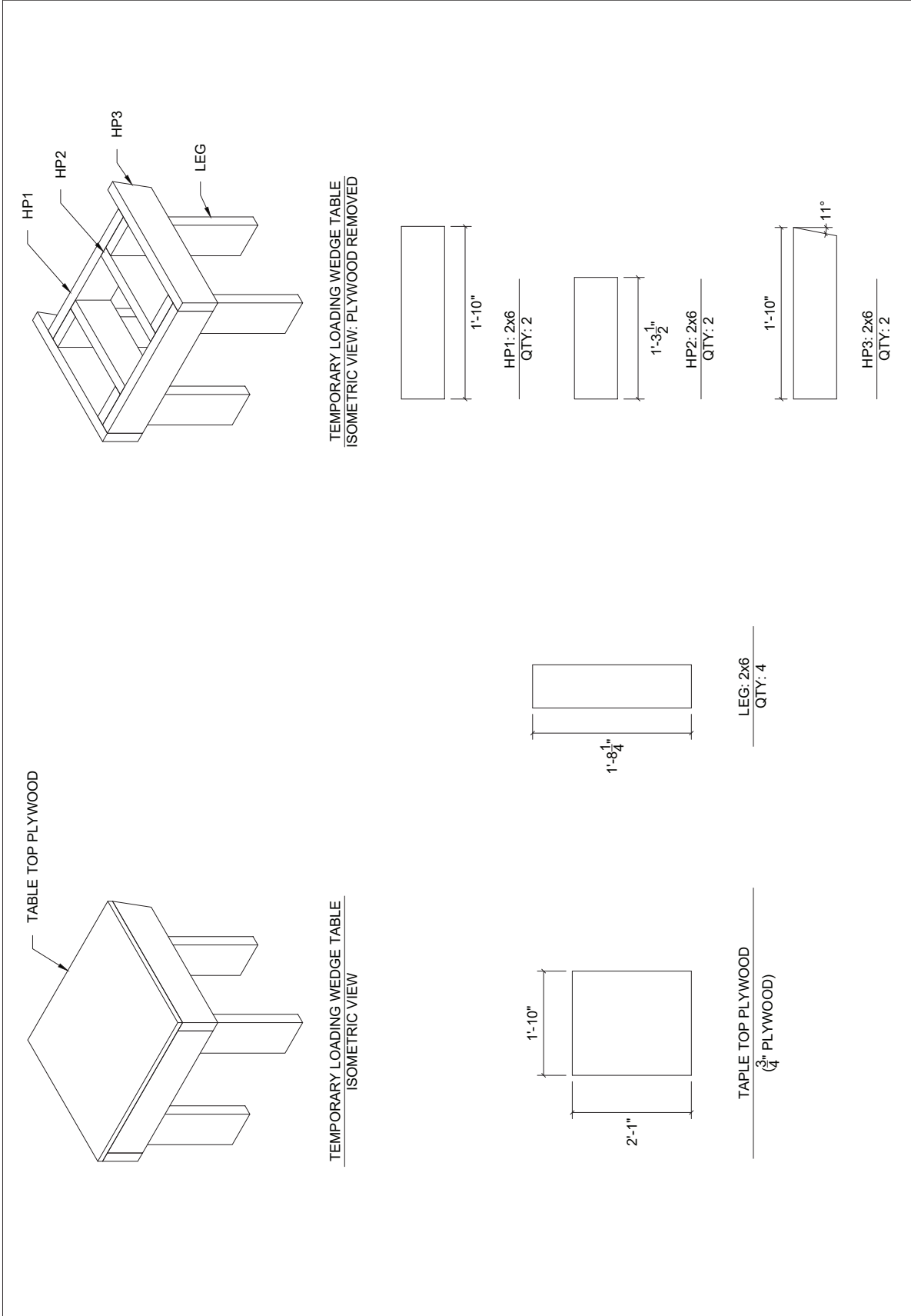
Reinforced Concrete Traffic Railings for Impact Loading		Revisions:
Specimen Anchoring Plan	2020-04-20	University of Florida



<i>Reinforced Concrete Traffic Railings for Impact Loading</i>		
<i>Specimen Anchoring Plan</i>	2020-04-20	<i>University of Florida</i>
Revisions:		



Reinforced Concrete Traffic Railings for Impact Loading		Revisions:
Specimen Anchoring Plan	2020-04-20	University of Florida



TEMPORARY LOADING WEDGE TABLE
ISOMETRIC VIEW: PLYWOOD REMOVED

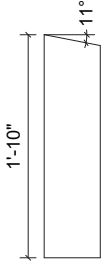
TEMPORARY LOADING WEDGE TABLE
ISOMETRIC VIEW



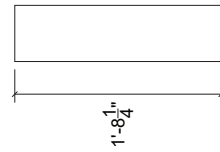
HP1: 2x6
QTY: 2



HP2: 2x6
QTY: 2



HP3: 2x6
QTY: 2



LEG: 2x6
QTY: 4

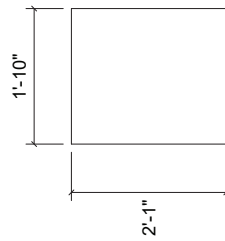
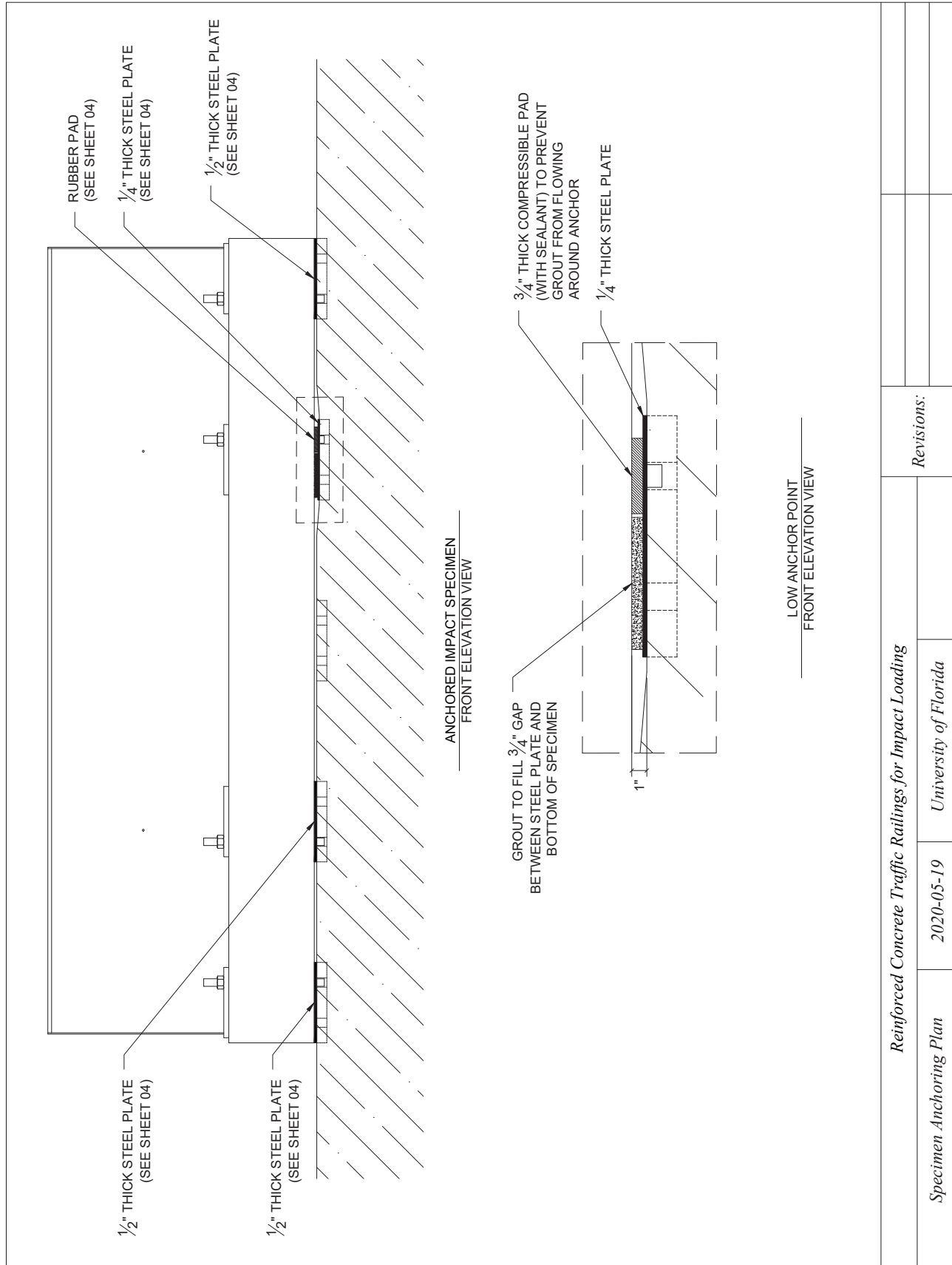


TABLE TOP PLYWOOD
(3/4" PLYWOOD)

Reinforced Concrete Traffic Railings for Impact Loading		Revisions:
Specimen Anchoring Plan	2020-04-20	
University of Florida		



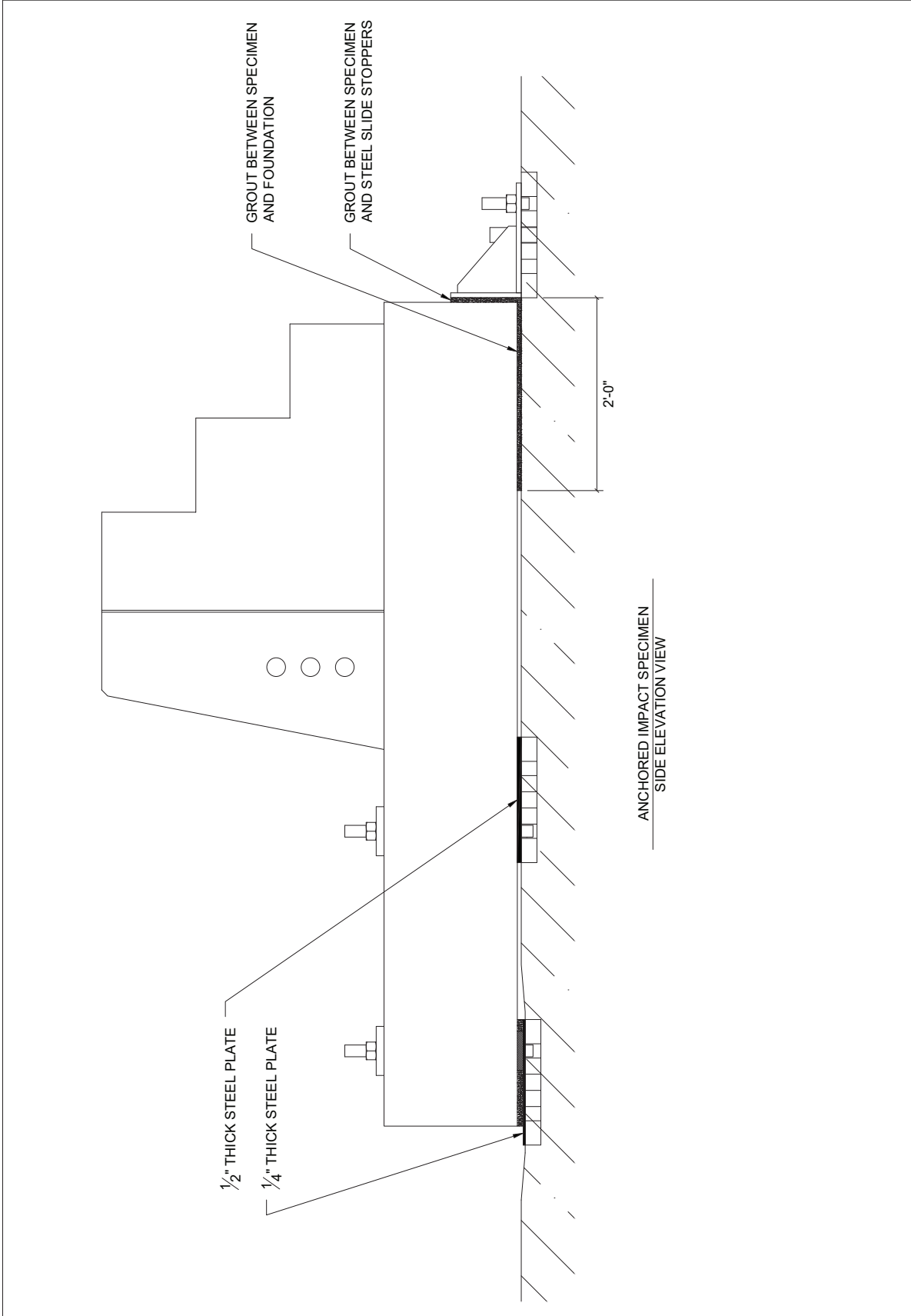
Reinforced Concrete Traffic Railings for Impact Loading

Specimen Anchoring Plan

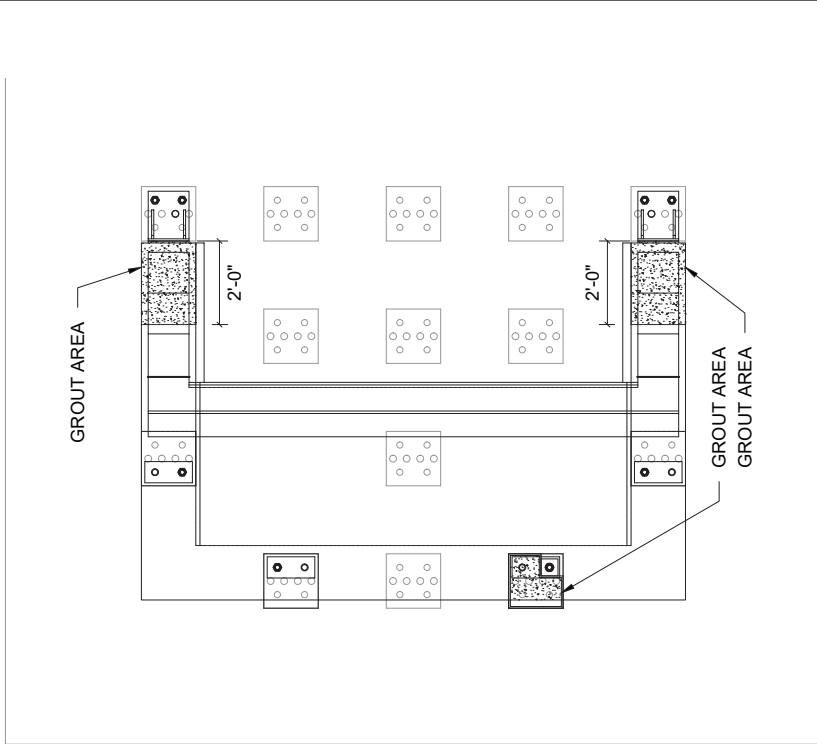
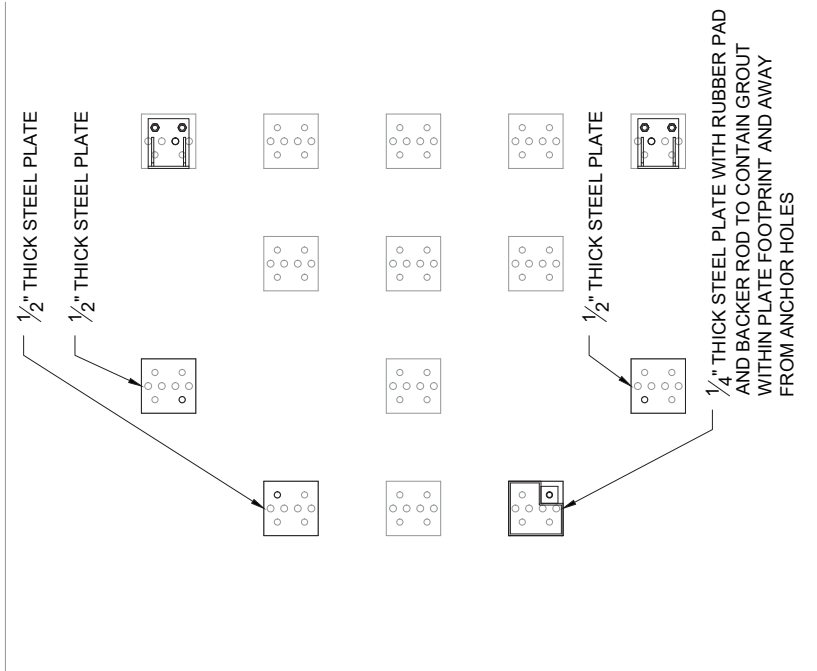
2020-05-19

University of Florida

Revisions:



<i>Reinforced Concrete Traffic Railings for Impact Loading</i>		<i>Revisions:</i>
<i>Specimen Anchoring Plan</i>	<i>2020-05-19</i>	<i>University of Florida</i>



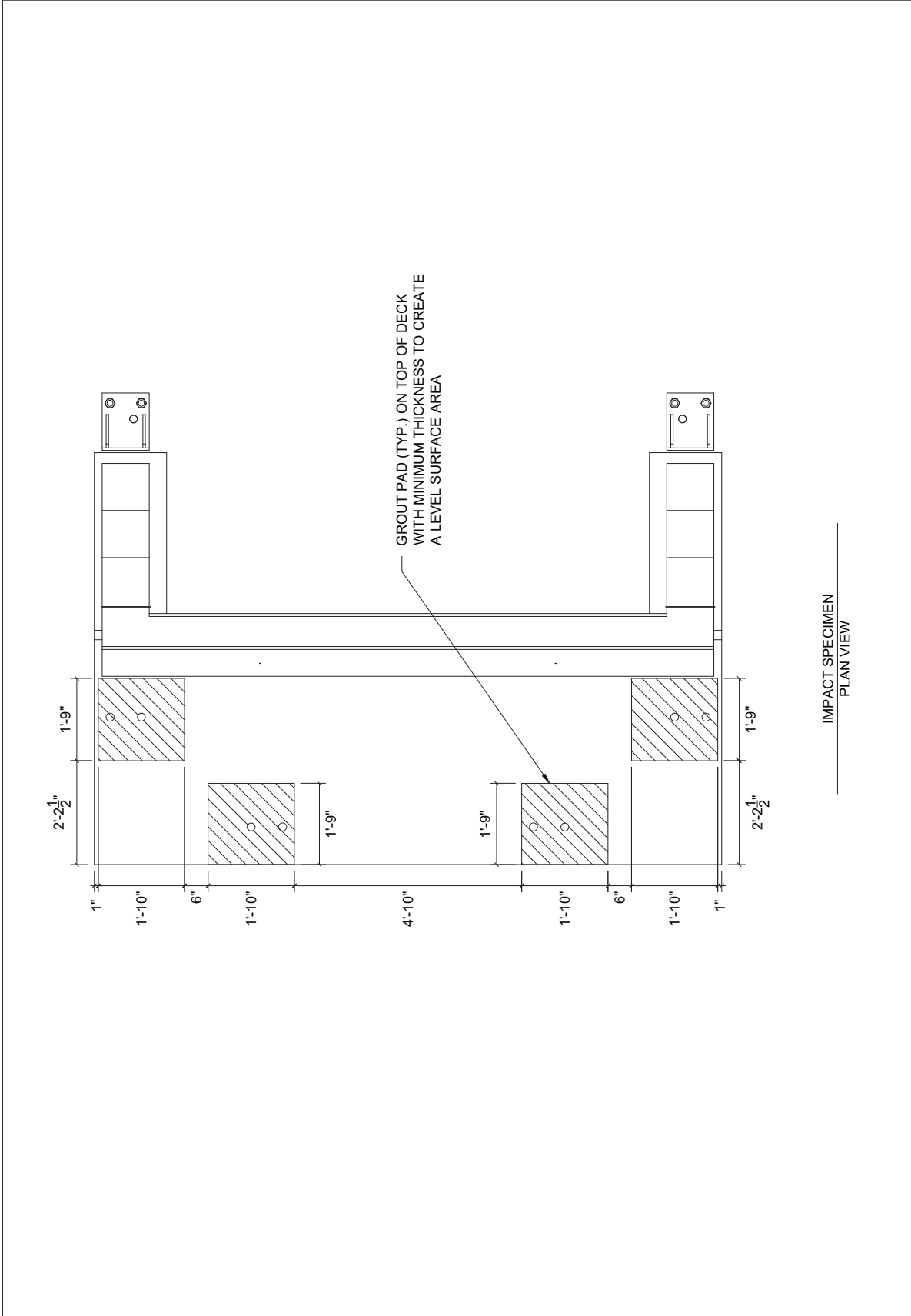
PLATES INSTALLED ONTO FOUNDATION
PLAN VIEW

SPECIMEN INSTALLED ONTO FOUNDATION
PLAN VIEW

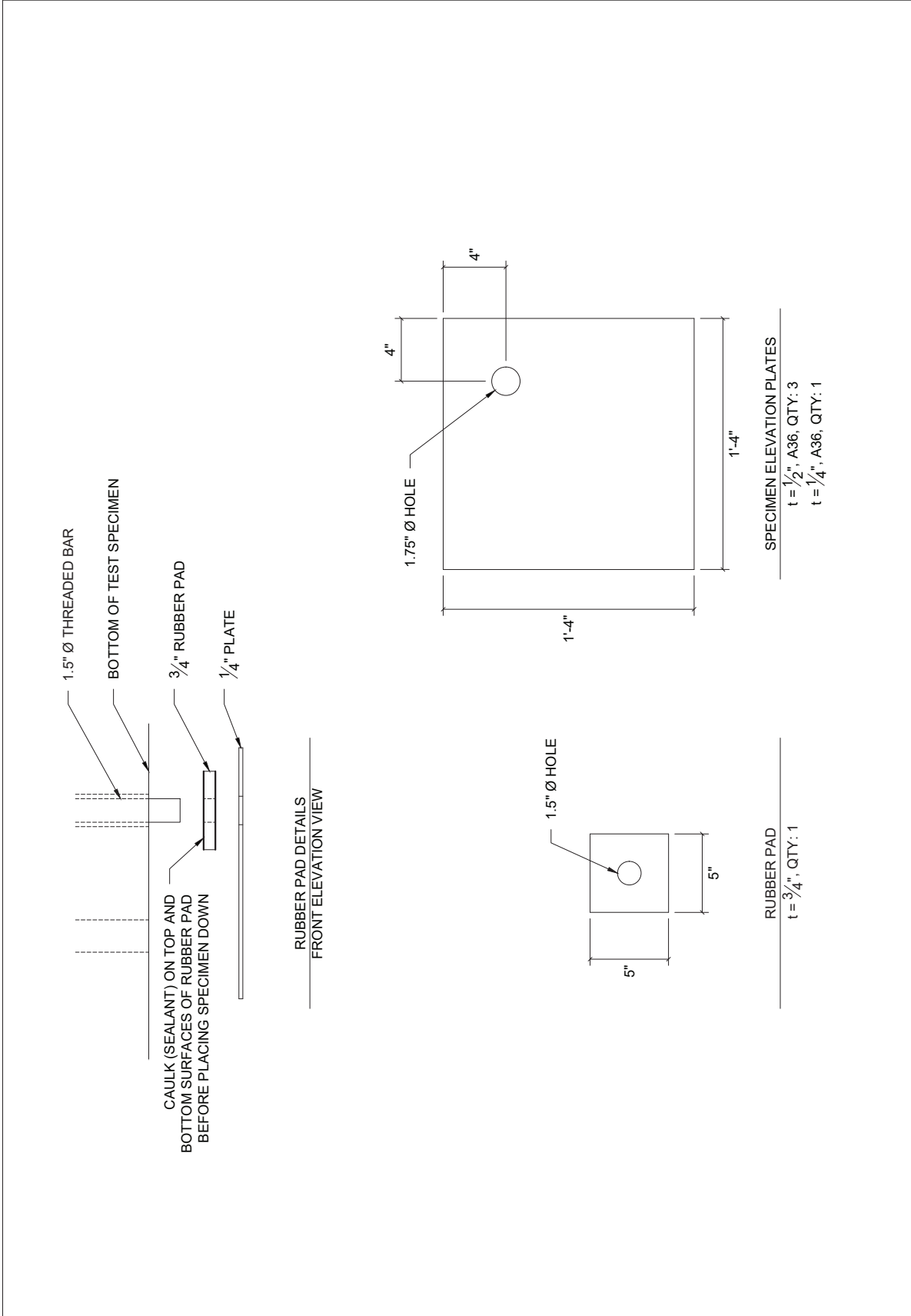
Sequencing:

- (1) Install backer rod and sealant around rubber pad on low anchor point with 1/4" steel plate (see Sheet 04)
- (2) With all steel plates installed, place specimen down
- (3) Hand tighten nuts on anchor bars to prevent specimen from rocking backward (since the specimen is elevated)
- (3) Post-tension the 3 anchor points with 1/2" plates beneath
- (4) Grout 4th anchor point (between 1/4" steel plate and specimen)
- (5) Let grout set
- (6) Post-tension 4th anchor point
- (7) Grout buttress regions

<i>Reinforced Concrete Traffic Railings for Impact Loading</i>		Revisions:
<i>Specimen Anchoring Plan</i>	2020-05-19	<i>University of Florida</i>



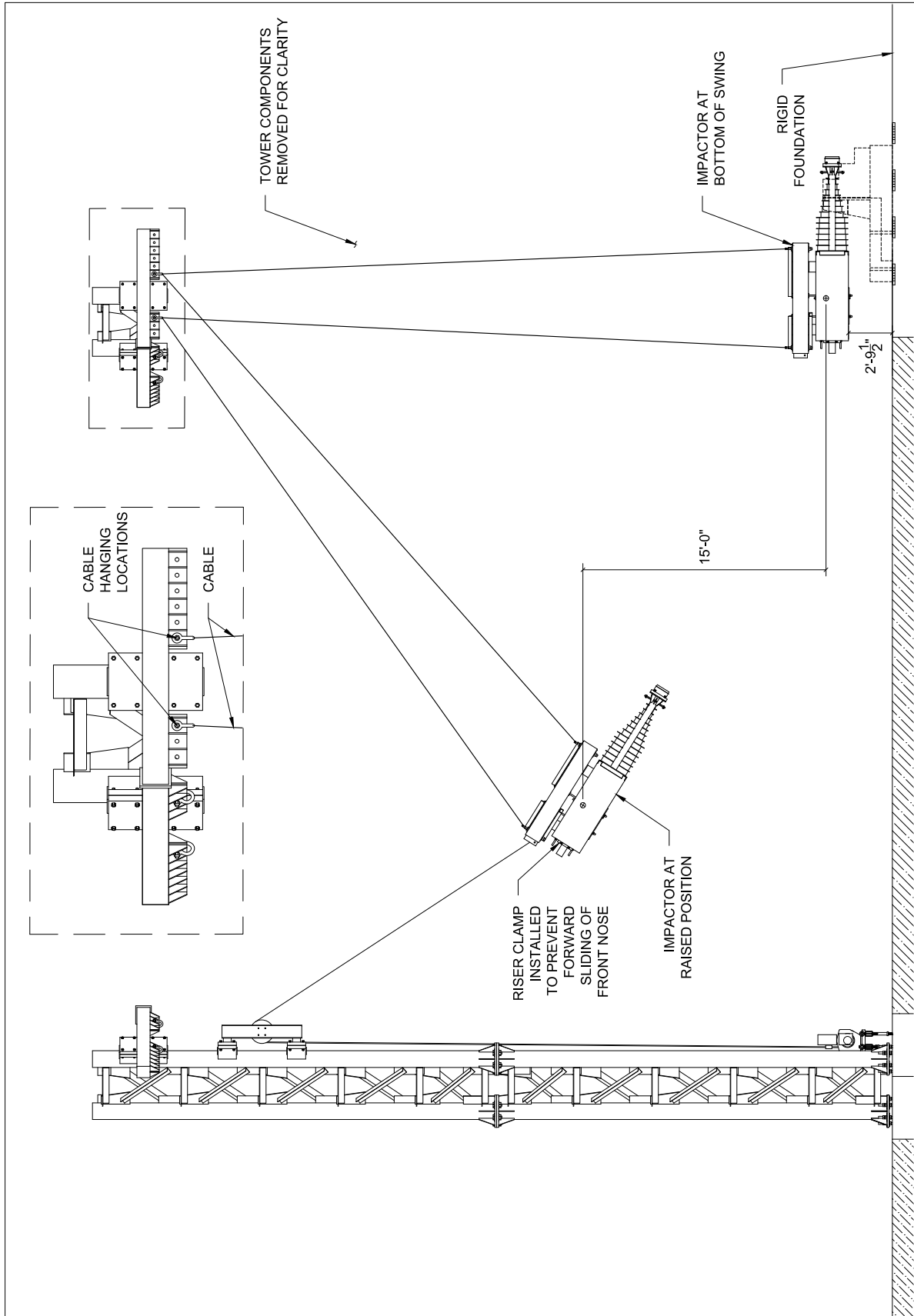
Reinforced Concrete Traffic Railings for Impact Loading		Revisions:
Specimen Anchoring Plan	2020-07-27	University of Florida



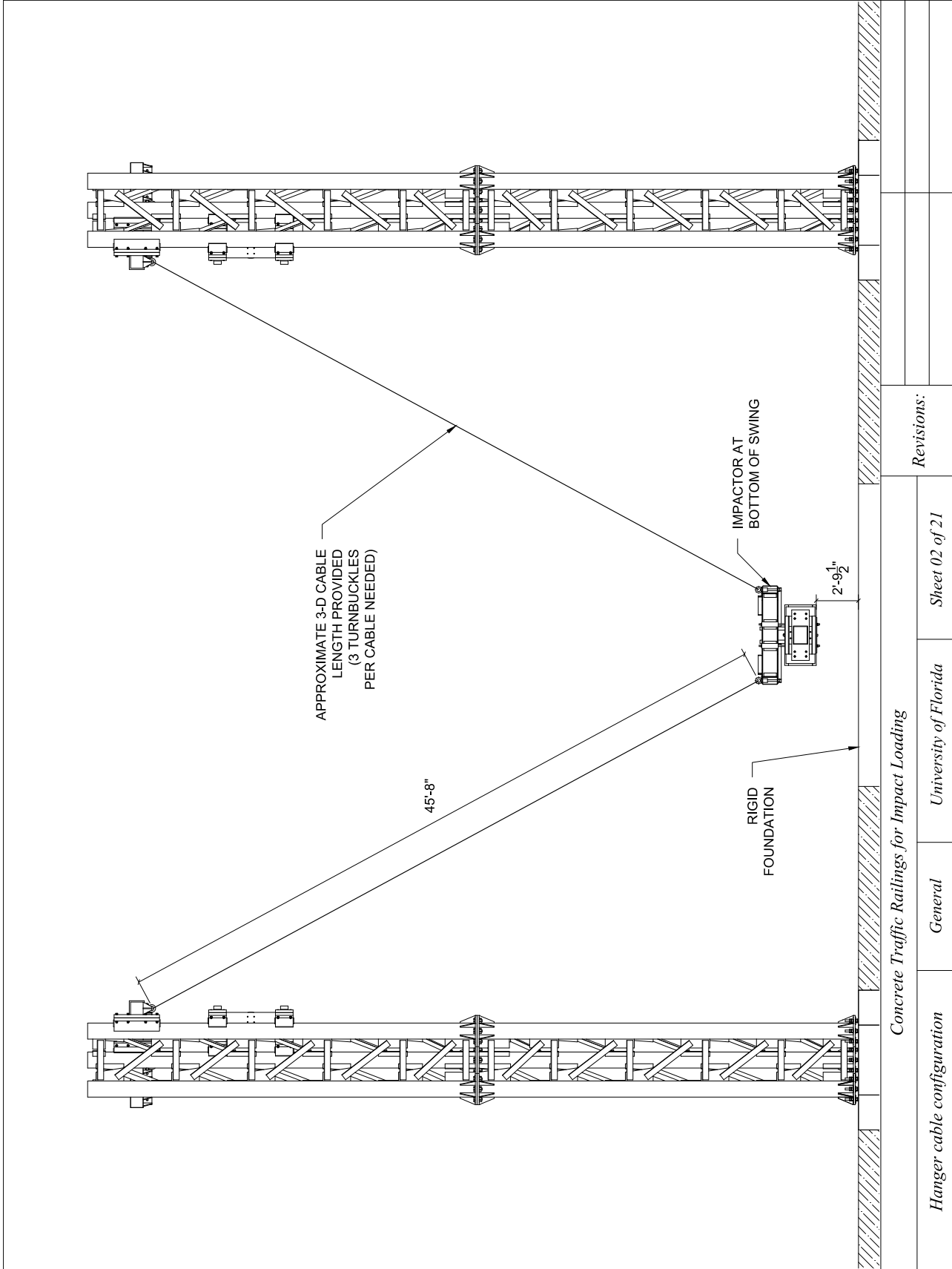
<i>Reinforced Concrete Traffic Railings for Impact Loading</i>		Revisions:
<i>Specimen Anchoring Plan</i>	2020-05-19	University of Florida

**APPENDIX H:
INSTRUMENTATION PLAN**

Presented in this appendix is the rail test specimen pendulum impact instrumentation plan.



<i>Concrete Traffic Railings for Impact Loading</i>		Revisions:
<i>Hanger cable configuration</i>	General	<i>University of Florida</i>
		<i>Sheet 01 of 21</i>



Revisions:

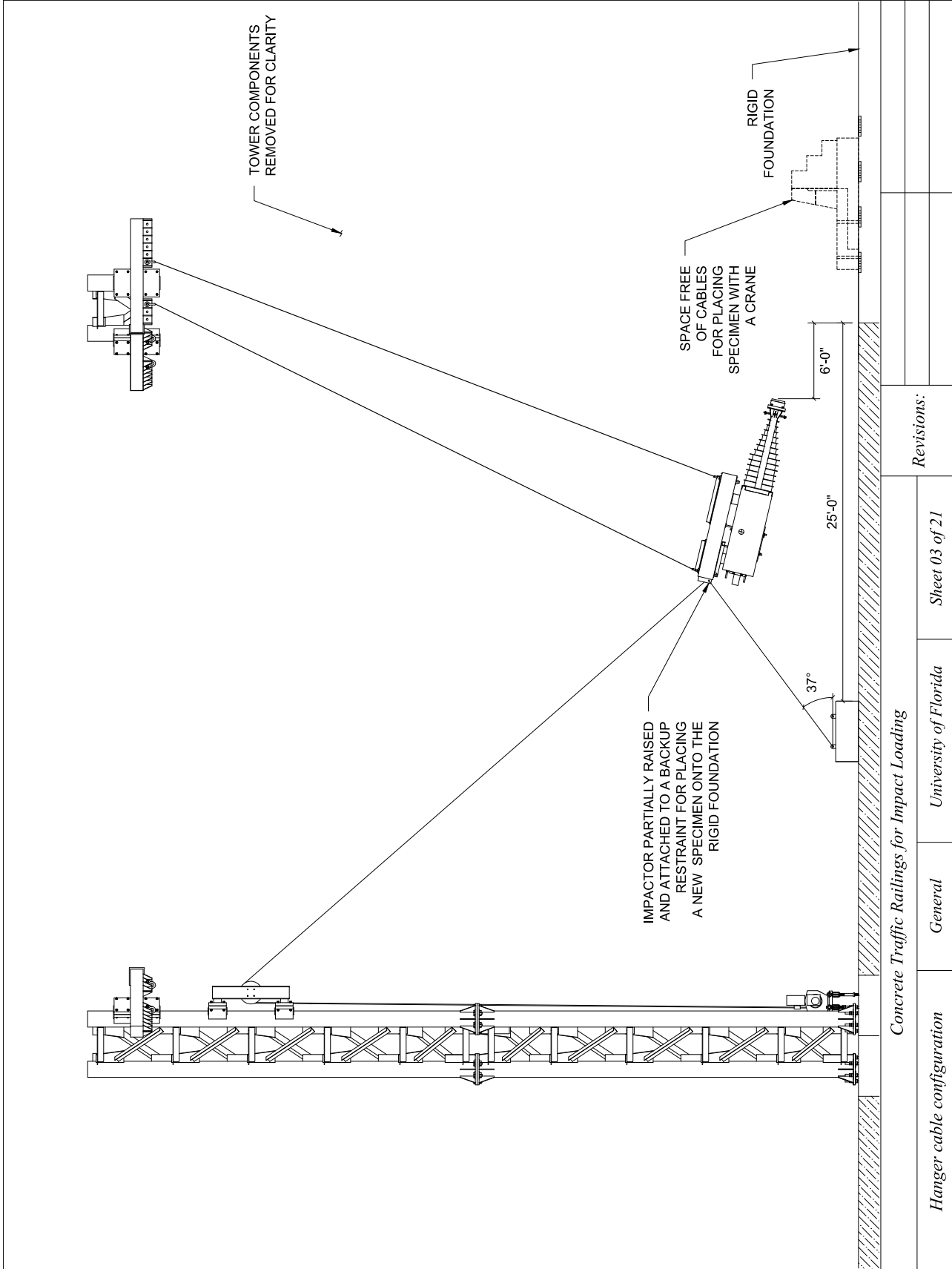
Sheet 02 of 21

University of Florida

General

Concrete Traffic Railings for Impact Loading

Hanger cable configuration



Concrete Traffic Railings for Impact Loading

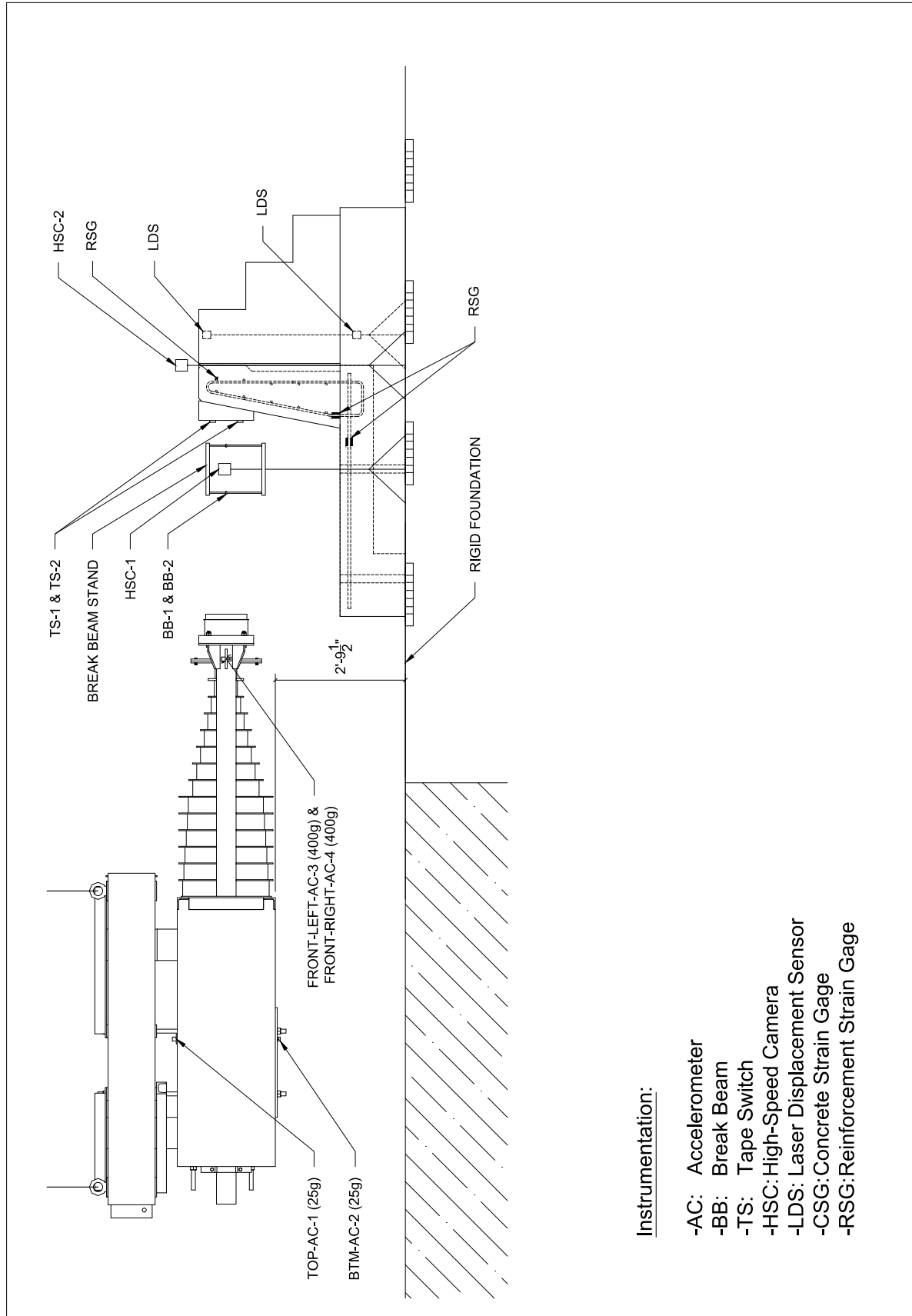
Hanger cable configuration

General

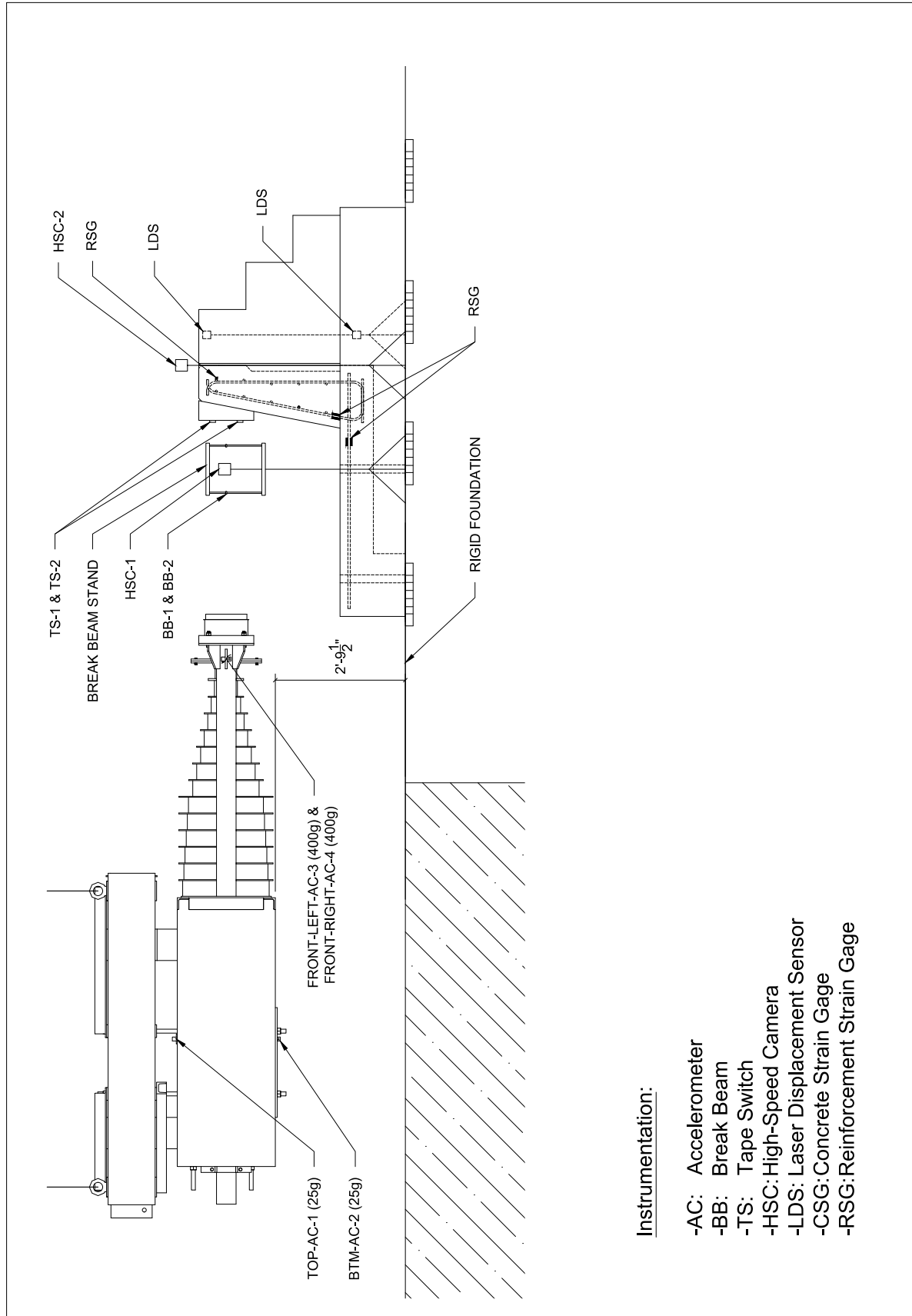
University of Florida

Sheet 03 of 21

Revisions:



<i>Concrete Traffic Railings for Impact Loading</i>		<i>Revisions:</i>
<i>Instrumentation Plan Overview</i>	<i>Steel COR/EOR</i>	<i>University of Florida</i>
<i>Sheet 04 of 21</i>		



Instrumentation:

- AC: Accelerometer
- BB: Break Beam
- TS: Tape Switch
- HSC: High-Speed Camera
- LDS: Laser Displacement Sensor
- CSG: Concrete Strain Gage
- RSG: Reinforcement Strain Gage

Concrete Traffic Railings for Impact Loading

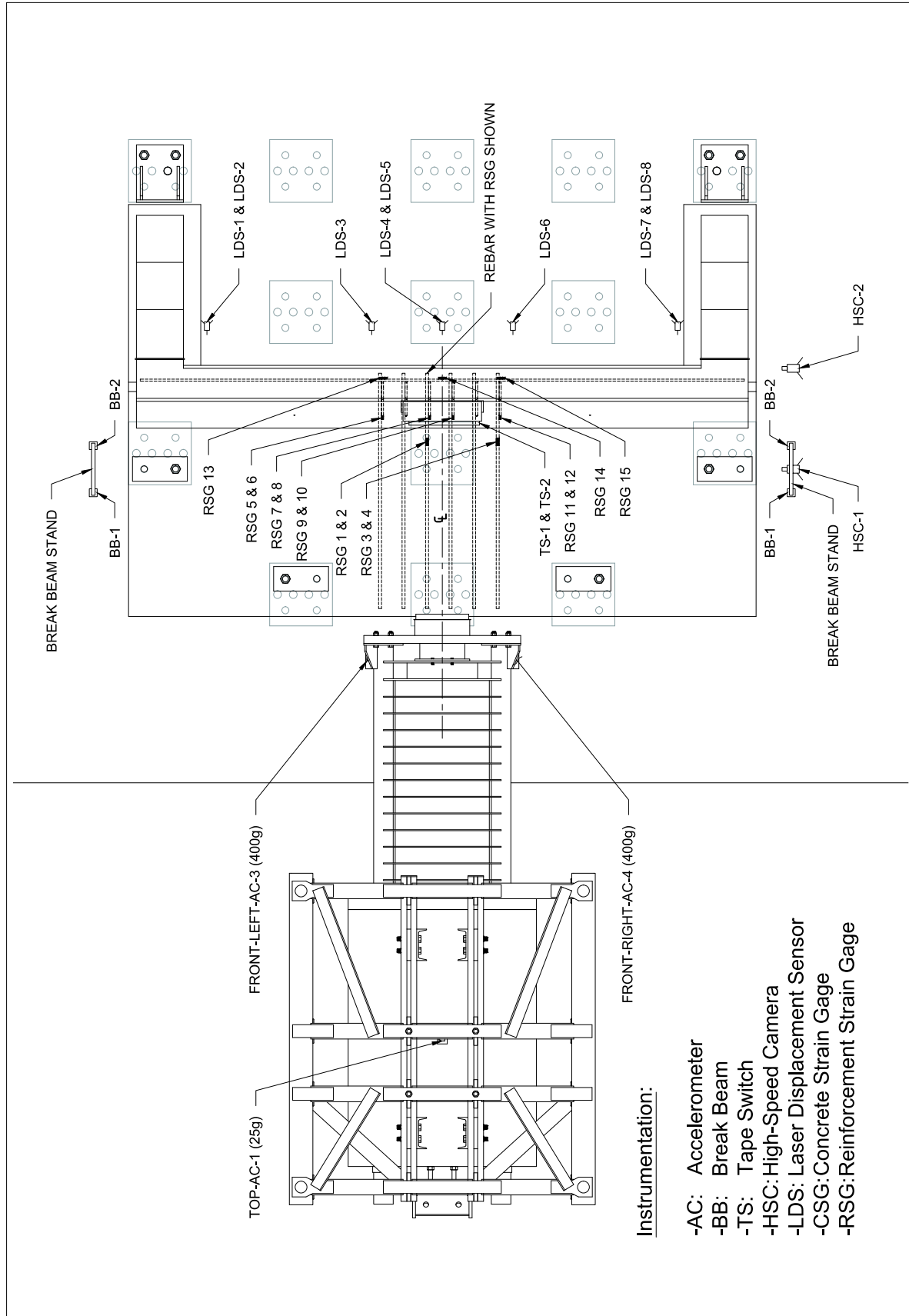
Instrumentation Plan Overview

GFRP COR/EOR

University of Florida

Sheet 05 of 21

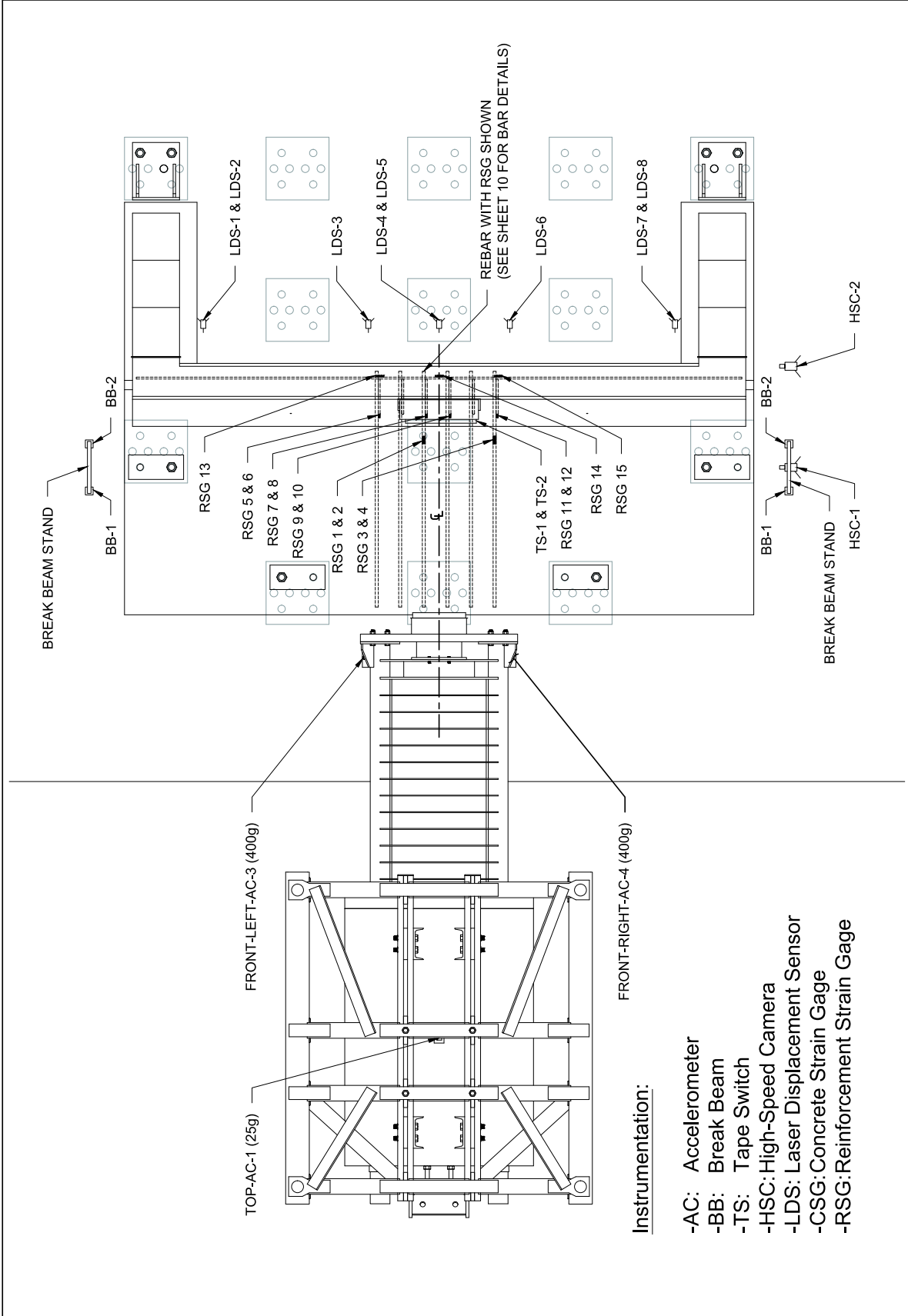
Revisions:



Instrumentation:

- AC: Accelerometer
- BB: Break Beam
- TS: Tape Switch
- HSC: High-Speed Camera
- LDS: Laser Displacement Sensor
- CSG: Concrete Strain Gage
- RSG: Reinforcement Strain Gage

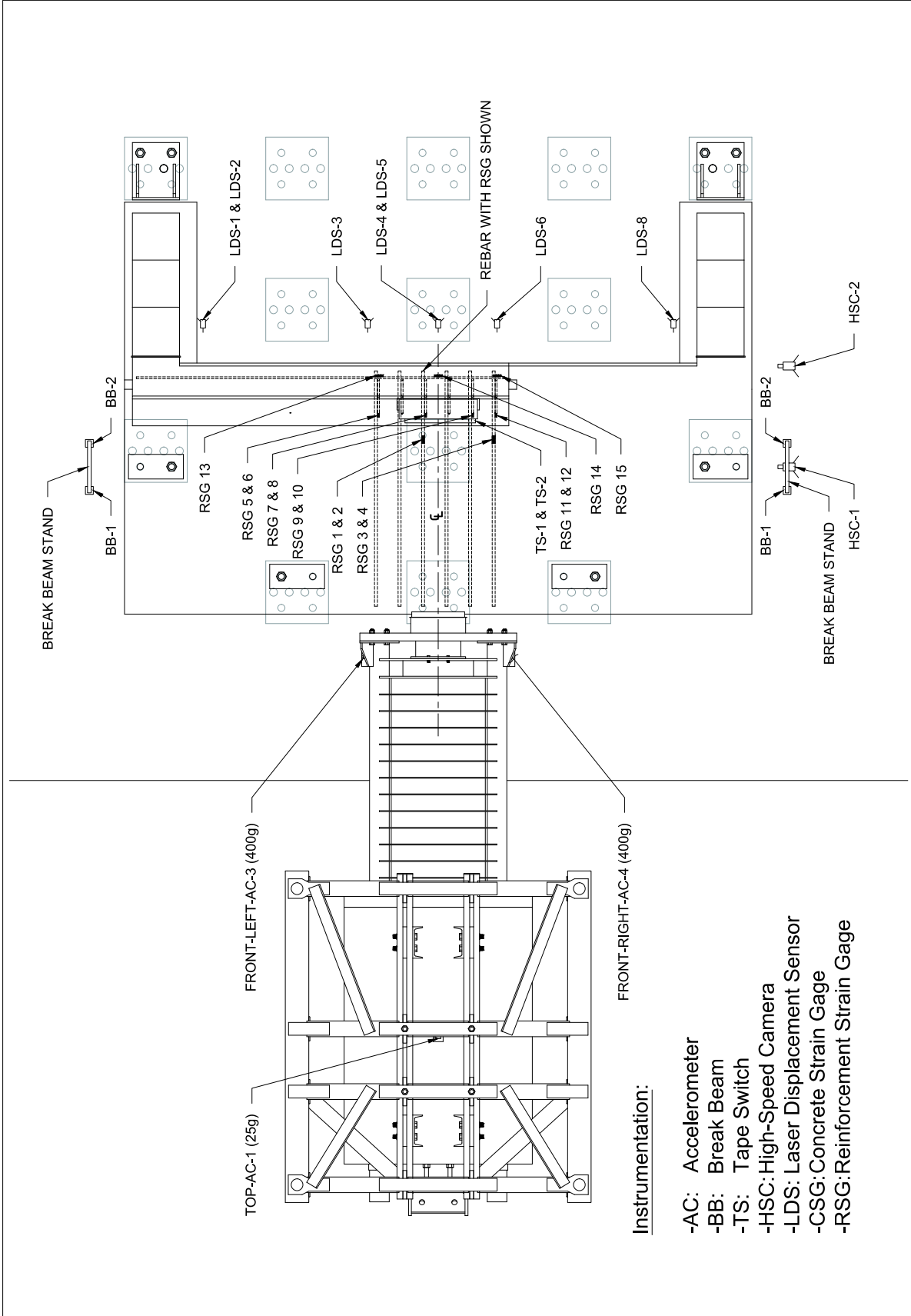
<i>Concrete Traffic Railings for Impact Loading</i>		<i>Revisions:</i>
<i>Instrumentation Plan Overview</i>	<i>Steel COR</i>	<i>University of Florida</i>
		<i>Sheet 06 of 21</i>



Instrumentation:

- AC: Accelerometer
- BB: Break Beam
- TS: Tape Switch
- HSC: High-Speed Camera
- LDS: Laser Displacement Sensor
- CSG: Concrete Strain Gage
- RSG: Reinforcement Strain Gage

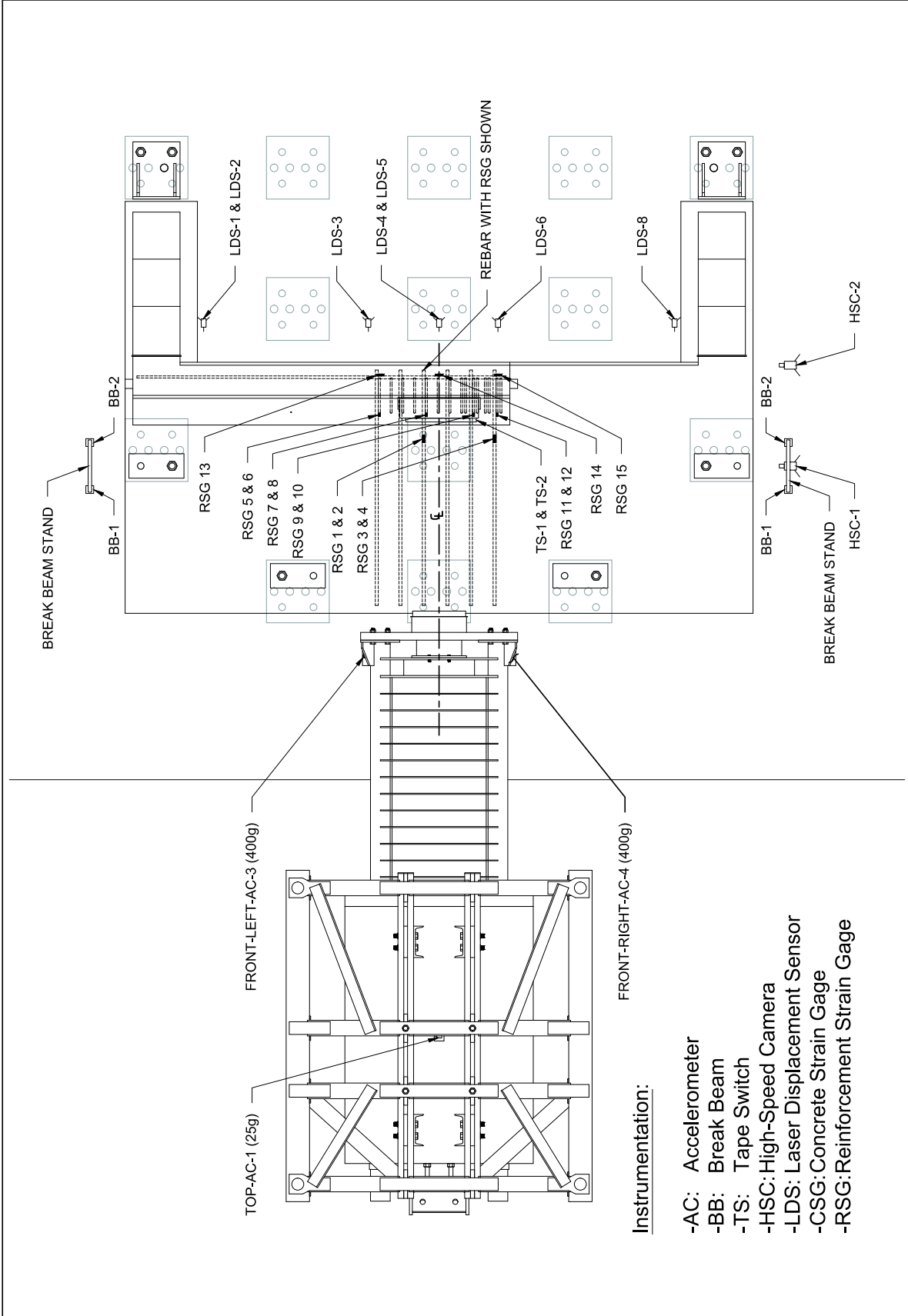
<i>Concrete Traffic Railings for Impact Loading</i>		<i>Revisions:</i>	
<i>Instrumentation Plan Overview</i>	<i>GFRP COR</i>	<i>University of Florida</i>	
		<i>Sheet 07 of 21</i>	



Instrumentation:

- AC: Accelerometer
- BB: Break Beam
- TS: Tape Switch
- HSC: High-Speed Camera
- LDS: Laser Displacement Sensor
- CSG: Concrete Strain Gage
- RSG: Reinforcement Strain Gage

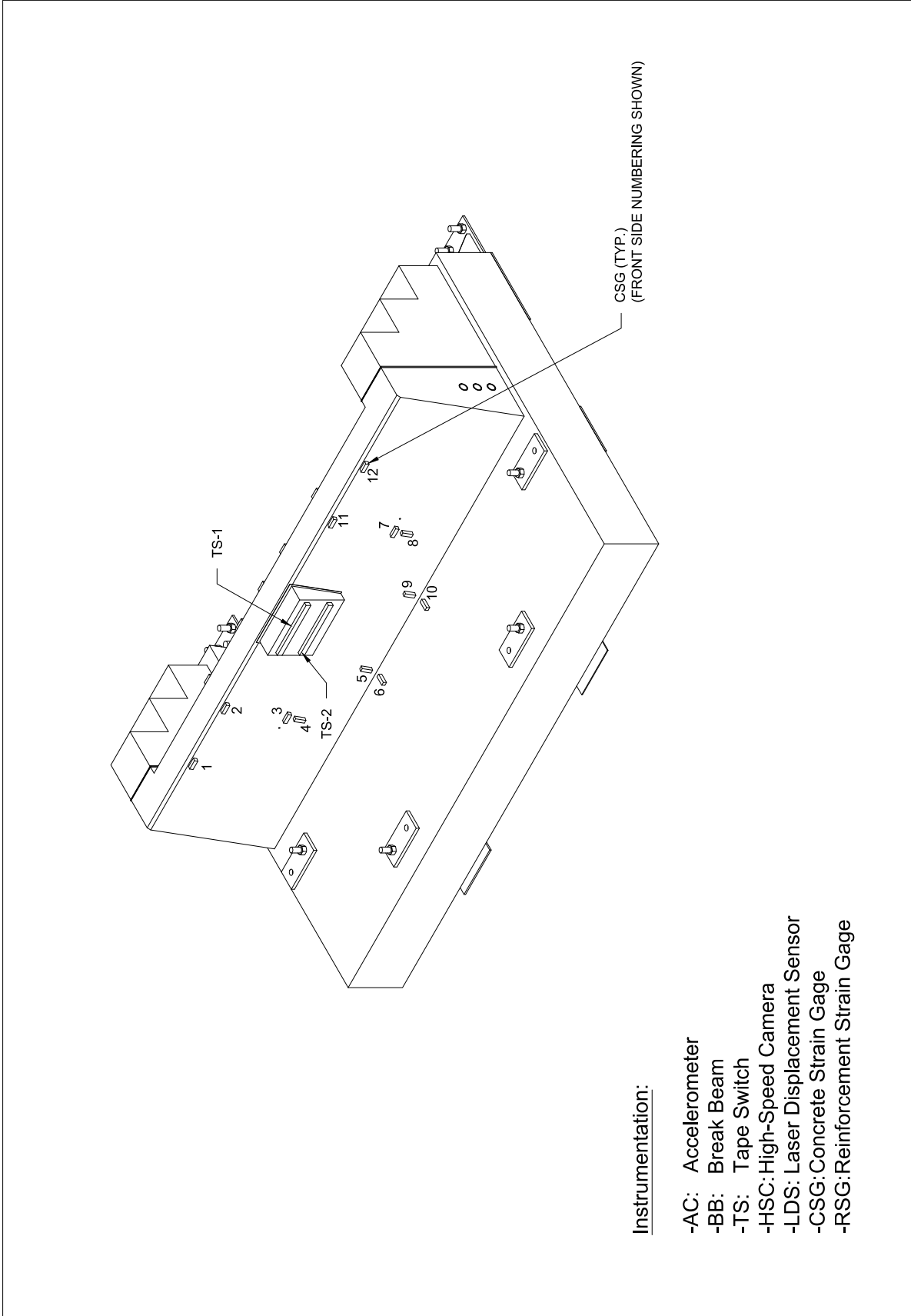
<i>Concrete Traffic Railings for Impact Loading</i>		<i>Revisions:</i>
<i>Instrumentation Plan Overview</i>	<i>Steel EOR</i>	<i>University of Florida</i>
		<i>Sheet 08 of 21</i>



Instrumentation:

- AC: Accelerometer
- BB: Break Beam
- TS: Tape Switch
- HSC: High-Speed Camera
- LDS: Laser Displacement Sensor
- CSG: Concrete Strain Gage
- RSG: Reinforcement Strain Gage

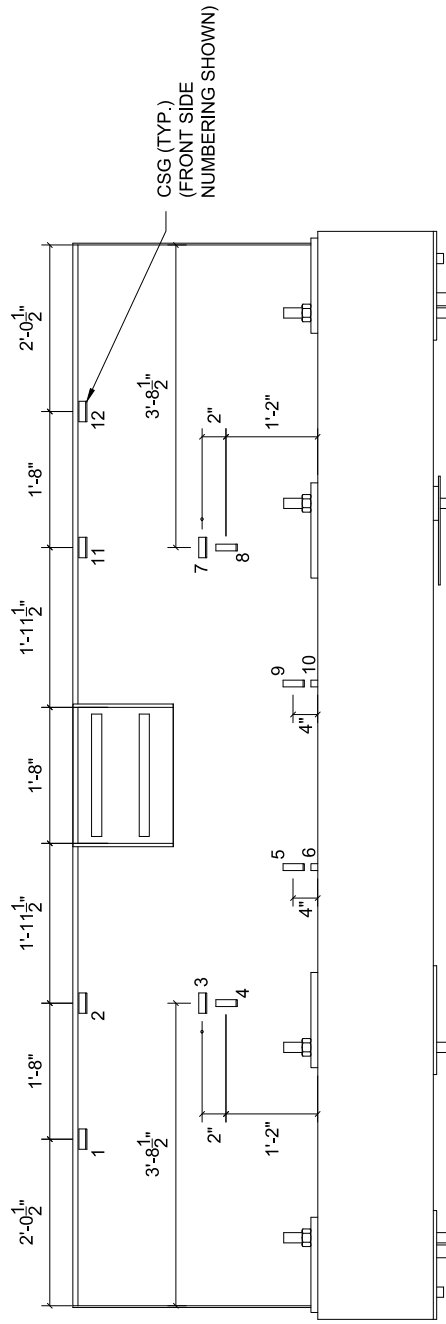
<i>Concrete Traffic Railings for Impact Loading</i>		<i>Revisions:</i>	
<i>Instrumentation Plan Overview</i>	<i>GFRP EOR</i>	<i>University of Florida</i>	
		<i>Sheet 09 of 21</i>	



Instrumentation:

- AC: Accelerometer
- BB: Break Beam
- TS: Tape Switch
- HSC: High-Speed Camera
- LDS: Laser Displacement Sensor
- CSG: Concrete Strain Gage
- RSG: Reinforcement Strain Gage

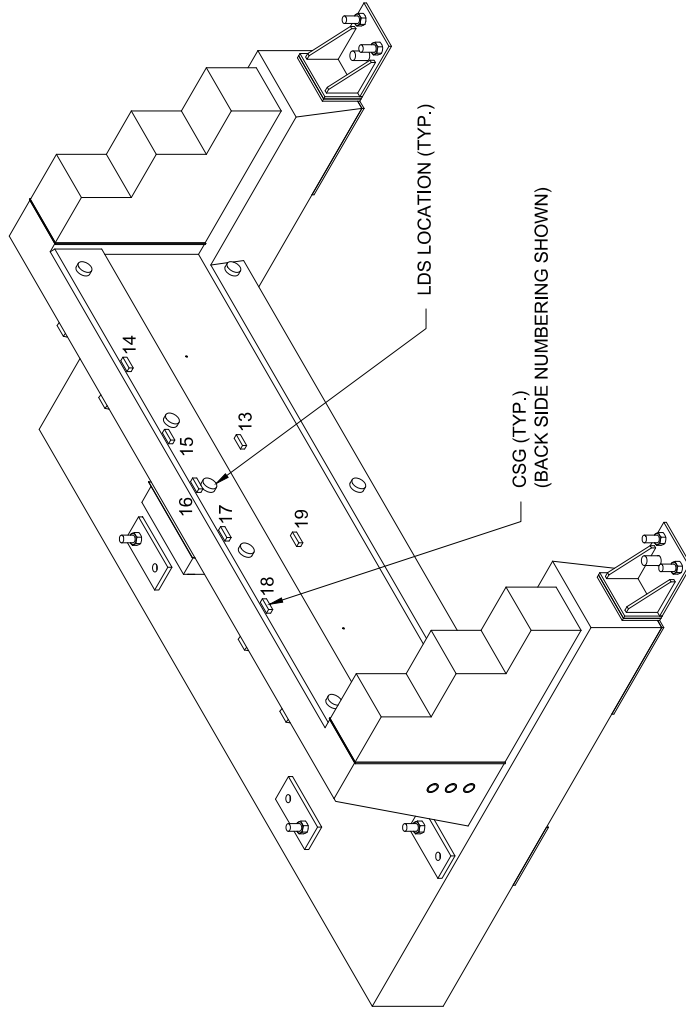
<i>Concrete Traffic Railings for Impact Loading</i>		Revisions:
<i>Concrete Instrumentation</i>	<i>Steel/GFRP COR</i>	<i>University of Florida</i>
	Sheet 10 of 21	



Instrumentation:

- AC: Accelerometer
- BB: Break Beam
- TS: Tape Switch
- HSC: High-Speed Camera
- LDS: Laser Displacement Sensor
- CSG: Concrete Strain Gage
- RSG: Reinforcement Strain Gage

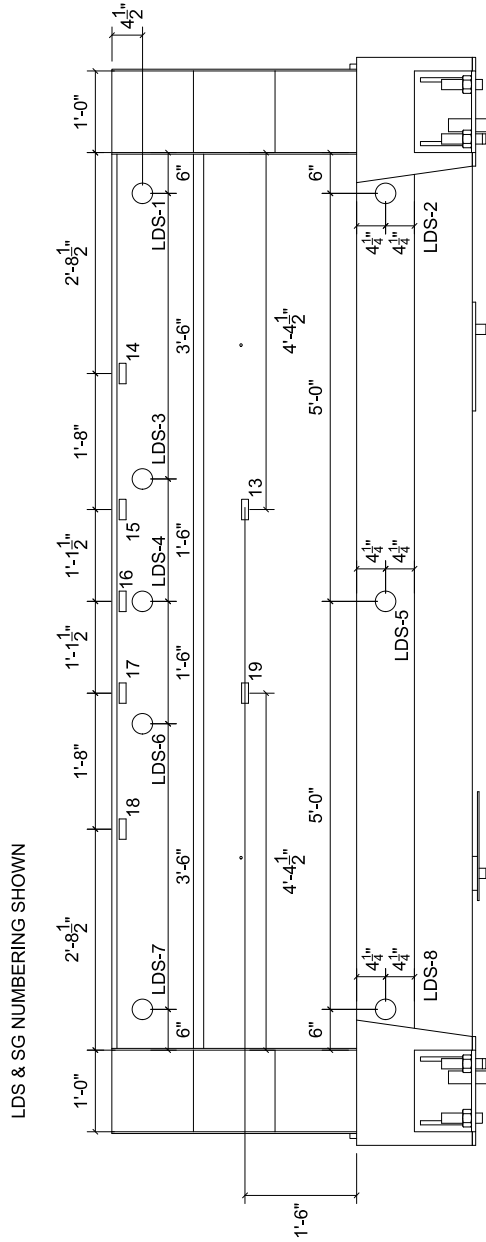
<i>Concrete Traffic Railings for Impact Loading</i>		<i>Revisions:</i>
<i>Concrete Instrumentation</i>	<i>Steel/GFRP COR</i>	<i>University of Florida</i>
	<i>Sheet 11 of 21</i>	



Instrumentation:

- AC: Accelerometer
- BB: Break Beam
- TS: Tape Switch
- HSC: High-Speed Camera
- LDS: Laser Displacement Sensor
- CSG: Concrete Strain Gage
- RSG: Reinforcement Strain Gage

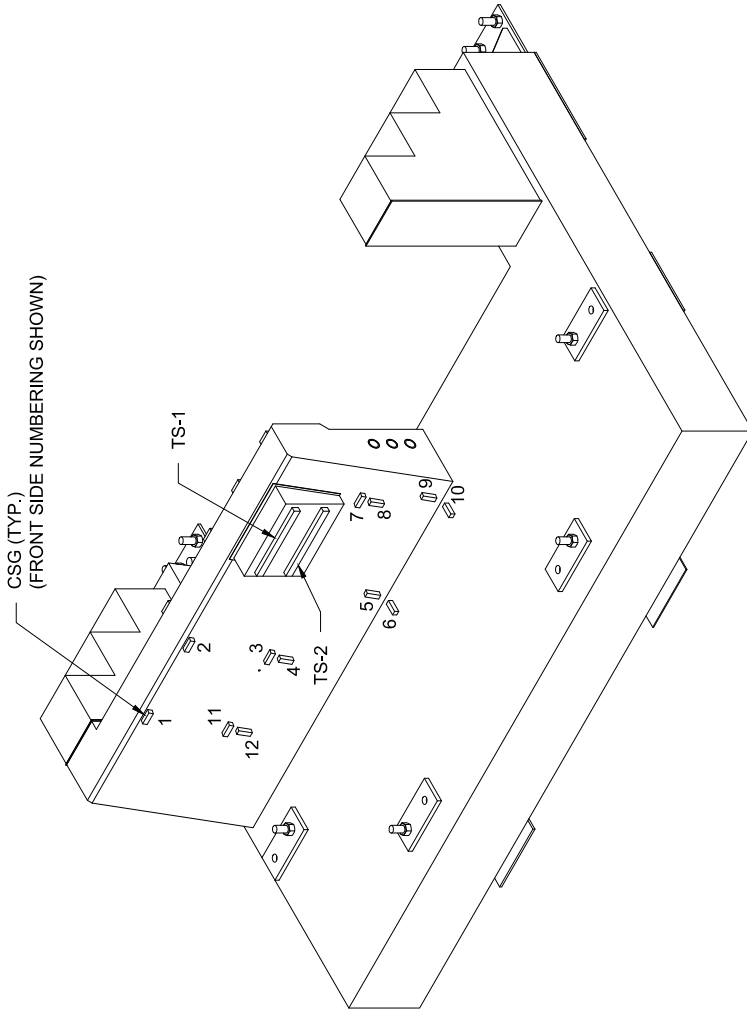
<i>Concrete Traffic Railings for Impact Loading</i>			<i>Revisions:</i>
<i>Concrete Instrumentation</i>	<i>Steel/GFRP COR</i>	<i>University of Florida</i>	<i>Sheet 12 of 21</i>



Instrumentation:

- AC: Accelerometer
- BB: Break Beam
- TS: Tape Switch
- HSC: High-Speed Camera
- LDS: Laser Displacement Sensor
- CSG: Concrete Strain Gage
- RSG: Reinforcement Strain Gage

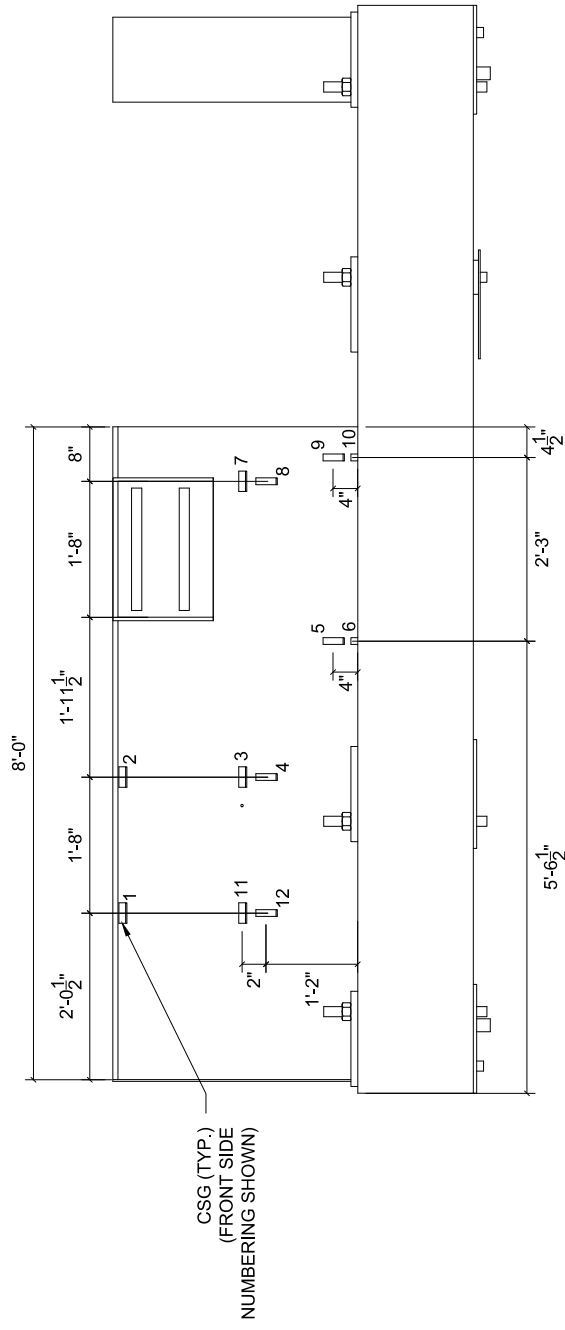
<i>Concrete Traffic Railings for Impact Loading</i>		<i>Revisions:</i>
<i>Concrete Instrumentation</i>	<i>Steel/GFRP COR</i>	<i>University of Florida</i>
	<i>Sheet 13 of 21</i>	



Instrumentation:

- AC: Accelerometer
- BB: Break Beam
- TS: Tape Switch
- HSC: High-Speed Camera
- LDS: Laser Displacement Sensor
- CSG: Concrete Strain Gage
- RSG: Reinforcement Strain Gage

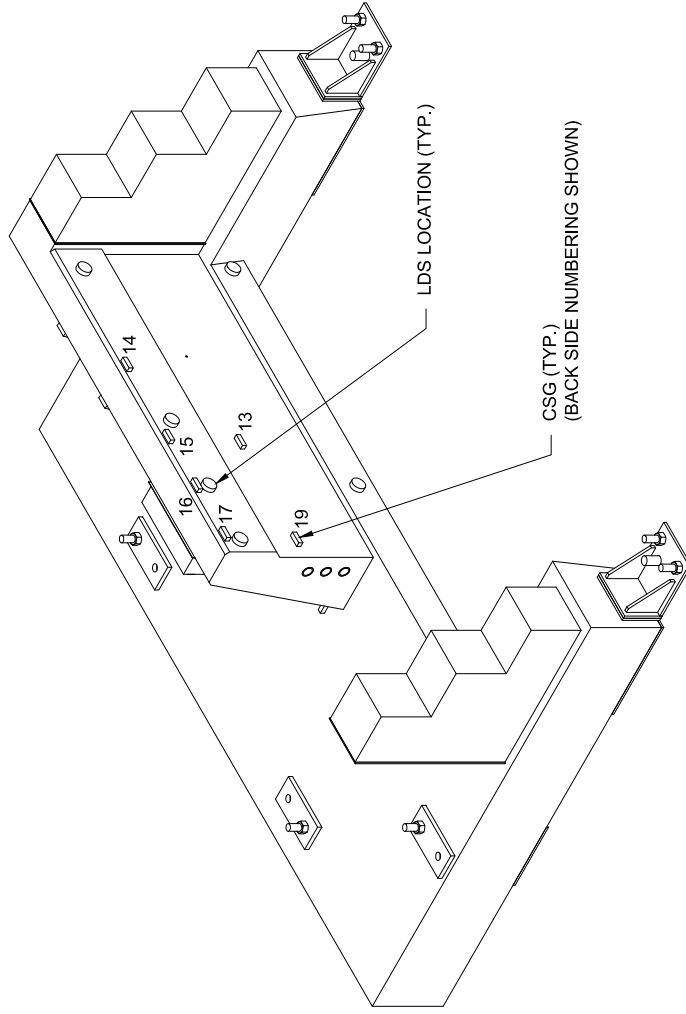
<i>Concrete Traffic Railings for Impact Loading</i>		<i>Revisions:</i>
<i>Concrete Instrumentation</i>	<i>Steel/GFRP EOR</i>	<i>University of Florida</i>
	<i>Sheet 14 of 21</i>	



Instrumentation:

- AC: Accelerometer
- BB: Break Beam
- TS: Tape Switch
- HSC: High-Speed Camera
- LDS: Laser Displacement Sensor
- CSG: Concrete Strain Gage
- RSG: Reinforcement Strain Gage

<i>Concrete Traffic Railings for Impact Loading</i>		<i>Revisions:</i>
<i>Concrete Instrumentation</i>	<i>Steel/GFRP EOR</i>	<i>University of Florida</i>
	<i>Sheet 15 of 21</i>	

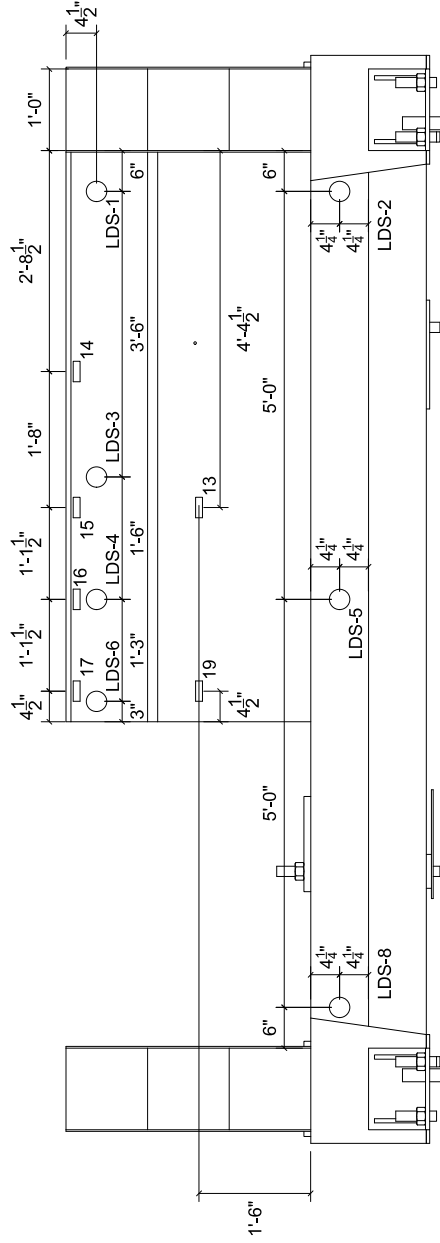


Instrumentation:

- AC: Accelerometer
- BB: Break Beam
- TS: Tape Switch
- HSC: High-Speed Camera
- LDS: Laser Displacement Sensor
- CSG: Concrete Strain Gage
- RSG: Reinforcement Strain Gage

<i>Concrete Traffic Railings for Impact Loading</i>		<i>Revisions:</i>
<i>Concrete Instrumentation</i>	<i>Steel/GFRP EOR</i>	<i>University of Florida</i>
	<i>Sheet 16 of 21</i>	

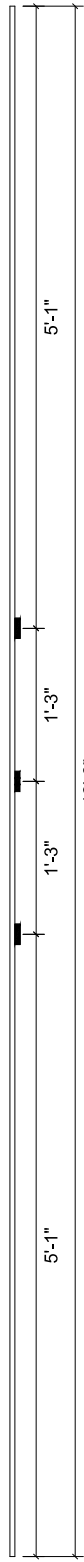
LDS & SG NUMBERING SHOWN



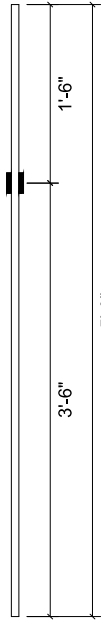
Instrumentation:

- AC: Accelerometer
- BB: Break Beam
- TS: Tape Switch
- HSC: High-Speed Camera
- LDS: Laser Displacement Sensor
- CSG: Concrete Strain Gage
- RSG: Reinforcement Strain Gage

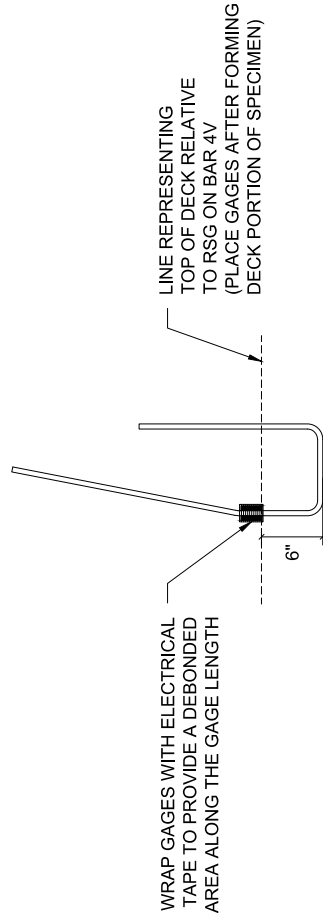
<i>Concrete Traffic Railings for Impact Loading</i>		<i>Revisions:</i>
<i>Concrete Instrumentation</i>	<i>Steel/GFRP EOR</i>	<i>University of Florida</i>
	<i>Sheet 17 of 21</i>	



BAR 4S: TOP LONGITUDINAL BAR IN RAILING
QTY: 1 BAR WITH 3 RSG (3 TOTAL)



BAR S601: TOP TRANSVERSE BAR IN DECK
QTY: 2 BARS EACH WITH 2 RSG (4 TOTAL)

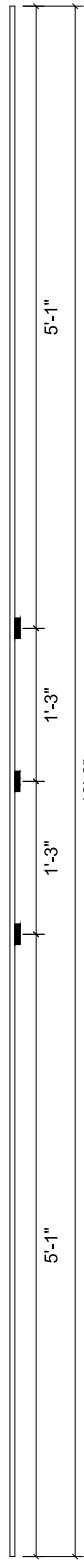


BAR 4V: CONNECTION BAR BETWEEN DECK AND RAIL
QTY: 4 BARS EACH WITH 2 RSG (8 TOTAL)

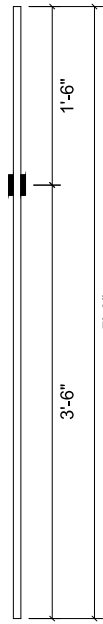
Instrumentation:

- AC: Accelerometer
- BB: Break Beam
- TS: Tape Switch
- HSC: High-Speed Camera
- LDS: Laser Displacement Sensor
- CSG: Concrete Strain Gage
- RSG: Reinforcement Strain Gage

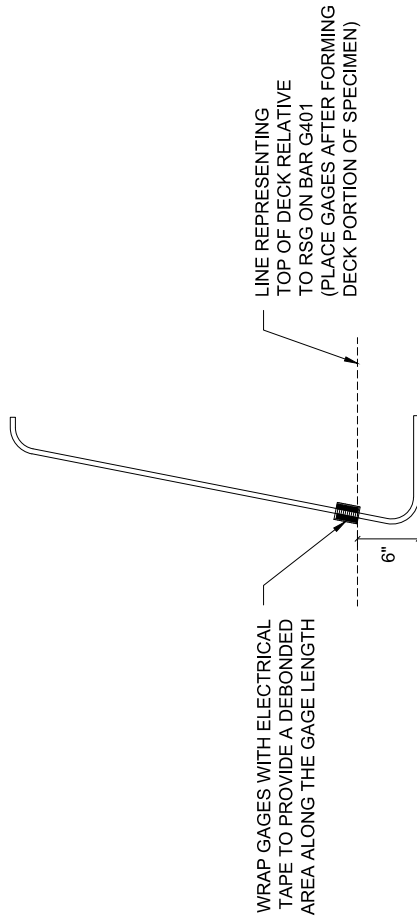
<i>Concrete Traffic Railings for Impact Loading</i>		
<i>Reinforcement Instrumentation</i>	<i>Steel COR</i>	<i>University of Florida</i>
	<i>Sheet 18 of 21</i>	<i>Revisions:</i>



BAR 4S: TOP LONGITUDINAL BAR IN RAILING
QTY: 1 BAR WITH 3 RSG (3 TOTAL)



BAR S601: TOP TRANSVERSE BAR IN DECK
QTY: 2 BARS EACH WITH 2 RSG (4 TOTAL)

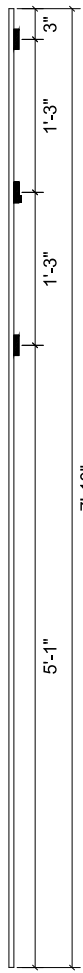


BAR G401: FRONT CONNECTION BAR BETWEEN DECK AND RAIL
QTY: 4 BARS EACH WITH 2 RSG (8 TOTAL)

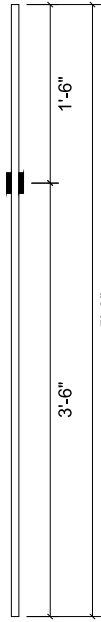
Instrumentation:

- AC: Accelerometer
- BB: Break Beam
- TS: Tape Switch
- HSC: High-Speed Camera
- LDS: Laser Displacement Sensor
- CSG: Concrete Strain Gage
- RSG: Reinforcement Strain Gage

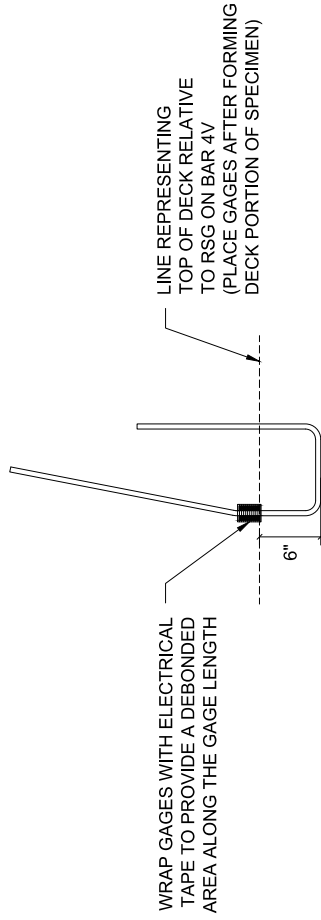
<i>Concrete Traffic Railings for Impact Loading</i>		
<i>Reinforcement Instrumentation</i>	<i>GFRP COR</i>	<i>University of Florida</i>
	<i>Sheet 19 of 21</i>	<i>Revisions:</i>



BAR 4SS: TOP LONGITUDINAL BAR IN RAILING
QTY: 1 BAR WITH 3 RSG (3 TOTAL)



BAR S601: TOP TRANSVERSE BAR IN DECK
QTY: 2 BARS EACH WITH 2 RSG (4 TOTAL)

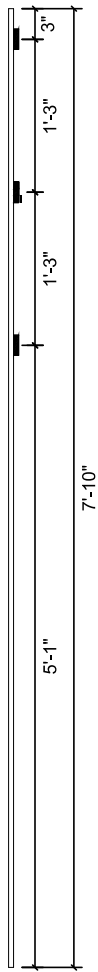


BAR 4V: CONNECTION BAR BETWEEN DECK AND RAIL
QTY: 4 BARS EACH WITH 2 RSG (8 TOTAL)

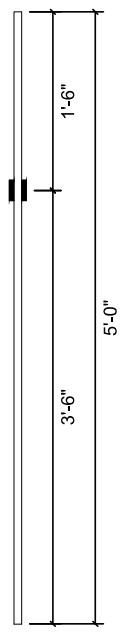
Instrumentation:

- AC: Accelerometer
- BB: Break Beam
- TS: Tape Switch
- HSC: High-Speed Camera
- LDS: Laser Displacement Sensor
- CSG: Concrete Strain Gage
- RSG: Reinforcement Strain Gage

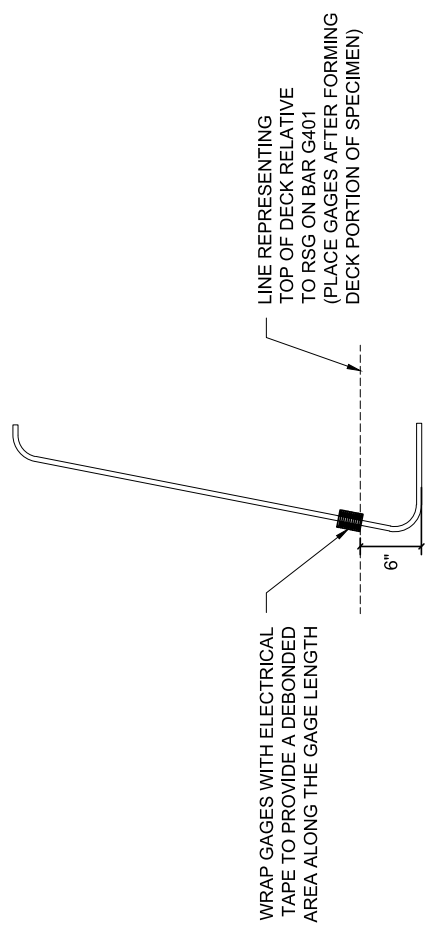
<i>Concrete Traffic Railings for Impact Loading</i>		
<i>Reinforcement Instrumentation</i>	<i>Steel EOR</i>	<i>University of Florida</i>
	<i>Sheet 20 of 21</i>	<i>Revisions:</i>



BAR #55: TOP LONGITUDINAL BAR IN RAILING
QTY: 1 BAR WITH 3 RSG (3 TOTAL)



BAR S601: TOP TRANSVERSE BAR IN DECK
QTY: 2 BARS EACH WITH 2 RSG (4 TOTAL)



BAR G401: FRONT CONNECTION BAR BETWEEN DECK AND RAIL
QTY: 4 BARS EACH WITH 2 RSG (8 TOTAL)

WRAP GAGES WITH ELECTRICAL TAPE TO PROVIDE A DEBONDED AREA ALONG THE GAGE LENGTH

Instrumentation:

- AC: Accelerometer
- BB: Break Beam
- TS: Tape Switch
- HSC: High-Speed Camera
- LDS: Laser Displacement Sensor
- CSG: Concrete Strain Gage
- RSG: Reinforcement Strain Gage

<i>Concrete Traffic Railings for Impact Loading</i>		
<i>Reinforcement Instrumentation</i>	<i>GFRP EOR</i>	<i>University of Florida</i>
	<i>Sheet 21 of 21</i>	<i>Revisions:</i>

**APPENDIX I:
HARDENED MECHANICAL PROPERTIES OF
RAIL CONCRETE MIXTURES**

Presented in this appendix are measured hardened mechanical properties of concrete test samples (4-in. x 8-in. cylinders) that were formed with the same concrete batches used to cast full-scale pendulum impact test specimens. Concrete compressive strengths are included for each of the impact test specimens at 28 days and at (or near) the day of pendulum impact testing.

Table I-1 Average compressive strength of concrete deck samples at 28 days

Related test specimen	Concrete placement location	Cast date	Test date	Age (days)	Avg. compressive strength (psi)
GFRP COR 1	Deck	4/13/2021	5/11/2021	28	4633
GFRP EOR 1	Deck	6/2/2021	6/30/2021	28	4064
GFRP EOR 2	Deck	9/8/2021	10/4/2021	28	7072
R/C COR 1	Deck	6/29/2020	7/27/2020	28	4542
R/C COR 2	Deck	8/31/2020	9/28/2020	28	5138
R/C EOR	Deck	2/17/2021	3/17/2021	28	4480

Table I-2 Average compressive strength of concrete deck samples near day of impact testing

Related test specimen	Concrete placement location	Cast date	Test date	Age (days)	Avg. compressive strength (psi)
GFRP COR 1	Deck	4/13/2021	6/4/2021	52	4239
GFRP EOR 1	Deck	6/2/2021	7/30/2021	58	4853
GFRP EOR 2	Deck	9/8/2021	11/10/2021	63	8943
R/C COR 1	Deck	6/29/2020	10/30/2020	123	5027
R/C COR 2	Deck	8/31/2020	12/9/2020	100	6677
R/C EOR	Deck	2/17/2021	4/6/2021	48	5332

Table I-3 Average compressive strength of concrete rail samples at 28 days

Related test specimen	Concrete placement location	Cast date	Test date	Age (days)	Avg. compressive strength (psi)
GFRP COR 1	Rail	5/4/2021	6/1/2021	28	3605
GFRP EOR 1	Rail	6/29/2021	7/28/2021	28	3831
GFRP EOR 2	Rail	10/11/2021	11/8/21	28	5031
R/C COR 1	Rail	7/16/2020	8/13/2020	28	4232
R/C COR 1	Rail	9/15/2020	10/13/2020	28	4105
R/C EOR	Rail	3/3/2021	3/31/2021	28	4474

Table I-4 Average compressive strength of concrete rail samples near day of testing

Related test specimen	Concrete placement location	Cast date	Test date	Age (days)	Avg. compressive strength (psi)
GFRP COR 1	Rail	5/4/2021	6/4/2021	31	4239
GFRP EOR 1	Rail	6/29/2021	7/30/2021	75	4020
GFRP EOR 2	Rail	10/11/2021	11/10/2021	34	4987
R/C COR 1	Rail	7/16/2020	10/30/2020	106	4972
R/C COR 1	Rail	9/15/2020	12/9/2020	85	5724
R/C EOR	Rail	3/3/2021	4/6/2021	34	4799